Author:
Townsend, Esther

Title:
Self-assembly of stimuli-responsive supramolecular nanostructures based on oligo(aniline) amphiphiles

Self-assembly of stimuli-responsive supramolecular nanostructures based on oligo(aniline) amphiphiles

Esther Jennie Townsend

School of Chemistry

University of Bristol

A dissertation submitted to the University of Bristol in accordance with the requirements for award of the degree of Doctor of Philosophy in Chemistry in the Faculty of Science.

May 2021

Words: Fifty-one thousand and seventy

ABSTRACT

Self-assembly is a valuable tool for the preparation of functional, supramolecular nanostructures from the bottom up. Liquid crystal mesophases are particularly attractive in this regard, with complex nanostructures that are readily adaptable to a diverse range of applications, from drug delivery vesicles to templates. Meanwhile, oligo(aniline)s are conjugated oligomers, with exciting switchable conductive and oxidative properties that can both benefit from and be used to direct self-assembled structures.

In this thesis, the effect of electroactive amphiphiles on the formation of monoolein cubic phases is explored and explained through discussion of their molecular packing parameters. Subsequently, an understanding of the ordered mesophases formed by a combination of amphiphiles and monoolein is used in the formation of well-defined, nanostructured polymers.

The preparation of single-tailed and bola-form tetra(aniline)-derived amphiphiles is described, with similar but chemically distinct structures chosen to provide different molecular packing parameters. The amphiphilic nature of the molecules, with their tetra(aniline) cores and alkyl tails terminated by cationic head groups, enabled their interaction with lipid bilayers. Small-angle X-ray scattering and UV-Vis/NIR absorption spectroscopy were used to probe the assemblies formed by the combinations of amphiphiles and lipids, which showed that transitions between cubic phases could be readily controlled by tuning of the amphiphiles' oxidation states and structures.

Different approaches for the synthesis of a polymerizable tetra(aniline)-derived amphiphile are also described, although with limited success owing to the formation of unwanted side products, which could not be removed by typical purification techniques. Instead, the binding of tetra(aniline)-amphiphiles is achieved through electrostatic interactions, using acids with multiple doping groups to non-covalently cross-link the amphiphiles in solution and within lipid cubic phases.

The facile manipulation of lipidic mesophases with electroactive amphiphiles is promising for the design of responsive architectures for many applications, while explorations of the templated assembly of oligo(aniline)s should guide further research into the design of responsive, porous polymers.

ACKNOWLEDGEMENTS

First and foremost, I would like to thank my supervisors, Professor Charl Faul and Dr Annela Seddon, for all they have done to guide and support me throughout my PhD. I am grateful to both for the time, patience and energy they have granted to me and my project. Their kindness and support will always be remembered.

I would like to acknowledge the EPSRC and the University of Bristol Alumni Association for financial support during this process. I would also like to thank the Bristol Centre for Functional Nanomaterials for the excellent training and support that I have received over the years. The BCFN are like a family and it has been a privilege to be counted among their members.

I am grateful to my collaborators, Dr Yang Li and Professor Kun Liu at Jilin University, Changchun, China. Discussions with both on the synthesis and polymerization of gemini monomers were highly instructive and valuable for directing my own work.

I have been lucky to be a part of two excellent research groups, who provided insight and expertise in both synthetic chemistry and X-ray scattering. The Faul research group were a source of fun, energy and inspiration. I would like to thank the Faul group members I have had the privilege to work with, particularly Dr Alex Bell, Dr Ben Mills, Dr Carl Hu, Dr Kazuyoshi Watanabe, Dr Maha Alotaibi, Dr Michael Dicker, Dr Djen Kuhnel, Veronica Del Angel Hernandez, Pongsathon Boonrod, Dr Henry Symons, Christian Romero, Nouf Zaghloul, Marcos Villeda Hernandez, Sam Deeks, Maximillian Hagemann, Ben Baker, Xue Fang, Basiram Brahma Narzary, Dr Sebastian Rochat and Neha Yadav. From the Seddon research group, I would like to acknowledge Chris Brasnett, whose expertise and support has been gratefully received throughout my PhD. I would also like to thank those project students I have had the pleasure to work with and mentor, Alex Byrne and Thomas Bott. Finally, I would like to express my gratitude to Dr Anna Slastanova in the Briscoe research group for providing access to and assisting with their freeze-dryer.

I owe family and friends a debt of gratitude. They have been a source of encouragement and strength throughout this process. I would like to thank my parents for their endless support, love and for their belief in my abilities. Christine Townsend deserves special thanks for proof-reading a thesis that may as well have been written in another language.

I dedicate this thesis to the Dr Townsends (and Dr Cawthornes) that have come before me.

DECLARATION

I declare that the work in this dissertation was carried out in accordance with the requirements of the University's *Regulations and Code of Practice for Research Degree Programmes and* that it has not been submitted for any other academic award. Except where indicated by specific reference in the text, the work is the candidate's own work. Work done in collaboration with, or with the assistance of, others, is indicated as such. Any views expressed in the dissertation are those of the author.

SIGNED: ..... DATE:.....

TABLE OF CONTENTS

CONTENTS

LIST OF FIGURES

LIST OF SCHEMES

LIST OF TABLES

LIST OF ABBREVIATIONS

Abbreviation	Full term
DOPC	1,2-Dioleoyl-sn-glycero-3-phosphocholine
NDS	1,5-Naphthalenedisulfonic acid
EDC	1-Ethyl-3-(3-dimethylaminopropyl)-carbodiimide
PI	2,2'-Azobis(2-methylpropionamidine) dihydrochloride
XPhos	2-Dicyclohexylphosphino-2',4',6'-triisopropylbiphenyl
CF	5(6)-Carboxyfluorescein
NH_2	Amine
AFM	Atomic force microscopy
V	Bicontinuous cubic
BEHP	Bis(ethyl hexyl) phosphate
CSA	Camphorsulfonic acid
CAC	Critical aggregation concentrations
CMC	Critical micelle concentration
dba	Dibenzylidneneacetone
DMF	Dimethylformamide
CPh_2	Diphenylmethylene
DBSA	Dodecylbenzenesulfonic acid
Pn3m	Double diamond
DLS	Dynamic light scattering
EB	Emeraldine base
ES	Emeraldine salt
GME	Glyceryl monooleyl ether
Ia3d	Gyroid
H_1	Hexagonal
HOMO	Highest occupied molecular orbital
HCl	Hydrochloric acid
H_2O_2	Hydrogen peroxide
L_α	Lamellar
LEB	Leucoemeraldine base
LUMO	Lowest unoccupied molecular orbital
LLC	Lyotropic liquid crystal
I_1	Micellar cubic
MO	Monoolein
NMR	Nuclear magnetic resonance
OANI	Oligo(aniline)
pp	Packing parameter
PPO	Pentaerythritol propoxylate
PB	Pernigraniline base
Ph	Phenyl
POM	Polarised optical microscopy
PANI	Poly(aniline)
PEG	Poly(ethylene glycol)
PNIPAM	Poly(N-isopropylacrylamide)

PDI	Polydispersity index
Im3m	Primitive
SEM	Scanning electron microscopy
SANS	Small-angle neutron scattering
SAXS	Small-angle X-ray scattering
L_3	Sponge
SPION	Superparamagnetic iron oxide nanoparticles
Boc	Tert-butyloxycarbonyl
TANI	Tetra(aniline)
TANI-C_{12}TAB	Tetra(aniline)-dodecyl trimethylammonium bromide
TANI-PTAB	Tetra(aniline)-pentyl trimethylammonium bromide
TANI-$(PTAB)_2$	Tetra(aniline)-(pentyl trimethylammonium bromide)$_2$
TANI-PTPB	Tetra(aniline)-pentyl trimethylphosphonium bromide
THF	Tetrahydrofuran
TLC	Thermotropic liquid crystal
TLC	Thin layer chromatography
TEM	Transmission electron microscopy
TFA	Trifluoroacetic acid
TMSI	Trimethylsilane iodide
TRIS-HCl	Trizma® hydrochloride
UV-Vis/NIR	Ultraviolet/visible/near-infrared
Z_{Ave}	Z-average

PUBLICATIONS

Some of the work outlined in this thesis forms the basis of publications that are in preparation or have been submitted.

Parts of Chapter 1 have been outlined in the following review paper, for which E. Townsend contributed to the research collection and wrote the main text, excluding the introduction.

> E. J. Townsend, M. Alotaibi, B. M. Mills, K. Watanabe, A. M. Seddon, C. F. J. Faul. Electroactive amphiphiles for addressable supramolecular nanostructures. *ChemNanoMat.* **4**, 741-752 (2018).

Most of Chapters 2, 3 and 4 form the basis of a forthcoming article:

> E. J. Townsend, M. Alotaibi, A. M. Seddon, C. F. J. Faul. Order transitions between bicontinuous cubic phases with pH-responsive electroactive amphiphiles. *In preparation.*

Additional publication:

> J. Chen, W. Yan, E. J. Townsend, J. Feng, L. Pan, V. Del Angel Hernandez, C. F. J. Faul. Tuneable surface area, porosity and function in conjugated microporous polymers. *Angew. Chem. Int. Ed.* **58**, 11715-11719 (2019).

1 INTRODUCTION

The desire to construct materials on the nanoscale has captivated researchers for decades, as the world strives towards the miniaturization of electronic devices, medicines, and environmental technologies. However, the construction of nanomaterials is often far more complex than their conceptualization.

There are two main fabrication approaches for the design of nanomaterials, which are top-down and bottom-up.[1] In top-down designs, nanometre-sized features are prepared from much larger materials, for example by etching. Meanwhile, with a bottom-up approach, molecules are designed to self-assemble into the desired structures with minimal external input, mimicking systems found in nature.[2] The latter approach can enable materials to be prepared with feature sizes not currently available to current lithographic approaches and can enable the design of soft systems that can respond to external stimuli, changing structure and function as required.[3] However, it is not often easy to prepare molecules that will organise into the desired shape under the correct conditions, particularly in mixed systems, as will be outlined in further detail in this chapter.

While much work has been done on understanding bottom-up approaches for material design,[4] challenges arise for each new system investigated. The work detailed in this thesis aims to develop an understanding of stimuli-responsive self-assembled systems and to use this knowledge to develop highly ordered polymer structures.

1.1 SELF-ASSEMBLY

Self-assembly has been described as "the spontaneous association of molecules under equilibrium conditions into stable, structurally well-defined aggregates joined by non-covalent bonds".[5] From this definition, two key features of self-assembly can be identified. The first is the spontaneity of assembly, where aggregates are formed from just intermolecular interactions and without the need of an external influence.[6] The second is that those interactions are non-covalent, which means that the aggregates are not fixed and can reversibly change form, providing dynamic and addressable structures.

Self-assembly is ubiquitous in nature and forms the basis for most biological systems. For example, phospholipids self-assemble into bilayers, which form the walls of living cells, owing to their cylindrical shape and amphiphilic nature. The interactions that drive the formation of the assemblies also provide self-healing properties and membrane fluidity, which are both key factors to maintaining healthy cells.[7] Another classic example is the tobacco mosaic virus, which is a rod-like particle consisting of an RNA chain surrounded by a helical array of identical protein subunits.[8] The proteins assemble due to a folding of the polypeptide chains into disk-like subunits, with a size that matches two turns of the RNA helix.

Inspired by nature, researchers have developed numerous strategies and designs using self-assembly techniques to build structures from the nanoscale to the macroscale,[9–12] finding applications in areas

such as self-healing materials,[13,14] electronic devices,[15,16] and drug delivery.[17–19] Such strategies utilize a "bottom-up" approach to produce assemblies with nanometre-sized features that are difficult to achieve with "top-down" approaches such as nanolithography.[20,21] Non-covalent interactions are favoured over covalent interactions, which often results in fewer steps being required to form large, stable structures.

The main types of non-covalent interactions involved in self-assembly are highlighted in Table 1.1, including their relative strengths, ranges and selectivities.[22] Typical covalent characteristics are included as a comparison. As a rule, non-covalent bonds are much weaker than covalent bonds, which is advantageous as this prevents structures from becoming trapped in one assembled structure.[23]

Table 1.1. Types of bonding available for self-assembly. Reproduced from Reference 22.

Type of interaction	Strength (kJ mol-1)	Range	Character
van der Waals	51	Short	Non-selective, non-directional
H-bonding	5-65	Short	Selective, directional
Coordination binding	50-200	Short	Directional
Amphiphilic	5-50	Short	Non-selective
Ionic	50-250	Long	Non-selective
Covalent	350	Short	Irreversible

Self-assembly usually arises as a result of multiple interactions, carefully balancing attractive and repulsive forces. Some interactions, such as van der Waals forces, are prevalent in all systems, providing attraction in a non-selective manner.[24] Meanwhile, forces such as hydrogen bonding or coordination interactions add complexity to structures, as their directionality and selectivity prevents random aggregation.[25,26]

Interactions between planar, aromatic compounds are also valuable for self-assembly.[27] Such interactions are often identified as "π-π interactions" and arise from a net favourable attraction between two π-systems, following the attraction of π-electrons and an α-framework and the repulsion of π-electrons.[28] Other non-covalent interactions can be used to strengthen π-π interactions and add complexity to the assembled structures.[29] For example, the interplay of π-π interactions and hydrogen-bonding interactions have been utilized to form wire-like structures of organic semiconductors.[30]

Finally, the strongest and furthest ranging interactions are ionic bonds, formed by oppositely charged atoms that are attracted to each other. The organization of ionic building blocks has been termed "ionic self-assembly".[22] Assembly occurs via a cooperative mechanism, where the initial bond formation stimulates further growth, and generally provides a facile route to form complex, hierarchical materials.

1.2 LIQUID CRYSTALS

Liquid crystals are a state of matter in which self-assembly plays a key role. As a state in between a solid and a liquid, liquid crystals are characterized by long-range orientation and fluidity. Molecules that form liquid-crystal phases are termed mesogens and they namely fall into two categories, thermotropic liquid crystals (TLCs), which rely upon heating for self-assembly, or lyotropic liquid crystals (LLCs), which require a solvent to induce organization.

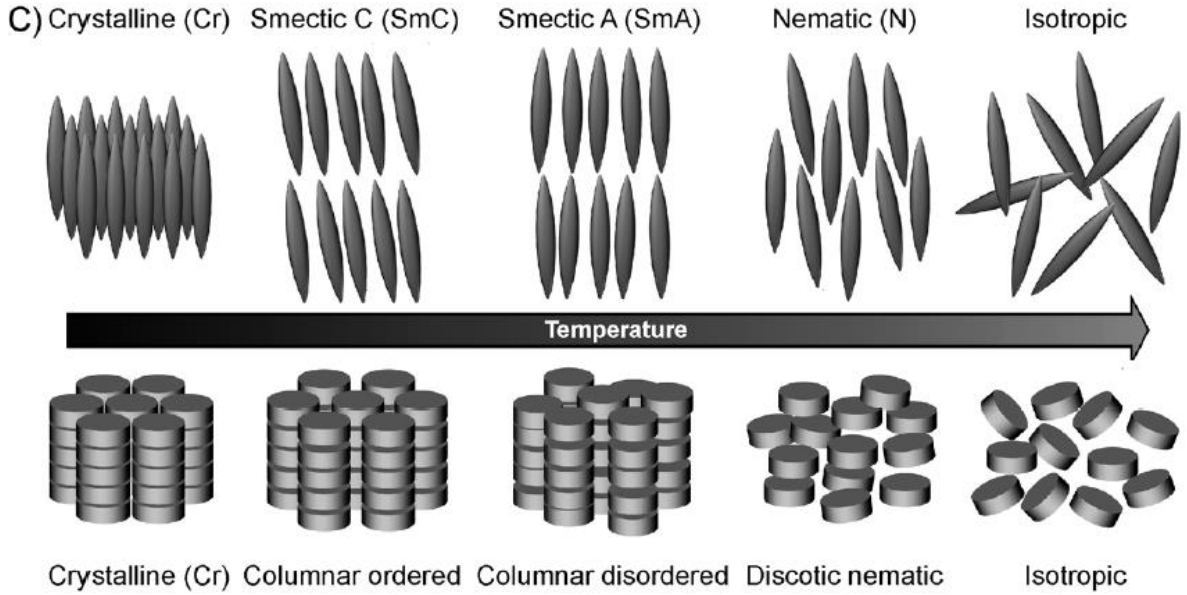

Figure 1.1. Schematic representation of temperature dependent calamitic and discotic mesophases. Adapted from Reference 31.

The difference between both types of liquid crystals arises from the structure of the mesogens. TLCs usually consist of rigid moieties connected to a flexible alkyl chain and can be grouped based on the shape of the mesogen, from rods (calamitic)[31] to discs (discotic)[32] and boards (sanidic),[33] each with different mesophase behaviour. Heating TLCs from the solid state leads to transitions between liquid crystal mesophases, before becoming fully isotropic. Typical thermotropic mesophases formed by calamitic and discotic liquid crystals can be found in Figure 1.1.[31] The nematic phase is the least ordered phase, with orientational order but no overall positional order. With further cooling the smectic phases are formed, providing positional order as layers that differ based on the alignment of the long axis of the mesogen relative to the layer.

1.2.1 Lyotropic liquid crystals

1.2.1.1 Amphiphiles and surfactants

Meanwhile, LLCs are formed from amphiphilic compounds, which contain two chemically distinct moieties within their structures, a hydrophobic tail and a hydrophilic headgroup.[34] Amphiphilic molecules form different complex structures in solution, depending on a range of factors including the

amphiphile concentration, solvent composition and temperature.[35] Amphiphiles are found in a variety of structures, with some typical forms shown in Figure 1.2.

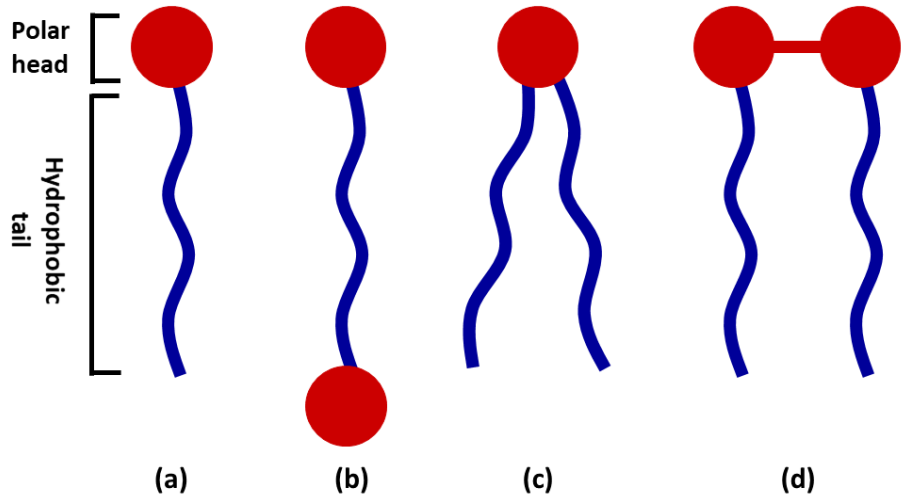

Figure 1.2. Structures of typical surfactants (a) single-tailed (b) bolaform (c) double-tailed (d) gemini.

The rearrangement of surfactant molecules to reduce the contact of hydrophobic segments with water is a result of the hydrophobic effect. The dissolution of a nonpolar molecule into water is a two-step process.[36] Firstly, a cavity must be introduced to the bulk solution to make space for the solute. Secondly, the solute is introduced, and the surrounding water molecules undergo a structuring process to form a "cage" around the nonpolar molecule. The new hydrogen bonds formed by the water "cage" enthalpically balance the hydrogen bonds broken in the formation of the cavity. Moreover, the increase in order of the water molecules upon structuring leads to a negative entropy change and therefore positive change in the Gibbs free energy, meaning that the dissolution is unfavourable.

The high entropic cost of introducing nonpolar solutes to water is minimised by the formation of aggregates. The release of the structured water surrounding individual solute molecules is associated with an increase in the system entropy. Meanwhile, the reformation of hydrogen bonds from the released water molecules with the bulk solution provides a favourable enthalpic contribution.[37] The size and the shape of aggregates formed is then driven by factors including the ionic strength and temperature of the solution, in addition to the surfactant shape.[38]

1.2.1.2 Packing parameter

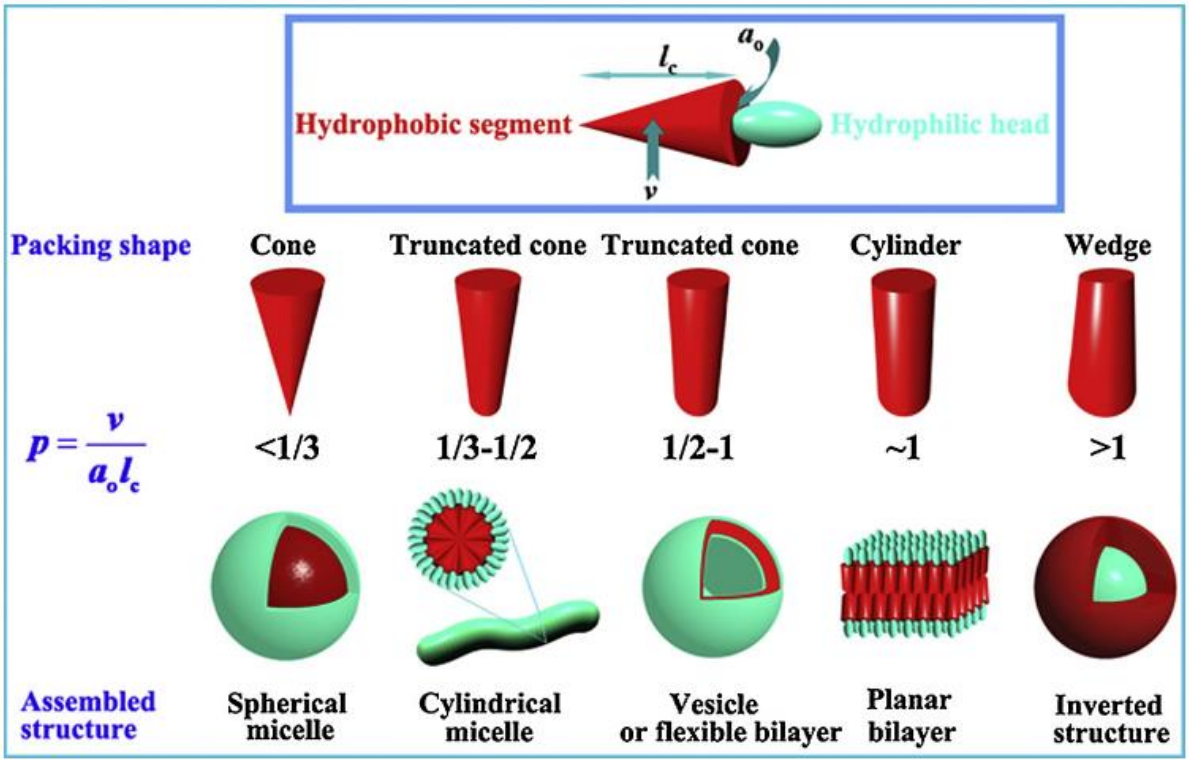

Figure 1.3. The effect of packing parameter (pp) on the self-assembled structures formed by amphiphiles. Reproduced from Reference 39.

The structures formed by amphiphiles in solution are governed by the molecular packing parameter (*pp*). An amphiphile's *pp* can be calculated from Equation 1, where v_0 is the volume of the hydrophobic section, l_0 is the critical length of the hydrophobic tail and a_e is the optimum head group area.[40]

$$pp = \frac{v_0}{a_e l_0} \qquad \textit{Equation 1}$$

The predicted structures with their corresponding *pp*s are given in Figure 1.3. Amphiphiles with $pp < \frac{1}{3}$ will preferentially form spherical micelles, while cylindrical micelles will be favoured for those with for $\frac{1}{3} \leq pp < \frac{1}{2}$, flexible bilayers and vesicles will form for $\frac{1}{2} \leq pp < 1$, and amphiphiles with $pp = 1$ will produce planar bilayers. Meanwhile, inverted micelles and other reversed phases will form when $pp > 1$.

Different morphologies can be obtained by careful consideration of the chemical composition. An amphiphile's *pp* can be increased by adding branching or unsaturation to the hydrophobic section or by functionalisation with multiple alkyl chains, thus increasing v_0 relative to a_e.[41] Meanwhile, different head groups and counterions are commonly used to tune the self-assembly of ionic and non-ionic amphiphiles by dramatically changing the effective head group area of the amphiphile.[42–44]

1.2.1.3 Typical mesophases formed by lyotropic liquid crystals

As previously mentioned, aggregate morphologies formed by amphiphiles depend on their concentration and the solution temperature. An example phase diagram for a typical amphiphile can be found in Figure 1.4, demonstrating mesophase formation as a factor of both. The Kraft point is highlighted on the diagram and is the temperature above which the solubility of an amphiphile increases, to the point where it can form micelles. Below the Kraft point, the amphiphile remains as an insoluble solid. Transitions between mesophases can occur with changes to temperature, however, the amphiphile concentration is the main driving force behind different assemblies.

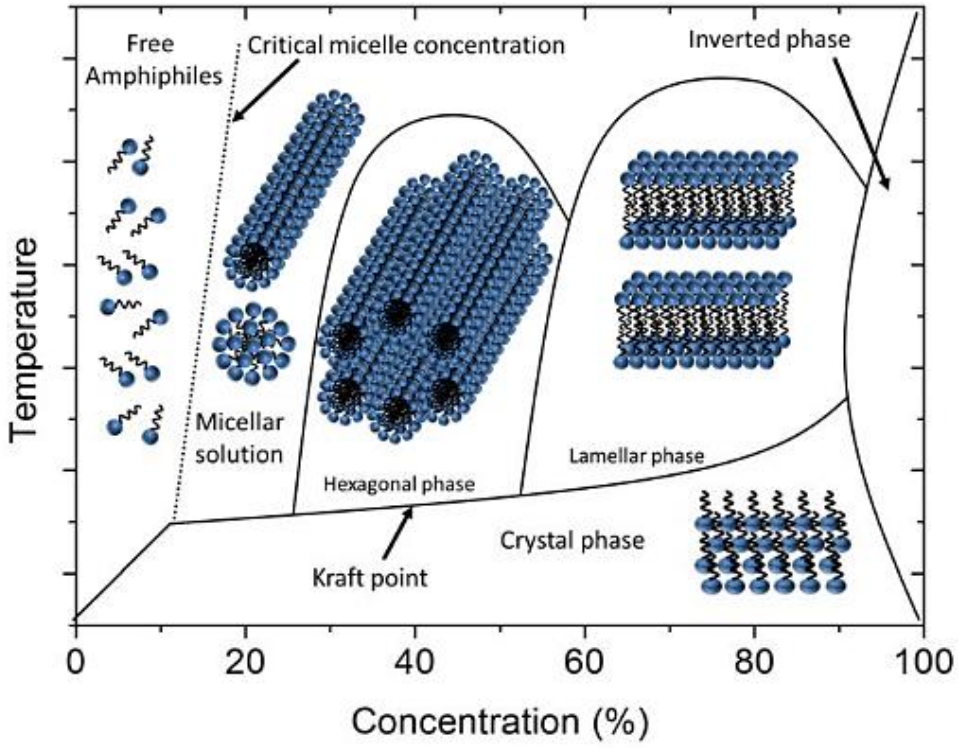

Figure 1.4. Example phase diagram for a lyotropic liquid crystal, showing phase changes as a function of temperature and concentration. Reproduced from Reference 45.

Figure 1.5 shows the typical mesophases formed by an amphiphile with increasing concentration. Initially, above the CMC, amphiphiles aggregate into micelles. These micelles are randomly dispersed in water, forming an isotropic phase. As the concentration increases, these micelles aggregate into a cubic lattice, known as the micellar cubic (I_1) phase. Increasing the concentration further produces the hexagonal (H_1) and lamellar (L_α) phases. For some amphiphiles, bicontinuous cubic phases present in between the hexagonal and lamellar phases. Bicontinuous cubic phases (V) are derived from a continuous bilayer structure with intertwined but separate hydrophobic and hydrophilic domains and will be discussed in further detail in the next section. Beyond the lamellar phase lie the inverse phases, which show the same structural arrangements as the normal phases but with the amphiphile arrangements reversed.

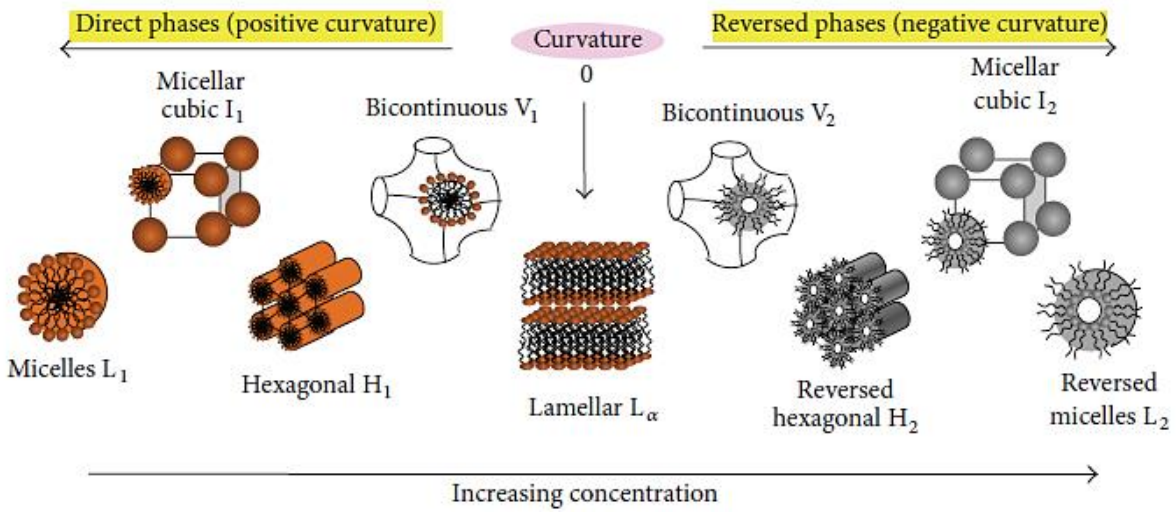

Figure 1.5. Typical phases formed by lyotropic liquid crystals upon increasing concentration. Reproduced from Reference 46.

1.2.2 Lipid self-assembly

Lipids are biological amphiphiles and can be widely found across the natural world. Indeed, lipids are found in all biological membranes, playing vital roles in the lives of cells, from maintaining the cell structure to cooperating with transmembrane proteins to transport materials across membranes.[47] Outside of biological applications, lipids have been the study of extensive research, due to their ability to self-assemble into complex nanostructures.

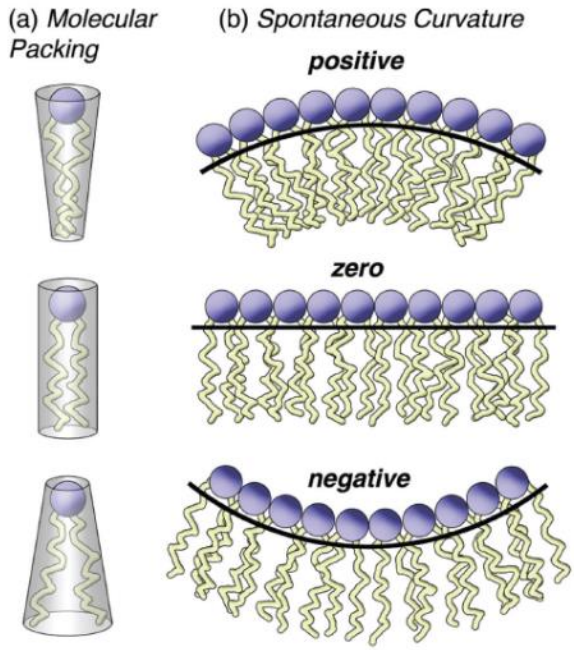

Figure 1.6. Molecular packing of lipids and their spontaneous curvature. Top: type I. Middle: type 0. Bottom: type II. Reproduced from Reference 48.

Owing to their amphiphilic character, lipids form the LLC phases highlighted in the previous section. Self-assembly of lipids into bilayer structures is driven by a need to protect the hydrophobic tails from

water with the hydrophilic head groups exposed.[49] The structures formed are governed by the solvent composition and external conditions, as well as the amphiphile's molecular shape or *pp* (Figure 1.6). Lipids with a *pp* < 1 are type I lipids and form structures with positive curvature, where the membrane curves towards water. Type 0 lipids have *pp* = 1 and form flat, lamellar-like phases. Meanwhile, type II lipids have *pp* > 1 and form membranes with negative curvature, where the membrane curves away from water.

Of the mesophases available to lipids, the inverse bicontinuous cubic phase has raised particular interest because of its continuous bilayer, which separates two discrete water channels. The bilayer forms a surface that has zero mean curvature and negative Gaussian curvature.[50] Three cubic phases can be identified from their crystallographic space groups, i.e., the double diamond (*Pn3m*), primitive (*Im3m*) and gyroid (*Ia3d*) phases. The *Pn3m* phase is predominantly formed in excess water conditions,[51] while the *Ia3d* phase forms under less hydrated conditions.[49] Meanwhile, the *Im3m* phase is more commonly observed when lipids are combined with additives.

The cubic phases can also be differentiated by their negative curvature. Figure 1.7 shows typical mesophases formed by lipids and demonstrates a trend of increasing negative curvature from the *Im3m* phase, to the *Pn3m* phase, followed by the *Ia3d* phase. Some lipids can present a flatter bicontinuous phase, with negative curvature in between the *Im3m* phase and lamellar phase, i.e., the sponge phase (L_3). The sponge phase, like the cubic phase, consists of a 3-D bilayer, which forms a barrier between two separate aqueous domains. However, unlike the cubic phase, the sponge phase is characterised by short-range order and long-range disorder.[50] The sponge phase is also much more fluid than the viscous cubic phase.

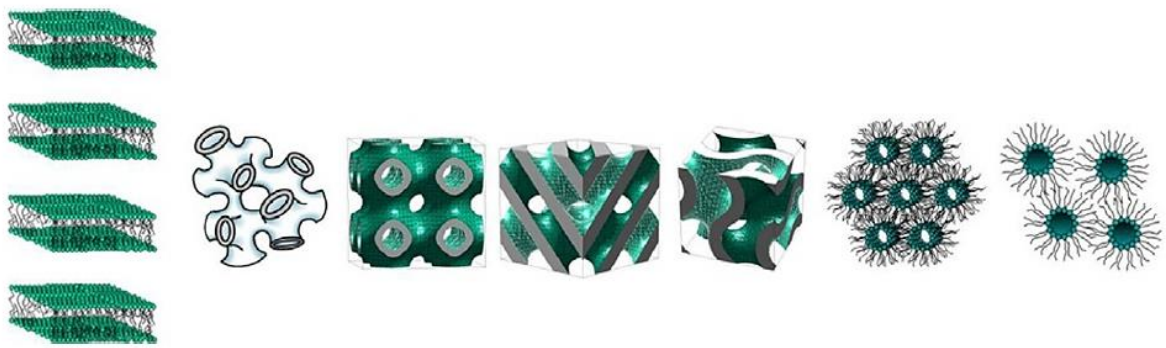

Figure 1.7. Lipidic mesophases displayed in order of increasing negative curvature. From left to right: Lamellar (L_α), sponge (L_3), primitive (Im3m), double diamond (Pn3m), gyroid (Ia3d), hexagonal (H_1) and isotropic micellar. Reproduced from Reference 49.

The dimensions and structures of the cubic and sponge phases can be readily controlled by manipulating the external conditions and by the introductions of additives. This addressability of both mesophases

have made them promising candidates for an extensive range of applications in areas such as model membranes,[47] electrochemistry,[52] biosensing,[53] biofuel cells,[54] templating[55] and protein crystallization.[56]

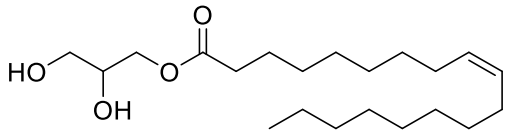

*Figure 1.8. Chemical structure of monoolein (**MO**).*

Monoolein (**MO**) is one of the most commonly utilized cubic phase-forming lipids (Figure 1.8). The presence of a *cis* double bond in its alkyl tail results in a $pp > 1$ and therefore results in the preferential formation of a stable *Pn3m* phase in excess water.[51] **MO** has attracted wide attention as it is non-toxic, biocompatible and biodegradable.[41] Many reports have focused on the effects of additives on the mesophase formation of **MO**, allowing it to be tailored for specific applications. For example, Duss et al. demonstrated that the aqueous channels of the *Pn3m* phase could be used as a template to control the growth of palladium nanoparticles.[57] The pore sizes could then be tuned with the use of poly(ethylene glycol) (**PEG**) to enable the controlled diffusion of reagents to the newly formed catalyst to be switched on and off.

Another common use of **MO** and indeed other lipidic cubic phases is the crystallization of membrane proteins. Protein crystals of sufficient quality to obtain structural information from have been grown in cubic phases, whose hydrophobic bilayers act as a suitable matrix to host protein molecules.[56] However, large proteins, which protrude into the water channels, can experience reduced mobility through the membrane and thus can prove difficult to crystallise. The sponge phase, which has larger water channels than the cubic phase and can be easily prepared with the use of different additives, has been shown to be a more suitable matrix for the growth of such large protein crystals.[58]

1.2.3 Manipulation of lipid self-assembly

Fine control over the complex nanostructures formed by lipids has been the subject of much research over recent years, having wide implications for many applications. For example, an understanding of how salts influence mesophase formation will benefit those attempting protein crystallization condition screenings.[59] Meanwhile, control over the macroscopic orientation of cubic phases will allow for the formation of superior, defect-free templates.[60,61]

However, of greater interest are those stimuli-responsive systems, which allow for switching between mesophases or altering of material properties, thus providing a means to switch on and off a desired function. This is particularly attractive for drug delivery, where targeted release would lower the overall drug concentrations required for patients, reducing possible side effects. The non-toxic nature of lipids and the presence of both hydrophobic and hydrophilic domains, capable of sequestering drugs, makes them attractive candidates for drug delivery vehicles. A review of lipidic liquid crystals and their role

as drug delivery and diagnostic tools is provided by Fong et al. (2011), which highlights stimuli-responsive systems.[62]

The diffusion and release of molecules from lipid mesophases is dependent on the phase identity. Phan et al. (2011) demonstrated that the release of a model hydrophilic drug from four lipidic mesophases was fastest from the *Pn3m* phase, followed by inverse micelles, the hexagonal phase and the micellar cubic phase, in that order.[63] The rapid release of a model drug from the cubic phase was attributed its relatively large and open water channels, promoting drug diffusion. This observation indicates that cubic phases are not suitable drug delivery vehicles, as the drug is likely to be released before reaching its intended target. However, the increased release rate could be beneficial if combined with a different mesophase and a triggered response mechanism, to induce a transition from a slow release to fast release mesophase at the target site.

Several release mechanisms have been explored in the literature and have been highlighted below. The first of interest is temperature. LLCs undergo structural changes with temperature and lipidic mesophases are no different. However, the structure properties can be adjusted with the use of additives. The *Pn3m* phase of pure **MO** experiences a de-swelling of the aqueous channels from 4.0 to 2.4 nm with increasing temperature from 20 °C to 65 °C.[64] However, with the addition of octyl glucoside, a greater difference in water channel sizes is observed. At low temperatures, the water channel diameter is 7.3 nm and de-swells to 3.1 nm upon heating.[64] It was proposed that this decrease in water channel diameter is the result of the "squeezing out" of the additive from the lipid bilayer upon heating, owing to an increase in the membrane curvature.

Manipulation of mesophase structures with temperature can also be performed using gold nanorods embedded in lipid hosts.[65,66] The nanorods respond to near-infrared light, becoming heated and effecting transitions to the hexagonal phase. When switched off (or with the application of a cooling pack), the mesophase transitions back to the cubic phase, releasing a contained drug.[66]

Magnetic fields can also be used as an external trigger and to direct materials to a target.[67] Superparamagnetic iron oxide nanoparticles (SPIONs) have been introduced to **MO** mesophases and have been shown to trigger a transition from the cubic phase to hexagonal phase in the presence of an alternating magnetic field, owing to localised heating.[68] The transition between mesophases could be used to switch on or off drug release. However, the SPION-embedded lipid mesophases were also suggested as hyperthermia treatments, providing heat when exposed to an alternating magnetic field at the target location.

Finally, pH-responsive additives can be added to lipid mesophases to induce transitions upon introduction to acidic environments.[69–71] Changes in pH occur naturally in the body and can be used as an internal trigger. Negrini and Mezzenga (2011) developed a system composed of monolinolein and linoleic acid, which underwent a transition from the *Im3m* phase to the hexagonal phase when

decreasing the pH to 2.[72] The transition between mesophases was attributed to linoleic acid, which is deprotonated at neutral pH and protonated under acidic conditions. The presence of a negative charge when deprotonated resulted in a larger effective head group area, due to electrostatic repulsion. Therefore, the *pp* of deprotonated linoleic acid was smaller than that of protonated linoleic acid, resulting in the preferential formation of the *Im3m* phase over the reverse hexagonal phase. The authors noted that the diffusion of drugs was four times faster in the *Im3m* phase than the hexagonal phase and proposed that the system be used to protect drugs taken orally from being released in the stomach, as shown in Figure 1.9.

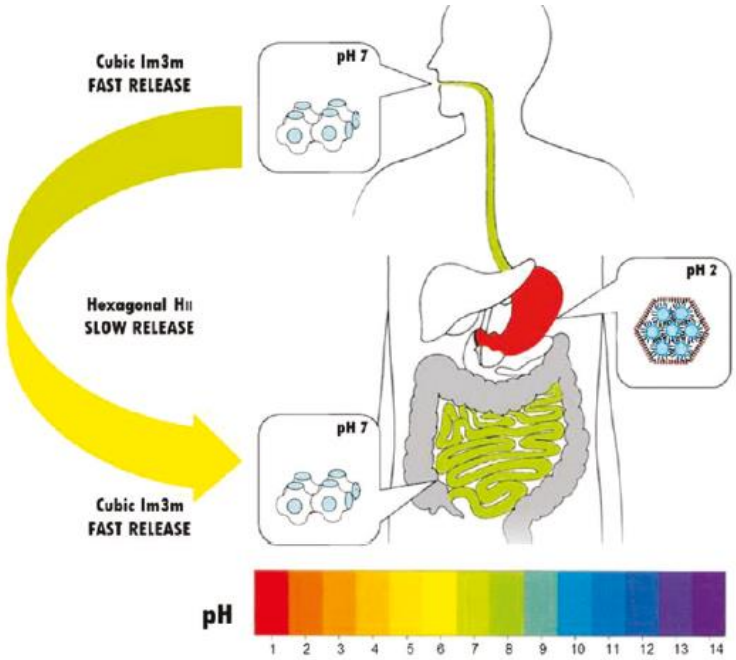

Figure 1.9. Schematic representation of pH-responsive drug delivery system, utilizing the difference in release speeds between the hexagonal and cubic phase. Reproduced from Reference 72.

A similar but inverted system has also been reported where a hexagonal to cubic transition occurred with lowered pH. In this system, monolinolein was combined with pyridinylmethyl linoleate, an amphiphile which becomes positively charged under acidic conditions. This again increases the effective head group area of the amphiphile, due to electrostatic repulsion, changing its *pp* and resulting in the formation of the cubic phase. The mesophases were explored as drug delivery vehicles for cancer treatments. In the acidic conditions surrounding cancer cells, mesophases loaded with an anti-cancer drug underwent a transition from the slow releasing hexagonal phase to the faster releasing cubic phase, resulting in the effective killing of the cancer cells.[73]

While many examples of stimuli-responsive lipidic mesophases focus on biomedical applications, their use does not have to be restricted to such areas. Control over the diffusion properties of bulk lipid mesophases would improve their function as size-selective molecular sieves. The introduction of sucrose stearate in a monolinolein/water system was shown to induce a transition from the *Pn3m* to

Im3m phase.[74] Further increasing the concentration of sugar ester led to a swelling of the water channels. The difference between *Pn3m* phase and swollen *Im3m* phase allowed for selective diffusion of small and large nanoparticles, dependent on the water channel diameter (Figure 1.10).

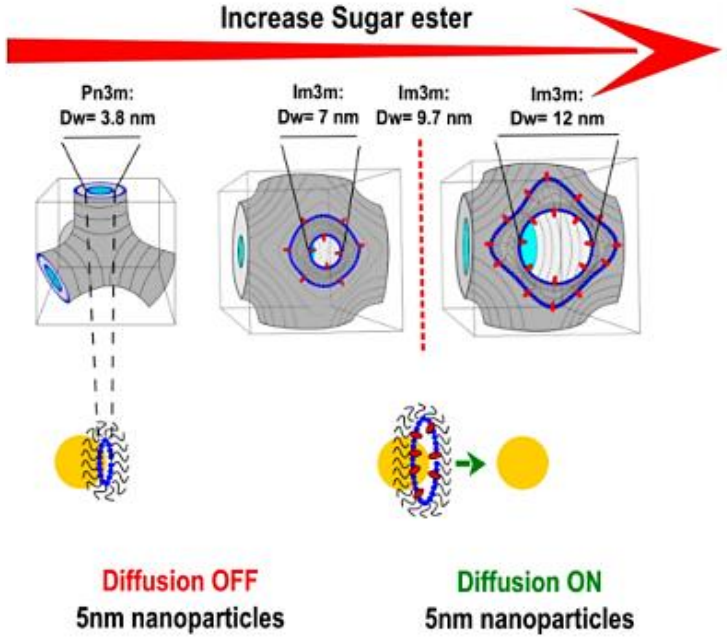

Figure 1.10. Controlling the pore width of cubic phases using a sugar ester, with effect on nanoparticle diffusion. Reproduced from Reference 74.

1.3 TEMPLATED SELF-ASSEMBLY

Liquid crystal engineering is an excellent way to build many different nanostructured materials from the ground up.[75] However, the fluidity and changing nature of liquid crystal mesophases can also be a drawback for many material applications, where mechanical strength and resistance to environmental changes is important.[76] To overcome this problem, polymer templating techniques have been applied, where well-ordered materials are used as structure directing agents to control the assembly of a growing polymer. Numerous templating strategies exist in the literature (see a review of polymer templating by Clapper et al. (2008)),[77] among which liquid crystal templating proves to be a promising candidate.

A survey of reviews (Gin et al. (1999),[76] Yun and Song (2017)[78] and Steer et al. (2017)),[79] highlights three main ways in which liquid crystals are used in polymer templating, which are 1) polymers as stabilizing agents for liquid crystals, 2) liquid crystals as templates and 3) polymerizable liquid crystals. In the first method, polymers are used to reinforce liquid crystal mesophases. A small quantity of a monomer (< 10 wt. %) and photoinitiator are dissolved in a liquid crystal, before photoinitiation to cross-link the monomer in situ. The polymer captures the mesophase structure, stabilising its properties.[80]

1.3.1 Liquid crystals as structure-directing agents

The second method uses liquid crystals as structure directing agents for polymer growth. Again, a monomer and initiator are dissolved in a liquid crystal mesophase, which directs the growth of the polymer following initiation. The template is then removed, yielding a well-structured polymer. Liquid crystal templates can generally be easily removed by washing with an appropriate solvent, in comparison to other templates such as block co-polymers, which may require harsh removal conditions including plasma etching or strong acids.[81,82]

Both thermotropic and lyotropic liquid crystals have been used as polymer templates. The growth of helical wires of polyacetylene from the polymerisation of acetylene gas in a chiral nematic TLC has been demonstrated by Akagi et al. (1998).[83] The polymer morphology could be readily controlled by adapting the mesophase parameters[84] and the technique easily applied to other polymers.[85,86]

Meanwhile, the variety of 3-D structures available to LLCs makes them attractive as templates. However, polymer templating in LLC mesophases does not often result in a direct 1:1 transfer of the template structure to the polymer.[76] This is because the polymer growth usually results in phase separation or demixing of the polymer from the liquid crystal phase, and/or the destruction of the template.[77] Instead, the template often acts to indirectly influence the polymer structure.

An example of how a mesophase can indirectly affect the growth of a polymer can be seen in Figure 1.11. The figure demonstrates schematically the formation of a highly porous polymer network by the polymerisation of a hydrophilic monomer in a hexagonal LLC phase.[87] The polymer demixes from the mesophase as it forms, although the growth remains directed by the anisotropic properties of the mesophase. As the polymer continues to grow, it forms a highly cross-linked network, with structural features much larger than the original mesophase. The polymer retained its structure after the template was removed and although it did not match the original mesophase, its highly regular, porous structure could be used as a size selective membrane.

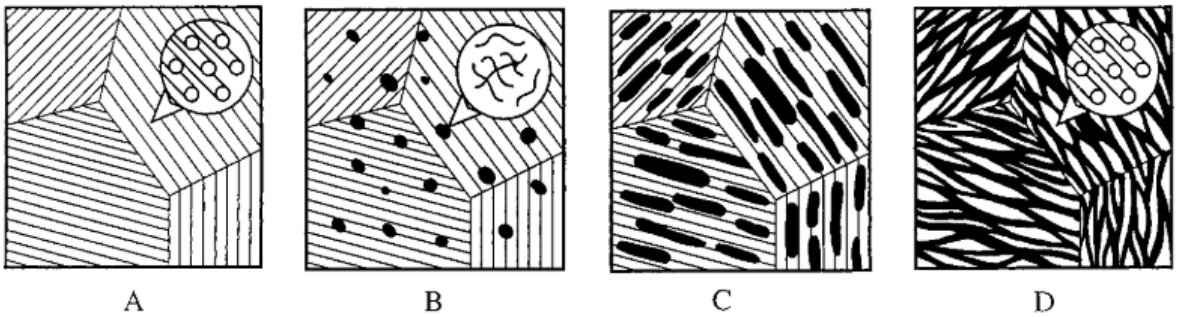

Figure 1.11. Scheme demonstrating the growth of a polymer in a hexagonal mesophase. a) A homogeneous hexagonal LLC phase is formed. b) Polymer begins to form and demixes from the mesophase. c) The polymer growth is directed by the anisotropic properties of the mesophase. d) Continued polymer growth leads to a cross-linked gel structure. Reproduced from Reference 87.

Similarly, structures formed by polysiloxane were dependent on the mesophase in which they were templated.[88] Rod-like particles were formed from hexagonal phases, while sheet-like particles were formed from lamellar phases. For both, the structures were several orders of magnitude larger than the original mesophase, demonstrating the indirect structural control of the template.

In the latter example, polymers were formed via a polycondensation reaction. The speed of polymerisation is a crucial factor in determining how well a growing polymer will retain the structure of its host matrix. Slower polymerisation reactions allow time for the polymer to phase separate from the template, while faster reactions enable the structure to be trapped before demixing can occur. In this regard, photopolymerisation is an ideal polymerisation technique. Both polymer initiation and growth occur very rapidly, reducing the likelihood of phase separation, and the use of light as a stimulus allows for targeted reactions to occur.[89] Additionally, as photopolymerisation is independent of temperature, it can be used with mesophases that exist within discrete temperature ranges.[77]

1.3.2 Reactive mesogens

In addition to the use of photoinitiated polymerisation reactions, the retention of LLC mesophase structures can be improved by using reactive mesogens.[90] This is the third method of liquid-crystal polymer templating and involves the use of mesogenic molecules that contain a reactive group in their structure, suitable for polymerisation reactions. As the monomers themselves are liquid crystals, they can self-assemble into different structures without the use of a host matrix. Rigidity and resilience to environmental changes can be induced by polymerisation of those assemblies (see Figure 1.12).[91]

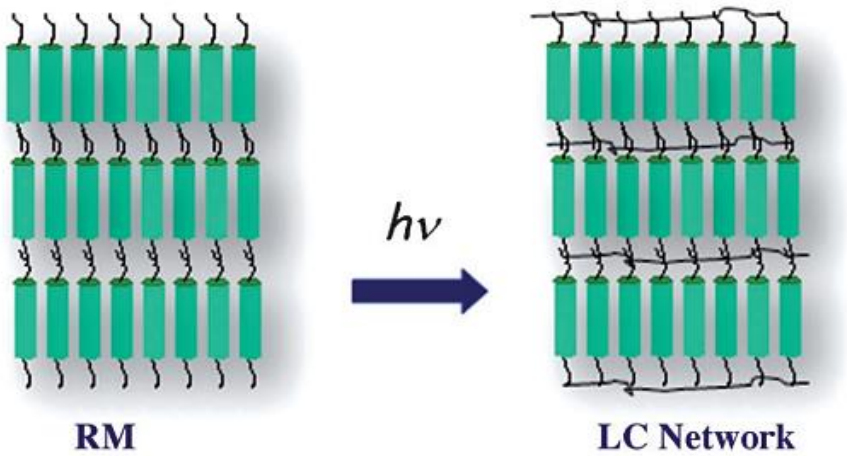

Figure 1.12. Formation of a well-defined polymer network by polymerisation of reactive mesogens (RM). Adapted from Reference 91.

Reactive LLCs have been the focus of much research in the past, with a range of successfully polymerised particles being found in the literature.[92] The bilayer structures formed by LLC mesogens can be readily cross-linked, owing to the separation of hydrophobic and hydrophilic moieties,

encouraging a high localised concentration of polymerizable groups in the centre of the bilayer. Indeed, this arrangement also serves well in thermotropic liquid crystals. Thiem et al. (2005) demonstrated that the polymerisation of smectic A phase of a reactive mesogen proceeded more quickly and with higher conversion than an isotropic phase, owing to the arrangement of the monomer into a layer structure.[93]

A fine example of the use reactive mesogens to make functional materials was reported recently by Li et al. (2019).[94] The authors developed a gemini monomer that self-assembled into bilayers on a substrate-water interface. The monomer could be readily adapted with a diverse range of functional groups and could be co-polymerised with the parent monomer, forming 2-D polymers with excellent material properties. The highly cross-linked nature of acrylate groups in the bilayer core endowed the polymer with good mechanical strength.

Meanwhile, mesophases with higher degrees of curvature have been polymerized, including the hexagonal and cubic phases.[95,96] The cubic phases in particular have been targeted, as the 3-D phases can be fixed by cross-linking, giving well-defined, highly-porous polymer networks, suitable for size-selective membranes, drug delivery or catalysis. A review on the formation of polymer networks synthesised by cubic-phase forming LLCs is given by Wiesenauer and Gin (2012).[97] They highlight the challenge of designing and synthesising reactive mesogens that will form cubic phases, and suggest that the simplest approach is to adapt a mesogen that will naturally form cubic phases, although this is not often successful. Nevertheless, 3-D polymer networks based on cubic phases can be produced with carefully experimentation. For example, gemini monomers bearing ammonium head groups and diene-terminated alkyl tails have been synthesised, which form cubic phases at elevated temperatures.[98] A stable polymer network has been formed by photoinitiation of the monomer assemblies and X-ray analysis has demonstrated the retention of the cubic phase structure.

There are advantages and disadvantages to using liquid crystals as structure directing agents or as reactive mesogens. The mesophases formed by common surfactants are well understood and may be easily adapted to tolerate the inclusion of monomers, while the synthesis of reactive mesogens that form the desired structures may be prohibitively expensive or complex.[99] However, problems of phase separation or template disruption usually result in indirect templating of the mesophase structure when liquid crystals are used as host matrices, while reactive mesogens more often allow for the original structure to be captured. It should be noted that the techniques need not be discrete. A combination of both utilizes non-reactive liquid crystals as hosts to direct the assembly of reactive mesogens, which can be polymerised with retention of the original mesophase structure after removal of the template.[100]

1.3.3 Lipidic mesophases as templates

The LLC phases formed by lipids have been widely explored as templates for functional materials. Their chemistry and self-assembly behaviour are well understood and can be readily controlled, allowing for a variety of structures to be templated with relative ease. In some cases, the lipids

themselves are subjected to polymerisation using reactive moieties in the lipid tails, ensuring stability with respect to changes in their environment.[55,101] This increased stability, in particular to changes in temperature and the presence of organic solvents, has allowed them to be used as nanoreactors.[55]

Lipidic mesophases have also been used to control the growth of metal nanowires. Again, the cubic phases have been viewed as attractive candidates in this regard, as the preparation of nanowires with controlled diameters and pore widths, in addition to good interwire connectivity, is important for electrical devices.[82] In recent years, members of the Squires group have focused on the electrochemical deposition of platinum nanowires in the *Pn3m* phases formed by phytantriol.[102–104] The lipid template can be easily removed by washing with ethanol, yielding a regular platinum lattice with a single diamond (*Fd3m*) morphology. The *Fd3m* structure arises from the deposition of platinum in only one of the two water channels, as the other is closed to the surrounding water. In a similar manner, palladium nanowires with *Fd3m* morphology have been grown by electrodeposition in phytantriol *Pn3m* phases,[105] while long and straight platinum nanowires can be grown from hexagonal phases.[106] In the latter example, the diameters of the nanowires are controlled by tuning of the aqueous pore diameter.

In addition to inorganic materials, organic polymers have been prepared using lipid mesophases as templates. Particles formed of cubic and hexagonal phases, or cubosomes and hexosomes, have been used as templates to form polymer particles.[107] Polymerisation of hydrophobic and hydrophilic monomers within these templates allow for the macroscopic structure to be retained after the template is removed, although the internal nanostructure is lost. Interestingly, the rigidity of the particles is governed by the hydrophobicity of the monomers, with hydrophobic monomers forming hard particles and hydrophilic monomers forming elastic, hydrogel particles.

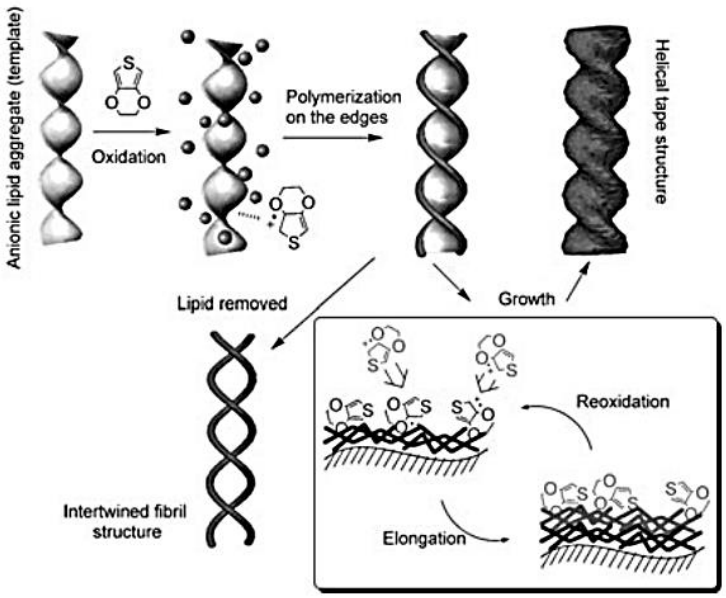

Figure 1.13. Scheme demonstrating the templated assembly of conjugated polymers by oxidative polymerisation. Reproduced from Reference 108.

Finally, helical conjugated polymers, including poly(ethylenedioxythiophene), poly(pyrrole) and poly(aniline), have been grown by oxidative polymerisation using a synthetic, chiral lipid as a template.[108] The anionic lipid assemblies interact with the cationic intermediates formed during oxidative polymerisation, directing the growth of the polymer along the lipid surface, as shown in Figure 1.13. The authors demonstrated that while the template was not removed and a lipid/polymer compositive was formed, the polymers demonstrated conductivity on par with those formed by similar polymerisation methods, while maintaining complex nanostructures.

1.4 CONDUCTING POLYMERS

Until late in the 20th century, conjugated polymers were viewed as insulators and were used in applications with that purpose in mind.[109] However, in 1977, it was found that poly(acetylene) could achieve metallic levels of conductivity upon doping with iodine, the discovery of which earned Shirakawa, MacDiarmid and Heeger the 2001 Nobel Prize in Chemistry.[110–112] Since that discovery, research into the development and understanding of conducting polymers has increased substantially.[113] Conjugated polymers combine the attractive properties of polymers (e.g. low cost, flexibility and processability) with the electrical properties of metals or inorganic semiconductors.[114]

1.4.1 Basis of conductivity in conjugated polymers

Conjugated polymers are characterised by alternating single and double bonds, giving a system of delocalised π-electrons. The simplest conjugated polymer is poly(acetylene), which can be used as a model to understand the origin of conductivity in other conjugated polymers. In poly(acetylene), each carbon is sp^2 hybridised with σ-bonds between neighbouring carbon atoms and an orthogonal π-bond network.

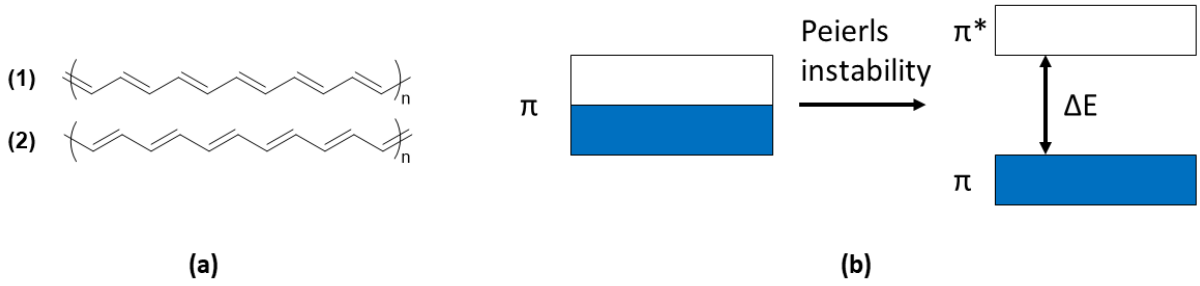

Figure 1.14. (a) Two degenerate forms of poly(acetylene) (b) Splitting of the π-band into π- and π-bands due to Peierls instability.*

In ideal poly(acetylene), it is expected that all C-C bonds are the same length, forming an arrangement where the π-electrons produce a half-filled π-band, giving rise to metallic conductivity. However, owing to Peierls instability, it is more energetically stable for the structure to remain as alternating single and double bonds, as has been demonstrated experimentally by NMR spectroscopy.[115] This phenomena

gives rise to two degenerate phases of poly(acetylene), as can be seen in Figure 1.14a, the result of which splits the π-band into two bands, a filled π-band and an empty π*-band (Figure 1.14b). The difference in energy between the highest occupied molecular orbital (HOMO) of the π-band and the lowest unoccupied molecular orbital (LUMO) of the π*-band is called the band gap. The size of the band gap determines the electrical and optical properties of the material. As its value decreases, the energy required to transition from the valence band (π) to conducting band (π*) decreases, improving the material's conductivity.

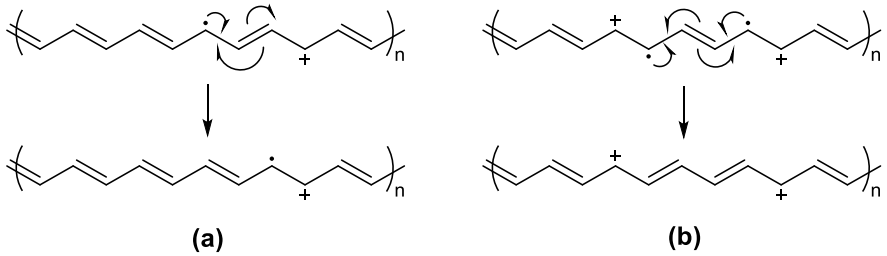

Figure 1.15. (a) Polaron formation by combining neutral and charged solitons (b) Bipolaron formation from the combination of two polarons.

Charge carriers can be introduced to improve the conductivity of conjugated polymers that would otherwise be insulators, owing to the size of their band gaps. The two degenerate forms of poly(acetylene) coexist within the polymer and meet at domain boundaries. This leads to defects known as solitons, which are neutral radical species that can travel along the backbone of the polymer. Positive solitons can be introduced by treatment with an oxidant, while negative solitons are formed with the use of a reductant. Positive and negative solitons can be treated as holes to the valence band or added electrons in the conducting band, respectively.

Charged solitons can also combine with neutral solitons to form polarons (Figure 1.15a). Neutral solitons have zero charge and a single spin. When combined with a charged soliton, which has charge and zero spin, they produce a polaron that has both charge and spin, existing in a triplet state. Meanwhile, bipolarons are formed by two solitons of like charge, or from two polarons that can pair to lower their energy (Figure 1.15b). Bipolarons have charge and no spin, existing as singlets. Conductivity arises as a result of these charge carriers, which are able to travel along the polymer. [112] It should be noted that disorder limits carrier mobility and that improved structural order will improve conductivity.

1.4.2 Polyaniline

Since its discovery in 1862,[116] poly(aniline), or **PANI**, has attracted much attention, owing to many factors including the low cost of its monomer, its facile and high-yielding polymerisation reactions, and good stability of the final polymer. In addition, **PANI** is attractive as it can exist in multiple oxidation states, each with a distinctive colour. The general composition of **PANI** is given in Figure 1.16. The

value of y can be varied from 1, producing the leucoemeraldine base state (LEB), to 0.5, giving the emeraldine base state (EB), to 0, producing the pernigraniline base state (PB).[117] These oxidation states are discrete and are interconverted without passing through any intermediate states.[118] The LEB state is highly susceptible to oxidation, producing the EB state with even minute amounts of oxygen, while the EB state is stable in air. It is therefore most practical to prepare **PANI** in the EB state and oxidise it or reduce it to the LEB or PB states as required.[119]

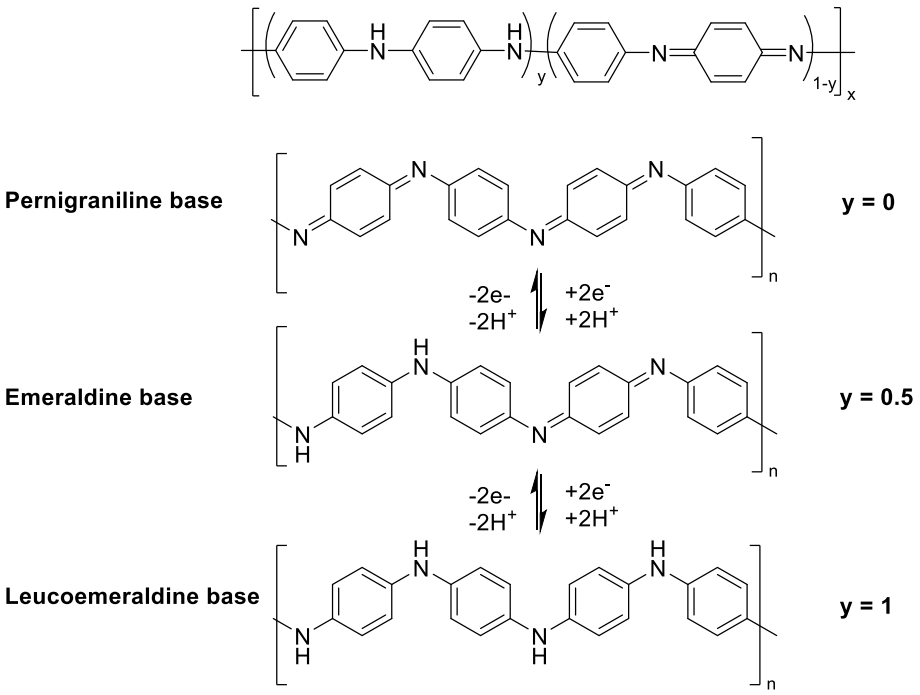

*Figure 1.16. Oxidation states of **PANI** and the transitions between states. The oxidation states are defined by the ratio of quinoid rings (1-y) to benzenoid rings (y).*

One of the main reasons that **PANI** has been the focus of extensive research is the presence of a fourth conductive state, the emeraldine salt (ES) state. The ES state can be accessed by either oxidative doping from the LEB state,[120] or by protonation of the EB state using doping acids. Conductivity in the ES state has reached values of up to 1,000 S cm^{-1},[121] although it has been predicted that the conductivity could be comparable to copper, if all charge carriers were available.[122]

The protonation process is outlined in Figure 1.17. Protonation preferentially occurs at the imine nitrogen atoms, as the amine nitrogen atoms are weaker bases.[123] A doubly charged, spinless bipolaron is formed, which undergoes an internal redox reaction and charge redistribution, producing a polaron lattice where there is one unpaired spin per repeat unit, giving a half-filled band.[112,124] Electrical conductivity occurs through a hopping mechanism, both intra- and inter-chain.[125] The protonation process is fully reversible with the addition of a base, reforming the insulating EB state.[126]

In addition to inducing metallic conductivity in **PANI**, dopants have been used to improve the solution processability of the polymer, utilizing the structures of different counterions to improve its solubility

in common solvents.[127] Dopants have also been used to improve the environmental stability and mechanical properties of **PANI**. Dufour et al. (2003) demonstrated that **PANI** doped with sulfosuccinates aggregated into lamellar-like structures, making it more stretchable and thermal stable.[128] Such dopant engineering has also been applied to improve electrical conductivity by changing the molecular conformation of **PANI** polymer chains from a compact coil arrangement to an expanded coil. This change is associated with increased crystallinity, which in turn is related to increased conductivity.[129] In addition, the expanded arrangement reduces π-conjugation defects that arise from ring twisting, improving charge transport properties.[123]

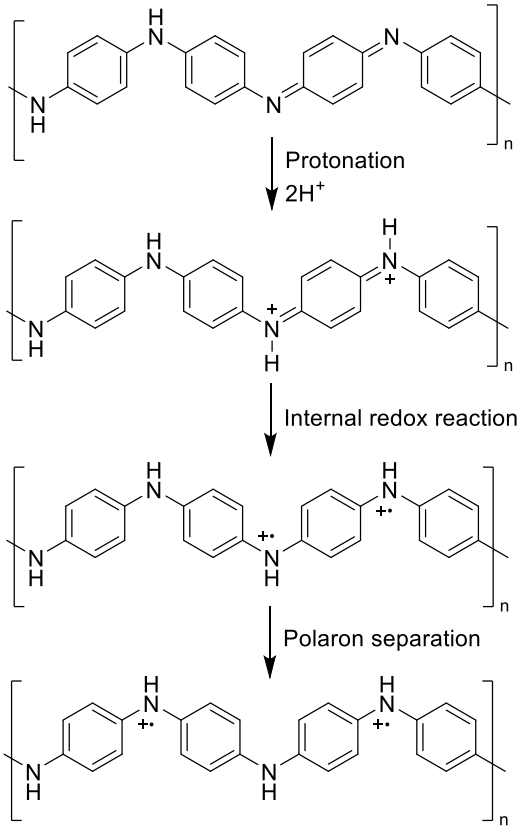

*Figure 1.17. Schematic representation of **PANI** doping by acids. Protonation of the imine nitrogen atoms leads to a bipolaron formation, which undergoes an internal redox reaction and charge redistribution, forming a polaron.*

1.4.3 The oligomer approach

With properties such as metallic-like conductivity upon doping and the accessibility of multiple oxidation states, **PANI** has attracted attention for many applications such as electrochromic devices,[130] transistors,[131] light emitting diodes,[132] bisensors[133] and chemical sensors.[134] However, in recent years the focus of much research has been the study of oligomers. An oligomer is a molecule made of only a few repeating units. Oligomers are of interest chiefly because they are more easily prepared, with higher degrees of purity and monodispersity, than their parent polymers.[135] These properties allow oligomers to act as model systems for longer polymers with the same repeating units, whose poorer solubilities and structural defects often hinder studies of their material properties.[136] This so called "oligomer

approach"[137] has proved valuable to extrapolate and predict the properties of polymers.[138,139] Indeed, highly pure oligo(aniline)s have been used to understand the isomeric behaviour expected of **PANI**, in which the presence of *cis/trans* isomers may hinder crystallinity and contribute to the lower than predicted conductivity achieved by the polymer.[140,141] Oligomers have also garnered interest of their own as functional materials, particularly in the area of organic electronics.[136,142]

1.4.4 Tetra(aniline)

Although oligo(aniline)s were initially developed as model systems to better understand the chemistry of the parent polymer, **PANI**, they have seen shown great promise as functional materials in their own right.[143] Indeed oligo(aniline)s have already been explored for applications in electronic devices[144,145] and photonic crystals.[146] Oligo(aniline)s have the same structure as **PANI**, although four aniline units are required to form the ES state. As such, the shortest oligo(aniline) that retains the same oxidative and chemical properties as **PANI** is the tetramer, tetra(aniline) (**TANI**).

TANI can be simply synthesised by the oxidative coupling of aniline dimers, using ferric chloride hexahydrate[147] or hydrogen peroxide as catalysts.[148] However, **TANI**s produced using this method will often be contaminated with higher molecular weight oligo(aniline)s such as hexamers or octamers, as the barrier to further reaction is often low. Alternative methods involve the Buchwald-Hartwig coupling of aryl amines and aryl bromides.[149,150] Protected dimers are used to ensure the selected synthesis at chosen locations allowing for highly pure, monodisperse oligo(aniline)s to be prepared. Typically, **TANI**s are end terminated by phenyl or amine moieties, the latter allowing for further functionalization of the oligo(aniline).[151]

As with **PANI**, **TANI** can be doped to the conductive ES state. The conductivity of **TANI** is lower than the parent polymer, although it is on par with other oligomer systems.[150] However, it has been noted that as the crystallinity of the bulk material increases, so does the conductivity. Indeed, it has been theorized that oligo(aniline)s may be more crystallizable than **PANI**, potentially giving rise to improved inter-molecular conductivity and therefore higher bulk conductivity.[140] Experiments with self-assembled **TANI** microstructures showed that conductivity in the structures is anisotropic, with higher conductivity along the π-π stacking direction.[152] Further evidence of anisotropic conductivity was demonstrated by single-crystalline **TANI** was grown using graphene as a guiding substrate. **TANI** crystals grew with a π-π stacking direction perpendicular to the substrate and conductivity was found to be highest in this vertical direction. The conductivity measurement of 12.3 S cm^{-1} was greater than any previously recorded measurement.[144]

1.4.5 Self-assembly of TANI

Research into the self-assembly of oligo(aniline)s has in part been driven by a desire to improve material properties such as conductivity. However, it has also been stimulated by an interest in preparing novel, switchable assemblies. Control over structure morphology can be achieved in many ways. One common

theme is the use of doping acids to control the material structure and dimensions.[145,152–154] Wang and colleagues (2012) found that single-crystalline **TANI** could be grown in the form of 1-D nanowires, 2-D nanoribbons and 3-D nanoplates or nanoflowers, using a solvent-exchange process and different dopants.[155] Powdered EB **TANI** was added to an organic solvent and aqueous acid, before leaving to rest for 4-5 days. The introduction of an acid produced the ES state, which lowered the solubility of the oligomer, resulting in a precipitate whose morphology was dependent on the acid. The single-crystalline growths showed improved conductivity over their bulk counterparts, owing to improved overlap of the π-electron density.

Dopants have also been utilized as plasticising agents to induce ionic self-assembly. **TANI** doped with an acid surfactant, bis(ethyl hexyl) phosphate (**BEHP**), forms lamellar structures owing to phase separation of the aromatic and alkyl regions.[156] Thin films formed of the **TANI-BEHP** complexes showed different assemblies than bulk material, highlighting the importance of material thickness in promoting structure formation, an important parameter in the construction of thin film electronic devices.[157]

An alternative method to control structure formation is by functionalising **TANI** with groups that induce long-range order. Rod-coil oligomers of **TANI** functionalised with alkyl chains have been prepared, which show different packing in the bilayer smectic structures depending on the oxidation state of the oligo(aniline).[158] The difference in packing between the LEB and EB states was attributed to additional amine-imine hydrogen bonding available to the latter state, which contributed to more efficient packing.

1.4.5.1 Amphiphilic oligo(aniline)s

Water is an excellent solvent to promote self-assembly. The hydrophobic effect is often a key driving force to direct the construction of complex structures.[37,159] Additionally, water is a green solvent and is non-toxic, allowing for sustainable and biocompatible materials to be prepared.

Despite such advantages, there are limited reports of amphiphilic **TANI**s. However, those that have been reported show exciting switchable behaviour, owing to the presence of multiple oxidation states. A review of electroactive amphiphiles has been recently published by Townsend et al. (2018), demonstrating the opportunity for materials with switchable structures or properties to be prepared for applications such as drug delivery systems, thin film formation, electrochromic devices or electronic devices.[160]

Transitions between oxidation states with the application of an oxidizing or reducing voltage often produce structural changes, owing to a difference in hydrogen-bonding interactions (as highlighted in the previous section). An amphiphilic rod-coil molecule comprised of **TANI** and **PEG** formed vesicles in the LEB state, which split into puck-like micelles upon oxidation to the EB state.[161] Similarly, an amphiphile composed of **TANI** and poly(N-isopropylacrylamide) (**PNIPAM**) formed vesicles that

were disrupted with the application of an oxidising voltage. Interestingly, the vesicles could also be disrupted by the addition of an acid, owing to the increase in solubility of the hydrophobic block upon doping to the ES state.[162] Both systems with **TANI-PEG** and **TANI-PNIPAM** were hailed as potential drug delivery systems, capable of releasing their contents with the application of an oxidising voltage or an acid.

Oxidation or doping can also produce functional changes to a material. A star-shaped rod-coil amphiphile has been prepared, composed of a benzene core and three **TANI-PEG** arms.[163] Thin films produced with this amphiphile showed switchable transitions in their colouration, from transparent to light green and dark blue with increasing voltage. The excellent electrochromic properties were attributed to the amphiphile's self-assembly into a cylindrical pattern, facilitating electronic charge transport.

Finally, the difference in conductivity between the EB and ES states has been exploited for the preparation of switchable electronic devices. Bell et al. (2015) developed an amphiphile, **TANI-PTAB**, from a rigid **TANI** core covalently bound to a trimethylammonium bromide head group by a flexible alkyl tail.[164] In the EB state, this amphiphile self-assembled into well-defined nanofibers. However, with the addition of enantiomerically pure camphorsulfonic acid (**CSA**), **TANI-PTAB** was doped to the ES state, forming helical nanowires whose handedness depended on the chirality of the acid. The conductivity of **CSA**-doped **TANI-PTAB** was 2.7 mS cm^{-1}, which while lower than crystalline **TANI** was still highly attractive when its simple processing methods were taken into consideration.

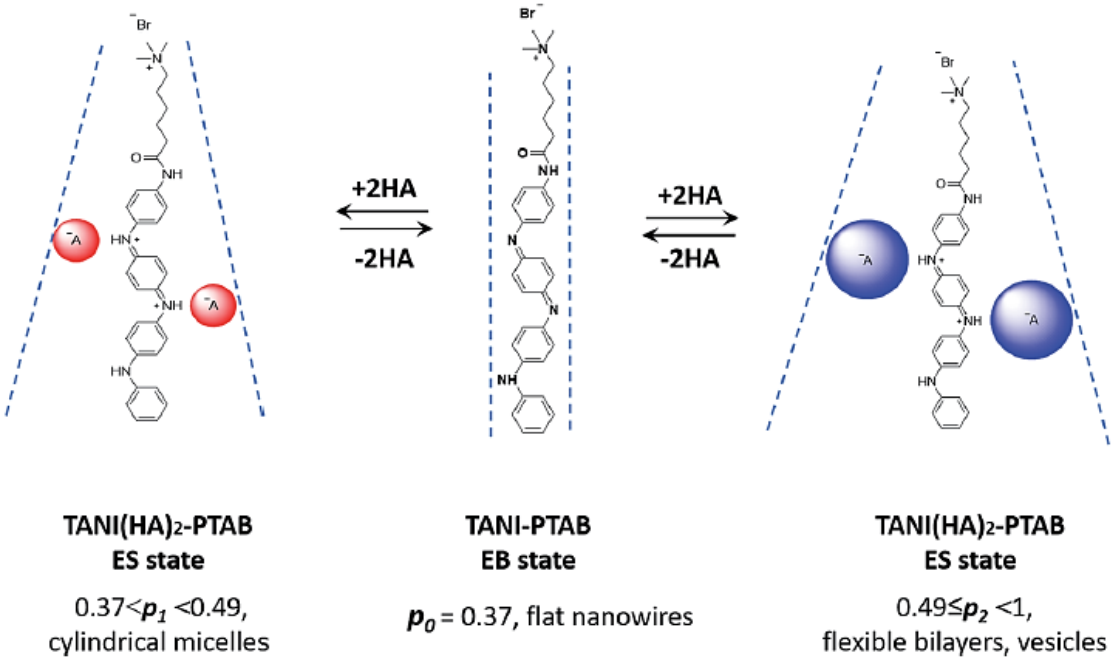

*Figure 1.18. Scheme demonstrating the addressable packing parameter approach, as applied to **TANI-PTAB**. Dopants are used to change the volume of the hydrophobic core, thereby reversibly tuning the packing parameter. Reproduced from Reference* 165.

Interestingly, further control over the self-assembled structures formed by **TANI-PTAB** could be achieved by utilizing different doping acids. Lyu et al. (2018) used an addressable *pp* approach to tune the self-assembly of **TANI-PTAB** (Figure 1.18). Acids of different volumes were used to dope the **TANI** core, thereby increasing the volume of the hydrophobic section and increasing the overall *pp* of the amphiphile. The authors demonstrated that small acids (i.e., hydrochloric acid) produced cylindrical micelles, while bulkier acids (i.e., trifluoroacetic acid) produced vesicles. These structures matched those expected from their calculated *pp*.[165]

Following this work, other **TANI**-derived amphiphiles were investigated, both single-tailed and bolaform, to explore how changes to the molecular structure and therefore their *pp* affected the self-assembly behaviour of such amphiphiles. Of those explored, most notable were a phosphonium amphiphile, **TANI-PTPB**, and a bolaamphiphile, **TANI-(PTAB)$_2$**.

TANI-PTPB is structurally analogous to **TANI-PTAB**, although bearing a trimethylphosphonium head group in place of a trimethylammonium one. In the EB state, **TANI-PTPB** self-assembled into nanofibers with occasional spherical structures.[166] The number of spherical structures increased with concentration, owing to a decrease in the head group surface area. Vesicular structures were also formed upon doping with **CSA**. Meanwhile, the bolaamphiphile, **TANI-(PTAB)$_2$**, is comprised of a **TANI** core and two flexible spacers terminated by trimethylammonium head groups. In contrast to the single-tailed analogue, EB **TANI-(PTAB)$_2$** self-assembled into spherical structures that swelled with the addition of acids.[166] For both amphiphiles, the self-assembly behaviour was fully reversible upon the addition of a base.

1.5 TEMPLATED ASSEMBLY OF PANI

While the above section highlights the progress of research into the self-assembly of oligo(aniline)s, limited attention has been given to the polymerisation of such structures or their templated assembly. As discussed in previous sections, the polymerisation of nanostructures adds stability and resilience to materials, while maintaining the order important to their function. Additionally, the use of templates can impart greater structural order to materials and allow for the production of otherwise unavailable architectures.

Improved structural order could benefit the conductivity of **PANI** and oligo(aniline)s, as structural defects can hinder charge transport. Meanwhile, 3-D porous architectures formed from nitrogen-rich conjugated polymers, which are structurally similar to **PANI**, have already proven valuable in the capture and storage of small molecules and as catalytic supports.[167,168] However, it can be difficult to tune the surface area and porosity of the polymers,[169] a problem which may be solved by judicious application of a template.

A few examples of **PANI** nanostructures grown in liquid crystal mesophases can be found in the literature. Conductive nanowires can find applications in nanodevices owing to their anisotropic structures, switchable conductivities, and flexibility. Huang et al. (2002) demonstrated the growth of long and straight **PANI** nanowires from a reverse phase hexagonal LLC.[170] The hexagonal phase was further ordered by the application of an external electric field, used in the electropolymerisation reaction. The nanowires formed had diameters much greater than the widths of the water channels of the hexagonal phase in which polymerisation occurred, indicating that the mesophase acted to indirectly control polymer growth.

Another example of indirect templating is the preparation of helical **PANI**, formed without the application of chiral dopant or template.[171] Figure 1.19 shows the growth of **PANI** helixes from multi-lamellar vesicles. **PANI** nanofibers are prepared by emulsion polymerisation of aniline with dodecylbenzenesulfonic acid (**DBSA**) and ammonium persulfate. **DBSA** and aniline form multi-lamellar vesicles in mixtures of water, methylbenzene and butanol. With the addition of ammonium persulfate, polymerisation starts to occur in the shell of the vesicles. As the polymer particles' molecular weights increase, the particles begin to aggregate and form longer nanofibers, directed by the liquid crystal. Mechanical stirring then promotes the twisting of the polymers into helixes.

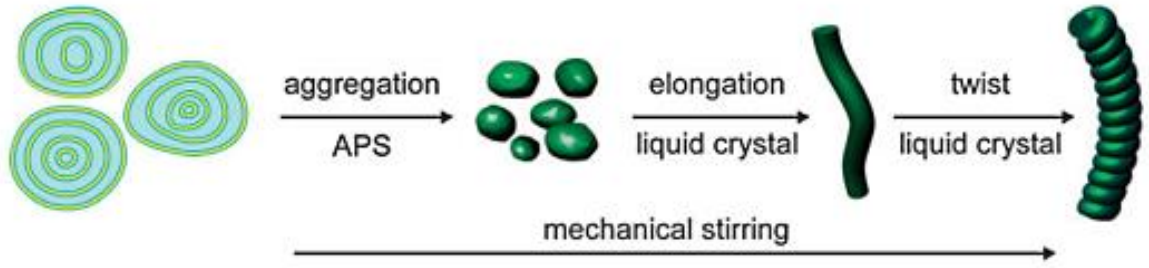

*Figure 1.19. Scheme showing formation of **PANI** helixes from multi-lamellar vesicles. Reproduced from Reference* 171.

Although LLC templating of **PANI** nanostructures appears to mainly involve indirect templating, a measure of control can be achieved by altering the template or the reaction conditions. Dutt et al. (2014) found that different **PANI** structures formed from swollen liquid crystal could be achieved by changing the rate of ammonium persulfate diffusion and by the application of different surfactants.[172] Stirring of the oxidant with the aniline-containing mesophase lead to the formation of spherical particles, while the slow diffusion of the oxidant led to the formation of rod-like structures.

1.6 CONCLUSIONS

In summary, self-assembly is a simple and efficient method of preparing highly ordered and complex structures from the bottom-up. Over the decades, the self-assembled systems formed by liquid crystals have played a key role in this regard, owing to their ease of preparation and ready adaptability for many

material applications. Numerous strategies have been applied to control the assemblies formed by liquid crystals, with those stimuli-responsive systems providing a facile, switchable method of controlling structure and function.

A diverse range of applications are available to self-assembled systems, from biomedical applications, to sensors, nanoreactors and indeed as templates themselves to prepare ordered materials. Templating can benefit many material applications, among them electronic devices, as the soft assemblies can be utilized to form more resilient and mechanically strong systems, bringing researchers ever closer to the goal of forming functional, defect-free, and complex materials.

1.7 THESIS OUTLINE

This thesis focuses on the design of stimuli-responsive supramolecular nanostructures based on electroactive amphiphiles. Such materials have promising applications in areas such as size-selective molecular sieves, drug delivery vehicles and templates. Their function is based on their capability to reversibly change form with the application of a stimulus, enabling their behaviour to be switched on and off.

The design of stimuli-responsive architectures is based on two approaches. In the first, tetra(aniline)-derived amphiphiles are introduced to a lipidic cubic phase and a packing parameter approach is used to tune the self-assembly behaviour of the mesophase. By careful control over the amphiphile's chemical structure, its packing parameter can be adapted to induce the desired structural changes to the lipid mesophase. Moreover, by application of an acid or a base, reversible changes in assembly can be achieved by altering the amphiphile's oxidation state.

In the second, lyotropic liquid crystals are used as structure-directing agents for polymerisation and as reactive mesogens, to encourage the formation of well-defined and responsive polymers. In this way, structural rigidity and resilience to environmental changes can be achieved, while maintaining functionality.

1.8 AIMS AND OBJECTIVES

The aim of this work was to develop an understanding of how an amphiphile's packing parameter can elicit structural changes to a mesophase and to use this understanding to prepare highly ordered and stimuli-responsive nanostructures from electroactive amphiphiles.

To achieve this aim, several objectives were identified:

- Synthesis of tetra(aniline)-derived amphiphiles that are structurally similar, but with key differences to produce varying packing parameters.

- Investigation of the effect of tetra(aniline)-derived amphiphiles on the self-assembled structures formed by monoolein, to determine how the shape of the amphiphile influences the membrane curvature of the lipid cubic phase.
- Investigate the effect of acid-doping, to ascertain whether pH can be used as a stimulus to induce structural changes in tetra(aniline)-containing lipid mesophases.
- Use polymerisation techniques to fix ordered mesophases, using liquid crystals as structure directing agents and as reactive mesogens, demonstrating the advantages of using both techniques to produce highly ordered, functional polymers.

The work towards the realization of these objectives is described in the following chapters:

In Chapter 2, the synthesis of tetra(aniline)-derived amphiphiles, comprised of tetra(aniline) cores and one or two cationic head groups, is outlined. The attempted synthesis of a polymerizable, tetra(aniline)-derived amphiphile is also explored, however, a fully realised product was not developed.

In Chapter 3, the effect of introducing the single-tailed amphiphile, **TANI-PTAB**, to monoolein cubic phases is investigated and the role of oxidation state is elucidated, using spectroscopic and scattering techniques.

In Chapter 4, the influence of different tetra(aniline)-derived amphiphiles on the mesophase formation of monoolein is explained using the packing parameter concept. Three tetra(aniline) amphiphiles that are structurally analogous to **TANI-PTAB** are explored and their effect on monoolein cubic phases determined by small-angle X-ray scattering.

Finally, in Chapter 5, two methods of preparing ordered polymers are outlined. In the first, a non-covalent polymerisation technique is explored, using doping acids to cross-link **TANI-PTAB** assemblies in water and within a lipid template. In the second, a lipid template is used as a host to direct the photopolymerisation of a gemini monomer.

1.9 REFERENCES

1. Silva, G. A. Introduction to Nanotechnology and Its Applications to Medicine. *Surg. Neurol.* **61**, 216–220 (2004).

2. Tu, R. S. & Tirrell, M. Bottom-up design of biomimetic assemblies. *Adv. Drug. Deliv. Rev.* **56**, 1537–1563 (2004).

3. Shimomura, M. & Sawadaishi, T. Bottom-up strategy of materials fabrication: a new trend in nanotechnology of soft materials. *Curr. Opin. Colloid Interface Sci.* **6**, 11–16 (2001).

4. Hamley, I. W. Nanotechnology with Soft Materials. *Angew. Chem. Int. Ed.* **42**, 1692–1712 (2003).

5. Seto, C. T. & Whitesides, G. M. Molecular Self-Assembly through Hydrogen Bonding: Supramolecular Aggregates Based on the Cyanuric Acid·Melamine Lattice. *J. Am. Chem. Soc.* **115**, 905–916 (1993).

6. Whitesides, G. M. & Grzybowski, B. Self-assembly at all scales. *Science* **295**, 2418–2421 (2002).

7. Alberts, B. *et al.* The Lipid Bilayer. *Molecular Biology of the Cell* (2002). Available at: https://www.ncbi.nlm.nih.gov/books/NBK26871. (Accessed: 9th April 2021)

8. Klug, A. From Macromolecules to Biological Assemblies(Nobel Lecture). *Angew. Chem. Int. Ed. Eng.* **22**, 565–582 (1983).

9. Cölfen, H. & Mann, S. Higher-Order Organization by Mesoscale Self-Assembly and Transformation of Hybrid Nanostructures. *Angew. Chem. Int. Ed.* **42**, 2350–2365 (2003).

10. Stupp, S. I. & Palmer, L. C. Supramolecular chemistry and self-assembly in organic materials design. *Chem. Mater.* **26**, 507–518 (2014).

11. Babu, S. S., Prasanthkumar, S. & Ajayaghosh, A. Self-assembled gelators for organic electronics. *Angew. Chem. Int. Ed.* **51**, 1766–1776 (2012).

12. Wang, C., Wang, Z. & Zhang, X. Superamphiphiles as building blocks for supramolecular engineering: Towards functional materials and surfaces. *Small* **7**, 1379–1383 (2011).

13. Cordier, P., Tournilhac, F., Soulié-Ziakovic, C. & Leibler, L. Self-healing and thermoreversible rubber from supramolecular assembly. *Nature* **451**, 977–80 (2008).

14. Burnworth, M. *et al.* Optically healable supramolecular polymers. *Nature* **472**, 334–337 (2011).

15. Li, X. *et al.* Uniform electroactive fibre-like micelle nanowires for organic electronics. *Nat. Commun.* **8**, 15909–15917 (2017).

16. Schenning, A. P. H. J. & Meijer, E. W. Supramolecular electronics; nanowires from self-assembled pi-conjugated systems. *Chem. Commun.* 3245–3258 (2005).

17. Yan, Q. *et al.* Voltage-responsive vesicles based on orthogonal assembly of two homopolymers. *J. Am. Chem. Soc.* **132**, 9268–9270 (2010).

18. Glavas, L., Odelius, K. & Albertsson, A.-C. Induced redox responsiveness and electroactivity for altering the properties of micelles without external stimuli. *Soft Matter* **10**, 4028–36 (2014).

19. Jacob, C., Safronov, A. Y., Wilson, S., Hill, H. A. O. & Booth, T. F. Synthesis, characterization and electrochemistry of a novel ruthenocene surfactant. *J. Electroanal. Chem.* **427**, 161–167 (1997).

20. Marencic, A. P. & Register, R. A. Controlling Order in Block Copolymer Thin Films for Nanopatterning Applications. *Annu. Rev. Chem. Biomol. Eng.* **1**, 277–297 (2010).

21. Sanders, D. P. Advances in Patterning Materials for 193 nm Immersion Lithography. *Chem. Rev.* **110**, 321–360 (2010).

22. Faul, C. F. J. & Antonietti, M. Ionic self-assembly: Facile synthesis of supramolecular materials. *Adv. Mater.* **15**, 673–683 (2003).

23. Antonietti, M. & Göltner, C. Superstructures of functional colloids: chemistry on the nanometer scale. *Angew. Chem. Int. Ed. Engl.* **36**, 910–928 (1997).

24. Hermann, J., Distasio Jr., R. A. & Tkatchenko, A. First-Principles Models for van der Waals Interactions in Molecules and Materials: Concepts, Theory, and Applications. *Chem. Rev.* **117**, 4714–4758 (2017).

25. Elemans, J. A. A. W., Rowan, A. E. & Nolte, R. J. M. Mastering molecular matter. Supramolecular architectures by hierarchical self-assembly. *J. Mater. Chem.* **13**, 2661–2670 (2003).

26. Ruokolainen, J. *et al.* Switching supramolecular polymeric materials with multiple length scales. *Science* **280**, 557–560 (1998).

27. Würthner, F. *et al.* Perylene Bisimide Dye Assemblies as Archetype Functional Supramolecular Materials. *Chem. Rev.* **116**, 962–1052 (2016).

28. Hunter, C. A & Sanders, J. K. M. The Nature of pi-pi Interactions. *J. Am. Chem. Soc.* **112**, 5525–5534 (1990).

29. Würthner, F. Perylene bisimide dyes as versatile building blocks for functional supramolecular architectures. *Chem. Commun.* 1564–1579 (2004).

30. González-Rodríguez, D. & Schenning, A. P. H. J. Hydrogen-bonded supramolecular π-functional materials. *Chem. Mater.* **23**, 310–325 (2011).

31. Fleischmann, E. K. & Zentel, R. Liquid-Crystalline Ordering as a Concept in Materials Science: From Semiconductors to Stimuli-Responsive Devices. *Angew. Chem. Int. Ed.* **52**, 8810–8827 (2013).

32. Destrade, C. *et al.* Disc-Like Mesogen Polymorphism. *Mol. Cryst. Liq. Crys.* **106**, 121–146 (1984).

33. Herrmann-Schonherr, O., Wendorff, J. H., Ringsdorf, H. & Tschirner, P. Structure of an aromatic polyamide with disc-like mesogens in the main chain. *Makromol. Chem., Rapid Commun.* **7**, 791–796 (1986).

34. Tschierske, C. Molecular self-organization of amphotropic liquid crystals. *Prog. Polym. Sci.* **21**, 775–852 (1996).

35. Huang, Y. & Gui, S. Factors affecting the structure of lyotropic liquid crystals and the correlation between structure and drug diffusion. *RSC Adv.* **8**, 6978–6987 (2018).

36. Silverstein, T. P. The Real Reason Why Oil and Water Don' t Mix. *J. Chem. Educ.* **75**, 116–118 (1998).

37. Biedermann, F., Nau, W. M. & Schneider, H.-J. The hydrophobic effect revisited-studies with supramolecular complexes imply high-energy water as a noncovalent driving force. *Angew. Chem. Int. Ed.* **53**, 11158–11171 (2014).

38. Nagarajan, R. & Ruckenstein, E. Theory of Surfactant Self-Assembly: A Predictive Molecular Thermodynamic Approach. *Langmuir* **7**, 2934–2969 (1991).

39. Zhang, J., Li, X. & Li, X. Stimuli-triggered structural engineering of synthetic and biological polymeric assemblies. *Prog. Polym. Sci.* **37**, 1130–1176 (2012).

40. Israelachvil, J. N. *et al.* Theory of Self-Assembly of Hydrocarbon Amphiphiles into Micelles and Bilayers. *J. Chem. Soc., Faraday Trans. 2* **72**, 1525–1568 (1976).

41. Fong, C., Le, T. & Drummond, C. J. Lyotropic liquid crystal engineering – ordered nanostructured small molecule amphiphile self-assembly materials by design. *Chem. Soc. Rev.* **41**, 1297–1322 (2012).

42. Gainanova, G. A. *et al.* Self-assembling systems based on amphiphilic

alkyltriphenylphosphonium bromides : Elucidation of the role of head group. *J. Colloid Interface Sci.* **367**, 327–336 (2012).

43. Bakshi, M. S., Singh, J., Singh, K. & Kaur, G. Mixed micelles of cationic gemini with tetraalkyl ammonium and phosphonium surfactants: the head group and hydrophobic tail contributions. *Colloids Surfaces A Physicochem. Eng. Asp.* **234**, 77–84 (2004).

44. Abdel-Rahem, R. The influence of hydrophobic counterions on micellar growth of ionic surfactants. *Adv. Colloid Interface Sci.* **141**, 24–36 (2008).

45. Dierking, I. & Al-Zangana, S. Lyotropic Liquid Crystal Phases from Anisotropic Nanomaterials. *Nanomaterials* **7**, 305 (2017).

46. Lombardo, D., Kiselev, M. A., Magazù, S. & Calandra, P. Amphiphiles Self-Assembly: Basic Concepts and Future Perspectives of Supramolecular Approaches. *Adv. Condens. Matter Phys.* **2015**, 151683 (2015).

47. Kulkarni, C. V., Ces, O., Templer, R. H. & Seddon, J. M. Pressure effects on a protein–lipid model membrane. *Soft Matter* **9**, 6525 (2013).

48. Brown, M. F. Curvature Forces in Membrane Lipid-Protein Interactions. *Biochemistry* **51**, 9782–9795 (2012).

49. Seddon, A. M. *Recent developments in the production, analysis, and applications of cubic phases formed by lipids*. *Advances in Planar Lipid Bilayers and Liposomes* **18**, (Academic Press, 2013).

50. Kulkarni, C. V., Wachter, W., Iglesias-Salto, G., Engelskirchen, S. & Ahualli, S. Monoolein: a magic lipid? *Phys. Chem. Chem. Phys.* **13**, 3004–3021 (2011).

51. van ‘t Hag, L., Gras, S. L., Conn, C. E. & Drummond, C. J. Lyotropic liquid crystal engineering moving beyond binary compositional space – ordered nanostructured amphiphile self-assembly materials by design. *Chem. Soc. Rev.* **46**, 2705–2731 (2017).

52. Nazaruk, E. *et al.* Properties of native and hydrophobic laccases immobilized in the liquid-crystalline cubic phase on electrodes. *J. Biol. Inorg. Chem.* **12**, 335–344 (2007).

53. Nazaruk, E., Bilewicz, R., Lindblom, G. & Lindholm-Sethson, B. Cubic phases in biosensing systems. *Anal. Bioanal. Chem.* **391**, 1569–1578 (2008).

54. Nazaruk, E. *et al.* Enzymatic biofuel cell based on electrodes modified with lipid liquid-crystalline cubic phases. *J. Power Sources* **183**, 533–538 (2008).

55. Manni, L. S., Fong, W.-K. & Mezzenga, R. Lipid-based mesophases as matrices for nanoscale

reactions. *Nanoscale Horizons* **5**, 914–927 (2020).

56. Caffrey, M. Crystallizing Membrane Proteins for Structure Determination: Use of Lipidic Mesophases. *Annu. Rev. Biophys.* **38**, 29–51 (2009).

57. Duss, M. *et al.* Lipidic Mesophase-Embedded Palladium Nanoparticles: Synthesis and Tunable Catalysts in Suzuki−Miyaura Cross-Coupling Reactions. *Langmuir* **35**, 120–127 (2019).

58. Cherezov, V., Clogston, J., Papiz, M. Z. & Caffrey, M. Room to move: Crystallizing membrane proteins in swollen lipidic mesophases. *J. Mol. Biol.* **357**, 1605–1618 (2006).

59. Brasnett, C., Longstaff, G., Compton, L. & Seddon, A. Effects of Cations on the Behaviour of Lipid Cubic Phases. *Sci. Rep.* **7**, 8229 (2017).

60. Oka, T. & Hojo, H. Single Crystallization of an Inverse Bicontinuous Cubic Phase of a Lipid. *Langmuir* **30**, 8253–8257 (2014).

61. Seddon, A. M., Lotze, G., Plivelic, T. S. & Squires, A. M. A highly oriented cubic phase formed by lipids under shear. *J. Am. Chem. Soc.* **133**, 13860–13863 (2011).

62. Fong, W. K., Negrini, R., Vallooran, J. J., Mezzenga, R. & Boyd, B. J. Responsive self-assembled nanostructured lipid systems for drug delivery and diagnostics. *J. Colloid Interface Sci.* **484**, 320–339 (2016).

63. Phan, S., Fong, W.-K., Kirby, N., Hanley, T. & Boyd, B. J. Evaluating the link between self-assembled mesophase structure and drug release. *Int. J. Pharm.* **421**, 176–182 (2011).

64. Angelov, B. *et al.* Small-angle neutron and X-ray scattering from amphiphilic stimuli-responsive diamond-type bicontinuous cubic phase. *J. Am. Chem. Soc.* **129**, 13474–13479 (2007).

65. Fong, W.-K., Hanley, T. L., Thierry, B., Kirby, N. & Boyd, B. J. Plasmonic Nanorods Provide Reversible Control over Nanostructure of Self-Assembled Drug Delivery Materials. *Langmuir* **26**, 6136–6139 (2010).

66. Fong, W.-K. *et al.* External manipulation of nanostructure in photoresponsive lipid depot matrix to control and predict drug release in vivo. *J. Control. Release* **228**, 67–73 (2016).

67. Szlezak, M. *et al.* Monoolein cubic phase gels and cubosomes doped with magnetic nanoparticles-hybrid materials for controlled drug release. *ACS Appl. Mater. Interfaces* **9**, 2796–2805 (2017).

68. Mendozza, M. *et al.* On the thermotropic and magnetotropic phase behavior of lipid liquid crystals containing magnetic nanoparticles. *Nanoscale* **10**, 3480–3488 (2018).

69. Bisset, N. B., Boyd, B. J. & Dong, Y. Da. Tailoring liquid crystalline lipid nanomaterials for controlled release of macromolecules. *Int. J. Pharm.* **495**, 241–248 (2015).

70. Kluzek, M. *et al.* Influence of a pH-sensitive polymer on the structure of monoolein cubosomes. *Soft Matter* **13**, 7571–7577 (2017).

71. Nazaruk, E. *et al.* Design and assembly of pH-sensitive lipidic cubic phase matrices for drug release. *Langmuir* **30**, 1383–1390 (2014).

72. Negrini, R. & Mezzenga, R. pH-responsive lyotropic liquid crystals for controlled drug delivery. *Langmuir* **27**, 5296–5303 (2011).

73. Negrini, R., Fong, W. K., Boyd, B. J. & Mezzenga, R. pH-responsive lyotropic liquid crystals and their potential therapeutic role in cancer treatment. *Chem. Commun.* **51**, 6671–6674 (2015).

74. Negrini, R. & Mezzenga, R. Diffusion, molecular separation, and drug delivery from lipid mesophases with tunable water channels. *Langmuir* **28**, 16455–16462 (2012).

75. Van Der Asdonk, P. *et al.* Patterning of Soft Matter across Multiple Length Scales. *Adv. Funct. Mater.* **26**, 2609–2616 (2016).

76. Gin, D. L., Gray, D. H., Smith, R. C. & Uni-, W. M. R. Polymerizable Liquid Crystals as Building Blocks for Functional, Nanostructured Materials. *Synlett* 1509–1522 (1999).

77. Clapper, J. D., Sievens-Figueroa, L. & Guymon, C. A. Photopolymerization in polymer templating. *Chem. Mater.* **20**, 768–781 (2008).

78. Yun, C.-J. & Song, J.-K. Functional films using reactive mesogens for display applications. *J. Inf. Disp.* **18**, 119–129 (2017).

79. Steer, D., Kang, M. & Leal, C. Soft nanostructured films for directing the assembly of functional materials. *Nanotechnology* **28**, 142001 (2017).

80. Dierking, I. Recent developments in polymer stabilised liquid crystals. *Polym. Chem.* **1**, 1153–1159 (2010).

81. Vignolini, S. *et al.* A 3D optical metamaterial made by self-assembly. *Adv. Mater.* **24**, 23–27 (2012).

82. Wang, D. *et al.* A general route to macroscopic hierarchical 3D nanowire networks. *Angew. Chem. Int. Ed.* **43**, 6169–6173 (2004).

83. Akagi, K. *et al.* Helical Polyacetylene Synthesized with a Chiral Nematic Reaction Field. *Science* **282**, 1683–1686 (1998).

84. Akagi, K. Helical polyacetylene: asymmetric polymerization in a chiral liquid-crystal field. *Chem. Rev.* **109**, 5354–401 (2009).

85. Park, J., Goh, M. & Akagi, K. Helical nylons and polyphthalamides synthesized by chiral interfacial polymerizations between chiral nematic liquid crystal and water layers. *Macromolecules* **47**, 2784–2795 (2014).

86. Goto, H. Doping-dedoping-driven optic effect of pi-conjugated polymers prepared in cholesteric-liquid-crystal electrolytes. *Phys. Rev. Lett.* **98**, 1–4 (2007).

87. Antonietti, M., Goltner, C. & Hentze, H.-P. Polymer Gels with a Micron-Sized, Layer-like Architecture by Polymerization in Lyotropic Cocogem Phases. *Langmuir* **14**, 2670–2676 (1998).

88. Wadekar, M. N., Pasricha, R., Gaikwad, A. B. & Kumaraswamy, G. Polymerization in Surfactant Liquid Crystalline Phases. *Chem. Mater.* **17**, 2460–2465 (2005).

89. Liu, D. & Broer, D. J. Liquid crystal polymer networks: preparation, properties, and applications of films with patterned molecular alignment. *Langmuir* **30**, 13499–13509 (2014).

90. Forney, B. S., Baguenard, C. & Guymon, C. A. Effects of controlling polymer nanostructure using photopolymerization within lyotropic liquid crystalline templates. *Chem. Mater.* **25**, 2950–2960 (2013).

91. Broer, D. J., Bastiaansen, C. M. W., Debije, M. G. & Schenning, A. P. H. J. Functional organic materials based on polymerized liquid-crystal monomers: Supramolecular hydrogen-bonded systems. *Angew. Chem. Int. Ed.* **51**, 7102–7109 (2012).

92. Gin, D. L., Gu, W., Pindzola, B. A. & Zhou, W.-J. Polymerized Lyotropic Liquid Crystal Assemblies for Materials Applications. *Acc. Chem. Res.* **34**, 973–980 (2001).

93. Thiem, H., Strohriegl, P., Shkunov, M. & Mcculloch, I. Photopolymerization of Reactive Mesogens. *Macromol.* **206**, 2153–2159 (2005).

94. Li, Y. *et al.* Two-dimensional polymers with versatile functionalities via gemini monomers. *Sci. Adv.* **5**, eaaw9120 (2019).

95. Pindzola, B. A., Hoag, B. P. & Gin, D. L. Polymerization of a Phosphonium Diene Amphiphile in the Regular Hexagonal Phase with Retention of Mesostructure. *J. Am. Chem. Soc.* **123**, 4617–4618 (2001).

96. Pindzola, B. A., Jin, J. & Gin, D. L. Cross-Linked Normal Hexagonal and Bicontinuous Cubic Assemblies via Polymerizable Gemini Amphiphiles. *J. Am. Chem. Soc.* **125**, 2940–2949 (2003).

97. Wiesenauer, B. R. & Gin, D. L. Nanoporous polymer materials based on self-organized, bicontinuous cubic lyotropic liquid crystal assemblies and their applications. *Polym. J.* **44**, 461–468 (2012).

98. Hatakeyama, E. S., Wiesenauer, B. R., Gabriel, C. J., Noble, R. D. & Gin, D. L. Nanoporous, Bicontinuous Cubic Lyotropic Liquid Crystal Networks via Polymerizable Gemini Ammonium Surfactants. *Chem. Mater.* **22**, 4525–4527 (2010).

99. Hentze, H.-P. & Kaler, E. W. Polymerization of and within self-organized media. *Curr. Opin. Colloid Interface Sci.* **8**, 164–178 (2003).

100. Wang, X., Bukusoglu, E. & Abbott, N. L. A Practical Guide to the Preparation of Liquid Crystal-Templated Microparticles. *Chem. Mater.* **29**, 53–61 (2017).

101. Srisiri, W. *et al.* Polymerization of the Inverted Hexagonal Phase. *J. Am. Chem. Soc.* **119**, 4866–4873 (1997).

102. Akbar, S., Elliott, J. M., Rittman, M. & Squires, A. M. Facile production of ordered 3D platinum nanowire networks with 'single diamond' bicontinuous cubic morphology. *Adv. Mater.* **25**, 1160–1164 (2013).

103. Richardson, S. J. *et al.* Aligned platinum nanowire networks from surface-oriented lipid cubic phase templates. *Nanoscale* **8**, 2850–2856 (2016).

104. Akbar, S., Elliott, J. M., Squires, A. M. & Anwar, A. Optimum conditions for electrochemical deposition of 3-D mesoporous platinum framework. *J. Nanopart. Res.* **22**, 170 (2020).

105. Burton, M. *et al.* Three-Dimensional Nanostructured Palladium with Single Diamond Architecture for Enhanced Catalytic Activity. *ACS Appl. Mater. Interfaces* **10**, 37087–37094 (2018).

106. Akbar, S., Boswell, J., Worsley, C., Elliott, J. M. & Squires, A. M. Ultrathin Uniform Platinum Nanowires via a Facile Route Using an Inverse Hexagonal Surfactant Phase Template. *Langmuir* **34**, 6991–6996 (2018).

107. Wang, H., Zetterlund, P. B., Boyer, C. & Spicer, P. T. Polymerization of cubosome and hexosome templates to produce complex microparticle shapes. *J. Colloid Interface Sci.* **546**, 240–250 (2019).

108. Hatano, T. *et al.* Helical structures of conjugate polymers created by oxidative polymerization using synthetic lipid assemblies as templates. *Chem. - A Eur. J.* **10**, 5067–5075 (2004).

109. Molapo, K. M. *et al.* Electronics of conjugated polymers (I): Polyaniline. *Int. J. Electrochem. Sci.* **7**, 11859–11875 (2012).

110. Shirakawa, H. The Discovery of Polyacetylene Film : The Dawning of an Era of Conducting Polymers (Nobel Lecture). *Angew. Chem. Int. Ed.* **40**, 2574–2580 (2001).

111. MacDiarmid, A. G. Synthetic Metals: A Novel Role for Organic Polymers (Nobel Lecture). *Angew. Chem. Int. Ed.* **40**, 2581–2590 (2001).

112. Heeger, A. J. Semiconducting and metallic polymers: The fourth generation of polymeric materials. *J. Phys. Chem. B* **105**, 8475–8491 (2001).

113. Heeger, A. J. Semiconducting polymers : the Third Generation. *Chem. Soc. Rev.* **39**, 2354–2371 (2010).

114. Morin, P.-O., Bura, T. & Leclerc, M. Realizing the full potential of conjugated polymers: innovation in polymer synthesis. *Mater. Horiz.* **3**, 11–20 (2016).

115. Yannoni, C. S. & Clarke, T. C. Molecular geometry of cis- and trans-polyacetylene by nutation NMR spectroscopy. *Phys. Rev. Lett.* **51**, 1191–1193 (1983).

116. Letheby, H. On the production of a blue substance by the electrolysis of sulphate of aniline. *J. Chem. Soc.* **15**, 161–163 (1862).

117. Shimano, J. Y. & MacDiarmid, A. G. Polyaniline, a dynamic block copolymer: Key to attaining its intrinsic conductivity? *Synth. Met.* **123**, 251–262 (2001).

118. Masters, J. G., Sun, Y., MacDiarmid, A. G. & Epstein, A. J. Polyaniline: Allowed oxidation states. *Synth. Met.* **41**, 715–718 (1991).

119. Pron, A. & Rannou, P. Processible conjugated polymers: From organic semiconductors to organic metals and superconductors. *Prog. Polym. Sci.* **27**, 135–190 (2002).

120. Ray, A. *et al.* Polyaniline: Doping, structure and derivatives. *Synth. Met.* **29**, 141–150 (1989).

121. Lee, K. *et al.* Metallic transport in polyaniline. *Nature* **441**, 65–68 (2006).

122. Kohlman, R. S. *et al.* Limits for Metallic Conductivity in Conducting Polymers. *Phys. Rev. Lett.* **78**, 3915–3918 (1997).

123. MacDiarmid, A. G. & Epstein, A. J. Secondary doping in polyaniline. *Synth. Met.* **69**, 85–92 (1995).

124. Stafstrom, S. *et al.* Polaron Lattice in Highly Conducting Polyaniline: Theoretical and Optical Studies. *Phys. Rev. Lett.* **59**, 1464–1467 (1987).

125. Bhadra, S., Khastgir, D., Singha, N. K. & Lee, J. H. Progress in preparation, processing and applications of polyaniline. *Prog. Polym. Sci.* **34**, 783–810 (2009).

126. Chiang, J.-C. & MacDiarmid, A. G. ‘Polyaniline’: Protonic acid doping of the emeraldine form to the metallic regime. *Synth. Met.* **13**, 193–205 (1986).

127. Cao, Y., Smith, P. & Heeger, A. J. Counter-ion induced processibility of conducting polyaniline and of conducting polyblends of polyaniline in bulk polymers. *Synth. Met.* **48**, 91–97 (1992).

128. Dufour, B. *et al.* Low Tg , Stretchable Polyaniline of Metallic-Type Conductivity : Role of Dopant Engineering in the Control of Polymer Supramolecular Organization and in the Tuning of Its Properties. *Chem. Mater.* **15**, 1587–1592 (2003).

129. MacDiarmid, A. G. & Epstein, A. J. The concept of secondary doping as applied to polyaniline. *Synth. Met.* **65**, 103–116 (1994).

130. Tarver, J. & Loo, Y.-L. Mesostructures of Polyaniline Films Affect Polyelectrochromic Switching. *Chem. Mater.* **23**, 4402–4409 (2011).

131. Yusoff, A. R. bin M. & Shuib, S. A. Metal-base transistor based on simple polyaniline electropolymerization. *Electrochim. Acta* **58**, 417–421 (2011).

132. Bejbouj, H. *et al.* Influence of the nature of polyaniline-based hole-injecting layer on polymer light emitting diode performances. *Mater. Sci. Eng. B* **166**, 185–189 (2010).

133. Yang, Y. & Mu, S. Bioelectrochemical Responses of the Polyaniline Horseradish Peroxidase Electrodes. *J. Electroanal. Chem.* **432**, 71–78 (1997).

134. Huang, J., Virji, S., Weiller, B. H. & Kaner, R. B. Polyaniline nanofibers: facile synthesis and chemical sensors. *J. Am. Chem. Soc.* **125**, 314–315 (2003).

135. Tour, J. M. Conjugated Macromolecules of Precise Length and Constitution. Organic Synthesis for the Construction of Nanoarchitectures. *Chem. Rev.* **96**, 537–554 (1996).

136. Martin, R. E. & Diederich, F. Linear Monodisperse pi-Conjugated Oligomers: Model Compounds for Polymers and More. *Angew. Chem. Int. Ed.* **38**, 1350–1377 (1999).

137. Muller, K. & Wegner, G. *Electronic Materials: The Oligomer Approach*. (Wiley-VCH, 1998).

138. Zade, Sanjio, S., Zamoshchik, N. & Bendikov, M. From Short Conjugated Oligomers to Conjugated Polymers. Lessons from Studies on Long Conjugated Oligomers. *Acc. Chem. Res.* **44**, 14–24 (2011).

139. Gierschner, J., Cornil, J. & Egelhaaf, H. J. Optical bandgaps of π-conjugated organic materials at the polymer limit: Experiment and theory. *Adv. Mater.* **19**, 173–191 (2007).

140. MacDiarmid, A. G., Zhou, Y. & Feng, J. Oligomers and isomers: new horizons in poly-

anilines. *Synth. Met.* **100**, 131–140 (1999).

141. Thomas, J. O. *et al.* Imaging the Predicted Isomerism of Oligo(aniline)s: A Scanning Tunneling Microscopy Study. *Small* **11**, 3430–3434 (2015).

142. Murphy, A. R. & Frechet, J. M. J. Organic Semiconducting Oligomers for Use in Thin Film Transistors. *Chem. Rev.* **107**, 1066–1096 (2007).

143. Wei, Z. & Faul, C. F. J. Aniline oligomers - Architecture, function and new opportunities for nanostructured materials. *Macromol. Rapid Commun.* **29**, 280–292 (2008).

144. Wang, Y. *et al.* Graphene-Assisted Solution Growth of Vertically Oriented Organic Semiconducting Single Crystals. *ACS Nano* **9**, 9486–9496 (2015).

145. Wang, Y., Tran, H. D., Liao, L., Duan, X. & Kaner, R. B. Nanoscale morphology, dimensional control, and electrical properties of oligoanilines. *J. Am. Chem. Soc.* **132**, 10365–10373 (2010).

146. Hu, Y. *et al.* Toward Direct Laser Writing of Actively Tuneable 3D Photonic Crystals. *Adv. Opt. Mater.* **5**, 1600458 (2017).

147. Zhang, W. J., Feng, J., MacDiarmid, A. G. & Epstein, A. J. Synthesis of oligomeric anilines. *Synth. Met.* **84**, 119–120 (1997).

148. Surwade, S. P. *et al.* Catalyst-Free Synthesis of Oligoanilines and Polyaniline Nanofibers Using H2O2. *J. Am. Chem. Soc.* **131**, 12528–12529 (2009).

149. Sadighi, J. P., Singer, R. A. & Buchwald, S. L. Palladium-Catalyzed Synthesis of Monodisperse, Controlled-Length, and Functionalized Oligoanilines. *J. Am. Chem. Soc.* **120**, 4960–4976 (1998).

150. Shao, Z. *et al.* Delineating poly(aniline) redox chemistry by using tailored oligo(aryleneamine)s: Towards oligo(aniline)-based organic semiconductors with tunable optoelectronic properties. *Chem. - A Eur. J.* **17**, 12512–12521 (2011).

151. Udeh, C. U., Fey, N. & Faul, C. F. J. Functional block-like structures from electroactive tetra(aniline) oligomers. *J. Mater. Chem.* **21**, 18137–18153 (2011).

152. Shao, Z. *et al.* Block-like electroactive oligo(aniline)s: anisotropic structures with anisotropic function. *J. Mater. Chem.* **22**, 16230–16234 (2012).

153. Lyu, W., Feng, J., Yan, W. & Faul, C. F. J. Self-assembly of tetra(aniline) nanowires in acidic aqueous media with ultrasonic irradiation. *J. Mater. Chem. C* **3**, 11945–11952 (2015).

154. Udeh, C. U., Rannou, P., Brown, B. P., Thomas, J. O. & Faul, C. F. J. Tuning structure and

function in tetra(aniline)-based rod–coil–rod architectures. *J. Mater. Chem. C* **1**, 6428 (2013).

155. Wang, Y. *et al.* Morphological and Dimensional Control via Hierarchical Assembly of Doped Oligoaniline Single Crystals. *J. Am. Chem. Soc.* **134**, 9251–9262 (2012).

156. Dane, T. G. *et al.* Structured oligo(aniline) nanofilms via ionic self-assembly. *Soft Matter* **8**, 2824 (2012).

157. Dane, T. G. *et al.* Oligo(aniline) nanofilms: from molecular architecture to microstructure. *Soft Matter* **9**, 10501 (2013).

158. Kim, H. & Park, J.-W. Self-assembly of rod-coils consisting of tetraaniline and alkyl chains in different oxidation states. *J. Mater. Chem.* **20**, 1186 (2010).

159. Chandler, D. Interfaces and the driving force of hydrophobic assembly. *Nature* **437**, 640–647 (2005).

160. Townsend, E. J. *et al.* Electroactive amphiphiles for addressable supramolecular nanostructures. *ChemNanoMat* **4**, 741–752 (2018).

161. Kim, H., Jeong, S.-M. & Park, J.-W. Electrical switching between vesicles and micelles via redox-responsive self-assembly of amphiphilic rod-coils. *J. Am. Chem. Soc.* **133**, 5206–5209 (2011).

162. Wu, Y. *et al.* New strategy for controlled release of drugs. Potential pinpoint targeting with multiresponsive tetraaniline diblock polymer vesicles: Site-directed burst release with voltage. *ACS Appl. Mater. Interfaces* **6**, 1470–1480 (2014).

163. Cao, L., Gong, C. & Yang, J. A Solution-Processable (Tetraaniline- b - Polyethylene Glycol) 3 Star-Shaped Rod-Coil Block Copolymer with Enhanced Electrochromic Properties. *Macromol. Rapid Commun.* **37**, 343–350 (2016).

164. Bell, O. A. *et al.* Self-Assembly of a Functional Oligo(Aniline)-Based Amphiphile into Helical Conductive Nanowires. *J. Am. Chem. Soc.* **137**, 14288–14294 (2015).

165. Lyu, W. *et al.* An addressable packing parameter approach for reversibly tuning the assembly of oligo(aniline)-based supra-amphiphiles. *Chem. Sci.* **9**, 4392–4401 (2018).

166. Alotaibi, M. M. Towards Aqueous Nanostructures Based on Oligo(aniline)s. (University of Bristol, 2019).

167. Liao, Y., Cheng, Z., Zuo, W., Thomas, A. & Faul, C. F. J. Nitrogen-Rich Conjugated Microporous Polymers: Facile Synthesis, Efficient Gas Storage, and Heterogeneous Catalysis. *ACS Appl. Mater. Interfaces* **9**, 38390–38400 (2017).

168. Pan, L. *et al.* Luminescent and Swellable Conjugated Microporous Polymers for Detecting Nitroaromatic Explosives and Removing Harmful Organic Vapors. *ACS Appl. Mater. Interfaces* **11**, 48352–48362 (2019).

169. Chen, J. *et al.* Porous Materials Tunable Surface Area , Porosity , and Function in Conjugated Microporous Polymers. *Angew. Chem. Int. Ed.* **58**, 11715–11719 (2019).

170. Huang, L. *et al.* Polyaniline nanowires by electropolymerization from liquid crystalline phases. *J. Mater. Chem.* **12**, 388–391 (2002).

171. Li, C. *et al.* Conductive polyaniline helixes self-assembled in the absence of chiral dopant. *Chem. Commun.* **49**, 1100–1102 (2013).

172. Dutt, S. & Siril, P. F. A novel approach for the synthesis of polyaniline nanostructures using swollen liquid crystal templates. *Mater. Lett.* **124**, 50–53 (2014).

2 SYNTHESIS OF OLIGO(ANILINE)-BASED AMPHIPHILES

2.1 INTRODUCTION

Oligo(aniline)s are linear chains of repeating aniline units that are covalently linked by *para*-C-N bonds. They are structurally analogous to poly(aniline) (**PANI**); however unlike the polymer, the number of repeating units is limited and as a result, it is easier to prepare oligo(aniline)s that are monodisperse and with high degrees of purity. As such, oligo(aniline)s have been used to provide insight into the behaviour of **PANI** and the relationship between chain length and material properties.[1–4]

Of the available oligo(aniline)s, tetra(aniline) (**TANI**) is the shortest oligomer that retains the oxidative and optical properties of **PANI**. There are many strategies used to synthesise **TANI**s, which allow for different molecular structures to be produced and for it to be functionalised as desired.[5] The end termination of **TANI**s is key, as it allows for subsequent reaction and functionalisation or will prevent further reaction as needed. There are three main categories of **TANI**, which are highlighted in Figure 2.1. These are phenyl-phenyl capped (**Ph/Ph TANI**), phenyl-amine capped (**Ph/NH_2 TANI**) and amine-amine capped (**NH_2/NH_2 TANI**). The presence of terminal amines provides a way to further functionalise the **TANI**s with subsequent reactions.

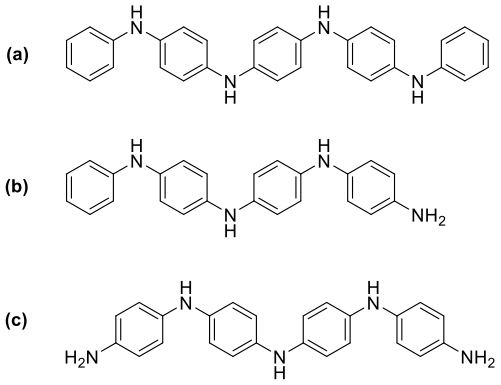

*Figure 2.1. Structures of three main **TANI**s based on end-functionality. (a) **Ph/Ph TANI**, (b) **Ph/NH_2 TANI**, (c) **NH_2/NH_2 TANI**.*

TANIs, and indeed other oligo(aniline)s and **PANI**, are fascinating owing to their ability to reversibly change oxidation state. There are three oxidation states that can be accessed interchangeably.[6,7] These are displayed in Figure 2.2. The leucoemeraldine base (LEB) is the fully reduced oxidation state. It is characteristically grey in colour and can produce the emeraldine salt (ES) state by oxidative doping with oxidants such as Cl_2 or I_2.[8] The emeraldine base (EB) is the partially (or half) oxidised state. It is typically purple in colour and consists of a mixture of benzenoid and quinoid aromatic rings, which exist at a ratio of 3 to 1. The two imine moieties are basic and can be protonated with strong acids (pKa < 2.5)[9] resulting in acid doping to the ES state. Finally, the pernigraniline base (PB) state can be

accessed with the use of a strong oxidant, resulting in the transformation of all benzenoid groups to quinoid groups. The PB state cannot be converted to the ES state, regardless of doping acid.

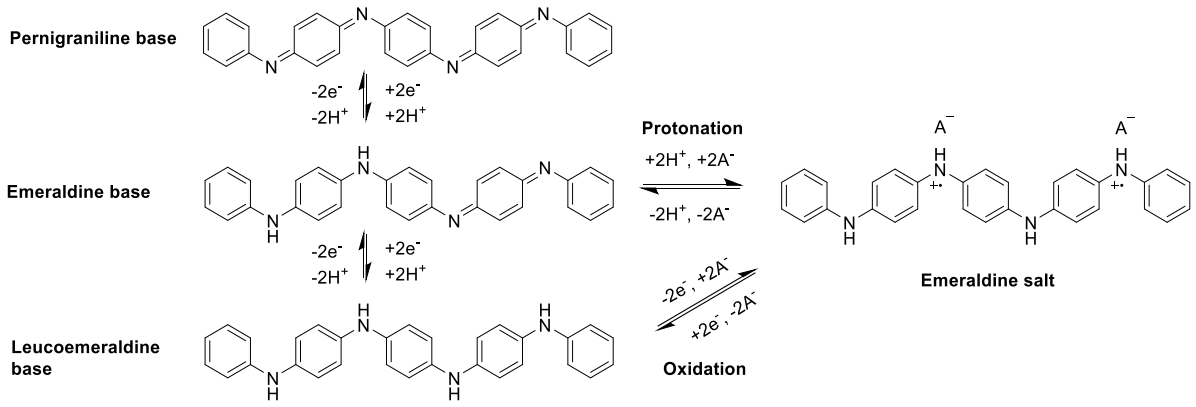

*Figure 2.2. Oxidation states of **TANI** and routes to the conducting emeraldine salt state.*

Combining oligo(aniline)s with different functional groups allows for them to be adapted for specific applications. The phenyl-amine and amine-amine end-capped **TANI**s have been functionalised with a variety of different groups, forming block-like compounds.[10] Of particular interest are water-soluble oligo(aniline)s, as these will allow for the preparation of biocompatible and sustainable materials. There have been several reports of the preparation of anionic amphiphilic oligo(aniline)s, typically prepared by the addition of poly(ethylene glycol) (**PEG**)[11–13] or poly(N-isopropylacrylamide) (**PNIPAM**)[14] blocks. Meanwhile, cationic single-tailed and bola-amphiphiles based on **TANI** have been the focus of the Faul research group and have been prepared by functionalising with ammonium and phosphonium headgroups.[15–17]

Other functional groups of interest are polymerizable groups. These allow for oligo(aniline)s to be transformed into polymeric structures, combining the well-defined structure and oxidative properties of the oligomer with the mechanical strength of polymers. Methacrylates and acrylates have been combined with **TANI**, which, when followed by free-radical polymerisation, lead to polymers containing **TANI** in the side chain or main chain.[18,19]

2.2 SYNTHESIS OF OLIGO(ANILINE)-DERIVED AMPHIPHILES

2.2.1 Boc-protected Ph/NH_2 TANI

Boc-protected **Ph/NH_2 TANI** (**6**) was used as a precursor in the synthesis of all single-tailed **TANI**-derived amphiphiles. **Ph/NH_2 TANI** can be synthesised through two main synthetic routes. The first route is an oxidative coupling method, in which aniline dimers are oxidatively coupled using hydrogen peroxide as a catalyst (Scheme 2.1).[20] However, this approach will often yield higher molecular weight oligomers such as hexamers or octamers as there is no barrier to further reaction of the tetramer once produced. Additionally, using this method, the oligo(aniline)s are produced in the EB state. This means

that the imines and secondary amines are available for further reaction, in addition to the terminal primary amine.

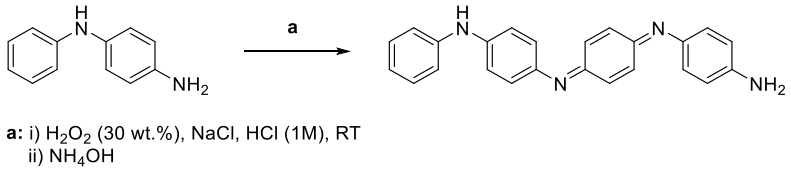

*Scheme 2.1. Oxidative synthesis of **Ph/NH₂ TANI** (EB).*

An alternative method involves the chemical synthesis of **Boc**-protected **Ph/NH₂ TANI** from protected di(aniline)s, where only the tetra(aniline) is prepared and all nitrogen groups are protected except for the reactive terminal amine. This route uses *tert*-butyloxycarbonyl (**Boc**) and diphenylmethylene (**CPh₂**) as orthogonal protecting groups to make selected amines unavailable for reaction and prevent the formation of unwanted side products. The two groups were chosen as each were chemically inert to the conditions required to remove the other. Benzophenone is readily coupled to amines through a condensation reaction and can be removed by hydrogenolysis. Meanwhile, **Boc**-groups can be attached by reaction with *di-tert*-butyl dicarbonate and removed by cleaving with trimethylsilane iodide (**TMSI**).[21]

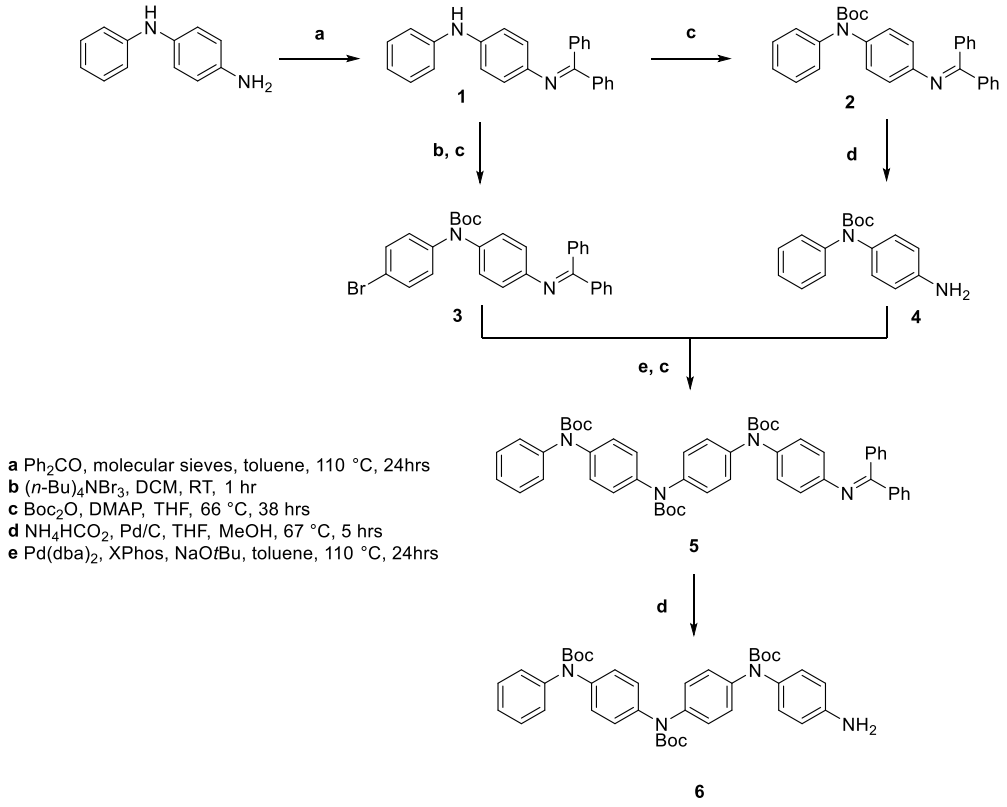

*Scheme 2.2. Synthetic route for **Boc**-protected **Ph/NH₂ TANI (6)**.*

In main, **Boc**-groups are stable under most of the conditions used in subsequent reactions to produce **TANI**-derived amphiphiles. **Boc**-groups are liable to cleave in the presence of acids or at high temperatures. Partial deprotection will occur above 100 °C and complete deprotection can be achieved in a few hours at temperatures above 140 °C.[19,22,23] However, in the absence of those conditions, **Boc**-groups provide increased solubility in common organic solvents and prevent changes in oxidation state until otherwise desired.[18]

The synthetic route for the preparation of **Boc**-protected **Ph/NH$_2$ TANI** was adapted from Chen and Benicewicz (2003) and is shown in Scheme 2.2.[18] *N*-Phenyl-*p*-phenylenediamine was initially protected with 1 molar equivalent of benzophenone. The product (**1**) was then either **Boc**-protected at the secondary amine (**2**) or was brominated before protection (**3**). **2** underwent hydrogenolysis to deprotect the terminal amine, making it available for a Buchwald-Hartwig cross-coupling reaction to produce **5**. Buchwald-Hartwig coupling reactions use a palladium catalyst to form C-N bonds and are commonly used to synthesise oligo(aniline)s.[21,24,25] Finally, the diphenylmethylene-protecting group on **5** was removed, producing the pure **Boc**-protected **Ph/NH$_2$ TANI** (**6**) that was used in subsequent reactions.

The purity of all precursors and products was confirmed by NMR spectroscopy and MALDI mass spectrometry (see Appendix A).

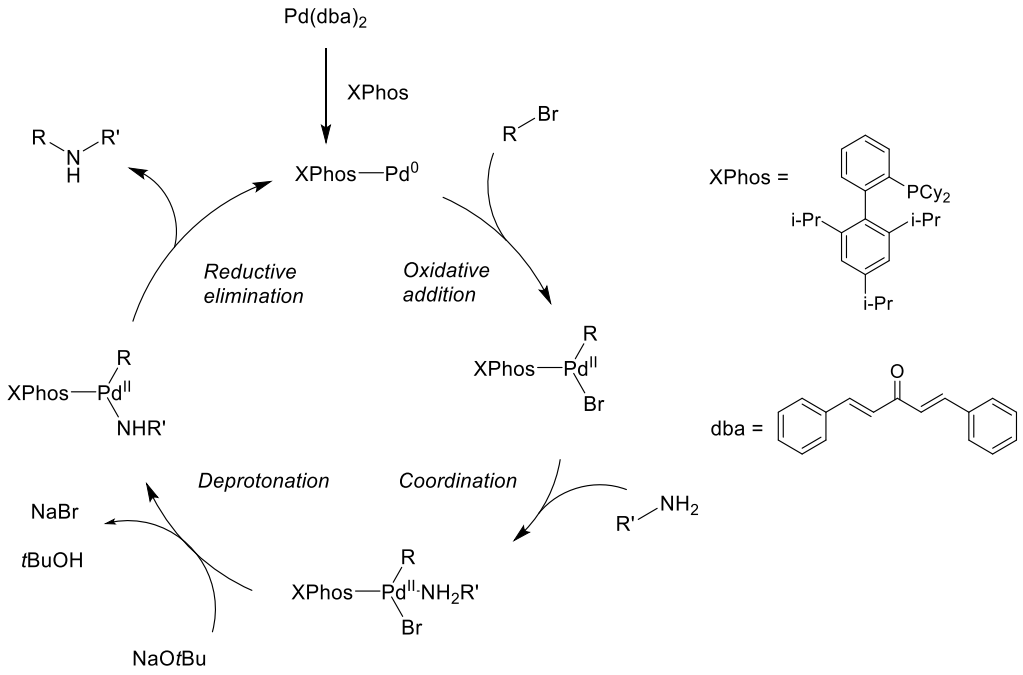

*Scheme 2.3. Mechanism for the Buchwald-Hartwig cross-coupling reaction, with structures of **dba** and **XPhos** included to the right of the scheme.*

The mechanism for the Buchwald-Hartwig coupling reaction is provided in Scheme 2.3. In the initial step, the palladium precatalyst undergoes ligand substitution, exchanging the two dibenzylideneacetone (**dba**) ligands for the bidentate 2-dicyclohexylphosphino-2',4',6'-triisopropylbiphenyl (**XPhos**) ligand.

XPhos promotes the formation of a reactive palladium catalyst owing to its steric bulk and strong electron-donating ability.[26] The catalyst then undergoes oxidative addition with the aryl-bromide, producing a Pd (II) species, followed by the coordination of the amine. The amine is then deprotonated with the use of a base such as sodium *tert*-butoxide before reductive elimination produces the aryl amine product and the catalyst is regenerated.[27]

2.2.2 TANI-PTAB

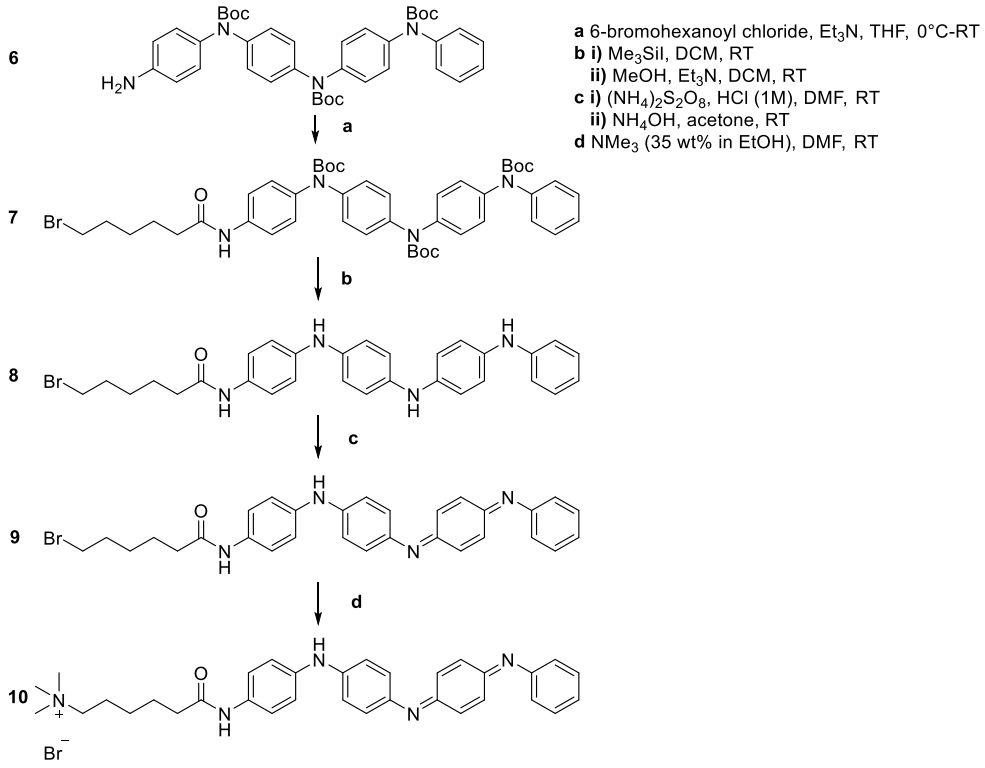

*Scheme 2.4. Synthetic route for EB **TANI-PTAB (10)** from **Boc**-protected **Ph/NH₂ TANI (6)**.*

The synthesis of EB **TANI**-pentyl trimethylammonium bromide (**TANI-PTAB**, **10**) was performed following the literature procedures with a few minor alterations outlined in the text below (Scheme 2.4).[15] Products from each step were identified by NMR spectroscopy and mass spectrometry (Appendix A). **Boc**-protected **Ph/NH₂ TANI** (**6**) was reacted at the primary terminal amine with 6-bromohexanoyl chloride which provided a flexible alkyl spacer between the cationic head group and the **TANI** core. The reaction produced **Boc**-protected **TANI-C₆Br** (**7**), which was purified by precipitation in hexane instead of the literature-recommended column chromatography.[15]

In the next step, **Boc**-deprotection was performed using **TMSI**. **TMSI** was used in place of strong acids as the latter could dope the deprotected **TANI** to the ES state. **Boc-TANI-C₆-Br** was dissolved in dichloromethane under a nitrogen atmosphere to prevent oxidation of the LEB state to the EB state. 3.6 molar equivalents of **TMSI** was added and the mixture stirred for 1 hour before 3.6 molar equivalents of anhydrous methanol was added. Care was taken to keep the quantity of methanol added as low as

possible, as excess methanol together with **TMSI** leads to the formation of acidic **HI**, which could dope the deprotected **TANI-C$_6$Br** and lower its purity and yield. Following this step, triethylamine was added to remove any acids that had formed and the precipitate was washed and dried. From this, LEB **TANI-C$_6$Br** (**8**) was obtained as a grey-purple solid in good yield (96 %).

LEB **TANI-C$_6$Br** was oxidised to the EB state using ammonium persulfate before quaternisation with trimethylamine to produce the amphiphilic EB **TANI-PTAB** (**10**). Deprotection and oxidation was performed before quaternisation to ensure inorganic by-products could be removed by washing with water, which would be difficult to do once the water-soluble amphiphile **TANI-PTAB** (EB) had been prepared.

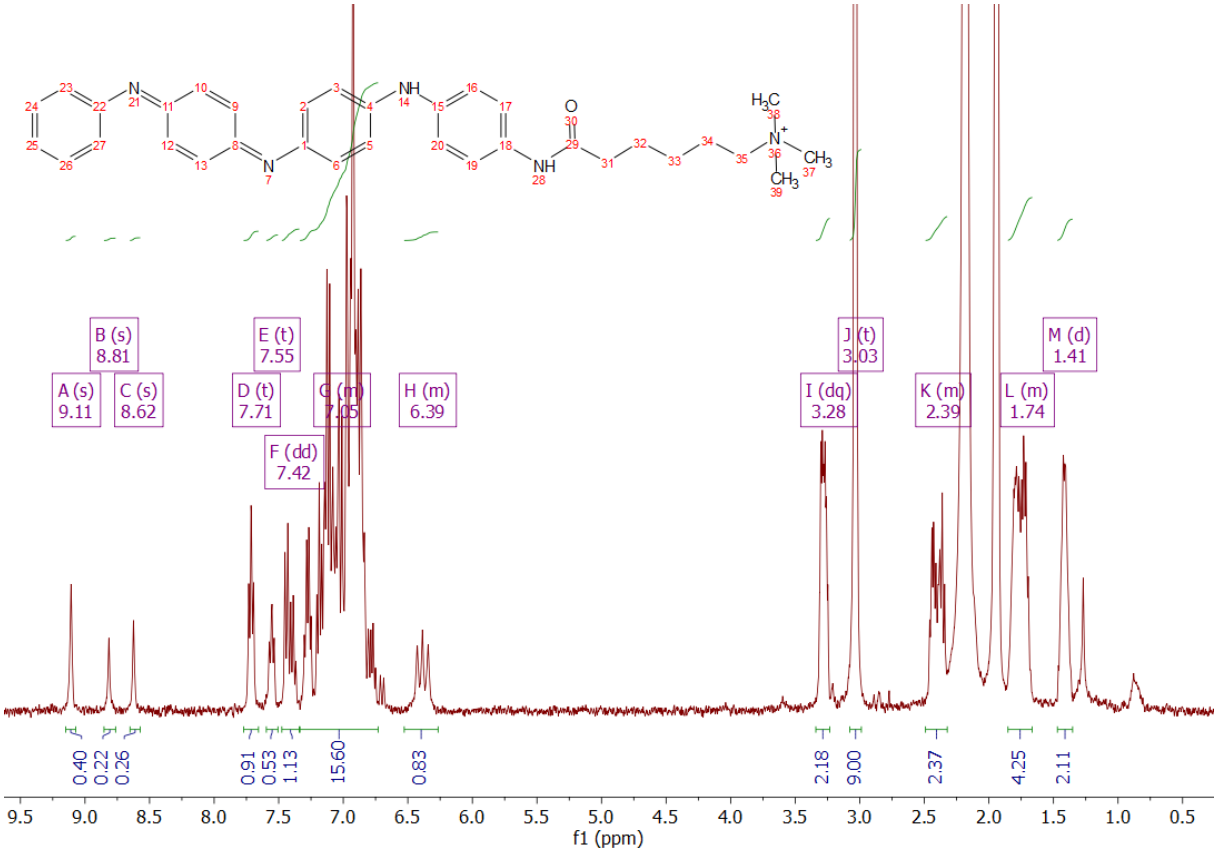

*Figure 2.3. ^{1}H NMR spectrum of EB **TANI-PTAB (10)** in acetonitrile-d$_3$.*

Quaternisation was performed by stirring EB **TANI-C$_6$Br** (**9**) with trimethylamine in dimethylformamide (DMF) for 5 days. After the reaction was complete, as confirmed by thin layer chromatography (TLC) analysis, the reaction mixture was added dropwise to ice-cold diethyl ether, causing the **TANI-PTAB** to precipitate. Yields were initially low as significant amounts of product was lost in this final step. Precipitation in diethyl ether was originally undertaken in beakers, where the product formed films on the glass walls that were difficult to remove for centrifugation and purification. The yield was improved when both the reaction and precipitation was performed in plastic centrifuge

tubes, allowing a suspension rather than a film to form. The suspension was collected by centrifugation and was dissolved in deionised water. Any insoluble materials were separated and the aqueous product was lyophilised, yielding a fluffy purple solid (59 %). The purity of the product was determined by ^{1}H NMR spectroscopy (Figure 2.3), mass spectrometry (Appendix A) and UV-Vis/NIR spectroscopy (Figure 2.4).

^{1}H NMR spectroscopy of EB **TANI-PTAB** was carried out in deuterated acetonitrile. The spectrum matched the literature and had no impurity peaks.[28] Quaternisation was confirmed by the appearance of a peak at 3.06 ppm with an integrated intensity of nine, which corresponded to the nine hydrogens of the trimethylammonium headgroup. It was noted that the amide proton was given as three peaks at 9.13, 8.84 and 8.65 ppm and there were additional aromatic proton peaks. This is due to the quinoid ring in the **TANI** core resulting in the presence of positional and *cis*/*trans* isomers. The *cis*/*trans* isomers can interconvert at room temperature, giving rise to multiple peaks in the ^{1}H NMR spectrum corresponding to the same **TANI** proton.[29]

After identification by NMR spectroscopy, a 1 mM solution of EB **TANI-PTAB** in water was prepared and analysed by UV-Vis/NIR spectroscopy to verify its oxidation state. EB **TANI-PTAB** was highly sensitive to acids and could become doped to the ES state during lyophilisation if the freeze-dryer had previously contained acidic compounds; extra care therefore had to be taken during the lyophilisation step. The EB state can be identified by two characteristic absorption peaks around 300 nm and 550 nm, corresponding to the $\pi \rightarrow \pi^*$ transition and molecular exciton transition, respectively.[30] Both peaks can be clearly observed in Figure 2.4. The presence of a shoulder peak at 490 nm was attributed to the formation of aggregates.[15] The **TANI** backbone is sequestered in the interior of the aggregate, away from the polar solvent. This results in a change in the polarity of the **TANI** environment, leading to a bathochromic shift in the peak position.

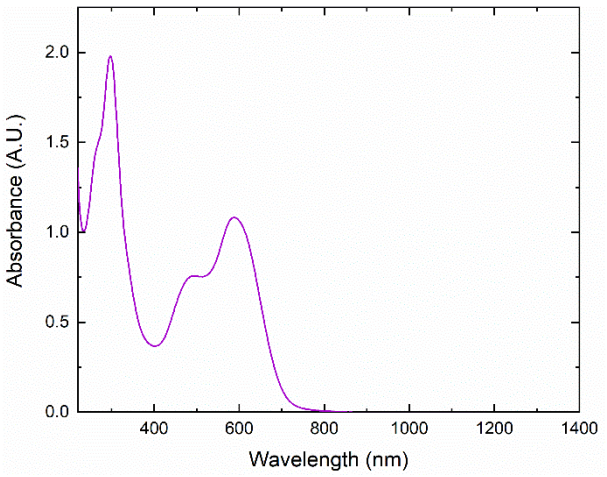

*Figure 2.4. UV-Vis/NIR spectrum for 1 mM **TANI-PTAB** in water, showing characteristic EB peaks.*

Peaks for **TANI** in the ES state are found around 440 nm and 780 nm, which correspond to the polaron → π* and π → polaron transitions, respectively.[31] Additionally, a peak at around 1000 nm may be present, corresponding to the bipolaronic doped state.[32] The structures of the polaronic and bipolaronic forms of **TANI-PTAB** can be found in Figure 2.5. No ES peaks were observed in the spectrum of **TANI-PTAB** (EB), indicating that the material was in the EB state only and no doping had occurred.

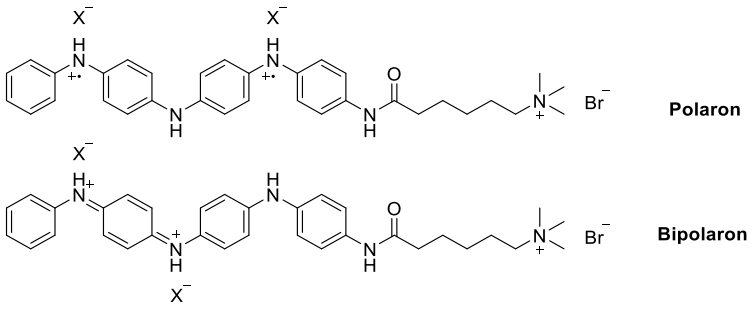

*Figure 2.5. Polaronic and bipolaronic forms of **TANI-PTAB**.*

2.2.3 TANI-C_{12}TAB

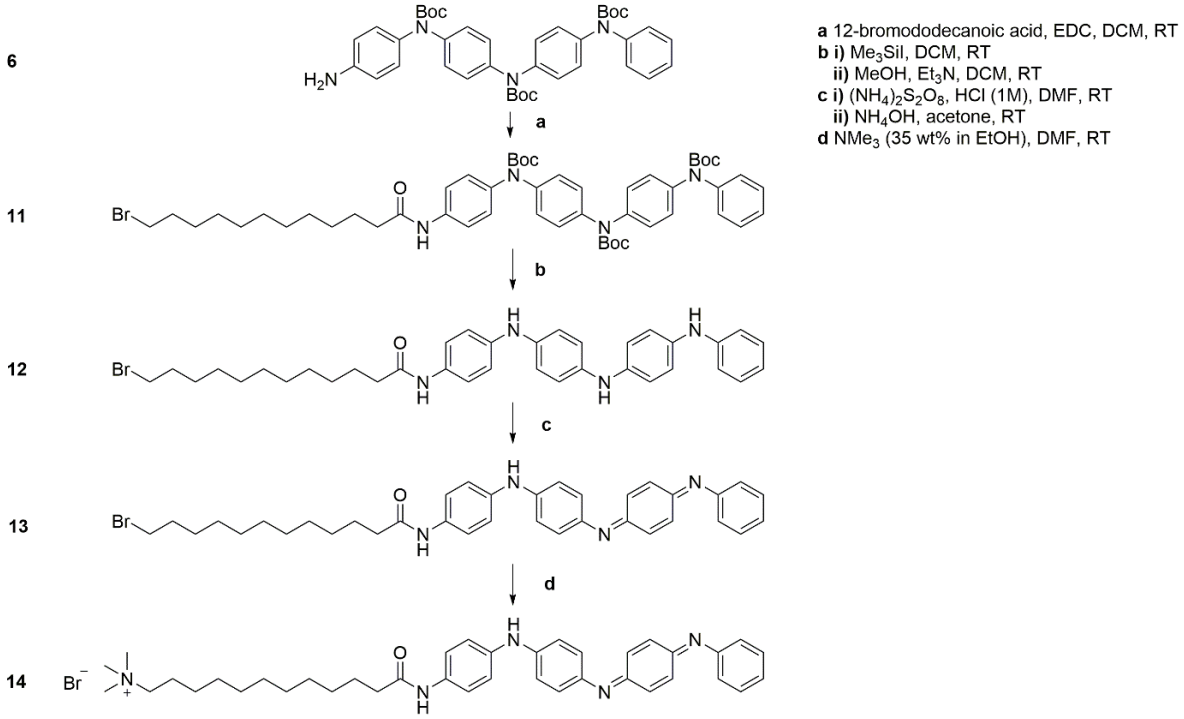

*Scheme 2.5. Synthetic route for **TANI-C_{12}TAB** (EB) from **Boc**-protected **Ph/NH_2 TANI (6)**.*

The synthetic route for EB **TANI**-dodecyl trimethylammonium bromide (**TANI-C_{12}TAB**, **14**) was developed by Watanabe in the Faul research group.[33] The method was adapted from the synthesis of EB **TANI-PTAB** (**10**) and was identical aside from the initial coupling reaction. A carboxylic acid, 12-bromododecanoic acid was used in place of 12-dodecanoyl chloride to provide the alkyl spacer for this reaction as it is more commercially available and is less reactive to water. The reaction scheme is shown in Scheme 2.5.

12-bromododecanoic acid was coupled to **Boc**-protected **Ph/NH$_2$ TANI** (**6**) using a 1-ethyl-3-(3-dimethylaminopropyl)-carbodiimide (**EDC**) coupling reaction. The reagents were dissolved in dichloromethane and were stirred overnight. After the reaction was complete, the solvent was removed and the residual solid was washed with plenty of water to remove any unreacted **EDC** and the byproduct ethyl-(*N'*,*N'*-dimethylamino) propyl urea. The solid was then recrystallised from methanol resulting in the product **Boc-TANI-C$_{12}$Br** (**11**) in good yield (90 %). The product was identified by NMR spectroscopy and mass spectrometry (Appendix A).

After addition of the alkyl-spacer, **Boc-TANI-C$_{12}$Br** was de-protected, oxidised and quaternised with trimethylamine, following the procedures outlined in Section 2.2.2. The experimental methods for these reactions are given in Section 2.4 and the full NMR spectroscopy spectra and mass spectrometry data are given in Appendix A.

The successful synthesis EB **TANI-C$_{12}$TAB** was confirmed by ^{1}H NMR spectroscopy (Figure 2.6) and UV-Vis/NIR spectroscopy (Figure 2.7). The NMR spectrum shows that the quaternisation of EB **TANI-C$_{12}$Br** (**13**) was successful, as evidenced by the appearance of a large peak at 3.00 ppm with a relative integration intensity of nine, corresponding to the nine hydrogen atoms on the trimethylammonium headgroup. The spectrum also displays the additional amide and aromatic proton peaks observed in the spectrum of **TANI-PTAB** (EB), caused by the presence of *cis*/*trans* isomers.

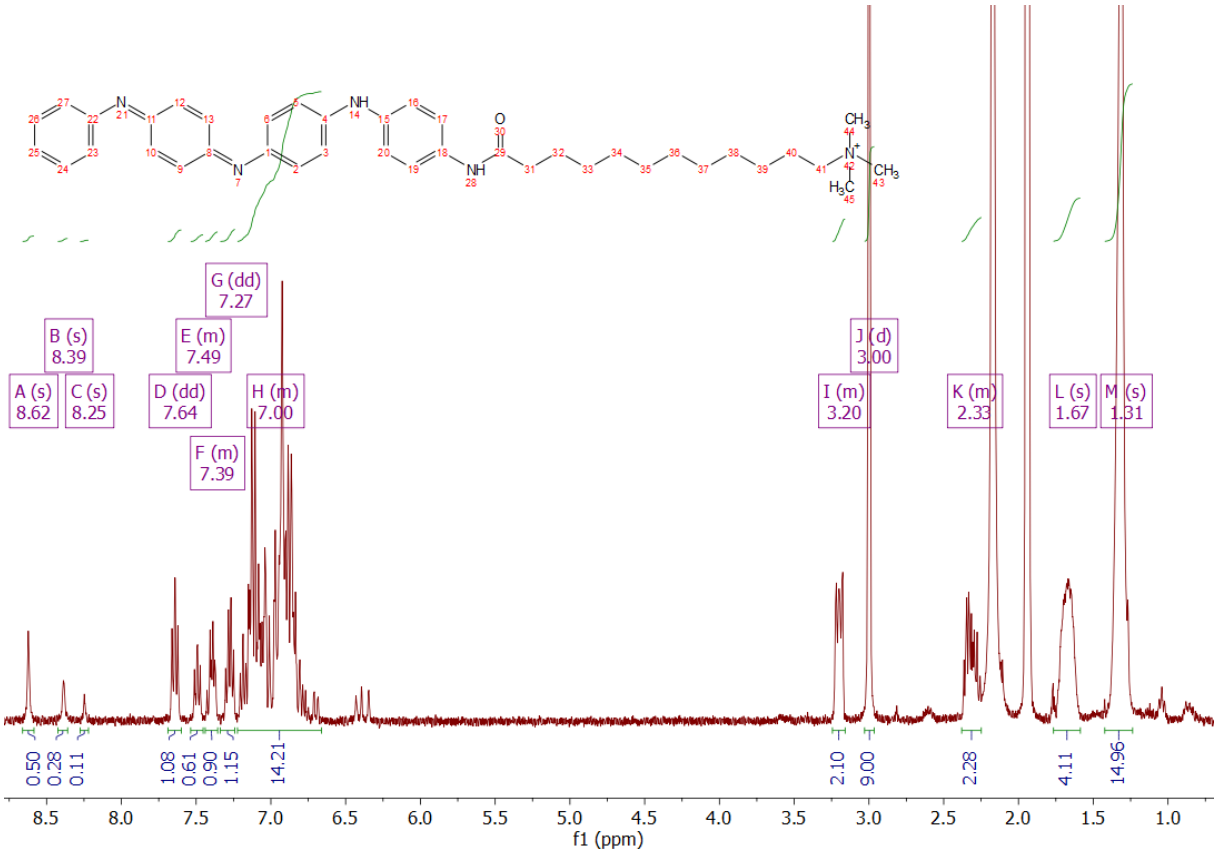

*Figure 2.6. ^{1}H NMR spectrum of EB **TANI-C$_{12}$TAB (14)** in acetonitrile-d$_3$.*

Finally, the UV-Vis/NIR spectroscopy spectrum confirmed the retention of the EB state during synthesis and lyophilisation. The characteristic peaks at 276 and 475 nm were present, in addition to a shoulder peak at 490 nm indicating aggregation. No ES state peaks were observed.

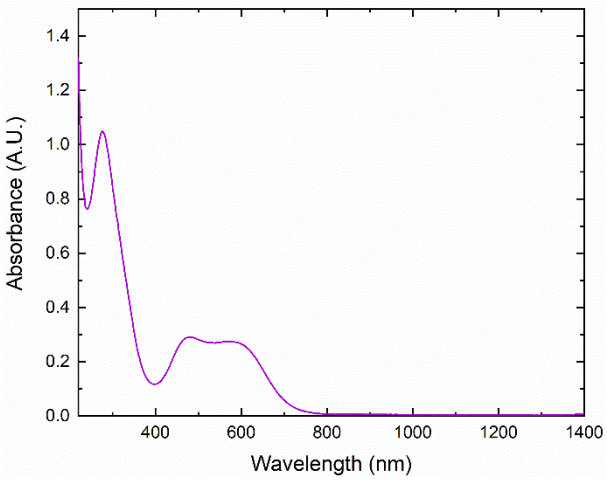

*Figure 2.7. UV-Vis/NIR spectrum for 1 mM EB **TANI-C$_{12}$TAB (14)** in water, showing characteristic EB peaks.*

2.2.4 TANI-PTPB

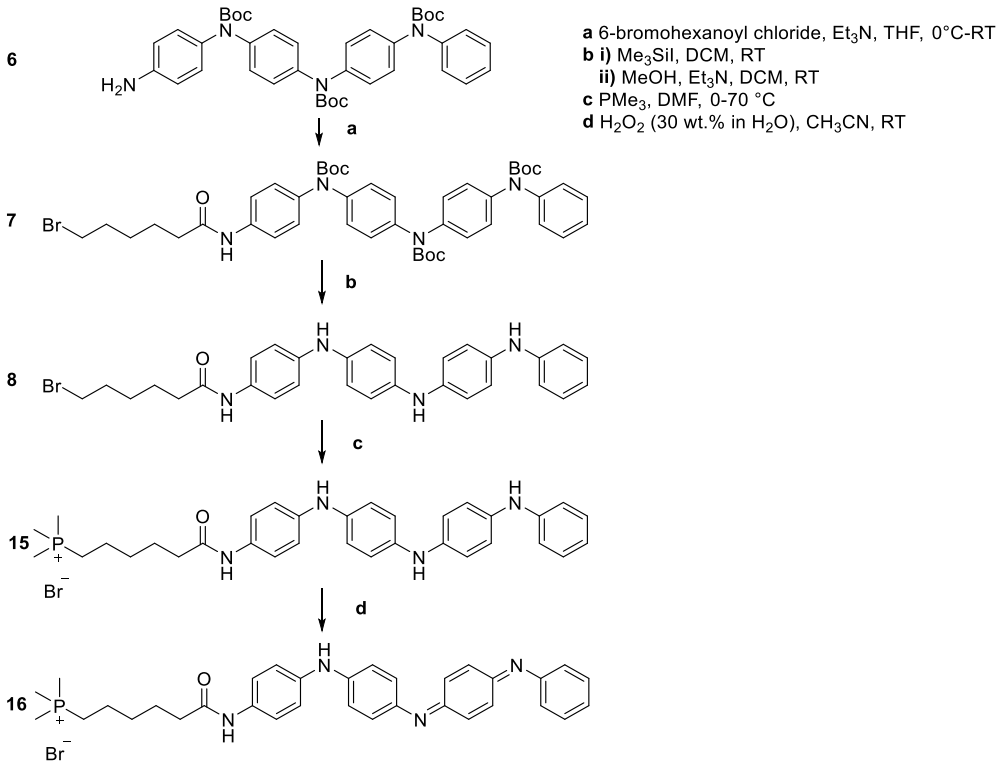

*Scheme 2.6.Reaction scheme for the preparation of EB **TANI-PTPB (16)** from **Boc**-protected **Ph/NH$_2$ TANI (6)**.*

The synthesis of EB **TANI-**pentyl trimethylphosphonium bromide (**TANI-PTPB**, **16**) was developed and performed by Alotaibi in the Faul research group.[17,34] All experiments using EB **TANI-PTPB** in this thesis used product synthesized by her.

The reaction scheme for the synthesis of EB **TANI-PTPB** is given in Scheme 2.6. In brief, **TANI-C_6Br** in the LEB state (**8**) was prepared as outlined in Section 2.2.2. Quaternisation was then performed with trimethylphosphine, using a heavy-walled flask as the reaction vessel in accordance with the safety precautions outlined in Section 2.4.15. The amphiphilic LEB **TANI-PTPB** (**15**) was then oxidised to the EB state using 30 wt.% H_2O_2. Quaternisation was carried out before oxidation as trimethylphosphine acted as a reducing agent, reducing any EB state material to the LEB state.

After oxidation, the solution was added dropwise to ice-cold diethyl ether and allowed to precipitate in a freezer overnight. The precipitate was collected by centrifugation and was washed with diethyl ether to remove any remaining acetonitrile and H_2O_2. Finally, the residue was taken up in deionised water, centrifuged to remove any water-insoluble impurities and lyophilised.

The full experimental procedure can be found in Section 2.4.15. The ^{1}H NMR spectroscopy and mass spectrometry spectra for EB **TANI-PTPB** can be found in Appendix A.

2.2.5 NH_2/NH_2 TANI

Synthesis of **NH_2/NH_2 TANI** (**19**) was performed in batches by members of the Faul group. In contrast to **Ph/NH_2 TANI** (**6**), **NH_2/NH_2 TANI** has two terminal amines that are available for functionalisation, symmetrically or asymmetrically. **NH_2/NH_2 TANI** is prepared via nucleophilic substitution in a stepwise fashion. The synthesis was originally reported by Kulszewicz-Bajer and colleagues (2004) who used 4,4′-diaminodiphenylamine sulfate and 4-nitrofluorobenzene to prepare **NO_2**-capped **TANI**.[35] The nitro groups could then be reduced using tin and concentrated hydrochloric acid, producing the arylamines. The drawback of this approach is that the **NH_2/NH_2 TANI** was prepared in the LEB state, which means the secondary amines were freely available. Therefore, subsequent reactions may not selectively occur at the primary amines. Additionally, the LEB state is also not stable and is liable to become oxidised in air.

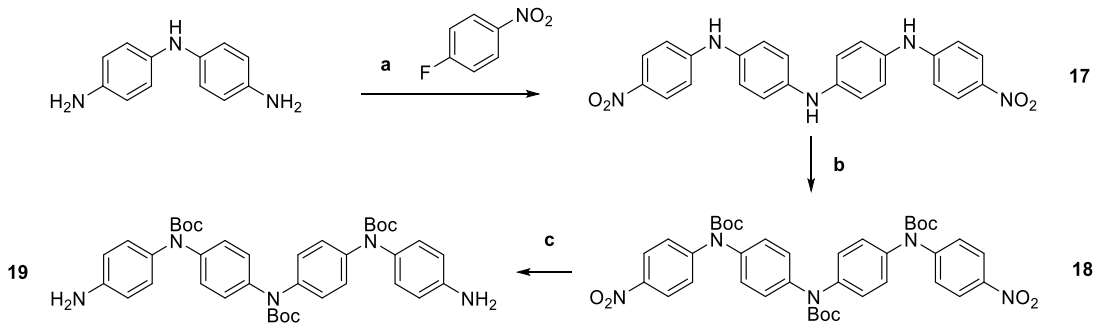

*Scheme 2.7. Synthetic route to prepare **Boc**-protected **NH_2/NH_2 TANI (19)**.*

To overcome these issues, a route to prepare **Boc**-protected **NH_2/NH_2 TANI** was developed by Eelkema and Anderson (2008).[36] The synthetic route is shown in Scheme 2.7. 4,4′-Diaminodiphenylamine sulfate was reacted with excess 4-nitrofluorobenzene as before to prepare **NO_2/NO_2 TANI** (**17**). The nitro groups in **NO_2/NO_2 TANI** could then act as protecting groups for the terminal amines, allowing **Boc**-protection to only occur at the secondary amines. Finally, the nitro groups were reduced using palladium on carbon and ammonium formate, yielding the **Boc**-protected **NH_2/NH_2 TANI**.

2.2.6 TANI-$(PTAB)_2$

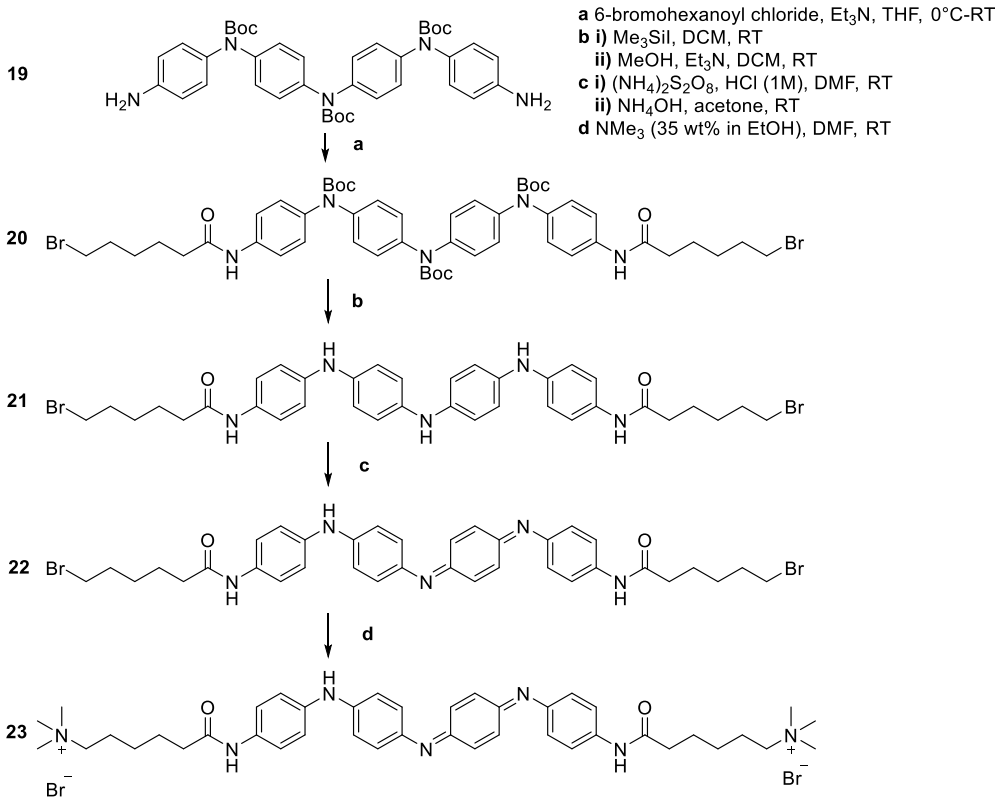

*Scheme 2.8. Synthetic route for EB **TANI-$(PTAB)_2$** (**23**) from **Boc**-protected **NH_2/NH_2 TANI** (**19**).*

The synthesis of EB **TANI**-(pentyl trimethylammonium bromide)$_2$ **TANI-$(PTAB)_2$** (**23**) was developed and performed by Alotaibi.[16,37] Most experiments using EB **TANI-$(PTAB)_2$** in this thesis used product synthesized by her, although the synthesis was repeated during this project when supplies diminished.

The reaction scheme for EB **TANI-$(PTAB)_2$** is shown in Scheme 2.8. In brief, **Boc**-protected **NH_2/NH_2 TANI** (**19**) was coupled with 2 equivalents of 6-bromohexanoyl chloride to produce a di-substituted **TANI** (**20**). The procedure then followed that outlined in Section 2.2.2. **20** was deprotected using **TMSI** before oxidation to the EB state with ammonium persulfate. The product was dissolved in dimethylformamide and quaternised with trimethylamine. Purification by washing with diethyl ether and water, followed by lyophilisation yielded EB **TANI-$(PTAB)_2$** as a fluffy blue solid with a typical yield of 55 %.

2.2.7 Asymmetric, polymerizable TANI-PTAB

2.2.7.1 From NH_2/NH_2 TANI (19)

The synthesis of an asymmetric polymerizable **TANI-PTAB** was one of the main objectives of this project and one that proved to be a challenge. Numerous synthetic routes were proposed and attempted, all of which proved unsuccessful due to the low reactivity of the starting materials, difficulty in purification or unwanted side reactions. Nevertheless, the attempted unsuccessful syntheses will be outlined below.

Initial experiments utilised **NH_2/NH_2 TANI** (**19**) as the starting material for subsequent reactions (Scheme 2.9). Acrylates were chosen as the polymerizable moiety for **TANI-PTAB** due to their previous successful use with other **TANI-**derived materials.[18,19]

The aim of the synthetic routes outlined in Scheme 2.9 was to react **NH_2/NH_2 TANI** with 1 molar equivalent of either a functional group (alkyl spacer or acrylate) or protecting group (benzophenone). This approach, in theory, should produce a mixture of mono- or di-substituted products that could be separated and the mono-substituted product collected for further reactions. The free terminal amine in the mono-substituted products could then be coupled with the remaining functional group, producing an asymmetric, polymerizable **TANI**. From this point, a polymerizable EB state **TANI-PTAB** (**MA-TANI-PTAB**), the structure of which can be seen in Figure 2.8, could be produced by following the **Boc**-deprotection, oxidation and quaternisation reactions outlined in Section 2.2.2.

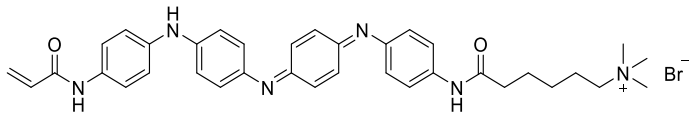

*Figure 2.8. Structure of EB **MA-TANI-PTAB**.*

However, a limitation of this route is that the quinoid moiety in the deprotected **MA-TANI-PTAB** could act as a free radical inhibitor, preventing free radical polymerisation.[18] Therefore, it may be preferable to first prepare a **Boc**-protected **MA-TANI-PTAB**, by quaternisation as the first step after addition of the acrylate and alkyl spacer. Then, after alignment and polymerisation in the template, the polymerised **TANI-PTAB** could be deprotected and oxidised to the EB state following the procedure outlined by Hu et al. (2017).[19] In this case, 3D structures of polymerised **TANI** were deprotected by heating to 140 °C, followed by oxidation to the EB state by submerging in aqueous hydrogen peroxide.

A **Boc**-protected **TANI-PTAB** has been previously prepared and while the self-assembly behaviour was not investigated, the amphiphile was surprisingly soluble in water, making it possible to incorporate it into the lipid template and a suitable compound to adapt for polymerisation.[38]

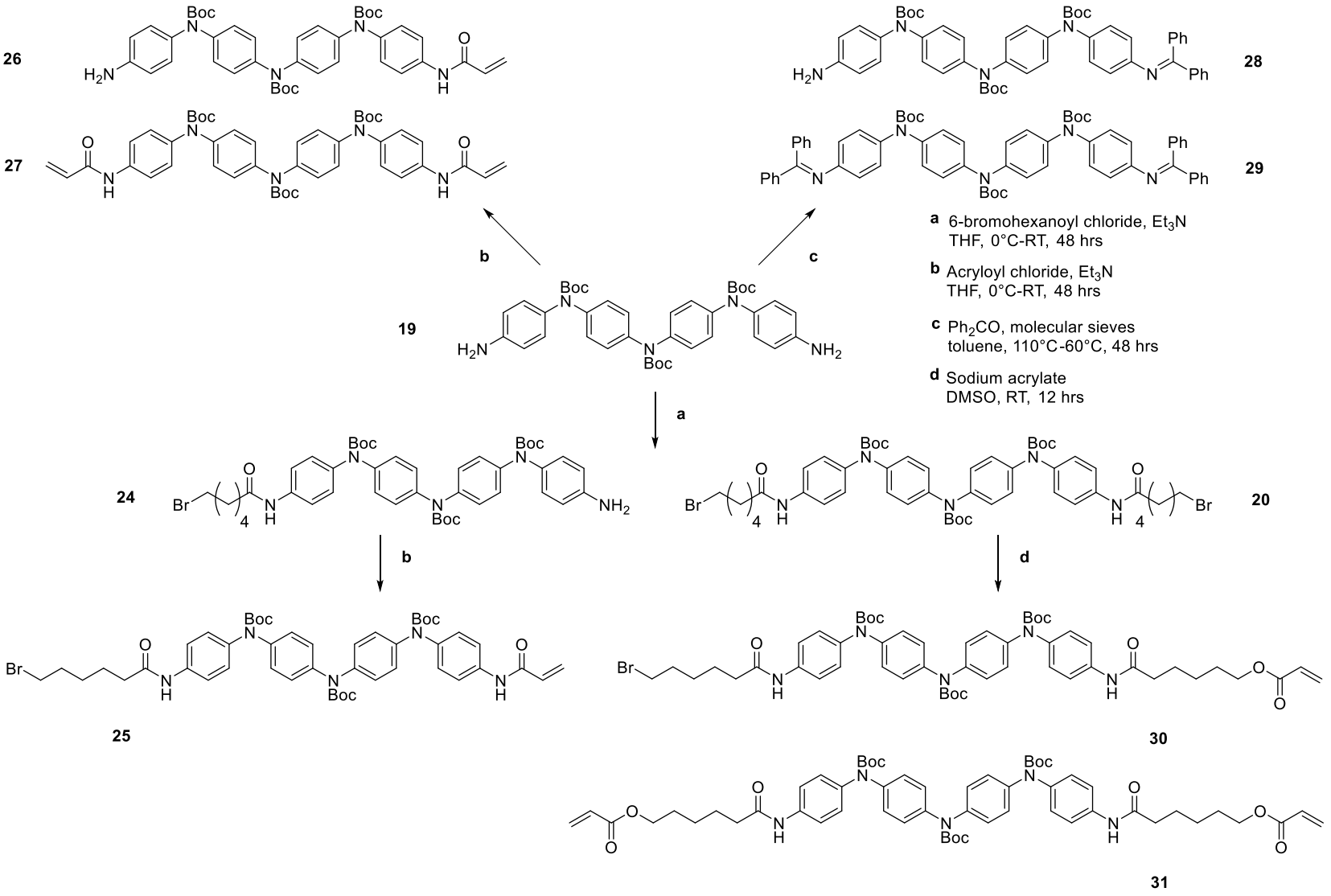

Scheme 2.9.Attempted synthetic routes for an asymmetric, polymerisable **TANI-PTAB**, starting from **NH_2/NH_2 TANI (19)**.

In the first route outlined in Scheme 2.9**,** 1 molar equivalent of 6-bromohexanoyl chloride was reacted with **NH_2/NH_2 TANI**. The theoretical main product of this reaction should be the mono-substituted **TANI-C_6Br** (**24**), which would have a free amine available for further addition of the polymerizable group. In practice, using 1 molar equivalent of 6-bromohexanoyl chloride produced a mixture of products, mono- and di-substituted **TANI-C_6Br** (**24** and **20**) with yields of 13 % and 26 % respectively. Both **TANI**s had similar retention times by column chromatography and were soluble in the same solvents, which made separation difficult and lowered the final yield.

Despite the low yield, enough **24** was produced for the second step, which was a reaction with acryloyl chloride following literature procedures.[19] **24** was placed under nitrogen and dissolved in anhydrous tetrahydrofuran (THF), before acryloyl chloride was added slowly and the mixture was left to stir and react for 24 hours. After this time, the reaction was stopped and ^{1}H NMR spectroscopy and mass spectrometry were used to determine the results of the reaction (Figure 2.9 and Figure 2.10).

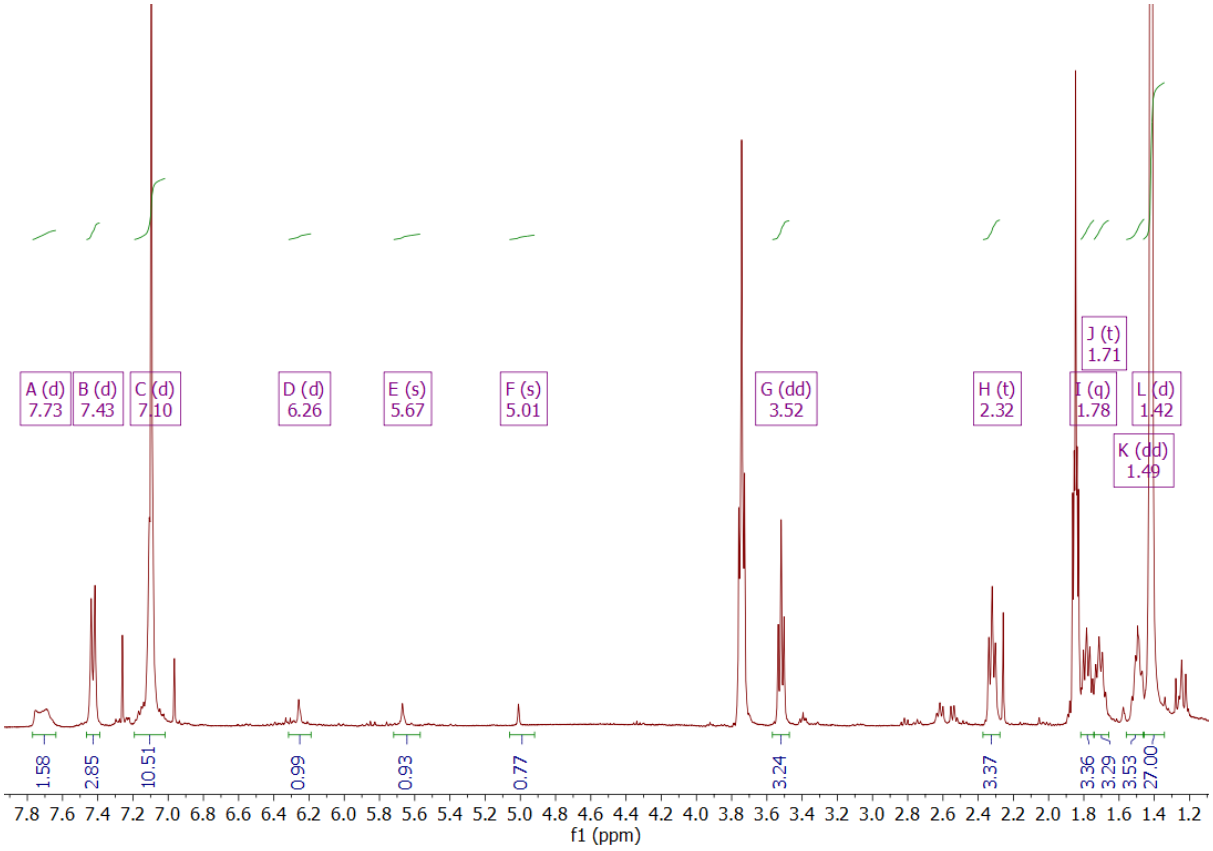

*Figure 2.9. ^{1}H NMR spectrum for **MA-TANI-C_6Br (25)** in $CDCl_3$.*

The ^{1}H NMR spectrum initially indicated the reaction was successful. Alkene proton peaks between 6.26-5.01 ppm were clearly visible, with the correct peak ratios relative to the aromatic proton peaks (1:16), indicating successful coupling of the acrylate. However, there were no peaks corresponding to the mass ion of **MA-TANI-C_6Br** (**25**) in the mass spectrometry spectrum (calculated *m/z:* 912.4). Instead, the main peaks that were identified belonged to the mass ion of **25**, if it had undergone a halogen

exchange reaction, where the bromide had been exchanged for chloride (**MA-TANI-C_6Cl**, calculated *m/z:* 890.4). This was unexpected, however, a brief literature search revealed that a primary alkyl chloride can be converted into an alkyl bromide or vice versa with the use of a quaternary ammonium salt.[39] It is possible that the triethylamine used in the synthesis of **25** was converted to an ammonium salt after reaction with acryloyl chloride and that this salt was in turn able to act as a catalyst for the halogen exchange reaction.

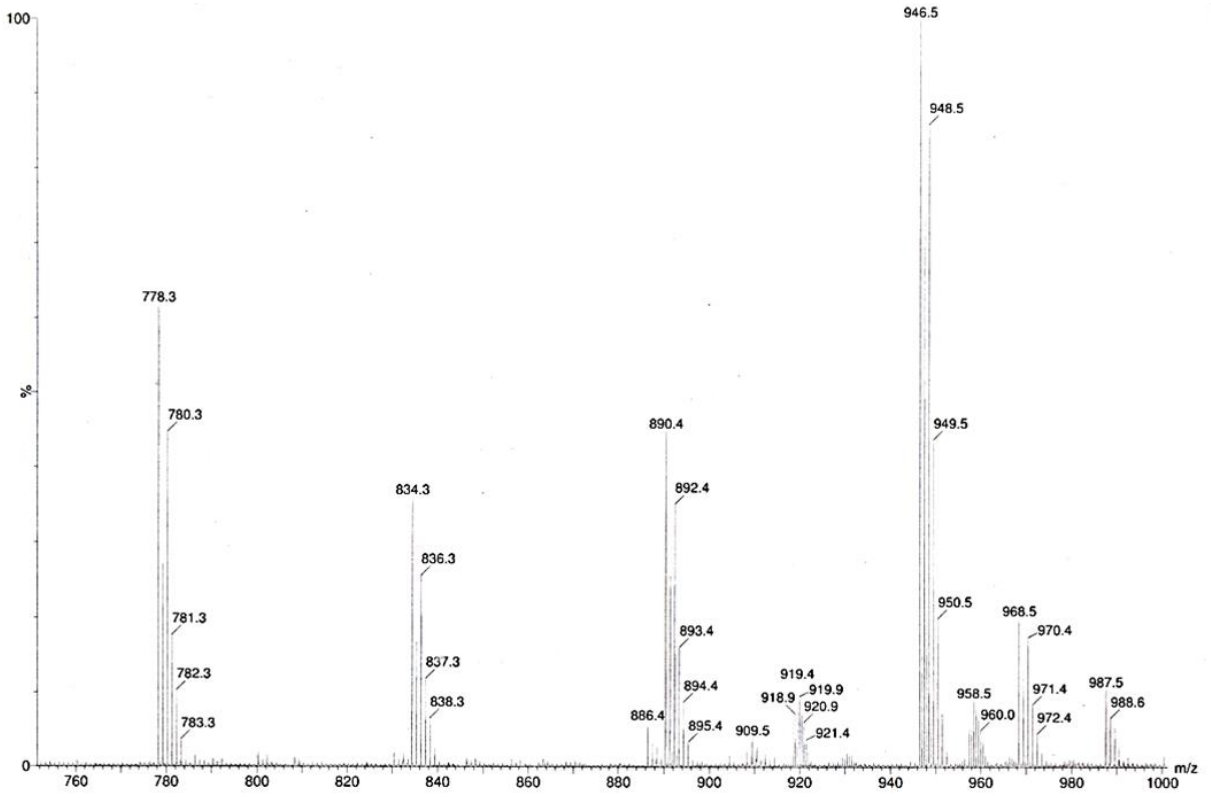

*Figure 2.10. Nanospray mass spectrum for **MA-TANI-C_6Br.** Expansion of area of interest.*

The halogen terminating the alkyl chain will become the counterion for the final **TANI** amphiphile. Different counterions can have a pronounced effect on an amphiphile's self-assembly, even between a bromide and a chloride.[40] To keep the self-assembly behaviour of **MA-TANI-PTAB** (EB) as close to **TANI-PTAB** (EB) possible, the same counterion (Br^-) should be used and halogen exchange during synthesis should be avoided.

To overcome this problem, an alternative route was developed where **NH_2/NH_2 TANI** was reacted with 1 molar equivalent of acryloyl chloride before subsequent purification and reaction with 6-bromohexanoyl chloride to prevent any possible exchange of bromide with chloride. It was expected that the first step of the reaction would produce a mixture of mono- (**26**) and di-substituted (**27**) **TANI** acrylates, as the reaction with 1 molar equivalent of 6-bromohexanoyl chloride had also produced a mixture of products. However, mass spectrometry revealed that only the di-substituted product (**27**) had been produced. A smaller quantity of acryloyl chloride may allow the production of **26** in addition to

27, however purification of **27** in the original reaction was not successful as the compound had very similar column retention times and solvent solubilities to **NH_2/NH_2 TANI** and it was therefore expected that it would also not be possible to purify a mixture of **26**, **27** and unreacted starting material.

The main difficulty with the above experiments was in purification. The reactions produced a mixture of products that were very similar to each other and the starting materials and could not be separated. Therefore, the next plan was to asymmetrically protect **NH_2/NH_2 TANI** with 1 molar equivalent of a bulky protecting group, which would produce a mono-substituted product that was chemically different enough from the starting material or di-substituted product to allow for simple separation and purification. The free amine remaining in the mono-substituted product could be reacted with acryloyl chloride before the protecting group is removed and the 6-bromo-hexanoyl chloride added. Benzophenone was chosen as the protecting group for this reaction, as it had previously been used in the synthesis of **Ph/NH_2 TANI** (**6**) (Section 2.2.1) and the reaction chemistry with **TANI** was known.

Benzophenone protection is often used in the synthesis of **TANI**s, protecting the primary amine in *N*-phenyl-*p*-phenylene diamine, and can be reduced using palladium-on-carbon and ammonium formate to re-form the amine.[18] However, it is important to note that the reaction with benzophenone occurs before **Boc**-protection of the secondary amines, unlike in the proposed reaction in Scheme 2.9 where the starting **NH_2/NH_2 TANI** is already **Boc**-protected.

Asymmetric benzophenone protection was attempted four times with varying experimental conditions. A summary of the conditions and results of each experiment can be found in Table 2.1. The first reaction was performed at 110 °C, under similar conditions to the protection of *N*-phenyl-*p*-phenylenediamine (Section 2.2.1). After reaction for 48 hours, the solution had changed colour from a pale yellow to dark green, which indicated that **Boc**-deprotection had occurred and the **TANI** had been doped to the ES state. Mass spectrometry analysis of the product after work-up showed that a mixture of mono- (**28**) and di-benzophenone (**29**) protected **TANI**s had been formed, although **Boc**-deprotection had also taken place (see Appendix A).

Boc-groups will partially decompose at temperatures above 100 °C, so it was theorized that leaving the reaction for 48 hours at elevated temperatures was the cause of the **Boc**-deprotection. Therefore, the second reaction attempt was performed at 70 °C. After 24 hours at this temperature TLC analysis indicated that the starting **TANI** had been consumed. The reaction was stopped, and the molecular sieves were washed with THF to recover the product, which was purified using column chromatography. Mass spectrometry (see Appendix A) revealed that mono- and di-protected products had been formed, although **Boc**-deprotection had occurred again.

While an asymmetrically protected **TANI** had been produced, it could not be used for subsequent reactions with 6-bromohexanoyl chloride or acryloyl chloride. This is because the secondary amines were no longer protected following the cleaving of the **Boc**-groups. Therefore, any reactions at the

primary amine could also occur at the secondary amines, resulting in unwanted side products. Similarly, **Boc**-protection of the secondary amines could not be re-applied after addition of the benzophenone, as the free primary amine in **28** would also be protected.

The reaction temperature was further lowered to 60 °C, to reduce the likelihood of **Boc**-deprotection due to reaction at elevated temperatures. The mixture was left to react for 48 hours, however TLC analysis after this time showed that no reaction had occurred, and the heating was stopped.

At this stage, it was determined that the molecular sieves were causing the **Boc**-deprotection, due to their mildly acidic nature.[41] **Boc**-groups are commonly cleaved by the use of strong acids such as trifluoroacetic acid (TFA) and hydrochloric acid (HCl). Such reactions are rapid and complete **Boc**-deprotection can be obtained in a few hours.[42–44] In the presence of a weak acid, such as the molecular sieves, deprotection will take longer. However, the above reactions took place over at least 24 hours, giving ample time for **Boc**-deprotection to occur. To prevent **Boc**-deprotection from occurring, a final reaction was performed at 70 °C without using molecular sieves. The reaction was left to heat for four days, however TLC analysis indicated that no reaction had occurred.

*Table 2.1. Summary of conditions and results for benzophenone-protection of **Boc**-protected **NH_2/NH_2 TANI (19)**.*

Experiment no.	Conditions	Results
1	110 °C, molecular sieves	Benzophenone protection, **Boc**-deprotection
2	70 °C, molecular sieves	Benzophenone protection, **Boc**-deprotection
3	60 °C, molecular sieves	No reaction
4	70 °C, no molecular sieves	No reaction

A final attempt at producing an asymmetric, polymerizable **TANI-PTAB** from **NH_2/NH_2 TANI** involved the selective substitution of **20** with sodium acrylate (see Scheme 2.9). **TANI**s bearing hexyl spacers functionalised with acrylate groups have been previously prepared in the Faul research group by first reacting **NH_2/NH_2 TANI** with 6-bromohexanoyl chloride, followed by nucleophilic substitution with sodium acrylate.[45] The author used 10 molar equivalents of sodium acrylate to encourage complete substitution of both alkyl bromides, therefore only 5 molar equivalents of sodium acrylate was used in this work to preferentially form the mono-substituted product. However, after the reaction was complete, mass spectrometry showed that a mixture of the mono- (**30**) and di-substituted (**31**) products had formed, which could not be separated due to their similar retention times by TLC and similar solvent solubilities.

2.2.7.2 From TANI-CPh_2 (5)

Until this point, the approach to synthesising an asymmetric, polymerizable **TANI-PTAB** had been to start with a symmetrical **NH_2/NH_2 TANI** and introduce asymmetry by reacting with 1 molar equivalent

of the desired reagent. However, as this had been unsuccessful, a different route was considered that started with an asymmetric **TANI**, which could be further reacted as desired. The asymmetric **TANI** chosen as the starting material was the benzophenone-protected **TANI** (**5**), which will be henceforth be referred to as **TANI-CPh$_2$**. Two routes for functionalisation of **TANI-CPh$_2$** were proposed and the reaction routes can be found in Scheme 2.10.

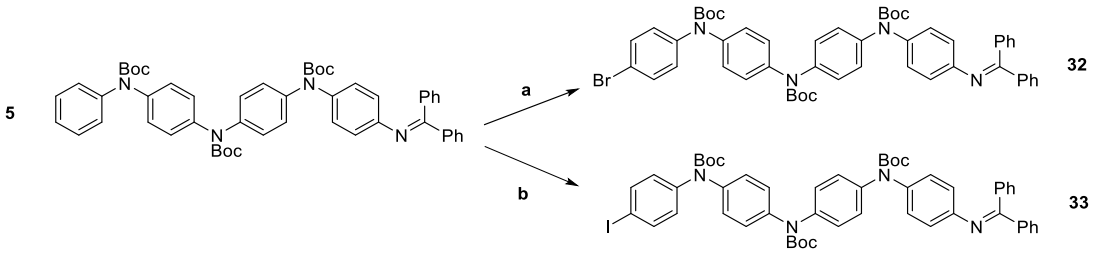

*Scheme 2.10. Attempted synthetic routes for an asymmetric polymerizable **TANI-PTAB**, starting from **TANI-CPh$_2$** (**5**).*

In the first reaction, **TANI-CPh$_2$** was reacted with tetra-n-butylammonium tribromide, with the aim of functionalising it with a reactive bromide. The bromide could be used in future Buchwald-Hartwig reactions with aminated functional groups, which would provide **TANI-CPh$_2$** with either an alkyl spacer or a polymerizable acrylate. Benzophenone deprotection could then be performed, freeing the terminal amine for further reactions.

Bromination of **TANI** precursors with tetra-n-butylammonium tribromide was one of the initial steps in the synthesis of **Ph/NH$_2$ TANI** (**6**) and was highly successful (Section 2.2.1). Therefore, initial reaction attempts used the same conditions of stirring **TANI-CPh$_2$** in dichloromethane with tetra-n-butylammonium tribromde at room temperature for 24 hours. However, no reaction occurred after this time. **TANI-CPh$_2$** is bulkier than the di(aniline) that is used in the synthesis of **Ph/NH$_2$ TANI** (**6**) and may be less reactive due to its size. Additionally, unlike in the previously used di(aniline), the secondary amine in **TANI-CPh$_2$** is **Boc**-protected and is therefore not available for use in the reaction mechanism, which may further hinder the reaction.

To encourage the reaction to occur, the reagents were dissolved in THF and heated to 40 °C. After TLC analysis showed that the **TANI-CPh$_2$** had been consumed, the product was purified by column chromatography. However, ^{1}H NMR spectroscopy and mass spectrometry revealed that while bromide had been added, the benzophenone-protecting group had been removed. This was a problem, as the newly formed terminal amine would be available during any Buchwald-Hartwig coupling reactions, leading to unwanted side products. The terminal amine could not be re-protected as previous reactions in Section 2.2.7.1 had shown that benzophenone-protection reactions with **Boc**-protected **TANI**s would lead to cleavage of the **Boc**-groups.

An alternative route that also used **TANI-CPh$_2$** as a starting material involved the *para*-iodination of the terminal phenyl group. Aryl iodides can be simply reacted with acrylamides by heating in the presence of a copper catalyst and a base.[46] This would provide a facile way to functionalise **TANI-CPh$_2$** with a polymerizable group, before benzophenone protection and subsequent addition of the alkyl spacer. The iodination procedure for **TANI-CPh$_2$** was adapted from Monnereau, Blart and Odobel (2005), who described a method of iodinating aniline derivatives using iodine dissolved in pyridine and dioxane.[47] Unfortunately, no reaction occurred using those conditions, perhaps due again to the bulky nature of **TANI-CPh$_2$**, which is much larger than the aniline derivatives used in the original paper.

2.2.8 MA-11-2-11-MA

After numerous attempts at synthesising an asymmetric, polymerizable **TANI-PTAB** with limited success, it was decided that a different method of functionalising the amphiphile with a polymerizable group was required. In previous attempts, the polymerizable group had been attached at the **TANI** core. As this approach had been unsuccessful, alternative reactive sites were explored.

Li et al. (2019) have prepared two-dimensional polymers by the polymerisation of amphiphilic, gemini monomers.[48] The monomer (**MA-11-2-11-MA**, **36**) consists of two hydrophilic heads, connected by a linker and with two hydrophobic tails each terminated by a methacrylate. When dissolved in water above the critical micelle concentration (CMC), the gemini surfactant assembled into bilayers around a suitable substrate. Using free-radical polymerisation, by heating in the presence of a photoinitiator, the bilayer structures could be trapped as a two-dimensional polymer film and could be removed from the substrate by careful etching.

Importantly for this work, the authors discovered that the monomer could be functionalised by replacing one of the alkyl tails and methacrylates with the desired functional group. The adapted monomer could be co-polymerised with **MA-11-2-11-MA**, forming similar bilayer polymer films to the parent monomer. The authors demonstrated the ease of this approach by functionalising the surfactant with fluorescent tags, which formed uniform films when polymerised around different substrates, where the fluorescence could be seen throughout the structure when probed by fluorescence microscopy.

While the authors had only reported the addition of fluorescent moieties to their gemini surfactant, the synthesis could be generalised to allow the addition of other functional groups, in particular **TANI**. The structure of such a gemini **TANI-PTAB** (**37**) is given Scheme 2.12.

The synthetic route for **MA-11-2-11-MA** is given in Scheme 2.11. 11-Bromoundecylmethacrylate (**34**) was synthesised by reaction of 11-bromo-1-undecanol with methacryloyl chloride at room temperature for 24 hours. **34** was then used to synthesise both **MA-11-2-11-MA** and its precursor, **MA-11-2** (**35**). Both reactions used the same starting materials, including trace quantities of 4-methoxyphenol, which was used as a polymerisation inhibitor, but used different solvents and reaction temperatures. The

gemini surfactant or precursor could be selectively prepared by changing the temperature of the reaction. A temperature of 45 °C would produce **MA-11-2**, while increasing the temperature to 80 °C would produce **MA-11-2-11-MA**.

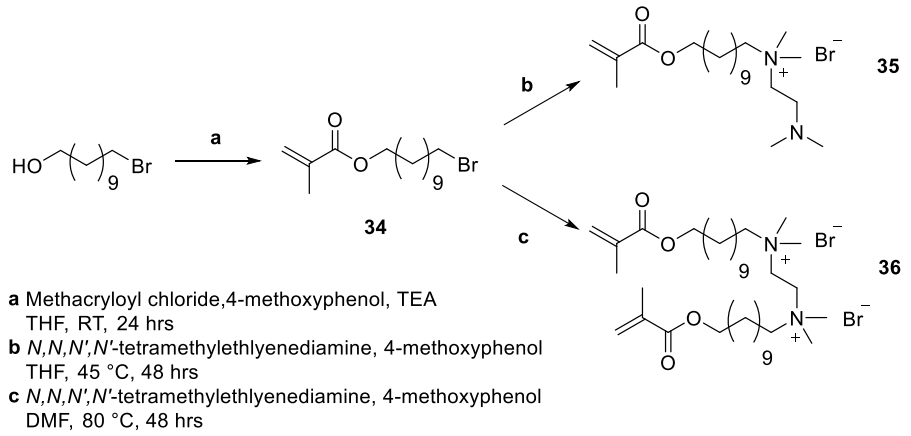

*Scheme 2.11. Synthetic route for **MA-11-2-11-MA (36)** and **MA-11-2 (35)**.*

34 was synthesised during the course of this work, as well as being donated by Yang Li (Jilin University, China) and Thomas Bott (University of Bristol). **MA-11-2** was prepared by Yang Li, while **MA-11-2-11-MA** was prepared by both Li and Bott. **34** and **MA-11-2** were used in the synthesis of a polymerizable, gemini **TANI-PTAB** while **MA-11-2-11-MA** was used to model the polymerisation of gemini monomers in the cubic phases of monoolein (Chapter 5).

2.2.8.1 Synthesis of MA-11-2-TANI-PTAB (37) from MA-11-2 (35)

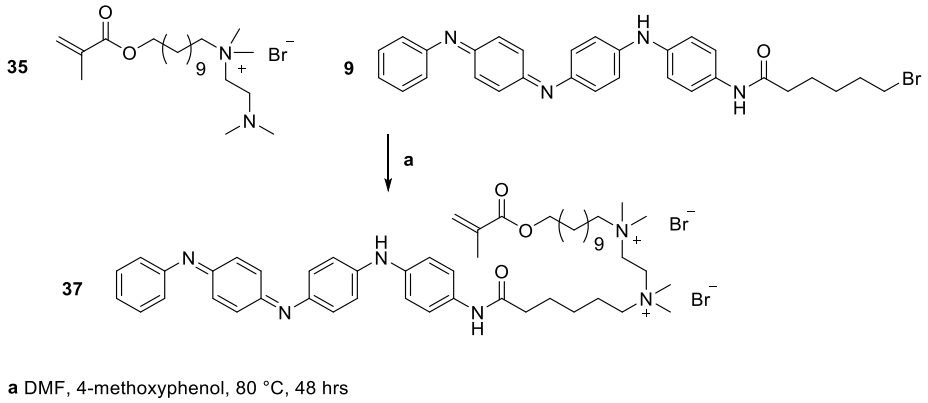

*Scheme 2.12. Synthetic route for EB **MA-11-2-TANI-PTAB** (37), using **MA-11-2 (34)** and **EB TANI-C$_6$Br (9)**.*

Several routes for the synthesis of EB **MA-11-2-TANI-PTAB** (**37**) were developed and attempted during this project. The first and simplest method involved reacting a **TANI-PTAB** precursor (**9**) with **MA-11-2** (**35**) by heating to 80 °C in DMF (Scheme 2.12). The quaternisation reaction was similar to the final step in the synthesis of **TANI-PTAB**, however the reaction involved the tertiary amine of **MA-11-2** instead of trimethylamine. The reaction was also heated, instead of taking place at room

temperature as Li et al. (2019) had determined that elevated reaction temperatures were required to encourage the formation of di-substituted products.[48] After reaction for 48 hours, a blue film had formed at the bottom of the reaction vessel. The heating was stopped, and the solvent was removed. Various solvents were used to attempt to dissolve the film for analysis, however it was not soluble in any of the solvents used (see Section 2.4.20).

The insoluble nature of the film suggested that it had formed a polymer network. 4-Methoxyphenol had been added as a polymerisation inhibitor, however, it is possible that an insufficient amount was added, and the methacrylate had polymerised due to prolonged heating. Additionally, while it was anticipated that the tertiary amine of **MA-11-2** would be the preferred reaction site, it is possible that the secondary amines in the **TANI** core could also be used in the reaction, forming a crosslinked network.

Therefore, a second synthetic route was explored that used a **Boc**-protected **TANI-PTAB** precursor (**7**), to prevent the secondary amines from participating in the quaternisation reaction (Scheme 2.13). It was also expected that the **Boc**-groups have the added benefits of improving the solubility of the product, allowing it to be more easily purified and analysed, and allowing the free-radical polymerisation of the final monomer, as the quinoid moiety in **TANI** is a free-radical inhibitor.[18] The reagents were dissolved in DMF and were heated for 48 hours. The reaction temperature was set at 60 °C to reduce the chance of **Boc**-deprotection due to prolonged heating.

The reaction was stopped after TLC indicated that **7** had been completely consumed. The solvent was removed, and the residue was washed with THF and water to remove any unreacted starting material. Mass spectrometry showed the doubly charged mass ion for the **Boc**-protected **MA-11-2-TANI-PTAB** (**38**), indicating that the reaction was successful. However, a peak for the unreacted starting reagent, **MA-11-2**, along with some heavier, unidentified peaks were also present, indicating that the product was not pure.

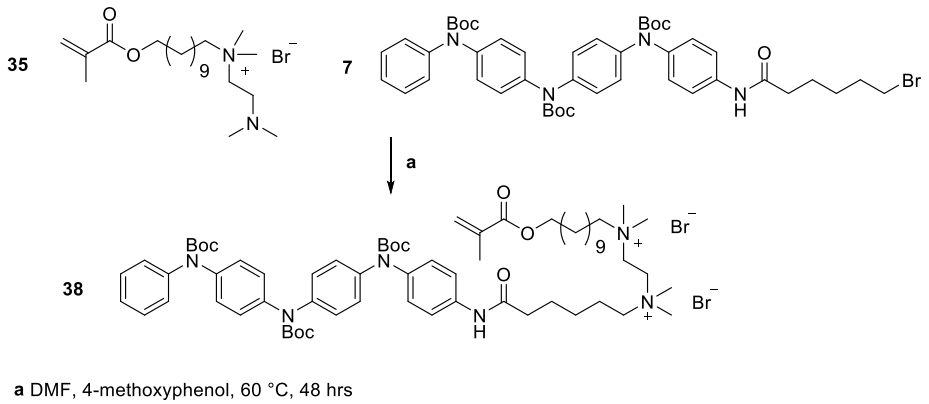

*Scheme 2.13. Synthetic route for **Boc-MA-11-2-TANI-PTAB (38)**, from **Boc-TANI-C6Br (7)** and **MA-11-2 (34)**.*

2.2.8.2 Synthesis of MA-11-2-TANI-PTAB (38) from Boc-protected TANI-C_6Br (7)

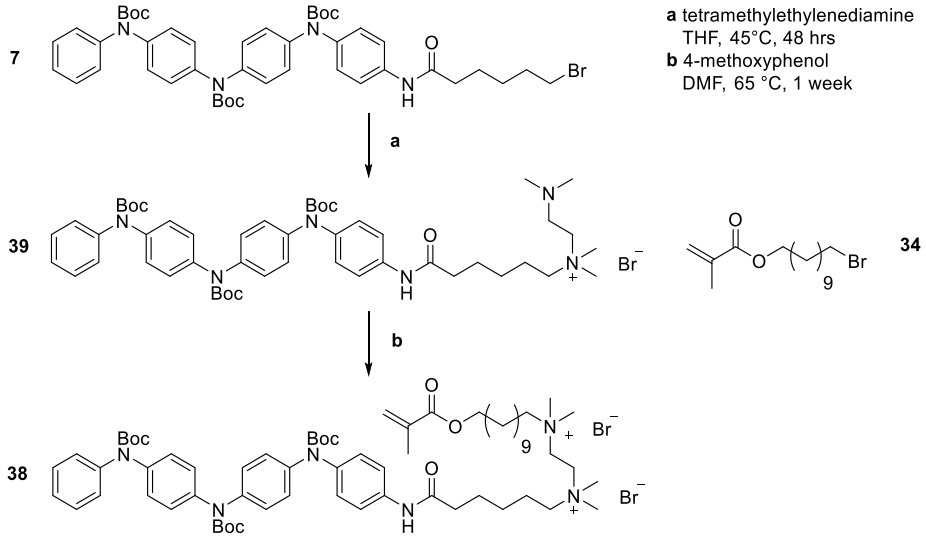

*Scheme 2.14. Synthetic route for **Boc-MA-11-2-TANI-PTAB (38)**, from **Boc-TANI-C_6Br (7)**, tetramethylethylenediamine and 11-bromoundecylmethacrylate (**34**)*

In another synthetic route, shown in Scheme 2.14, a mono-substituted amphiphile was prepared by reacting **Boc-TANI-C_6Br** (**7**) with tetramethylethylenediamine before the addition of the methacrylate tail. It was anticipated that this route would allow for easier purification as any unreacted **TANI** reagents or by-products formed in the synthesis of **39** could be removed by recrystallisation or column chromatography, without needing to take precautions to prevent polymerisation of the methacrylate group. In the second step, any unreacted **34** could be removed by washing with THF or hexane.

Boc-TANI-C_6Br was dissolved in THF along with a large excess of tetramethylethylenediamine (>100 eq.). A large excess of the diamine was required to encourage the formation of the mono-substituted product over the di-substituted product. The mixture was heated to 45 °C to again encourage the formation of the mono-substituted product. After reaction for 24 hours, TLC showed that **Boc-TANI-C_6Br** had been completely consumed. The solvent was removed, and the residue was washed with diethyl ether before being precipitated from hexane. Mass spectrometry and ^{1}H NMR spectroscopy (Appendix A) showed that only the mono-substituted product (**39**) had been formed and no further purification was required.

In the second step, **39** was reacted with **34** by heating in DMF at 65 °C for 1 week. A low reaction temperature was again chosen to reduce the potential for **Boc**-deprotection due to prolonged heating. After 1 week, the reaction was stopped and the solvent was removed. The residue was purified by washing with diethyl ether and precipitation from hexane. The product was identified by mass spectrometry, which showed a mixture of unreacted **39** in addition to **Boc**-protected **MA-11-2-TANI-PTAB** (**38**). A few attempts were made to separate them, however, the attempts were hindered by the charged nature of both starting material and product. For both TLC and reverse phase TLC, **Boc**-

protected **MA-11-2-TANI-PTAB** and **39** did not move from the baseline regardless of the solvent used to separate them, which meant that they could not be separated by column chromatography. Both were also soluble in the same solvents, which meant they could not be separated by recrystallisation.

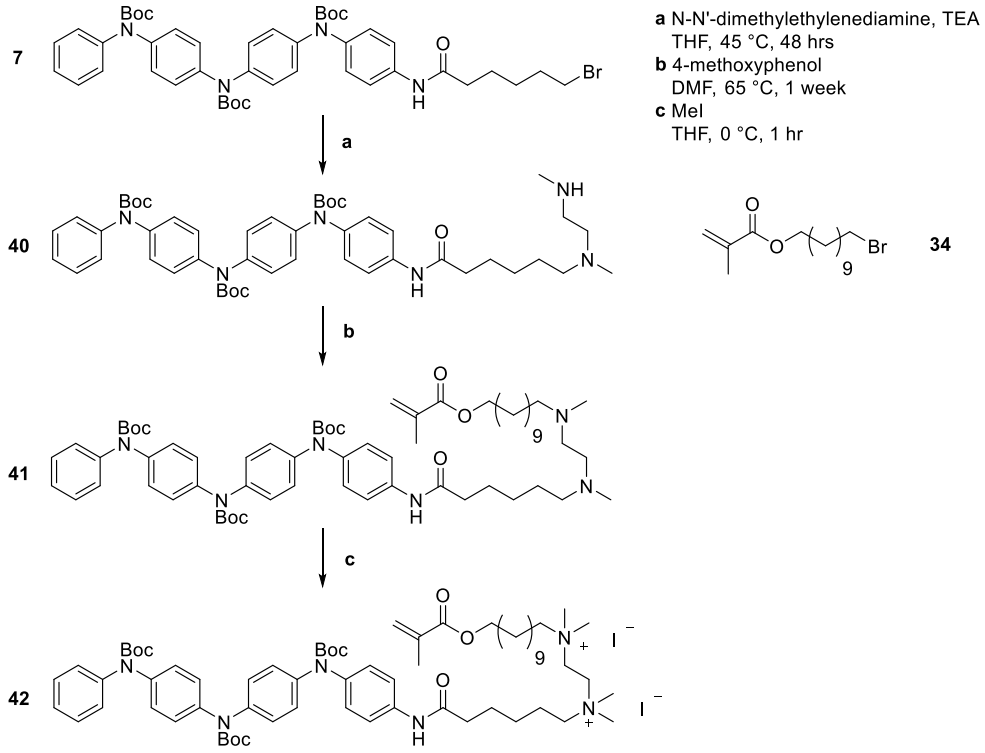

*Scheme 2.15. Synthetic route for **Boc**-protected **MA-11-TANI-PTAI (42)** starting from **Boc-TANI-C$_6$Br (7)**.*

As the charged nature of the starting materials and product were hindering purification, a final synthetic route was proposed, where starting materials and precursors remained uncharged until the final step (Scheme 2.15). In this method, **Boc-TANI-C$_6$Br** would be reacted with *N-N'*-dimethylethylenediamine to provide the terminal, tertiary amine, before the addition of the methacrylate. The tertiary amines formed in **41** could then be converted into quaternary ammonium salts in a Menshutkin reaction, by reaction with iodomethane.[49]

The first two steps were similar to those used in the synthesis of the charged **Boc-MA-11-TANI-PTAB** (Scheme 2.14). **Boc-TANI-C$_6$Br** was coupled with *N-N'*-dimethylethylenediamine using a large excess of the starting amine (> 10 eq.) and low reaction temperature to encourage the formation of the singly-substituted product over the doubly-substituted product. After the reaction was complete and the solvent was removed, the product was simply purified by washing with copious quantities of water to remove any salts, followed by precipitation from hexane.

The methacrylate group was then added by heating **40** with **34** to 65 °C in DMF for one week. The temperature was kept below 70 °C to reduce the chance of **Boc**-deprotection and 4-methoxyphenol was added as a free-radical polymerisation inhibitor. After one week, the reaction was stopped, and the

product was purified by washing with water and precipitation from hexane. Mass spectrometry was used to identify the products that had formed. A peak at 1089.7 m/z corresponding to the product molecular ion was observed along with a couple of other unidentifiable peaks. Thin layer chromatography (normal and reverse phase) was used to try and separate the mixture of compounds, however, all spots stayed close to the baseline regardless of which eluents were used and so purification by column chromatography was not possible.

2.3 CONCLUSIONS

The two main focuses of this chapter are the syntheses of electroactive amphiphiles based on tetra(aniline) (**TANI**) and the syntheses of polymerizable, amphiphilic **TANI**s.

In the first part, the syntheses of **TANI**-derived amphiphiles are described following the literature procedures and methods developed within the Faul group. **Ph/NH_2 TANI** was used as a precursor for the synthesis of single-tailed **TANI** amphiphiles. The synthesis of **Ph/NH_2 TANI** depends on the use of *tert*-butyloxycarbonyl (**Boc**) and diphenylmethylene (**CPh_2**) for the protection of secondary and primary amines, respectively, which allows for the stepwise synthesis of a highly pure material. From this starting block, **TANI-PTAB**, **TANI-C_{12}TAB** and **TANI-PTPB** were prepared by functionalising with either a C6 or C12 alkyl spacer before removal of the **Boc**-groups. This was then followed by either oxidation to the EB state and quaternisation with trimethylamine for **TANI-PTAB** and **TANI-C_{12}TAB** or by functionalising with trimethylphosphine followed by oxidation to the EB state for **TANI-PTPB**.

In a similar manner, a bola-amphiphile, **TANI-$(PTAB)_2$**, was prepared by synthesising **NH_2/NH_2 TANI** from **Boc**-protected precursors before functionalisation with two alkyl spacers, oxidation and quaternisation with trimethylamine.

In the second part, several methods to prepare polymerizable, amphiphilic **TANI**s were evaluated. The different approaches can be grouped depending on either the **TANI** precursor used in the reaction, or by the desired final product.

In the first group, **Boc**-protected **NH_2/NH_2 TANI** was coupled with 1 molar equivalent of either an alkyl spacer, acrylate or diphenylmethylene. In all cases, the reactions produced a mixture of mono- and di-substituted products that were difficult to separate, making further reactions impossible. Additionally, the presence of activated molecular sieves in the reaction with benzophenone led to **Boc**-deprotection, which meant that while a mono-substituted product was formed, any subsequent reactions could take place at the uncovered secondary amines in addition to the primary amine.

In the second group, the aim was to functionalise **TANI-CPh_2** with either bromide or iodide, for use in Buchwald-Hartwig cross coupling reactions or copper thiophenecarboxylate catalysed *N*-arylation

reactions, respectively. Bromination with tetra-n-butylammonium tribromide was partially successful. While bromide had been successfully added, benzophenone deprotection had occurred, limiting further reactions. Meanwhile, no iodination reactions occurred under the conditions used.

In the third group, the focus was the preparation of a polymerizable, gemini **TANI-PTAB** using precursors developed by Li and colleagues at Jilin University for the synthesis of the gemini monomer **MA-11-2-11-MA.** Initial experiments aimed to couple the **MA-11-2-11-MA** precursor, **MA-11-2**, with **Boc-**protected **TANI-C_6Br**. While mass spectrometry showed that the reaction was successful, the product was contaminated with unreacted starting materials, which could not be removed due to difficulties in purification caused by the charged nature of the reagents and product. Difficulties in purification due to charged starting materials and products limited the success of an alternative reaction route, where **Boc-**protected **TANI-C_6Br** was aminated, forming a quaternary ammonium cation, before functionalisation with an acrylate. Therefore, a final route was explored where **Boc**-protected **TANI-C_6Br** was aminated to a tertiary amine before functionalisation with an acrylate. However, this too could not be readily purified and so the final quaternisation step with iodomethane was not attempted.

In summary, a series of electroactive amphiphiles derived from **TANI** were prepared, bearing cationic trimethylammonium or trimethylphosphonium head groups. The purities of **TANI-PTAB**, **TANI-C_{12}TAB, TANI-PTPB** and **TANI-(PTAB)** were confirmed by ^{1}H NMR spectrometry and UV-Vis/NIR spectroscopy, demonstrating their readiness for use in subsequent experiments. Meanwhile, the synthesis of a polymerizable, single-tailed **TANI**-amphiphile was attempted, using either **NH_2/NH_2 TANI** or **TANI-CPh_2**. However, success was limited by the formation of unwanted side products that could not be removed by common purification techniques. Alternative routes to produce a polymerizable, gemini **TANI**-amphiphile were explored, using **TANI-C_6Br** and **MA-11-2-11-MA** precursors, however again with limited success due to the difficulties in separating starting materials from products. Although a polymerizable **TANI-**amphiphile was not produced in this work, it is hoped that the outlined reactions and details of **TANI** chemistry will provide a stepping-stone for future projects.

2.4 MATERIALS AND METHODS

2.4.1 Reagents

Reagents were purchased from Sigma-Aldrich UK and were used as received. Molecular sieves were activated by heating to 200 °C overnight under vacuum.

2.4.2 NMR spectrometry

^{1}H NMR experiments were performed using either a 400 MHz Varian VNMR 400, 400 MHz Jeol ECZ400 or 400 MHz Jeol ECS400 spectrometer and were referenced to deuterated solvents.

2.4.3 Mass spectrometry

Mass spectrometry was conducted using either a Bruker microOTOF II or Thermo Scientific Orbitrap Elite for electrospray ionisation time-of-flight (ESI-TOF), and a Waters Synapt G2S for nanospray ionisation.

2.4.4 UV-Vis spectroscopy

UV-Vis/NIR absorption spectra were collected using a Shimadzu UV2600 spectrophotometer with integrating sphere attachment. Spectra were recorded using a 1 mm path length quartz cuvette due to the strongly absorbing nature of the solutions. Spectra of water, water/**PPO** or water/**PPO**/**MO** baselines were subtracted from the data as required.

Sponge phases were prepared using 40 % (w/w) **MO** and 60 % (v/v) lyotrope, where the lyotrope contained 20 % (v/v) **PPO** for all experiments except for those with pure **MO**, which used 25 % (v/v) **PPO**.

2.4.5 Small-angle X-ray scattering

Monoolein (**MO**) was both received as a gift from Danisco and was purchased from Sigma-Aldrich.

MO cubic phases containing **PPO** and EB or ES state **TANI-**amphiphiles were prepared in the following manner. A stock solution of EB **TANI-**amphiphile was diluted with water and **PPO** (24 µL) to prepare a 96 µL solution at the desired concentration. The solution was mixed with 80 mg of **MO** to produce the sponge phase. 40 µL of the **TANI-**amphiphile-doped sponge phase was loaded into a borosilicate glass capillary (1.5 mm, Capillary Tube Supplies Ltd), followed by either 40 µL of deionised water for retention of the EB state or 40 µL of aqueous acid (4 eq.) for doping to the ES state. The capillary was centrifuged at 2000 rpm for 60 seconds to encourage water diffusion and hydration to the cubic phase. The capillary was then sealed with UV-curable adhesive (Norland Optical Adhesive) for 30 minutes and the sample left to equilibrate for 48 hours.

For **MO** cubic phases containing EB **TANI-PTAB** only, the desired concentration of EB **TANI-PTAB** was prepared in 120 µL of ethanol and was used to dissolve 80 mg of **MO**. 40 µL of the mixture was loaded into a borosilicate glass capillary, which was placed in a fumehood to allow the solvent to slowly evaporate over two weeks. After this time, the capillary was placed under vacuum for a further 24 hours to ensure complete removal of the solvent. 40 µL of deionised water was loaded into the capillary, followed by centrifugation at 2000 rpm for 60 seconds. The capillary was sealed with UV-curable adhesive for 30 minutes and the sample left to equilibrate for a minimum of 24 hours.

Small-angle X-ray scattering data were collected using a SAXSLAB Ganesha 300XL instrument at room temperature over a Q-range of 0.015-0.65 $Å^{-1}$, with an exposure time of 600 seconds per sample.

2.4.6 Carboxyfluorescein leakage assay

1,2-Dioleoyl-sn-glycero-3-phosphocholine (**DOPC**) in chloroform (25 mg/mL) was purchased from Avanti® Polar Lipids, Inc. and was used to prepare unilamellar vesicles for efflux measurements.

5(6)-carboxyfluorescein (**CF**), Trizma® hydrochloride (**TRIS-HCl**), sodium chloride (NaOH) and sodium hydroxide (NaOH) were purchased from Sigma-Aldrich and were used as received in the preparation of internal and elution buffers. Sephadex™ G-25 M and Triton X-100 were also purchased from Sigma-Aldrich and were used as a gel filtration column and to determine the final fluorescence intensity during efflux measurements, respectively.

An internal buffer was prepared consisting of **CF** (50 mM), **TRIS-HCl** (10 mM), NaCl (10 mM) and NaOH (ca. 80 mM) to adjust the pH to 7.4, and was used for vesicle formation. The solution was covered in foil and was stored at 4 °C when not in use.

An elution buffer was prepared using **TRIS-HCl** (10 mM), NaCl (107 mM) and NaOH (ca. 0.75 mM) to adjust the pH to 7.4. This solution was also stored at 4 °C when not in use.

Vesicle preparation method and efflux measurements followed procedures outlined by Stanley (2011).[50]

Vesicle preparation:

A 500 µL solution of **DOPC** (12.5 mM) in chloroform was prepared and pipetted into a 10 mL round bottom flask. The solvent was removed by evaporation using a stream of nitrogen, resulting in a thin film. The flask was then dried under vacuum for a minimum of 1 hour. The lipid film was then hydrated with 500 µL of the internal buffer solution for 10 minutes, before the flask was vortexed to remove the lipid film from the glass wall. 10 freeze-thaw cycles were performed to disrupt the formation of multilamellar species, followed by extrusion 28 times through a polycarbonate membrane (100 nm diameter pore size).

After extrusion, any **CF** remaining in the surrounding solution was removed using a gel filtration column. The column was packed with Sephadex™ G-25 M and washed with 5-10 column volumes of deionised water (ca. 25 mL), followed by 3 column volumes of the elution buffer (ca. 10 mL). 200 µL of the vesicle solution was loaded onto the column and was separated from the free dye with more elution buffer. The collected vesicle solution had a lipid concentration of approximately 2 mM, which was diluted to 0.2 mM for efflux measurements.

Microplate well set-up:

For efflux measurements, 150 µL of **CF**-loaded vesicles (0.2 mM) was pipetted into a microplate well. 150 µL of water or elution buffer was added for the control experiments, to provide the fluorescence intensity at 0 mM and the fluorescence intensity in the absence of an agent, respectively. To determine

the final fluorescence intensity, 150 µL of elution buffer was added along with 1 % (v/v) of Triton X-100.

For efflux measurements using **TANI-PTAB** in the EB and ES states, either 150 µL of EB **TANI-PTAB** was added to the microplate well, or 75 µL of EB **TANI-PTAB** and 75 µL of acid (2 molar eq.).

Efflux measurements:

An excitation wavelength of 490 nm and emission wavelength of 516 nm were chosen for kinetic experiments. 5 nm excitation and emission slits were used, along with a medium scan rate and a photomultiplier tube (PMT) detector voltage of 500 V. Efflux measurements were taken by recording the fluorescence intensity at 516 nm over a 6-hour period, with scans performed at 60 second intervals.

2.4.7 Dynamic light scattering

Dynamic light scattering experiments were performed using a Malvern Autosizer 4800 DLS, at an angle of 90 °, using a 532 nm laser.

DOPC vesicles were prepared in a similar manner to the preparation of vesicles for **CF** leakage assays. A **DOPC** lipid film was prepared by drying a solution of **DOPC** in chloroform (12.5 mM, 500 µL) within a round bottom flask. The film was hydrated with 500 µL of the elution buffer for 10 minutes, before the flask was vortexed to remove the film from the glass walls of the flask. 10 freeze-thaw cycles were performed to disrupt the formation of multilamellar species, followed by extrusion 28 times through a polycarbonate membrane (100 nm diameter pore size) to form large unilamellar vesicles. The lipid concentration after extrusion was 12.5 mM. A 0.2 mM solution was then prepared by taking 160 µL of the 12.5 mM solution and diluting with 9840 µL of deionised water. The diluted solution was used in DLS experiments within one hour of preparation, to reduce the likelihood of vesicle disruption over time.

For DLS experiments, 1 mL of the 0.2 mM **DOPC** solution was diluted to 0.1 mM with 1 mL of either water or elution buffer for the control experiments, or 1 mL of EB **TANI-PTAB**. Measurements were taken at 30-minute intervals for 4 hours.

2.4.8 Transmission electron microscopy

Transmission electron microscopy (TEM) images were obtained using a JEOL 1400 TEM with a tungsten filament, operating at a frequency of 120 kV and equipped with an Orius SC 200 (Gatan) camera using Digital Micrograph GMS 3 image software.

TANI-amphiphile solutions (EB and ES) were sonicated for one minute prior to use. TEM samples were then prepared by depositing 5 µL of the **TANI-**amphiphile solutions on a carbon-coated glow-discharged copper grid and allowing them to rest for 20 seconds. The solvent was then removed by absorbing with filter paper. The samples were then stained using uranyl acetate (1 %, 5 µL) by

depositing the solution on the TEM grid, leaving for 30 seconds, and then removing excess solution with more filter paper. The grids were left to dry at room temperature overnight before analysis.

2.4.9 Polarised optical microscopy

Polarised optical microscopy images were obtained using an Olympus BX50 microscope fitted with an Olympus C-5060 digital camera.

2.4.10 Polymerisation of MA-11-2-11-MA in MO cubic phases

30 mM stock solutions of **MA-11-2-11-MA** and 2,2'-azobis(2-methylpropionamidine) dihydrochloride (**PI**) in deionised water were prepared and were stored in the fridge when not in use.

Sponge phases were prepared by mixing **PPO** with water (for control experiments using just **MA-11-2-11-MA**) or water and **PI** (for control experiments using just **PI** or for polymerisation experiments with **MA-11-2-11-MA** and **PI**), before adding to **MO** and stirring to produce a homogenous sponge phase. A heat gun was used to dissolve the stock solution of **MA-11-2-11-MA** and the appropriate volume was quickly added to the sponge phase before re-precipitation could occur. The sponge phase was stirred again using a vortex mixer before 40 µL of the mixture was pipetted into a borosilicate glass capillary tube. 40 µL of water was added via centrifugation at 2000 rpm for 60 seconds, and the capillary was sealed with a UV-curable adhesive. The capillary tube holder was wrapped in aluminium foil to reduce the likelihood of polymerisation due to the UV-light during the 30-minute curing of the glue.

Samples were kept in the dark for the 48-hour equilibration period, to prevent any photo-initiated polymerisation. SAXS patterns were then collected to identify the phases that were formed. The capillaries were marked to ensure that re-analysis would be performed on the same section.

After a further 24 hours, capillaries containing both **MA-11-2-11-MA** and **PI** were placed in a UV-reactor and were irradiated with 310-380 nm light for 2 hours, to induce photo-polymerisation. The samples were left to rest for another 24 hours, before identification of the phase structure using SAXS.

2.4.11 Chemical characterisation data

All spectra pertaining to compounds synthesised in this work can be found in Appendix A.

2.4.12 Ph/NH_2 TANI

The syntheses of **1** and **2** were done in large batches by various group members as common precursors for many other projects. Typical experimental procedures and characterisation data for both are provided below.

1 and **2** were used in the syntheses of **3** and **4**, which were done during a separate project.[51] The experimental procedures and characterisation data for both reactions are provided below. **3** and **4** were used to prepare **5** in this work.

4-((diphenylmethylene)amino)-*N*-phenylaniline (1)

N-phenyl-*p*-phenylene diamine and benzophenone (1 eq.) were added to a flask containing activated molecular sieves (3 Å), before being placed under nitrogen. Anhydrous toluene was added, and the mixture was refluxed for 24 hours. After cooling to room temperature, the mixture was filtered, and the molecular sieves were washed with THF until clear. The organic fractions were combined and concentrated. The resulting oil was washed with methanol, filtered and dried. The remaining solid was recrystallised from methanol (70%).

^{1}H NMR (400 MHz, $CDCl_3$): δ 7.75 (d, *J* = 7.2 Hz, 2H), 7.48-7.39 (m, 3H), 7.32-7.28 (m, 3H), 7.24-7.15 (m, 4H), 6.95 (d, *J* = 8.1 Hz, 2H), 6.90-6.85 (m, 3H), 6.69 (d, *J* = 8.6 Hz, 2H), 5.56 (s, 1H).

(*m/z*): [M + H]+ calcd., 349.17; found, 349.17.

tert-butyl (4-((diphenylmethylene)amino)phenyl)(phenyl)carbamate (2)

1, di-tert-butyl dicarbonate (1.2 eq.) and dimethylaminopyridine (0.1 eq.) were weighed into a flask and protected under nitrogen. Anhydrous THF was added, and the solution was refluxed for 24 hours. The mixture was cooled to room temperature and an excess of ethanol was added. The mixture was placed in a fridge for 12 hours, followed by filtration yielding pale yellow crystals (78%).

^{1}H NMR (400 MHz, $CDCl_3$): δ 7.74-7.72 (m, 2H), 7.48-7.44 (m, 1H), 7.41-7.36 (m, 2H), 7.27-7.23 (m, 5H), 7.15-7.08 (m, 5H), 6.98-6.95 (m, 2H), 6.68-6.64 (m, 2H), 1.39 (s, 9H).

(*m/z*): [M+H]+ calcd., 449.2; found, 449.2; [M+Na]+ calcd., 471.2; found, 471.2; [M+K]+ calcd., 487.2; found, 487.2.

tert-butyl (4-bromophenyl)(4-((diphenylmethylene)amino)phenyl)carbamate (3)

1 (5.05 g, 14.3 mmol) was dissolved in dichloromethane (100 mL) before tetrabutylammonium tribromide (1.1 eq., 7.59 g) was added. After stirring for one hour, sodium sulfite (aq. 22 %, 50 mM) was added and the solution stirred for 30 minutes. Sodium hydroxide (2 M, 50 mL) was added, and the solution stirred for a further 30 minutes. The organic phase was separated, washed with water, dried over anhydrous $MgSO_4$ and concentrated. The residue was placed in a flask, along with di-tert-butyl dicarbonate (1.1 eq., 3.51 g) and dimethylaminopyridine (0.1 eq., 0.175 g), and was protected under nitrogen. The solids were dissolved in anhydrous THF (200 mL) and the mixture was refluxed for 38 hours. After the reaction was complete, the mixture was cooled to room temperature and ethanol (300 mL) was added, causing the precipitation of yellow crystals. After filtration, the supernatant was dried, and the residue recrystallised from 9:1 methanol/ethyl acetate. The crystals were combined with those precipitated from ethanol (5.323 g, 86%).

^{1}H NMR (400 MHz, $CDCl_3$): δ 7.76-7.73 (m, 2H), 7.50-7.46 (m, 1H), 7.43-7.34 (m, 4H), 7.31-7.27 (m, 2H), 7.26-7.23 (m, 1H), 7.13-7.10 (m, 2H), 7.04-7.01 (m, 2H), 6.96-6.92 (m, 2H), 6.70-6.66 (m, 2H), 1.39 (s, 9H).

(*m/z*): [M+H]+ calcd., 529.1; found, 529.1; [M+Na]+ calcd., 551.1; found, 551.1.

tert-butyl (4-aminophenyl)(phenyl)carbamate (4)

2 (10 g, 22.3 mmol), ammonium formate (12 eq., 16.9 g) and palladium-on-carbon (2.5 % mol, 0.593 g) were weighed into a flask and protected under nitrogen. Anhydrous THF (100 mL) and anhydrous methanol (250 mL) were added, and the mixture was heated at 67 °C for 5 hours. After cooling to room temperature, the solvents were removed, and the residue was dissolved in dichloromethane before being filtered through celite. The filtrate was dried under reduced pressure and the residue stirred in hexane before a final filtration, leaving an off-white powder (5.395 g, 85.08%).

^{1}H NMR (400 MHz, $CDCl_3$): δ 7.29-7.26 (m, 1H), 7.26-7.25 (m, 1H), 7.23-7.20 (m, 2H), 7.13-7.09 (m, 1H), 7.01-6.97 (m, 2H), 6.64-6.60 (m, 2H), 3.63 (s, 2H), 1.44 (s, 9H).

(*m/z*): [M+H]+ calcd., 285.2; found, 285.2; [M+Na]+ calcd., 307.1; found, 307.1.

tert-butyl (4-((tert-butoxycarbonyl)(4-((tert-butoxycarbonyl)(4-((diphenylmethylene)amino)phenyl)amino)phenyl)amino)phenyl)(phenyl)carbamate, TANI-CPh_2 (5)

4 (1.2 eq., 0.41 g), **3** (0.635 g, 1.20 mmol), $Pd(dba)_2$ (0.014 g, 2% mol), XPhos (0.012 g, 2% mol) and NaOtBu (2 eq., 0.231 g) were weighed into a flask and were protected under nitrogen. Anhydrous toluene (50 mL) was added, and the mixture refluxed at 110 °C for 24 hours. After the reaction was complete, the solution was cooled to room temperature, filtered through celite and dried. The residue was dissolved in dichloromethane, washed with water, and dried over $MgSO_4$.

The solvent was then removed by evaporation and the residue was dissolved in THF (100 mL). Di-tert-butyl dicarbonate (1.3 eq., 0.341 g) and dimethylaminopyridine (0.1 eq., 0.015 g) were added and the solution was heated at 66 °C for 36 hours. The solvent was then removed, and the product was washed with cold methanol and was filtered, yielding **5** (42%).

^{1}H NMR (400 MHz, $CDCl_3$): δ 7.75-7.73 (m, 2H), 7.49-7.45 (m, 1H), 7.43-7.38 (m, 2H), 7.32-7.26 (m, 3H), 7.26-7.10 (m, 11H), 7.08 (s, 4H), 6.96-6.94 (m, 2H), 6.67-6.65 (m, 2H), 1.44-1.38 (m, 27H).

(*m/z*): [M+H]+ calcd., 831.4; found, 831.4; [M+Na]+ calcd., 853.4; found, 853.4.

Ph/NH_2 TANI (6)

5 (0.5 g, 0.6 mmol), palladium on carbon (13 mg, 10% Pd content, 2% mol) and ammonium formate (10 eq., 0.36 g) were weighed into a flask and protected under nitrogen. Anhydrous THF (30 mL) and

anhydrous methanol (75 mL) were added, and the solution was refluxed at 67 °C for 6 hours. After the reaction was complete, the solvent was removed, and the residue dissolved in dichloromethane before filtering through celite. The filtrate was dried and stirred in hexane for 3 hours, before further filtration and drying to produce **6** (73%).

^{1}H NMR (400 MHz, $CDCl_3$): δ 7.32-7.28 (m, 2H), 7.20-7.07 (m, 11H), 6.97-6.94 (m, 2H), 6.64-6.61 (m, 2H), 3.64 (s, 1H), 1.43-1.42 (m, 27H).

(*m/z*): [M+H]+ calcd., 667.4; found, 667.3; [M+Na]+ calcd., 689.3; found, 689.3.

2.4.13 TANI-PTAB (EB)

tert-butyl (4-(6-bromohexanamido)phenyl)(4-((tert-butoxycarbonyl)(4-((tertbutoxycarbonyl)(phenyl)amino)phenyl)amino)phenyl)carbamate, Boc-TANI-C_6Br (7)

6 (1.63 g, 2.4 mmol) was dissolved in anhydrous THF (140 mL), under a nitrogen atmosphere and was cooled to 0 °C. Triethylamine was added (5 eq., 1.24 g), followed dropwise by a solution of 6-bromohexanoyl chloride (1.05 eq., 0.548 mg) in THF (10 mL). Once the addition was complete, the ice bath was removed, and the solution allowed to warm to room temperature. After TLC confirmed reaction of the starting amine was complete (48 hrs), the solvent was removed, and the residue dissolved in ethyl acetate. The solution was washed with HCl (1 M, 15 mL), NaOH (1 M, 15 mL) and brine (15 mL), before drying over $MgSO_4$ and removing the solvent to yield the crude product. The product was purified by column chromatography (silica gel, 1:1 ethyl acetate:n-hexane) to yield the product **7** (85%).

^{1}H NMR (400 MHz, DMSO-d_6): δ 9.92 (s, 1H), 7.56-7.54 (m, 2H), 7.36-7.32 (m, 2H), 7.22-7.11 (m, 13H), 3.53 (t, *J* = 6.6 Hz, 2H), 2.30 (t, *J* = 7.1 Hz, 2H), 1.82 (q, *J* = 7.2 Hz, 2H), 1.60 (q, *J* = 7.2 Hz, 2H), 1.47-1.39 (m, 2H), 1.36 (m, 27H).

(*m/z*): [M+Na]+ calcd., 865.3; found, 865.3; [M+K]+ calcd., 881.3; found, 881.3.

6-bromo-N-(4-((4-((4-(phenylamino)phenyl)amino)phenyl)amino)phenyl)hexanamide (8)

7 (1 g, 1.19 mmol) was dissolved in anhydrous dichloromethane (25 mL) under a nitrogen atmosphere before the dropwise addition of trimethylsilane iodide (3.6 eq., 0.85 g). The mixture was stirred for 1 hour before anhydrous methanol (3.6 eq., 0.17 mL) was added dropwise, causing the precipitation of a pale solid. The mixture was stirred for a further 30 minutes before triethylamine (1.7 mL) was added causing a pale purple colour to develop. The mixture was stirred for 15 minutes before centrifugation to collect the precipitate. The precipitate was washed with dichloromethane (1 x 30 mL) and diethyl ether (2 x 30 mL). The precipitate was dried in a vacuum overnight to yield pure **8** (96%).

^{1}H NMR (400 MHz, DMSO-d_6): δ 9.59 (s, 1H), 7.73 (s, 1H), 7.64 (s, 1H), 7.59 (s, 1H), 7.36 (d, *J* = 9.0 Hz, 2H), 7.12 (t, *J* = 7.6 Hz, 2H), 6.97-6.84 (m, 12H), 6.64 (t, *J* = 7.2 Hz, 1H), 3.52 (t, *J* = 6.7 Hz, 2H), 2.23 (t, *J* = 7.2 Hz, 2H), 1.88 (q, *J* = 7.3 Hz, 2H), 1.81 (q, *J* = 7.3 Hz, 2H), 1.40 (q, *J* = 6.9 Hz, 2H).

(*m/z*): [M+H]+ calcd., 543.2; found, 543.2; [M+K]+ calcd., 581.1; found, 581.1.

6-bromo-N-(4-(((1E,4E)-4-((4-(phenylamino)phenyl)imino)cyclohexa-2,5-dien-1-ylidene)amino)phenyl)hexanamide (9)

8 (0.460 g, 0.85 mmol) was dissolved in DMF (46 mL) and stirred while a solution of ammonium persulfate (1 eq., 0.193 g) in HCl (1 M, 31 mL) was added dropwise causing a dark green precipitate to develop. The mixture was stirred for 30 minutes, followed by centrifugation to collect the precipitate. The precipitate was washed with acetone (3 x 30 mL), before being suspended in acetone (460 mL). Ammonium hydroxide (2 M, 61 mL) was added, changing the mixture from green to dark purple. The mixture was stirred for 15 minutes before the acetone was removed under vacuum, leaving an aqueous suspension of a dark blue solid. The solid was collected by centrifugation and was washed with copious amounts of water, followed by drying under vacuum to yield **9** (48%).

^{1}H NMR (400 MHz, DMSO-d_6): δ 9.91 (s, 1H), 7.68-7.54 (m, 2H), 7.37-7.25 (m, 2H), 7.15-6.88 (m, 13H), 3.55 (t, *J* = 6.8 Hz, 2H), 2.31 (t, *J* = 7.3 Hz, 2H), 1.84 (q, *J* = 7.3 Hz, 2H), 1.62 (q, *J* = 6.9 Hz, 2H), 1.43 (q, *J* = 7.7 Hz, 2H).

(*m/z*): [M+H]+ calcd., 541.2; found, 543.2; [M+Na]+ calcd., 563.2; found, 565.1.

EB TANI-PTAB (10)

9 (0.22 g, 0.37 mmol) was loaded into a plastic centrifuge tube and dissolved in DMF (10 mL), before the addition of trimethylamine (>10 eq., 35 wt.% in ethanol, 1.25 mL). The mixture was stirred until TLC analysis showed no starting material (100 % ethyl acetate), approx. 48 hrs. When complete, the DMF solution was added dropwise to ice-cold diethyl ether (300 mL), contained in plastic centrifuge tubes. The product was left to precipitate in a freezer overnight. The suspension was centrifuged and washed with diethyl ether. The residue was dried in a vacuum before dissolving in deionised water (300 mL). The solutions were centrifuged to remove any water-insoluble impurities and the supernatant lyophilised to give the product **10** as a fluffy blue solid (59%).

^{1}H NMR (400 MHz, acetonitrile-d_3): δ 9.11 (s, 1H), 8.81 (s, 1H), 8.62 (s, 1H), 7.73-7.69 (m, 1H), 7.57-7.53 (m, 1H), 7.45-7.37 (m, 1H), 7.30-6.69 (m, 16H), 6.43-6.34 (m, 1H), 3.31-3.25 (m, 2H), 3.04-3.03 (m, 9H), 2.46-2.34 (m, 2H), 1.80-1.69 (m, 4H), 1.42-1.40 (m, 2H).

(*m/z*): [M-Br]+ calcd., 520.3; found, 522.3.

2.4.14 TANI-C_{12}TAB (EB)

tert-butyl (4-(12-bromododecanamido)phenyl)(4-((tert-butoxycarbonyl)(4-((tert-butoxycarbonyl)(phenyl)amino)phenyl)amino)phenyl)carbamate (11)

6 (300 mg, 0.45 mmol), 12-bromododecanoic acid (1.5 eq., 188 mg) and 1-ethyl-3-(3-dimethylaminopropyl)-carbodiimide hydrochloride (1.5 eq., 105 mg) were mixed in anhydrous dichloromethane (5 mL) at 0 °C under a nitrogen atmosphere. The reaction mixture was warmed to room temperature and stirred overnight. After evaporating the solvent, the residue was washed by water 10 times before being recrystallized from methanol, yielding **11** as a white powder (90%).

^{1}H NMR (400 MHz, $CDCl_3$): δ 7.46 (d, *J* = 8.6 Hz, 2H), 7.32-7.28 (m, 2H), 7.20-7.11 (m, 14H), 3.40 (t, *J* = 6.7 Hz, 2H), 2.34 (t, *J* = 7.5 Hz, 2H), 1.85 (q, *J* = 7.5 Hz, 2H), 1.71 (m, 2H), 1.45-1.42 (m, 30H), 1.31-1.26 (m, 16H).

(*m/z*): [M+Na]+ calcd., 949.4; found, 951.4.

12-bromo-N-(4-((4-((4-(phenylamino)phenyl)amino)phenyl)amino)phenyl)dodecanamide (12)

11 (0.34 g, 0.37 mmol) was placed in a nitrogen atmosphere and dissolved in anhydrous dichloromethane (8 mL). Trimethylsilane iodide (3.6 eq., 0.188 mL) was slowly added and the mixture stirred for 1 hour before anhydrous methanol (3.6 eq., 0.05 mL) was added dropwise, causing the precipitation of a pale solid. The mixture was stirred for a further 30 minutes before triethylamine (0.5 mL) was added causing a pale purple colour to develop. The mixture was stirred for 15 minutes before centrifugation to collect the precipitate. The precipitate was washed with dichloromethane (1 x 30 mL) and diethyl ether (2 x 30 mL) before being dried in a vacuum overnight to yield pure **12** (81%).

^{1}H NMR (400 MHz, DMSO-d_6): δ 9.60 (s, 1H), 7.75 (s, 1H), 7.66 (s, 1H), 7.61 (s, 1H), 7.39-7.36 (m, 2H), 7.16-7.12 (m, 2H), 6.99-6.86 (m, 12H), 6.69-6.65 (m, 1H), 3.51 (t, *J* = 6.7 Hz, 2H), 2.23 (t, *J* = 7.3 Hz, 2H), 1.80-1.74 (m, 2H), 1.56-1.54 (m, 2H), 1.38-1.34 (m, 2H), 1.28-1.26 (m, 13H).

(*m/z*): [M+H]+ calcd., 627.3; found, 627.3.

12-bromo-N-(4-((4-(((1E,4E)-4-(phenylimino)cyclohexa-2,5-dien-1-ylidene)amino)phenyl)amino)phenyl)dodecanamide (13)

12 (0.058 g, 0.092 mmol) was dissolved in DMF (6 mL) before a solution of ammonium persulfate (21 mg, 1 eq.) in HCl (1 M, 4 mL) was added dropwise with stirring. The mixture was stirred for 30 minutes, followed by centrifugation to collect the precipitate. The precipitate was washed with acetone (3x) before being suspended in acetone (58 mL). Ammonium hydroxide (2M, 8 mL) was added, and the mixture was stirred for a further 15 minutes. The acetone was evaporated under vacuum and the resulting aqueous suspension was collected by centrifugation. The product was washed with water and dried under vacuum, yielding **13** as a dark blue solid (77%).

^{1}H NMR (400 MHz, DMSO-d_6): δ 9.94-9.73 (m, 1H), 8.43-8.36 (m, 1H), 7.64-6.89 (m, 18H), 3.51 (t, *J* = 7.1 Hz, 2H), 2.29 (m, 2H), 1.80-1.76 (m, 2H), 1.36-1.26 (m, 16H).

(*m/z*): [M+H]+ calcd., 625.3; found, 625.3.

EB TANI-C_{12}TAB (14)

13 (0.131 g, 0.21 mmol) was loaded into a plastic centrifuge tube and dissolved in DMF (5 mL), before trimethylamine was added (35 wt.% in ethanol, 0.5 mL, >10 eq.). The mixture was stirred until TLC analysis showed no starting material (100% ethyl acetate), approx. 48 hrs. When complete, the DMF solution was added dropwise to ice-cold diethyl ether (250 mL), contained in plastic centrifuge tubes. The product was left to precipitate in a freezer overnight. The suspension was centrifuged and washed with diethyl ether. The residue was dried in a vacuum before dissolving in deionised water (250 mL). The solutions were centrifuged to remove any water-insoluble impurities and the supernatant lyophilised to give the product **14** as a fluffy blue solid (75%).

^{1}H NMR (400 MHz, acetonitrile-d_3): δ 8.62 (s, 1H), 8.39 (s, 1H), 8.25 (s, 1H), 7.66-7.62 (m, 1H), 7.49-7.47 (m, 1H), 7.41-7.37 (m, 1H), 7.30-7.25 (m, 1H), 7.21-6.68 (m, 14H), 3.22-3.17 (m, 2H), 3.00 (s, 9H), 2.36-2.28 (m, 2H), 1.67 (m, 4H), 1.31-1.27 (m, 15H).

(*m/z*): [M-Br]+ calcd., 604.4; found, 604.4

2.4.15 EB TANI-PTPB (16)

The synthesis of **TANI-PTPB** (EB) was done by Alotaibi.[17,34] All experiments using **TANI-PTPB** (EB) in this thesis used product donated by her.

In a typical procedure,[34] a solution of **8** in DMF was prepared in a thick-walled flask, under a nitrogen atmosphere at 0 °C. Trimethylphosphine is pyrophoric and may decompose explosively when heated. Therefore, a thick-walled flask was used as a reaction vessel and a blast shield was put in place around the reaction to protect against accidents. Trimethylphosphine (1.5 eq., 1 M in toluene) was added to the solution, before the flask was tightly sealed and placed behind a blast shield. The flask was heated to 70 °C using an oil bath for at least 16 hrs. After cooling to 0 °C, the remaining trimethylphosphine was removed under vacuum before the mixture was poured into a large quantity of cold diethyl ether. The product was left to precipitate in a freezer, before being collected by centrifugation and washing with diethyl ether to yield **15** (70%).

15 was then dissolved in acetonitrile and H_2O_2 (30 wt.% in water, >12 eq.) was added. The solution was stirred for 2-3 hours, before being added to ice-cold diethyl ether, dropwise. The solution was left to fully precipitate overnight in a freezer. The precipitate was collected by centrifugation and was washed by diethyl ether. The residue was dried in a vacuum oven, then dissolved in deionised water. The

solution was centrifuged to remove any water-insoluble impurities and the supernatant lyophilised to give the product **16.**

(*m/z*): [M-Br]+ calcd., 537.3; found, 537.3.

^{1}H NMR (400 MHz, DMSO-d_6): δ 10.09 (s, 1H), 8.47-8.39 (m, 1H), 7.67-6.82 (m, 14H), 2.39-2.32 (m, 2H), 2.19-2.15 (m, 2H), 1.86-1.79 (m, 9H), 1.64 (m, 2H), 1.54 (m, 2H), 1.44-1.39 (m, 2H).

2.4.16 NH_2/NH_2 TANI (19)

The syntheses of **NO_2/NO_2 TANI** (**18**) and **NH_2/NH_2 TANI** (**19**) were performed in batches by various group members, as precursors for other projects. The synthesis and characterisation of these materials are given below. **NH_2/NH_2 TANI** (**19**) was used as prepared in following reactions in this work.

N^1-(4-nitrophenyl)-N^4-(4-((4-nitrophenyl)amino)phenyl)benzene-1,4-diamine (17)

4,4-Diaminophenylamine sulfate and 4-fluoronitrobenzene (10 eq.) were weighed into a flask and protected under nitrogen. DMSO and triethylamine (4.5 eq.) were added, and the solution was heated at 90 °C for 24 hours. After cooling to room temperature, the solution was poured into deionised water and stirred for a further 15 minutes. The resulting precipitate was filtered, washed with water and chloroform, and dried under vacuum. The crude product (**17**) was then purified by recrystallisation from methanol (49%).

^{1}H NMR (400 MHz, DMSO-d_6): δ 9.11 (s, 2H), 8.21 (s, 1H), 8.06-8.04 (m, 4H), 7.15-7.09 (m, 8H), 6.92-6.90 (m, 4H).

(*m/z*): [M+H]+ calcd., 442.2; found, 442.2; [M+Na]+ calcd., 464.1; found, 464.1; [M+K]+ calcd., 480.1; found, 480.1.

tert-butyl (4-((tert-butoxycarbonyl)(4-((tert-butoxycarbonyl)(4-nitrophenyl)amino)phenyl)amino)phenyl)(4-nitrophenyl)carbamate (18)

17, di-tert-butyl dicarbonate (4.5 eq.) and dimethylaminopyridine were dissolved in anhydrous THF, under a nitrogen atmosphere. The solution was refluxed overnight, before being cooled and diluted with dichloromethane. The organic phase was washed with HCl (1 M) and NaOH (1 M), dried over $MgSO_4$ and the solvent removed. The product (**18**) was obtained after recrystallisation from methanol (85 %).

^{1}H NMR (400 MHz, $CDCl_3$): δ 8.16-8.12 (m, 4H), 7.38-7.34 (m, 4H), 7.25-7.23 (m, 4H), 7.16-7.12 (m, 4H), 1.46 (s, 27H).

(*m/z*): [M+Na]+ calcd., 764.3; found, 764.3.

NH_2/NH_2 TANI (19)

18, palladium on carbon (10 % Pd content, 5 % Pd) and ammonium formate (20 eq.) were weighed into a flask and protected under nitrogen. Anhydrous THF and methanol were added and the mixture was refluxed overnight or until TLC analysis (1:1 ethyl acetate:hexane) confirmed the reaction was complete. The reaction was cooled to room temperature and the solvent removed. The residue was dissolved in dichloromethane and filtered through celite. The solvent was dried, leaving the crude product (**19**), which was recrystallised from methanol (63%).

^{1}H NMR (400 MHz, $CDCl_3$): δ 7.14-7.06 (m, 8H), 6.97-6.95 (m, 4H), 6.62-6.60 (m, 4H), 3.64 (s, 4H), 1.44-1.42 (m, 27H).

(*m/z*): [M+Na]+ calcd., 704.3; found, 704.3; [M+K]+ calcd., 720.3, found, 720.3.

2.4.17 TANI $(PTAB)_2$ (23)

The synthesis of EB **TANI-$(PTAB)_2$** (**23**) was developed and performed by Alotaibi.[34,37] Most experiments using EB **TANI-$(PTAB)_2$** (**23**) in this work involved product donated by her. However, the synthesis was repeated from existing stocks of **20** (prepared by Alotaibi) during this project to produce enough EB **TANI-$(PTAB)_2$** (**23**) for all experiments.

tert-butyl (4-(6-bromohexanamido)phenyl)(4-((4-((4-(6-bromohexanamido)phenyl)(tert-butoxycarbonyl)amino)phenyl)(tert-butoxycarbonyl)amino)phenyl)carbamate (20)

In a typical procedure, **19** was dissolved in anhydrous THF, under a nitrogen atmosphere. The mixture was cooled to 0 °C using an ice bath and triethylamine (5 eq.) was added. A solution of 6-bromohexanoyl chloride (1 eq.) in anhydrous THF was added dropwise, and the solution allowed to warm to room temperature. After the reaction overnight, the solvent was removed, and the residue dissolved in ethyl acetate. The organic phase was washed with HCl (1 M), NaOH (1 M) and brine, before drying over $MgSO_4$ and removal of the solvent. The crude product was purified by flash column chromatography (silica gel, 1:1 hexane: ethyl acetate), followed by stirring in hexane overnight and filtration to obtain the pure **20** (88%).

^{1}H NMR (400 MHz, DMSO-d_6): δ 9.92 (s, 2H), 7.56-7.54 (m, 4H), 7.14-7.11 (m, 12H), 3.55-3.52 (m, 4H), 2.31-2.28 (m, 4H), 1.86-1.78 (m, 4H), 1.64-1.51 (m, 4H), 1.43-1.39 (m, 4H), 1.36 (s, 27H).

(*m/z*): [M+Na]+ calcd., 1056.3; found, 1058.3.

N,N'-(((azanediylbis(4,1-phenylene))bis(azanediyl))bis(4,1-phenylene))bis(6-bromohexanamide) (21)

Trimethylsilane iodide (3.6 eq., 0.5 mL) was slowly added to a solution of **20** (1 g, 0.97 mmol) in anhydrous dichloromethane (100 mL). The mixture was stirred for 1 hour before anhydrous methanol

(3.6 eq., 0.14 mL) was added dropwise causing precipitation. The mixture was then stirred for a further 30 minutes, before triethylamine (2 mL) was added and the mixture stirred for a final 15 minutes. The precipitate was collected by centrifugation and washed with dichloromethane (1 x 30 mL) and diethyl ether (2 x 30 mL), before drying overnight in a vacuum oven, yielding **21** (86%).

^{1}H NMR (400 MHz, DMSO-d_6): δ 9.60 (s, 2H), 7.64 (s, 2H), 7.56 (s, 1H), 7.38-7.35 (m, 4H), 6.95-6.90 (m, 8H), 6.88-6.85 (m, 4H), 3.56-3.52 (m, 4H), 2.27-2.23 (m, 4H), 1.86-1.79 (m, 4H), 1.64-1.56 (m, 4H), 1.45-1.38 (m, 4H).

(*m/z*): [M+H]+ calcd., 734.2; found, 735.2.

6-bromo-N-(4-(((1E,4E)-4-((4-((4-(6-bromohexanamido)phenyl)amino)phenyl)imino)cyclohexa-2,5-dien-1-ylidene)amino)phenyl)hexanamide (22)

21 (0.612 g, 0.83 mmol) was dissolved in DMF (61 mL) and stirred while ammonium persulfate (1 eq., 0.19 g) in HCl (1 M, 41 mL) was added dropwise. The mixture was stirred for 30 minutes, followed by centrifugation to collect the precipitate, which was washed with acetone (3 x 30 mL), before being suspended in acetone (610 mL). Ammonium hydroxide (2 M, 81 mL) was added, and the mixture was stirred for 15 minutes before the acetone was removed under vacuum, leaving an aqueous suspension. The solid was collected by centrifugation and was washed with copious amounts of water, followed by drying under vacuum to yield **22** (50%).

^{1}H NMR (400 MHz, DMSO-d_6): δ 9.97 (d, *J* = 2.3 Hz, 1H), 9.76 (d, *J* = 2.4 Hz, 1H), 9.62 (s, 1H), 8.36 (d, *J* = 3.1 Hz, 1H), 7.66-7.62 (m, 2H), 7.51-7.48 (m, 2H), 7.37 (d, *J* = 9.0 Hz, 1H), 7.15-6.82 (m, 13H), 3.57-3.53 (m, 4H), 2.35-2.23 (m, 4H), 1.86-1.80 (m, 4H), 1.63-1.59 (m, 4H), 1.45-1.41 (m, 4H).

(*m/z*): [M+H]+ calcd., 732.1; found, 735.2.

TANI-(PTAB)$_2$ (23)

22 (0.305 g, 0.42 mmol) was dissolved in DMF (12 mL) and triethylamine (>10 eq., 35 wt.% in ethanol, 1.17 mL) was added. The mixture was stirred until TLC analysis showed no starting material (100 % ethyl acetate). When the reaction was complete, the DMF solution was added dropwise to ice-cold diethyl ether (400 mL) and was left to fully precipitate overnight in the freezer. The suspension was then centrifuged and washed with further diethyl ether to remove any residual DMF. The residue was dried under vacuum before being dissolved in deionised water (250 mL). The solution was centrifuged to remove any water-insoluble impurities and the supernatant decanted and lyophilised to give the product **23** (55%).

^{1}H NMR (400 MHz, DMSO-d_6): δ 9.90 (s, 1H), 8.44 (s, 1H), 7.68-6.81 (m, 11H), 3.30-3.27 (m, 4H), 3.05 (s, 18H), 2.35-2.32 (m, 3H).

(*m/z*): [M-2Br]2+ calcd., 345.7; found, 345.7.

2.4.18 MA-TANI-PTAB from NH_2/NH_2 TANI

NH_2-TANI-C_6Br (24)

19 (1.00 g, 1.47 mmol) was dissolved in anhydrous THF (190 mL), under a nitrogen atmosphere and was cooled to 0 °C. Triethylamine was added (5 eq., 0.743 g), followed dropwise by a solution of 6-bromohexanoyl chloride (1 eq., 0.313 mg) in THF (10 mL). Once the addition was complete, the ice bath was removed, and the solution allowed to warm to room temperature. After reaction for 48 hours, the solvent was removed, and the residue dissolved in ethyl acetate. The solution was washed with HCl (1 M, 20 mL), NaOH (1 M, 20 mL) and brine (20 mL), before drying over $MgSO_4$ and removing the solvent to yield the mixture of crude products. The mono- and di-substituted products were separated by column chromatography (silica gel, 2:1 ethyl acetate:n-hexane) to yield **24** (13%) and **20** (26%).

24 ^{1}H NMR (400 MHz, $CDCl_3$): δ 7.60 (s, 1H), 7.42 (d, *J* = 9.2 Hz, 2H), 7.14-7.06 (m, 10H), 6.96-6.93 (m, 2H), 6.61-6.58 (m, 2H), 3.41-3.38 (m, 2H), 2.32-2.29 (m, 2H), 1.91-1.84 (m, 2H), 1.73-1.67 (m, 2H), 1.51-1.47 (m, 2H), 1.42-1.41 (m, 27H).

24 (*m/z*): [M+H]+ calcd., 858.3; found, 858.3; [M+Na]+ calcd., 880.3; found, 880.3.

MA-TANI-C_6Br (25)

24 (0.1 g, 0.12 mmol) was placed under nitrogen in an ice-bath and was dissolved in anhydrous THF (10 mL). Triethylamine (5 eq., 0.059 g) was added, followed dropwise by acryloyl chloride (1.2 eq., 0.013 g). The solution was allowed to warm to room temperature and was left to stir for 48 hrs. After the reaction was complete, the solvent was evaporated and the residue was dissolved in minimal ethyl acetate and washed with HCl (1 M, 40 mL), NaOH (1 M, 40 mL) and brine (40 mL). The organic layer was extracted, dried over $MgSO_4$ and the solvent was removed. The resulting powder was purified by dissolving in minimal ethyl acetate and precipitating in hexane.

^{1}H NMR spectroscopy showed that the acrylate had been successfully attached, however, mass spectrometry indicated that a halogen exchange had occurred.

^{1}H NMR (400 MHz, $CDCl_3$): δ 7.75-7.70 (m, 2H), 7.44-7.42 (m, 3H), 7.12-7.07 (m, 11H), 6.26 (s, 1H), 5.67 (s, 1H), 5.01 (s, 1H), 3.54-3.50 (m, 3H), 2.34-2.30 (m, 3H), 1.80-1.75 (m, 3H), 1.73-1.69 (m, 3H), 1.51-1.47 (m, 4H), 1.42-1.41 (m, 27H).

(*m/z*): [M -Br, +Cl, +Na]+ calcd., 890.4; found, 890.4; [M -Br, +Cl, +NEt_3]+ calcd., 968.5; found, 968.5.

MA-TANI-NH_2 (26)

19 (0.2 g, 0.29 mmol) was placed under nitrogen and dissolved in anhydrous THF (20 mL), before being placed in an ice bath. Triethylamine (5 eq., 0.148 g) was added, followed dropwise by acryloyl

chloride (1 eq., 0.026 g). The solution was allowed to warm to room temperature and left to stir for 48 hours. After the reaction was complete, the solvent was removed and the residue dissolved in ethyl acetate followed by washing with HCl (1 M, 15 mL), NaOH (1 M, 15 mL) and brine (15 mL). The organic phase was extracted, dried over $MgSO_4$ and the solvent removed. The crude product was purified by column chromatography (10:1 DCM/MeOH), yielding only the di-substituted product, **27**.

27 (*m/z*): [M -Me_3, +H]+ calcd., 734.3; found, 734.3; [M+H]+ calcd., 790.4; found, 790.4.

NH_2/CPh_2 TANI (28)

Activated molecular sieves (500 mg), **19** (0.1 g, 0.15 mmol) and benzophenone (0.9 eq., 0.24 g) were placed in a flask and were protected under nitrogen. Anhydrous toluene (20 mL) was added, and the mixture was refluxed at 110 °C for 48 hours. After cooling to room temperature, the mixture was filtered, and the molecular sieves were washed with THF until the solution was clear. The organic fractions were combined and concentrated. The resulting oil was dark green in colour, indicating **Boc**-deprotection and doping had occurred.

(*m/z*): [**28** -Boc_3, +H]+ calcd., 546.3; found, 546.3; [**29** -Boc_3, +H]+ calcd., 710.3; found, 710.3.

The above procedure was repeated at 70 °C for 24 hours to prevent **Boc**-decomposition due to temperature. However, although both mono- and di-substituted products were produced, **Boc**-deprotection and doping occurred. The deprotected **28** and **29** were separated by column chromatography (1:2 ethyl acetate/hexane).

28 ^{1}H NMR (400 MHz, $CDCl_3$): δ 7.73-7.70 (m, 2H), 7.46-7.36 (m, 3H), 7.30-7.28 (m, 3H), 7.16-7.14 (m, 2H), 6.99-6.80 (m, 7H), 6.75-6.73 (m, 2H), 6.66-6.63 (m, 4H).

28 (*m/z*): [M -**Boc**$_3$, +H]+ calcd., 546.3; found, 546.3.

29 ^{1}H NMR (400 MHz, $CDCl_3$): δ 7.73-7.71 (m, 4H), 7.44-7.37 (m, 6H) 7.31-7.28 (m, 5H), 7.16-7.14 (m, 5H), 7.00-6.65 (m, 16H).

29 (*m/z*): [M -**Boc**$_3$, +H]+ calcd., 710.3; found 710.3.

The reaction temperature was further lowered to 60 °C, however TLC analysis after 48 hours showed that no reaction had occurred.

The above procedure was also repeated at 70 °C without the use of activated molecular sieves, to prevent **Boc**-decomposition. However, TLC analysis after 4 days indicated no reaction had occurred.

MA-C_6-TANI-C_6-Br (30)

20 (0.1 g, 0.01 mmol) and sodium acrylate (5 eq., 0.045 g) were dissolved in DMSO (10 mL) and were stirred at room temperature overnight. After the reaction completion was confirmed by TLC (1:1

petroleum ether/ethyl acetate), the reaction mixture was poured into deionised water (70 mL) causing a white precipitate to form. The precipitate was collected by centrifugation and was washed with water (3 x 25 mL), before drying overnight under vacuum.

Mass spectrometry showed weak peaks for both mono- and di-substituted products (**30** and **31**).

(*m/z*): [**31**+H]+ calcd., 1018.5; found, 1018.5; [**30**+H]+ calcd., 1026.4; found, 1026.4; [**31**+Na]+ calcd., 1040.5; found, 1040.5; [**30**+Na]+ calcd., 1048.4; found, 1048.4; [**31**+K]+ calcd., 1056.5; found, 1056.5; [**30**+K]+ calcd., 1064.4; found, 1064.4.

2.4.19 MA-TANI-PTAB from TANI-CPh_2 (5)

Br-TANI-CPh_2 (32)

5 (0.1 g, 0.12 mmol) was dissolved in dichloromethane (10 mL) and tetra-*n*-butylammonium tribromide (0.75 eq., 0.043 g) was added. The mixture was stirred at room temperature for 24 hours before sodium sulphite (aq. 22 %, 1 mL) was added. The mixture was stirred for a further 30 minutes before NaOH (1 M, 1 mL) was added. The mixture was separated, and the organic phase was washed with water (3 x 5 mL), followed by drying over $MgSO_4$. ^{1}H NMR of the product indicated no reaction had occurred.

The above procedure was repeated using THF in place of dichloromethane and heating to 40 °C. After reaction for 24 hours, the reaction was cooled to room temperature before sodium sulphite (aq. 22%, 1 mL) was added. The mixture was stirred for 30 minutes before NaOH (1 M, 1 mL) was added. The mixture was separated, and the aqueous phase was washed with water (3 x 5 mL), followed by drying over $MgSO_4$. The product was purified by column chromatography (1:1 hexane/ethyl acetate), yielding a benzophenone-deprotected **32.**

^{1}H NMR (400 MHz, DMSO-d_6): δ 7.36-7.32 (m, 2H), 7.22-7.12 (m, 12H), 6.93 (dd, *J* = 8.7, 2.3 Hz, 1H), 6.74 (d, *J* = 8.6 Hz, 1H), 5.35 (s, 2H), 1.36-1.35 (m, 27H).

(*m/z*): [M -CPh_2, +Br, +H]+ calcd., 577.1; found, 579.1; [M -CPh_2, +Br, +Na]+ calcd., 764.2; found, 769.3.

I-TANI-CPh_2 (33)

5 (0.1 g, 0.12 mmol) was dissolved in dioxane (5 mL) and pyridine (5 mL) and the mixture was cooled to 0 °C. Iodine (3 eq., 91 mg) was added and the mixture was stirred for 5 hours, after which the ice bath was removed. The solution was stirred for a further hour at room temperature. A saturated solution of sodium thiosulfate was added until the solution was no longer brown. The product was extracted with dichloromethane and was washed with water. After drying, the product was filtered through a silica plug using THF before drying. ^{1}H NMR spectroscopy indicated no reaction had occurred.

2.4.20 MA-11-2-TANI-PTAB from MA-11-2 (35)

The synthesis of **MA-11-2-11-MA** (**36**) and its precursors was developed by Yang Li and colleagues.[48] 11-Bromoundecylmethacrylate (**34**) was synthesised for this work, as well as being donated by Yang Li (Jilin University, China) and Thomas Bott (University of Bristol). **MA-11-2** (**35**) was prepared by Yang Li, while **MA-11-2-11-MA** (**36**) was prepared by both Yang Li and Thomas Bott.

11-Bromoundecylmethacrylate (34)

11-Bromo-1-undecanol (0.3 g, 1.19 mmol) and 4-methoxyphenol (trace) were placed under nitrogen and dissolved in anhydrous THF (15 mL). Triethylamine (1.25 eq., 0.151 g) was added, followed dropwise by methacryloyl chloride (1.2 eq., 0.15 g). The reaction mixture was stirred for 24 hours at room temperature. After the reaction was complete, the solvent was removed and the residue dissolved in ethyl acetate and washed with HCl (1 M, 15 mL), NaOH (1 M, 15 mL) and brine (15 mL). The organic layer was extracted, dried over $MgSO_4$ and the solvent removed, yielding **34** (40%).

^{1}H NMR (400 MHz, $CDCl_3$): δ 6.09 (m, 1H), 5.54 (m, 1H), 4.13 (t, *J* = 6.6 Hz, 2H), 3.40 (t, *J* = 7.0 Hz, 2H), 1.94 (m, 3H), 1.89-1.81 (m, 2H), 1.70-1.63 (m, 2H), 1.44-1.28 (m, 16H).

(*m/z*): [M+Na]+ calcd., 341.1; found, 341.1.

MA-11-2 (35)

In a typical procedure, **34**, *N,N,N',N'*-tetramethylethylenediamine (1.25 eq.) and 4-methoxyphenol (trace) were dissolved in THF under a nitrogen atmosphere. The reaction mixture was stirred for 48 hours at 45 °C before the solvent was removed and the residue was washed with diethyl ether to remove excess reactants. The product (**35**) was further purified by elution with THF, yielding a white solid.

^{1}H NMR (400 MHz, $CDCl_3$): δ 6.09-6.08 (m, 1H), 5.55-5.54 (m, 1H), 4.13 (t, *J* = 6.8 Hz, 2H), 3.83-3.80 (m, 2H), 3.63-3.58 (m, 2H), 3.44 (s, 6H), 2.77 (t, *J* = 5.9 Hz, 2H), 2.29 (s, 6H), 1.94-1.93 (m, 3H), 1.75-1.72 (m, 2H), 1.66-1.63 (m, 2H), 1.36-1.28 (m, 14H).

(*m/z*): [M-Br]+ calcd., 355.3; found, 355.3.

MA-11-2-11-MA (36)

In a typical procedure, **34** (3 eq.), *N,N,N',N'*-tetramethylethylenediamine and 4-methoxyphenol (trace) were dissolved in DMF under a nitrogen atmosphere. The mixture was heated at 80 °C for 48 hours, before the solvent was removed and the residue was washed with THF to remove excess reactants and any **35** that had been produced. Further purification was carried out by recrystallisation from water, yielding **36**.

^{1}H NMR (400 MHz, $CDCl_3$): δ 6.09-6.08 (m, 2H), 5.55-5.54 (m, 2H), 4.75 (s, 4H), 4.13 (t, *J* = 6.8 Hz, 4H), 3.73-3.69 (m, 4H), 3.51 (s, 12H), 1.94-1.93 (m, 6H), 1.84-1.80 (m, 4H), 1.70-1.63 (m, 4H), 1.37-1.27 (m, 28H).

(*m/z*): [M-2Br]2+ calcd., 297.3; found, 297.3; [M-Br]+ calcd., 673.5; found, 673.5.

EB MA-11-2-TANI-PTAB (37)

9 (0.03 g, 0.05 mmol), **35** (1.25 eq., 0.03 g) and 4-methoxyphenol (trace) were dissolved in DMF (2 mL) under a nitrogen atmosphere. After reaction at 80 °C for 48 hours, the solvent was removed, and the residue was washed with THF, before attempted dissolution in chloroform, DMSO, acetonitrile, water and acetone. The residue formed an insoluble blue film that was not identified.

Boc-MA-11-2-TANI-PTAB (38)

7 (0.047 g, 0.06 mmol), **35** (1.25 eq., 0.03 g) and 4-methoxyphenol (trace) were dissolved in DMF (2 mL) under a nitrogen atmosphere. After reaction at 60 °C for 48 hours, the solvent was removed, and the residue was washed with THF and water. Mass spectrometry showed that a mixture of product (**38**) and starting material (**35**) was present.

(*m/z*): [M-2Br]2+ calcd., 559.4; found, 559.5, [**35**-Br]+ calcd., 355.3; found, 355.4.

NMe_3-2-TANI-PTAB (39)

7 (0.07 g, 0.083 mmol) and tetramethylethylenediamine (100 eq., 1.24 mL) were dissolved in THF (3 mL) under a nitrogen atmosphere. After reaction at 45 °C for 24 hours, the solvent was removed by evaporation and the obtained residue was washed with diethyl ether (30 mL). The remaining solid was then dissolved in minimal acetone and was added dropwise to stirring hexane, causing a white precipitate to form. The precipitate was collected and dried yielding **39** (75%).

^{1}H NMR (400 MHz, $CDCl_3$): δ 9.93 (s, 1H), 7.82 (d, *J* = 9.0 Hz, 2H), 7.31-7.27 (m, 2H), 7.18-7.06 (m, 13H), 3.57-3.50 (m, 4H), 3.21 (s, 6H), 2.65 (t, *J* = 5.3 Hz, 2H), 2.58 (t, *J* = 7.2 Hz, 2H), 2.23 (s, 6H), 1.80-1.77 (m, 4H), 1.44-1.38 (m, 30H), 1.29-1.24 (m, 4H).

(*m/z*): [M]+ calcd., 879.5; found, 879.5.

Boc-MA-11-2-TANI-PTAB (38)

39 (0.05 g, 0.05 mmol), **34** (1.5 eq., 0.045 g) and 4-methoxyphenol (trace) were dissolved in DMF (2 mL) under a nitrogen atmosphere. The mixture was heated at 65 °C for 1 week. After this time, the solvent was removed by evaporation and the residue washed with diethyl ether. The product was then dissolved in minimal acetone before being added dropwise to stirring hexane, forming a white precipitate. The precipitate was collected and dried, before analysis by mass spectrometry, which showed a mixture of **38** and unreacted **39**.

(*m/z*): [**38**]2+ calcd., 559.4; found, 559.4; [**39**]+ calcd., 879.5; found, 879.5; [**38**+Br-]+ calcd., 1197.7; found, 1199.7.

NMe-2-NMe-TANI (40)

7 (0.1 g, 0.12 mmol), *N-N'*-dimethylethylenediamine (10 eq., 0.104 g) and triethylamine (1.5 eq., 0.018 g) were dissolved in THF (6 mL) under a nitrogen atmosphere. After reaction at 45 °C for 48 hours the solvent was removed, and the residue was washed with water (10 x 10 mL). The crude product was stirred in hexane for 1 hour. The solid product was collected and dried in a vacuum, yielding **40** as a white powder (35%).

^{1}H NMR (400 MHz, $CDCl_3$): δ 8.46 (s, 1H), 7.58-7.56 (m, 2H), 7.31-7.27 (m, 2H), 7.19-7.09 (m 14H), 2.85-2.82 (m, 2H), 2.64-2.61 (m, 2H), 2.55 (s, 3H), 2.41-2.36 (m, 4H), 2.21 (3, 3H), 1.74-1.67 (m 2H), 1.54-1.49 (m, 3H), 1.43-1.36 (m, 28H).

(*m/z*): [M+H]+ calcd., 851.5; found, 851.5.

MA-11-2-NMe-TANI (41)

40 (50 mg), **34** (1.5 eq., 18 mg) and 4-methoxyphenol (trace) were dissolved in DMF (2 mL) under a nitrogen atmosphere. The mixture was heated at 65 °C for 1 week, after which the solvent was removed by evaporation and the residue was washed with water (5 x 10 mL). The product was finally purified by stirring in hexane for 48 hrs. Mass spectrometry showed that **41** had been prepared, however it was contaminated with unidentified impurities that could not be removed by recrystallisation or column chromatography.

(*m/z*): [M+H]+ calcd., 1089.7; found, 1089.7.

2.5 REFERENCES

1. Lu, F. L., Wudl, F., Nowak, M. & Heeger, A. J. Phenyl-Capped Octaaniline (COA): An Excellent Model for Polyaniline. *J. Am. Chem. Soc.* **108**, 8311–8313 (1986).

2. Payerne, R., Rannou, P., Djurado, D., Genoud, F. & Travers, J. P. New insight on local electronic transport properties of poly(aniline): A comparative study of oligo(aniline) model compound and polymer using spin dynamics techniques. *Synth. Met.* **152**, 193–196 (2005).

3. Muller, K. & Wegner, G. *Electronic Materials: The Oligomer Approach*. (Wiley-VCH, 1998).

4. Shacklette, L. W., Wolf, J. F., Gould, S. & Baughman, R. H. Structure and properties of polyaniline as modeled by single-crystal oligomers. *J. Chem. Phys.* **88**, 3955–3961 (1988).

5. Wei, Z. & Faul, C. F. J. Aniline oligomers - Architecture, function and new opportunities for nanostructured materials. *Macromol. Rapid Commun.* **29**, 280–292 (2008).

6. Kang, E., Neoh, K. G. & Tan, K. L. Polyaniline: A polymer with many interesting intrinsic redox states. *Prog. Polym. Sci.* **23**, 277–324 (1998).

7. Masters, J. G., Sun, Y., MacDiarmid, A. G. & Epstein, A. J. Polyaniline: Allowed oxidation states. *Synth. Met.* **41**, 715–718 (1991).

8. Ray, A. *et al.* Polyaniline: Doping, structure and derivatives. *Synth. Met.* **29**, 141–150 (1989).

9. Hatchett, D. W., Josowicz, M. & Janata, J. Acid Doping of Polyaniline : Spectroscopic and Electrochemical Studies. *J. Phys. Chem. B* **103**, 10992–10998 (1999).

10. Udeh, C. U., Fey, N. & Faul, C. F. J. Functional block-like structures from electroactive tetra(aniline) oligomers. *J. Mater. Chem.* **21**, 18137–18153 (2011).

11. Kim, H., Jeong, S.-M. & Park, J.-W. Electrical switching between vesicles and micelles via redox-responsive self-assembly of amphiphilic rod-coils. *J. Am. Chem. Soc.* **133**, 5206–5209 (2011).

12. Cao, L., Gong, C. & Yang, J. A Solution-Processable (Tetraaniline- b - Polyethylene Glycol) 3 Star-Shaped Rod-Coil Block Copolymer with Enhanced Electrochromic Properties. *Macromol. Rapid Commun.* **37**, 343–350 (2016).

13. Khalily, M. A. *et al.* Fabrication of Supramolecular n/p-Nanowires via Coassembly of Oppositely Charged Peptide-Chromophore Systems in Aqueous Media. *ACS Nano* **11**, 6881–6892 (2017).

14. Wu, Y. *et al.* New strategy for controlled release of drugs. Potential pinpoint targeting with multiresponsive tetraaniline diblock polymer vesicles: Site-directed burst release with voltage.

ACS Appl. Mater. Interfaces **6**, 1470–1480 (2014).

15. Bell, O. A. *et al.* Self-Assembly of a Functional Oligo(Aniline)-Based Amphiphile into Helical Conductive Nanowires. *J. Am. Chem. Soc.* **137**, 14288–14294 (2015).

16. Alotaibi, M. M. *et al.* Synthesis and tunable self-assembly of electroactive bolaamphiphiles based on oligo(aniline)s. *Submitted*

17. Alotaibi, M. M. *et al.* Tunable self-assembled nanostructures from electroactive amphiphiles. *Prep.*

18. Chen, R. & Benicewicz, B. C. Preparation and properties of poly(methacrylamide)s containing oligoaniline side chains. *Macromolecules* **36**, 6333–6339 (2003).

19. Hu, Y. *et al.* Toward Direct Laser Writing of Actively Tuneable 3D Photonic Crystals. *Adv. Opt. Mater.* **5**, 1600458 (2017).

20. Surwade, S. P., Agnihotra, S. R., Dua, V., Manohar, N. & Jain, S. Catalyst-Free Synthesis of Oligoanilines and Polyaniline Nanofibers Using H2O2. *J. Am. Chem. Soc.* **131**, 12528–12529 (2009).

21. Sadighi, J. P., Singer, R. A. & Buchwald, S. L. Palladium-Catalyzed Synthesis of Monodisperse, Controlled-Length, and Functionalized Oligoanilines. *J. Am. Chem. Soc.* **120**, 4960–4976 (1998).

22. Rawal, V. H. & Cava, M. P. Thermolytic Removal of t-Butyloxycarbonyl (BOC) Protecting Group on Indoles and Pyrroles. *Tetrahedron Lett.* **26**, 6141–6142 (1985).

23. Choy, J., Jaime-Figueroa, S., Jiang, L. & Wagner, P. Novel Practical Deprotection of N-Boc Compounds Using Fluorinated Alcohols. *Synth. Commun.* **38**, 3840–3853 (2008).

24. Shao, Z. *et al.* Delineating poly(aniline) redox chemistry by using tailored oligo(aryleneamine)s: Towards oligo(aniline)-based organic semiconductors with tunable optoelectronic properties. *Chem. - A Eur. J.* **17**, 12512–12521 (2011).

25. Singer, R. A., Sadighi, J. P. & Buchwald, S. L. A general synthesis of end-functionalized oligoanilines via palladium-catalyzed amination. *J. Am. Chem. Soc.* **120**, 213–214 (1998).

26. Surry, D. S. & Buchwald, S. L. Biaryl Phosphane Ligands in Palladium-Catalyzed Amination. *Angew. Chemie Int. Ed.* **47**, 6338–6361 (2008).

27. Schlummer, B. & Scholz, U. Palladium-Catalyzed C-N and C-O Coupling – A Practical Guide from an Industrial Vantage Point. *Adv. Synth. Catal.* **346**, 1599–1626 (2004).

28. Lyu, W. *et al.* An addressable packing parameter approach for reversibly tuning the assembly

of oligo(aniline)-based supra-amphiphiles. *Chem. Sci.* **9**, 4392–4401 (2018).

29. MacDiarmid, A. G., Zhou, Y. & Feng, J. Oligomers and isomers: new horizons in poly-anilines. *Synth. Met.* **100**, 131–140 (1999).

30. de Albuquerque, J. E., Mattoso, L. H. C., Faria, R. M., Masters, J. G. & MacDiarmid, A. G. Study of the interconversion of polyaniline oxidation states by optical absorption spectroscopy. *Synth. Met.* **146**, 1–10 (2004).

31. Xia, Y., Wiesinger, J. M., MacDiarmid, A. G. & Epstein, A. J. Camphorsulfonic Acid Fully Doped Polyaniline Emeraldine Salt: Conformations in Different Solvents Studied by an Ultraviolet/Visible/Near-Infrared Spectroscopic Method. *Chem. Mater.* **7**, 443–445 (1995).

32. Mills, B. M. *et al.* Tipping the polaron-bipolaron balance: concentration and spin effects in doped oligo(aniline)s observed by UV-vis-NIR and TD-DFT. *Mol. Syst. Des. Eng.* **4**, 103–109 (2019).

33. Watanabe, K. Personal Communication - Faul Research Group.

34. Alotaibi, M. M. Towards Aqueous Nanostructures Based on Oligo(aniline)s. (University of Bristol, 2019).

35. Kulszewicz-Bajer, I., Rozalska, I. & Kurylek, M. Synthesis and spectroscopic properties of aniline tetramers. Comparative studies. *New. J. Chem.* **28**, 669–675 (2004).

36. Eelkema, R. & Anderson, H. L. Synthesis of End-Functionalized Polyanilines. *Macrolecules* **41**, 9930–9933 (2008).

37. Alotaibi, M. *et al.* Synthesis and tunable self-assembly of electroactive bolaamphiphiles based on oligo(aniline)s. *Prep.*

38. Bell, O. A. Synthesis, self-assembly and applications of functional amphiphiles based on oligo(aniline). (University of Bristol, 2015).

39. Hahn, R. C. Homogeneous Nucleophile Exchange. 1. Simple, High-Yield Synthesis of Some Heterodihalides. *J. Org. Chem.* **53**, 1331–1333 (1988).

40. Abdel-Rahem, R. The influence of hydrophobic counterions on micellar growth of ionic surfactants. *Adv. Colloid Interface Sci.* **141**, 24–36 (2008).

41. Asakura, N., Hirokane, T., Hoshida, H. & Yamada, H. Molecular sieves 5A as an acidic reagent: The discovery and applications. *Tetrahedron Lett.* **52**, 534–537 (2011).

42. Wang, X. J. *et al.* Dual-responsive vesicles formed by an amphiphile containing two tetrathiafulvalene units in aqueous solution. *Org. Biomol. Chem.* **14**, 65–68 (2016).

43. Han, G., Tamaki, M. & Hruby, V. J. Fast , efficient and selective deprotection of the tert - butoxycarbonyl (Boc) group using HCl / dioxane (4 M). *J. Pept. Res.* **58**, 338–341 (2001).

44. Hartwig, S., Nguyen, M. M. & Hecht, S. Exponential growth of functional poly(glutamic acid) dendrimers with variable stereochemistry. *Polym. Chem.* **1**, 69–71 (2010).

45. Hu, Y. Functional 3D Architectures Based on Oligo(aniline)s. (University of Bristol, 2016).

46. Quan, Z. J., Xia, H. D., Zhang, Z., Da, Y. X. & Wang, X. C. Ligand-free CuTC-catalyzed N-arylation of amides, anilines and 4-aminoantipyrine: Synthesis of N-arylacrylamides, 4-amido-N-phenylbenzamides and 4-amino(N-phenyl)antipyrenes. *Appl. Organomet. Chem.* **28**, 81–85 (2014).

47. Monnereau, C., Blart, E. & Odobel, F. A cheap and efficient method for selective para - iodination of aniline derivatives. *Tetrahedron Lett.* **46**, 5421–5423 (2005).

48. Li, Y. *et al.* Two-dimensional polymers with versatile functionalities via gemini monomers. *Sci. Adv.* **5**, eaaw9120 (2019).

49. Semsarilar, M., Ladmiral, V., Blanazs, A. & Armes, S. P. Cationic Polyelectrolyte-Stabilized Nanoparticles via RAFT Aqueous Dispersion Polymerization. *Langmuir* **29**, 7416–7424 (2013).

50. Stanley, C. E. Development of high-throughput technologies for the study of drug-membrane interactions. (University of Bristol, 2011).

51. Townsend, E. J. Synthesis and Investigations of Polymerisable Oligo(aniline)s in Liquid-Crystalline Media. (University of Bristol, 2016).

3 TEMPLATED SELF-ASSEMBLY OF TANI-PTAB IN LIPID BICONTINUOUS CUBIC PHASES

3.1 INTRODUCTION

Self-assembly is a valuable tool to prepare soft nanostructures, using a bottom-up approach to control the design of materials over multiple length scales. This approach can allow for tailoring of self-assembled constructs with desirable characteristics, such as improved conductivity,[1,2] self-healing,[3] self-regulation and emergent self-replication,[4] or switchable structures,[5–7] expanding their potential applications to new fields.

The self-assembly of lipids is an area of particular interest, as they are capable of forming well-defined 1-, 2- and 3-D structures in aqueous media, depending on the chosen lipid and external conditions.[8] Among such 3-D mesophases are the inverse bicontinuous cubic phases (including the primitive (*Im3m*), double diamond (*Pn3m*) and gyroid (*Ia3d*)), which all consist of a continuous lipid bilayer surrounded by two water channel networks. The diameters of the water channels are highly uniform, and the dimensions can be readily tuned by controlling the temperature or by the incorporation of additives.[9,10] Therefore, such materials have attracted attention for many applications, such as biosensors or biofuels,[11–13] substrates for the crystallisation of membrane proteins[10,14,15] or as delivery mechanisms for hydrophobic drugs.[16–18]

For these applications, control over the structure is of the utmost importance, as material properties differ noticeably between mesophases. For example, the release of drugs from lipidic mesophases is complex and highly dependent on the lipid structure, particularly for hydrophilic molecules which are mainly contained in the water channels.[19] Phan et al. (2011) conducted a study of the release rates for four lipidic mesophases and found that the cubic phase was significantly faster than the inverse hexagonal phase, micellar cubic phase and inverse micelles, reducing its suitability for sustained drug release.[20] However, this difference in release rates has been targeted for controlled release systems. Using triggers such as pH,[21–23] light[24–26] or electromagnetic energy,[16,27] the mesophase can be switched from a slow release to a fast release system, allowing for targeted delivery of the payload.

Control over the mesophase dimensions is also valuable for other applications. The ability to swell cubic phases can allow for the crystallization of large proteins, which would otherwise be excluded from the mesophase.[10] Meanwhile, the fine-tuning of water channel dimensions in biosensor devices allows researchers to exclude contaminants or increase the selectivity of the sensor.[12]

3-D cubic phases are also used as templates to prepare other well-defined nanostructures, for applications such as electronic devices. The well-ordered, interconnected, porous nature of cubic

phases, with easily controlled aqueous channel diameters and lattice parameters, makes them highly attractive for the growth of conductive nanowires. While much research has focused on the preparation of metal nanowires,[28–30] researchers have also utilized cubic phases to control the growth of conjugated polymers.[31,32]

One polymer that has benefitted from templating is poly(aniline) (**PANI**).[33–35] **PANI** is a conjugated polymer that can exist in multiple oxidation states, including a conductive state that is accessed by acid doping.[36] The conductivity of **PANI** is highly dependent on the material order, as defects and breaks in conjugation can negatively impact charge transport through the polymer network.[37] Indeed, difficulties in preparing high purity and crystalline **PANI** have led many researchers to explore oligomers of the polymer, including tetra(aniline) (**TANI**).[38] **TANI** retains the attractive oxidative and conductive properties of **PANI**, while being easier to prepare. Investigations into the preparation of highly ordered **TANI**-based materials by self-assembly techniques have demonstrated that control over the nanostructure dramatically improves the material properties.[39,40]

TANI-PTAB is a **TANI-**derived amphiphile that self-assembles in water into nanofibers when in the emeraldine base (EB) state.[41] Interestingly, the self-assembly behaviour can be tuned by the addition of acids, transitioning to vesicles or cylindrical micelles when doped to the emeraldine salt (ES) state, owing to a change in packing parameter (*pp*).[42] This transition is fully reversible, reverting to nanofibers with the addition of a base.

While the formation of such 1-D or 2-D structures is interesting, some applications for **TANI-PTAB** may benefit from additional order or from the formation of 3-D structures. Oligo(aniline)s typically have lower conductivities than poly(aniline), however, it has been theorised that charge transport could be improved by increasing the crystallinity of the oligomer, eventually surpassing the parent polymer.[43] Additionally, porous materials prepared by the templating of **TANI-PTAB** in lipidic cubic phases could be used in applications such as sensing or CO_2 capture and conversion, following the example of conjugated microporous polymers prepared from aniline derivatives.[44–46]

The incorporation of **TANI-PTAB** into lipidic cubic phases has two-fold benefits. Firstly, the change in oxidation state upon the addition of an acid or base would introduce a switchable element to the mesophase, allowing for the structure and phase dimensions to be readily controlled. Secondly, the highly ordered cubic phases could be used as a template to impart further order to **TANI-PTAB** assemblies, expanding their potential applications.

3.2 RESULTS AND DISCUSSION

3.2.1 Preparation of MO sponge and cubic phases

Cubic phases containing **TANI-**amphiphiles were prepared via dilution of the sponge phase, which was accessed with the addition of pentaerythritol propoxylate (**PPO**). Additives such as **PPO** can be used to access a wide range of mesophases with monoolein (**MO**), including the disordered sponge phase, and can be used to tune the phase dimensions such as the lattice parameters.[10] The sponge phase can be considered as a disordered cubic phase, containing short-range order but long-range disorder.[47] Unlike the stiff cubic phase, the sponge phase is less viscous and flows like a liquid, allowing it to be more easily manipulated. Cherezov (2006) investigated a selection of additives and their effects on the phase behaviour of **MO**.[10] Samples were prepared using a mixture of 40 % (w/w) lipid and 60 % (w/w) lyotrope, where the lyotrope consisted of water and **PPO**. Lyotrope mixtures containing less than 10 % (v/v) **PPO** resulted in the formation of the *Pm3m* phase. Meanwhile, mixtures containing 12-22 % (v/v) **PPO** formed the sponge phase, while higher concentrations of **PPO** formed a lamellar phase.

In this work, all sponge phases were formed using a mixture of 40 % (w/w) **MO** and 60 % (w/w) lyotrope, where the lyotrope was 20 % (v/v) **PPO**. 40 µL of the sponge mixture was pipetted into a capillary tube and diluted with 40 µL of deionised water under centrifugation. After dilution, the lyotrope contained 7.5 % (v/v) **PPO**, resulting in a transition to the *Pn3m* phase in the absence of any other factors. Order, and any orientation displayed by the mesophase was determined by small-angle X-ray scattering (SAXS).

The type of cubic phase formed by **MO** containing **PPO**, with and without **TANI-**amphiphiles, was identified by the positions of the Bragg peaks in the 1-D scattering patterns (i.e., Figure 3.1c). The ratios of the peak positions on the q-scale have values that depend on the mesophase. Typical cubic phases formed by **MO** are the *Pm3m* phase and the *Im3m* phase, which have peak ratios of √2, √3, √4, √6, √8, √9 and √2, √4, √6, √8, √10, √12, respectively.[48] The lattice parameters for the prepared cubic phases were calculated in the following manner. The q values ($Å^{-1}$) for each peak were converted to d values (Å) using the following equation:

$$d = \frac{2\pi}{q}$$

The d values for each peak were then multiplied by the respective peak ratio to get the d-spacings, from which an average was taken for the lattice parameter of the mesophase. An example calculation for EB **TANI-PTAB** (2 mM) in **MO** with **PPO** is given in Table B.2 of Appendix B.

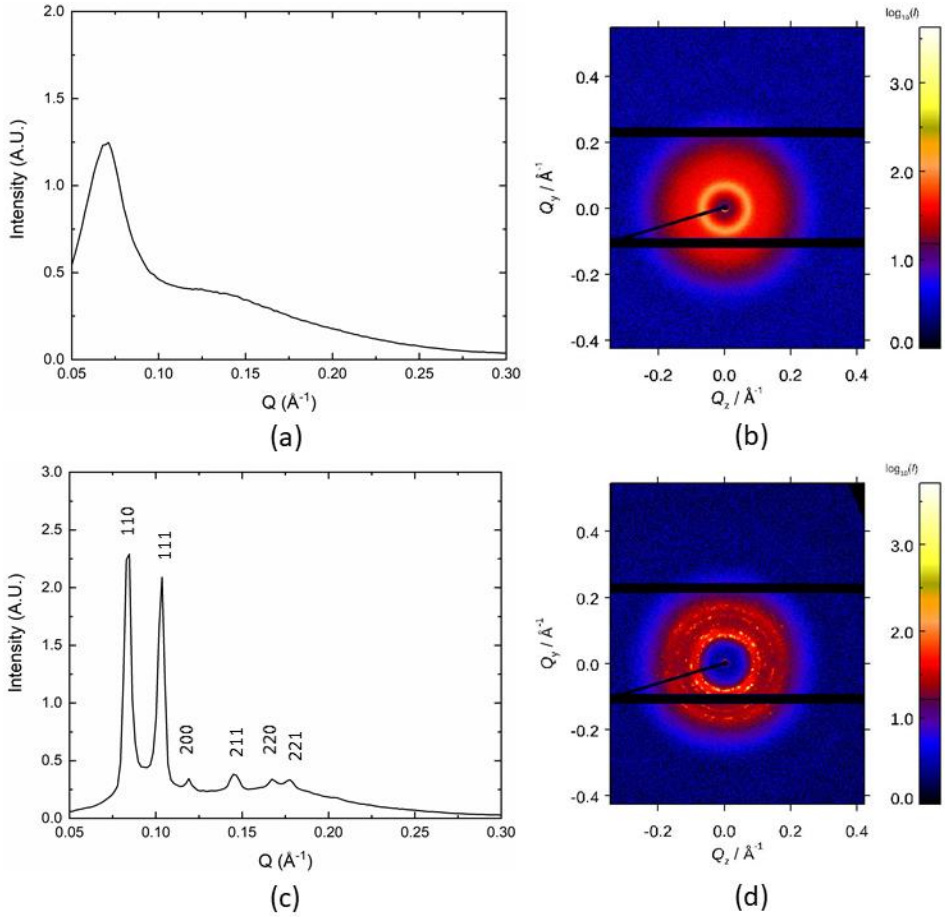

*Figure 3.1. 1-D and 2-D SAXS patterns for the **MO**/**PPO** (a, b) sponge phase and (c, d) Pn3m phase.*

The 1-D and 2-D scattering patterns for *Pn3m* and sponge phases prepared with the above method are given in Figure 3.1. The correlation length for the disordered sponge phase was 9.1 nm, while the lattice parameter for the cubic phase was 10.6 nm. The latter value was typical of **MO** *Pn3m* phases formed with the above method, as can be seen from Table B.1 in Appendix B, which shows the average calculated lattice parameter over six samples was 10.75 nm.

The preparation of cubic phases via the sponge phase may appear to be a circuitous route, however, initial experiments in this project demonstrated that this was the most efficient and reproducible method to produce **TANI-PTAB**-containing mesophases. An alternative method was briefly explored, where **TANI-PTAB** and **MO** were mixed in ethanol and dried together to form a film that was hydrated to produce cubic phases. This method will be discussed in greater detail in Section 3.2.7, however, the samples required very long equilibration times (> 1 month) to form stable phases and the results were inconsistent. Meanwhile, the use of **PPO** allowed for reproducible cubic phases to be prepared within 48 hours.

In preparing cubic phases by dilution of the sponge phase under centrifugation, it was noted that the method occasionally produced highly aligned phases. The 2-D scattering patterns of aligned cubic

phases prepared with just **MO** and **PPO** or **MO**, **PPO** and EB **TANI-PTAB** are given in Figure 3.2b and d, respectively, and show well-defined diffraction spots, indicating that the samples were highly orientated. Both aligned phases showed larger lattice parameters in comparison to more randomly oriented cubic phases, which suggested that alignment causes a slight swelling of the mesophase.

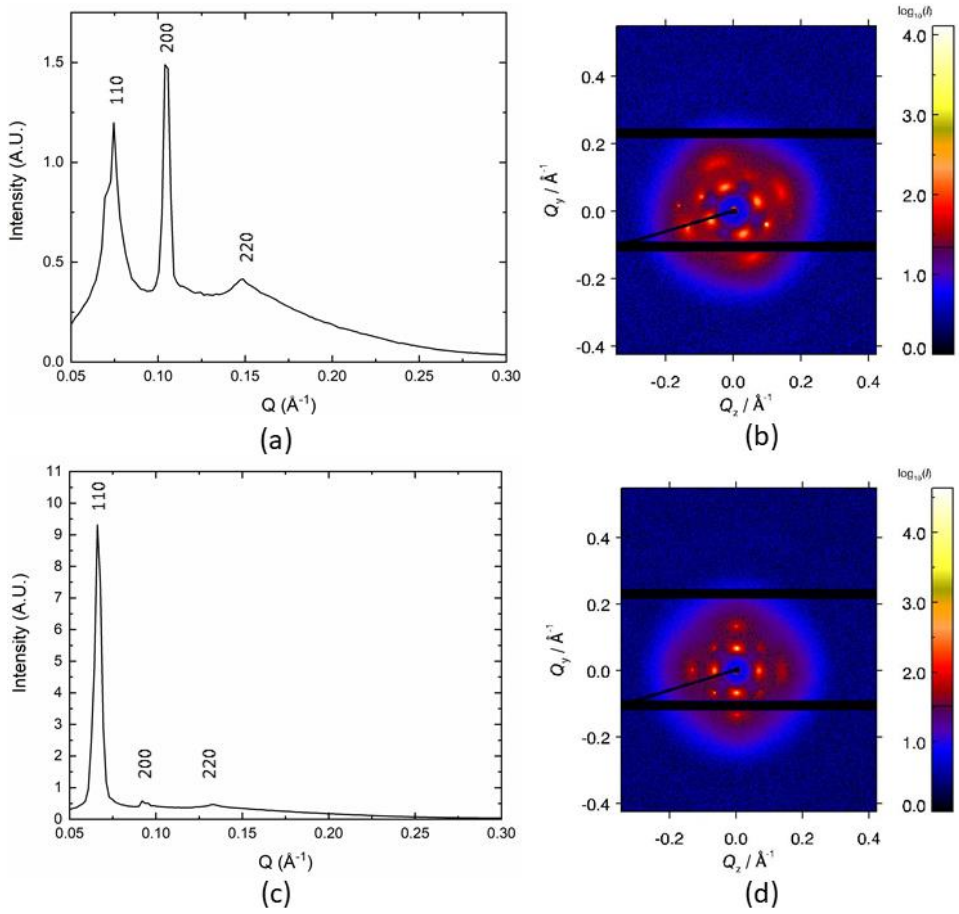

*Figure 3.2. 1-D and 2-D scattering patterns for (a, b) aligned Pn3m phase prepared with **MO/PPO**, calculated lattice parameter: 12.0 nm (c, d) aligned Pn3m phase prepared with EB **TANI-PTAB** (0.8 mM) in **MO/PPO**, calculated lattice parameter: 13.4 nm.*

The potential to add further order to **MO** cubic phases by alignment with rotational shear was briefly considered in order to improve their properties as templates. The aim of templating is to use a well-defined 3-D structure to impart order over multiple length scales to less ordered materials such as 2-D nanofibers, which may have short-range orientation but be macroscopically disordered. The ideal template would be single crystalline or monodomain, as the presence of internal domain boundaries in polydomain materials can negatively impact the template's diffusion and transport properties, conductivity, and mechanical properties. This holds true when using lipids as a template[28,49] or indeed as a material itself for applications such as size selective molecular sieves and catalysis[50,51] or electronic devices[28,52] where the diffusion, transport and mechanical properties play a vital role.

A few methods of lipid alignment have been described in the literature, including the dilution of the sponge to the cubic phase by shear flow or by simple diffusion.[53,54] However, while those methods demonstrated an aligned cubic phase could be repeatably produced, samples prepared with our method of dilution under centrifugation showed alignment in less than 1 in 10 samples. Indeed, most cubic phases were randomly oriented, and it was not clear what factors influenced alignment as all samples were prepared following the same procedure.

As alignment could not be predicted or controlled, any long-range order was largely ignored in this work. While a highly oriented cubic phase would have been valuable, had the scope of this project focused solely on templating, for most of the investigations carried out in this work alignment was not necessary. Therefore, no further analysis of long-range order and orientation was performed.

3.2.2 Spectroscopic investigations of TANI-PTAB in MO/PPO

The UV-Vis/NIR absorption spectra of EB **TANI-PTAB** in water and with **PPO** or **PPO**/**MO** were collected to determine whether the oxidation state of the amphiphile was affected by the different additives. The sample preparation methods for each mixture are given in Chapter 2, Section 2.4.4. Samples were analysed in the sponge phase rather than the cubic phase, as the sponge phase was more easily prepared and loaded into a cuvette. The same ratios of lipid-to-lyotrope and **PPO**-to-water/**TANI-PTAB** were used in the UV-Vis spectroscopy experiments as were used for SAXS measurements. **MO** and a **TANI-PTAB**/**PPO**/water mixture were stirred until they formed a homogenous sponge phase that was analysed as prepared.

The UV-Vis/NIR absorption spectra for EB **TANI-PTAB** (1 mM) in water, with **PPO**, and with **PPO** and **MO** are shown in Figure 3.3. **TANI-PTAB** in water showed peaks characteristic of the EB state at approximately 300 and 585 nm, which correspond to the $\pi \rightarrow \pi^*$ transition and molecular exciton transition, respectively.[55] A shoulder at 490 nm was also present and was attributed to aggregation of amphiphile in solution.[56]

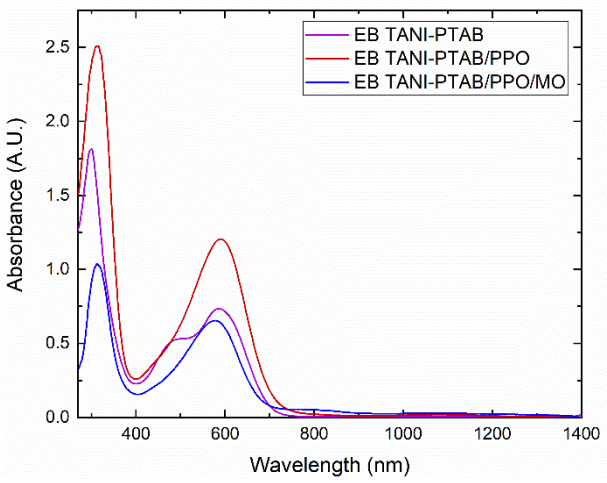

*Figure 3.3. UV-Vis/NIR absorption spectra for EB **TANI-PTAB** (1 mM) in water, with **PPO**, and with **PPO**/**MO**.*

EB peaks at approximately 300 nm and 580 nm were also observed for **TANI-PTAB** in the presence of **PPO** and **MO**/**PPO**. A slight bathochromic shift in λ_{max} from 585 nm to 590 nm was observed with the addition of **PPO**. This is likely to be a solvatochromic effect, due to a change in the polarity of the chromophore's environment by the addition of **PPO**. It has been noted that EB **TANI-PTAB** experiences a bathochromic shift when the solvent's polarity was decreased by the addition of THF.[56] A decrease in polarity that leads to a bathochromic shift is known as negative solvatochromism, and is caused by the ground-state molecule being better stabilised than the excited state with increasing solvent polarity.[57] Additionally, the shoulder at 490 nm disappeared upon addition of **PPO**, which indicated that aggregation of the amphiphile had been disrupted by the polymer. The same disappearance of the shoulder can be observed with low concentrations of EB **TANI-PTAB**, below the critical micelle concentration (CMC) (1 x 10^{-4} M), as can be seen in Figure 3.4.

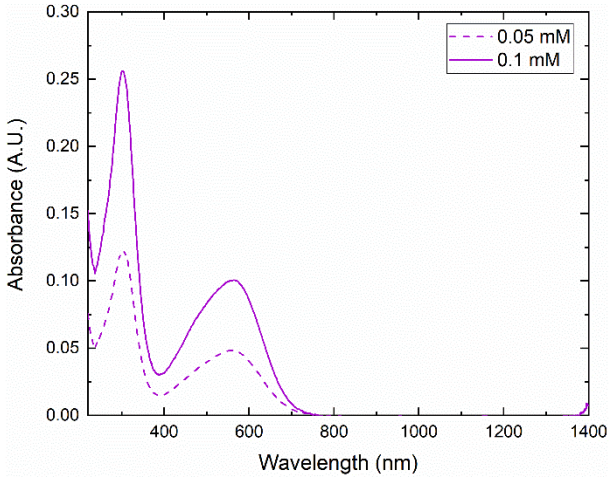

*Figure 3.4. UV-Vis/NIR absorption spectra for EB **TANI-PTAB** (0.05 and 0.1 mM) in water below the CMC.*

Meanwhile, the UV-Vis/NIR absorption spectrum for EB **TANI-PTAB** in **MO**/**PPO** showed a slight hypsochromic shift in the λ_{max} to 575 nm, along with the disappearance of the shoulder. The disappearance of the shoulder and the shift to shorter wavelengths indicated a decrease in conjugation, which suggested that some aggregation was lost as **TANI-PTAB** was incorporated into the lipid bilayer.

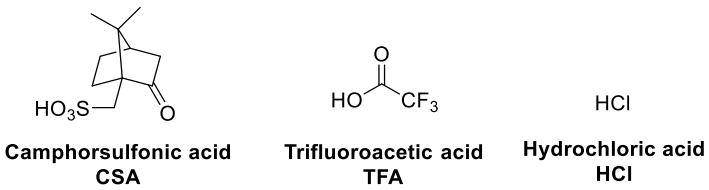

*Figure 3.5. Structures of camphorsulfonic acid (**CSA**), trifluoroacetic acid (**TFA**), and hydrochloric acid (**HCl**).*

After investigation of the EB state, attention was turned to the ES state of **TANI-PTAB**. Three acids were chosen for this study: camphorsulfonic acid (**CSA**), trifluoroacetic acid (**TFA**) and hydrochloric acid (**HCl**). The structures of the acids are given in Figure 3.5. All three had been previously shown to

dope **TANI-PTAB** and induce different changes in its self-assembly behaviour, due to their varied sizes altering the amphiphile's pp.[42]

Mixtures for UV-Vis/NIR spectroscopy experiments were prepared similarly to those made with **TANI-PTAB** in the EB state. Samples were again prepared in the sponge phase, for ease of preparation and analysis. EB **TANI-PTAB** was mixed with **PPO** and water, before being added to **MO** and stirred to form a homogenous mixture. Aqueous acid was then added and the UV-Vis/NIR absorption spectrum was collected. The samples were analysed again after 48 hours, to determine whether any de-doping had occurred.

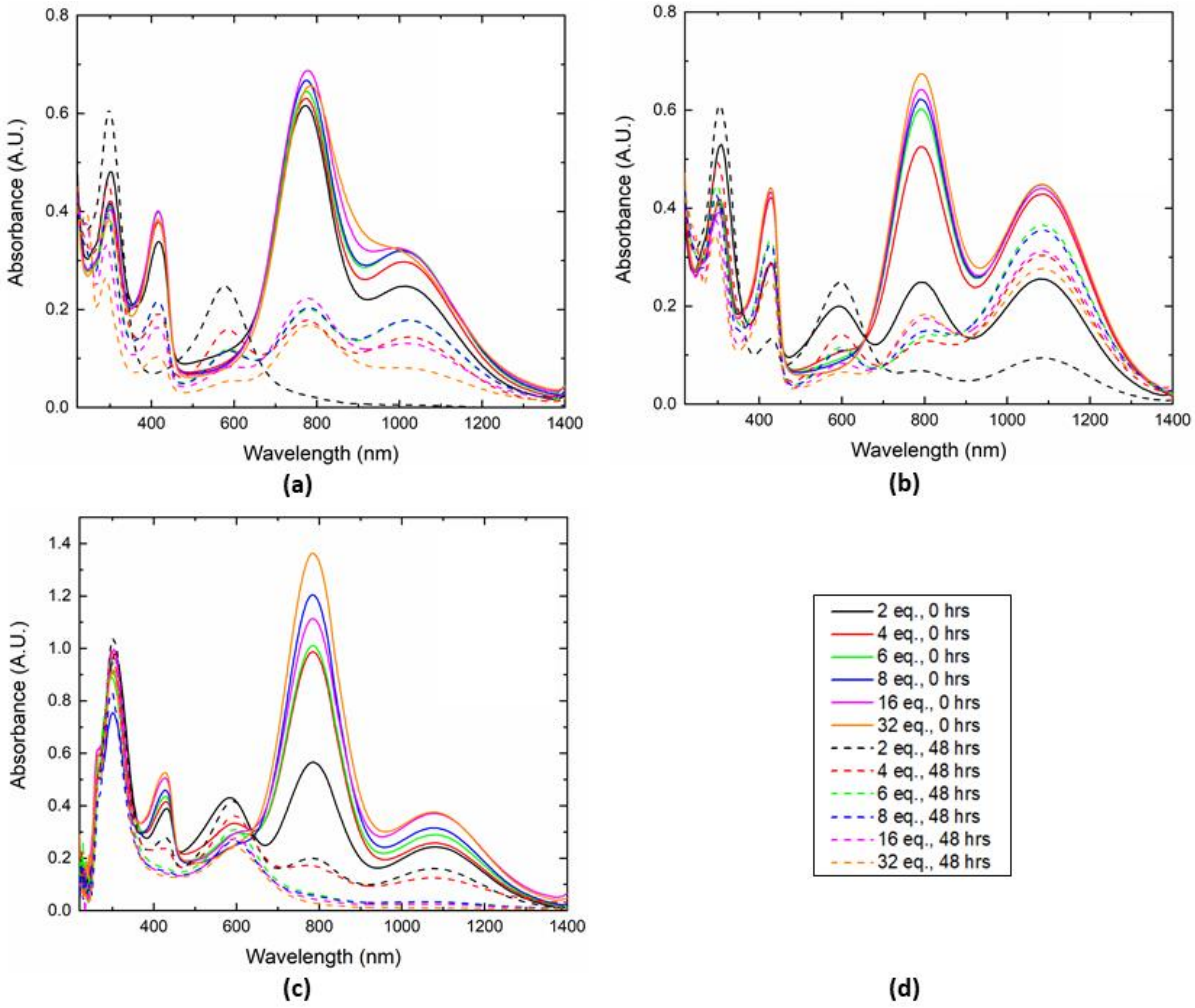

*Figure 3.6. UV-Vis/NIR absorption spectra of ES **TANI-PTAB** (0.25 mM) doped with 2-32 eq. of **CSA**. (a) in water (b) in water/**PPO** (c) in water/**PPO**/**MO** (d) legend. Spectra recorded at 0 and 48 hrs.*

The UV-Vis/NIR spectroscopy spectra for ES **TANI-PTAB** in water, with and without **PPO**, can be found in Figure 3.6 (doped with **CSA**) and Appendix B (doped with **TFA** and **HCl**). A molar ratio of at least 1:2 **TANI-PTAB**-to-acid was used, to ensure that doping at both imine sites occurred (Figure 3.7). A visible colour change from purple to green was observed immediately upon addition of all three acids, indicating the change in oxidation state.

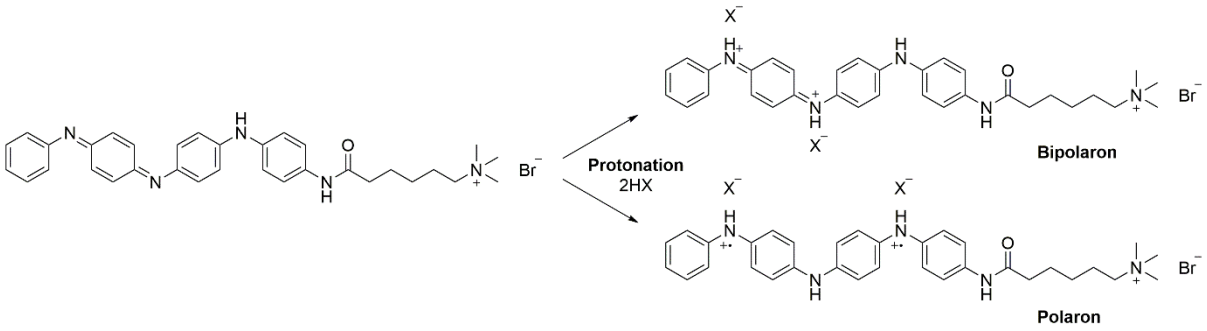

*Figure 3.7. Polaronic (triplet) and bipolaronic (singlet) forms of ES **TANI-PTAB**.*

Figure 3.6a in the main text, along with Figure B.1a and B.2a in Appendix B, show that **TANI-PTAB** doped with 2 molar equivalents of acids in water retained a small EB peak at 585 nm, indicating that the amphiphile was partially doped. However, **TANI-PTAB** solutions doped with 4 molar equivalents of acid showed complete conversion to the ES state, as evidenced by the disappearance of the EB peak and appearance of ES peaks at 750 and 1050 nm, corresponding to the polaron and bipolaron doped states, respectively.[58] The structures of the polaronic (or triplet), and bipolaronic (or singlet), forms of **TANI-PTAB** can be found in Figure 3.7. The intensity of the bipolaron peak with respect to the polaron peak increased with the concentration of the doping acid. This trend is consistent with literature studies of both doped states, which have shown that the polaron form is predominant at intermediate acid concentrations, while the bipolaron form is favoured with high concentrations of the dopant.[58] The polaron-to-bipolaron transition has been attributed to the increased screening of the two positive charges by the acidic counterions, allowing them to be spatially closer together.

The solutions became de-doped over time. After 48 hours, the EB peak had begun to reappear and the ES peaks had reduced in intensity, disappearing completely with low concentrations of acid (< 4 molar eq.). However, with a greater ratio of acid-to-**TANI-PTAB** (4:1 and above), the ES peaks remained prominent in comparison to the weaker-in-intensity EB peaks, indicating that the solutions stayed doped longer.

A similar trend was observed in the presence of **PPO** (see Figure 3.6b in the main text and Figure B.1b and B.2b in Appendix B)**. TANI-PTAB** was only partially doped with 2 molar equivalents of all three acids. However, with increasing acid concentration, complete conversion to the ES state was noted with the disappearance of the EB peak and the appearance of two peaks around 800 and 1100 nm, corresponding to the polaron and bipolaron doped states, respectively. The bipolaron state appeared to be more stable in the presence of **PPO** than in solutions with just water. Indeed, after 48 hours the bipolaron peaks were more intense than the polaron peaks for all acids. The **PPO** molecules may be acting to screen the positive charges on the imine nitrogen atoms, allowing the bipolaronic state to be more favoured, similar to the effect of increasing the acid concentration. The solutions again became

partially de-doped after 48 hours, although the de-doping was reduced with higher concentrations of acid.

Finally, the absorption spectra for acid-doped **TANI-PTAB** in **MO** sponge phases were recorded. The results for **CSA-**doped **TANI-PTAB** in the sponge phase are given in Figure 3.6c, while the results for samples doped with **TFA** and **HCl** are given in Figures B.1c and B.2c in Appendix B. **TANI-PTAB** became partially doped immediately after the addition of each acid, although there was greater conversion to the ES state with increased acid concentration. However, a transition back to the EB state was observed after 48 hours. Intriguingly, mixtures containing lower concentrations of acid showed increased retention of the ES state after this time, in contrast to solutions of ES **TANI-PTAB** prepared in just water or water and **PPO**. This was unexpected, as it was assumed that higher concentrations of acid would allow doping to be retained longer because more acid molecules should be available in the surrounding solution for doping.

The sponge and cubic phases consist of a hydrophobic lipid bilayer, surrounded by interconnecting water channels. When introduced to such mesophases, amphiphilic molecules are often incorporated into the lipid bilayer while acids tend to be found in the water channels.[8] It is likely that the amphiphilic **TANI-PTAB** will also be found within the bilayer, with the hydrophobic **TANI** core shielded from the water among the lipid hydrocarbon tails and with the hydrophilic trimethylammonium head group found at the lipid/water interface. It is therefore unclear by what mechanism the **TANI-PTAB** molecules are becoming doped, as acids are not expected to partition into the hydrophobic bilayer. Some possible mechanisms are discussed in Section 3.2.4.2, such as the formation of pore-like openings in the bilayer or the partitioning of **TANI-PTAB** into the water channels.

In the above UV-Vis absorption experiments, samples with **MO** were prepared in the sponge phase. As noted earlier, the sponge phase was chosen as it is more fluid than the cubic phase and could be more readily loaded into a cuvette for analysis. The results from the sponge phase were then used to predict the redox behaviour of **TANI-PTAB** in the cubic phase. It is likely that there is a difference in the rate at which acids diffuse through the sponge and cubic phases to dope the amphiphile. Different diffusion rates between mesophases are commonly reported in the literature.[21,23,59] The aqueous channels of the sponge phase are more dilated than the cubic phases, allowing for more rapid diffusion of additives.[60] Indeed, there are differences even between the cubic phases. Negrini and Mezzenga (2012) utilised the difference in water channel diameters between the narrower *Pn3m* and wider *Im3m* phases to control the diffusion behaviour of small molecules through the mesophases.[61] Sucrose stearate was used to tune the water channel diameter of the lipid bicontinuous cubic phase, allowing for diffusion to be switched on and off.

With the above in mind, 4 molar equivalents of acid were chosen to dope **TANI**-derived amphiphiles in subsequent SAXS experiments and samples were left to equilibrate for 48 hours. 4 molar equivalents

of each acid were selected as they showed the most complete doping at 0 and 48 hours, and samples were left to equilibrate for 48 hours to allow for diffusion and doping to occur. Doping in cubic phases was confirmed by a visual colour change from purple to green. Further discussion of sample preparation for doped samples can be found in Section 3.2.4.2.

3.2.3 Small-angle X-ray scattering investigations of EB TANI-PTAB in MO cubic phases

After UV-Vis/NIR spectroscopy confirmed that EB state **TANI-PTAB** was oxidatively stable in **MO**/**PPO** mixtures and could be doped to the ES state with a variety of acids, the amphiphile's effect on **MO** cubic phases was investigated by SAXS. Much research has been done on the effect of different additives on the phase behaviour of **MO** and similar lipids, which can be found in a comprehensive review by van't Hag et al. (2017).[8] In this review, amphiphiles were noted as being encapsulated in the lipid bilayer to some degree, owing to their partially hydrophobic nature. Their effect on the lipid phase behaviour was then rationalised by their *pp*. Amphiphiles with a $pp < 1$ when mixed with a cubic phase forming lipid ($pp > 1$) formed flatter phases, such as the lamellar phase, as the combined *pp* was closer to 1. Amphiphiles with a $pp >> 1$ in combination with the same lipids formed more negatively curved phases, such as the hexagonal and micellar phases.

As mentioned in the previous section, it was expected that EB **TANI-PTAB** would be at least partially encapsulated by the lipid bilayer, due to its amphiphilic nature. Transmission electron microscopy (TEM) and atomic force microscopy (AFM) have been previously utilised to show that above the CMC (1×10^{-4} M) EB **TANI-PTAB** forms nanofibers that are 3 nm in diameter and are several microns long.[41] The average diameter of the nanofibers is approximately the length of one EB **TANI-PTAB** molecule, which was calculated to be 2.9 nm.[56] This is on the same length scale as the bilayer thickness and water channel diameter of **MO** in the *Pn3m* phase under excess water conditions, which are 3.2 nm and 5.1 nm, respectively.[8] The similarity in dimensions indicated that EB **TANI-PTAB** could be incorporated into the mesophase, in contrast to larger amphiphiles, which are often excluded from lipidic cubic phases.[62,63] Furthermore, the *pp* of EB **TANI-PTAB** had previously been calculated as 0.37.[42] Therefore, it was expected that the addition of this amphiphile will have a flattening effect on the cubic phases of **MO**, resulting in the formation of the less negatively curved *Im3m* phase or sponge phase.

A detailed method for the preparation of SAXS samples containing **TANI-PTAB** is given in Chapter 2, Section 2.4.5, while the key steps are highlighted in Figure 3.8. In brief, a known concentration of EB **TANI-PTAB** was prepared in a solution of water and **PPO**, before being mixed with **MO** to form the sponge phase. 40 µL of the sponge mixture was pipetted into a borosilicate glass capillary tube, followed by 40 µL of deionised water. The capillary was placed in a centrifuge at 2000 rpm for 60 seconds, encouraging the water to penetrate the sponge phase, diluting it to the cubic phase and inducing

alignment. The mixtures were left to hydrate for 48 hours, giving enough time for transitions between mesophases to occur.

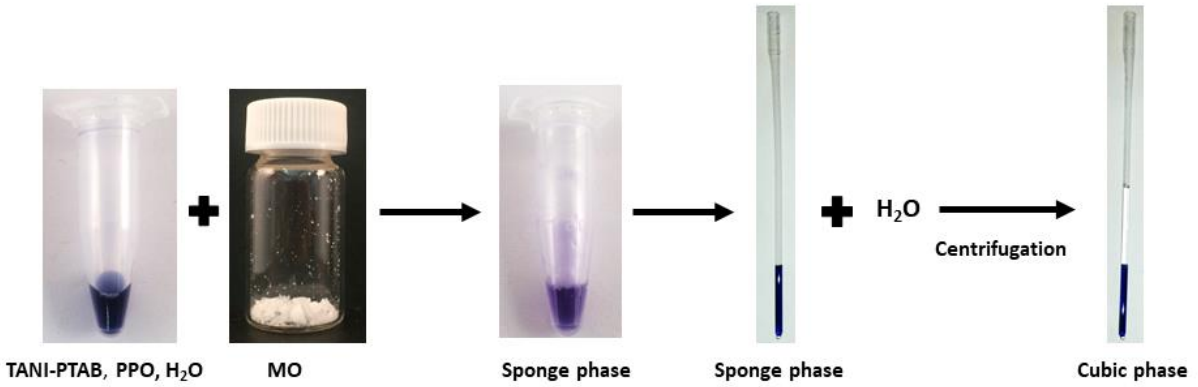

*Figure 3.8. Preparation of **MO** cubic phases containing EB **TANI-PTAB** and **PPO.***

The reported **TANI-PTAB** concentrations given in all SAXS experiments were the initial concentrations used in the preparation of the sponge phase as the final concentration after diluting with water to the cubic phase could not be accurately reported. As can be seen in Figure 3.8, the added water did not completely mix with the sponge phase. Instead, dilution only occurred at the sponge/water interface, which was the area then investigated by SAXS. As the quantity of water that had penetrated the sponge phase was unknown, the new **TANI-PTAB** concentration at the interface could not be calculated. Therefore, to compare the results of different runs, the initial **TANI-PTAB** concentration was reported as a standard.

In the absence of **TANI-PTAB**, **MO** with **PPO** formed the *Pn3m* phase with typical lattice parameters around 10.75 nm (Section 3.2.1), following the previously outlined preparation method. As the concentration of **PPO** was kept constant for all experiments, it was expected that any deviation from the lattice parameter and phase assignment was due to the addition of **TANI-PTAB**.

The results for the effect of EB **TANI-PTAB** concentration on **MO** with **PPO** over eight experiments are given in Figure 3.9. At low concentrations of **TANI-PTAB** (< 3 mM), **MO** formed the *Pn3m* phase with a lattice parameter of around 11 nm. This is slightly larger than that of phases without **TANI-PTAB**, however as noted in previous sections, the presence of additives is known to swell the mesophase. At higher concentrations of **TANI-PTAB** (> 9 mM), a transition to the *Im3m* phase with a larger lattice parameter was observed. This transition from the more negatively curved *Pn3m* phase to the less negatively curved *Im3m* phase was expected, owing to the flattening effect of **TANI-PTAB** (*pp* < 1) when combined with **MO** (*pp* > 1), which became more pronounced as the concentration of the amphiphile increased.

With EB **TANI-PTAB** concentrations between 3 and 9 mM, either the *Pn3m* or the *Im3m* phase were observed. The phases were discrete, rather than a mix of both within the same sample. Instead, it appeared that the concentration at which the transition to the *Im3m* phase occurred was variable. Discussion of the factors that may account for the differences between mesophase nanostructure within the same concentration range is given in Section 3.2.5.

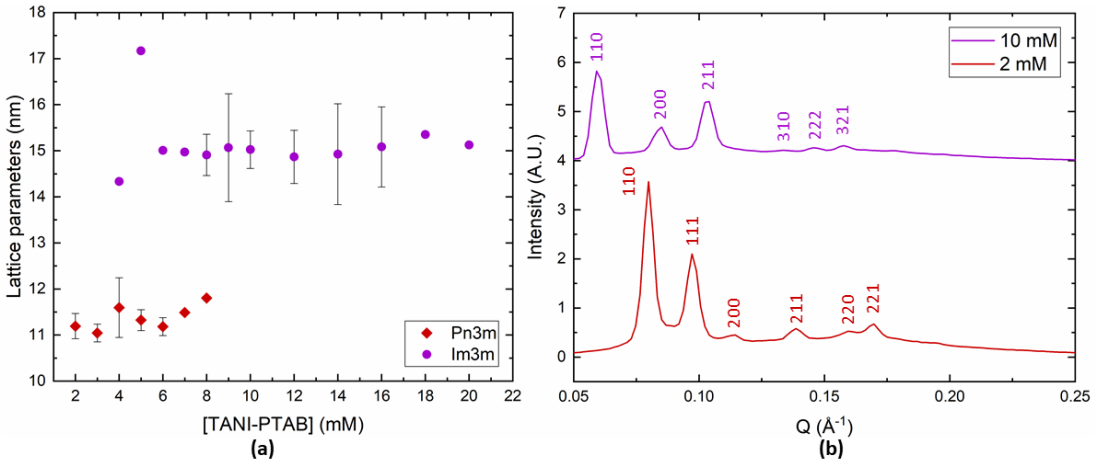

*Figure 3.9. (a) Lattice parameters for **MO** cubic phases prepared with **PPO** and EB **TANI-PTAB** (2-20 mM). Results combined from eight experiments. (b) 1-D scattering patterns for **MO** cubic phases containing 2 and 10 mM **TANI-PTAB** (EB), showing peaks for the Pn3m and Im3m.*

3.2.4 Small-angle X-ray scattering investigations of ES TANI-PTAB in MO cubic phases

3.2.4.1 Effect of pH on MO cubic phases

After investigating the effect of EB **TANI-PTAB** on the phase behaviour of **MO**, attention was turned to the ES state. Following the results of the UV-Vis spectroscopy experiments outlined in Section 3.2.2, samples were doped with 4 molar equivalents of either **CSA**, **TFA** or **HCl**. However, before doping of **TANI-PTAB** in **MO** was attempted, the effect of introducing these acids to the cubic phases was first explored.

Full SAXS sample preparation details are given in Chapter 2, Section 2.4.5. A **MO** sponge phase was prepared with **PPO** and pipetted into a capillary tube, followed by aqueous acid at the desired concentration. The capillary was placed in a centrifuge at 2000 rpm for 60 seconds, before the mixture was left to hydrate for 48 hours. The mesophase structure and lattice parameters were then identified by SAXS.

The results for the addition of **CSA**, **TFA** and **HCl** are given in Figure 3.10. Typically, pH has limited effect on the cubic phase, beyond a small increase in lattice parameter with increasing pH.[64–66] **MO** forms the *Pn3m* cubic phase with all three acids, regardless of the concentration. Mixtures prepared with **CSA** appear slightly swollen, with lattice parameters closer to 11.5 nm, in comparison to **TFA** and **HCl**, which have lattice parameters around 11.1 and 10.9 nm, respectively. The calculated lattice

parameters for all are close to that obtained from **MO** with **PPO** without any other additives (10.75 nm, Section 3.2.1), which indicate that the acids have little effect on the mesophase dimensions, as anticipated.

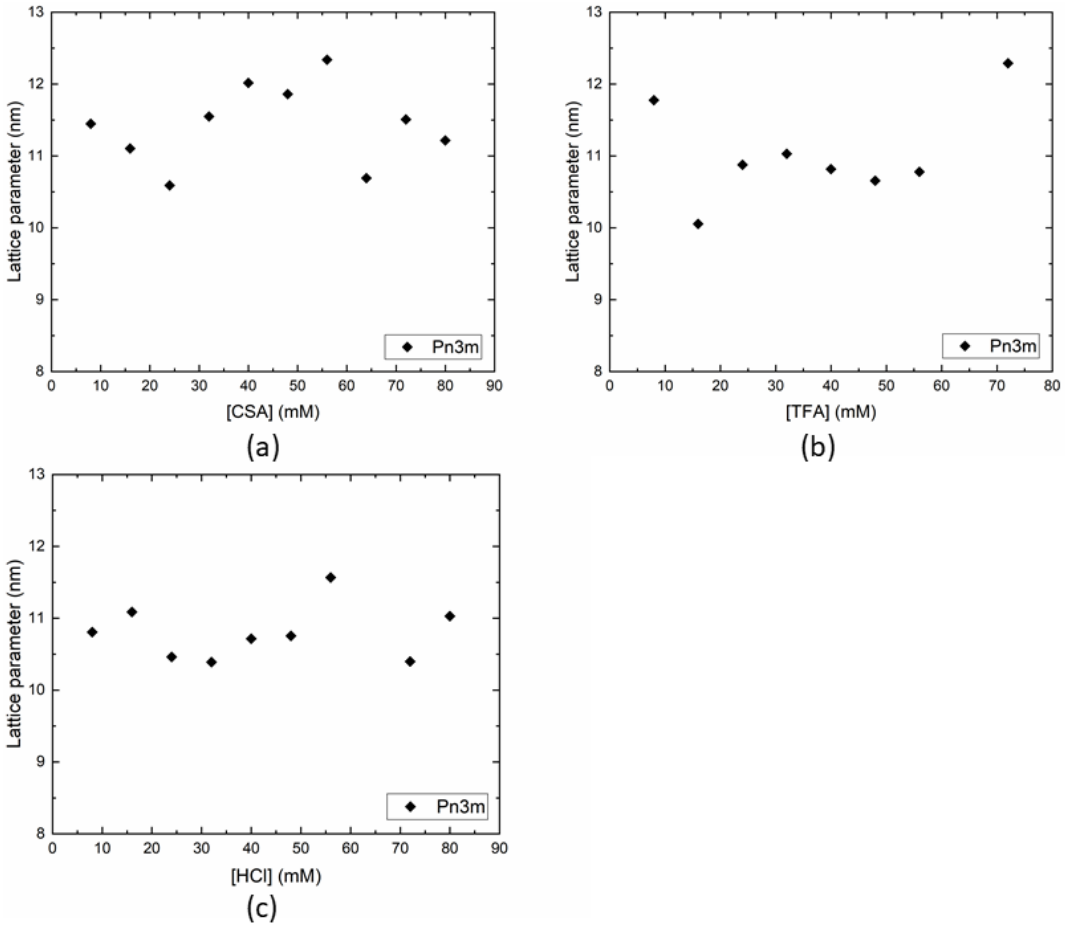

*Figure 3.10. Lattice parameters for **MO** with **PPO** and acids (a) **CSA**, (b) **TFA** and (c) **HCl**.*

Slight variations in lattice parameters can be observed between each acid concentration. As the acids should not be influencing the mesophase structure and the preparation conditions should be the same between each sample, it is likely that the sources of variation come from random and systematic errors (see Section 3.2.5).

3.2.4.2 Effect of ES TANI-PTAB on MO cubic phases

After the control experiments were complete and indicated that the inclusion of acids had limited effect on the mesophase structure, samples containing **TANI-PTAB** in the ES state were investigated. The preparation method was similar to that of samples prepared in the EB state (see Chapter 2, Section 2.4.5 for full details). **MO**/**PPO** sponge phases containing EB **TANI-PTAB** were prepared and loaded into a capillary tube, followed by 4 molar equivalents of aqueous acid. The capillaries were centrifuged to encourage hydration before being left to equilibrate over a 48-hour period.

Doping occurred during this time and was assumed by a visible colour change from dark purple to green (see Figure 3.11). This assumption was supported by the results of the UV-Vis spectroscopy experiments, which indicated that **TANI-PTAB** in **MO**/**PPO** would be in the ES state 48 hours after the addition of a doping acid (Section 3.2.2).

*Figure 3.11. ES **TANI-PTAB** (2 mM) in **MO/PPO** doped with 8 mM **CSA** at (a) 0 hrs (b) 48 hrs.*

The SAXS results for cubic phases formed in the presence of **TANI-PTAB** when doped with **CSA**, **TFA** and **HCl** are given in Figure 3.12. The *Pn3m* phase was formed at all **TANI-PTAB** concentrations, irrespective of the doping acid. The lattice parameters appear mostly constant across all concentrations, with the average lattice parameters for samples doped with **CSA**, **TFA** and **HCl** being 11.4 nm, 11.2 nm and 11.3 nm, respectively.

The samples were left to hydrate for 48 hours before analysis, which was sufficient time for most to transition from the sponge phase to *Pn3m* phase. However, a few samples produced broad peaks in the 1-D scattering patterns or had larger lattice parameters, in particular those containing 8 and 10 mM **TANI-PTAB** doped with **TFA**, which suggested they needed longer to equilibrate. A longer hydration time was considered but as **TANI-PTAB** would de-dope after a few days the time was kept at 48 hours.

The change in mesophase, from the *Im3m* phase in the EB state to the *Pn3m* phase in the ES state, can be understood by considering the change in the amphiphile's *pp*. In the EB state, **TANI-PTAB** has a *pp* of 0.37. However, when doped with **CSA**, **TFA** and **HCl**, the *pp* increases to 0.73, 0.49 and 0.41, respectively, as the dopants increase the volume of the hydrophobic section.[42] This leads to a transition in water from flat nanofibers to cylindrical micelles or vesicles. The increased *pp* of the doped **TANI-PTAB**, when combined with **MO** (*pp* > 1) will have less of a flattening effect on the membrane curvature than the EB state and the *Pn3m* phase will be retained at all assessed concentrations.

The above description of how the doping of **TANI-PTAB** and subsequent change in *pp* results in the *Pn3m* phase with **MO** is one possible explanation for the observed change. As an amphiphile, **TANI-PTAB** is expected to lie in the lipid bilayer. This can be seen experimentally by the transformation to

the *Im3m* phase when EB **TANI-PTAB** is added to **MO**. The addition of dopants changes the *pp* of **TANI-PTAB** in water and the transition to the *Pn3m* phase upon doping in **MO** is consistent with what would be expected with a similar increase in *pp* of the amphiphile within the lipid membrane. However, the acids used for doping are highly hydrophilic and would not be expected to partition into the hydrophobic bilayer for doping to occur, which calls into question the validity of this theory.

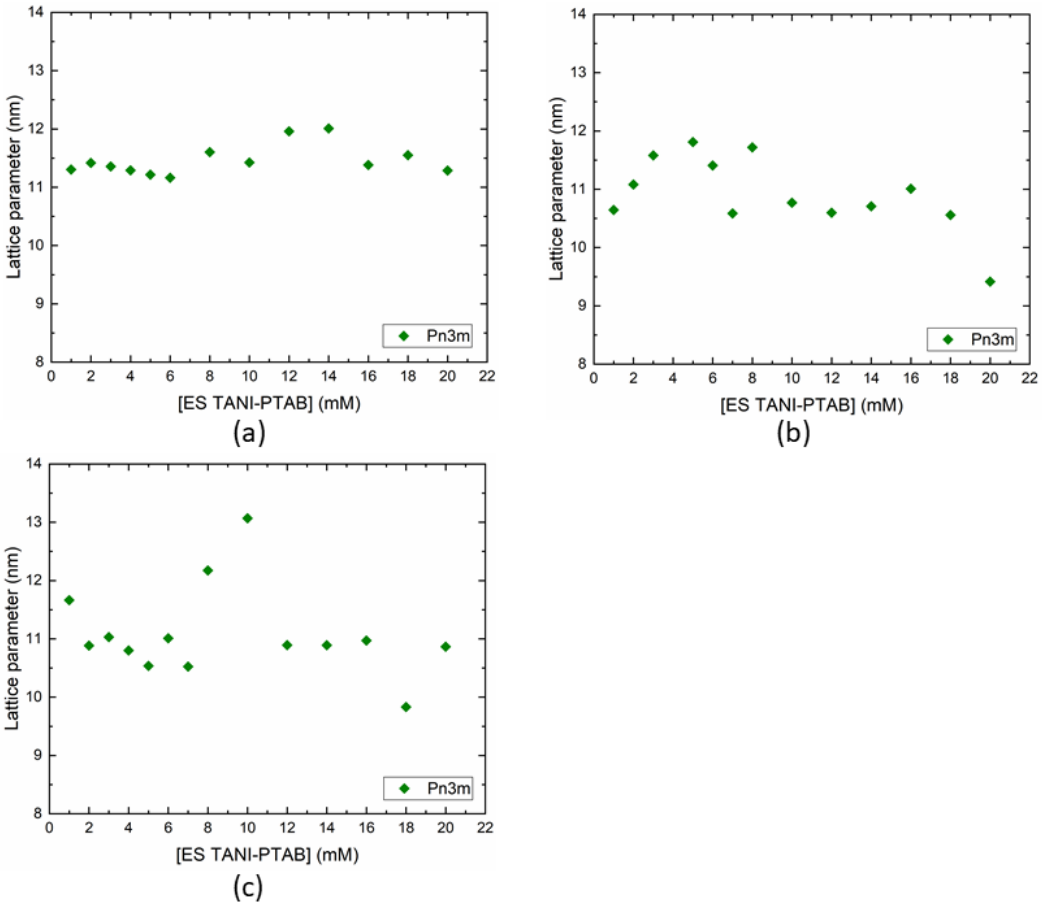

*Figure 3.12. Lattice parameters for **MO** prepared with **PPO** and **TANI-PTAB** (ES), doped with 4 molar equivalents of (a) **CSA** (b) **TFA** and (c) **HCl**.*

Possible explanations for how doping can occur in this case have been considered. It is possible that the acids can partition into the bilayer, despite the hydrophobic environment. Additionally, the **TANI-PTAB** molecules could be aggregating and forming a pore-like opening in the bilayer, allowing the acids to enter and act as dopants. Alternatively, it is possible that **TANI-PTAB** partitions into the water channels upon doping as the acids allow it to be more hydrophilic. In that case, the transition to the *Pn3m* phase could be due to the removal of **TANI-PTAB** from the bilayer and not to do with the amphiphile's change in *pp*.

3.2.5 Factors influencing cubic phase nanostructure

In the previous experiments, some variation was observed in lattice parameters between samples of the same cubic phase, which did not appear to follow a pattern with **TANI-PTAB** concentration. For example, the lattice parameters for *Pn3m* phases containing **TANI-PTAB** doped with different acids increased or decreased at random across all reported concentrations (Figure 3.12). Additionally, for experiments with EB **TANI-PTAB**, the concentration at which the *Im3m* phase appeared was between 4 and 9 mM and differed across each experiment, again without an immediately notable cause (Figure 3.9). This section aims to discuss some possible causes for these observations.

All samples were prepared in the same manner. **TANI-PTAB** was mixed with **PPO**, water and **MO** to form the sponge phase, which was transferred to a capillary tube. Further water or aqueous acid was added and the capillary was centrifuged for one minute at 2000 rpm to encourage hydration to the cubic phase. The sample was then left to equilibrate for two days prior to analysis by SAXS. There are a few potential sources of variation that can be found in this preparation method, such as the centrifuge settings, instrumentation error and hydration time, all of which may influence the phase behaviour of **MO**.

The first condition that was explored was hydration time. Confirmation that 48 hours was sufficient time for **MO** to fully transition from the sponge phase to the cubic phases was required, as larger or smaller than expected lattice parameters or the presence of extra peaks could indicate that the samples did not have enough time to equilibrate. Cubic phases containing 2-9 mM of EB **TANI-PTAB** were prepared and analysed after 48 hours and at two weeks, the results of which can be found in Figure 3.13 (a, b). The *Pn3m* phase was observed for **TANI-PTAB** concentrations below 8 mM, while the *Im3m* phase was identified at 9 mM for both time frames. There was little variation in the lattice parameters after the additional hydration time, which indicated that 48 hours was sufficient for the mesophase to reach equilibrium.

The centrifuge settings were also considered, as a faster spin speed or longer centrifuge time could allow for more rapid diffusion of the water into the sponge phase, which in turn could result in the cubic phase reaching equilibrium earlier. To test this hypothesis, two centrifuge settings were changed. In the first, the spin speed was set to 3000 rpm, while the centrifuge time was kept at one minute. In the second, the spin speed was set to 2000 rpm, while the time was increased to five minutes. The results for both are given in Figure 3.13 (c, d). At the higher spin speed, there was greater variation in the lattice parameters for the *Pn3m* phase. Additionally, while the *Im3m* phase appeared at the same concentration as the slower spin speed (9 mM), peaks for the *Pn3m* phase were also present. With the longer centrifuge time, there was less variation in the lattice parameters for the *Pn3m* phase and peaks for the *Im3m* phase initially appeared at 8 mM before becoming the predominant phase at 9 mM.

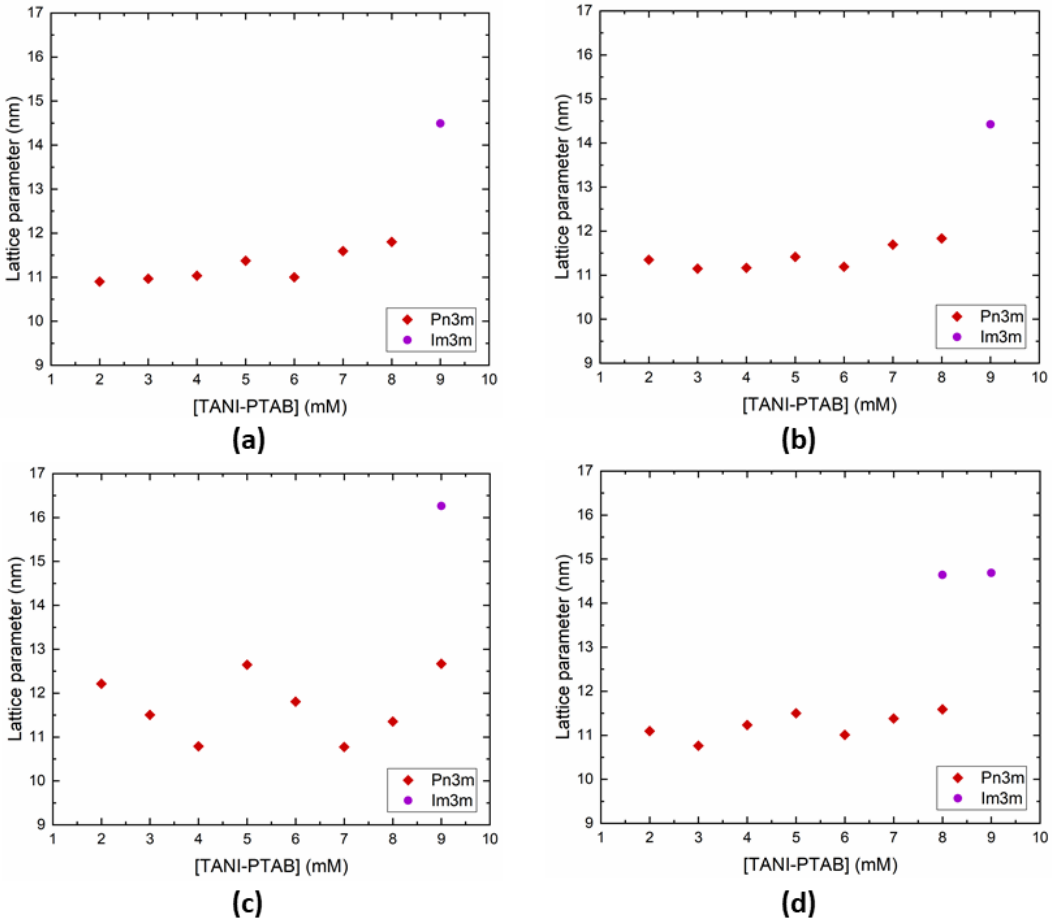

*Figure 3.13. Lattice parameters for **MO/PPO** with EB **TANI-PTAB** (2-9 mM) prepared under different conditions. (a) Centrifuge settings: 2000 rpm, 1 min. Hydration time: 48 hours (b) Centrifuge settings: 2000 rpm, 1 min. Hydration time: 2 weeks (c) Centrifuge settings: 3000 rpm, 1 min. Hydration time: 48 hours (d) Centrifuge settings: 2000 rpm, 5 minutes. Hydration time: 48 hours.*

The centrifuge speed appeared to have the greatest effect on the lattice parameters, as *Pn3m* mesophases prepared using spin speeds of 3000 rpm had lattice parameters of around 11.5 nm ± 1 nm, while the variation for samples prepared at 2000 rpm was much smaller. Meanwhile, centrifuge time had limited effect on the lattice parameters, with the main difference being the formation of the *Im3m* phase at a lower concentration.

Other factors that could cause variation between samples are systematic and random errors. Systematic errors are consistent and repeatable, often arising from poorly calibrated equipment. The reported systematic errors for the 10, 100 and 200 µL Gilson pipettes used in these experiments at their highest volumes are ± 0.1, 0.8 and 1.6 µL, respectively, and the average volumes measured by properly calibrated pipettes will not vary from the set volume outside of these ranges.[67] As the pipettes and balance utilised in the preparation of SAXS samples were calibrated, and should not vary in measurements to an appreciable degree, it was not expected that systematic error was the cause of the observed variation.

Meanwhile, random errors vary unpredictably between samples and can occur from instrument limitations, the environment, and variations in procedure. While systematic error can often be corrected and minimised, sources of random error are harder to identify. For example, changes in lab humidity could result in a difference in water content and air currents across balances can affect weight measurements, which could cause marked differences between experiments. As the difference in lattice parameters between samples does not appear to follow a pattern, it is likely that the variation is due to unidentified random errors.

While errors and variations in centrifuge settings could account for slight differences in lattice parameters between samples of the same cubic phase, it seemed unlikely that they were responsible for the difference in concentration at which the *Im3m* phase was formed. To determine the cause of this difference, the concentration at which the *Im3m* phase formed was plotted as a factor of time. As can be seen from Figure 3.14, the required **TANI-PTAB** concentration for this transition increased from around 4 mM to 9 mM over two years, which indicated obvious change during this time. As the sample preparation conditions had been consistent, attention was turned to the components making up the cubic phases.

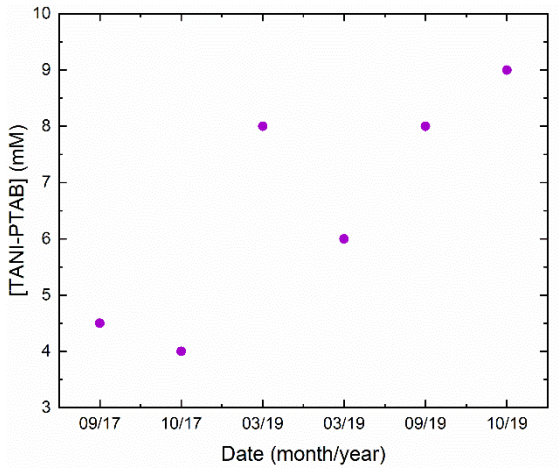

*Figure 3.14. EB **TANI-PTAB** concentration at which the Im3m phase formed from 2017 to 2019.*

The oxidation state of EB **TANI-PTAB** in **MO** sponge phases was determined by UV-Vis/NIR spectroscopy to see whether any doping was occurring over time (Figure 3.15). A slight ES peak at around 800 nm was observed with sponge phases prepared in October 2019. This peak became noticeably more pronounced in samples prepared from February 2020 onwards, although the EB peak was predominant, indicating that samples were only partially doped.

Doping of **TANI-PTAB** could explain the observed difference in phase behaviour between batches. As noted in Section 3.2.4, the addition of dopants increases the *pp* of **TANI-PTAB**, so it has less of a flattening effect on the membrane curvature of **MO** than the EB state and resulting in the formation of the *Pn3m* phase. Therefore, it was expected that **MO** containing partially doped **TANI-PTAB** would

require a higher concentration of the amphiphile to produce the *Im3m* phase in comparison to **MO** prepared with **TANI-PTAB** in the EB state only.

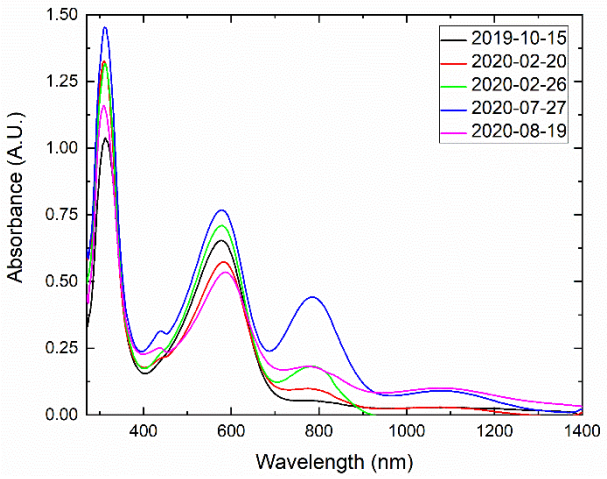

*Figure 3.15. UV-Vis/NIR absorption spectra for EB **TANI-PTAB** (1 mM) in **MO/PPO** sponge phase, prepared from 2019-2020.*

TANI-PTAB, **PPO** and **MO** were investigated to determine the origin of the dopant. The purities of **TANI-PTAB** solutions used to prepare SAXS samples were determined by ^{1}H NMR spectroscopy and UV-Vis/NIR spectroscopy prior to use in all experiments. Any partially doped samples were discarded. Additionally, the UV-Vis/NIR absorption spectrum of EB **TANI-PTAB** with **PPO** was collected and confirmed that **PPO** did not act as a dopant (Figure 3.3). Therefore, it appeared that **MO** was acting as a dopant for **TANI-PTAB**.

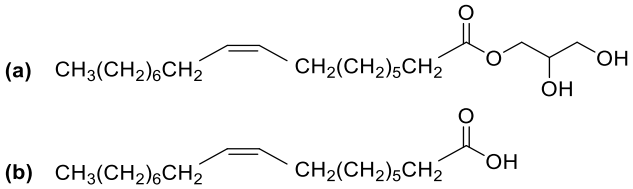

*Figure 3.16. Structures of (a) **MO** (b) oleic acid.*

The structure of **MO** is given in Figure 3.16. The lipid consists of a glycerol head group attached to a hydrocarbon chain by an ester bond. This ester bond can be hydrolysed to produce a carboxylic acid. In this case, the cleavage of the ester bond in **MO** will produce oleic acid. Carboxylic acids are typically poor dopants for **PANI** and oligo(aniline)s, owing to their high pKas. Indeed, the pKa of oleic acid is 5.02. However, partial doping can occur with weak acids and oleic acid has been used as a dopant for **PANI**, increasing the polymer's solubility in organic solvents and resulting in a conductivity of 1.3 x 10^{-2} S/cm.[68]

While the hydrolysis of esters typically requires the presence of a strong acid or base as a catalyst, it is possible that cleavage of the ester bond in **MO** had been slowly occurring over the years due to water

in the air, resulting in a higher concentration of carboxylic acids at the end of this project than at the start. Indeed, the decomposition of **MO** into oleic acid and glycerol with prolonged storage has been previously noted and highlighted as a drawback for applications that require long term stability.[69]

A bottle of pure **MO** was obtained and used as a comparison with the original bottle of **MO**, which had been generously donated by Danisco. The high cost of the pure lipid limited the number of experiments that could be done, however, the mass spectra of both bottles were collected and compared. As can be seen in Figure B.4 of Appendix B, the mass spectrum for the original bottle of **MO** contains a peak that corresponds to the molecular ion of oleic acid (*m/z*: 282.3), in addition to the molecular ion peak for **MO** with sodium (*m/z*: 379.3). Meanwhile, the mass spectrum for pure **MO** is much clearer, with the predominant feature being the molecular ion peak for **MO** with sodium (Figure B.5 of Appendix B).

3.2.6 Small-angle X-ray scattering investigations of TANI-PTAB in pure MO cubic phases

The phase behaviour of pure **MO** with **TANI-PTAB** was briefly investigated and compared with the previous results, to determine the effect of the amphiphile in the EB and ES oxidation states without the concern of doping due to the presence of oleic acid. It was expected that the phase diagram of pure **MO** would be different to that of **MO** donated by Danisco as there were fewer impurities present. Therefore, the addition of **TANI-PTAB** may not produce the *Pn3m* and *Im3m* phases at the same concentrations as with previous experiments. However, using the *pp* theory, it was expected that EB **TANI-PTAB** would form the *Im3m* phase or flatter phases with **MO**, while doping to the ES state would result in the *Pn3m* phase.

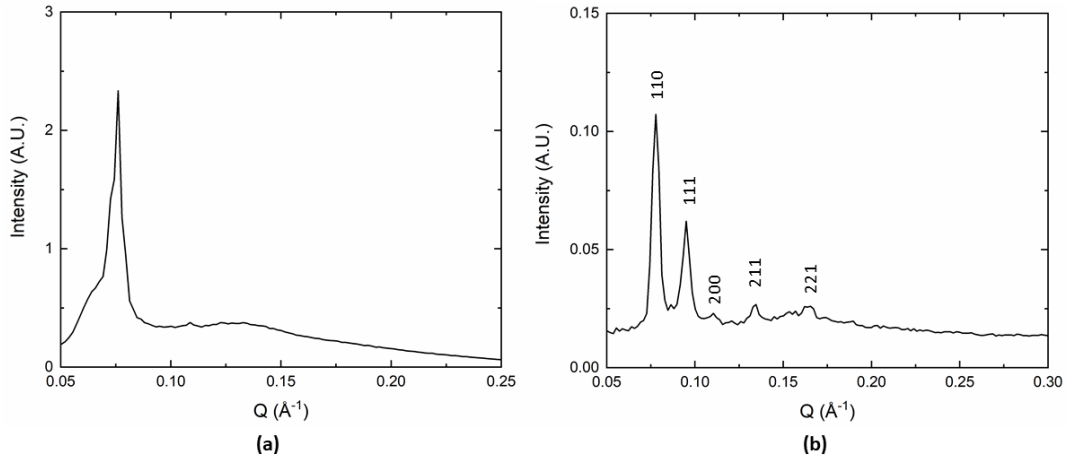

*Figure 3.17. 1-D scattering pattern for **MO** prepared with (a) 20 % (v/v) **PPO** (b) 25 % (v/v) **PPO**.*

To begin, the *Pn3m* phase was formed with the addition of just **PPO** and water, to determine the mesophase structure of **MO** prepared without **TANI-PTAB**. 25 % (v/v) **PPO** was used in the lyotrope mixture, instead of 20 % (v/v) **PPO**, as the latter concentration did not produce the distinct Bragg scattering peaks expected of *Pn3m* phase. The 1-D scattering plots for mesophases prepared with both **PPO** concentrations are shown in Figure 3.17. The calculated lattice parameter for the *Pn3m* phase

formed with 25 % (v/v) **PPO** is 11.4 nm. This value is close to the average lattice parameter obtained when forming *Pn3m* phases with **MO** donated by Danisco (10.8 nm), although it should be noted that a direct comparison is not possible as the latter used less **PPO** to form the same phase and contained impurities that would influence the phase behaviour. Nevertheless, it was shown that a cubic phase could be formed with the pure **MO** using the same preparation method as before, although with a greater quantity of **PPO**.

The next step was the addition of EB **TANI-PTAB**. Prior to any SAXS experiments, a sponge phase containing EB **TANI-PTAB** (1 mM) was prepared and analysed by UV-Vis/NIR spectroscopy to determine whether any doping occurred with the pure **MO**. The absorbance of a sponge phase prepared without **TANI-PTAB**, and with 25 % (v/v) **PPO**, was used as a background and was subtracted from the data. The absorbance spectrum is given in Figure 3.18. Unlike sponge phases formed with **MO** donated by Danisco, the pure **MO** sponge phase was highly opaque, resulting in a baseline below zero when background subtracted from that containing EB **TANI-PTAB**. However, while a characteristic EB peak at 590 nm was clearly visible, there were no peaks that corresponded to the ES state, suggesting that no doping occurred with the pure **MO**.

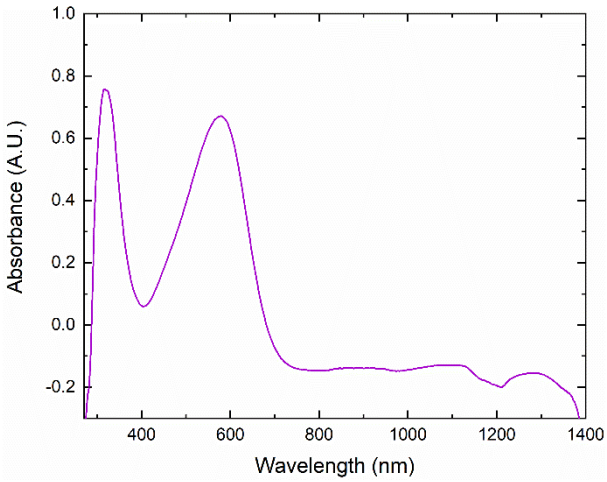

*Figure 3.18. UV-Vis/NIR absorption spectrum for EB **TANI-PTAB** (1 mM) in a sponge phase formed by pure **MO**.*

After UV-Vis/NIR spectroscopy confirmed that the pure **MO** did not dope **TANI-PTAB**, cubic phases with both were prepared and the phase behaviour was identified by SAXS. The lattice parameters for samples prepared with EB **TANI-PTAB** (2-10 mM) in addition to the 1-D scattering plots for samples containing 2 and 4 mM **TANI-PTAB** are shown in Figure 3.19. As with previous experiments, the *Pn3m* phase formed at low concentrations of **TANI-PTAB**, while the *Im3m* phase was produced at concentrations above 4 mM. However, the lattice parameters for these cubic phases were swollen in comparison to earlier experiments, with values of around 16 nm and 18 nm recorded for the *Pn3m* and the *Im3m* phases, respectively. The 1-D scattering patterns reflect the reason for the larger lattice parameters (Figure 3.19b). The peaks are broad and are poorly defined, particularly for the sample

prepared with 2 mM **TANI-PTAB**. This result indicates that the samples may not have had long enough to transition from the sponge phase to their respective cubic phases. A longer equilibration time could allow for the transition to go to completion and may result in smaller lattice parameters, however due to time constraints it was not possible to re-analyse these samples at a later date.

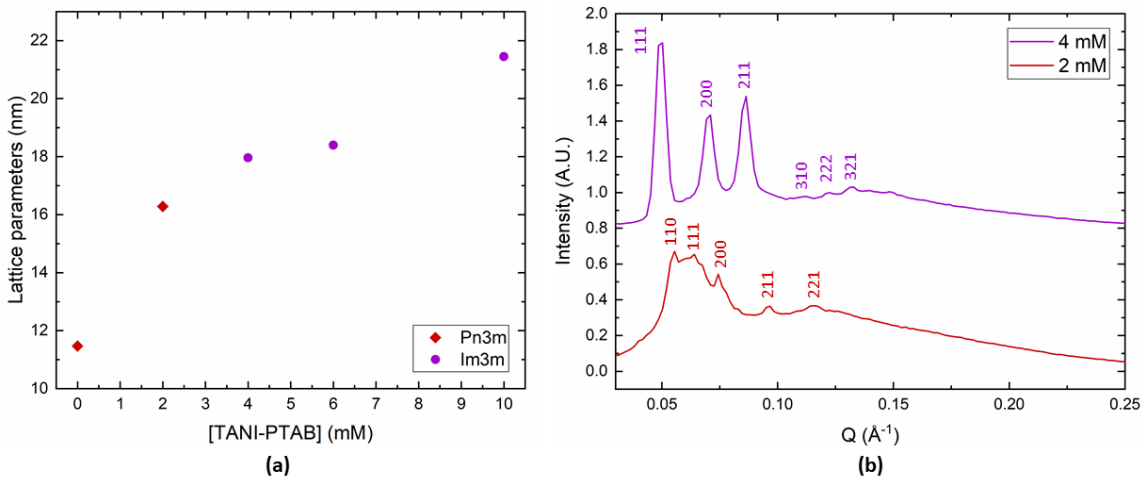

*Figure 3.19. (a) Lattice parameters for pure **MO** with EB **TANI-PTAB** (2-10 mM) (b) 1-D scattering patterns for samples with 2 and 4 mM EB **TANI-PTAB**.*

Following experiments in the EB state, samples doped with 4 molar equivalents of **CSA** were prepared, to determine the effect of increasing the *pp* of **TANI-PTAB** when incorporated into pure **MO**. The lattice parameters for samples containing 2-10 mM **TANI-PTAB** and the 1-D scattering plot for 6 mM **TANI-PTAB** can be found in Figure 3.20. Upon doping, the *Pn3m* phase was formed at all **TANI-PTAB** concentrations, as expected from previous experiments. However, the lattice parameters were again swollen to around 16 nm and the 1-D scattering plot shows that while the peaks corresponding to the Pn3m phase are present, they are broad and poorly defined, making it difficult to be confident of the mesophase parameters and indicating that a longer hydration time was required. Again, due to time constraints, it was not possible to re-analyse these samples at a later date, although it should be noted that it is likely that de-doping would occur with a longer hydration time and therefore a mixture of EB and ES state **TANI-PTAB** would be present.

Without a more detailed study of the phase diagram of pure **MO** and with the poor data quality of samples containing both EB and ES state **TANI-PTAB**, it is difficult to come to any conclusions as to the effect of introducing the amphiphile to mesophases prepared with the pure lipid. However, it was generally clear that the addition of **TANI-PTAB** resulted in the formation of the *Im3m* phase and that by acid doping, a transition to the *Pn3m* phase was observed, which supports the previously reported results.

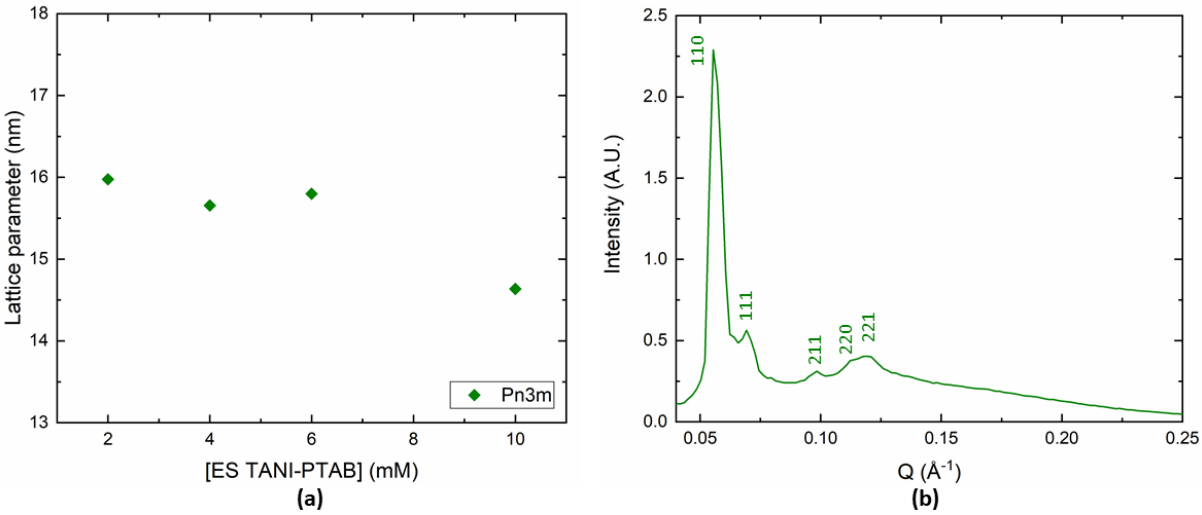

*Figure 3.20. (a) Lattice parameters for pure **MO** with ES **TANI-PTAB** (2-10 mM), doped with **CSA** (4 eq.) (b) 1-D scattering pattern for pure **MO** with ES **TANI-PTAB** (6 mM), doped with **CSA** (4 eq.).*

3.2.7 Small-angle X-ray scattering investigations of TANI-PTAB in MO cubic phases, prepared without PPO

An alternative method to prepare **MO**/**TANI-PTAB** cubic phases without the use of **PPO** was briefly explored. The aim was to find a simpler method to prepare cubic phases that did not involve the weighing of small quantities of the viscous liquid **PPO**, which was a time-consuming process. It was also anticipated that the results would provide further insight into the effect of **TANI-PTAB** on the membrane curvature of **MO** without the influence of other additives. It was expected that a higher concentration of EB **TANI-PTAB** would be required to form the *Im3m* phase as there would be no **PPO** present to have an additional flattening effect on the mesophase.

The preparation method was adapted from that outlined by Brasnett et al. (2017).[70] Full experimental details are outlined in Chapter 2, Section 2.4.5. As these experiments were performed earlier in the project, the **MO** used was that provided by Danisco. **MO** and EB **TANI-PTAB** were dissolved in ethanol and pipetted into a capillary tube. The solvent was allowed to evaporate in air for 48 hours before being placed under vacuum for one week. After drying, water was added under centrifugation at 2000 rpm for one minute and the samples were left to equilibrate before analysis by SAXS.

In the first set of experiments, samples were left for equilibrate for one week before the mesophase structure was identified by SAXS. The lattice parameters and phase identification for these can be found in Figure 3.21. The *Pn3m* phase was formed at concentrations below 5 mM, while the *Im3m* phase was formed at higher concentrations. This matched the behaviour of **MO** when prepared with **TANI-PTAB** and **PPO**, which suggested that the transition to the *Im3m* phase was solely dependent on **TANI-PTAB.** However, while the Bragg peak positions could be identified in the 1-D scattering plots, the peaks were broad and poorly defined, which suggested the samples needed longer to hydrate and reduced confidence in the phase identification.

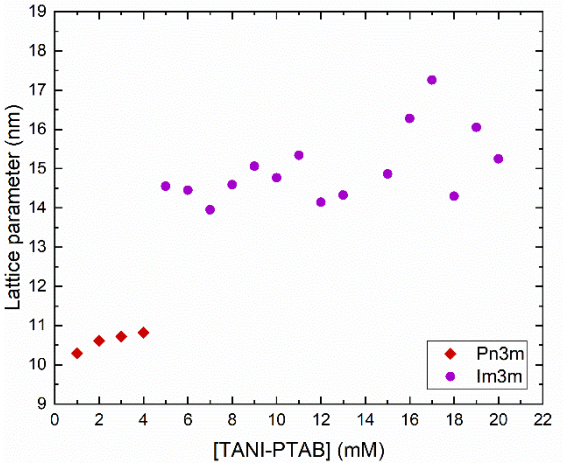

*Figure 3.21. Lattice parameters for **MO** with EB **TANI-PTAB** (1-20 mM), prepared without **PPO**.*

The experiment was repeated and the samples were left to equilibrate for nine days before identification by SAXS to see whether a longer hydration time would produce better defined peaks. The results for this experiment can be found in Figure 3.22a. The *Ia3d* phase was formed with all concentrations of EB **TANI-PTAB**, which indicated that the samples were not fully hydrated. The *Ia3d* phase typically forms with a lower water content and can be transformed into the *Im3m* or *Pn3m* phases with increasing hydration.[71,72] Therefore, the samples were allowed to hydrate for a further twelve days before re-analysis. The results after this time are given in Figure 3.22b. The *Pn3m* phase formed with concentrations lower than 14 mM, while peaks corresponding to the *Im3m* phase were observed at higher concentrations.

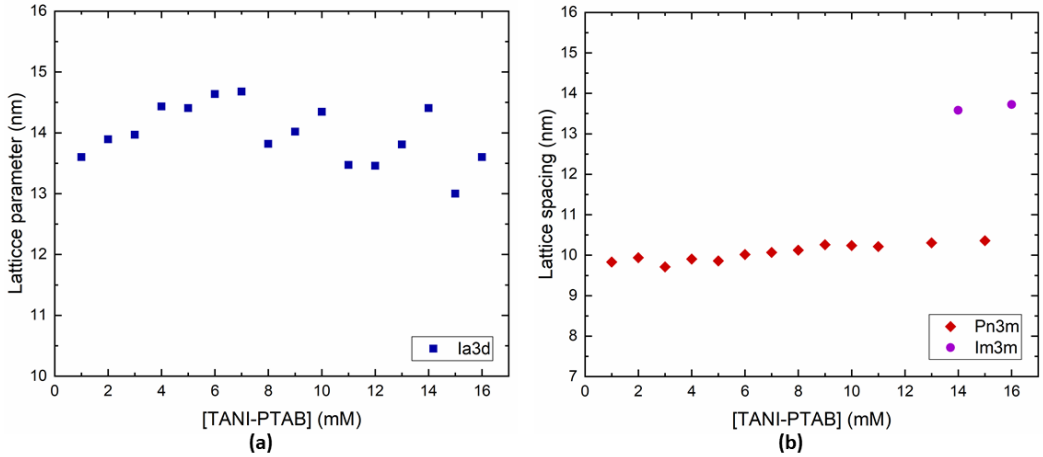

*Figure 3.22. Lattice parameters for **MO** with EB **TANI-PTAB** (1-16 mM), prepared without **PPO**, (a) after nine days (b) after 21 days.*

These results initially appeared to follow the earlier proposed pattern, which was that the addition of **TANI-PTAB** would form the *Im3m* phase at higher concentrations than samples that included **PPO**. However, the samples that formed the *Im3m* phase displayed additional peaks that could correspond to the *Pn3m* phase (see Figure B.3 in Appendix B), which indicated that they may still require longer

hydration times to finish transitioning between mesophases and the *Im3m* assignment may not be accurate.

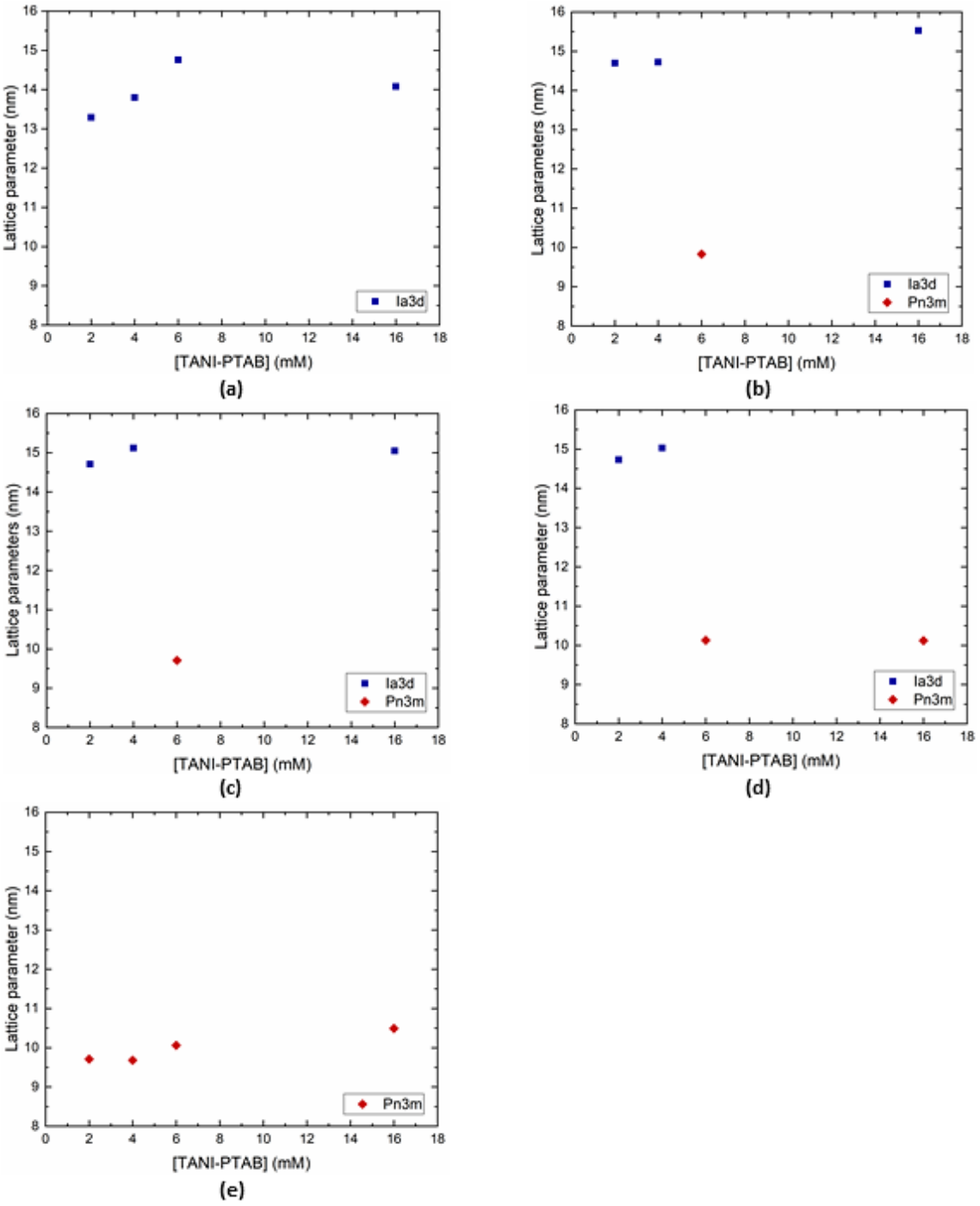

*Figure 3.23. Lattice parameters for **MO** with EB **TANI-PTAB** (1-16 mM), prepared without **PPO**. (a) 24 hours (b) 48 hours (c) 72 hours (d) 96 hours (e) 168 hours.*

A more detailed study of how the mesophase changes with time was undertaken, to gain more insight into how cubic phases form with hydration. Samples with four EB **TANI-PTAB** concentrations (2, 4, 6 and 16 mM) were prepared and were hydrated by centrifugation at 2000 rpm for one minute. The

mesophase structure was identified by SAXS over one week. The lattice parameters and phase identification for each time measurement are given in Figure 3.23.

After 24 hours, the *Ia3d* phase had formed for all **TANI-PTAB** concentrations, which indicated that, unsurprisingly, the samples needed longer to hydrate. After 48 hours, the *Pn3m* phase had formed with 6 mM of **TANI-PTAB**, however lower and higher concentrations remained in the *Ia3d* phase. The *Pn3m* phase formed with 16 mM of **TANI-PTAB** at 96 hours and with 2 and 4 mM at 168 hours. This contrasts with the results of the previous experiments, where the *Im3m* or *Ia3d* phase had formed with higher concentrations of **TANI-PTAB** and calls into question the validity of the results.

Over the three experiments, no obvious pattern for what cubic phase would form at which **TANI-PTAB** concentration was observed. The phase behaviour appeared random, with the same **TANI-PTAB** concentration producing the *Ia3d, Im3m* and *Pn3m* phases at similar time frames. Additionally, the hydration time appeared to produce inconsistent results. All experiments required further hydration, with even the samples measured at three weeks requiring longer to equilibrate.

As the results appeared to be different with each experiment, it was suggested that **TANI-PTAB** was not homogenously distributed in the **MO** mesophase and instead may be aggregating in the lipid bilayer upon drying. Different phases may form at each concentration due to variation in the amount of aggregation, which would affect the membrane curvature producing different cubic phases. Aggregation of **TANI-PTAB** may additionally be leading to pore-like openings in the bilayer, allowing for penetration of hydrophilic molecules such as acids and doping to occur, as was suggested in Section 3.2.4.2.

From the above results, it was clear that hydrating **MO** cubic phases with **TANI-PTAB** is highly challenging. Therefore, the use of additives **PPO** to produce the sponge phase before hydration to the cubic phases was preferred as this method led to reproducible results. Additionally, as the hydration time for cubic phases prepared without additives spanned weeks, it was not a practical method to prepare such materials, particularly if doping was required. De-doping occurs with **TANI-PTAB** after a few days and would certainly occur before the cubic phase reached an equilibrium. Following these results, all experiments used **PPO** in addition to **TANI** amphiphiles, to overcome these difficulties.

3.2.8 Carboxyfluorescein leakage assay

Carboxyfluorescein (**CF**) leakage assays were utilized to further explore the question of whether **TANI-PTAB** was aggregating and forming pore-like openings in the lipid membrane, allowing acids to partition into the hydrophobic bilayer. Leakage assays are a commonly used technique to determine the extent by which the introduction of an external molecule perturbs a lipid bilayer and measure the efflux of an encapsulated dye over time. Numerous examples of leakage assays can be found in the literature, with main applications in areas such as dye-release systems for targeted fluorescence imaging,[73,74] the

development of controlled drug-release in liposomes[75–77] or to investigate the effects of exogeneous species on a membrane.[78–82]

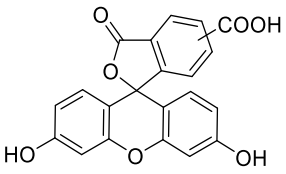

*Figure 3.24. Molecular structure of 5(6)-carboxyfluorescein (**CF**).*

CF is a derivative of fluorescein, which contains in its structure an additional carboxyl group in the 5- or 6- position, as can be seen in Figure 3.24. This additional carboxyl moiety reduces the molecule's ability to partition into hydrophobic environments, allowing for greater retention within lipid vesicles and making it more suitable for leakage assays.[83] **CF** additionally displays interesting fluorescence behaviour, emitting green light when excited. However, at high concentrations (50-200 mM), the fluorescence emission is self-quenched due to the formation of non-fluorescent dimers.[74,84]

This phenomenon is utilized in leakage assays and is represented in Scheme 3.1. Lipid vesicles are prepared containing **CF** at a concentration where the fluorescence is quenched. A membrane-perturbing species, such as EB **TANI-PTAB**, is then introduced, resulting in the formation of pores or total membrane destabilisation and thus the release of the dye into the surrounding solution. As the dye is diluted, an increase in fluorescence output is observed and from this increase, the percentage of dye release can be quantified and the species' influence on the membrane be inferred.

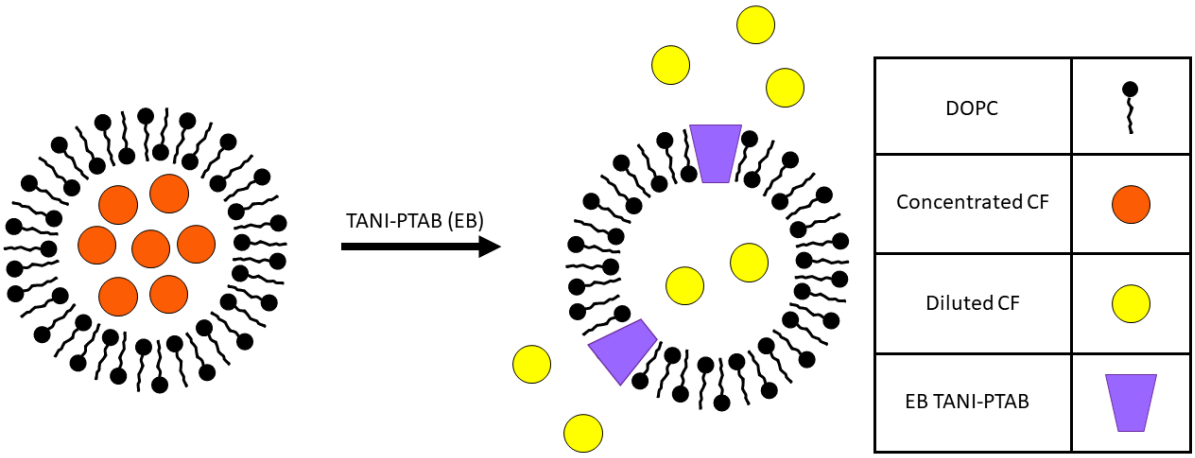

*Scheme 3.1. Schematic representation of pore formation upon addition of EB **TANI-PTAB** to **CF**-containing **DOPC** vesicles.*

1,2-dioleoyl-sn-glycero-3-phosphocholine (**DOPC**) was used in place of **MO** for the leakage assays, as it forms vesicles in excess water. The vesicles have a bilayer structure and it was expected that EB **TANI-PTAB** would insert into the lipid membrane due to its amphiphilic nature, potentially aggregating and forming pore-like openings (as with the proposed mechanism for **TANI-PTAB** with **MO** in Section 3.2.4.2), resulting in dye release.

The preparation of vesicles for leakage assay experiments followed the method outlined by Stanley (2011).[85] The full experimental details are given in Chapter 2, Section 2.4.6. In brief, a solution of 12.5 mM **DOPC** in chloroform was added to a round bottom flask and the solvent evaporated using a gentle stream of nitrogen, leaving a lipid film. The flask was placed under vacuum to ensure complete removal of the solvent before the film was hydrated using an internal buffer solution containing **CF**. The flask was vortexed to remove the lipid film from the glass walls before ten freeze-thaw cycles were performed with liquid nitrogen to disrupt the formation of multilamellar vesicles. The solution was then extruded through a polycarbonate membrane to form unilamellar vesicles. Finally, a gel filtration column was used to separate the **CF**-containing vesicles from the free dye, yielding a solution with a lipid concentration of approximately 2 mM, which was diluted to 0.2 mM for efflux experiments. The solution was then further diluted to 0.1 mM with **TANI-PTAB** solutions for leakage measurements and UV-Vis/NIR absorption spectroscopy analysis.

The UV-Vis/NIR absorption spectra of **CF** and EB **TANI-PTAB** were collected before any leakage experiments were performed, to confirm that no change in oxidation state occurred upon addition of the amphiphile to the dye-loaded vesicles. While the pKa of **CF** is 6.5, and it would not be expected to dope **TANI-PTAB**, weak acids have been previously shown to produce the ES state with **TANI**s and therefore confirmation was required before continuing the experiments.

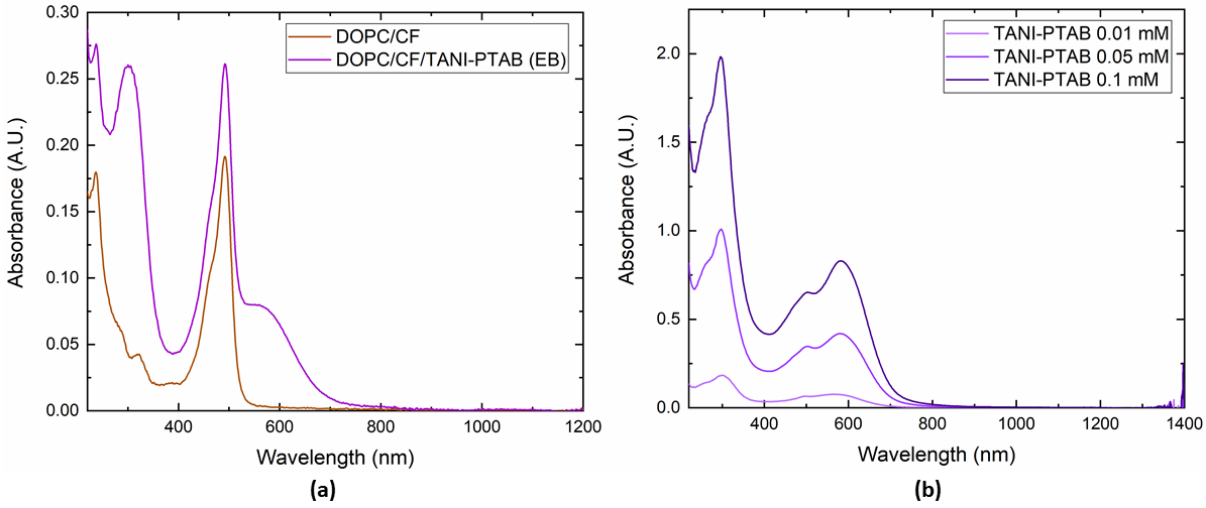

*Figure 3.25. UV-Vis/NIR absorption spectra for (a) **CF**-containing **DOPC** vesicles (0.1 mM) and EB **TANI-PTAB** (0.01 mM), with water subtracted from the baseline (b) **CF**-containing **DOPC** vesicles (0.1 mM) and EB **TANI-PTAB** (0.1-0.01 mM), with **DOPC**, **CF** and water subtracted from the baseline.*

The UV-Vis/NIR absorption spectra for **CF**-containing **DOPC** vesicles, alone and with EB **TANI-PTAB**, where water was used for baseline correction, are given in Figure 3.25a. **CF** displayed an absorption maximum of 490 nm, while a peak for only EB-state **TANI-PTAB** at 560 nm was observed. The EB peaks were more clearly observed when the absorbance spectrum of **DOPC** and **CF** was used for the baseline correction (Figure 3.25b). As the **TANI-PTAB** concentration increased, the peak at 560

nm experienced a bathochromic shift and a shoulder peak became more prominent, indicating an increase in conjugation length and therefore an increase in **TANI-PTAB** aggregation, despite the concentrations being below the CMC (0.1 mM). This was attributed to the presence of salts in the buffer used to prepare and stabilise the **DOPC** vesicles, which encouraged **TANI-PTAB** aggregation.

Following the results of the UV-Vis experiments, which confirmed that no doping occurred when EB **TANI-PTAB** was added to dye-loaded vesicles, leakage assays were performed to determine whether the amphiphile interacts with the lipid membrane and causes **CF** release, either by forming pore-like openings or causing complete membrane disruption. As a general method, 150 µL of the dye-loaded vesicles (0.2 mM) was added to a microwell plate, followed by 150 µL of the analyte solution, which diluted both to half of their initial concentrations. **CF** release was then monitored by measuring the fluorescence intensity at 516 nm over six hours. An example efflux graph can be found in Figure 3.26. The initial fluorescence intensity is seen at time zero. After the addition of an analyte, the fluorescence intensity increases and can be monitored at specific time points to get f(t). The final fluorescence intensity (f_{inf}) after complete disruption of the vesicles is obtained after the addition of 1 % (v/v) Triton-X 100. Meanwhile, the initial fluorescence intensity (f_0) is obtained after measuring the vesicle suspension when diluted with the elution buffer solution.

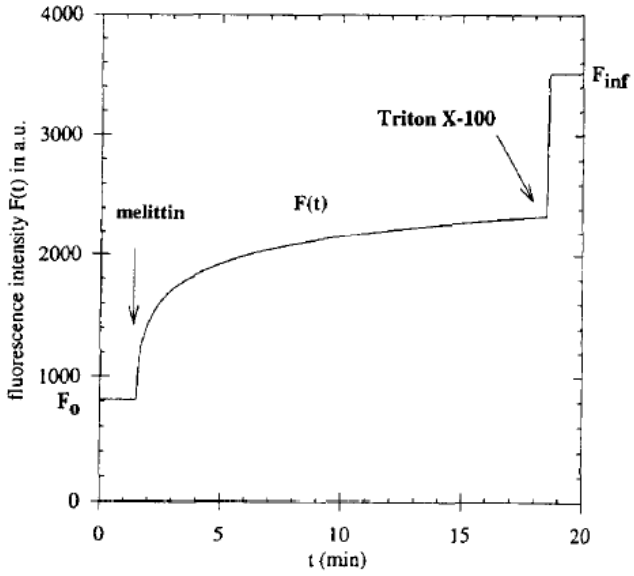

*Figure 3.26. Example graph demonstrating change in fluorescence intensity with the addition of an external species, here melittin, to lipid vesicles containing **CF**. Image reproduced from Rex (1996).*[86]

To normalise the data and allow for comparison between experiments, an efflux function (see Equation 2) was implemented.[86] This gives a result where the efflux function (E(t)) is between 0 and 1. The percent of **CF** leakage was then obtained using Equation 3.

$$E(t) = (f_{inf} - f(t))/(f_{inf} - f_0) \quad \textit{Equation 2}$$

$$\% \text{ CF leakage} = 1 - (E(t) * 100) \quad \textit{Equation 3}$$

Additionally, the rate of **CF** release was obtained by plotting the percentage of **CF** leakage as a function of time. A line of best fit was applied over the first twenty minutes, using a linear regression model, and the rate of release was obtained from the slope of the line.

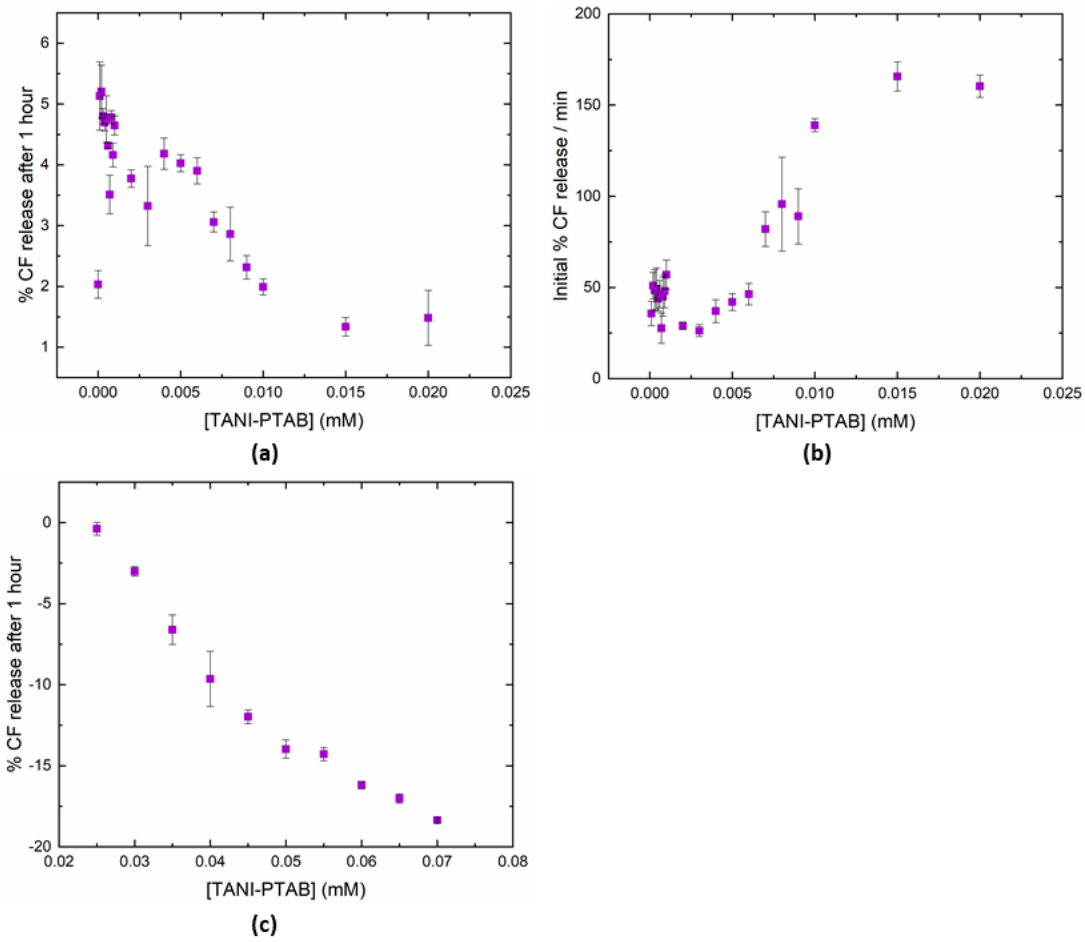

*Figure 3.27. Effect of EB **TANI-PTAB** on **CF** leakage from **DOPC** vesicles (a) % **CF** release after 1 hour for 0-0.02 mM **TANI-PTAB** (b) Initial % **CF** release per minute for 0-0.02 mM **TANI-PTAB** (c) % **CF** release after 1 hour for 0.025-0.07 mM **TANI-PTAB.***

The results for the effect of introducing EB **TANI-PTAB** to dye-containing **DOPC** vesicles are given in Figure 3.27, which shows plots for the percent of **CF** release after one hour and the initial percent of **CF** release per minute. As a control, the percentage of **CF** release after the addition of deionised water (i.e., 0 mM **TANI-PTAB**) was calculated to be approximately 2 %. The addition of EB **TANI-PTAB** initially resulted in increased **CF** release than the control (Figure 3.27a). However, as the **TANI-PTAB** concentration increased, the percentage of **CF** release began to decrease, eventually being surpassed by the control at concentrations above 0.009 mM. The fluorescence output continued to decrease with

increasing **TANI-PTAB** concentration, giving a negative calculated percentage of **CF** release (Figure 3.27c).

This negative trend is counter-intuitive, as if **TANI-PTAB** did interact with the **DOPC** bilayer, it would be expected that a higher concentration of the amphiphile would result in the formation of more pores or the complete disruption of vesicles, leading to greater dye release and an increase in the fluorescence output, not less. A negative fluorescence output would also not be expected if **TANI-PTAB** was simply not interacting with the vesicles, as the **CF** should remain encapsulated by the **DOPC** vesicles at the same self-quenching concentration.

As the **TANI-PTAB** concentration increased, the solution became darker, due to the deep purple colour of the EB state amphiphile. It is possible that the dark colour of the solution prevented the emitted light from being accurately recorded, resulting in negative results. Additionally, **CF** has an emission wavelength maximum of 517 nm,[87] which is in the range where EB **TANI-PTAB** absorbs. This could result in quenching of the emitted radiation, where higher concentrations of **TANI-PTAB** would lead to increased quenching of the **CF** fluorescence.

As low concentrations of **TANI-PTAB** resulted in increased dye-release than the control, it was possible that higher concentrations resulted in greater **CF** leakage, which was not accurately recorded due to quenching by the EB-state **TANI-PTAB**. Indeed, the plotted release rates (Figure 3.27b) showed a positive trend, suggesting faster dye-release with increasing **TANI-PTAB** concentration, although the data may not be accurate due to the fluorescence quenching.

To overcome this issue, acids were introduced to dope the **TANI-**amphiphile to the ES state and move its absorbance maxima to longer wavelengths. It was also hoped that the change in oxidation state would result in a change in **CF** release, providing a controlled release mechanism by the application of an acid or base.

The UV-Vis/NIR absorption spectra for **TANI-PTAB** doped with **TFA** and **CSA**, which were baseline corrected with **CF**-containing **DOPC** vesicles, are given in Figure 3.28. In the presence of the lipid, dye, and the elution buffer, which was used as the solvent, **TANI-PTAB** required a larger quantity of acid to become doped. An ES peak at around 800 nm only appeared with 32 molar equivalents of either **TFA** or **CSA**, when a sharp decrease in absorbance at 490 nm was also noted. The most soluble form of **CF** is the trivalent anion, which exist in a pH range of 7-11.[87] The internal and elution buffers were adjusted to pH 7.4 before vesicle formation to encourage **CF** dissolution. However, when high concentrations of **TFA** and **CSA** were added to the UV-Vis solutions, the overall pH was lowered and the solubility of the dye decreased, resulting in the observed decrease in absorbance.

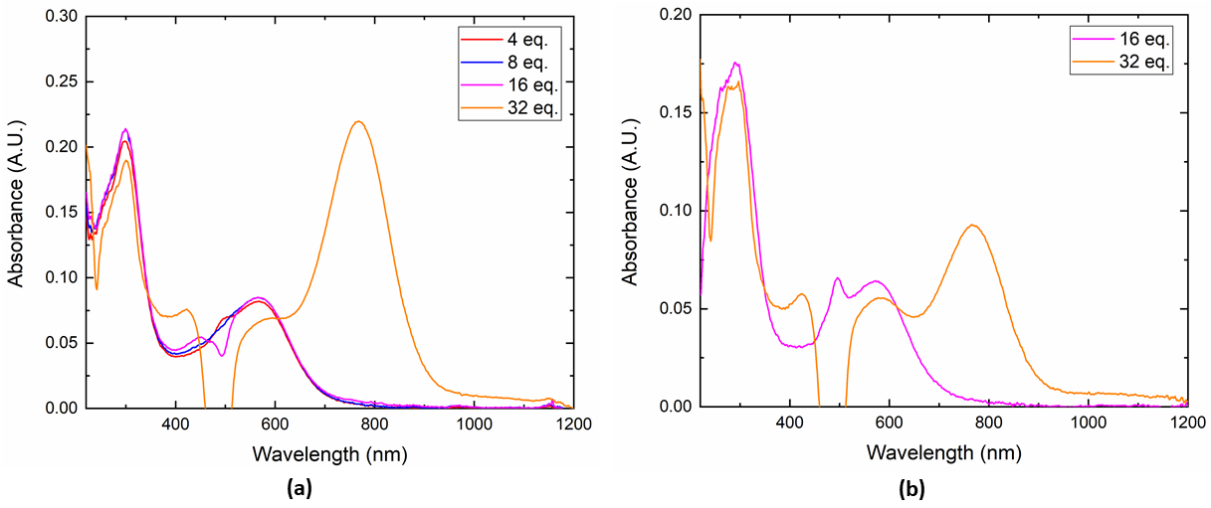

*Figure 3.28. UV-Vis/NIR absorption spectra for **TANI-PTAB** (0.1 mM) doped with (a) **TFA** and (b) **CSA**. The spectra are baseline corrected with **CF**-containing **DOPC** vesicles (0.1 mM).*

The same decrease in **CF** solubility was noted when performing leakage assays with dye-loaded vesicles and **TFA** or **CSA** (Figure 3.29). It appeared that the addition of both acids also disrupts the vesicle formation, as could be seen by the initially higher percentage of dye release than the control. However, as the concentration of acid increased, the fluorescence output decreased, eventually giving a negative release measurement for **TFA**. **TFA** is a stronger acid than **CSA**, which have pKas of 0.23 and 1.2, respectively. Therefore, a lower concentration of **TFA** is required to lower the pH of the solution sufficiently to cause **CF** to precipitate.

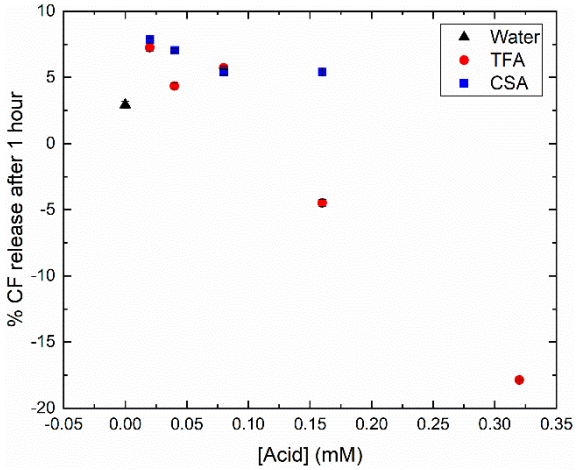

*Figure 3.29. Effect of **TFA** and **CSA** addition to **CF**-loaded **DOPC** vesicles (0.1 mM). % **CF** release reported after 1 hour.*

Leakage assays with **TANI-PTAB** doped with **TFA** and **CSA** were performed, to determine their combined effect on **CF** release (Figure 3.30). A low concentration of each acid (2 molar equivalents) was chosen to reduce the amount of **CF** precipitation due to lowered pH. However, from the results of the UV-Vis experiments (Figure 3.28), it was clear that this was not sufficient to dope **TANI-PTAB** and the solution remained purple. The results of the leakage assays suggest that a slightly greater amount

of dye was released with low concentrations of the "doped" **TANI-PTAB**, however, this was likely to be due to the combined separate effects of EB **TANI-PTAB** and the acids. A negative trend was observed with increasing **TANI-PTAB** concentration, which could be due to quenching from the EB state and the increased pH that occurred with increasing acid concentration. The release rates did not show any trend with concentration.

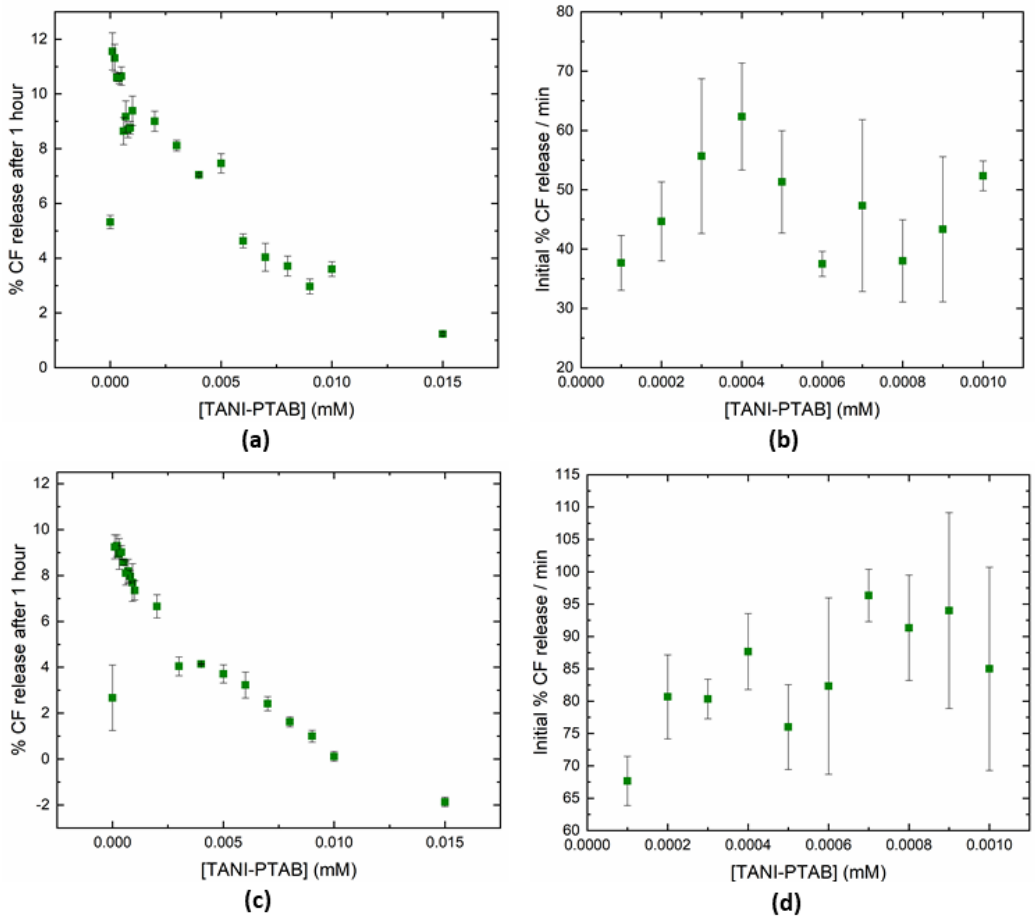

*Figure 3.30. Effect of **TANI-PTAB** and acids on the leakage of **CF** from **DOPC** vesicles (0.1 mM). (a) % **CF** release after 1 hour and (b) Initial % **CF** release per minute with **TANI-PTAB** and 2 molar equivalents of **CSA**. (c) % **CF** release after 1 hour and (d) Initial % **CF** release per minute with **TANI-PTAB** and 2 molar equivalents of **TFA**.*

Limited conclusions can be drawn from the results of these leakage assays. It appears that EB **TANI-PTAB** does interact with a **DOPC** membrane, resulting in **CF** release at concentrations below 0.01 mM. However, the results are hampered by the quenching of **CF** fluorescence emission by **TANI-PTAB** and the reduced solubility of the dye upon addition of acids. The mechanism of release cannot be identified, either pore formation due to aggregation of **TANI-PTAB** or membrane dissolution, and therefore no parallels can be drawn for the behaviour of the amphiphile in **MO** cubic phases.

3.2.9 Dynamic light scattering

An alternative method to probe the change in vesicle structure after the introduction of **TANI-PTAB** is dynamic light scattering (DLS). With this technique, a measure of vesicle size can be collected over a period of time, allowing for a change in size or polydispersity to be recorded dynamically. An additional benefit to this technique is that it does not require a dye for vesicle disruption to be identified, which means that any quenching of fluorescence by **TANI-PTAB** is not a limiting factor. Indeed, it is preferable to not use a fluorescent dye when analysing structures with DLS as the technique relies on scattered light from an incident laser beam to determine the hydrodynamic radius of nanoparticles, which can be absorbed and re-emitted by fluorescent particles affecting the measured signal.[88]

DOPC vesicles were prepared similarly to those used in **CF** leakage assays, however, the elution buffer was used to initially hydrate the lipid film in place of the internal buffer, eliminating the addition of the dye. After hydration, the **DOPC** solution underwent multiple freeze-thaw cycles to disrupt any multilamellar vesicles, before extrusion through a polycarbonate membrane (100 nm diameter pore size). After extrusion, the lipid solution was diluted to 0.2 mM with deionised water. For DLS experiments, 1 mL of vesicle solution was further diluted to 0.1 mM with 1 mL of analyte solution. Measurements were taken at 30-minute intervals for four hours.

*Table 3.1. Z-Averages and PDIs for **DOPC** vesicles (0.1 mM) after the addition of elution buffer, water or EB **TANI-PTAB** (0.01 mM)*

	Elution buffer		**Water**		**EB TANI-PTAB (0.01 mM)**	
Time (mins)	**Z_{Ave} (nm)**	**PDI**	**Z_{Ave} (nm)**	**PDI**	**Z_{Ave} (nm)**	**PDI**
30	117.1	0.149	104.1	0.480	131.4	0.106
60	120.0	0.077	120.7	0.102	129.1	0.146
90	117.4	0.149	119.9	0.134	112.4	0.440
120	118.0	0.162	120.8	0.123	114.9	0.312
150	117.9	0.098	118.9	0.171	110.7	0.387
180	102.1	0.463	121.9	0.154	102.3	0.590
210	102.9	0.449	119.3	0.157	103.4	0.584
240	102.2	0.456	103.9	0.503	107.2	0.521

Water and elution buffer were added to the vesicle solution as controls and were compared to the addition of 0.01 mM EB **TANI-PTAB**, the results of which can be found in Table 3.1. The Z-average (Z_{Ave}) is the intensity weighted mean hydrodynamic size of a collection of particles, while the polydispersity index (PDI) gives an indication of the width of the overall distribution for each peak. With DLS, a PDI below 0.1 usually indicates a highly monodisperse sample, while a value above 0.4 indicates a highly polydisperse sample and values in between are moderately disperse.

The results in Table 3.1 indicate that vesicles in the presence of EB **TANI-PTAB** were initially swollen (ca. 130 nm after 60 minutes) in comparison to vesicles diluted with water or elution buffer (ca. 120 nm after 60 minutes), which may be due to the incorporation of the amphiphile into the lipid bilayer. However, after 90 minutes, the Z-average for vesicles containing **TANI-PTAB** had decreased to 112 nm and the PDI had increased, which indicated that the mixture had become more polydisperse. The Z-average continued to decrease with time and the PDI increased, indicating that a mixture of particle sizes was present, possibly due to the disruption of the vesicles into smaller particles. In comparison, solutions diluted with water and elution buffer were stable for longer, only experiencing a decrease in particle size and increase in PDI after three hours.

The results suggest that **TANI-PTAB** does interact with **DOPC** vesicles, initially by swelling the particle sizes before causing vesicle disruption and formation of smaller, polydisperse aggregates. However, the sample size was limited and so it is not reasonable to use the results to predict the outcome of future experiments. With additional time, the experiments would have been repeated, using different **TANI-PTAB** concentrations and adding dopants to provide a more detailed comparison with the leakage assays and demonstrate the effect of changing oxidation state on vesicle size. Similar experiments could be performed using SAXS, which could provide further insight into the morphological changes of the **DOPC** vesicles with the addition of **TANI-PTAB** over time. Finally, cryo-transmission electron microscopy (cryo-TEM) could be used to probe the physical changes to the vesicles. The freezing process would prevent the visualisation of vesicle disruption over real time, however, by analysing samples prepared at different time intervals, it would be possible to directly observe the difference between **DOPC** vesicles alone, with the addition of **TANI-PTAB** and after certain time increments.

3.3 CONCLUSIONS

In this chapter, the effect of introducing **TANI-PTAB**, in both the emeraldine base (EB) and emeraldine salt (ES) oxidation states, on lipid self-assemblies was investigated. Cubic phases were prepared from monoolein (**MO**) by first preparing the sponge phase using pentaerythritol propoxylate (**PPO**), before dilution to the cubic phase under centrifugation. This preparation method was chosen over a simpler method (i.e., hydration of films formed by drying **MO** and **TANI-PTAB** together), as it produced reproducible results within 48 hours.

EB **TANI-PTAB** was incorporated into **MO** sponge and cubic phases and the oxidation state in the sponge phase was confirmed by UV-Vis/NIR spectroscopy. A loss of aggregation was noted after addition to the sponge phase, as evident by the absence of a shoulder in the UV-Vis/NIR absorption spectrum, however this was attributed to the incorporation of the amphiphile into the lipid bilayer. The *Im3m* phase was formed upon increasing EB **TANI-PTAB** concentration, due to the combination of the amphiphile's packing parameter ($pp < 1$) with that of **MO** ($pp > 1$).

A change in mesophase was noted upon doping **TANI-PTAB** to the ES state. The addition of doping acids increases the volume of the hydrophobic **TANI-PTAB** core, resulting in an increase in the amphiphile's *pp*. When combined with **MO**, this increase in *pp* resulted in the formation of the *Pn3m* phase at all ES **TANI-PTAB** concentrations. The mechanism by which the **TANI-PTAB** molecules, which are sequestered in the hydrophobic lipid bilayer, became doped by the hydrophilic acids was also discussed and a few theories, such as the formation of pores or the partitioning of **TANI-PTAB** into the water channels, were put forward.

The formation of pores by **TANI-PTAB** was further explored using carboxyfluorescein (**CF**) leakage assays and dynamic light scattering. The results suggested that the introduction of **TANI-PTAB** did result in membrane disruption, however, further experimentation was required to draw conclusive results due to the limited number of experiments performed and the potential quenching of **CF** fluorescence by EB **TANI-PTAB**.

Finally, the variation in concentration at which the *Im3m* phase formed with EB **TANI-PTAB** was explored. It was discovered that the **MO** used in the majority of UV-Vis/NIR spectroscopy and SAXS experiments had partially degraded over time, resulting in the formation of oleic acid. Despite it being a weak acid, it was proposed that the oleic acid was partially doping **TANI-PTAB** in **MO** cubic phases, as evidenced by the presence of ES peaks in UV-Vis/NIR absorption spectra, and that the mixture of EB and ES states was influencing the mesophase behaviour.

In summary, EB and ES state **TANI-PTAB** were introduced to **MO** cubic phases and the resulting effect on the mesophase structure was recorded. The results appeared dependent on the amphiphile's *pp*. The EB state, with a *pp* of 0.37, produced the *Im3m* phase when combined with **MO**. However, the *Pn3m* phase was formed upon acid doping and subsequent increase in *pp*. This change with doping provides a switchable method to control the phase behaviour of **MO** by simple application of an acid or base, allowing the structure to be tuned for the desired application.

3.4 REFERENCES

1. Ruokolainen, J. *et al.* Switching supramolecular polymeric materials with multiple length scales. *Science* **280**, 557–560 (1998).

2. Li, X. *et al.* Uniform electroactive fibre-like micelle nanowires for organic electronics. *Nat. Commun.* **8**, 15909–15917 (2017).

3. Cordier, P., Tournilhac, F., Soulié-Ziakovic, C. & Leibler, L. Self-healing and thermoreversible rubber from supramolecular assembly. *Nature* **451**, 977–80 (2008).

4. Ilday, S., Makey, G. & Akguc, G. B. Rich complex behaviour of self-assembled nanoparticles far from equilibrium. *Nat. Commun.* **8**, 14942–14952 (2017).

5. Yan, Q. *et al.* Voltage-responsive vesicles based on orthogonal assembly of two homopolymers. *J. Am. Chem. Soc.* **132**, 9268–9270 (2010).

6. Van Dijk, E. H., Myles, D. J. T., Van Der Veen, M. H. & Hummelen, J. C. Synthesis and properties of an anthraquinone-based redox switch for molecular electronics. *Org. Lett.* **8**, 2333–2336 (2006).

7. She, S. *et al.* Buildup of Redox-Responsive Hybrid from Polyoxometalate and Redox-Active Conducting Oligomer: Its Self-Assemblies with Controllable Morphologies. *Chem. - A Eur. J.* **23**, 14860–14865 (2017).

8. van 't Hag, L., Gras, S. L., Conn, C. E. & Drummond, C. J. Lyotropic liquid crystal engineering moving beyond binary compositional space – ordered nanostructured amphiphile self-assembly materials by design. *Chem. Soc. Rev.* **46**, 2705–2731 (2017).

9. Qiu, H. & Caffrey, M. The phase diagram of the monoolein/water system: Metastability and equilibrium aspects. *Biomaterials* **21**, 223–234 (2000).

10. Cherezov, V., Clogston, J., Papiz, M. Z. & Caffrey, M. Room to move: Crystallizing membrane proteins in swollen lipidic mesophases. *J. Mol. Biol.* **357**, 1605–1618 (2006).

11. Nazaruk, E. *et al.* Enzymatic biofuel cell based on electrodes modified with lipid liquid-crystalline cubic phases. *J. Power Sources* **183**, 533–538 (2008).

12. Nazaruk, E., Bilewicz, R., Lindblom, G. & Lindholm-Sethson, B. Cubic phases in biosensing systems. *Anal. Bioanal. Chem.* **391**, 1569–1578 (2008).

13. Nazaruk, E. *et al.* Properties of native and hydrophobic laccases immobilized in the liquid-crystalline cubic phase on electrodes. *J. Biol. Inorg. Chem.* **12**, 335–344 (2007).

14. Hag, L. Van *et al.* In Meso Crystallization: Compatibility of Different Lipid Bicontinuous

Cubic Mesophases with the Cubic Crystallization Screen in Aqueous Solution. *Cryst. Growth Des.* **14**, 1771–1781 (2014).

15. Caffrey, M. Crystallizing Membrane Proteins for Structure Determination: Use of Lipidic Mesophases. *Annu. Rev. Biophys.* **38**, 29–51 (2009).

16. Szlezak, M. *et al.* Monoolein cubic phase gels and cubosomes doped with magnetic nanoparticles-hybrid materials for controlled drug release. *ACS Appl. Mater. Interfaces* **9**, 2796–2805 (2017).

17. Nazaruk, E., Górecka, E., Osornio, Y. M., Landau, E. M. & Bilewicz, R. Charged additives modify drug release rates from lipidic cubic phase carriers by modulating electrostatic interactions. *J. Electroanal. Chem.* **819**, 269–274 (2018).

18. Rahanyan-Kägi, N., Aleandri, S., Speziale, C., Mezzenga, R. & Landau, E. M. Stimuli-responsive lipidic cubic phase: Triggered release and sequestration of guest molecules. *Chem. - A Eur. J.* **21**, 1873–1877 (2015).

19. Fong, W. K., Negrini, R., Vallooran, J. J., Mezzenga, R. & Boyd, B. J. Responsive self-assembled nanostructured lipid systems for drug delivery and diagnostics. *J. Colloid Interface Sci.* **484**, 320–339 (2016).

20. Phan, S., Fong, W.-K., Kirby, N., Hanley, T. & Boyd, B. J. Evaluating the link between self-assembled mesophase structure and drug release. *Int. J. Pharm.* **421**, 176–182 (2011).

21. Negrini, R. & Mezzenga, R. pH-responsive lyotropic liquid crystals for controlled drug delivery. *Langmuir* **27**, 5296–5303 (2011).

22. Negrini, R., Fong, W. K., Boyd, B. J. & Mezzenga, R. pH-responsive lyotropic liquid crystals and their potential therapeutic role in cancer treatment. *Chem. Commun.* **51**, 6671–6674 (2015).

23. Bisset, N. B., Boyd, B. J. & Dong, Y. Da. Tailoring liquid crystalline lipid nanomaterials for controlled release of macromolecules. *Int. J. Pharm.* **495**, 241–248 (2015).

24. Fong, W.-K., Hanley, T. L., Thierry, B., Kirby, N. & Boyd, B. J. Plasmonic Nanorods Provide Reversible Control over Nanostructure of Self-Assembled Drug Delivery Materials. *Langmuir* **26**, 6136–6139 (2010).

25. Aleandri, S., Speziale, C., Mezzenga, R. & Landau, E. M. Design of Light-Triggered Lyotropic Liquid Crystal Mesophases and Their Application as Molecular Switches in ‘On Demand’ Release. *Langmuir* **31**, 6981–6987 (2015).

26. Fong, W.-K. *et al.* External manipulation of nanostructure in photoresponsive lipid depot

matrix to control and predict drug release in vivo. *J. Control. Release* **228**, 67–73 (2016).

27. Mendozza, M. *et al.* On the thermotropic and magnetotropic phase behavior of lipid liquid crystals containing magnetic nanoparticles. *Nanoscale* **10**, 3480–3488 (2018).

28. Akbar, S., Elliott, J. M., Rittman, M. & Squires, A. M. Facile production of ordered 3D platinum nanowire networks with 'single diamond' bicontinuous cubic morphology. *Adv. Mater.* **25**, 1160–1164 (2013).

29. Richardson, S. J. *et al.* Aligned platinum nanowire networks from surface-oriented lipid cubic phase templates. *Nanoscale* **8**, 2850–2856 (2016).

30. Burton, M. *et al.* Three-Dimensional Nanostructured Palladium with Single Diamond Architecture for Enhanced Catalytic Activity. *ACS Appl. Mater. Interfaces* **10**, 37087–37094 (2018).

31. Dehmel, R., Nicolas, A., Scherer, M. R. J. & Steiner, U. 3D Nanostructured Conjugated Polymers for Optical Applications. *Adv. Funct. Mater.* **25**, 6900–6905 (2015).

32. Cho, W. *et al.* Synthesis and characterization of bicontinuous cubic poly(3,4-ethylene dioxythiophene) gyroid (PEDOT GYR) gels. *Phys. Chem. Chem. Phys.* **17**, 5115–5123 (2015).

33. Khiew, P. S., Radiman, S., Huang, N. M., Kan, C. S. & Ahmad, M. S. In situ polymerization of conducting polyaniline in bicontinuous cubic phase of lyotropic liquid crystal. *Colloids Surfaces A Physicochem. Eng. Asp.* **247**, 35–40 (2004).

34. Huang, L. *et al.* Polyaniline nanowires by electropolymerization from liquid crystalline phases. *J. Mater. Chem.* **12**, 388–391 (2002).

35. Li, C. *et al.* Conductive polyaniline helixes self-assembled in the absence of chiral dopant. *Chem. Commun.* **49**, 1100–1102 (2013).

36. Shimano, J. Y. & MacDiarmid, A. G. Polyaniline, a dynamic block copolymer: Key to attaining its intrinsic conductivity? *Synth. Met.* **123**, 251–262 (2001).

37. MacDiarmid, A. G. & Epstein, A. J. Secondary doping in polyaniline. *Synth. Met.* **69**, 85–92 (1995).

38. Wei, Z. & Faul, C. F. J. Aniline oligomers - Architecture, function and new opportunities for nanostructured materials. *Macromol. Rapid Commun.* **29**, 280–292 (2008).

39. Wang, Y. *et al.* Morphological and dimensional control via hierarchical assembly of doped oligoaniline single crystals. *J. Am. Chem. Soc.* **134**, 9251–9262 (2012).

40. Wang, Y. *et al.* Graphene-Assisted Solution Growth of Vertically Oriented Organic

Semiconducting Single Crystals. *ACS Nano* **9**, 9486–9496 (2015).

41. Bell, O. A. *et al.* Self-Assembly of a Functional Oligo(Aniline)-Based Amphiphile into Helical Conductive Nanowires. *J. Am. Chem. Soc.* **137**, 14288–14294 (2015).

42. Lyu, W. *et al.* An addressable packing parameter approach for reversibly tuning the assembly of oligo(aniline)-based supra-amphiphiles. *Chem. Sci.* **9**, 4392–4401 (2018).

43. MacDiarmid, A. G., Zhou, Y. & Feng, J. Oligomers and isomers: new horizons in poly-anilines. *Synth. Met.* **100**, 131–140 (1999).

44. Liao, Y., Cheng, Z., Zuo, W., Thomas, A. & Faul, C. F. J. Nitrogen-Rich Conjugated Microporous Polymers: Facile Synthesis, Efficient Gas Storage, and Heterogeneous Catalysis. *ACS Appl. Mater. Interfaces* **9**, 38390–38400 (2017).

45. Chen, J. *et al.* Porous Materials Tunable Surface Area , Porosity , and Function in Conjugated Microporous Polymers. *Angew. Chem. Int. Ed.* **58**, 11715–11719 (2019).

46. Pan, L. *et al.* Luminescent and Swellable Conjugated Microporous Polymers for Detecting Nitroaromatic Explosives and Removing Harmful Organic Vapors. *ACS Appl. Mater. Interfaces* **11**, 48352–48362 (2019).

47. Porte, G. Isotropic phases of bilayers. *Curr. Opin. Colloid Interface Sci.* **1**, 345–349 (1996).

48. Kulkarni, C. V., Wachter, W., Iglesias-Salto, G., Engelskirchen, S. & Ahualli, S. Monoolein: a magic lipid? *Phys. Chem. Chem. Phys.* **13**, 3004–3021 (2011).

49. Bennett, N. *et al.* Mesoporous tertiary oxides via a novel amphiphilic approach. *APL Mater.* **4**, 015701 (2016).

50. Negrini, R. & Mezzenga, R. Diffusion, molecular separation, and drug delivery from lipid mesophases with tunable water channels. *Langmuir* **28**, 16455–16462 (2012).

51. Holyst, R. Infinite networks of surfaces. *Nat. Mater.* **4**, 510–511 (2005).

52. Wang, D. *et al.* A general route to macroscopic hierarchical 3D nanowire networks. *Angew. Chem. Int. Ed.* **43**, 6169–6173 (2004).

53. Seddon, A. M., Lotze, G., Plivelic, T. S. & Squires, A. M. A highly oriented cubic phase formed by lipids under shear. *J. Am. Chem. Soc.* **133**, 13860–13863 (2011).

54. Oka, T. & Hojo, H. Single Crystallization of an Inverse Bicontinuous Cubic Phase of a Lipid. *Langmuir* **30**, 8253–8257 (2014).

55. de Albuquerque, J. E., Mattoso, L. H. C., Faria, R. M., Masters, J. G. & MacDiarmid, A. G.

Study of the interconversion of polyaniline oxidation states by optical absorption spectroscopy. *Synth. Met.* **146**, 1–10 (2004).

56. Bell, O. A. *et al.* Self-assembly of a functional oligo(aniline)-based amphiphile into helical conductive nanowires. *J. Am. Chem. Soc.* **137**, 14288–14294 (2015).

57. Reichardt, C. Solvatochromic Dyes as Solvent Polarity Indicators. *Chem. Rev.* **94**, 2319–2358 (1994).

58. Mills, B. M. *et al.* Tipping the polaron-bipolaron balance: concentration and spin effects in doped oligo(aniline)s observed by UV-vis-NIR and TD-DFT. *Mol. Syst. Des. Eng.* **4**, 103–109 (2019).

59. Nazaruk, E. *et al.* Lyotropic Cubic Phases for Drug Delivery: Diffusion and Sustained Release from the Mesophase Evaluated by Electrochemical Methods. *Langmuir* **31**, 12753–12761 (2015).

60. Caffrey, M. A comprehensive review of the lipid cubic phase or in meso method for crystallizing membrane and soluble proteins and complexes. *Acta Crystallogr. Sect. F Struct. Biol. Commun.* **71**, 3–18 (2015).

61. Negrini, R. & Mezzenga, R. Diffusion, molecular separation, and drug delivery from lipid mesophases with tunable water channels. *Langmuir* **28**, 16455–16462 (2012).

62. Zhai, J. *et al.* Lipid–PEG Conjugates Sterically Stabilize and Reduce the Toxicity of Phytantriol-Based Lyotropic Liquid Crystalline Nanoparticles. *Langmuir* **31**, 10871–10880 (2015).

63. Mezzenga, R. *et al.* Polysaccharide-Induced Order-to-Order Transitions in Lyotropic Liquid Crystals. *Langmuir* **21**, 6165–6169 (2005).

64. Vargas, R., Mateu, L. & Romero, A. The effect of increasing concentrations of precipitating salts used to crystallize proteins on the structure of the lipidic Q 224 cubic phase. *Chem. Phys. Lipids* **127**, 103–111 (2004).

65. Conn, C. E. *et al.* High-throughput analysis of the structural evolution of the monoolein cubic phase in situ under crystallogenesis conditions. *Soft Matter* **8**, 2310–2321 (2012).

66. Yaghmur, A., Rappolt, M., Østergaard, J., Larsen, C. & Larsen, S. W. Characterization of Bupivacaine-Loaded Formulations Based on Liquid Crystalline phases and Microemulsions : The Effect of Lipid Composition. *Langmuir* **28**, 2881–2889 (2012).

67. Gilson. Pipetman (R). (2018). Available at: https://gb.gilson.com/pub/static/frontend/Gilson/customtheme/en_US/images/docs/PIPETMA

NG_BROC_2018.pdf. (Accessed: 13th January 2021)

68. Liu, P. Synthesis and characterization of organo-soluble conducting polyaniline doped with oleic acid. *Synth. Met.* **159**, 148–152 (2009).

69. Fong, C., Le, T. & Drummond, C. J. Lyotropic liquid crystal engineering – ordered nanostructured small molecule amphiphile self-assembly materials by design. *Chem. Soc. Rev.* **41**, 1297–1322 (2012).

70. Brasnett, C., Longstaff, G., Compton, L. & Seddon, A. Effects of Cations on the Behaviour of Lipid Cubic Phases. *Sci. Rep.* **7**, 8229 (2017).

71. Templer, R. H., Seddon, J. M., Warrender, N. A., Syrykh, A. & Huang, Z. Inverse Bicontinuous Cubic Phases in 2 : 1 Fatty Acid / Phosphatidylcholine Mixtures . The Effects of Chain Length , Hydration , and Temperature. *J. Phys. Chem. B* **102**, 7251–7261 (1998).

72. Seddon, A. M., Hallett, J., Beddoes, C., Plivelic, T. S. & Squires, A. M. Experimental confirmation of transformation pathways between inverse double diamond and gyroid cubic phases. *Langmuir* **30**, 5705–5710 (2014).

73. Begu, S., Mordon, S., Desmettre, T. & Devoisselle, J. M. Fluorescence imaging method for in vivo pH monitoring during liposomes uptake in rat liver using a pH-sensitive fluorescent dye. *J. Biomed. Opt.* **10**, 024008 (2005).

74. Mordon, S., Devoisselle, J. M., Begu, S. & Desmettre, T. Laser-Induced Release of Liposome-Encapsulated Dye : A New Diagnostic Tool. *Lasers Med. Sci.* **13**, 181–188 (1998).

75. Li, L. *et al.* Triggered content release from optimized stealth thermosensitive liposomes using mild hyperthermia. *J. Control. Release* **143**, 274–279 (2010).

76. Tai, L.-A. *et al.* Thermosensitive liposomes entrapping iron oxide nanoparticles for controllable drug release. *Nanotechnology* **20**, 135101 (2009).

77. Gao, X. *et al.* Controllable Synthesis of a Smart Multifunctional Nanoscale Metal − Organic Framework for Magnetic Resonance / Optical Imaging and Targeted Drug Delivery. *ACS Appl. Mater. Interfaces* **9**, 3455–3462 (2017).

78. Ambroggio, E. E., Separovic, F., Bowie, J. H., Fidelio, G. D. & Bagatolli, L. A. Direct Visualization of Membrane Leakage Induced by the Antibiotic Peptides: Maculatin, Citropin, and Aurein. *Biophys. J.* **89**, 1874–1881 (2005).

79. Gregory, S. M., Cavenaugh, A., Journigan, V., Pokorny, A. & Almeida, P. F. F. A Quantitative Model for the All-or-None Permeabilization of Phospholipid Vesicles by the Antimicrobial Peptide Cecropin A. *Biophys. J.* **94**, 1667–1680 (2008).

80. Pokorny, A. & Almeida, P. F. F. Kinetics of Dye Efflux and Lipid Flip-Flop Induced by δ -Lysin in Phosphatidylcholine Vesicles and the Mechanism of Graded Release by Amphipathic, a-Helical Peptides. *Biochemistry* **43**, 8846–8857 (2004).

81. Yandek, L. E. *et al.* Mechanism of the Cell-Penetrating Peptide Transportan 10 Permeation of Lipid Bilayers. *Biophys. J.* **92**, 2434–2444 (2007).

82. Ladokhin, A. S. Leakage of Membrane Vesicle Contents: Determination of Mechanism Using Fluorescence Requenching. *Biophys. J.* **69**, 1964–1971 (1995).

83. Grimes, P. A., Stone, R. A., Laties, A. M. & Li, W. Carboxyfluorescein A Probe Of The Blood-Ocular Barriers With Lower Membrane Permeability Than Fluorescein. *Arch. Ophthalmol.* **100**, 635–639 (1982).

84. Chen, R. F. & Knutson, J. R. Mechanism of Fluorescence Concentration Quenching of Carboxyfluorescein in Liposomes : Energy Transfer to Nonfluorescent Dimers. *Anal. Biochem.* **77**, 61–77 (1988).

85. Stanley, C. E. Development of high-throughput technologies for the study of drug-membrane interactions. (University of Bristol, 2011).

86. Rex, S. Pore formation induced by the peptide melittin in different lipid vesicle membranes. *Biophys. Chem.* **58**, 75–85 (1996).

87. Weinstein, J. N., Blumenthal, R. & Klausner, R. D. Carboxyfluorescein leakage assay for lipoprotein-liposome interaction. *Methods Enzymol.* **128**, 657–668 (1986).

88. Geißler, D. *et al.* Effect of fluorescent staining on size measurements of polymeric nanoparticles using DLS and SAXS. *Anal. Methods* **7**, 9785–9790 (2015).

4 TEMPLATED SELF-ASSEMBLY OF OTHER OLIGO(ANILINE)-DERIVED AMPHIPHILES IN LIPID BICONTINUOUS CUBIC PHASES

4.1 INTRODUCTION

The concept of a molecular packing parameter (*pp*) was first introduced by Israelachvili, Mitchell and Ninham in 1976, and has since been widely used to predict and explain the self-assembly behaviour of amphiphiles.[1–5] An amphiphile's *pp* can be calculated from Equation 1, where v_0 is the volume of the hydrophobic section, l_0 is the hydrophobic tail length and a_e is optimum head group area.[6]

$$pp = v_0/a_e l_0 \qquad \textit{Equation 1}$$

The *pp* model predicts that spherical micelles will be preferred when $pp < \frac{1}{3}$, cylindrical micelles will be formed for $\frac{1}{3} \leq pp < \frac{1}{2}$, flexible bilayers or vesicles will be favoured for $\frac{1}{2} \leq pp < 1$, planar bilayers are produced when $pp = 1$ and inverted micelles are formed when $pp > 1$.[7]

When the concept of *pp* was first introduced, it was believed that the hydrophobic tail length had no role in determining the self-assembled structures formed by common amphiphiles, as the ratio of v_0/l_0 is a constant that is independent of tail length.[6] Therefore, the optimum head group area was expected to be solely responsible for the shape and size of any aggregates formed. However, on the contrary, Nagarajan (2002) demonstrated that the tail does exert a great deal of influence over the self-assemblies, by altering the ionic strength of the solution and thereby changing the optimum head group area and overall packing, or by affecting transitions between assemblies.[6] Indeed, numerous studies have shown that the amphiphile tail length influences properties such as the critical micelle concentration (CMC) and aggregate dimensions and structure, and should not be ignored when predicting self-assembly behaviour.[8–12]

Meanwhile, changes to the optimal head group area are commonly used to tune the self-assembly behaviour of an amphiphile and can come in many forms, including simple changes to solution temperature, concentration and the presence of additives.[13] The head groups of ionic amphiphiles can vary dramatically in size, from relatively small groups such as trimethylammonium salts to much more sterically hindered triphenylphosphonium salts, and can be increased by the addition of branched substituents.[14–16] Similarly, the typical halide counterions can be exchanged with bulkier, organic counterions, whose hydrophobic character allows them to penetrate the surface of a micelle and bind strongly, facilitating self-assembly.[17,18]

The length of the hydrophobic tail and the optimum head group area are not only used to control the self-assembly behaviour of single-tailed amphiphiles but also that of bolaamphiphiles, which are

formed from two hydrophilic heads connected by a hydrophobic core. The presence of two hydrophilic head groups makes bolaamphiphiles an interesting class of molecules, which can form a variety of self-assemblies depending on their structure.[19–21] Typically, the additional hydrophilic head group increases the solubility of the amphiphile in water when compared with conventional amphiphiles and can lower its CMC.[22,23]

The self-assembly behaviour of bolaamphiphiles can be predicted to an extent using the *pp* concept. The additional head group prevents the calculation of the *pp* in the same manner as single-tailed amphiphiles, however, researchers have shown that aggregate morphology can be predicted by changing factors such as the optimum head group area and have related such changes to the *pp*.[3,24] Indeed, morphological changes can be predicted with bolaamphiphiles based on oligo(aniline)s (**OANI**s), where the volume of the hydrophobic section can be tuned by the addition of doping acids.[25,26]

Recently, researchers in the Faul research group have synthesised a variety of **TANI**-amphiphiles inspired by **TANI-PTAB**, focusing on the length of the hydrophobic section,[27] the optimum head group area,[28] and the formation of bolaamphiphiles.[28] Of those studied, three were chosen to be incorporated into monoolein (**MO**) cubic phases; **TANI-C_{12}TAB**, **TANI-PTPB** and **TANI-$(PTAB)_2$**. It was anticipated that their different structures, in comparison with **TANI-PTAB**, would each distinctly influence the membrane curvature of **MO**, providing more insight into the role of *pp* on the overall phase behaviour and allowing for precise control over the final structural dimensions.

4.2 Results and Discussion

4.2.1 Self-assembly of TANI-C_{12}TAB in water

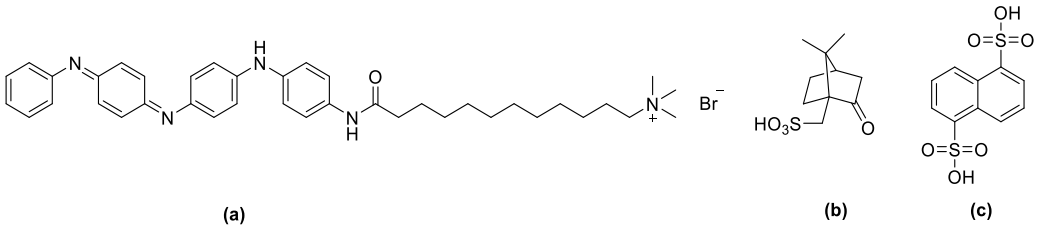

*Figure 4.1. Structures of (a) EB **TANI-C_{12}TAB** (b) camphorsulfonic acid (**CSA**) (c) 1,5-naphthalenedisulfonic acid (**NDS**).*

The first **TANI**-derived amphiphile to be considered in this chapter is **TANI-C_{12}TAB**. Structurally, this amphiphile is analogous to **TANI-PTAB**, however with a twelve-carbon alkyl tail instead of six (Figure 4.1). This increase in tail length should have a noticeable effect on the self-assembly behaviour of the amphiphile if the concept of *pp* is used as a predictor. As the tail length increases, the *pp* should decrease, resulting in more spherical structures being favoured.

The self-assembly behaviour of **TANI-C_{12}TAB** in water has previously been explored using UV-Vis/NIR absorption spectroscopy and transmission electron microscopy (TEM) by Watanabe in the Faul research group,[27] and has been repeated in this project for completeness.

4.2.1.1 Spectroscopic investigations of TANI-C_{12}TAB in water

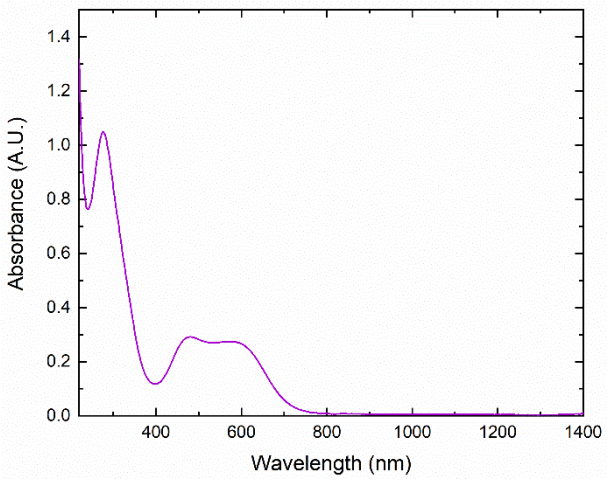

*Figure 4.2. UV-Vis/NIR absorption spectrum for EB **TANI-C_{12}TAB** (1 mM) in water.*

The CMC of EB **TANI-C_{12}TAB** is 1 x 10^{-4} M, as determined by Watanabe in the Faul research group, and is the same as EB **TANI-PTAB**.[27,29] However, EB **TANI-C_{12}TAB** is less soluble than EB **TANI-PTAB**, requiring longer sonication times (> 1 hour) to fully dissolve. This was attributed to the increase in the alkyl tail length and overall length of the hydrophobic section, resulting in a reduction in the amphiphile's solubility in water.

The UV-Vis/NIR absorption spectrum for EB **TANI-C_{12}TAB** (1 mM) in water was collected and can be found in Figure 4.2. Two peaks at 270 nm and 580 nm were clearly visible, corresponding to the π-π* transition and molecular exciton transition, respectively.[30] A shoulder peak at 480 nm was also present, and was attributed to the formation of aggregates, in the same manner as EB **TANI-PTAB**.[29]

The UV-Vis/NIR absorption spectra for **TANI-C_{12}TAB** doped with camphorsulfonic acid (**CSA**) and 1,5-naphthalenedisulfonic acid (**NDS**) in water were also collected. **CSA** and **NDS** were chosen for their large volumes (217.05 $Å^3$ and 230.54 $Å^3$, respectively)[28] to effect a greater change in the volume of the hydrophobic section of **TANI-C_{12}TAB** upon doping and therefore a bigger difference in its self-assembly behaviour. Both acids have been used to reversibly tune the self-assembled structures of **TANI**-amphiphiles in water, to great effect.[4,29,31] In addition, **NDS** is a diacid, which means it has the potential to non-covalently cross-link **TANI**-amphiphiles, in water or indeed within a template, and add rigidity to any self-assembled structures.

The UV-Vis/NIR absorption spectra for **TANI-C_{12}TAB** (0.25 mM) doped with **CSA** are given in Figure 4.3a. A molar ratio of at least 2:1 **CSA**-to-**TANI-C_{12}TAB** was chosen to ensure that protonation

occurred at both imine nitrogen atoms. However, despite the presence of a peak at 760 nm corresponding to a polaron transition typical of the ES state,[32] the presence of EB peaks at 480 and 580 nm indicated that this molar ratio was not sufficient for complete conversion to the ES state. However, as the acid concentration increased, the EB peaks became less prominent and the polaron peak increased in intensity, which indicated more complete doping.

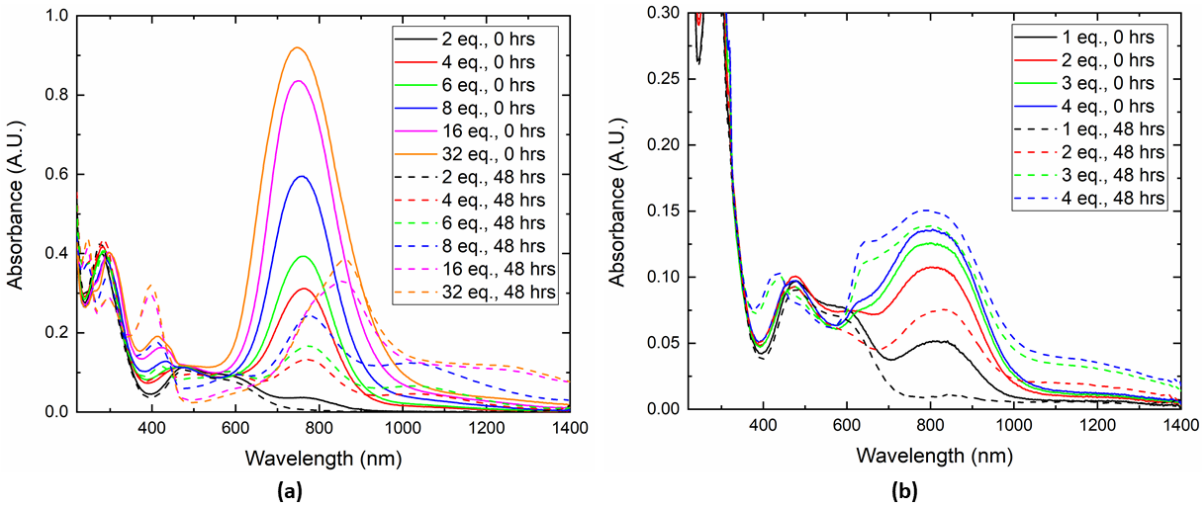

*Figure 4.3. UV-Vis/NIR absorption spectra for ES **TANI-C$_{12}$TAB** (0.25 mM) in water, doped with (a) **CSA** and (b) **NDS**.*

The solutions were left for 48 hours to determine whether de-doping occurred after this time. Solutions with higher acid concentrations (> 8 molar eq.) showed better retention of the ES state over the 48-hour period, with weaker or no EB peaks observed in the absorption spectra. Meanwhile, a bipolaron peak at 1020 nm also appeared in solutions doped with 4 molar equivalents of **CSA** and above. Both the polaron and bipolaron peaks experienced a bathochromic shift with increasing acid concentration over time. Bathochromic shifts are often indicative of an increase in conjugation length in conjugated polymers, [33–35] which suggested that the addition of **CSA** to **TANI-C$_{12}$TAB** may induce the formation of long wire-like structures similar to **CSA**-doped **TANI-PTAB**.[36]

Meanwhile, the UV-Vis/NIR absorption spectra for **TANI-C$_{12}$TAB** (0.25 mM) doped with **NDS** are given in Figure 4.3b. As each molecule of **NDS** contains two acidic sites available for doping (see Figure 4.1), a molar ratio of at least 1:1 **TANI-C$_{12}$TAB**-to-**NDS** was chosen to ensure doping at both imine nitrogen atoms. However, as with **CSA**, complete doping did not occur with low concentrations of **NDS**. Indeed, three molar equivalents of **NDS** were required for the disappearance of the EB peak at 580 nm. Again, the solutions were left for 48 hours to determine the extent of de-doping over time and it was found that solutions containing 3 molar equivalents of **NDS** or above did not show a re-emergence of the EB peaks, indicating that the ES state was retained.

4.2.1.2 Microscopy studies of TANI-C_{12}TAB in water

4.2.1.2.1 Polarised optical microscopy (POM)

Polarised optical microscopy (POM) was used to observed aggregates formed by **TANI-C_{12}TAB** in water. With a typical POM set-up, two polarising filters are placed below and above the specimen, with their vibration directions oriented at 90° angles to each other. Light from the microscope passes through the first filter, becoming polarised in one direction, before passing through the specimen and reaching the second filter. With isotropic samples, the slide will appear dark, as the light is not correctly oriented to pass through the second filter. However, birefringent, anisotropic samples will rotate the plane polarised light, changing its vibration direction and allowing it to pass through the second filter and giving a bright image. A 4 mM solution of EB **TANI-C_{12}TAB** was prepared by briefly mixing the solid in deionised water before sonication for 5 minutes. After this time, **TANI-C_{12}TAB** appeared to the naked eye to be completely dissolved, giving a dark purple solution. However, POM demonstrated that a suspension of birefringent particles had instead been formed (Figure 4.4a).

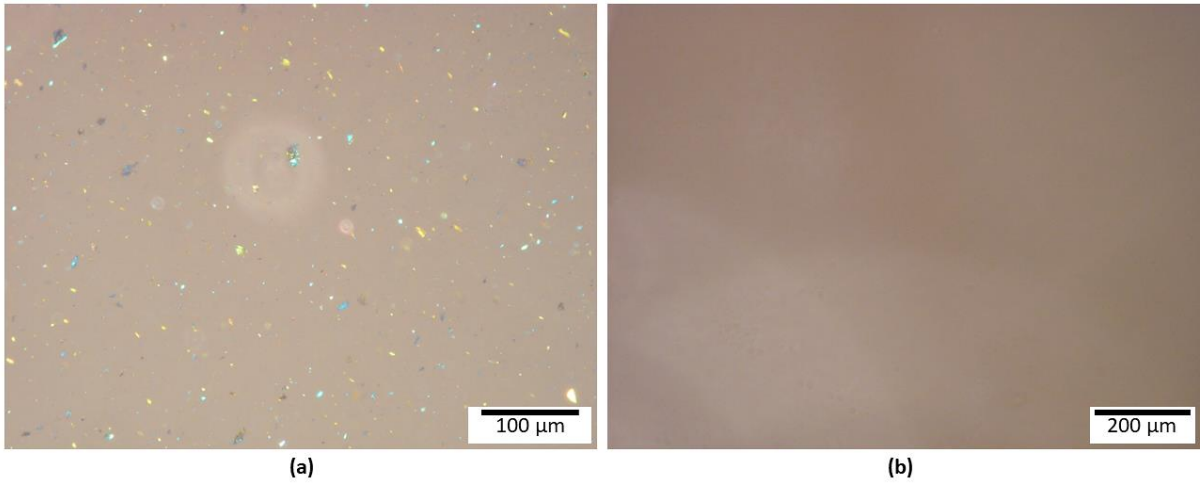

*Figure 4.4. POM image of aqueous EB **TANI-C_{12}TAB** (4 mM) (a) After sonication for 5 minutes (b) After resting for one month.*

Due to the increase in the alkyl tail length, the solubility of **TANI-C_{12}TAB** was reduced in comparison to **TANI-PTAB**. Therefore, longer sonication times (> 1 hour) were required to fully dissolve the suspension. Alternatively, leaving the solution to rest for over one week allowed for dissolution to occur (Figure 4.4b). However, unlike EB **TANI-PTAB**,[36] fully-dissolved EB **TANI-C_{12}TAB** did not form birefringent textures above the CMC, indicating that it did not self-assemble into liquid crystal mesophases. It should be noted that regions of the slide containing isotropic materials were not fully dark, as would be expected owing to the presence of the two polarising filters. This is because the crossed polarisers may not have been at an exact 90° angle, as previous microscope users had manually adjusted the settings to allow for the viewing of isotropic specimens.

The self-assembly of doped **TANI-C_{12}TAB** was also investigated by POM. Dopants have long been used to plasticise and improve the solution processability of **PANI**, resulting in complexes with high degrees of order and orientation.[37–41] Similar work has been done with **OANI**s, which have shown that factors such as the dopant or oligomer length play an important role in inducing liquid crystalline or crystalline order.[42–45] Figure 4.5a shows a POM image of ES **TANI-C_{12}TAB** (4 mM) doped with **CSA** (16 mM). While the bulk solution did not show any liquid-crystalline phases, a Schlieren texture typical of a nematic phase was observed at the periphery of the glass cover slips where solvent evaporation occurred, indicating that a higher amphiphile concentration was required for aggregation to occur. The observed Schlieren texture matched similar textures produced by chromonic liquid crystals.[46] Chromonic liquid crystals are a class of lyotropic liquid crystals and are formed from soluble aromatic compounds, which aggregate into columns in a face-to-face manner. At lower concentrations, these columnar aggregates align parallel to each other with no long-range positional order, forming a nematic (N) phase. However, at higher concentrations, the columns are arranged in a hexagonal array, forming a hexagonal (M) phase.

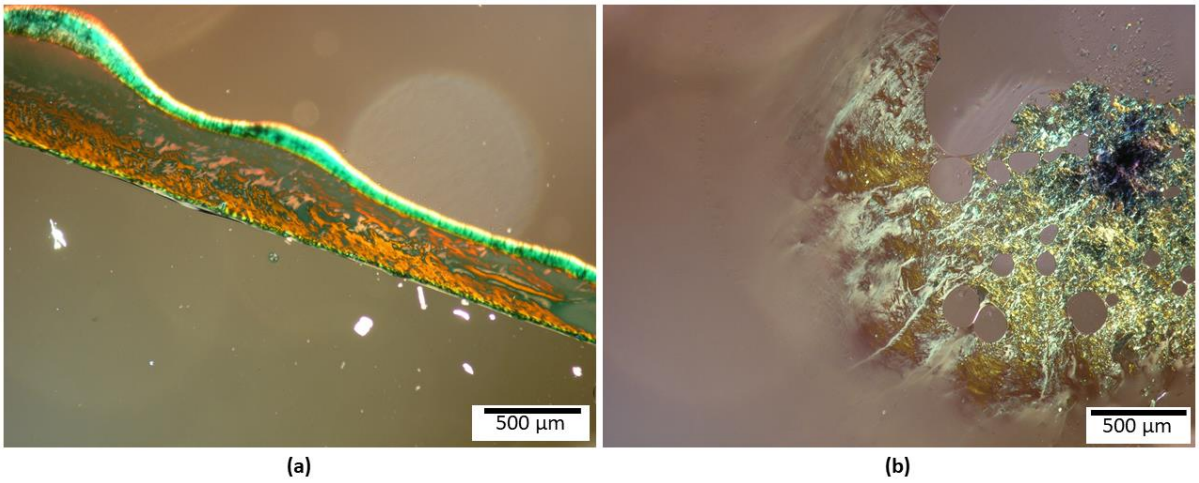

*Figure 4.5. (a) POM image of aqueous ES **TANI-C_{12}TAB** (4 mM), doped with 4 molar equivalents of **CSA**. Image taken at drying edges. (b) POM image of ES **TANI-C_{12}TAB** concentration gradient formed with aqueous **CSA** (16 mM).*

A concentration gradient was prepared with **TANI-C_{12}TAB** and **CSA**, to provide further confirmation of concentration-induced liquid crystallinity. Solid **TANI-C_{12}TAB** was placed on a glass slide and was covered by a glass coverslip. Aqueous **CSA** (16 mM) was pipetted underneath the coverslip, solubilizing the **TANI-C_{12}TAB** flakes and producing a concentration gradient, which can be seen in Figure 4.5b. A Schlieren texture was observed at the edges of the concentration gradient, typical of the N phase.[47,48] Meanwhile, a more grainy and ill-defined texture was observed at regions with higher **TANI-C_{12}TAB** concentrations, matching reported textures for the M phase.[47,48]

Finally, the structures formed by ES **TANI-C_{12}TAB** (4 mM) doped with 4 molar equivalents of **NDS** were identified. As **NDS** is a diacid, it acts as an effective cross-linker, non-covalently bonding

molecules of **TANI-C_{12}TAB**. Figure 4.6 shows that micrometre-sized aggregates are formed, which were weakly birefringent and were not soluble in water.

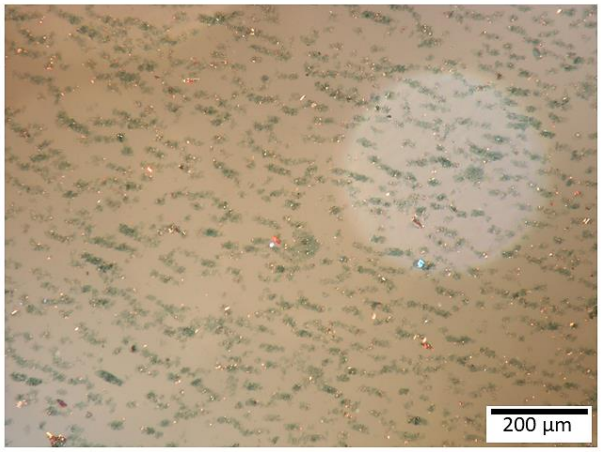

*Figure 4.6. POM image of aqueous ES **TANI-C_{12}TAB** (4 mM), doped with 4 molar equivalents of **NDS**.*

4.2.1.2.2 Transmission electron microscopy (TEM)

From the POM images, it was clear that self-assembly of **TANI-C_{12}TAB** had occurred, at least for solutions doped with **CSA**. Therefore, transmission electron microscopy (TEM) was used to directly observe the structures formed in solution by EB and ES state **TANI-C_{12}TAB**. **TANI-C_{12}TAB** solutions were sonicated for five minutes prior to dropping on a carbon-coated glow-discharged copper grid. Samples were negatively stained with uranyl acetate (1 %), which acts to add contrast to organic materials.[49]

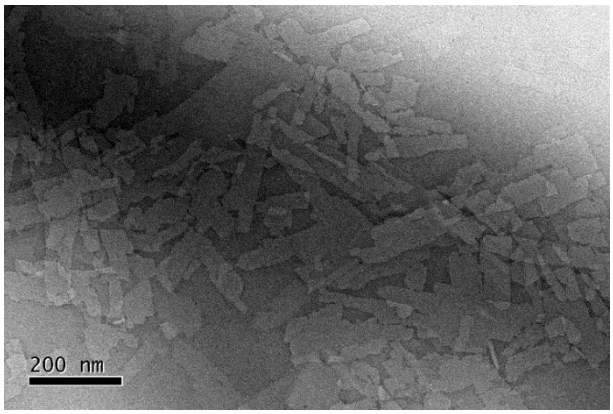

*Figure 4.7. TEM image of EB **TANI-C_{12}TAB** solution (1 mM) stained with 1 % uranyl acetate.*

Plate-like aggregates were observed for the EB state (Figure 4.7), which likely indicates that the amphiphile was not fully dissolved. The results from POM observations have shown that longer sonication times are required for complete dissolution of EB **TANI-C_{12}TAB**, otherwise micrometre or smaller particulates remain in solution. While POM images also showed that no mesophases formed after longer sonication times, it would be valuable to repeat the TEM experiments with fully dissolved EB **TANI-C_{12}TAB**, to confirm whether any structures form on the nanoscale.

Meanwhile, TEM images of ES **TANI-C_{12}TAB** doped with **CSA** show large numbers of highly anisotropic nanofibers, which have widths of approximately 5 nm and are several micrometres long (Figure 4.8). The structure dimensions are like that of **CSA**-doped **TANI-PTAB**, which formed elongated nanofibers that were approximately 6 nm in diameter and were wider than the 3 nm in diameter nanofibers formed in the EB state. The increase in nanofiber width upon doping of **TANI-PTAB** was attributed to the inclusion of the **CSA** counterions into the aggregate structure. It is likely that **CSA**-doped **TANI-C_{12}TAB** forms aggregates in a similar manner.

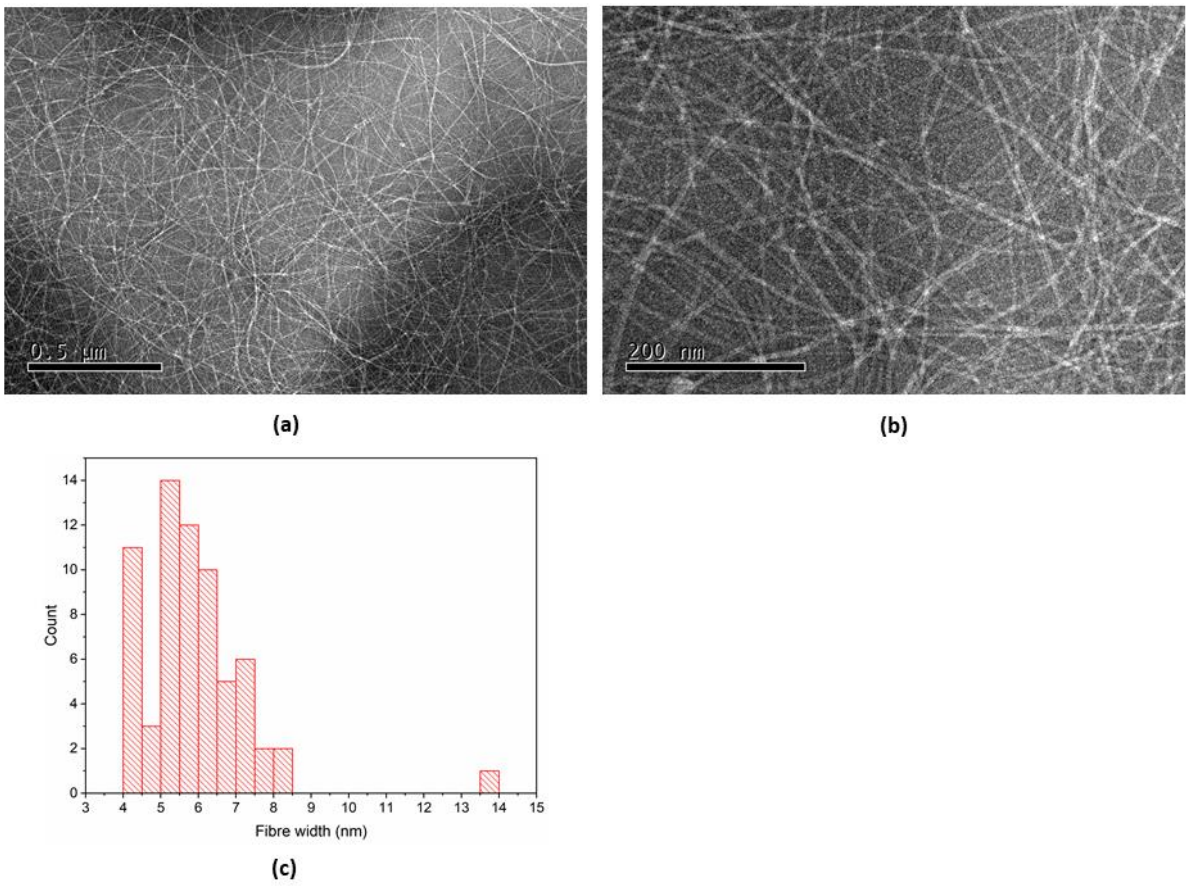

*Figure 4.8. TEM images (a) and (b) of ES **TANI-C_{12}TAB** (1 mM) solutions doped with 4 molar equivalents of **CSA**, stained with 1 % uranyl acetate (c) histogram showing fiber widths measured by analysis of TEM images.*

The nanofibers formed with the addition of **CSA** do not match the structures that are expected to form with the addition of a bulky dopant, using the *pp* model. It would be expected that the increase in the volume of the hydrophobic section, owing to the presence of the bulky acid, would result in the formation of lamellar or vesicular structures. Lyu et al. (2018) suggested that the formation of nanofibers, which were also observed with **CSA**-doped **TANI-PTAB**, was due to the fit of **CSA** into a molecular cavity formed between phenyl rings and additional hydrogen-bonding interactions with the **TANI** backbone, resulting in the formation of nanowire structures.[4,29]

4.2.1.3 Conclusions from aqueous experiments

The self-assembled structures formed by **TANI-C_{12}TAB** in aqueous media were briefly explored. In comparison to EB **TANI-PTAB**, EB **TANI-C_{12}TAB** was less soluble in water, requiring long sonication times (> 1 hour) or resting times (> 1 week) for complete dissolution. It was expected that EB **TANI-C_{12}TAB** would self-assemble into nanofibers like those formed by EB **TANI-PTAB**, owing to their comparable structures and therefore likely similar aggregation behaviour. Indeed, the UV-Vis/NIR absorption spectrum of EB **TANI-C_{12}TAB** matched that of EB **TANI-PTAB**, displaying peaks that indicated the formation of aggregates. However, the reduced solubility of EB **TANI-C_{12}TAB** hindered investigation of potential assemblies by POM and TEM, which had been prepared by sonication in water for only 5 minutes and showed undissolved, plate-like aggregates.

The solubility of **TANI-C_{12}TAB** was improved by doping with **CSA**, which had an additional effect of inducing the formation of liquid-crystal phases. The UV-Vis/NIR absorption spectra of **TANI-C_{12}TAB** showed a bathochromic shift with increasing concentrations of **CSA**, indicating an increase in conjugation length due to the formation of long aggregates. Further evidence of aggregation was observed by POM, which showed the formation of nematic liquid-crystal mesophases, and TEM, which revealed the presence of long nanofibers.

The role of *pp* on the self-assembly behaviour of **TANI-C_{12}TAB** was not easily determined from the above results. The reduced solubility hindered observations of the structures formed with EB **TANI-C_{12}TAB**, and therefore the effect of increasing the chain length and subsequent decrease in *pp* was not clear. Meanwhile, increasing the *pp* by doping with **CSA** did not result in the predicted formation of vesicular structures, instead forming nanofibers, due to secondary interactions of the acid with the **OANI** backbone. Nevertheless, it was hoped that there would be a significant difference in the behaviour of the longer amphiphile in comparison with **TANI-PTAB** when incorporated into **MO** cubic phases, and that the concept of *pp* could be used to predict the mesophase structure.

4.2.2 Investigations of TANI-C_{12}TAB in MO cubic phases

4.2.2.1 Spectroscopic investigations of TANI-C_{12}TAB in water and PPO

The UV-Vis/NIR absorption spectra of EB and ES **TANI-C_{12}TAB** in the presence of **PPO** were collected to determine whether there were any changes to the oxidation states when mixed with the additive. The spectrum for EB **TANI-C_{12}TAB** with **PPO** is given in Figure 4.9. A characteristic EB peak at 590 nm was clearly visible, in addition to a slight shoulder peak at 475 nm. The shoulder peak was less prominent than that of EB **TANI-C_{12}TAB** in water, indicating a loss of aggregation due to the introduction of **PPO**.

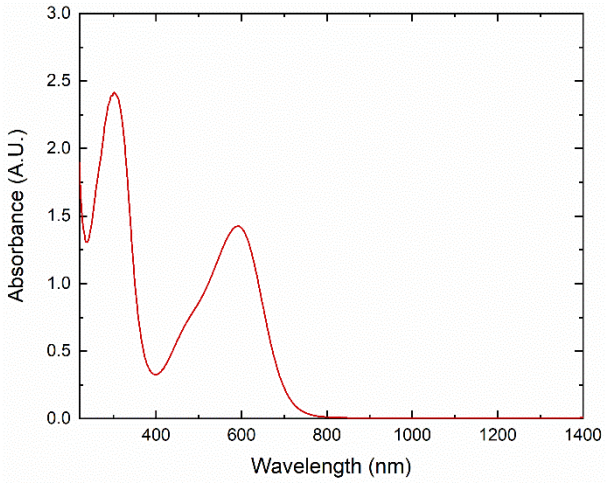

*Figure 4.9. UV-Vis/NIR absorption spectrum for EB **TANI-C$_{12}$TAB** (1 mM) in water, with **PPO**.*

With the addition of **CSA** or **NDS**, peaks at around 800 nm and 1100 nm appeared, corresponding to the polaron and bipolaron states, respectively (Figure 4.10). For both acids, EB peaks were present at the lowest acid concentrations, although a greater conversion to the ES state was noted with increasing acid concentrations. De-doping also occurred for both acids after 48 hours, although higher acid concentrations showed greater retention of the ES peaks.

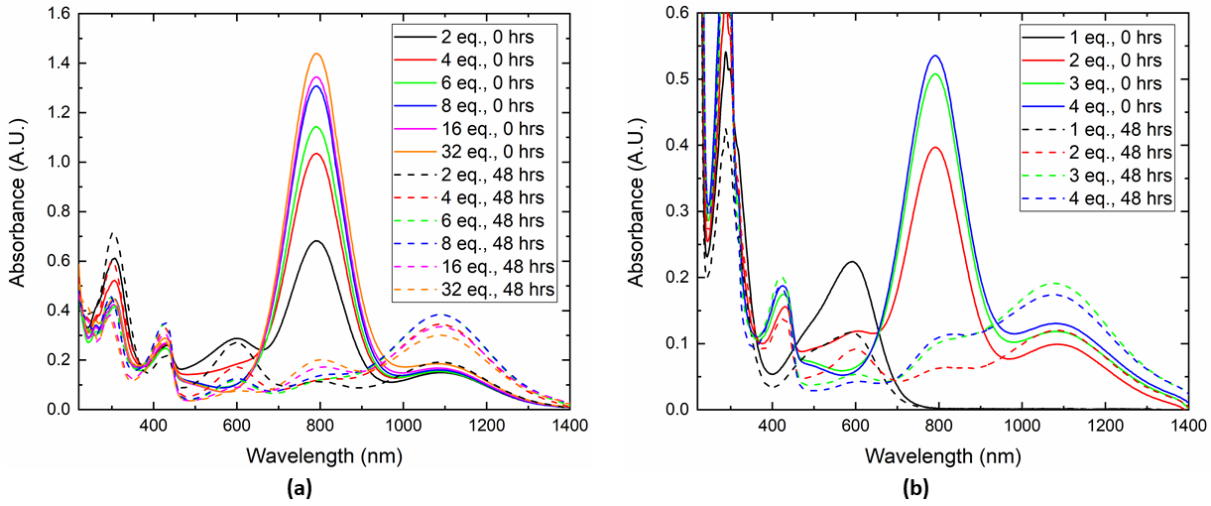

*Figure 4.10. UV-Vis/NIR absorption spectra for ES **TANI-C$_{12}$TAB** (0.25 mM) in water/**PPO**, doped with (a) **CSA** and (b) **NDS**.*

Unlike ES **TANI-C$_{12}$TAB** in water, the spectra for ES **TANI-C$_{12}$TAB** with **PPO** did not show bathochromic shifts with increasing acid concentrations or tailing of the bipolaron peaks, indicating that the aggregation induced by the addition of acids in water was disrupted by presence of **PPO**. However, the presence of **PPO** did act to stabilize the bipolaron state, as evident by the prominent peaks at 1100 nm after 48 hours. The stabilization was probably due to a charge screening mechanism, similar to that proposed by Mills et al. (2019) due to high acid concentrations.[32]

The UV-Vis/NIR absorption spectra for EB and ES **TANI-C$_{12}$TAB** in **MO** sponge phases were not collected due to the partial decomposition of **MO** observed towards the end of this project (discussed in Chapter 3, Section 3.2.5), which would prevent accurate measurements of the oxidation states. However, the redox behaviour of **TANI-C$_{12}$TAB** in **MO** was expected to mimic that of **TANI-PTAB**, due to the structural similarities and the concurrent behaviour in water and **PPO**. Indeed, as the redox behaviour was anticipated to be the same, small-angle X-ray scattering (SAXS) experiments with EB and ES **TANI-C$_{12}$TAB**, using the same preparation conditions and acid concentrations as with **TANI-PTAB**, were performed before any spectroscopic investigations were undertaken and before any decomposition of **MO** was observed.

4.2.2.2 Small-angle X-ray scattering investigations of TANI-C$_{12}$TAB in MO cubic phases

The effect of introducing **TANI-C$_{12}$TAB** to **MO** cubic phases was determined by SAXS. With the increase in tail length, relative to **TANI-PTAB**, the *pp* of **TANI-C$_{12}$TAB** should decrease. This should result in an increased flattening effect on the membrane curvature of **MO** and therefore a lower concentration of this amphiphile should be required to form the *Im3m* phase.

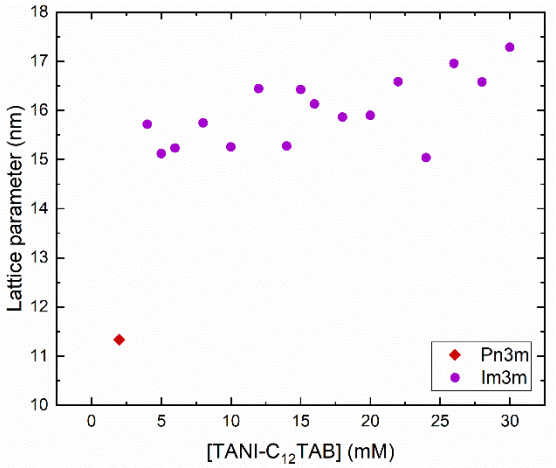

*Figure 4.11. Lattice parameters for **MO** cubic phases prepared with **PPO** and EB **TANI-C$_{12}$TAB** (2-30 mM).*

The results for the addition of EB **TANI-C$_{12}$TAB** (2-30 mM) to **MO** cubic phases are given in Figure 4.11, while representative 1-D scattering patterns can be found in Figure C.1a in Appendix C. All *Pn3m* and *Im3m* phases showed characteristic scattering features. The results showed that the *Im3m* phase does indeed form at lower concentrations than with the addition of EB **TANI-PTAB**, with the less negatively curved phase occurring at 4 mM **TANI-C$_{12}$TAB**. Additionally, an increase in lattice parameter was noted with increasing **TANI-C$_{12}$TAB** concentrations. A swelling of the cubic phase nanostructure is usually associated with the flattening of the lipid membrane, and could result in a transition to flatter sponge or lamellar phases with increasing additive concentrations.[50] However, the increase in lattice parameters could equally result from insufficient hydration times. Samples prepared

with **TANI-C$_{12}$TAB** concentrations above 25 mM gave broad scattering peaks in the 1-D scattering plots, which indicated that they may require longer to equilibrate.

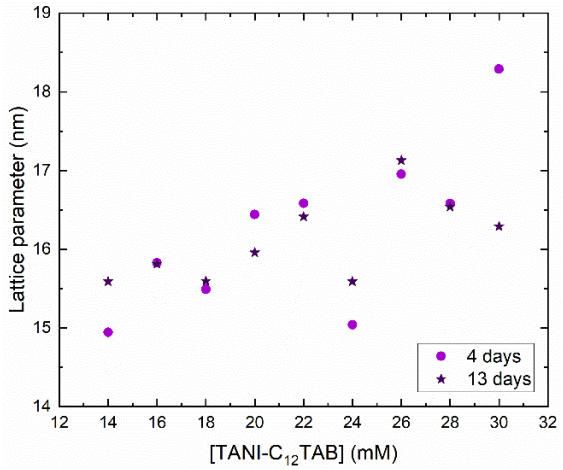

*Figure 4.12. Lattice parameters for **MO** cubic phases prepared with **PPO** and EB **TANI-C$_{12}$TAB** (14-30 mM), measured 4 and 13 days after preparation.*

Cubic phases containing high concentrations of **TANI-C$_{12}$TAB** (14-30 mM) were analysed at two time intervals to determine whether additional time was required for the samples to finish hydrating (Figure 4.12). The cubic phases were prepared and were left to hydrate for four days, before analysis by SAXS. The same samples were then left for a further nine days before re-analysis, giving a total equilibration time of thirteen days. Apart from the cubic phase containing 30 mM **TANI-C$_{12}$TAB**, the mesophases showed little difference in lattice parameters with the additional hydration time, indicating that they reached an equilibrium by the four-day analysis window and were not likely to transform further.

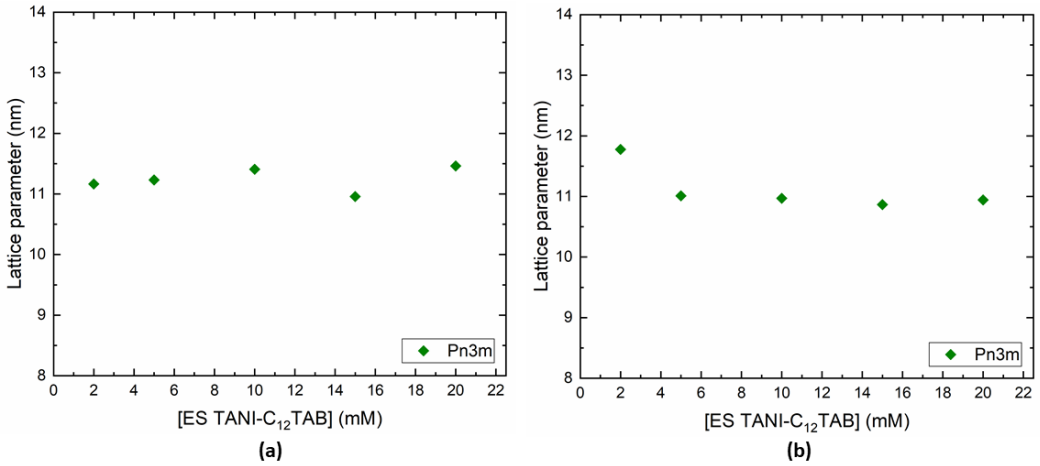

*Figure 4.13. Lattice parameters for **MO** cubic phases prepared with **PPO** and ES **TANI-C$_{12}$TAB** (2-20 mM), doped with 4 molar equivalents of (a) **CSA** (b) **NDS**.*

An increase in lattice parameter with concentration was noted again, irrespective of hydration time, which suggested that the cause was the flattening effect of EB **TANI-C$_{12}$TAB** on the lipid bilayer. Lipid mesophases containing higher concentrations of EB **TANI-C$_{12}$TAB** were considered, to determine

whether transitions to flatter sponge or lamellar phases would then occur. However, due to the limited solubility of **TANI-C_{12}TAB** in water, it was not possible to prepare accurate stock solutions of high enough concentrations to prepare such mesophases.

Following experiments in the EB state, **TANI-C_{12}TAB** was doped in-situ using 4 molar equivalents of either **CSA** or **NDS**. Doping was assumed by a visual colour change from purple to green with the addition of either acid. It was expected that the increase in volume of the hydrophobic section upon doping would result in an increase in the *pp* of **TANI-C_{12}TAB**, thus resulting the preferential formation of the more negatively curved *Pn3m* phase. The results in Figure 4.13 show that indeed the *Pn3m* phase formed at all concentrations of ES **TANI-C_{12}TAB**, as determined by the Bragg scattering peaks identified in the SAXS patterns (see Figure C.1b in Appendix C for a representative scattering pattern). It should be noted that (as discussed in Chapter 3) the exact mechanism of doping is unknown and the transition to the *Pn3m* phase could be due to the partitioning of **TANI-**amphiphiles into the water channels with doping, instead of as a result of changing *pp* within the lipid bilayer.

4.2.3 Investigations of TANI-PTPB in MO cubic phases

Following investigations into the effect of increasing the length of the hydrophobic section, attention was turned to the effect of the hydrophilic head group, exploring the difference between a trimethylammonium bromide and a trimethylphosphonium bromide. Phosphonium amphiphiles are less commonly studied than ammonium amphiphiles, owing to their comparatively difficult synthesis and limited availability of starting phosphines.[12,51] However, the properties of phosphonium amphiphiles do allow for applications less suited to their ammonium analogues. For example, their increased antimicrobial activity and reduced cytotoxicity makes them suitable for biomedical devices.[52–54]

The use of different head groups also changes the self-assembly behaviour between otherwise structurally analogous amphiphiles. The critical aggregation concentrations (CAC) of phosphonium amphiphiles are often lower than similar ammonium amphiphiles.[14] In terms of *pp*, the change from nitrogen to phosphorous should also result in an increase in the optimum head group area of the amphiphile, due to an increase in atomic radius and bond lengths (the length of a carbon-nitrogen bond is 1.48 Å while a carbon-phosphorous bond is 1.84 Å)[55]. The increase in head group area should result in a smaller *pp* in comparison to ammonium analogues.

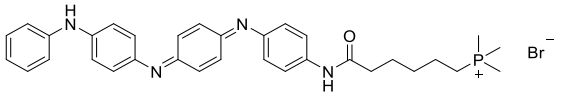

*Figure 4.14. Structure of EB **TANI-PTPB**.*

A phosphonium-amphiphile (**TANI-PTPB**), which is structurally analogous to **TANI-PTAB**, has been prepared, the structure of which can be found in Figure 4.14. In water, EB **TANI-PTPB** predominately self-assembles into nanofibers, although some spherical structures are also formed.[28] The number of

spherical structures increases with concentration, which was attributed to a decrease in the surface area of the head groups and subsequent increase in *pp*. When doped with **CSA**, **TANI-PTPB** forms vesicles, which can be transformed back into nanofibers with the addition of a base.

While the *pp* of **TANI-PTPB** has not been calculated, its self-assembly behaviour is similar to that of **TANI-PTAB**, with the formation of nanofibers in the EB state and vesicles in the ES state, which suggests that their *pp*s are close. However, the formation of some spherical structures in the EB state with **TANI-PTPB** shows that there is a slight difference in self-assembly with the increase in head group size, which may lead to a difference in the mesophase behaviour of **MO** when combined with **TANI-PTPB**.

4.2.3.1 Spectroscopic investigations of TANI-PTPB in water and with PPO

The UV-Vis/NIR absorption spectra for EB and ES **TANI-PTPB** were collected as a comparison with **TANI-PTAB** and **TANI-C_{12}TAB**, to determine whether there was any difference in absorption with the trimethylphosphonium head group. The absorption spectra for EB **TANI-PTPB** in water and with **PPO** are given in Figure 4.15. For both conditions, characteristic EB peaks at 300 and 590 nm were observed, corresponding to the π-π* transition and molecular exciton transition, respectively.[30] As with **TANI-PTAB** and **TANI-C_{12}TAB**, a shoulder peak at 487 nm was observed for **TANI-PTPB** in water, indicating aggregation, and was disrupted with the addition of **PPO**.

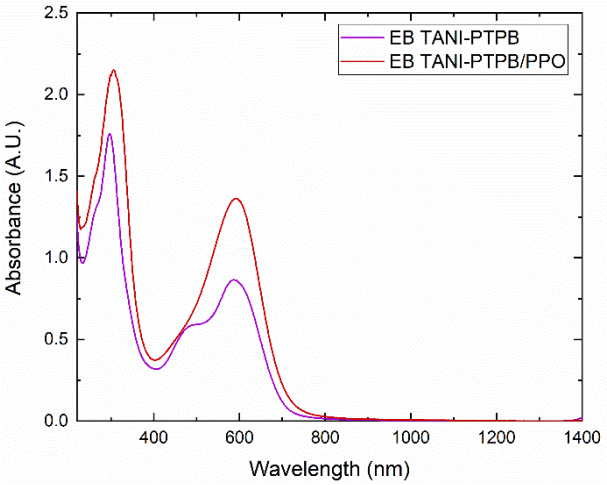

*Figure 4.15. UV-Vis/NIR absorption spectra for EB **TANI-PTPB** (1 mM) in water and with **PPO**.*

The absorption spectra for ES **TANI-PTPB** doped with **CSA** are given in Figure 4.16. In water, complete conversion to the ES state was observed with 2 molar equivalents of acid, as evident by the presence of a polaron peak at 762 nm and the absence of an EB peak at 590 nm. As with the previously explored **TANI**-amphiphiles, de-doping occurred after 48 hours, although this effect was reduced with higher acid concentrations. Similar absorption spectra were observed with **TANI-PTPB** in the presence of **PPO**, although a higher concentration of **CSA** was initially required to ensure complete doping.

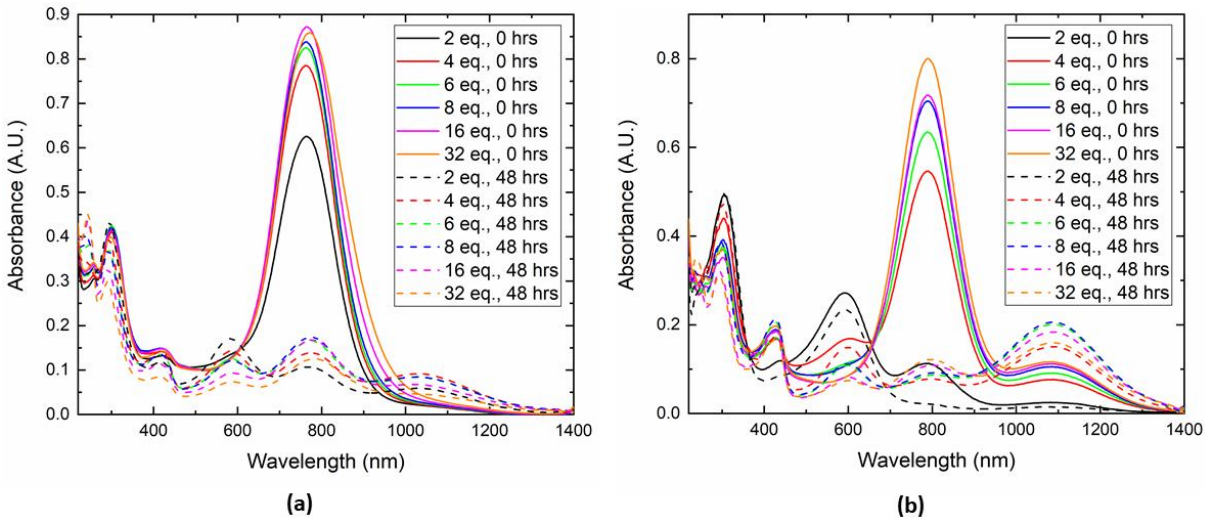

*Figure 4.16. UV-Vis/NIR absorption spectra for ES **TANI-PTPB** (0.25 mM) doped with **CSA** (a) in water (b) in water and **PPO**.*

Meanwhile, the absorption spectra for ES **TANI-PTPB** doped with **NDS** in water can be seen in Figure 4.17a. A minimum of 2 molar equivalents of **NDS** were required for doping to occur, producing a polaron peak at 764 nm. Visible cross-linking occurred with high acid concentrations (> 3 molar equivalents), resulting in weaker absorbance due to the precipitation of **TANI-PTPB** from solution and subsequent reduction in concentration. This effect was more apparent after 48 hours, where EB and ES peaks were observed with 2 molar equivalents of **NDS** and very weak peaks were observed with higher acid concentrations due to precipitation of cross-linked aggregates. The introduction of **PPO** appeared to disrupt the cross-linking process and no precipitation was observed in the presence of this additive (Figure 4.17b).

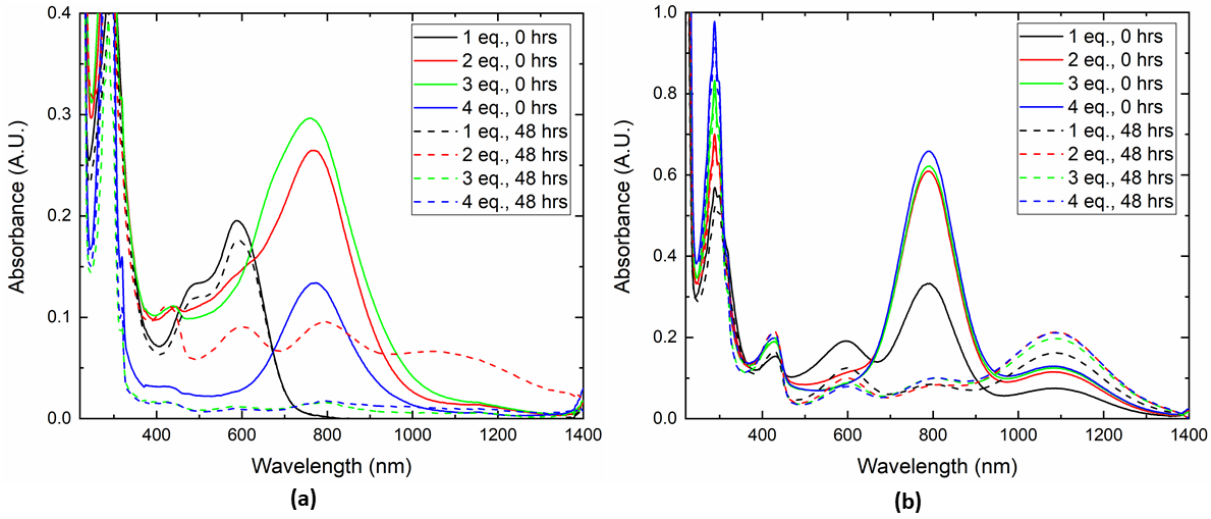

*Figure 4.17. UV-Vis/NIR absorption spectra for ES **TANI-PTPB** (0.25 mM) doped with **NDS** (a) in water (b) in water and **PPO**.*

As with **TANI-C$_{12}$TAB**, the absorbance spectra for **TANI-PTPB** in **MO** sponge phases were not collected as partial **MO** decomposition had occurred before analysis was attempted. However, as the **TANI** backbone was unchanged, it was anticipated that the oxidative behaviour of **TANI-PTPB** in **MO** would match that of **TANI-PTAB**. Again, SAXS experiments utilising the same preparation conditions and acid concentrations were performed before any spectroscopic investigations were undertaken and before any decomposition of **MO** was noted.

4.2.3.2 Small-angle X-ray scattering investigations of TANI-PTPB in MO cubic phases

EB **TANI-PTPB** was incorporated into **MO** cubic phases and the effect on the membrane curvature was identified by SAXS. As previously mentioned, the increase in head group size from an ammonium moiety to a phosphonium moiety was expected to decrease the amphiphile's *pp*, which should result in the formation of the *Im3m* phase at lower concentrations, as with EB **TANI-C$_{12}$TAB**. However, previous experiments have also shown that the self-assembly behaviour of **TANI-PTPB** in water is like that of **TANI-PTAB**, indicating that their *pp*'s are similar and therefore no difference in mesophase structure may be expected.[28]

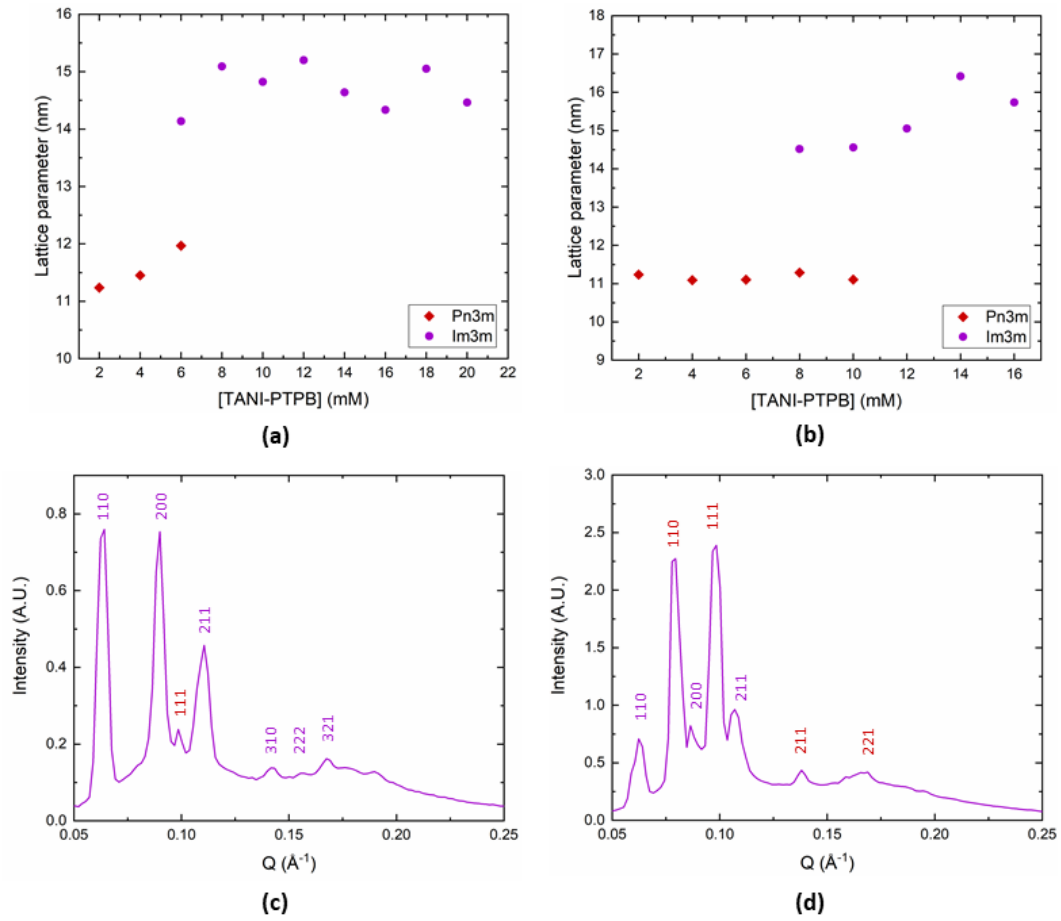

*Figure 4.18. Lattice parameters for EB **TANI-PTPB** in **MO** with **PPO**. (a) After hydration for 48 hours (b) After hydration for 1 month (c) 1-D scattering pattern for 6 mM **TANI-PTPB** after hydration for 48 hours (d) 1-D scattering pattern for 8 mM **TANI-PTPB** after hydration for 1 month.*

The average lattice parameters for cubic phases containing EB **TANI-PTPB** after hydration for 48 hours are given in Figure 4.18a. The results show that, like **TANI-PTAB** and **TANI-C$_{12}$TAB**, the *Pn3m* phase formed at low **TANI-PTPB** concentrations, while the *Im3m* phase was produced at high concentrations. However, unlike the other amphiphiles which showed discrete phases, samples containing 6 mM **TANI-PTPB** displayed a mixture of peaks from both the *Pn3m* and *Im3m* phases (see Figure 4.18c). This indicated that a longer hydration time was required, to ensure that the samples had sufficient time to transition between mesophases.

Therefore, the cubic phases were re-analysed after one month (Figure 4.18b). Analysis of the SAXS patterns showed that after the additional time, the *Pn3m* phase persisted to higher concentrations of **TANI-PTPB**, while peaks for the *Im3m* phase were only present at concentrations above 8 mM. However, again mixed phases were formed with **TANI-PTPB** concentrations around the transition concentration, which suggested that further time was required for the samples to reach equilibrium.

The effect of doping was also explored, using 4 molar equivalents of **CSA** or 2 molar equivalents of the diacid, **NDS** (Figure 4.19). Doping was confirmed by a visible colour change from purple to green and the cubic phase was identified by characteristic Bragg peaks (see representative scattering pattern in Figure C.2, Appendix C). As with **TANI-PTAB** and **TANI-C$_{12}$TAB**, the *Pn3m* phase formed at all ES **TANI-PTPB** concentrations, although the peaks for most samples were broad or poorly defined, which indicated that additional hydration time was required. However, as visible de-doping occurred after 48 hours, it was not possible to leave the samples to equilibrate further as the ES state would not be retained.

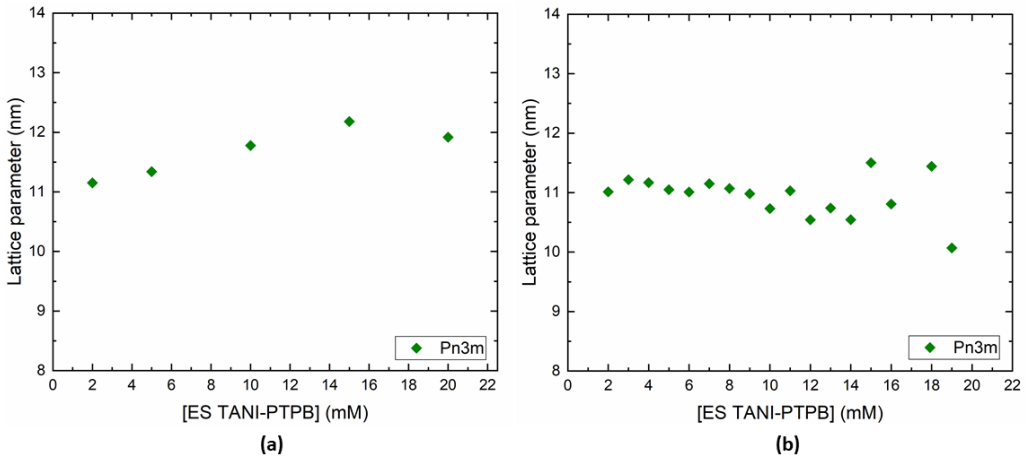

*Figure 4.19. Lattice parameters for ES **TANI-PTPB** in **MO** with **PPO**, (a) doped with 4 molar equivalents of **CSA** (b) doped with 2 molar equivalents of **NDS**.*

The above results demonstrated that the influence of **TANI-PTPB** on the mesophase structure of **MO** was like that of **TANI-PTAB**. In the EB state, the *Pn3m* phase formed at low concentrations and a transition to the *Im3m* phase occurred at a similar concentration to **TANI-PTAB**. This fits with

conclusions drawn from observations of both amphiphiles in water, which indicated that their *pp*s were similar and that there may be no difference in **MO** phase behaviour with the increase in head group size. In addition, doping led to the formation of the *Pn3m* phase at all concentrations, which could be attributed to an increase in *pp* due to the increase in the volume of the hydrophobic section upon doping, or to the partitioning of the amphiphile into the water channels. However, **MO** cubic phases containing **TANI-PTPB** differed in the longer equilibration times required to form a stable mesophase in comparison to cubic phases containing **TANI-PTAB**. It was unclear why the introduction of a phosphonium-based amphiphile would dramatically change the time taken to reach equilibrium. It may be of interest to explore this observation further, to expand our understanding of the influence of cationic amphiphiles on the stability of lipidic mesophases.

4.2.4 Investigations of TANI-(PTAB)$_2$ in MO cubic phases

The final amphiphile to be explored in this chapter is a bolaamphiphile, **TANI-(PTAB)$_2$**, which consists of a **TANI** core and two alkyl tails terminated by trimethylammonium head groups (Figure 4.20). The self-assembly behaviour of **TANI-(PTAB)$_2$** in water has been reported by Alotabi (2019).[28] In the EB state, **TANI-(PTAB)$_2$** self-assembled into spherical nanostructures, which were approximately 22 nm in diameter. The addition of monoacids, such as **CSA** or **TFA**, led to a slight swelling of the spheres, resulting in diameters of approximately 28 nm. However, the addition of a diacid, **NDS**, induced the formation of nanofibers, which could be transformed back into spheres with the addition of a base. This change in self-assembly with upon doping could again provide a dynamic method to tune the morphology of **MO** cubic phases when mixed with **TANI-(PTAB)$_2$**.

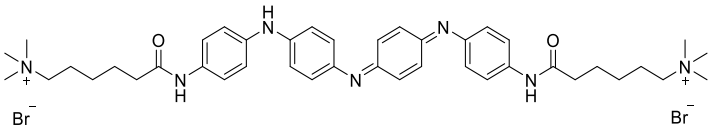

*Figure 4.20. Structure of EB **TANI-(PTAB)$_2$**.*

4.2.4.1 Spectroscopic investigations of TANI-(PTAB)$_2$ in MO cubic phases

The UV-Vis/NIR absorption spectra for **TANI-(PTAB)$_2$** were collected to confirm the redox behaviour of the amphiphile in water and with **PPO** prior to incorporation into **MO** cubic phases. In the EB state, two peaks at approximately 310 and 590 nm were observed in both conditions, corresponding to the π-π* transition and molecular exciton transition, respectively (Figure 4.21).[30]

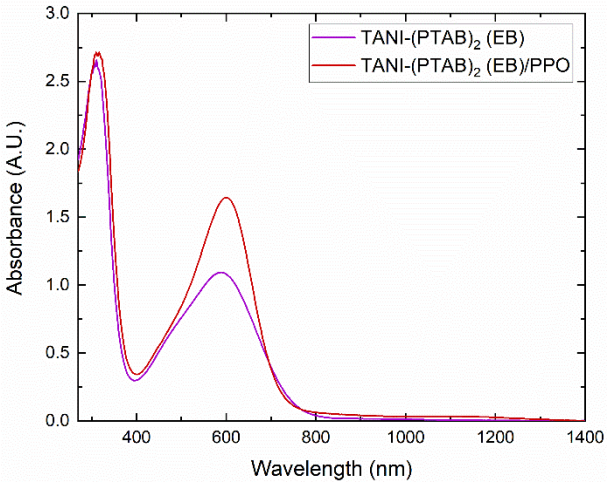

*Figure 4.21. UV-Vis/NIR absorption spectra for EB **TANI-(PTAB)$_2$** (1 mM) in water and with **PPO**.*

NDS was then chosen as a dopant to produce the ES state (Figure 4.22). As previously mentioned, **NDS** is a bulky acid that produced nanofibers with **TANI-(PTAB)$_2$**, therefore it was expected that this acid would induce the greatest change in phase behaviour with **MO** over other previously explored acids (e.g., **CSA** or **TFA**). The UV-Vis/NIR spectra for **TANI-(PTAB)$_2$** in water doped with **NDS** show peaks at 770 nm and 1100 nm, corresponding to the polaron and bipolaron states, respectively.[32] De-doping occurred after 48 hours for the solution doped with 1 molar equivalent of **NDS**, however solutions with higher concentrations of the diacid remained doped for longer, perhaps due to the strong cross-linking nature of the acid, which could fix the dopant in place. Extensive cross-linking was apparent by the tailing of the bipolaron peak, which indicated an extension of the conjugation length. Tailing of the ES peaks was not observed for solutions prepared with **PPO**, indicating that the cross-linking may be disrupted. However, as with other doped **TANI-**amphiphiles, the bipolaron state was stabilised by the presence of **PPO**, producing more prominent peaks at 1100 nm after 48 hours.

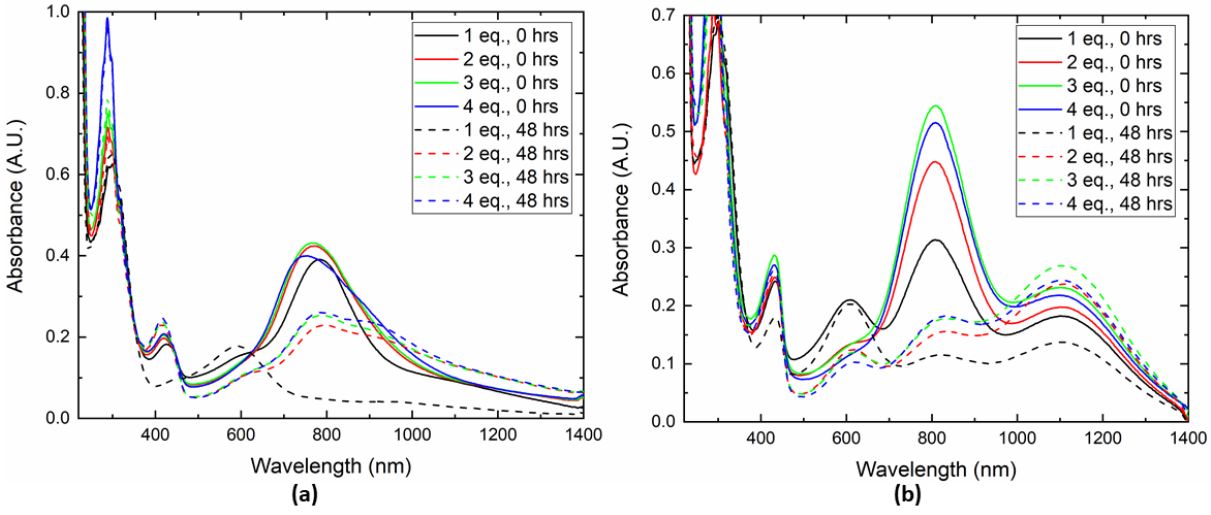

*Figure 4.22. UV-Vis/NIR absorption spectra for ES **TANI-(PTAB)$_2$** (0.25 mM) doped with **NDS** (a) in water (b) in water with **PPO**.*

4.2.4.2 Small-angle X-ray scattering investigations of TANI-(PTAB)$_2$ in MO cubic phases

As previously mentioned, *pp* calculations for bolaamphiphiles are complicated by the presence of an additional hydrophilic head group. Therefore, the *pp*s of EB and ES **TANI-(PTAB)$_2$** have not been calculated and could not be used to predict the effect of incorporating the amphiphile into **MO** cubic phases. However, observations of the self-assembly behaviour of **TANI-(PTAB)$_2$** in water could be used to hypothesise the effect it may have on the mesophase structure. In water, EB **TANI-(PTAB)$_2$** self-assembles into spherical structures, much like ES **TANI-PTAB**. As **MO** with ES **TANI-PTAB** preferentially forms the *Pn3m* phase, it is likely that the same phase will be formed with the addition of EB **TANI-(PTAB)$_2$**. Indeed, Figure 4.23a shows that the *Pn3m* phase was formed at all EB **TANI-(PTAB)$_2$** concentrations, with all SAXS patterns showing characteristic *Pn3m* features (see typical spectrum in Figure C.3a, Appendix C). The average lattice parameter of cubic phases containing **TANI-(PTAB)$_2$** was 11.4 nm, which was slightly swollen in comparison to that of **MO** prepared with just **PPO** and water (10.75 nm, Chapter 3 Section 3.2.1), however this was not unexpected as additives are known to swell the mesophase.[50,56]

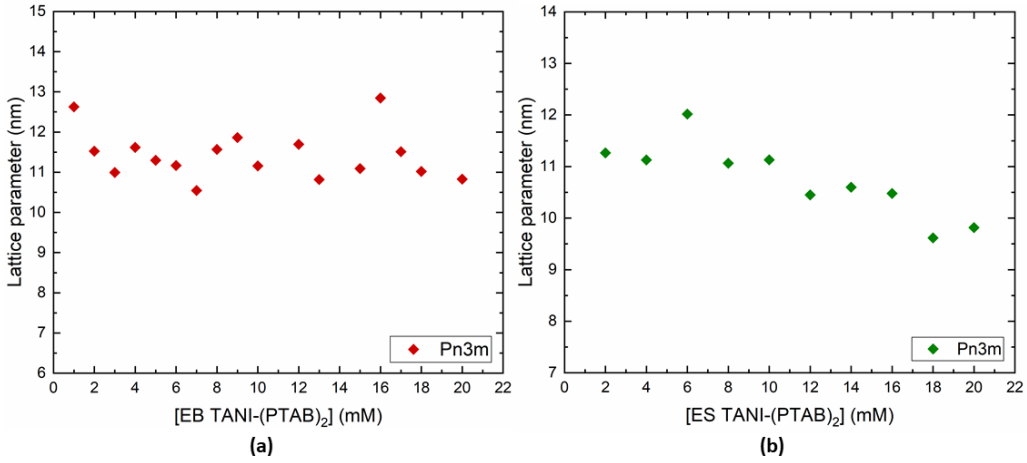

*Figure 4.23. Lattice parameters for **TANI-(PTAB)$_2$** in **MO** with **PPO** in the (a) EB state (b) ES state, doped with 4 molar equivalents of **NDS**.*

Following the results in the EB state, **TANI-(PTAB)$_2$** was doped to the ES state with 4 molar equivalents of **NDS**. Hypothetically, the addition of a bulky dopant should increase the volume of the hydrophobic section of **TANI-(PTAB)$_2$**, which should increase its overall *pp* resulting in the formation of more negatively curved phases when combined with **MO**. Figure 4.23b shows that while the *Pn3m* phase was again formed, a decrease in lattice parameter was observed with increasing ES **TANI-(PTAB)$_2$** concentration. Such a trend usually is explained by an increase in negative curvature and could precede a transition to the hexagonal phase.[50] Again a typical scattering pattern for **MO** with ES **TANI-(PTAB)$_2$** can be observed in Figure C.3b (Appendix C), showing characteristic Bragg scattering peaks for the *Pn3m* phase.

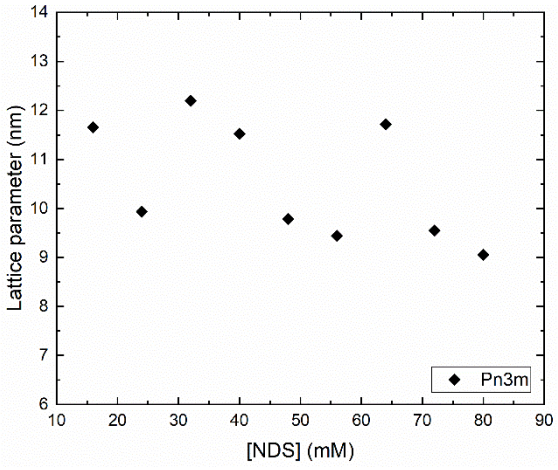

*Figure 4.24. Lattice parameters for **MO** with **PPO** and **NDS** (16-80 mM).*

This result initially appeared to answer the question of where **TANI**-amphiphiles are situated after doping (i.e., in the lipid bilayer or in the water channels), as the negative trend was proposed to be due to an increase in the *pp* of **TANI-(PTAB)$_2$** in the bilayer, which would affect the packing of **MO** molecules. However, **MO** cubic phases prepared with equivalent concentrations of **NDS** also show a negative trend in the lattice parameters with increasing concentration, indicating that this effect may be a product of the acid and not **TANI-(PTAB)$_2$** (Figure 4.24).

NDS is a strong acid, with a pKa of -2.8, and is relatively larger than other acids used in this work (i.e., **HCl** or **TFA**). Typically, pH has minimal effect on the cubic phase nanostructure, beyond a slight increase in lattice parameter with increasing pH.[57–59] However, amphiphilic acids such as oleic acid or linoleic acid do lead to transitions to more negatively curved phases, due to their larger size ($pp > 1$).[50] The aromatic nature of **NDS** may allow it to interact with the lipid bilayer in a similar manner, resulting in the decrease in lattice parameter as its concentration increases.

One thing to note is that the decrease in lattice parameter was only observed with the introduction of **NDS** alone or with **NDS** and **TANI-(PTAB)$_2$**. No noticeable negative trend with concentration was observed for **NDS**-doped **TANI-C$_{12}$TAB** (Figure 4.13b), **TANI-PTPB** (Figure 4.19b) or **TANI-PTAB** (Figure 8a, Chapter 5). It may be that the non-covalent interactions with between **NDS** and the single-tailed **TANI**-amphiphiles take priority over any interactions between **NDS** and **MO**, resulting in the same phase behaviour being observed as when doping with monoacids such as **CSA** or **HCl**.

The reason for the decrease in lattice parameter with **NDS**-doped **TANI-(PTAB)$_2$** is yet unclear. Doping was assumed to be successful, owing to a visible colour change from purple to green. Therefore, this observation is expected to be due to an interplay of **NDS** with **TANI-(PTAB)$_2$** rather than the effect of each component independently. However, whether this is the result of an increase in *pp* within the bilayer or an effect of doping in the aqueous channels of **MO** still needs to be determined.

4.2.5 Investigations of TANI-amphiphiles in pure MO

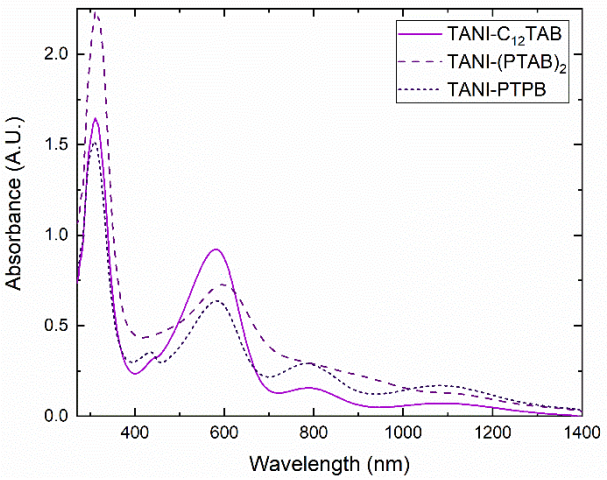

*Figure 4.25. UV-Vis/NIR absorption spectra for EB **TANI-C$_{12}$TAB**, **TANI-(PTAB)$_2$** and **TANI-PTPB** (1 mM) in **MO** and **PPO**, collected in January 2020.*

After observing that **TANI-PTAB** was becoming doped from partially degraded **MO** (Chapter 3, Section 3.2.5), the UV-Vis/NIR absorption spectra for EB state **TANI-C$_{12}$TAB**, **TANI-PTPB** and **TANI-(PTAB)$_2$** in **MO** were collected, to determine whether doping was occurring with all amphiphiles. The spectra are given in Figure 4.25 and showed significant ES peaks at approximately 800 and 1100 nm for all three **TANI**-amphiphiles, which indicated that they were partially doped.

Subsequently, all previously collected data were re-examined to determine whether there was a noticeable difference in phase behaviour over time. However, unlike **TANI-PTAB**, the effect of partial doping with **TANI-C$_{12}$TAB**, **TANI-PTPB** and **TANI-(PTAB)$_2$** on the mesophase structure of **MO** was less clear. Figure 4.26 shows the concentrations at which the *Im3m* phase formed with **TANI-C$_{12}$TAB** and **TANI-PTPB**, between 2018 and 2020. For **TANI-C$_{12}$TAB**, no change in transition concentration was observed over time, suggesting that any partial doping did not affect the mesophase structure.

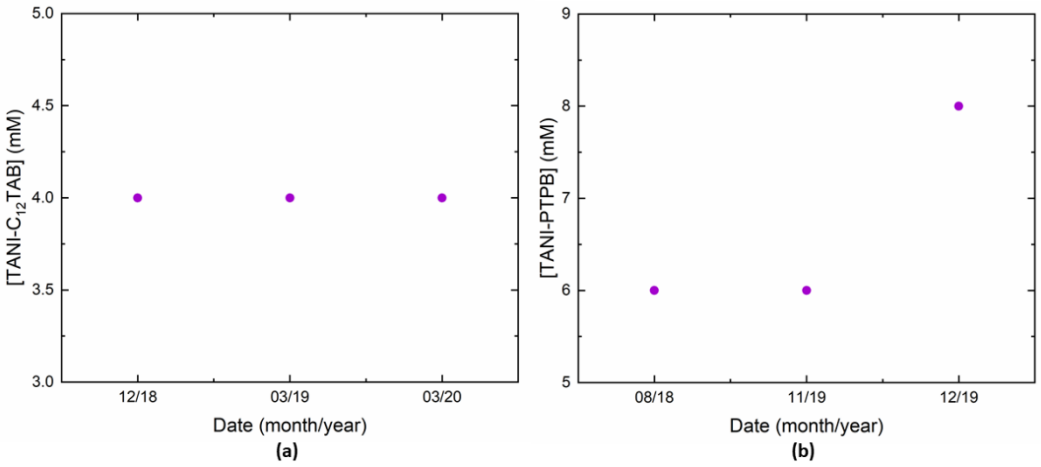

*Figure 4.26. Concentrations at which the Im3m phase formed over time with (a) EB **TANI-C$_{12}$TAB** (b) EB **TANI-PTPB**.*

Meanwhile, **TANI-PTPB** showed an increase in transition concentration from 6 mM to 8 mM between November and December in 2019. While this difference could be related to an increase in partial doping due to continued degradation of **MO**, it should be noted that as cubic phases containing **TANI-PTPB** required longer to equilibrate the difference could be due to incomplete transitions between mesophases. Finally, no noticeable effect of partial doping on cubic phases containing **TANI-(PTAB)$_2$** was observed, as the *Pn3m* phase was formed for both the EB and ES states and therefore no change in phase behaviour over time was recorded.

It was unclear as to why **MO** cubic phases containing **TANI-PTAB** were more sensitive to partial doping than those containing **TANI-C$_{12}$TAB** or **TANI-PTPB**, as the **TANI** core for all three amphiphiles was the same and should be equally likely to become doped over time. However, it should be noted that for **TANI-PTAB**, the biggest difference in transition concentration occurred between October 2017 (*Im3m* phase formed at 4 mM) and March 2019 (*Im3m* phase formed at 8 mM) (see Figure 14, Chapter 3). It is possible that **MO** degradation occurred within this timeframe and that the initial experiments were of predominantly EB state **TANI-PTAB** and later experiments were partially doped. In that case, it could be assumed that **TANI-PTPB** and **TANI-C$_{12}$TAB** in **MO** cubic phases prepared in August and December 2018 (Figure 4.26) were already partially doped and therefore no major difference in phase behaviour would be noted over time.

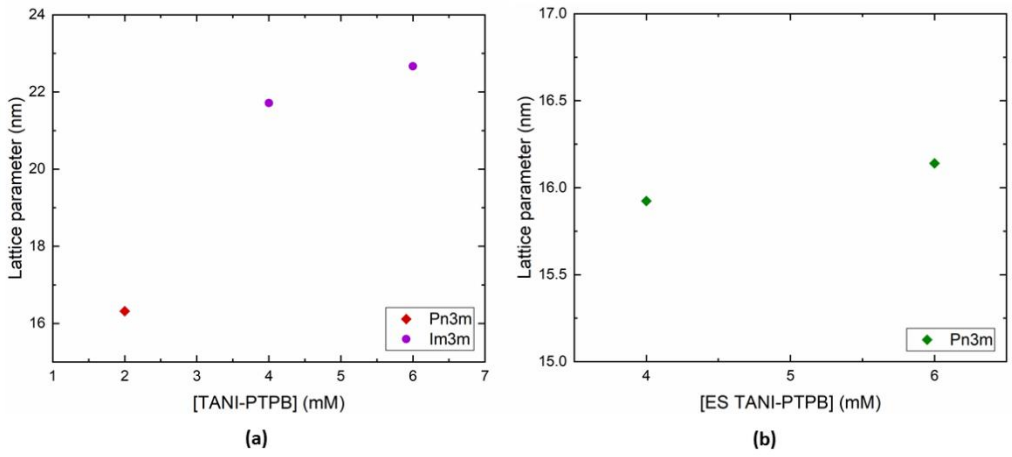

*Figure 4.27. Lattice parameters for **TANI-PTPB** in pure **MO** with **PPO** (a) EB state (b) ES state doped with 4 molar equivalents of **CSA**.*

Cubic phases containing **TANI**-amphiphiles were prepared with pure **MO**, to separate the effects of the amphiphiles and any partial doping. Limited stocks of pure **MO** were available, reducing the number of experiments that could be performed. Nevertheless, cubic phases containing 2 to 6 mM **TANI-PTPB** were prepared, in the EB state and doped to the ES state with 4 molar equivalents of **CSA** (Figure 4.27). The results were similar to those observed with the addition of **TANI-PTAB** to pure **MO** (Figures 19 and 20, Chapter 3), in that the *Im3m* phase was formed with 4 mM of both amphiphiles in the EB state, while the *Pn3m* phase was predominant upon doping. The similarities in the effects of **TANI-PTPB**

and **TANI-PTAB** were also consistent with the observations of both amphiphiles when combined with **MO** donated by Danisco, supporting the conclusion that the change in head group size had limited effect on the overall phase behaviour.

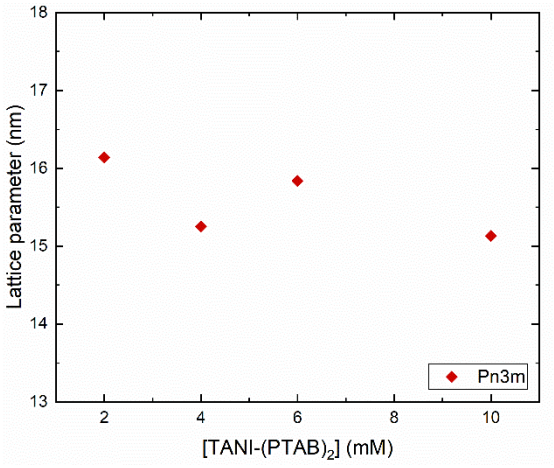

*Figure 4.28. Lattice parameters for EB **TANI-(PTAB)$_2$** in pure **MO** with **PPO**.*

Next, cubic phases containing EB **TANI-(PTAB)$_2$** were prepared (Figure 4.28). As with samples made with **MO** donated by Danisco, the *Pn3m* phase was formed with all **TANI-(PTAB)$_2$** concentrations in conjunction with pure **MO**, which suggested that any effect of partial doping in the former lipid was minimal.

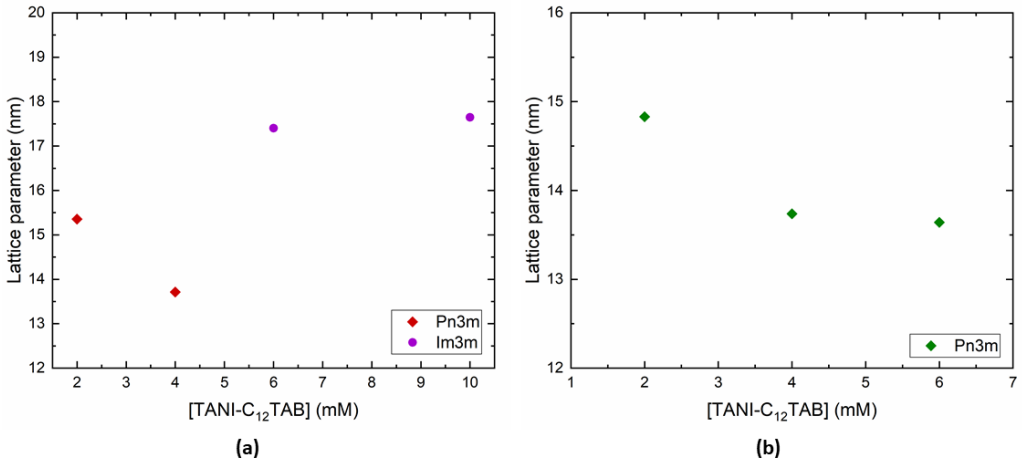

*Figure 4.29. Lattice parameters for **TANI-C$_{12}$TAB** in pure **MO** with **PPO** (a) EB state (b) ES state doped with 4 molar equivalents of **CSA**.*

Finally, the effect of **TANI-C$_{12}$TAB** on cubic phases prepared with pure **MO** was explored. It was expected that the addition of low concentrations of EB **TANI-C$_{12}$TAB** would result in the formation of the *Pn3m* phase, while increasing the amphiphile concentration would result in a transition to the *Im3m* phase. As the *pp* of **TANI-C$_{12}$TAB** is lower than that of **TANI-PTAB**, it was also expected that this transition would occur at a lower concentration, supporting the results obtained using **MO** donated by

Danisco. However, the results in Figure 4.29 show that instead the transition to the *Im3m* phase occurred at 6 mM **TANI-C_{12}TAB**, a higher concentration than **TANI-PTAB** (4 mM). The reason for this discrepancy was not immediately clear and due to time constraints and limited stocks of pure **MO**, it was not explored further.

As with samples prepared using **TANI-PTAB**, cubic phases formed with pure **MO** and the three **TANI**-amphiphiles explored in this chapter displayed swollen lattice parameters and produced broad or indistinct peaks in the 1-D scattering plots, which indicated that a longer hydration time was required. Such features reduced the confidence in the calculated lattice parameters and phase identification as it was likely that both would change over time. However, it was generally clear that the addition of single-tailed **TANI**-amphiphiles in the EB state led to the formation of the *Im3m* phase, while doping resulted in a transformation to the *Pn3m* phase. Meanwhile, the addition of EB **TANI-$(PTAB)_2$**, which in water self-assembles into spherical structures reminiscent of ES **TANI-PTAB**, resulted in the formation of the *Pn3m* phase. In these ways, the self-assembly behaviour of all explored amphiphiles in pure **MO** matched their recorded behaviour in **MO** donated by Danisco and showed that transitions between cubic phases can be readily controlled by the simple application of an acid or base.

4.3 CONCLUSIONS

In this chapter, the self-assembly behaviour of **TANI-C_{12}TAB** in water was explored and compared with **TANI-PTAB**. Additionally, the effect of introducing tetra(aniline) (**TANI**)-derived amphiphiles with different packing parameters (*pp*) to monoolein (**MO**) cubic phases was investigated.

The self-assembled structures formed by **TANI-C_{12}TAB** in water were explored by polarised optical microscopy (POM) and transmission electron microscopy (TEM). Investigations of the EB state were hindered by the reduced solubility of the amphiphile in comparison to the shorter **TANI-PTAB**, resulting in observations of microplates in solutions that had not been given sufficient time for dissolution. However, the addition of camphorsulfonic acid (**CSA**) improved the solubility of **TANI-C_{12}TAB**, resulting in observations of nematic liquid crystal phases by POM and elongated nanofibers by TEM. Similar observations have been noted for **CSA**-doped **TANI-PTAB**, which suggested a similar model of aggregation in doped **TANI-C_{12}TAB**, using cofacial stacking of the **TANI** core with **CSA** counterions embedded in the structure.

Following investigations of the amphiphile in water, **TANI-C_{12}TAB** was incorporated into **MO** cubic phases and its effect on the overall structure was determined. A transition to the *Im3m* phase was noted with 4 mM EB-state **TANI-C_{12}TAB**, a lower concentration than with **TANI-PTAB**. This difference was attributed to the decrease in *pp* that occurred with the longer hydrophobic tail and was also proposed to be responsible for the increase in lattice parameter that was noted with increasing **TANI-C_{12}TAB** concentration, indicating a possible transition to flatter phases if it was further increased. As with **TANI-**

PTAB, the addition of dopants resulted in the *Pn3m* phase at all concentrations, although it was unclear as to whether this was due to the increase in *pp* upon doping in the membrane or the partitioning of **TANI-C_{12}TAB** into the water channels for doping in a more hydrophilic environment.

Attention was then turned to **TANI-PTPB**, to determine how changing the hydrophilic head group to a trimethylphosphonium bromide would affect its influence on the membrane curvature of **MO**. Cubic phases were prepared with both EB and ES state **TANI-PTPB** and showed little difference in phase behaviour in comparison to **TANI-PTAB**. These results suggested that the change in *pp* with the different head group had limited effect on the cubic phase formation, outside of the extended equilibration times required to form a stable mesophase.

Next, the effect of incorporating **TANI-$(PTAB)_2$** into **MO** cubic phases was investigated. As EB **TANI-$(PTAB)_2$** in water formed spherical structures, much like ES **TANI-PTAB**, it was predicted that it would also produce the *Pn3m* phase at all concentrations, which was found to be the case. Upon doping with naphthalenedisulfonic acid (**NDS**), the *Pn3m* phase was again formed, however, with a negative trend in lattice parameters with increasing concentration, indicating an eventual transition to the hexagonal phase.

Finally, the effect of partial doping over time was explored. As the results in Chapter 3 had shown that **TANI-PTAB** had become doped by partially degraded **MO** over the past three years, which had affected the cubic phase formation, it was anticipated that the other **TANI-**amphiphiles may have been similarly affected. However, no difference in mesophase formation was noted for **TANI-C_{12}TAB** and **TANI-PTPB**, which was attributed to the delay in beginning experiments with those amphiphiles, to the point where degradation and doping may have already begun. As a comparison, cubic phases were prepared with pure **MO** and all three amphiphiles, which showed similar behaviour to previous experiments, with the *Im3m* phase formed in the EB state and *Pn3m* phase formed with doping.

In summary, cubic phases containing three **TANI-**amphiphiles were prepared and demonstrated that the mesophase structure and dimensions could be predicted and tuned using the *pp* concept. This provides a very simple method to control the cubic phases of **MO**, with reversible transitions available between the *Im3m* and *Pn3m* phases upon doping and de-doping and gives a basis for future experiments with other **TANI-**amphiphiles that may allow other mesophases to be accessed.

4.4 REFERENCES

1. Israelachvil, J. N. *et al.* Theory of Self-Assembly of Hydrocarbon Amphiphiles into Micelles and Bilayers. *J. Chem. Soc., Faraday Trans. 2* **72**, 1525–1568 (1976).

2. Song, S., Song, A. & Hao, J. Self-assembled structures of amphiphiles regulated via implanting external stimuli. *RSC Adv.* **4**, 41864–41875 (2014).

3. Yan, Y. *et al.* Molecular Packing Parameter in Bolaamphiphile Solutions: Adjustment of Aggregate Morphology by Modifying the Solution Conditions. *J. Phys. Chem. B* **111**, 2225–2230 (2007).

4. Lyu, W. *et al.* An addressable packing parameter approach for reversibly tuning the assembly of oligo(aniline)-based supra-amphiphiles. *Chem. Sci.* **9**, 4392–4401 (2018).

5. Negrini, R. & Mezzenga, R. pH-responsive lyotropic liquid crystals for controlled drug delivery. *Langmuir* **27**, 5296–5303 (2011).

6. Nagarajan, R. Self-Assembly: The Neglected Role of the Surfactant Tail. *Langmuir* **18**, 31–38 (2002).

7. Balazs, D. A. & Godbey, W. T. Liposomes for Use in Gene Delivery. *J. Drug Deliv.* **2011**, 326497 (2011).

8. Akbay, C. & Shamsi, S. A. Polymeric sulfated surfactants with varied hydrocarbon tail: I. Synthesis, characterization, and application in micellar electrokinetic chromatography. *Electrophoresis* **25**, 622–634 (2004).

9. Fanun, M. Surfactant Chain Length Effect on the Structural Parameters of Nonionic Microemulsions. *J. Dispers. Sci. Technol.* **29**, 289–296 (2008).

10. Svensson, A., Norrman, J. & Piculell, L. Phase Behavior of Polyion-Surfactant Ion Complex Salts: Effects of Surfactant Chain Length and Polyion Length. *J. Phys. Chem. B* **110**, 10332–10340 (2006).

11. Akpinar, E., Canioz, C., Turkmen, M., Reis, D. & Neto, A. M. F. Effect of the surfactant alkyl chain length on the stabilisation of lyotropic nematic phases. *Liq. Cryst.* **45**, 219–229 (2018).

12. Gamarra, A., Urpi, L., Matrinez de Ilarduya, A. & Munoz-Guerra, S. Crystalline structure and thermotropic behaviour of alkyltrimethylphosphonium amphiphiles. *Phys. Chem. Chem. Phys.* **19**, 4370–4382 (2017).

13. Svenson, S. Controlling surfactant self-assembly. *Curr. Opin. Colloid Interface Sci.* **9**, 201–212 (2004).

14. Gainanova, G. A. *et al.* Self-assembling systems based on amphiphilic alkyltriphenylphosphonium bromides : Elucidation of the role of head group. *J. Colloid Interface Sci.* **367**, 327–336 (2012).

15. Jurasin, D., Habus, I. & Filipovic-Vincekovic, N. Role of the alkyl chain number and head groups location on surfactants self-assembly in aqueous solutions. *Colloids Surfaces A Physicochem. Eng. Asp.* **368**, 119–128 (2010).

16. Bakshi, M. S., Singh, J., Singh, K. & Kaur, G. Mixed micelles of cationic gemini with tetraalkyl ammonium and phosphonium surfactants: the head group and hydrophobic tail contributions. *Colloids Surfaces A Physicochem. Eng. Asp.* **234**, 77–84 (2004).

17. Abdel-Rahem, R. The influence of hydrophobic counterions on micellar growth of ionic surfactants. *Adv. Colloid Interface Sci.* **141**, 24–36 (2008).

18. Raghavan, S. R. & Kaler, E. W. Highly viscoelastic wormlike micellar solutions formed by cationic surfactants with long unsaturated tails. *Langmuir* **17**, 300–306 (2001).

19. Wu, G., Thomas, J., Smet, M., Wang, Z. & Zhang, X. Controlling the self-assembly of cationic bolaamphiphiles: hydrotropic counteranions determine the aggregated structures. *Chem. Sci* **5**, 3267–3274 (2014).

20. Wu, G. *et al.* Bolaamphiphiles Bearing Bipyridine as Mesogenic Core: Rational Exploitation of Molecular Architectures for Controlled Self-Assembly. *Langmuir* **28**, 5023–5030 (2012).

21. Mizoshita, N. & Seki, T. Organised structures of flexible bolaamphiphiles with trisiloxane spacers: three- and two-dimensional molecular assemblies with different molecular conformation. *Soft Matter* **2**, 157–165 (2006).

22. Wang, G., Wang, C., Wang, Z. & Zhang, X. Bolaform Superamphiphile Based on a Dynamic Covalent Bond and Its Self-Assembly in Water. *Langmuir* **27**, 12375–12380 (2011).

23. da Silva, E. R. *et al.* Self-Assembled Arginine-Capped Peptide Bolaamphiphile Nanosheets for Cell Culture and Controlled Wettability Surfaces. *Biomacromolecules* **16**, 3180–3190 (2015).

24. Nagarajan, R. Self-assembly of bola amphiphiles. *Chem. Eng. Comm.* **55**, 251–273 (2007).

25. Yang, R. *et al.* Synthesis, electrochemical properties and inhibition performance of water-soluble self-doped oligoaniline derivative. *Electrochim. Acta* **93**, 107–113 (2013).

26. Hu, J. *et al.* pH/Potential-Responsive Large Aggregates from the Spontaneous Self-Assembly of a Triblock Copolymer in Water. *Langmuir* 13376–13382 (2008).

27. Watanabe, K. Personal Communication - Faul Research Group.

28. Alotaibi, M. M. Towards Aqueous Nanostructures Based on Oligo(aniline)s. (University of Bristol, 2019).

29. Bell, O. A. *et al.* Self-assembly of a functional oligo(aniline)-based amphiphile into helical conductive nanowires. *J. Am. Chem. Soc.* **137**, 14288–14294 (2015).

30. de Albuquerque, J. E., Mattoso, L. H. C., Faria, R. M., Masters, J. G. & MacDiarmid, A. G. Study of the interconversion of polyaniline oxidation states by optical absorption spectroscopy. *Synth. Met.* **146**, 1–10 (2004).

31. Alotaibi, M. M. *et al.* Synthesis and tunable self-assembly of electroactive bolaamphiphiles based on oligo(aniline)s. *Submitted*

32. Mills, B. M. *et al.* Tipping the polaron-bipolaron balance: concentration and spin effects in doped oligo(aniline)s observed by UV-vis-NIR and TD-DFT. *Mol. Syst. Des. Eng.* **4**, 103–109 (2019).

33. Martin, R. E. & Diederich, F. Linear Monodisperse pi-Conjugated Oligomers: Model Compounds for Polymers and More. *Angew. Chem. Int. Ed.* **38**, 1350–1377 (1999).

34. Meier, H., Gerold, J., Kolshorn, H. & Bastian, M. Extension of Conjugation Leading to Bathochromic or Hypsochromic Effects in OPV Series. *Chem. Eur. J.* **10**, 360–370 (2004).

35. Ickenroth, D., Weissmann, S., Rumpf, N. & Meier, H. Monodisperse Oligo (2,5-dipropoxy-1,4-phenyleneethynylene)s. *Eur. J. Org. Chem.* 2808–2814 (2002).

36. Bell, O. A. *et al.* Self-Assembly of a Functional Oligo(Aniline)-Based Amphiphile into Helical Conductive Nanowires. *J. Am. Chem. Soc.* **137**, 14288–14294 (2015).

37. Cao, Y., Smith, P. & Heeger, A. J. Counter-ion induced processibility of conducting polyaniline and of conducting polyblends of polyaniline in bulk polymers. *Synth. Met.* **48**, 91–97 (1992).

38. Paul, R. K. & Pillai, C. K. S. Melt/solution processable conducting polyaniline with novel sulfonic acid dopants and its thermoplastic blends. *Synth. Met.* **114**, 27–35 (2000).

39. Dufour, B. *et al.* Low Tg , Stretchable Polyaniline of Metallic-Type Conductivity : Role of Dopant Engineering in the Control of Polymer Supramolecular Organization and in the Tuning of Its Properties. *Chem. Mater.* **15**, 1587–1592 (2003).

40. Olinga, T. E., Fraysse, J., Travers, J. P., Dufresne, A. & Pron, A. Highly Conducting and Solution-Processable Polyaniline Obtained via Protonation with a New Sulfonic Acid Containing Plasticizing Functional Groups. *Macrolecules* **33**, 2107–2113 (2000).

41. Zheng, W. *et al.* Self-assembly of the electroactive complexes of polyaniline and surfactant. *Macromol. Chem. Phys.* **196**, 2443–2462 (1995).

42. Wei, Z., Laitinen, T., Smarsly, B., Ikkala, O. & Faul, C. F. J. Self-assembly and electrical conductivity transitions in conjugated oligoaniline - Surfactant complexes. *Angew. Chemie - Int. Ed.* **44**, 751–756 (2005).

43. Dane, T. G. *et al.* Oligo(aniline) nanofilms: from molecular architecture to microstructure. *Soft Matter* **9**, 10501 (2013).

44. Dane, T. G. *et al.* Structured oligo(aniline) nanofilms via ionic self-assembly. *Soft Matter* **8**, 2824 (2012).

45. Wang, Y., Tran, H. D., Liao, L., Duan, X. & Kaner, R. B. Nanoscale morphology, dimensional control, and electrical properties of oligoanilines. *J. Am. Chem. Soc.* **132**, 10365–10373 (2010).

46. Lydon, J. Chromonic review. *J. Mater. Chem.* **20**, 10071–10099 (2010).

47. Attwood, T. K., Lydon, J. E. & Jones, F. The chromonic phases of dyes. *Liq. Cryst.* **1**, 499–507 (1986).

48. Tam-Chang, S.-W. & Huang, L. Chromonic liquid crystals: properties and applications as functional materials. *Chem. Commun.* 1957–1967 (2008).

49. Watson, M. L. Staining of Tissue Sections for Electron Microscopy with Heavy Metals. *J. Biophys. Biochem. Cytol.* **4**, 475–478 (1958).

50. van 't Hag, L., Gras, S. L., Conn, C. E. & Drummond, C. J. Lyotropic liquid crystal engineering moving beyond binary compositional space – ordered nanostructured amphiphile self-assembly materials by design. *Chem. Soc. Rev.* **46**, 2705–2731 (2017).

51. Kanazawa, A., Tsutsumi, O., Ikeda, T. & Nagase, Y. Novel Thermotropic Liquid Crystals without a Rigid Core Formed by Amphiphiles Having Phosphonium Ions. *J. Am. Chem. Soc.* **119**, 7670–7675 (1997).

52. Xue, Y., Xiao, H. & Zhang, Y. Antimicrobial Polymeric Materials with Quaternary Ammonium and Phosphonium Salts. *Int. J. Mol. Sci.* **16**, 3626–3655 (2015).

53. Kanazawa, A., Ikeda, T. & Endo, T. Synthesis and Antimicrobial Activity of Dimethyl- and Trimethyl-Substituted Phosphonium Salts with Alkyl Chains of Various Lengths. *Antimicrob. Agents Chemother.* **38**, 945–952 (1994).

54. Cieniecka-Roslonkeiwicz, A. *et al.* Synthesis , anti-microbial activities and anti-electrostatic

properties of phosphonium-based ionic liquids. *Green Chem.* **7**, 855–862 (2005).

55. Schnee, V. P. & Palmer, C. P. Characterization of a cationic phosphonium surfactant for micellar electrokinetic chromatography : Using the linear solvation energy relationships model. *Electrophoresis* **29**, 761–766 (2008).

56. Cherezov, V., Clogston, J., Papiz, M. Z. & Caffrey, M. Room to move: Crystallizing membrane proteins in swollen lipidic mesophases. *J. Mol. Biol.* **357**, 1605–1618 (2006).

57. Conn, C. E. *et al.* High-throughput analysis of the structural evolution of the monoolein cubic phase in situ under crystallogenesis conditions. *Soft Matter* **8**, 2310–2321 (2012).

58. Yaghmur, A., Rappolt, M., Østergaard, J., Larsen, C. & Larsen, S. W. Characterization of Bupivacaine-Loaded Formulations Based on Liquid Crystalline phases and Microemulsions : The Effect of Lipid Composition. *Langmuir* **28**, 2881–2889 (2012).

59. Vargas, R., Mateu, L. & Romero, A. The effect of increasing concentrations of precipitating salts used to crystallize proteins on the structure of the lipidic Q 224 cubic phase. *Chem. Phys. Lipids* **127**, 103–111 (2004).

5 POLYMERISATION OF TEMPLATED TANI-PTAB

5.1 INTRODUCTION

Using the concept of self-assembly, researchers have been able to design many complex structures with fine control over the material nanostructure and dimensions.[1,2] While the formation of self-assembled materials is often advantageous, owing to their reversibility and addressability, some applications require greater stability and mechanical strength.[3] One way this can be achieved is by polymerisation, which acts to fix the self-assembled structures while providing the desired rigidity and resilience to environmental changes.[4]

There are many methods to impart long-range order and orientation to polymeric materials, however the two that will be focused on in this chapter are the use of liquid crystals as structure-directing agents for reactive monomers and the use of reactive mesogens, which are mesogens that are themselves capable of polymerisation.

When using ordered mesophases as templates, the reactive monomer and initiators are dispersed in a liquid-crystal phase followed by polymerisation to capture the material structure. The removal of the template reveals the ordered polymer. Numerous examples of liquid-crystal templating can be found in the literature, with thermotropic or lyotropic liquid crystals being used to control the growth of complex polymer structures.[5–9] Such materials can then find applications as templates,[10] platforms for catalysis,[10] liquid crystal displays,[11] organic electronics[11,12] or nanoporous membranes.[13]

However, this method of polymer templating does not often result in the direct 1:1 transfer of the template structure to the final polymer.[14] Indeed, templated polymerisation within a mesophase often results in demixing or phase separation of the growing polymer.[15] Instead, the template acts to indirectly control the polymer structure, producing larger or different features to the mesophase. For example, polyaniline (**PANI**) nanofibers grown within a hexagonal phase were found to be much bigger than the diameter of the cylindrical micelles of the mesophase, which collapsed during the polymer growth.[16–18] Meanwhile, **PANI** helixes have been grown from multi-lamellar vesicles, demonstrating that ordered structures obtained by templated polymerisation can be very different from the initial mesophase.[19]

To overcome structure loss during templating, researchers often use photoinitiation to start polymer growth. Photopolymerisation is a very rapid polymerisation technique that uses light to initiate and propagate polymerisation reactions and is often used in the preparation of liquid crystal polymer networks.[20] Photoinitiation is preferable over the commonly used thermal initiation as temperature, which may affect the mesophase formation, is not an issue. Additionally, photoinitiation can occur rapidly enough that the template features are captured by the polymer before phase separation or template disruption can occur.[21]

Meanwhile, the use of reactive mesogens eliminates the requirement for a template to produce complex structures. The monomers themselves self-assemble into the desired constructs, which are then frozen in place by polymerisation.[22–25] In such cases, alignment and order are often retained, although a cross-linker may be required for stability.[26,27] Photopolymerisation is again often a valuable tool to capture the nanostructures, as it can take place before any potential phase changes due to the polymer growth.

The use of either templates or reactive mesogens to prepare complex polymer structures have their own advantages or disadvantages. As the structure of the template is usually independent of the monomer, different 3-D architectures can be easily accessed by adjusting the template conditions without adapting the reactive species. However, phase separation and demixing of the growing polymer often occurs when templating, resulting in indirect control over the mesostructure. Additionally, the monomer may need functionalising to solubilize it within the template phase, adding extra synthetic steps that may be complex.[28] Meanwhile, the use of reactive mesogens avoids miscibility problems prior to and during polymerisation and often results in liquid crystal structure being carried over to the final polymer.[10,29] However, the synthesis of a suitable mesogenic monomer may not be simple and the monomer may not form 3-D structures under the explored conditions, resulting in a template being required.

In this chapter, two methods of preparing polymer structures were investigated. In the first, acids with multiple acidic groups were used to non-covalently bond **TANI-PTAB** molecules in water and within a lipidic cubic phase. The use of doping acids as a binding agent aimed to eliminate the need to functionalise **TANI-PTAB** with a reactive group, which had proved difficult (see Chapter 2 and Section 5.2.3). Additionally, as the electrostatic interactions were reversible by the addition of a base, switchable structures that in the ES state were mechanically more stable could be produced. In the second, a more classic templating method was utilized, with a reactive gemini monomer being templated within a lipidic cubic phase. The aim of this second route was to demonstrate the growth of a simple polymer within a *Im3m* phase and use it as a model system to predict the growth of more complex polymers.

5.2 Results and Discussion

5.2.1 Non-covalent polymerisation of TANI-PTAB in water using acids with multiple acidic groups

As discussed above, the use of cross-linking dopants provides a method to simply add rigidity to **PANI** and **OANI** assemblies, without functionalising the compounds with polymerizable groups. Two acids were chosen for this work, naphthalenedisulfonic acid (**NDS**) and phytic acid (Figure 5.1). Phytic acid has been previously used in the synthesis of **PANI** polymer hydrogels, with the cross-linking effects of the multiple acidic groups adding mechanical strength to the polymers.[30,31] Indeed, the dynamic hydrogen bonding and electrostatic interactions even allowed for self-healing properties, reforming a

polymer film with little to no external input.[32,33] Meanwhile, **NDS** has been found to direct the morphology of **PANI** nanostructures, owing to the aromatic rings within both structures, and has been used to form fused nanowires when combined with **TANI-(PTAB)$_2$**.[34,35]

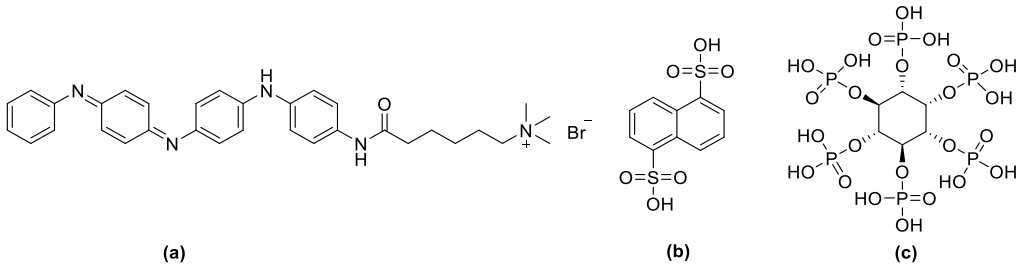

*Figure 5.1. Structures of (a) **TANI-PTAB** (b) naphthalenedisulfonic acid (**NDS**) (c) phytic acid.*

Investigations into the non-covalent polymerisation of **TANI-PTAB** in water using acids with multiple acidic sites were carried out in collaboration with Alex Byrne during an undergraduate BSc research project. The results of his work can be found in his thesis, entitled "Towards Organisational Control of Electroactive Amphiphiles",[36] and some UV-Vis/NIR absorption spectroscopy, polarised optical microscopy (POM) and transmission electron microscopy (TEM) experiments of **TANI-PTAB** doped with **NDS** have been replicated in this work. However, while Bryne used phytic acid as a cross-linking dopant for **TANI-C$_{12}$TAB**, the doping of **TANI-PTAB** with phytic acid is novel to this work.

5.2.1.1 Spectroscopic investigations of ES TANI-PTAB in water

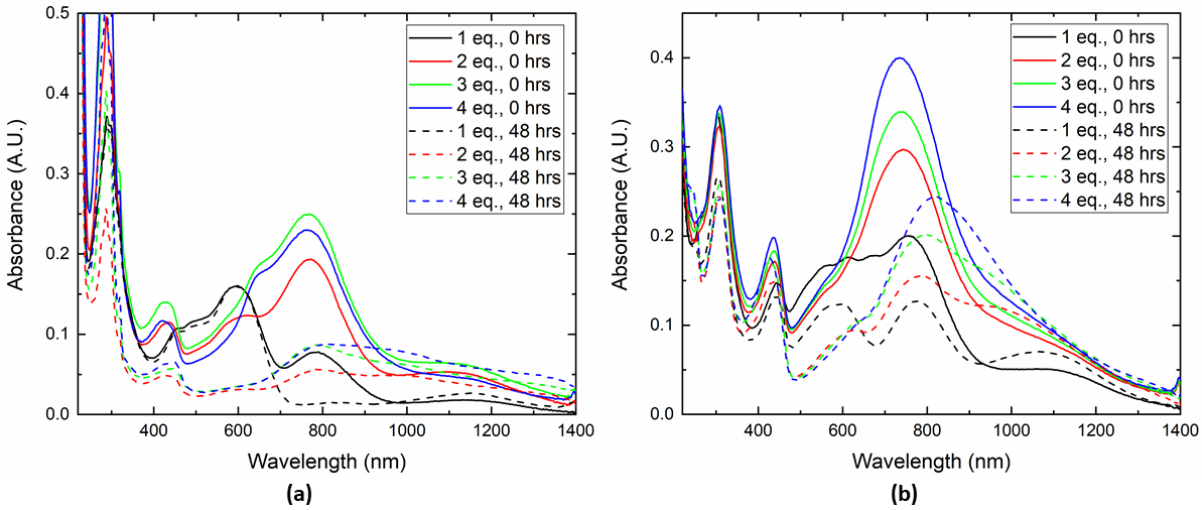

*Figure 5.2. UV-Vis/NIR absorption spectra for ES **TANI-PTAB** (0.25 mM) in water doped with (a) **NDS** (b) phytic acid. Spectra collected at 0 and 48 hours.*

The UV-Vis/NIR absorption spectra for ES **TANI-PTAB** doped with **NDS** and phytic acid were collected to determine the acid concentration required for complete doping. Figure 5.2a shows the absorption spectra for **TANI-PTAB** doped with increasing concentrations of **NDS**, immediately after preparation and after resting for 48 hours. **NDS** contains in its structure two sulfonic acid moieties

(Figure 5.1b), which means that only 1 molar equivalent of **NDS** should be required to ensure complete doping at both imine nitrogen atoms in **TANI-PTAB**. However, the absorption spectrum shows that at this lowest acid concentration, the EB peaks at 490 and 585 nm were still prominent in comparison to the polaron and bipolaron peaks at 784 and 1140 nm, respectively, which indicated that a higher acid concentration was necessary for complete conversion to the ES state. The EB peaks disappeared with 3 molar equivalents and above of **NDS**, while the ES peaks increased in intensity.

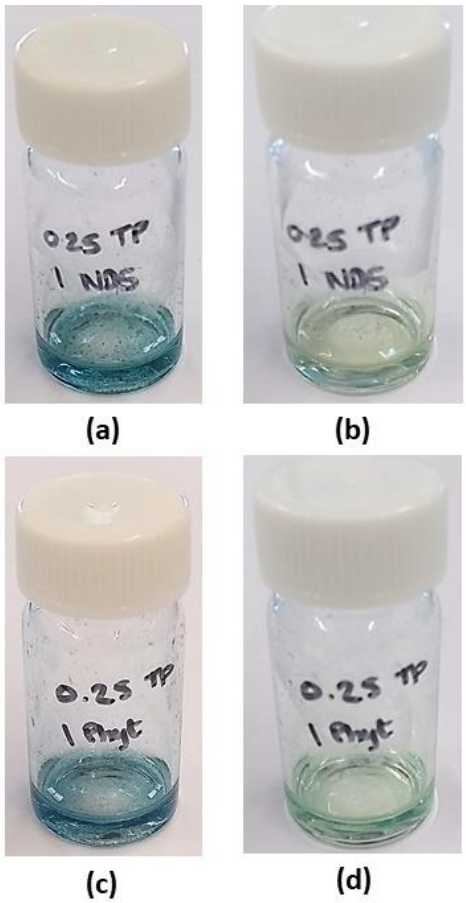

*Figure 5.3. ES **TANI-PTAB** (0.25 mM) in water, doped with 4 molar equivalents of (a, b) **NDS** and (c, d) Phytic acid. (a) and (c) taken at 0 hours. (b) and (d) taken after 48 hours.*

Concurrently, it was noted that green-blue precipitates formed with the two highest acid concentrations (Figure 5.3a), which were attributed to the non-covalent cross-linking of **TANI-PTAB** molecules by the diacid. After 48 hours, the precipitates had settled to the bottom of the vials, forming thin films and leaving a pale green solution (Figure 5.3b). The vials were agitated to redisperse the precipitates into solution and the absorbance spectra were collected again. The spectra for solutions after this time showed that de-doping occurred for the lowest acid concentration, however, for higher concentrations no re-emergence of the EB peaks were noted. The improved retention of the ES state with time, in comparison to monoacids such as **CSA** or **HCl** (Chapter 3), was attributed to the cross-linking nature

of **NDS**. Cross-linking was also evident by the tailing of the polaron and bipolaron peaks, indicating an increase in conjugation length.

Meanwhile, phytic acid contains six acidic moieties in its structure, meaning that one molecule of the acid should be sufficient for complete doping of three molecules of **TANI-PTAB** (Figure 5.1c). However, Figure 5.2b showed that even with 1 molar equivalent of phytic acid, an EB peak at 570 nm persisted, indicating that a higher concentration of the acid was required for complete conversion to the ES state. The degree of protonation for **PANI-** and **OANI-**based materials depends on the solution pH.[37] While theoretically 1 molar equivalent of phytic acid should be enough for all imine nitrogen atoms to be protonated, the acid concentration may not lower the solution pH sufficiently for complete doping to occur. Meanwhile, with 2 molar equivalents of the acid and above, only polaron and bipolaron peaks were present at approximately 750 and 1100 nm, respectively, indicating complete conversion to the ES state.

As with **NDS**, blue-green precipitates were observed in vials containing phytic acid-doped **TANI-PTAB** (Figure 5.3c), which were also attributed to the cross-linking abilities of the acid. After 48 hours, the precipitates had settled, forming a film at the bottom of the vials and leaving a pale-green solution (Figure 5.3d). The absorption spectra were collected again after agitating the vials to redisperse the films (Figure 5.2b) and showed that no de-doping occurred after the 48-hour period, indicating that the cross-linking dopants have better retention of the ES state over time. Additionally, the polaron peaks experienced a bathochromic shift that was more prominent with increasing acid concentration, and was attributed to the extension in conjugation length in the polymer owing to the cross-linking effect of phytic acid.[38,39]

5.2.1.2 Microscopy studies of ES TANI-PTAB in water

5.2.1.2.1 Polarised optical microscopy (POM)

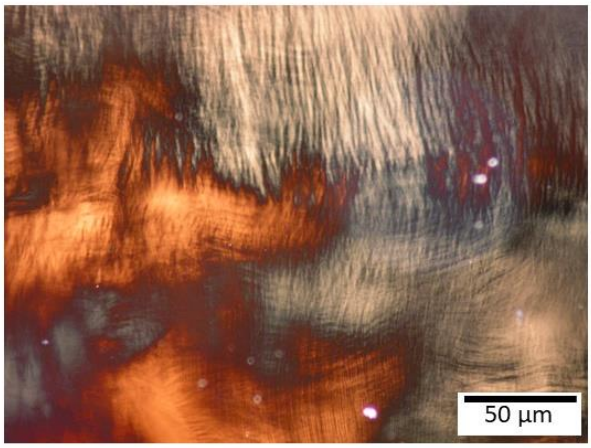

*Figure 5.4. POM image of EB **TANI-PTAB** (4 mM) in water.*

The structures formed by **TANI-PTAB** doped with **NDS** and phytic acid were explored further using microscopy techniques, beginning with polarised optical microscopy (POM). As can be seen in Figure 5.4, EB **TANI-PTAB** in water displays Schlieren-like textures, matching those formed by chromonic liquid crystals.[40,41] Chromonic liquid crystals are formed from aromatic compounds, which aggregate into columns, typically at low concentrations. These columns either align parallel to each other with no long-range order, forming a nematic phase, or arrange in a hexagonal array, forming a hexagonal phase. It was hoped that the cross-linking dopants would be able to trap the columnar aggregates, adding structural rigidity while maintaining the self-assembled structures.

Figure 5.5 shows POM images of **TANI-PTAB** doped with 4 molar equivalents of **NDS** and 2 molar equivalents of phytic acid. The acid concentrations were chosen following UV-Vis/NIR absorption experiments, to ensure that complete doping would be achieved. For both acids, blue-green micrometre-sized aggregates formed. With **NDS**, the aggregates were only weakly birefringent, which indicated that some internal order had been lost after doping. Meanwhile, with phytic acid, the fibre-like aggregates formed by **TANI-PTAB** exhibited stronger birefringence, which indicated more ordered assemblies than with the diacid. As noted in Section 4.2.1.2.1, Chapter 4, sections of the slide bearing isotropic solutions were not fully dark as the crossed polarisers were not at an exact 90° angle (owing to manual adjustments made by other microscope users).

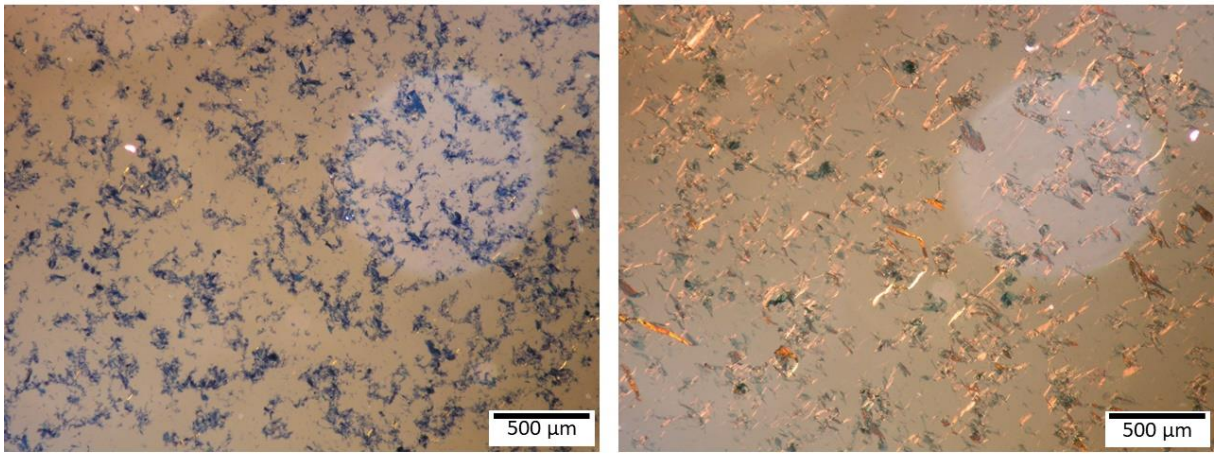

*Figure 5.5. POM images of aqueous ES **TANI-PTAB** (4 mM), doped with (a) 4 molar equivalents of **NDS** (b) 2 molar equivalents of phytic acid.*

5.2.1.2.2 Transmission electron microscopy (TEM)

Transmission electron microscopy (TEM) was used to further probe the internal structures of the doped **TANI-PTAB** aggregates. Solutions of ES **TANI-PTAB** (0.01 mM) doped with 4 molar equivalents of each acid were sonicated for one minute prior to deposition on carbon-coated glow-discharged copper grids and were negatively stained with uranyl acetate (1 %) to provide contrast.[42]

After doping with **NDS**, **TANI-PTAB** formed fibres that were approximately 17 nm in diameter and several micrometres long (Figure 5.6a). Closer inspection of the aggregates (Figure 5.6b) indicated that they were formed from bundles of nanofibers, although as the structures were resistant to staining it was difficult to distinguish individual nanofibers within the aggregates to confirm this. However, as the length of a single **TANI-PTAB** molecule has been calculated to be 2.9 nm,[40] and the observed doped fibres are much wider than this, it is likely that they are formed from aggregating nanofibers.

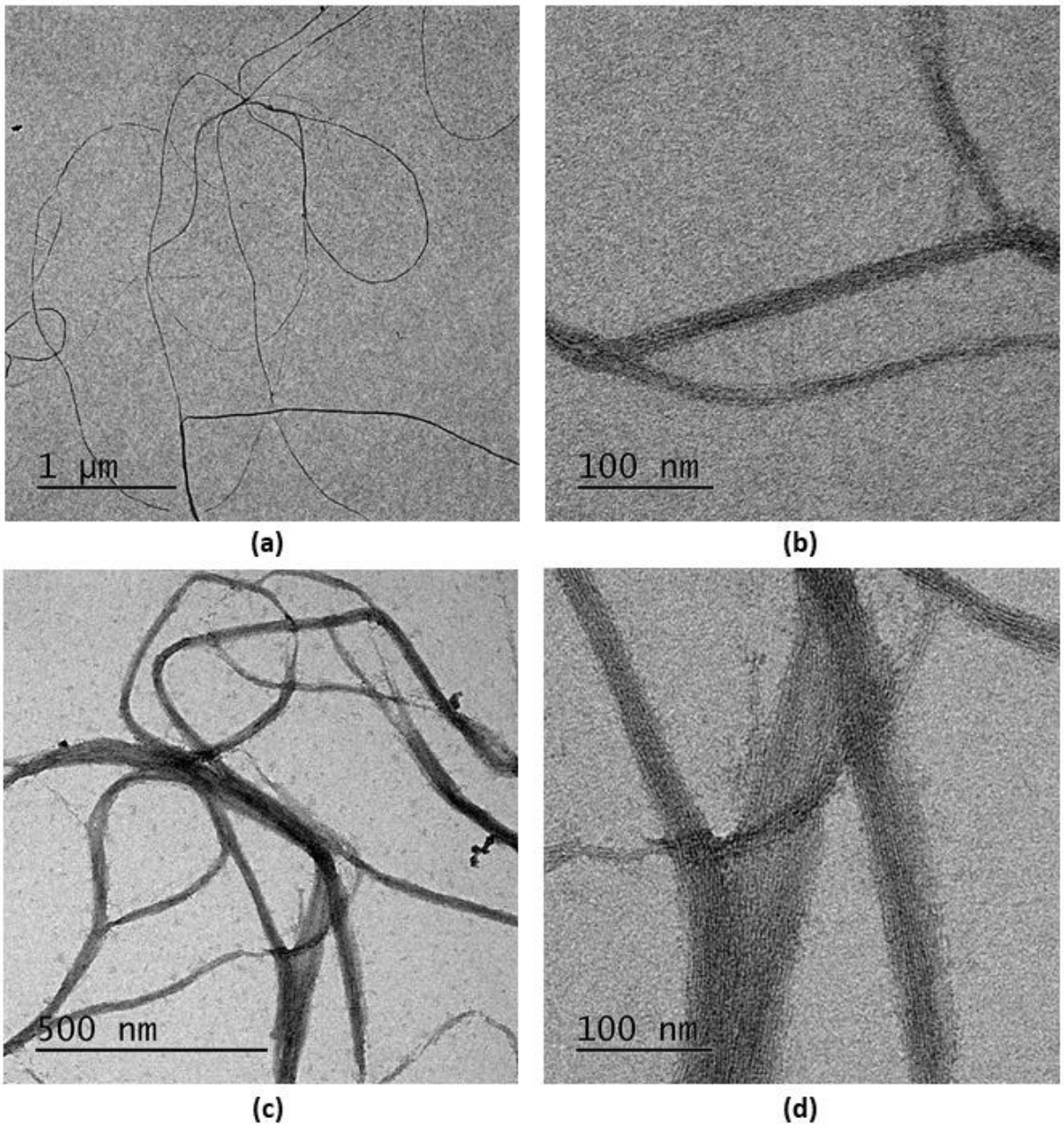

*Figure 5.6. TEM images ES **TANI-PTAB** (0.01 mM) solutions doped with 4 molar equivalents of (a, b) **NDS** and (c, d) phytic acid. Stained with 1 % uranyl acetate.*

Meanwhile, Figure 5.6c shows that **TANI-PTAB** doped with phytic acid formed ribbon-like structures, which were of varying widths. The measured ribbons were anywhere between 14 and 70 nm in diameter.

These structures also appeared to be formed from aggregated nanofibers (Figure 5.6d), however, again the images were not clear enough to fully distinguish individual fibres.

The difference in the structures formed after doping with **NDS** or phytic acid is likely due to the number of acidic sites on each acid. Phytic acid has three times the number of acidic sites in comparison to **NDS**, which would allow it to bond with more **TANI-PTAB** molecules at once, forming a more widely cross-linked material. This is supported by literature reports where **NDS** has been used to form fibre-like structures with **TANI**-amphiphiles,[35] while phytic acid is often used to form densely cross-linked polymer hydrogels.[30,32,33]

5.2.1.3 Conclusions from doping experiments in water

The use of **NDS** and phytic acid as dopants for **TANI-PTAB** resulted in the formation of aggregates that were visible to the naked eye. UV-Vis/NIR absorption spectroscopy demonstrated that the aggregates showed better retention of the doped ES state than acids with only one acidic moiety, over a 48-hour period, which was attributed to the cross-linking effects of the acids. Meanwhile, POM showed the formation of micrometre-sized aggregates, which upon closer inspection by TEM were revealed to be fibrous and ribbon-like structures for **NDS** and phytic acid, respectively.

TEM investigations were hindered by poor electron contrast, which made it difficult to determine the whether the fibres were formed from bundles of nanofibers or were formed by some other mechanism. In addition, the micrometre-sized structures were too big for TEM to be ideally used. For future experiments, techniques such as atomic force microscopy (AFM) or scanning electron microscopy (SEM) may be valuable to determine the aggregate morphology. Byrne utilized SEM to investigate the structures formed by doped **TANI**-amphiphiles,[36] however, as the sample preparation was time-consuming and required freeze-drying with ramping temperatures, similar experiments were not performed in this work.

5.2.2 Non-covalent polymerisation of TANI-PTAB in MO cubic phases

5.2.2.1 Spectroscopic investigations of TANI-PTAB with PPO

Following investigations into the non-covalent cross-linking of **TANI-PTAB** in water, attention was turned to the application of the same process within a lipid template. While experiments in water had demonstrated the formation of 1-D nanofibers and 2-D nanoribbons, it was hoped that the use of a cubic phase template would allow for a 3-D polymer network for be prepared. As with previous experiments investigating the doping of **TANI**-amphiphiles in monoolein (**MO**) (Chapters 3 and 4), the UV-Vis/NIR absorption spectra for **TANI-PTAB** doped with **NDS** and phytic acid in the presence of **PPO** were collected to infer the quantity of acid required for conversion to the ES state.

The absorption spectra for **TANI-PTAB** doped with **NDS** and phytic acid in the presence of **PPO** are given in Figure 5.7 (a and b, respectively). Complete conversion to the ES state was observed with 3

molar equivalents of **NDS** or 1 molar equivalent of phytic acid, as evident by the absence of EB peaks at 600 nm. De-doping occurred with the lowest **NDS** concentration after 48 hours, however, all other **NDS** concentrations and all phytic acid concentrations showed little re-emergence of the EB peaks, indicating the stability of the ES state over time. Additionally, the bipolaron peaks at approximately 1080 nm became more prominent after 48 hours for both acids, which was attributed to a charge screening effect from **PPO**, as noted in previous chapters.

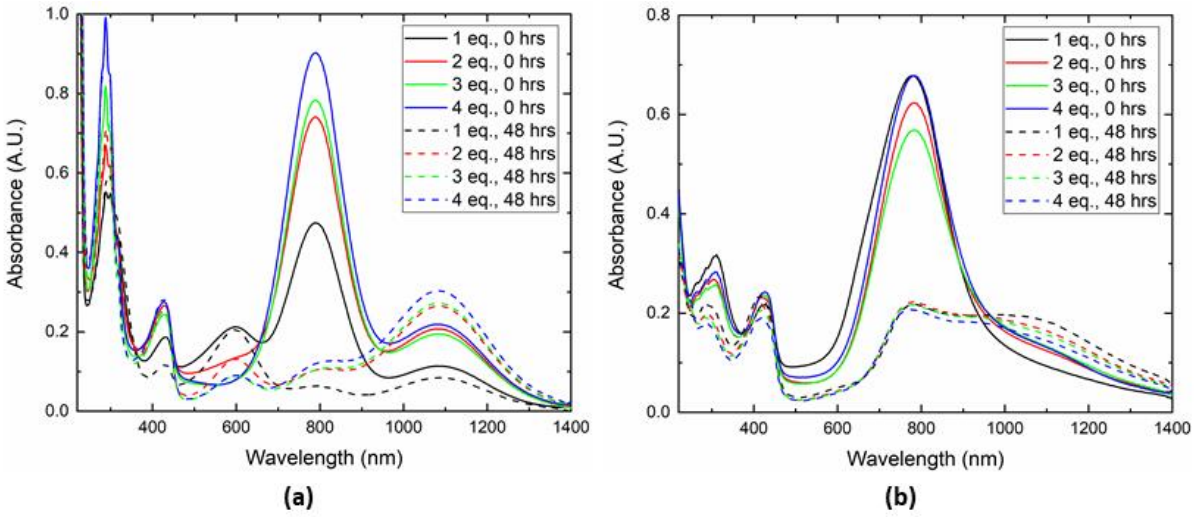

*Figure 5.7. UV-Vis/NIR absorption spectra for ES **TANI-PTAB** (0.25 mM), doped with (a) **NDS**, with **PPO** (b) phytic acid, with **PPO**.*

SAXS experiments were performed using 4 molar equivalents of **NDS** and phytic acid, as experiments in water had indicated this concentration was sufficient to ensure doping at 0 and 48 hours and experiments with monoacids (**CSA**, **HCl** and **TFA**) had used the same concentrations. Doping was assumed based on a visible colour change from purple to green. The UV-Vis/NIR absorption spectra for ES **TANI-PTAB** doped with either acid in **MO** sponge phases were not collected owing to the partial decomposition of **MO** discussed in previous chapters (Chapter 3, Section 3.2.5), although SAXS experiments were completed prior to any recorded lipid degradation.

5.2.2.2 Small-angle X-ray scattering investigations of TANI-PTAB in MO cubic phases

Prior to investigations into the non-covalent polymerisation of **TANI-PTAB** in **MO** cubic phases, the effects of both cross-linking dopants on the mesophase behaviour of the lipid were investigated. As mentioned in previous chapters, pH typically has limited effect on the cubic phase nanostructure.[43–45] Indeed, SAXS patterns for both acids show peaks characteristic of the *Pn3m* phase (see representative scattering patterns in Figure D.1, Appendix D). However, as can be seen in Figure 5.8, the addition of **NDS** and phytic acid both led to a decrease in lattice parameters with increasing acid concentration. Such trends usually precede a transition to more negatively curved phases, such as the hexagonal phase, which could be expected to form if the acid concentrations were further increased.[46]

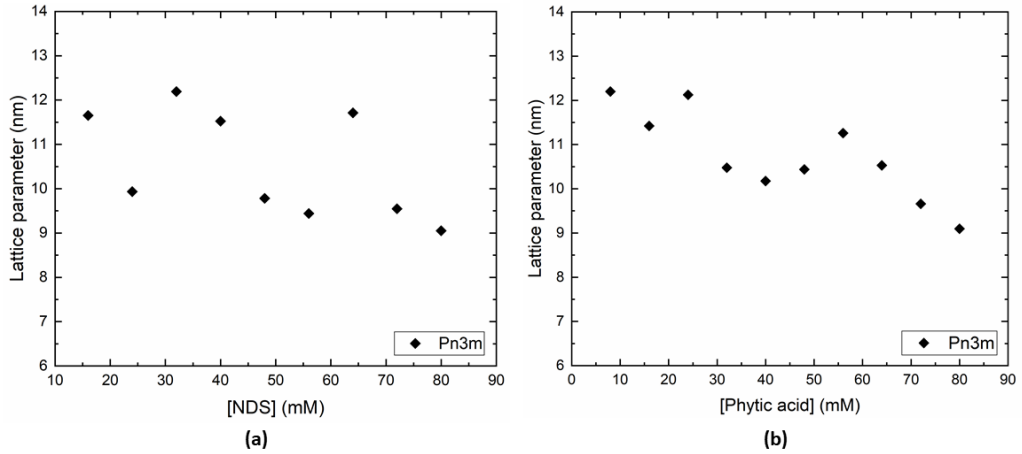

*Figure 5.8. Lattice parameters for **MO** cubic phases containing 10-80 mM of (a) **NDS** and (b) phytic acid.*

While both **NDS** and phytic acid are strong acids, with pKas of -2.8 and 0.14, respectively, the decrease in pH was not believed to be the cause of this change. Indeed, other acids used in this work (**CSA**, **HCl** and **TFA**) with similar pKas had no effect on **MO** mesophase formation suggesting another factor was at play. Instead, the trend may be related to the bulky, amphiphilic nature of both acids. Some large acids, such as oleic acid, lead to transitions to more negatively curved phases owing to their amphiphilic character.[46] It may be that phytic acid and in particular **NDS**, with its aromatic core, interact with the lipid membrane and affect its curvature in a similar manner.

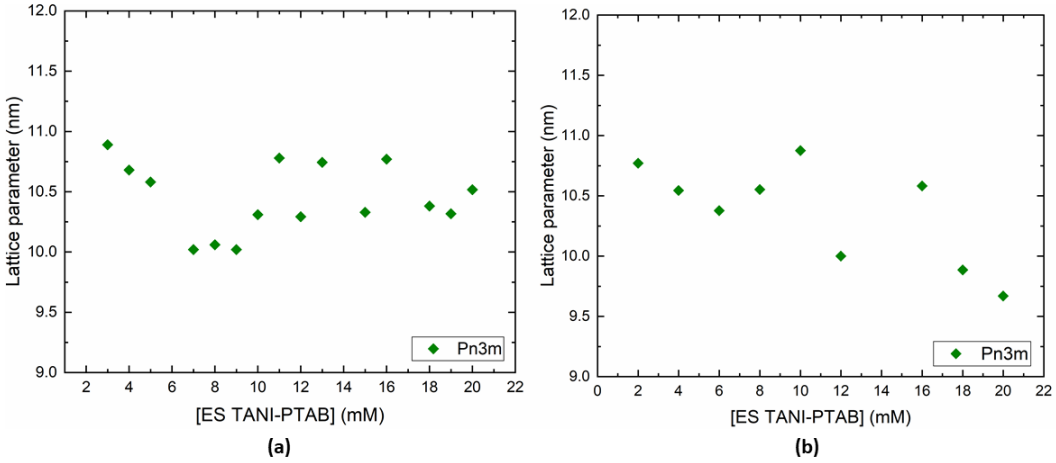

*Figure 5.9. Lattice parameters for **MO** cubic phases containing ES **TANI-PTAB** (2-20 mM) doped with 4 molar equivalents of (a) **NDS** (b) phytic acid.*

Following the control experiments with both acids, cubic phases containing **TANI-PTAB** doped with **NDS** and phytic acid were prepared. 4 molar equivalents of each acid were chosen for each sample, as UV-Vis/NIR absorption experiments had shown that this produced only ES-state **TANI-PTAB** in water and with **PPO** at 0 and 48 hours. Cubic phases containing **TANI-PTAB** doped with **NDS** and phytic acid were prepared following the procedures outlined in Chapter 2. The production of the ES state after

hydration for 48 hours was assumed based on a colour change from purple (characteristic of the EB state) to green (characteristic of the ES state).

The lattice parameters and phase identification for **NDS**-doped **TANI-PTAB** are given in Figure 5.9a. The *Pn3m* phase was formed at all **TANI-PTAB** concentrations, with an average lattice parameter of 10.4 nm. The results matched findings from **TANI-PTAB** doped with the monoacids, **CSA**, **HCl** and **TFA**, (Chapter 3) and therefore the same mechanisms for self-assembly were proposed, which were either an increase in *pp* with the addition of dopants within the lipid bilayer or the partitioning of **TANI-PTAB** into the aqueous channels and subsequent doping.

Interestingly, no negative trend in lattice parameter was noted with increasing concentrations of **TANI-PTAB** and **NDS**, as had been observed with the acid alone. From previous experiments with the diacid (Chapter 4), it appeared that doping single-tailed **TANI**-amphiphiles with **NDS** resulted in the *Pn3m* phase with no noticeable difference in lattice parameters. It was assumed that the non-covalent interactions between **TANI**-amphiphiles and **NDS** took priority over interactions between **NDS** and **MO**, negating any effect of the acid on the membrane curvature.

Meanwhile, the lattice parameters and phase identification for cubic phases prepared with phytic acid and **TANI-PTAB** are given in Figure 5.9b. As with samples doped with **NDS**, the addition of phytic acid resulted in the formation of the *Pn3m* phase at all **TANI-PTAB** concentrations. However, unlike **NDS**, samples doped with phytic acid displayed a negative trend in lattice parameters with increasing concentration, following control experiments with the acid alone.

With 4 moles of acid to each mole of **TANI-PTAB**, phytic acid is in high excess of what should be required for complete doping to the ES state. Therefore, it may be that in the prepared cubic phases, not all phytic acid molecules were involved in doping and instead were interacting with the lipid membrane, producing the observed trend.

*Figure 5.10. Photos of capillaries containing **MO** cubic phases prepared with phytic acid-doped **TANI-PTAB**. Left: 6 mM, Right: 8 mM.*

Interestingly, while **TANI-PTAB** doped with **NDS**, **CSA**, **HCl** or **TFA** produced visually homogeneous, dark-green cubic phases, samples prepared with phytic acid showed clear phase separation. Figure 5.10 is a photo of capillaries containing 6 and 8 mM **TANI-PTAB** doped with phytic acid. The dark green regions indicate higher concentrations of ES **TANI-PTAB**.

As the acids had been previously utilized to cross-link **TANI-PTAB** in water, it was hoped that similar non-covalent polymerisation of the amphiphile would occur after addition of the acids to **MO** cubic phases. While there had been no indicators of cross-linking with **NDS**, the phase separation observed with phytic acid suggested a cross-linking effect with the latter acid in the template.

Direct templating of lyotropic liquid crystal phases is rare, particularly with slower polymerisation techniques such as electrochemical or thermal polymerisation.[14] Instead, the template usually acts to indirectly control the polymer growth into an ordered structure. In such cases, demixing and phase separation of the growing polymer usually occurs, often with the destruction of the template.[15] The slow diffusion of phytic acid into the **MO**/**TANI-PTAB** mixture likely precludes any rapid "freezing" of the cubic phase nanostructure and it would therefore be expected that while the phase separated polymer may be ordered, it would not have the same mesostructure as the template.

The SAXS patterns for **MO** with phytic acid-doped **TANI-PTAB** did not provide any details as to the final cross-linked **TANI** structure, as any scattering from the polymer was overwhelmed by the scattering from the lipid. Determining what structures, if any, were formed by cross-linking of the amphiphile required the removal of the template by washing with ethanol, followed by analysis of the polymer structure by SAXS, TEM and SEM. However, as the cubic phases were prepared and sealed within a capillary tube, removal of the template in this work was not possible.

5.2.3 Covalent polymerisation of amphiphiles in MO cubic phases

Following experiments exploring the non-covalent polymerisation of templated **TANI-PTAB**, avenues to covalently link **TANI-**amphiphiles were investigated. Acrylates were chosen as polymerizable moieties, as they can be rapidly polymerised using light and have been previously utilised to form polymers from **TANI** monomers.[47,48] Many synthetic routes to produce a polymerizable **TANI-**amphiphile were attempted in this project, with limited success. In brief, the synthesis of a single-tailed polymerizable **TANI-PTAB** was attempted by the asymmetric substitution of **NH_2/NH_2 TANI** or by the functionalisation of **TANI-CPh_2**. Both methods were impeded by the formation of undesired side-products that could not be removed by common purification techniques. Difficulties in purification again hindered the synthesis of a polymerizable gemini **TANI-**amphiphile from **TANI-C_6Br** and the precursors of a gemini surfactant, as the starting materials could not be separated from the products. Full experimental details and greater discussion of the different routes and their outcomes are given in Chapter 2 and will not be covered further in this chapter.

5.2.3.1 Polymerization of MA-11-2-11-MA in MO/PPO

As a polymerizable **TANI**-amphiphile had not been successfully synthesised, the use of **MO** cubic phases as a template for stimuli-responsive electroactive amphiphiles could not be explored. However, the final synthetic route attempted used a gemini surfactant terminated by methacrylate groups as the basis of its design. This gemini surfactant, known as **MA-11-2-11-MA** (Figure 5.11a), has been used to prepare polymer films and coatings by the polymerisation of the monomer around suitable substrates.[49] Free-standing polymer films could be achieved by subsequent etching of the substrates with hydrofluoric acid.

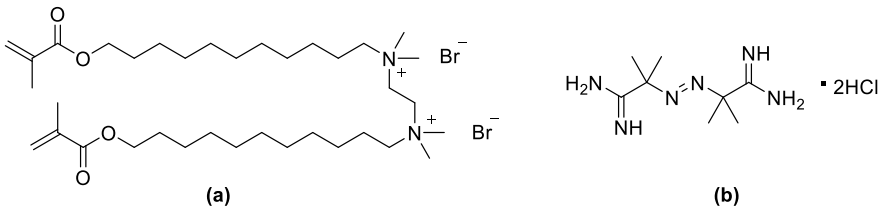

*Figure 5.11. Structures of (a) **MA-11-2-11-MA** (b) 2,2'-azobis(2-methylpropionamidine) dihydrochloride (**PI**).*

MA-11-2-11-MA was designed with a short alkyl linker of two methylene groups between the hydrophilic head groups, as a short linker would result in a higher *pp* and thus encourage the formation of flat bilayers on a substrate interface and cylindrical micelles in solution.[50,51] Additional evidence for the formation of flat bilayers by **MA-11-2-11-MA** arose from POM analysis of a film prepared by drop-casting and drying of the monomer solution on a glass slide, revealing a smectic-type birefringent texture that implied the formation of lamellar structures as the solvent evaporated.

A research project was developed by Esther Townsend to investigate the lyotropic liquid-crystalline behaviour of **MA-11-2-11-MA** in water and to polymerise such mesophases in solution. This project was carried out by Thomas Bott as an undergraduate MSci research project in collaboration with Esther Townsend. The results can be found in "Gemini Surfactant to 3D Polymers" and formed the basis for the polymerisation reactions performed in this work.[52]

Bott determined that **MA-11-2-11-MA** (200 mM) forms a lamellar mesophase at 25 °C upon cooling from 65 °C. With the addition of a photoinitiator, 2,2'-azobis(2-methylpropionamidine) dihydrochloride (**PI**, Figure 5.11b), a polymer film could be prepared by the irradiation of the monomer solution using UV-light. The rate of photopolymerisation increased with the ratio of **PI**-to-**MA-11-2-11-MA**, from 10 minutes with a 1:8 ratio to 5 minutes with a 1:1 ratio. The polymer films retained the lamellar character of the monomer solution.

As the self-assembly behaviour and the polymerisation conditions for **MA-11-2-11-MA** in water were well understood, it was decided to combine the surfactant with **MO** and to use it as a model system to explore the polymerisation of organic monomers in bicontinuous lipidic cubic phases. The full experimental details for the preparation of cubic phases with **MA-11-2-11-MA** and **PI** are given in

Chapter 2. Sponge phases were prepared before the addition of **MA-11-2-11-MA**, as the reduced solubility of the surfactant at room temperature led to its precipitation from solution when added to the lyotrope mixture before combining with **MO**.

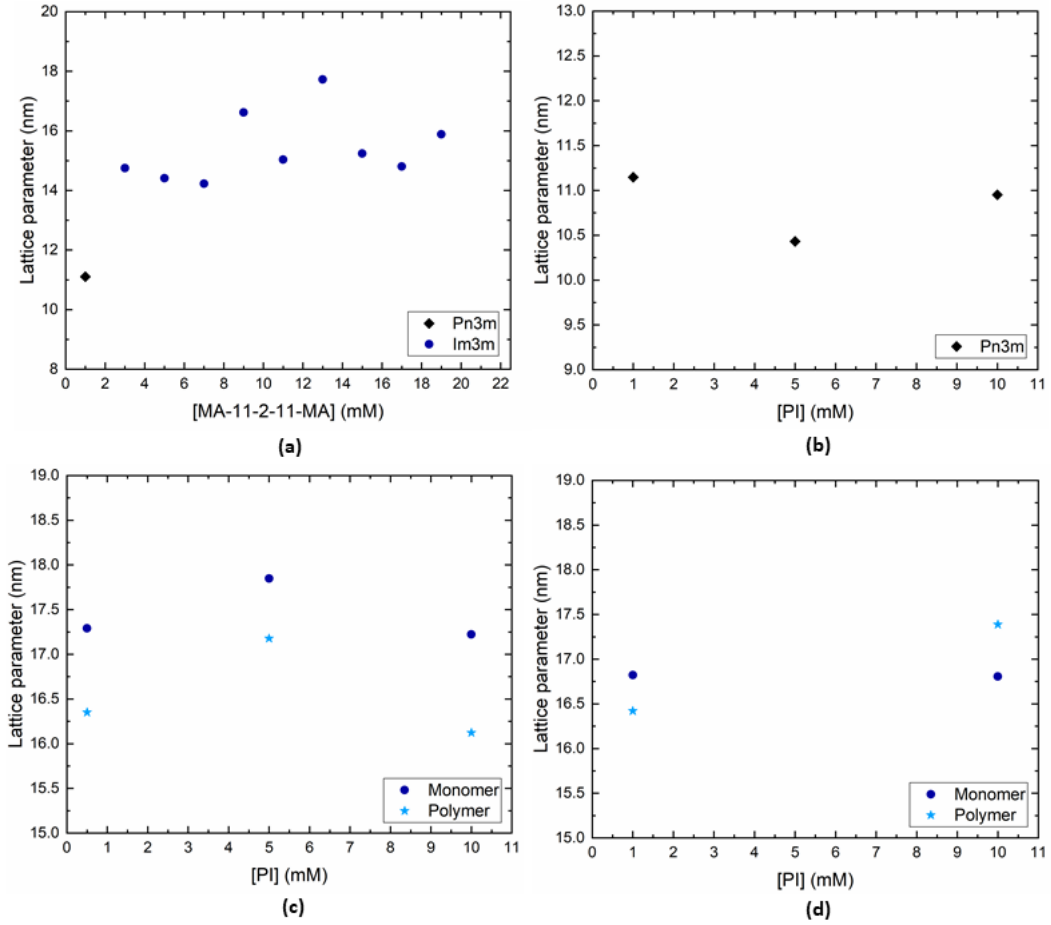

*Figure 5.12. Lattice parameters for **MO** cubic phases prepared with (a) **MA-11-2-11-MA** (1-20 mM) (b) **PI** (1-10 mM) (c) **MA-11-2-11-MA** (10 mM) and **PI** (0.5-10 mM), before and after photo-polymerisation (d) **MA-11-2-11-MA** (20 mM) and **PI** (1-10 mM), before and after polymerisation.*

In preliminary experiments, increasing concentrations of **MA-11-2-11-MA** were added to **MO** cubic phases without the addition of **PI**, to determine the influence of the gemini surfactant on the mesophase structure alone (Figure 5.12a). It was found that the *Pn3m* phase formed with the addition of 1 mM **MA-11-2-11-MA**, however, concentrations above 3 mM produced the *Im3m* phase, as determined by characteristic scattering patterns (see Figure D.2 in Appendix D for example spectra). The transition to the less negatively curved *Im3m* phase with **MA-11-2-11-MA** was explained by the *pp* of the gemini surfactant, which had been designed to result in the formation of flat bilayers and was therefore expected to have a flattening effect on the membrane curvature of **MO.** The behaviour was also reminiscent of that induced by the addition of single-tailed **TANI-**amphiphiles, which in the EB state form flat nanowire structures and may have a similar *pp* to **MA-11-2-11-MA**.

Next, the effect of the photoinitiator was explored to determine whether it would affect the phase behaviour of **MO**. As Bott had shown that the rate of photopolymerisation was dependent on the photoinitiator concentration, a range of **PI** concentrations from 1 to 10 mM were included (Figure 5.12b). The *Pn3m* phase was formed for all investigated concentrations, which indicated that the addition of the photoinitiator would not produce any competing effects on the mesophase structure in combination with **MA-11-2-11-MA**.

Finally, cubic phases were prepared with both **MA-11-2-11-MA** and **PI** and initial polymerisation experiments were attempted. Two **MA-11-2-11-MA** concentrations were chosen, to determine whether the monomer concentration affected the degree of polymerisation. The higher the monomer concentration, the greater the likelihood of there being adjacent molecules close enough in space for polymerisation to be successful. With 10 and 20 mM **MA-11-2-11-MA**, the ratios of monomer to **MO** are approximately 1:187 and 1:94, respectively. The lipid-to-monomer ratio is heavily skewed towards the lipid and if the monomer is homogenously distributed, the probability of adjacent monomers is low, which may hinder polymerisation. However, the distribution of **MA-11-2-11-MA** in **MO** is unknown and it may be that aggregates of the monomer within the bilayer are favourable, increasing the chance of polymerisation. Ideally, the concentration of **MA-11-2-11-2-MA** would be increased to improve the ratio of the monomer relative to **MO**, however, owing to time constraints and limited availability of **MA-11-2-11-MA**, it was not possible to do so in this work. The concentration of **PI** was also varied from 1:20 to 1:1 **PI**-to-**MA-11-2-11-MA**, to determine whether this would also affect the degree of polymerisation.

Cubic phases containing monomeric **MA-11-2-11-MA** were kept in the dark when not in use, to prevent early photoinitiation. Samples were left to hydrate for 48 hours after preparation to ensure complete conversion from the sponge phase to the *Im3m* phase had occurred before identification using SAXS. The capillaries were marked to enable the same section of the cubic phase to be reanalysed after polymerisation. Owing to reduced equipment access, samples were left for 24 hours after analysis before polymerisation. The capillaries were transferred to a UV-reactor and were irradiated with light (310-380 nm) for 2 hours, which was expected to be sufficient for photoinitiation to occur. Indeed, polymerisation with **PI** can usually be accomplished in a matter of hours by thermal initiation or in under an hour by photoinitiation.[49,53–55] Following polymerisation, the capillaries were left to rest for a further 24 hours before analysis again by SAXS.

The lattice parameters associated with the *Im3m* phases formed with **MA-11-2-11-MA** (10 and 20 mM) before and after polymerisation can found in Figure 5.12c and d. The *Im3m* phase was retained post-polymerisation, although a significant decrease in lattice parameter of at least 0.5 nm was noted for most samples. This decrease is likely a result of the additional 48 hours hydration time between analysis of the monomer state and polymer and suggests that the cubic phases had not reached an equilibrium

before polymerisation. The sample containing 20 mM **MA-11-2-11-MA** and 10 mM **PI** was the only cubic phase that experienced an increase in lattice parameter after polymerisation. The swelling of the lattice parameter could indicate the growth of a polymer, which only occurred with the highest monomer and photoinitiator concentration.

Again, it is worth noting that the direct templating of a lyotropic liquid crystal microstructure is rare.[14] Typically, the growth of polymers within a mesophase results in demixing and phase separation, which usually results in indirect structural control and the destruction of the template.[15] As photopolymerisation proceeds rapidly, it is sometimes possible to trap the template structure before phase separation of the polymer or the disruption of the template can occur, however this is often the exception and not the rule.[20]

In some cases, the lyotropic liquid crystal phase will coexist with the demixed polymer, so there are no noticeable differences in diffraction patterns before and after polymerisation.[4] For this reason, the diffraction patterns obtained by SAXS cannot be used to identify any microstructures formed by templated polymers until after purification. As **MO** is soluble in ethanol, templated polymers formed by **MA-11-2-11-MA** should be readily purified by washing with the solvent, following which the degree of polymerisation could be explored by IR and ^{1}H NMR spectroscopy and the polymer structure could be identified by SAXS, TEM and SEM. However, as the above polymerisation experiments were performed in sealed capillary tubes, subsequent purification and analysis was not possible.

Overall, it is likely that no polymerisation of **MA-11-2-11-MA** in **MO** cubic phases occurred. This was indicated by the absence of any meaningful changes to the template structure after polymerisation and the low monomer concentration. Another complication was the choice of photoinitiator. **PI** is often used as a free-radical source in hydrophilic environments,[56] which means it may not have been available within the hydrophobic compartment of the lipid bilayer for photoinitiation of **MA-11-2-11-MA**. An initiator that is preferentially situated in hydrophobic environments may have been preferred, such as 2,2'-azobis(2,4-dimethylvaleronitrile).[57] However, owing to time constraints at the close of this project, experiments with other photoinitiators could not be explored.

5.3 CONCLUSIONS

In this chapter, two methods to polymerise and therefore capture the self-assembled structures formed by amphiphiles were investigated. In the first method, acids with multiple acidic groups were used to non-covalently bond **TANI-PTAB** using electrostatic interactions, fixing the aggregate formations in water and within a template. In the second method, the acrylate groups on a gemini monomer were polymerised by photoinitiation, again attempting to capture a template structure.

In the first part, **TANI-PTAB** was doped using either 1,5-naphthalenedisulfonic acid (**NDS**) or phytic acid and the structures formed were explored. It was expected that a 1:1 ratio of **NDS**-to-**TANI-PTAB**

and a 1:3 ratio of phytic acid-to-**TANI-PTAB** would be required for full conversion to the ES state, owing to the number of acidic sites relative to imine nitrogen atoms. However, UV-Vis/NIR absorption experiments demonstrated that higher acid concentrations were necessary, which was attributed to the lower pH required for complete protonation. Aggregates visible with the naked eye were observed with both acids and were investigated by polarised optical microscopy (POM) and transmission electron microscopy (TEM). POM demonstrated the formation of micrometre-sized aggregates that were weakly birefringent, indicating some order was retained after doping. Meanwhile, TEM showed that fibrous structures were formed with the addition of **NDS,** while ribbon-like structures were prepared with phytic acid. The difference in structures was attributed to the cross-linking capabilities of both acids. **NDS** with two acidic moieties facilitated the formation of elongated nanofibers, while phytic acid with six acidic sites facilitated the formation of more densely cross-linked and wider aggregates.

Following experiments in water and the formation of 1- and 2-D structures upon doping, attention was turned to doping within a template, with the aim of preparing complex 3-D architectures using non-covalent interactions. The addition of **NDS** and phytic acid to **MO** cubic phases resulted in a decrease in lattice parameter with increasing acid concentration, indicating that both acids increased the negative curvature of the lipid bilayer. However, the combination of **TANI-PTAB** and **NDS** led to the formation of the *Pn3m* phase with no significant variation in lattice parameter with concentration, indicating that the electrostatic interactions between **TANI-PTAB** and **NDS** took precedence over interactions between **NDS** and **MO**.

Meanwhile, doping **TANI-PTAB** with phytic acid in **MO** led to the formation of *Pn3m* phases that showed a negative trend in lattice parameters with increasing concentration. This was attributed to the possibly higher than necessary concentration of phytic acid, resulting in only a portion of the acid molecules being involved in doping while the remainder were left to interact with the bilayer. Interestingly, clear phase separation was observed upon doping, which could indicate the formation of a cross-linked polymer within the template. However, as the templated polymer was contained within a sealed capillary tube, it was not possible to remove the template by washing and determine what structures had formed.

Finally, experiments were undertaken to explore the covalent polymerisation of a gemini monomer (**MA-11-2-11-MA**) using **MO** cubic phases as a template. The addition of **MA-11-2-11-MA** to **MO** resulted in the formation of the *Im3m* phase, owing to the flattening effect of the surfactant, which had been selected due to its inclination to form lamellar phases. Subsequently, *Im3m* phases containing varying concentrations of **MA-11-2-11-MA** and a photoinitiator (**PI**) were formed and were analysed prior to and after exposure to UV light. The recorded lattice parameters decreased following polymerisation, which was attributed to the additional hydration time experienced between analyses. Polymerisation was not believed to have occurred, owing to the hydrophilicity of **PI**, which would result

in it being located in the water channels while the monomer would be sequestered in the hydrophobic lipid bilayer.

To summarise, non-covalent and covalent methods of polymerising amphiphiles were explored, with and without templates. **NDS** and phytic acid were successfully used to cross-link **TANI-PTAB** in water, resulting in the formation of nanofibers or nanoribbons. The application of the same process using **MO** as template was more difficult, owing to the interaction of the acids with the lipid bilayer and the inability to remove the template post-polymerisation. Meanwhile, the addition of **MA-11-2-11-MA** was successfully used to induce the formation of the *Im3m* phase, however its photoinitiated polymerisation was hindered by the differences in hydrophobicity of the monomer and the **PI**.

5.4 REFERENCES

1. Stupp, S. I. & Palmer, L. C. Supramolecular chemistry and self-assembly in organic materials design. *Chem. Mater.* **26**, 507–518 (2014).

2. Wang, C., Wang, Z. & Zhang, X. Superamphiphiles as building blocks for supramolecular engineering: Towards functional materials and surfaces. *Small* **7**, 1379–1383 (2011).

3. Miller, S. A, Ding, J. H. & Gin, D. L. Nanostructured materials based on polymerizable amphiphiles. *Curr. Opin. Colloid Interface Sci.* **4**, 338–347 (1999).

4. Hentze, H.-P. & Kaler, E. W. Polymerization of and within self-organized media. *Curr. Opin. Colloid Interface Sci.* **8**, 164–178 (2003).

5. Akagi, K. *et al.* Highly conductive polyacetylene film prepared by the liquid crystal polymerization method under magnetic field. *Synth. Met.* **17**, 241–246 (1987).

6. Goto, H. Doping-dedoping-driven optic effect of pi-conjugated polymers prepared in cholesteric-liquid-crystal electrolytes. *Phys. Rev. Lett.* **98**, 1–4 (2007).

7. Goto, H. & Akagi, K. Optically Active Electrochromism of Poly(3,4-ethylenedioxythiophene) Synthesized by Electrochemical Polymerization in Lyotropic Liquid Crystal of Hydroxypropyl Cellulose/ Water: Active Control of Optical Activity. *Chem. Mater.* **18**, 255–262 (2006).

8. Akagi, K. *et al.* Helical Polyacetylene Synthesized with a Chiral Nematic Reaction Field. *Science* **282**, 1683–1686 (1998).

9. Wadekar, M. N., Pasricha, R., Gaikwad, A. B. & Kumaraswamy, G. Polymerization in Surfactant Liquid Crystalline Phases. *Chem. Mater.* **17**, 2460–2465 (2005).

10. Gin, D. L., Gu, W., Pindzola, B. A. & Zhou, W.-J. Polymerized Lyotropic Liquid Crystal Assemblies for Materials Applications. *Acc. Chem. Res.* **34**, 973–980 (2001).

11. Yun, C.-J. & Song, J.-K. Functional films using reactive mesogens for display applications. *J. Inf. Disp.* **18**, 119–129 (2017).

12. O'Neill, M. & Kelly, S. M. Ordered materials for organic electronics and photonics. *Adv. Mater.* **23**, 566–584 (2011).

13. Wang, G., Garvey, C. J., Zhao, H., Huang, K. & Kong, L. Toward the Fabrication of Advanced Nanofiltration Membranes by Controlling Morphologies and Mesochannel Orientations of Hexagonal Lyotropic Liquid Crystals. *Membranes (Basel).* **7**, 37 (2017).

14. Gin, D. L., Gray, D. H., Smith, R. C. & Uni-, W. M. R. Polymerizable Liquid Crystals as Building Blocks for Functional, Nanostructured Materials. *Synlett* 1509–1522 (1999).

15. Hentze, H.-P. & Antonietti, M. Template synthesis of porous organic polymers. *Curr. Opin. Solid State Mater. Sci.* **5**, 343–353 (2001).

16. Dutt, S. & Siril, P. F. A novel approach for the synthesis of polyaniline nanostructures using swollen liquid crystal templates. *Mater. Lett.* **124**, 50–53 (2014).

17. Dutt, S. & Siril, P. F. Controlling the morphology of polyaniline–platinum nanocomposites using swollen liquid crystal templates. *Synth. Met.* **209**, 82–90 (2015).

18. Huang, L. *et al.* Polyaniline nanowires by electropolymerization from liquid crystalline phases. *J. Mater. Chem.* **12**, 388–391 (2002).

19. Li, C. *et al.* Conductive polyaniline helixes self-assembled in the absence of chiral dopant. *Chem. Commun.* **49**, 1100–1102 (2013).

20. Liu, D. & Broer, D. J. Liquid crystal polymer networks: preparation, properties, and applications of films with patterned molecular alignment. *Langmuir* **30**, 13499–13509 (2014).

21. Clapper, J. D., Sievens-Figueroa, L. & Guymon, C. A. Photopolymerization in polymer templating. *Chem. Mater.* **20**, 768–781 (2008).

22. Srisiri, W. *et al.* Stabilization of a Bicontinuous Cubic Phase from Polymerizable Monoacylglycerol and Diacylglycerol. *Langmuir* **14**, 1921–1926 (1998).

23. Srisiri, W. *et al.* Polymerization of the Inverted Hexagonal Phase. *J. Am. Chem. Soc.* **119**, 4866–4873 (1997).

24. Antonietti, M., Goltner, C. & Hentze, H.-P. Polymer Gels with a Micron-Sized, Layer-like Architecture by Polymerization in Lyotropic Cocogem Phases. *Langmuir* **14**, 2670–2676 (1998).

25. Broer, D. J., Bastiaansen, C. M. W., Debije, M. G. & Schenning, A. P. H. J. Functional organic materials based on polymerized liquid-crystal monomers: Supramolecular hydrogen-bonded systems. *Angew. Chem. Int. Ed.* **51**, 7102–7109 (2012).

26. Broer, D. J., Gossinks, R. G. & Hikmet, R. A. M. Oriented polymer networks obtained by photopolymerization of liquid-crystalline monomers. *Macromol. Mater. Eng.* **183**, 45–66 (1990).

27. Thiem, H., Strohriegl, P., Shkunov, M. & Mcculloch, I. Photopolymerization of Reactive Mesogens. *Macromol.* **206**, 2153–2159 (2005).

28. Park, J., Yu, T., Inagaki, T. & Akagi, K. Helical Network Polymers Exhibiting Circularly Polarized Luminescence with Thermal Stability. Synthesis via Photo-Cross-Link

Polymerizations of Methacrylate Derivatives in a Chiral Nematic Liquid Crystal. *Macromolecules* **48**, 1930–1940 (2015).

29. Schenning, A. P. H. J., Gonzalez-Lemus, Y. C., Shishmanova, I. K. & Broer, D. J. Nanoporous membranes based on liquid crystalline polymers. *Liq. Cryst.* **38**, 1627–1639 (2011).

30. Pan, L. *et al.* Hierarchical nanostructured conducting polymer hydrogel with high electrochemical activity. *Proc. Natl. Acad. Sci.* **109**, 9287–9292 (2012).

31. Wang, Z. *et al.* Extremely stretchable and electrically conductive hydrogels with dually synergistic networks for wearable strain sensors. *J. Mater. Chem. C* **6**, 9200–9207 (2018).

32. Wang, T. *et al.* A Self-Healable, Highly Stretchable, and Solution Processable Conductive Polymer Composite for Ultrasensitive Strain and Pressure Sensing. *Adv. Funct. Mater.* **28**, 170551 (2018).

33. Lu, Y. *et al.* Ultrastretchable Conductive Polymer Complex as a Strain Sensor with a Repeatable Autonomous Self-Healing Ability. *ACS Appl. Mater. Interfaces* **11**, 20453–20464 (2019).

34. Huang, J. I. E. & Wan, M. Polyaniline Doped with Different Sulfonic Acids by in Situ Doping Polymerization. *J. Polym. Sci. Part A Polym. Chem.* **37**, 1277–1284 (1999).

35. Alotaibi, M. M. Towards Aqueous Nanostructures Based on Oligo(aniline)s. (University of Bristol, 2019).

36. Byrne, A. Towards Organisational Control of Electroactive Amphiphiles. (2018).

37. Ray, A., Richter, A. F., MacDiarmid, A. G. & Epstein, A. J. Polyaniline: protonation/deprotonation of amine and imine sites. *Synth. Met.* **29**, 151–156 (1989).

38. Martin, R. E. & Diederich, F. Linear Monodisperse pi-Conjugated Oligomers: Model Compounds for Polymers and More. *Angew. Chem. Int. Ed.* **38**, 1350–1377 (1999).

39. Meier, H., Gerold, J., Kolshorn, H. & Bastian, M. Extension of Conjugation Leading to Bathochromic or Hypsochromic Effects in OPV Series. *Chem. Eur. J.* **10**, 360–370 (2004).

40. Bell, O. A. *et al.* Self-Assembly of a Functional Oligo(Aniline)-Based Amphiphile into Helical Conductive Nanowires. *J. Am. Chem. Soc.* **137**, 14288–14294 (2015).

41. Lydon, J. Chromonic review. *J. Mater. Chem.* **20**, 10071–10099 (2010).

42. Watson, M. L. Staining of Tissue Sections for Electron Microscopy with Heavy Metals. *J. Biophys. Biochem. Cytol.* **4**, 475–478 (1958).

43. Vargas, R., Mateu, L. & Romero, A. The effect of increasing concentrations of precipitating salts used to crystallize proteins on the structure of the lipidic Q 224 cubic phase. *Chem. Phys. Lipids* **127**, 103–111 (2004).

44. Conn, C. E. *et al.* High-throughput analysis of the structural evolution of the monoolein cubic phase in situ under crystallogenesis conditions. *Soft Matter* **8**, 2310–2321 (2012).

45. Yaghmur, A., Rappolt, M., Østergaard, J., Larsen, C. & Larsen, S. W. Characterization of Bupivacaine-Loaded Formulations Based on Liquid Crystalline phases and Microemulsions : The Effect of Lipid Composition. *Langmuir* **28**, 2881–2889 (2012).

46. van 't Hag, L., Gras, S. L., Conn, C. E. & Drummond, C. J. Lyotropic liquid crystal engineering moving beyond binary compositional space – ordered nanostructured amphiphile self-assembly materials by design. *Chem. Soc. Rev.* **46**, 2705–2731 (2017).

47. Chen, R. & Benicewicz, B. C. Preparation and properties of poly(methacrylamide)s containing oligoaniline side chains. *Macromolecules* **36**, 6333–6339 (2003).

48. Hu, Y. *et al.* Toward Direct Laser Writing of Actively Tuneable 3D Photonic Crystals. *Adv. Opt. Mater.* **5**, 1600458 (2017).

49. Li, Y. *et al.* Two-dimensional polymers with versatile functionalities via gemini monomers. *Sci. Adv.* **5**, eaaw9120 (2019).

50. Manne, S. *et al.* Gemini Surfactants at Solid-Liquid Interfaces: Control of Interfacial Aggregate Geometry. *Langmuir* **13**, 6382–6387 (1997).

51. Duval, F. P., Zana, R. & Warr, G. G. Adsorbed Layer Structure of Cationic Gemini and Corresponding Monomeric Surfactants on Mica. *Langmuir* 1143–1149 (2006).

52. Bott, T. Gemini Surfactant to 3D Polymers. (2020).

53. Wang, J. *et al.* Large scale synthesis of single-chain/colloid Janus nanoparticles with tunable composition. *Chem. Commun.* **56**, 3875–3878 (2020).

54. Lee, C.-F., Chou, Y.-H. & Chiu, W.-Y. Synthesis and Morphology of Fe3O4/polystyrene/poly(isopropylacrylamide-co-methyl acrylate acid) Magnetic Composite Latex – 2,2'-Azobis (2-methylpropionamidine) Dihydrochloride as Initiator. *J. Polym. Sci. Part A Polym. Chem.* **45**, 3912–3921 (2007).

55. Lee, C.-F., Wen, C.-J. & Chiu, W.-Y. Synthesis of Poly (chitosan-N -isopropylacrylamide) Complex Particles with the Method of Soapless Dispersion. *J. Polym. Sci. Part A Polym. Chem.* **41**, 2053–2063 (2003).

56. Yoshida, Y., Itoh, N., Saito, Y., Hayakawa, M. & Niki, E. Application of Water-Soluble Radical Initiator, Dihydrochloride, to a Study of Oxidative Stress Application of Water-Soluble Radical Initiator, 2,2'-Azobis-[2-(2-imidazolin-2-yl)propane] Dihydrochloride, to a Study of Oxidative Stress. *Free Radic. Res.* **38**, 375–384 (2004).

57. Niki, E., Kawakami, A., Yamamoto, Y. & Kamiya, Y. Oxidation of lipids. VIII. Synergistic inhibition of oxidation of phosphatidylcholine liposome in aqueous dispersion by vitamin E and vitamin C. *Bull. Chem. Soc. Jpn.* **58**, 1971–1975 (1985).

6 CONCLUSIONS AND FUTURE OUTLOOK

6.1 CONCLUSIONS

The aims of this project were twofold. The first was to understand how an amphiphile's packing parameter (*pp*) can direct the self-assembly of lipidic mesophases, by the incorporation of tetra(aniline) (**TANI**)-derived amphiphiles into monoolein (**MO**) cubic phases. The second aim was to use this understanding to prepare well-defined, stimuli-responsive nanostructures from those **TANI**-amphiphiles and their polymerizable analogues, using **MO** as a structure-directing template.

The work began with the synthesis of single-tailed and bola-form **TANI**-amphiphiles. The single-tailed amphiphiles, **TANI-PTAB**, **TANI-C_{12}TAB** and **TANI-PTPB**, were synthesised from the same precursor, **Ph/NH_2 TANI**. **Ph/NH_2 TANI** was functionalised with an alkyl spacer of the desired length (C6 or C12), before oxidation and quaternisation with trimethylamine for **TANI-PTAB** and **TANI-C_{12}TAB**, or quaternisation with trimethylphosphine prior to oxidation for **TANI-PTPB**. **TANI-(PTAB)$_2$** was prepared by functionalisation of **NH_2/NH_2 TANI** with two alkyl spacers, followed by oxidation to the EB state and quaternisation with trimethylamine. Following the synthesis of **TANI-PTAB**, work on an analogous polymerizable amphiphile was untaken, with limited success. Numerous methods of synthesising polymerizable **TANI**-amphiphiles were attempted, which were hindered by the formation of unwanted side products that, along with the starting reagents, could not be separated by common purification techniques.

Despite setbacks to the synthesis of a polymerizable **TANI-**amphiphile, investigations began into the role of an amphiphile's *pp* in determining the structure formation of **MO** cubic phases. The first amphiphile explored was **TANI-PTAB**, consisting of a C6 alkyl spacer separating a **TANI** core and a trimethylammonium head group. Low concentrations of EB **TANI-PTAB** led to the formation of the *Pn3m* phase. However, increasing the amphiphile concentration induced a transition to the *Im3m* phase. The change in cubic phase was attributed to the flattening effect of **TANI-PTAB**, owing to the combination of the amphiphile's *pp* ($pp < 1$) with that of **MO** ($pp > 1$).

The transition to less negatively curved phases could be prevented by the addition of doping acids, resulting in the formation of the *Pn3m* phase at all ES **TANI-PTAB** concentrations. The mechanism by which ES **TANI-PTAB** influenced the membrane curvature of **MO** was less easily explained than EB **TANI-PTAB.** Using the *pp* concept, it was expected that the addition of dopants would increase the volume of the **TANI** core, thus increasing the amphiphile's *pp*. The increased *pp* would have less of a flattening effect than the EB state, resulting in the preferential formation of the *Pn3m* phase. However, the **TANI-PTAB** molecules were expected to be sequestered in the hydrophobic domain of the lipid bilayer, away from the hydrophilic acids in the aqueous channels. Therefore, an alternative theory was

put forward, where the **TANI-PTAB** molecules partitioned into the water channels to become doped and the change in mesophase was due to the removal of the amphiphiles from the membrane.

Following experiments with **TANI-PTAB**, three other **TANI-**amphiphiles (**TANI-C_{12}TAB**, **TANI-PTPB** and **TANI-$(PTAB)_2$**) were explored in relation to their effect on **MO**. The amphiphiles were chosen owing to their similar but different chemical structures. **TANI-C_{12}TAB** was prepared with a longer (C12) alkyl chain. The increased tail length was predicted to decrease the amphiphile's *pp*, resulting in the formation of the *Im3m* phase at lower concentrations than **TANI-PTAB**, as was observed. Meanwhile, changing the cationic head group from a trimethylammonium bromide to a trimethylphosphonium bromide appeared to have limited effect on the cubic phase formation. Both **TANI-PTPB** and **TANI-PTAB** produced the *Im3m* phase at similar concentrations, suggesting that the slight increase in head group size was not sufficient to alter the mesophase behaviour. As with **TANI-PTAB**, doping both **TANI-C_{12}TAB** and **TANI-PTPB** to the ES state resulted in transitions back to the *Pn3m* phase.

Finally, it was shown that the introduction of EB **TANI-$(PTAB)_2$** to **MO** resulted in the formation of the *Pn3m* phase, regardless of concentration. While the *pp* of EB **TANI-$(PTAB)_2$** could not be easily calculated and used to interpret its effect on mesophase formation, this behaviour was predicted from observations the amphiphile in water. Like ES **TANI-PTAB**, EB **TANI-$(PTAB)_2$** formed spherical structures in water and therefore a similar effect on the membrane curvature was expected for both amphiphiles. Doping **TANI-$(PTAB)_2$** with naphthalenedisulfonic acid (**NDS**) again led to the *Pn3m* phase, although a negative trend in lattice parameters was noted, indicating an eventual transition to the more negatively curved hexagonal phase.

After investigations into the role of *pp* in influencing the formation of different cubic phases, attention was turned to methods of templating amphiphiles for the preparation of highly ordered polymers. In the first method, cross-linking acids were used to non-covalently bond **TANI-PTAB** assemblies in water, using electrostatic interactions to fix aggregate formations. **NDS** and phytic acid were used to dope **TANI-PTAB** assemblies, resulting in the formation of fibrous and ribbon-like structures, respectively. The same acids were used to cross-link **TANI-PTAB** molecules within **MO** cubic phases. No appreciable difference was noted in cubic phases prepared with **NDS**, although phases doped with phytic acid showed clear phase separation of the doped amphiphile. However, the exact structures formed from **TANI-PTAB** doped with phytic acid could not be distinguished as the template could not be removed, owing to the sample being prepared in a sealed capillary tube. A similar problem occurred with the second templating method, which was the photopolymerisation of a gemini monomer within a **MO** mesophase. The monomer, **MA-11-2-11-MA**, induced a transition to the *Im3m* phase and was photopolymerised by exposure to UV-light for 2 hours. No noticeable change in mesophase structure was observed after polymerisation and the template could not be removed to determine the extent of

polymerisation, limiting any conclusions that could be drawn as to the successful transfer of template structure to polymer.

In summary, this thesis aimed to provide a deeper understanding into the role of molecular packing parameter in determining the influence of an electroactive amphiphile on lipidic mesophases. It was demonstrated that mesophase behaviour could be controlled by careful design of the amphiphile structure or by application of an acid, the latter providing a way to reversibly transition between cubic phases. The opportunity to manipulate such mesophase mixtures enables their usage in drug delivery systems or as size-selective molecular sieves, where control over dimensions is crucial for function. Furthermore, excellent strides were taken towards the development of templated polymers, which while not fully realised in this work, could be achieved with further experimentation and will be valuable for the design of responsive, nanoporous polymer films.

6.2 FUTURE OUTLOOK

6.2.1 Understanding and directing MO cubic phase formation with TANI-amphiphiles

While the effect of **TANI**-amphiphiles on **MO** cubic phase formation could be predicted to an extent from the amphiphile structure and oxidation state, the exact mechanism by which they influenced the membrane curvature was unknown. Single-tailed EB **TANI-**amphiphiles induced the formation of the *Im3m* phase, which was explained by their insertion into the lipid bilayer and subsequent flattening of the membrane, owing to their lower *pp*s. Meanwhile, the addition of dopants resulted in a transition to the *Pn3m* phase. This transition was originally attributed to the increase in the amphiphiles' *pp*s upon doping. However, as acids were unlikely to penetrate the hydrophobic bilayer, it was proposed that the **TANI-**amphiphiles partitioned into the water channels of the cubic phase when doped and that was the removal of the amphiphiles from the bilayer that triggered the re-formation of the *Pn3m* phase.

For many applications, such as catalysis, molecular separation, and templating, it important that the water channels within cubic phases are clear, enabling unimpeded diffusion of materials throughout the mesophase. While it is expected that EB **TANI-**amphiphiles are located within the lipid bilayer, amphiphiles in the ES state may partition into the water channels, hindering diffusion and potentially interfering with processes that occur in the aqueous domains. Therefore, an understanding of the location of EB and ES **TANI-**amphiphiles in lipidic mesophases is key when using them as stimuli-responsive molecules for material applications.

Various methods could be applied to understand the behaviour of EB and ES **TANI**-amphiphiles in lipidic cubic phases. One possible avenue is to utilize computer simulations to model the behaviour of such systems. Molecular dynamics modelling has been used to simulate the cubic phase formation of **MO** and water.[1] While the developments of a stable, model cubic phase was not facile, the authors demonstrated that the packing of **MO** molecules within the bilayer structure could eventually be

determined. Meanwhile, the preferred location of proteins in lipidic cubic phases have been explored by computer simulations, which suggest that they tend to aggregate at flat points within a *Pn3m* phase.[2] Similar calculations could be applied to determine the preferred location of **TANI-PTAB** molecules within **MO** cubic phases. Computer modelling approaches were briefly explored for this project, however, the size and relative complexity of **TANI-PTAB** would make it a highly computationally expensive calculation, which would require extensive time to develop a working model and it was therefore not pursued further.

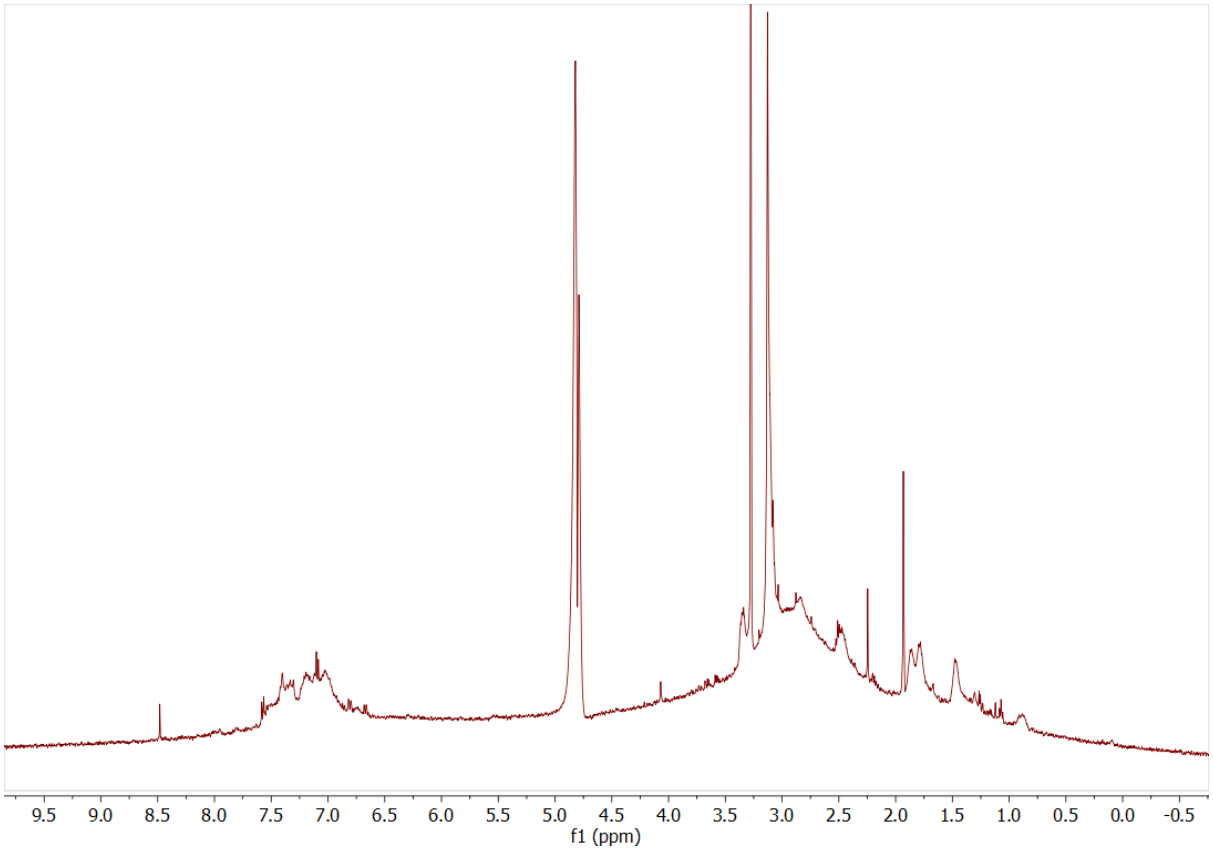

*Figure 6.1. ^{1}H NMR spectrum of EB **TANI-PTAB** in D_2O.*

Additionally, NMR spectroscopy techniques could be utilized to follow the partitioning of **TANI-**amphiphiles between the lipid bilayer and the water channels. Evenbratt and colleagues (2013) used ^{1}H NMR spectroscopy to determine the partitioning of 1,5-pentanediol in the cubic phase of glyceryl monooleyl ether (**GME**).[3] The authors used differences in the chemical shifts of 1,5-pentanediol to determine the distribution of the molecule in the aqueous and lipid domains, from which the partition coefficient could be simply calculated. Again, during this project diffusion NMR spectroscopy experiments were explored to determine the partitioning of **TANI-PTAB** molecules into the lipid bilayer. However, a drawback of this approach is that a ^{1}H NMR spectrum of **TANI-PTAB** in D_2O is required as a benchmark to determine the chemical shift change upon introduction to lipid mesophases.

The aggregation of **TANI-PTAB** molecules at even low concentrations resulted in severe signal broadening, meaning that an adequate baseline could not be obtained (Figure 6.1).

Finally, the behaviour of **TANI-**amphiphiles in **MO** could be visualised by contrast-matched small-angle neutron scattering (SANS), which could be used to verify the results of computational studies. This technique has been successfully utilized to determine the location of biomolecules within lipidic cubic phases.[4,5] Deuterated lipids are perfectly contrasted-matched with D_2O, so that the only recorded scattering arises from the embedded proteins and peptides. The intensity ratio of the first two Bragg peaks can then provide information on the preferred locations of the biomolecules. The synthesis of a fully deuterated **MO** has been described by van't Hag and colleagues (2019)[5] and could be replicated for experiments with **TANI-**amphiphiles. By contrast-matching the lipid and solvent, the remaining scattering would provide information into the preferential location of EB and ES **TANI-**amphiphiles and whether the amphiphile is homogeneously distributed in the membrane or is aggregating within the bilayer.

With a better understanding of how **TANI-**amphiphiles effect the mesophase formation of **MO**, attention can be turned to the fine control over its structure and dimensions by adaptation of the **TANI-**amphiphile's chemical structure. The functionalisation of **TANI** with alkyl spacers and cationic head groups following procedures outlined in this work is relatively simple and could be adapted to produce amphiphiles with different *pp*s. In addition to single-tailed and bola-form amphiphiles already demonstrated in this work, a gemini analogue of **TANI-PTAB** could be prepared by reaction of **TANI-C_6Br** with tetramethylethylenediamine, following similar procedures as outlined in Chapter 2, Section 2.2.8.2. Gemini surfactants have lower critical micelle concentrations than their single-tailed counterparts,[6] forming micelles whose size and shape is dependent on the alkyl spacer connecting the head groups.[7] The length of the spacer can be easily increased, allowing the *pp* of the gemini amphiphile to be readily tuned for different applications.

6.2.2 Templated assembly of ordered electroactive polymers

The preparation of highly ordered, responsive polymers was only briefly touched upon towards the end of this project but provides plenty of opportunities for further work. The synthesis of a polymerizable **TANI-**amphiphile ultimately proved to be highly difficult, however non-covalent methods of cross-linking **TANI-PTAB** in water and within a lipid template appeared to be more successful. The phase separation observed with cubic phases containing phytic acid-doped **TANI-PTAB** is particularly intriguing, as it may indicate the formation of a polymer, whose structure may be directed by the surrounding lipid template.

To explore the templated polymer structures further, a method of removing the lipid must be developed, in which case it may be advantageous to use a flow cell. A cubic phase containing **TANI-PTAB** doped with phytic acid can be prepared within a flow cell and analysed by small-angle X-ray scattering

(SAXS). Subsequently, ethanol can be used to wash away the lipid template, leaving the templated polymer in the cell and enabling the remaining structure to be identified by SAXS. An added benefit of flow cells is that they could enable the monitoring of phase changes with oxidation state, by feeding through aqueous acids and bases, which is not currently available with the current closed capillary set-up.

It is worth considering that the electrostatic interactions between acid and **TANI-**amphiphile may not be strong enough to withstand washing with ethanol, resulting in de-doping and the break-up of the polymer structure. Phytic acid-doped poly(aniline) (**PANI**) and **TANI** assemblies are generally stable in water, however, their integrity in the presence of organic solvents is less certain.[8,9] It may be advisable to use a polymeric dopant to maintain the polymer structure during processing. For example, poly(acrylic) acid has been used as a dopant for **PANI**, increasing the mechanical stability of the prepared polymer films and showing greater retention of the ES state over monomeric acids.[10,11] Templated self-assembly of **TANI-**amphiphile nanofibers could be achieved using a polymerizable dopant, in place of a polymerizable **TANI-**amphiphile. **MO** cubic phases containing EB **TANI-PTAB** could be prepared and be doped with a monomeric acid and a suitable initiator. After doping, photopolymerisation of the acid could be achieved by initiation with UV-light, forming a polymeric dopant, which should trap the **TANI-**amphiphile assemblies through electrostatic interactions.

6.3 REFERENCES

1. Marrink, S. J. & Tieleman, D. P. Molecular dynamics simulation of a lipid diamond cubic phase. *J. Am. Chem. Soc.* **123**, 12383–12391 (2001).

2. Grabe, M., Neu, J., Oster, G. & Nollert, P. Protein Interactions and Membrane Geometry. *Biophys. J.* **84**, 854–868 (2003).

3. Evenbratt, H., Nordstierna, L., Ericson, M. B. & Engström, S. Cubic and sponge phases in ether lipid-solvent-water ternary systems: Phase behavior and NMR characterization. *Langmuir* **29**, 13058–13065 (2013).

4. van'T Hag, L. *et al.* Using SANS with Contrast-Matched Lipid Bicontinuous Cubic Phases to Determine the Location of Encapsulated Peptides, Proteins, and Other Biomolecules. *J. Phys. Chem. Lett.* **7**, 2862–2866 (2016).

5. van't Hag, L. *et al.* Protein-Eye View of the in Meso Crystallization Mechanism. *Langmuir* **35**, 8344–8356 (2019).

6. Zana, R. Dimeric and oligomeric surfactants. Behavior at interfaces and in aqueous solution: a review. *Adv. Colloid Interface Sci.* **97**, 205–253 (2002).

7. Manne, S. *et al.* Gemini Surfactants at Solid-Liquid Interfaces: Control of Interfacial Aggregate Geometry. *Langmuir* **13**, 6382–6387 (1997).

8. Pan, L. *et al.* Hierarchical nanostructured conducting polymer hydrogel with high electrochemical activity. *Proc. Natl. Acad. Sci.* **109**, 9287–9292 (2012).

9. Wang, Z. *et al.* Extremely stretchable and electrically conductive hydrogels with dually synergistic networks for wearable strain sensors. *J. Mater. Chem. C* **6**, 9200–9207 (2018).

10. Wang, T. *et al.* A Self-Healable, Highly Stretchable, and Solution Processable Conductive Polymer Composite for Ultrasensitive Strain and Pressure Sensing. *Adv. Funct. Mater.* **28**, 170551 (2018).

11. Hu, H., Saniger, J. M. & Banuelos, J. G. Thin films of polyaniline-polyacrylic acid composite by chemical bath deposition. *Thin Solid Films* **347**, 241–247 (1999).

APPENDIX A

SYNTHESIS OF PH/NH_2 TANI

4-((diphenylmethylene)amino)-*N*-phenylaniline (1)

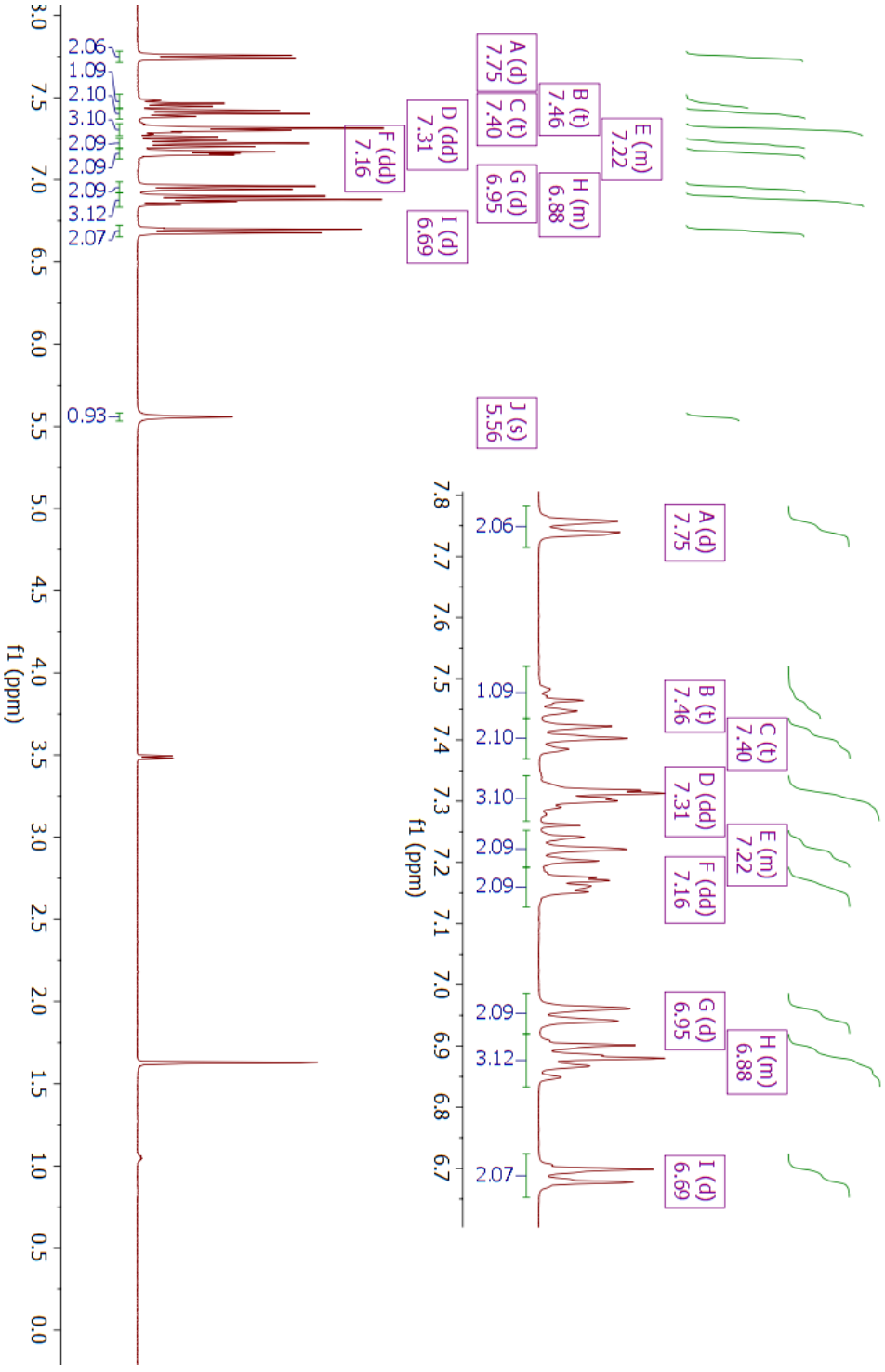

Figure A.1. ***4-((diphenylmethylene)amino)-N-phenylaniline (1) ^{1}H NMR spectrum in $CDCl_3$***

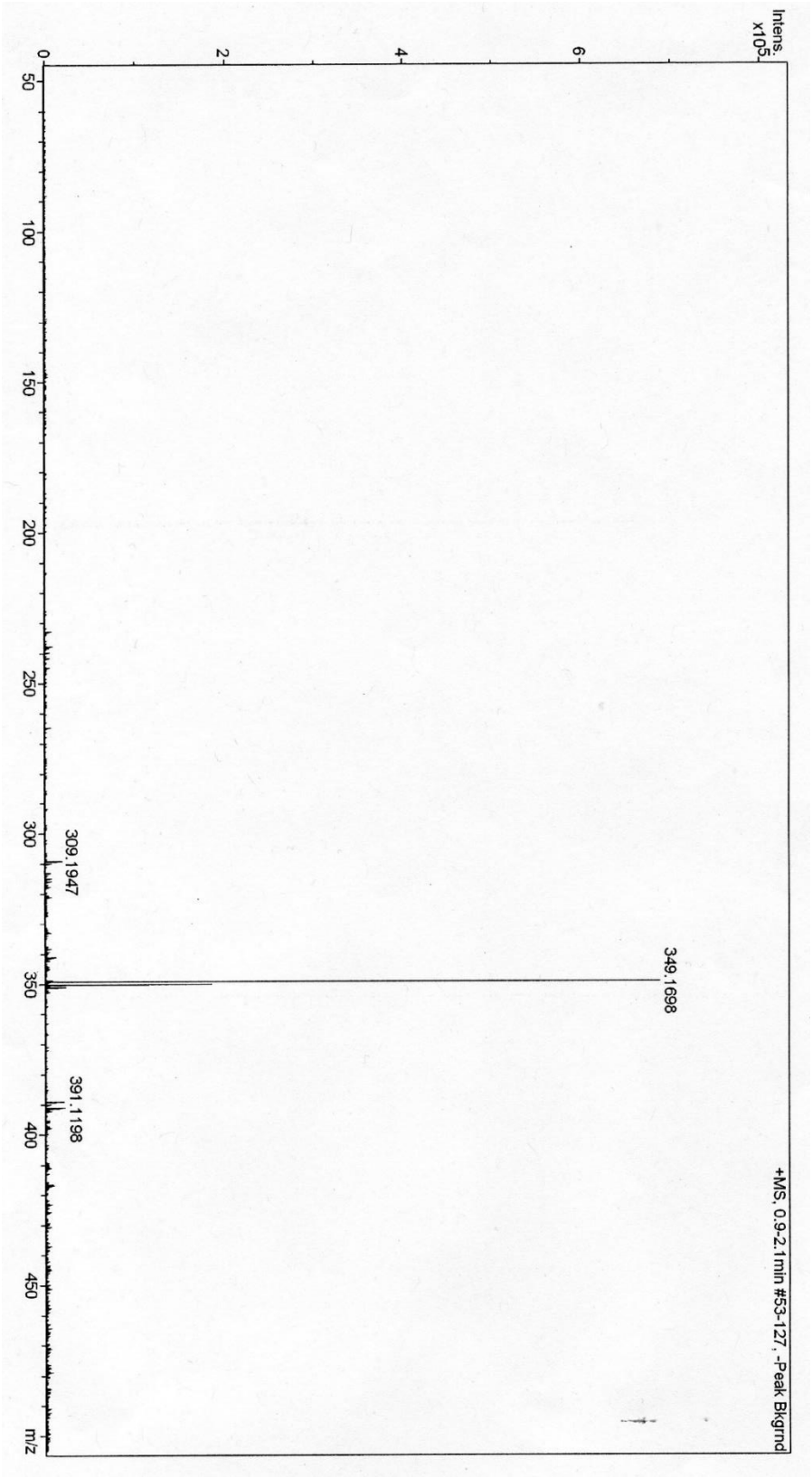

Figure A.2. ***4-((diphenylmethylene)amino)-N-phenylaniline (1) Mass spectrometry***

tert-butyl (4-((diphenylmethylene)amino)phenyl)(phenyl)carbamate (2)

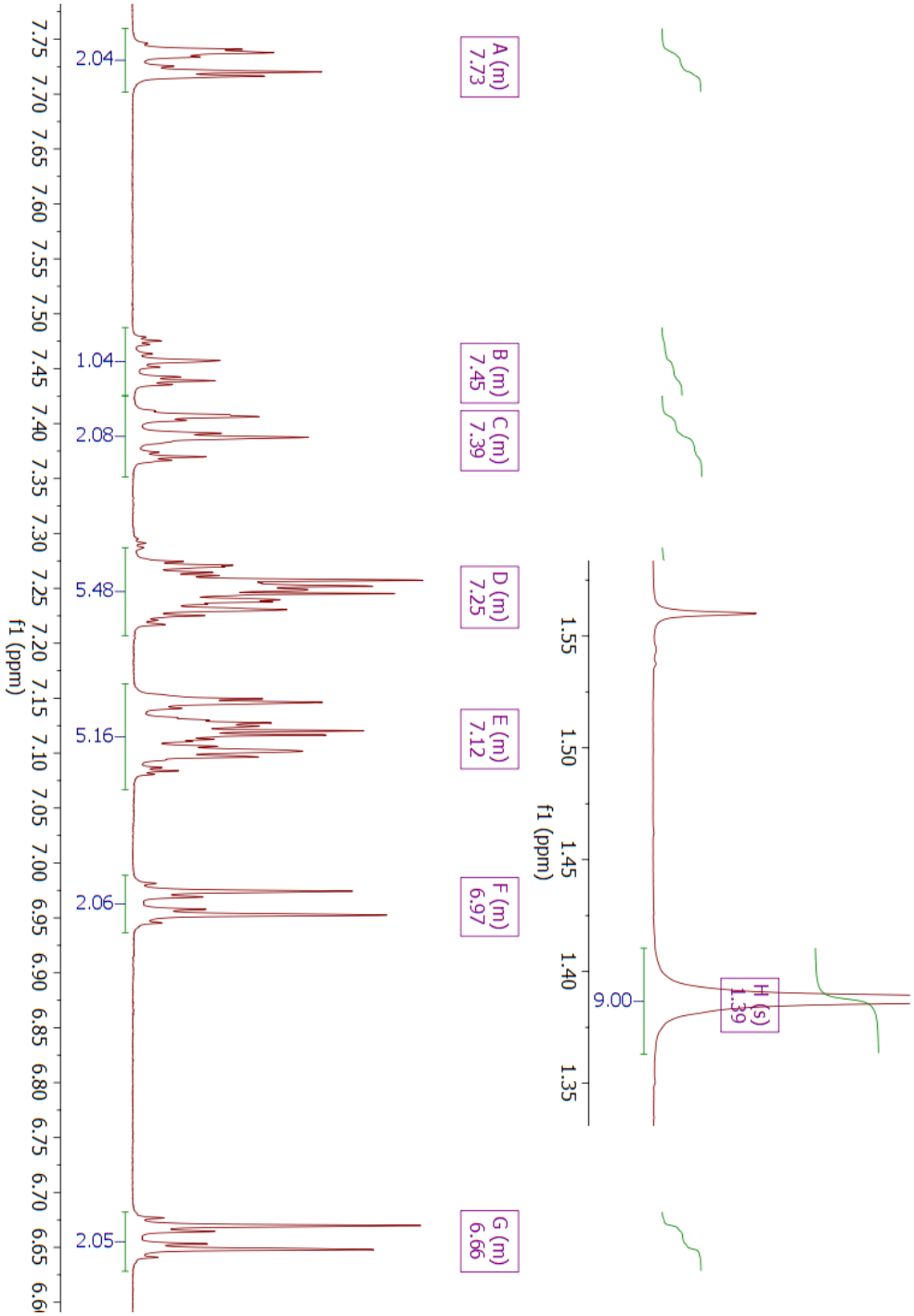

Figure A.3. ***tert-butyl (4-((diphenylmethylene)amino)phenyl)(phenyl)carbamate (2) ^{1}H NMR spectrum in $CDCl_3$***

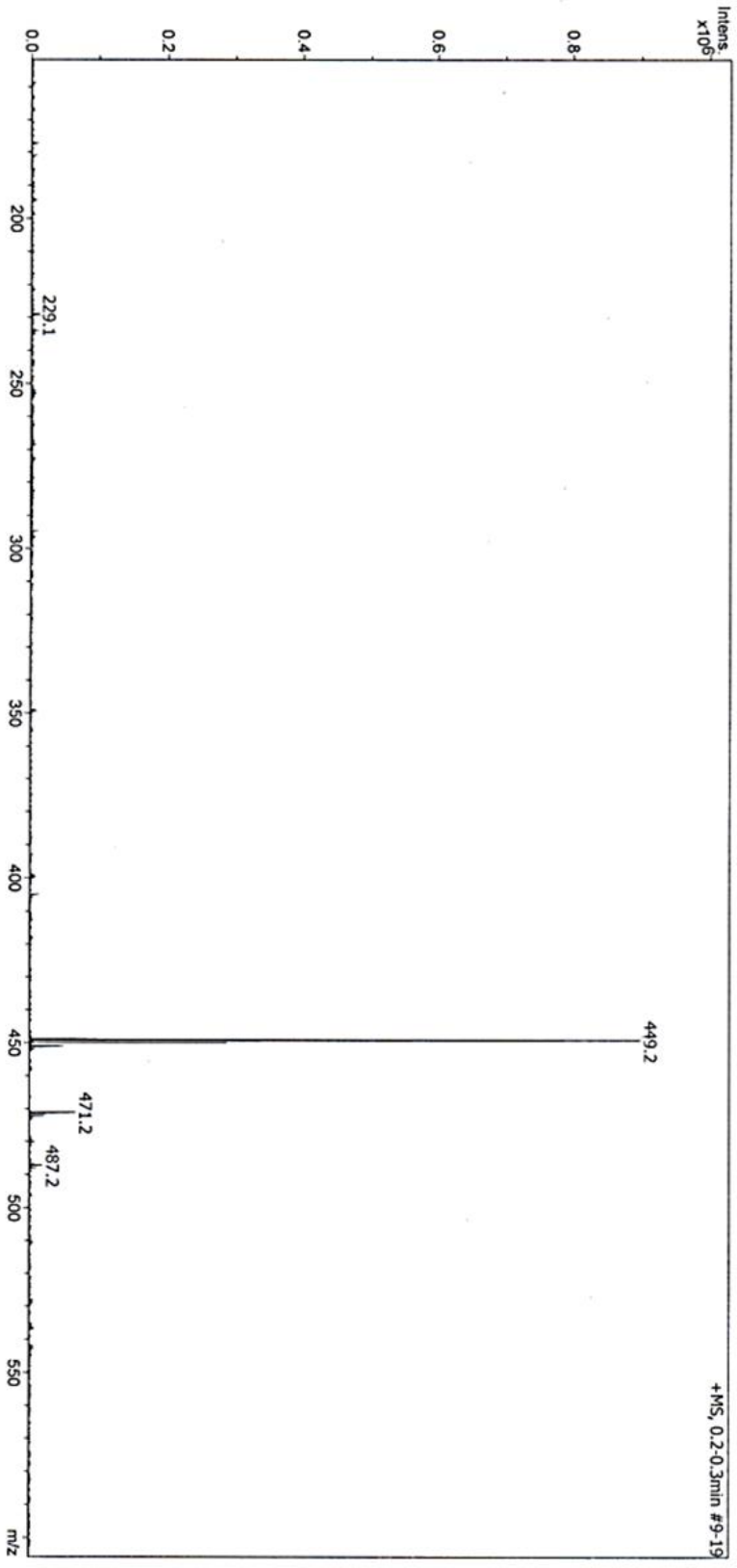

Figure A.4. ***tert-butyl (4-((diphenylmethylene)amino)phenyl)(phenyl)carbamate (2) Mass spectrometry***

tert-butyl (4-bromophenyl)(4-((diphenylmethylene)amino)phenyl)carbamate (3)

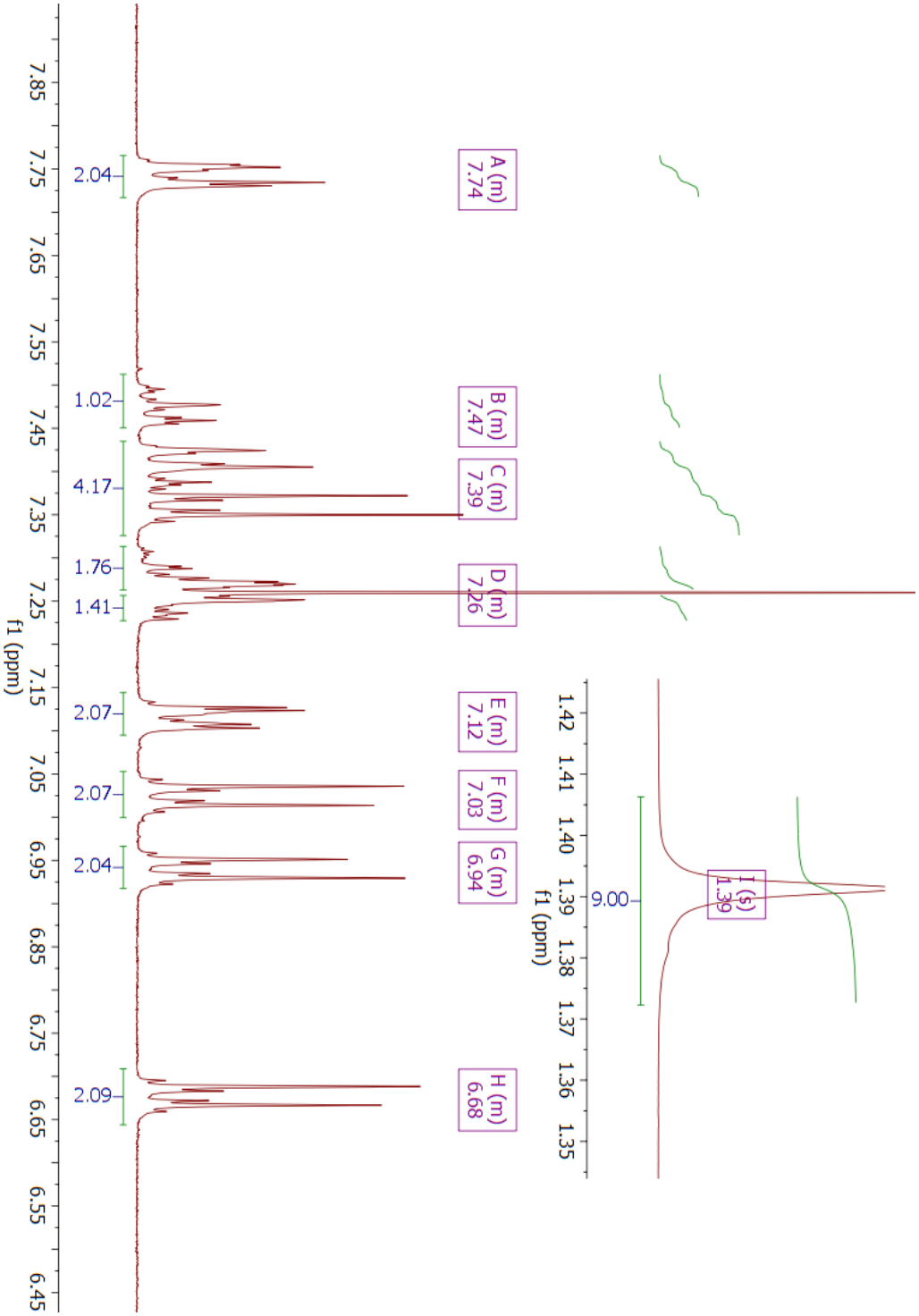

Figure A.5. ***tert-butyl (4-bromophenyl)(4-((diphenylmethylene)amino)phenyl)carbamate (3) ^{1}H NMR spectrum in $CDCl_3$***

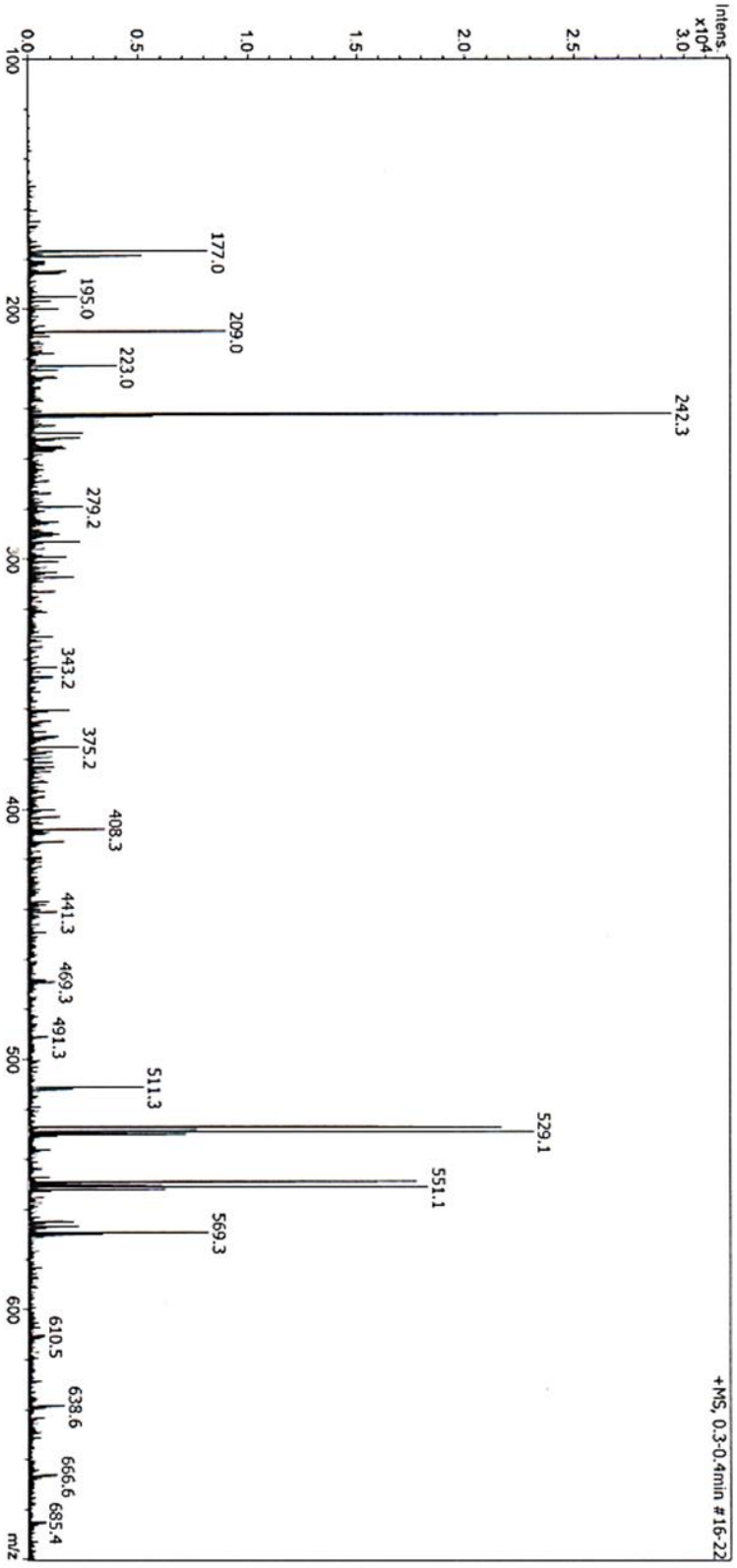

Figure A.6. ***tert-butyl (4-bromophenyl)(4-((diphenylmethylene)amino)phenyl)carbamate (3) Mass spectrometry***

tert-butyl (4-aminophenyl)(phenyl)carbamate (4)

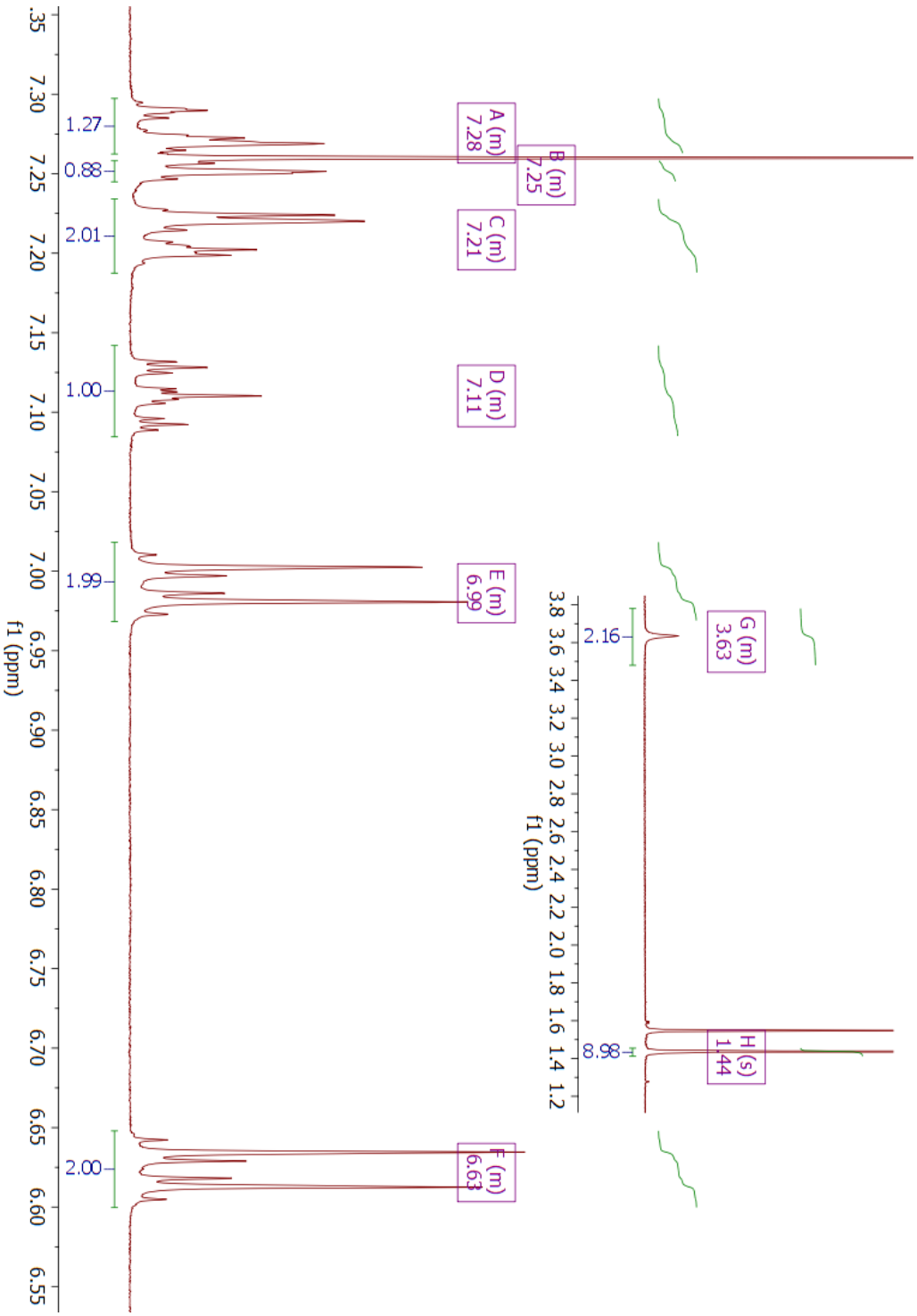

Figure A.7. ***tert-butyl (4-aminophenyl)(phenyl)carbamate (4) ^{1}H NMR spectrum in $CDCl_3$***

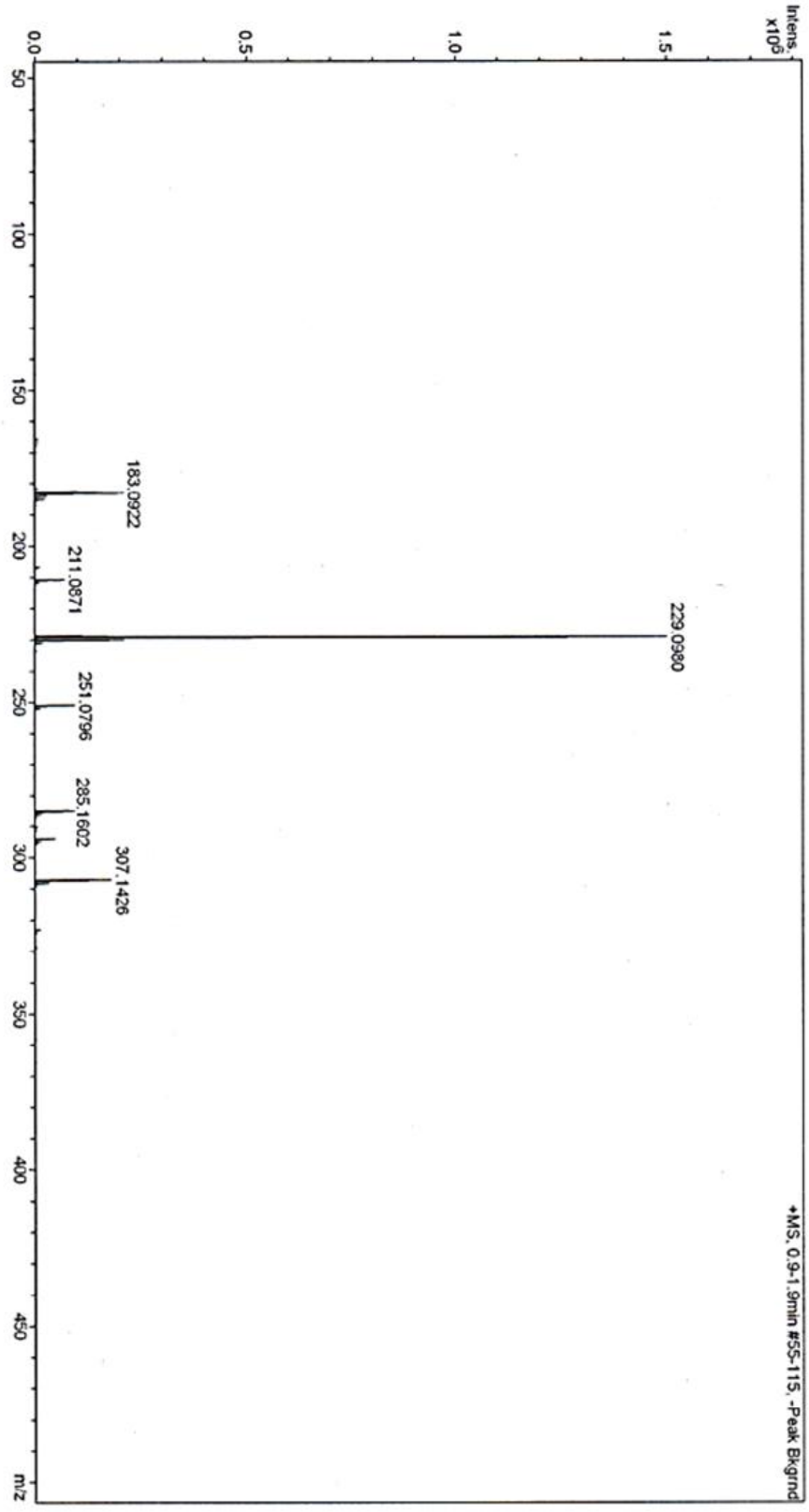

Figure A.8. ***tert-butyl (4-aminophenyl)(phenyl)carbamate (4) Mass spectrometry***

tert-butyl (4-((tert-butoxycarbonyl)(4-((tert-butoxycarbonyl)(4-((diphenylmethylene)amino)phenyl)amino)phenyl)amino)phenyl)(phenyl)carbamate (5)

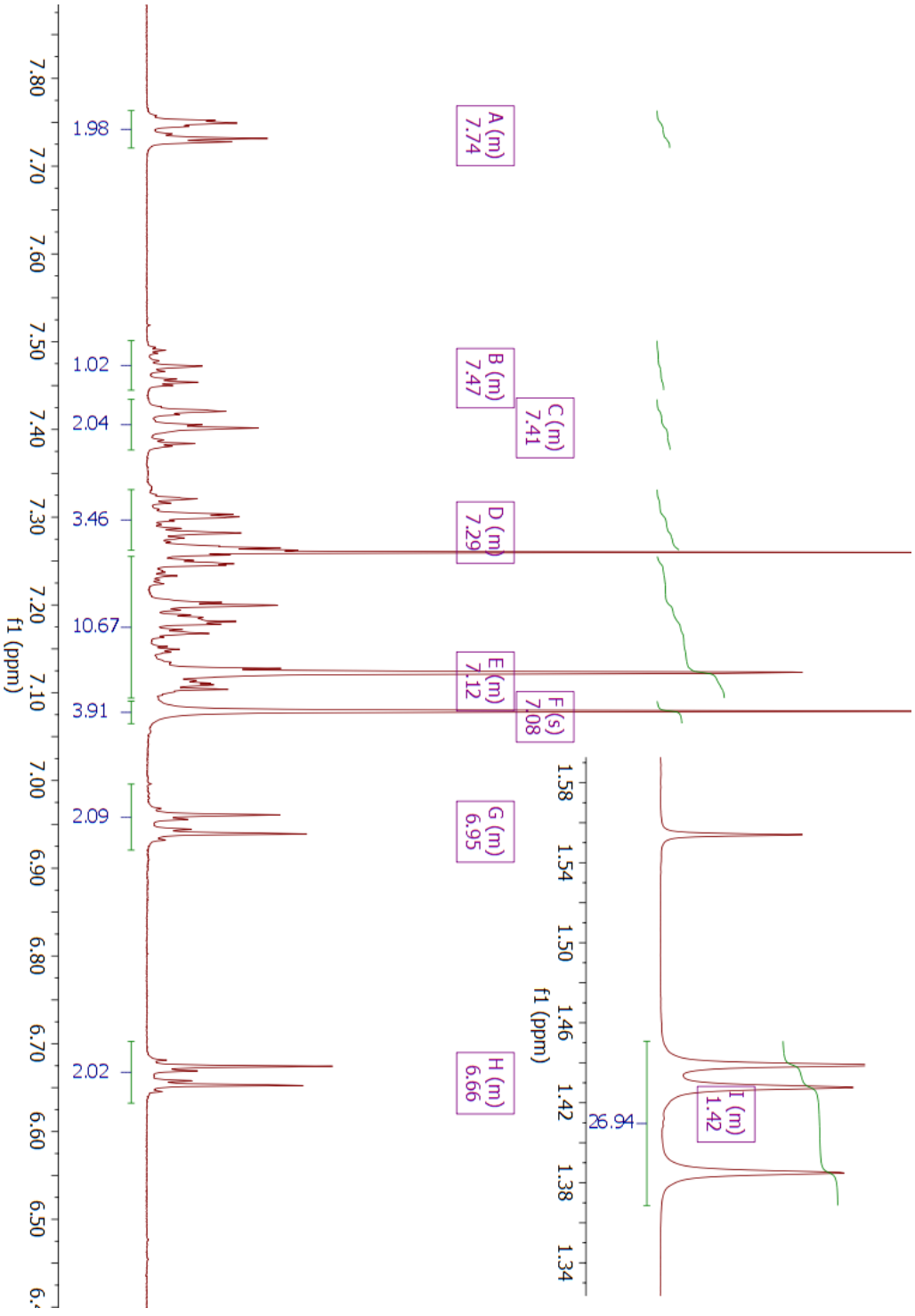

Figure A.9. ***tert-butyl (4-((tert-butoxycarbonyl)(4-((tert-butoxycarbonyl)(4-((diphenylmethylene)amino)phenyl)amino)phenyl)amino)phenyl)(phenyl)carbamate (5) ^{1}H NMR spectrum in $CDCl_3$***

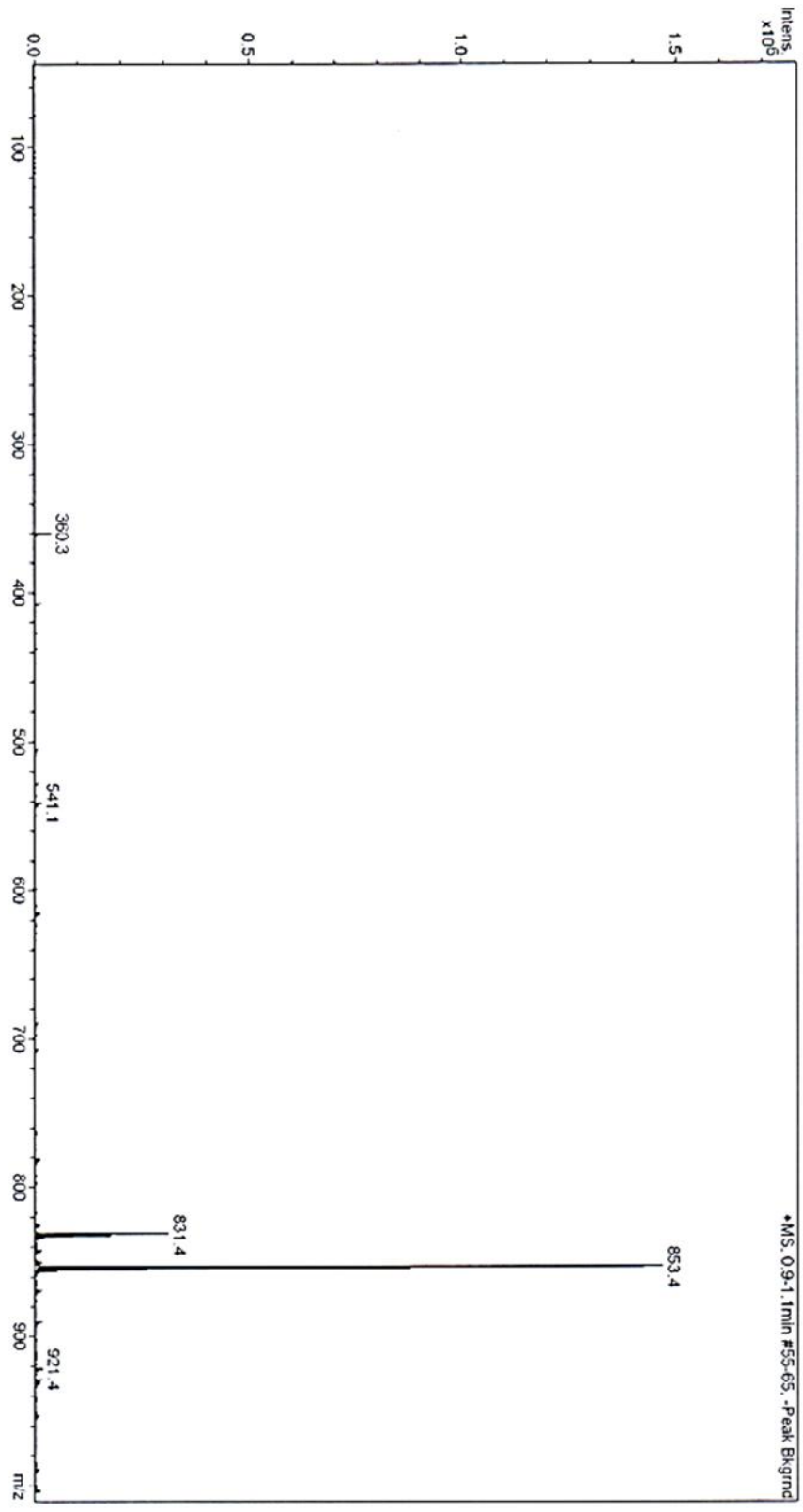

Figure A.10. ***tert-butyl (4-((tert-butoxycarbonyl)(4-((tert-butoxycarbonyl)(4-((diphenylmethylene)amino)phenyl)amino)phenyl)amino)phenyl)(phenyl)carbamate (5) Mass spectrometry***

Ph/NH_2 TANI (6)

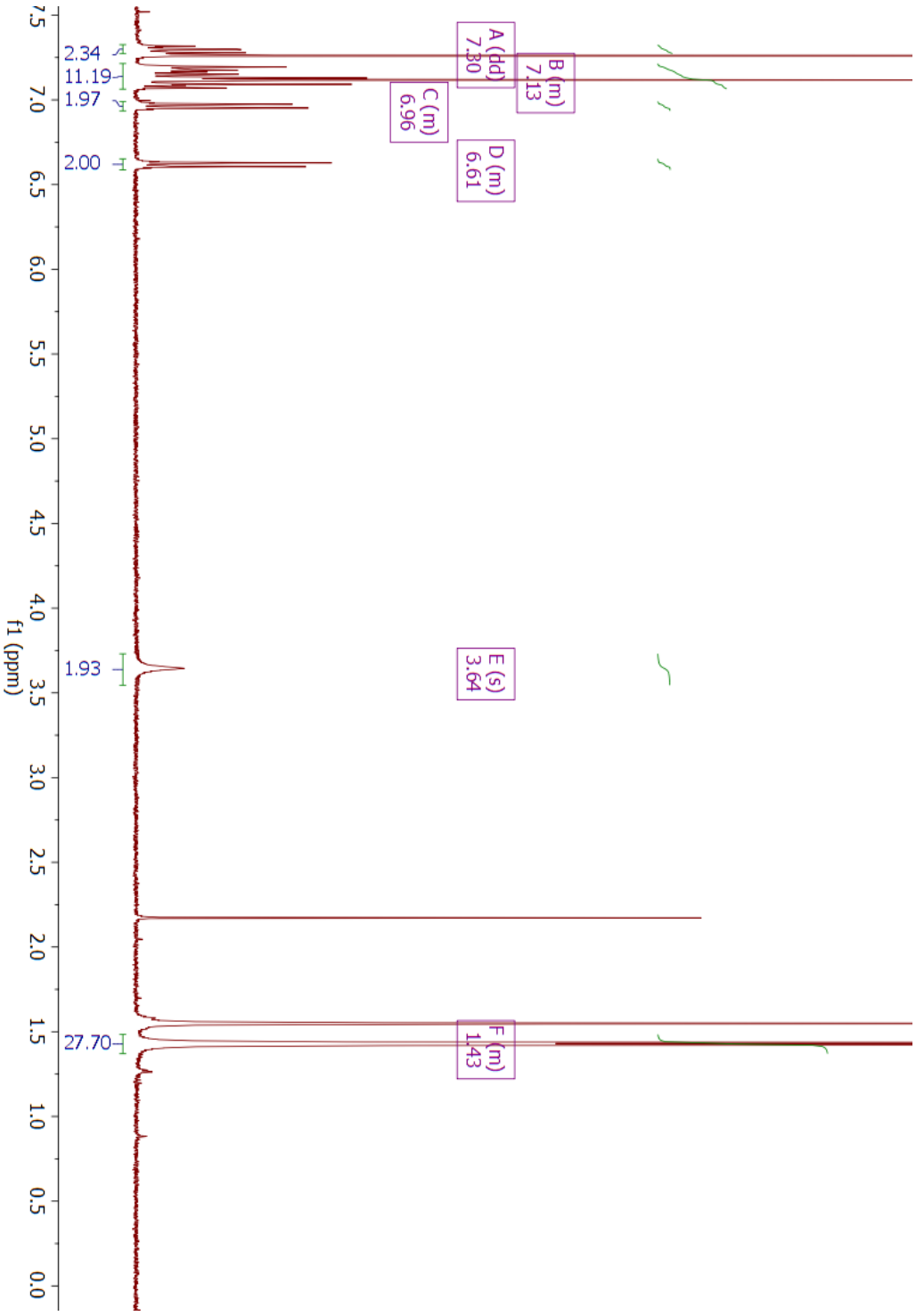

Figure A.11. ***Ph/NH_2 TANI (6) ^{1}H NMR spectrum in $CDCl_3$***

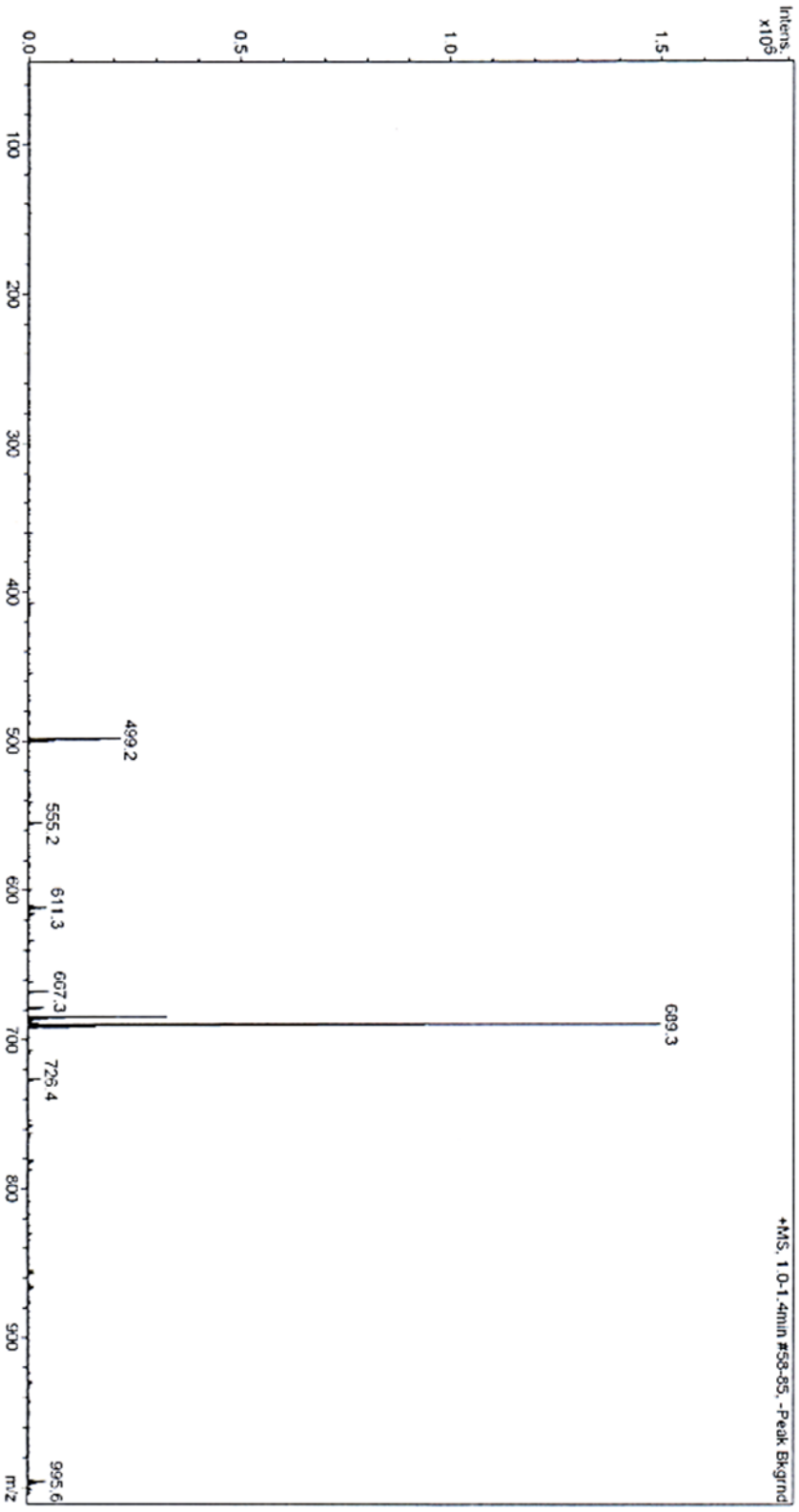

Figure A.12. ***Ph/NH₂ TANI (6) Mass spectrometry***

SYNTHESIS OF TANI-PTAB (EB)

tert-butyl (4-(6-bromohexanamido)phenyl)(4-((tert-butoxycarbonyl)(4-((tertbutoxycarbonyl)(phenyl)amino)phenyl)amino)phenyl)carbamate (7)

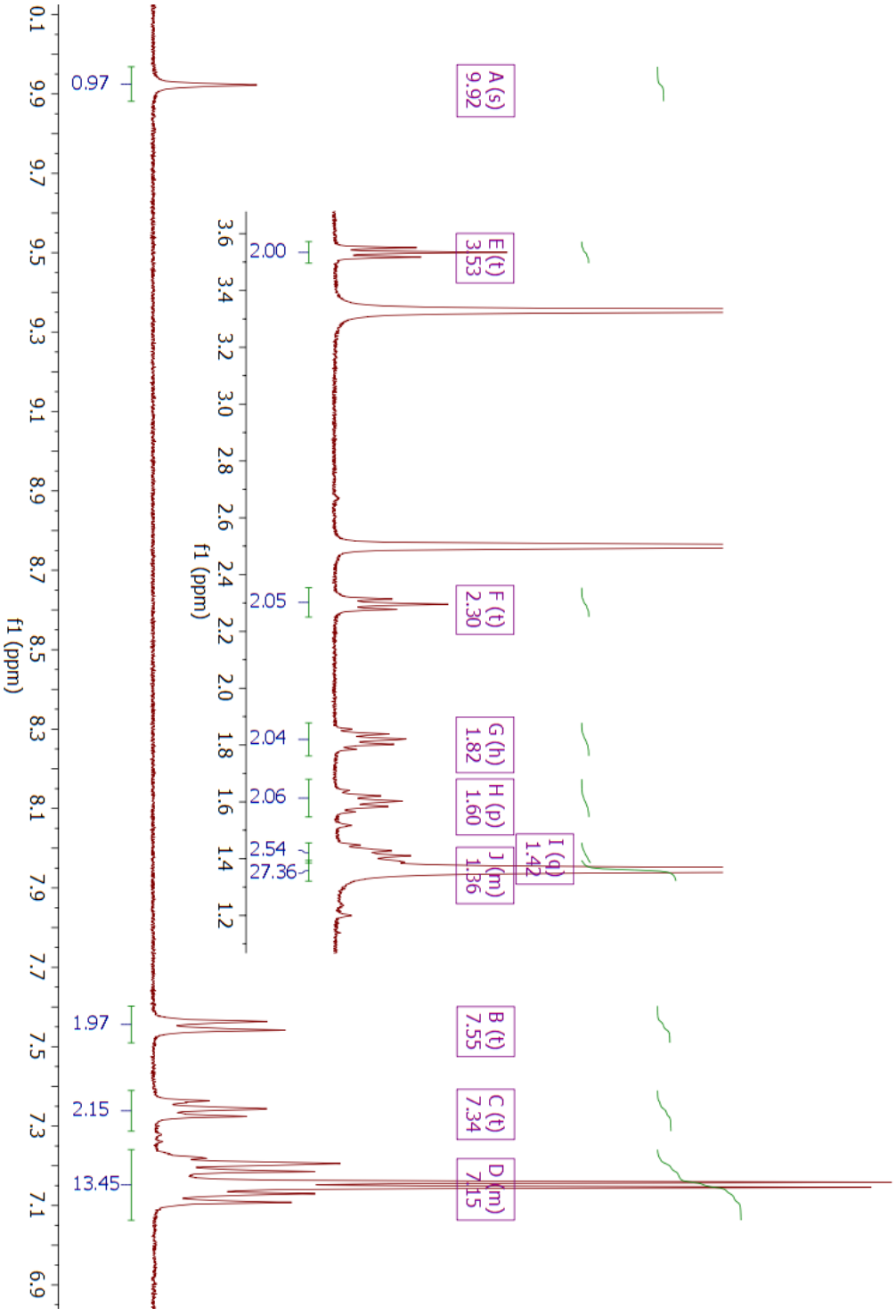

Figure A.13. ***tert-butyl (4-(6-bromohexanamido)phenyl)(4-((tert-butoxycarbonyl)(4-((tertbutoxycarbonyl)(phenyl)amino)phenyl)amino)phenyl)carbamate (7) ^{1}H NMR spectrum in DMSO-d_6***

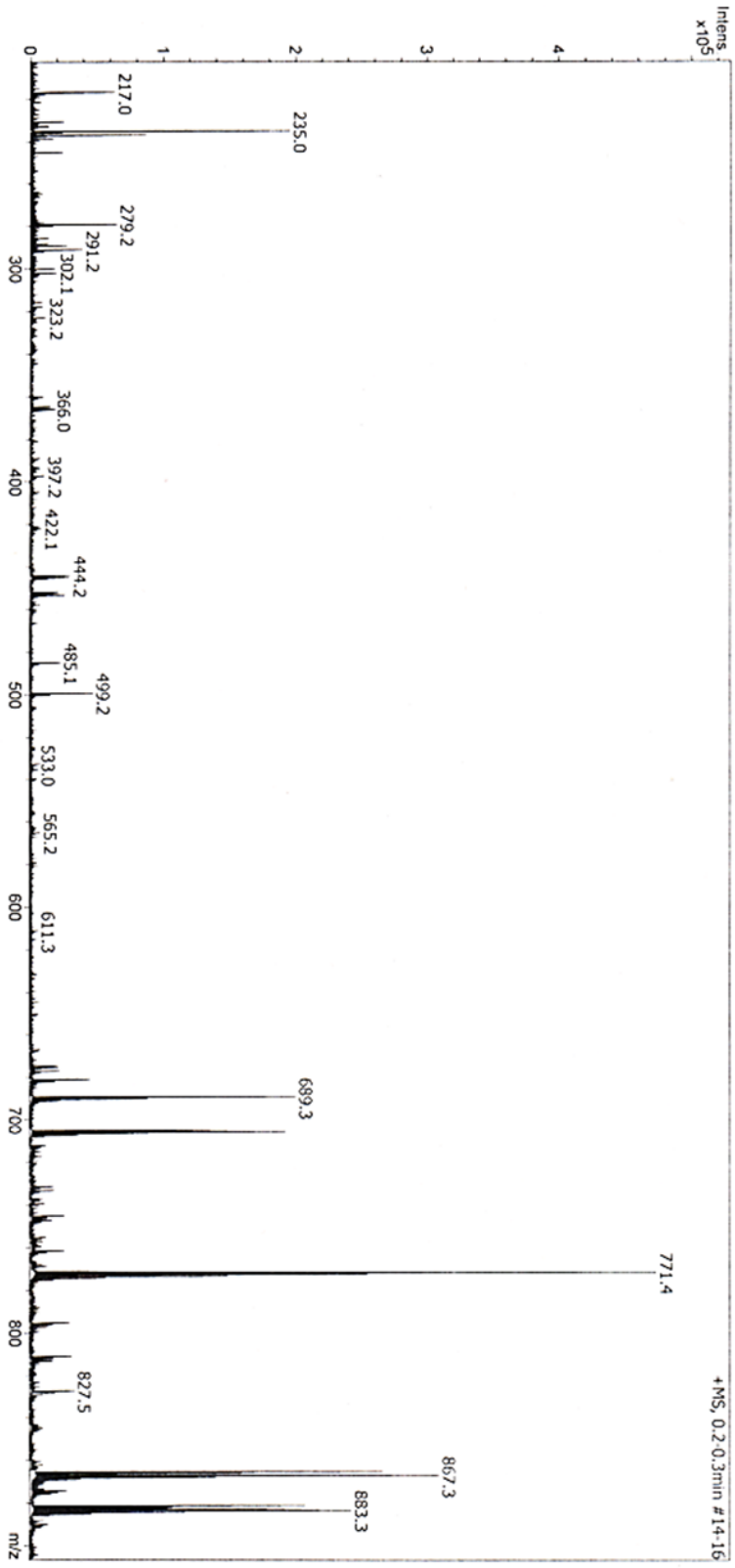

Figure A.14. ***tert-butyl (4-(6-bromohexanamido)phenyl)(4-((tert-butoxycarbonyl)(4-((tertbutoxycarbonyl)(phenyl)amino)phenyl)amino)phenyl)carbamate (7) Mass spectrometry***

6-bromo-N-(4-((4-((4-(phenylamino)phenyl)amino)phenyl)amino)phenyl)hexanamide (8)

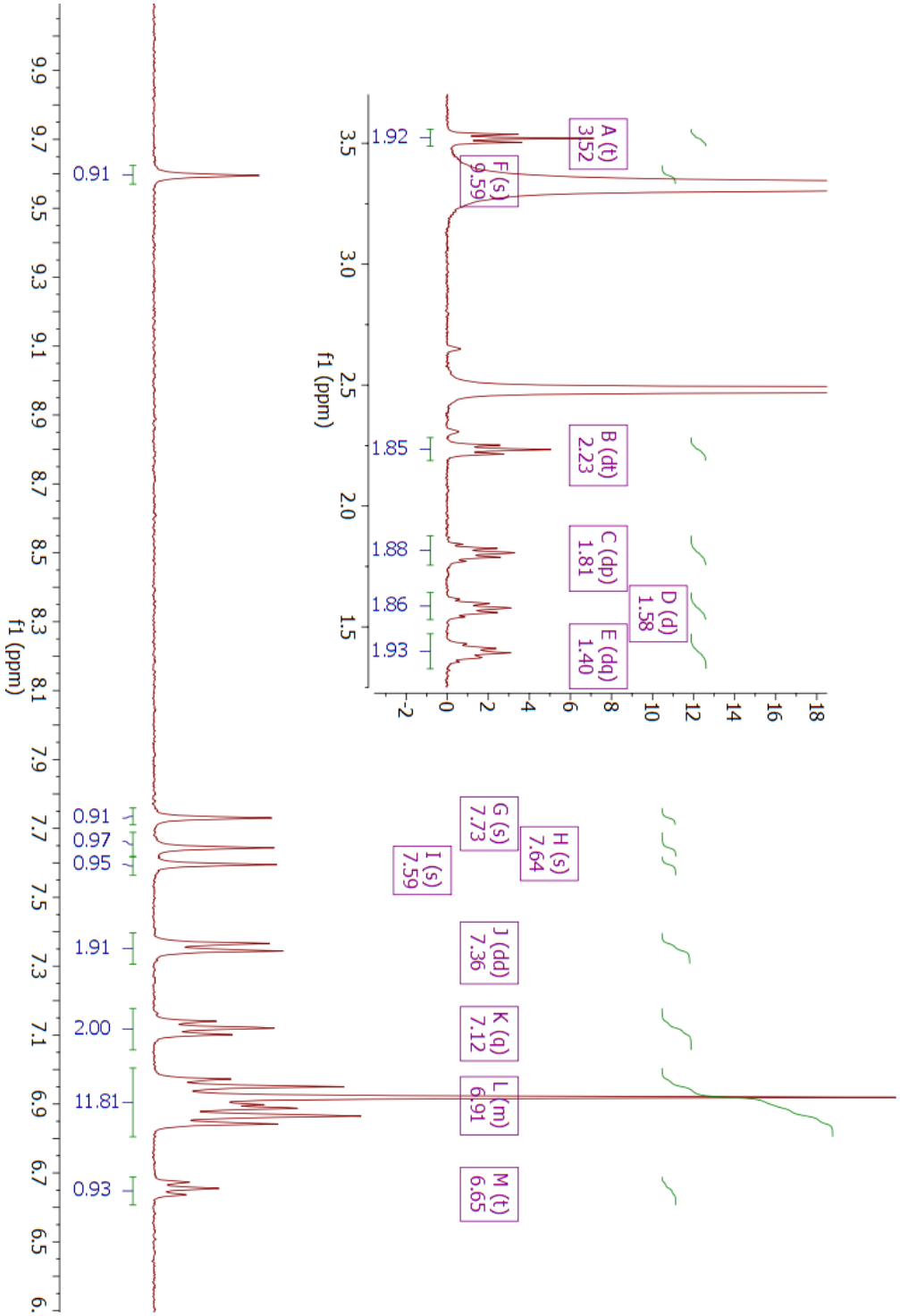

Figure A.15. ***6-bromo-N-(4-((4-((4-(phenylamino)phenyl)amino)phenyl)amino)phenyl)hexanamide (8) ^{1}H NMR spectrum in DMSO-d_6***

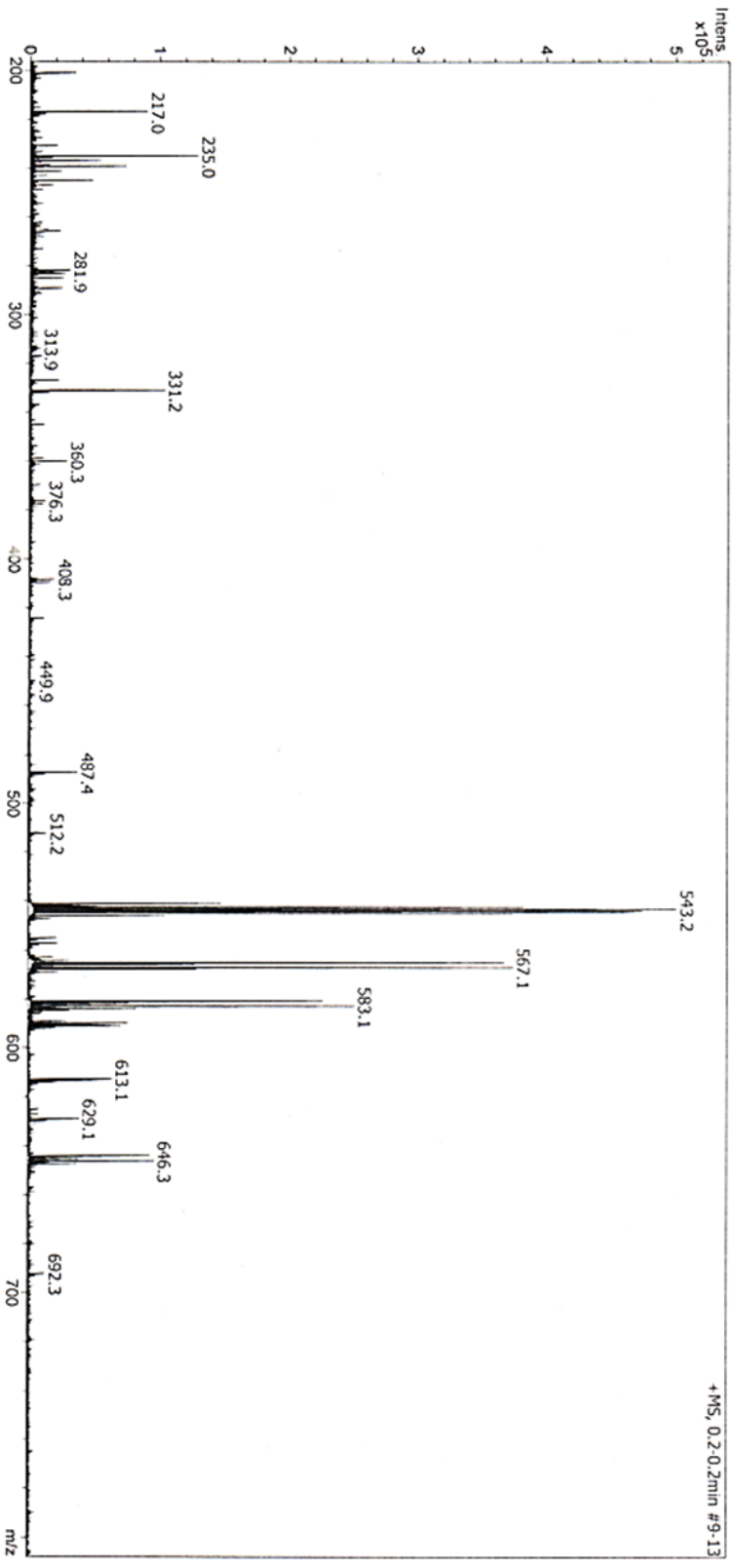

Figure A.16. ***6-bromo-N-(4-((4-((4-(phenylamino)phenyl)amino)phenyl)amino)phenyl)hexanamide (8) Mass spectrometry***

6-bromo-N-(4-(((1E,4E)-4-((4-(phenylamino)phenyl)imino)cyclohexa-2,5-dien-1-ylidene)amino)phenyl)hexanamide (9)

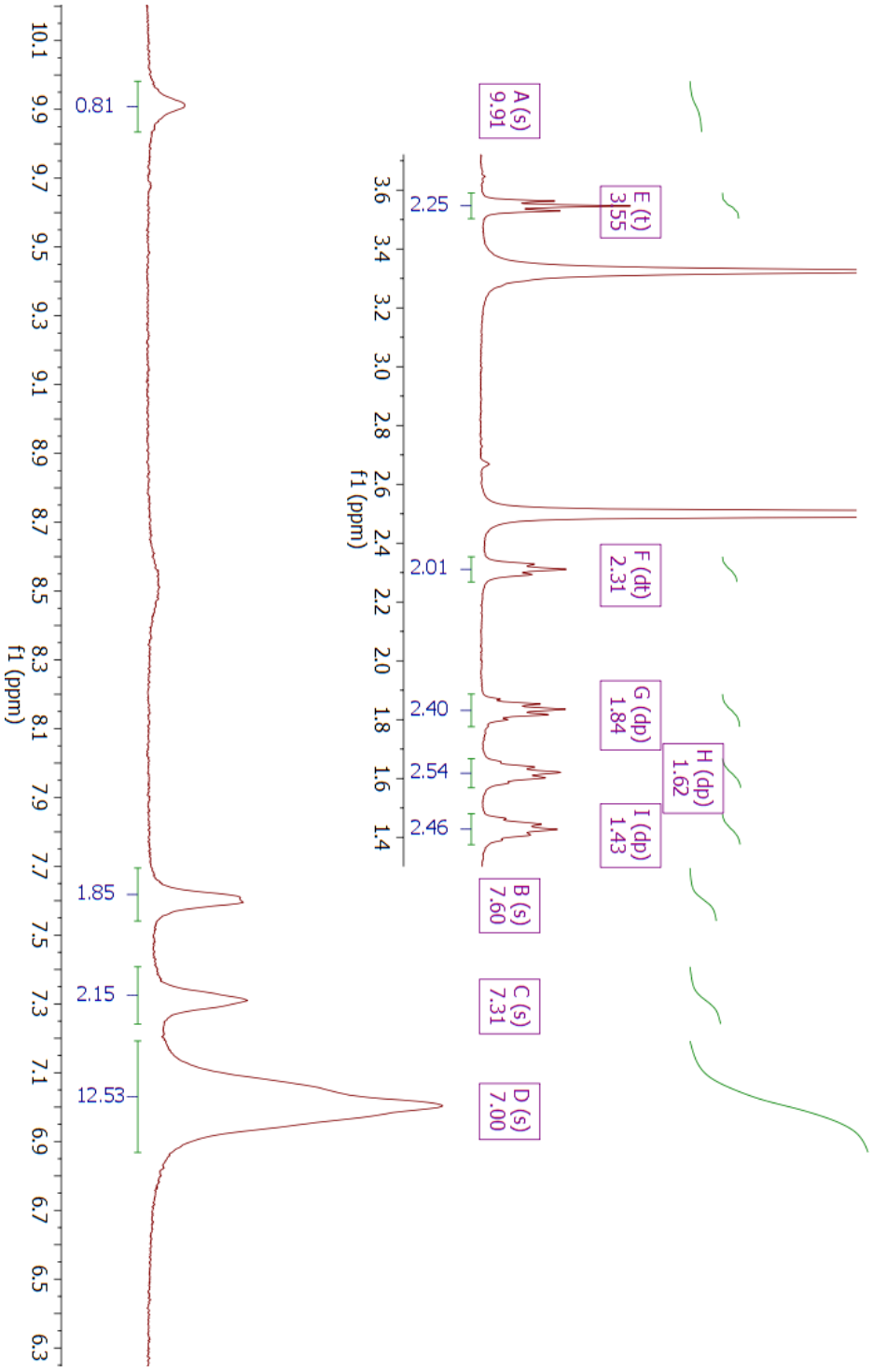

Figure A.17. ***6-bromo-N-(4-(((1E,4E)-4-((4-(phenylamino)phenyl)imino)cyclohexa-2,5-dien-1-ylidene)amino)phenyl)hexanamide (9) ^{1}H NMR spectrum in DMSO-d_6***

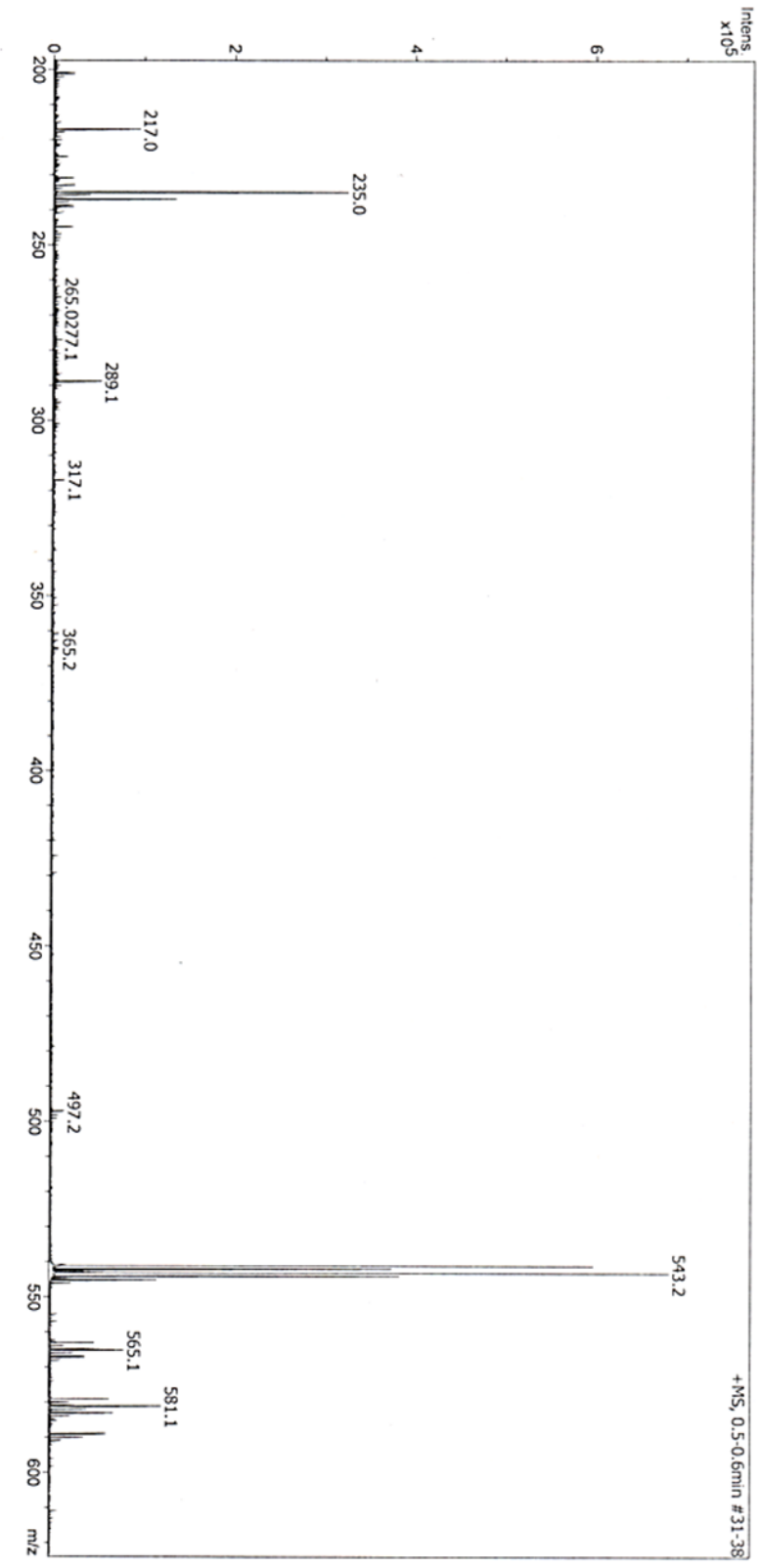

Figure A.18. ***6-bromo-N-(4-(((1E,4E)-4-((4-(phenylamino)phenyl)imino)cyclohexa-2,5-dien-1-ylidene)amino)phenyl)hexanamide (9) Mass spectrometry***

EB TANI-PTAB (10)

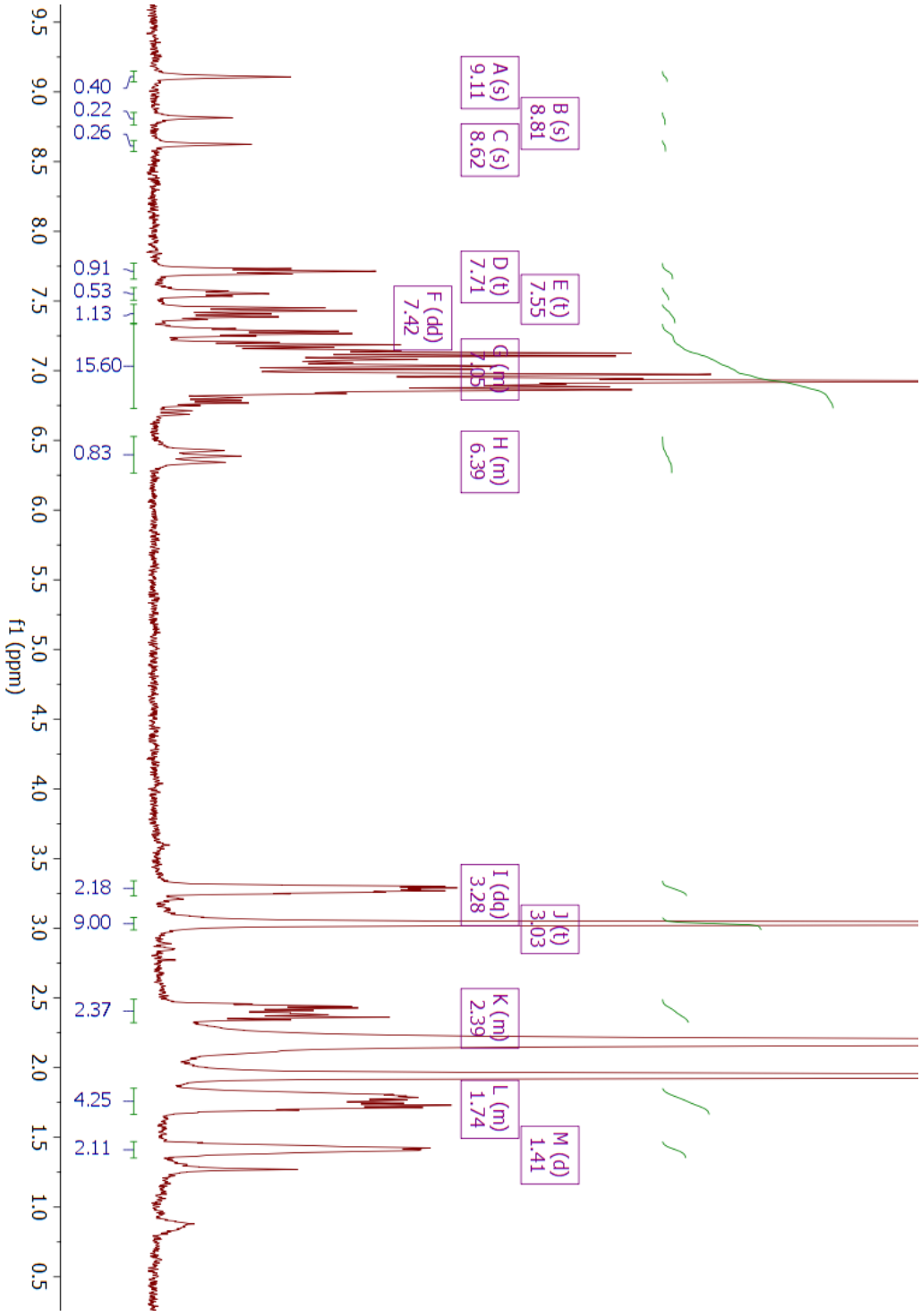

Figure A.19. ***EB TANI-PTAB (10) ^{1}H NMR spectrum in acetonitrile-d$_3$***

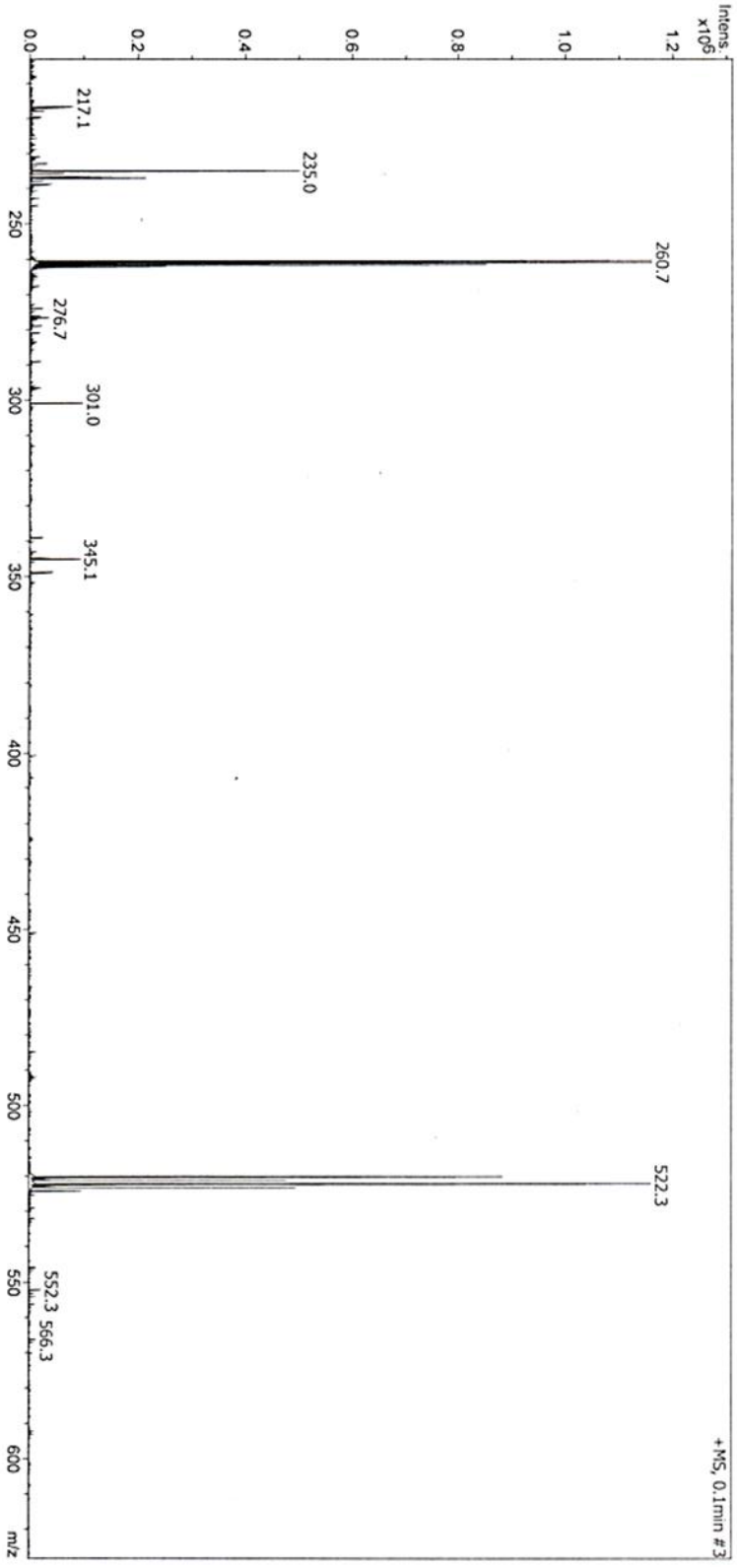

Figure A.20. ***EB TANI-PTAB (10) Mass spectrometry***

SYNTHESIS OF TANI-C_{12}TAB (EB)

tert-butyl (4-(12-bromododecanamido)phenyl)(4-((tert-butoxycarbonyl)(4-((tert-butoxycarbonyl)(phenyl)amino)phenyl)amino)phenyl)carbamate (11)

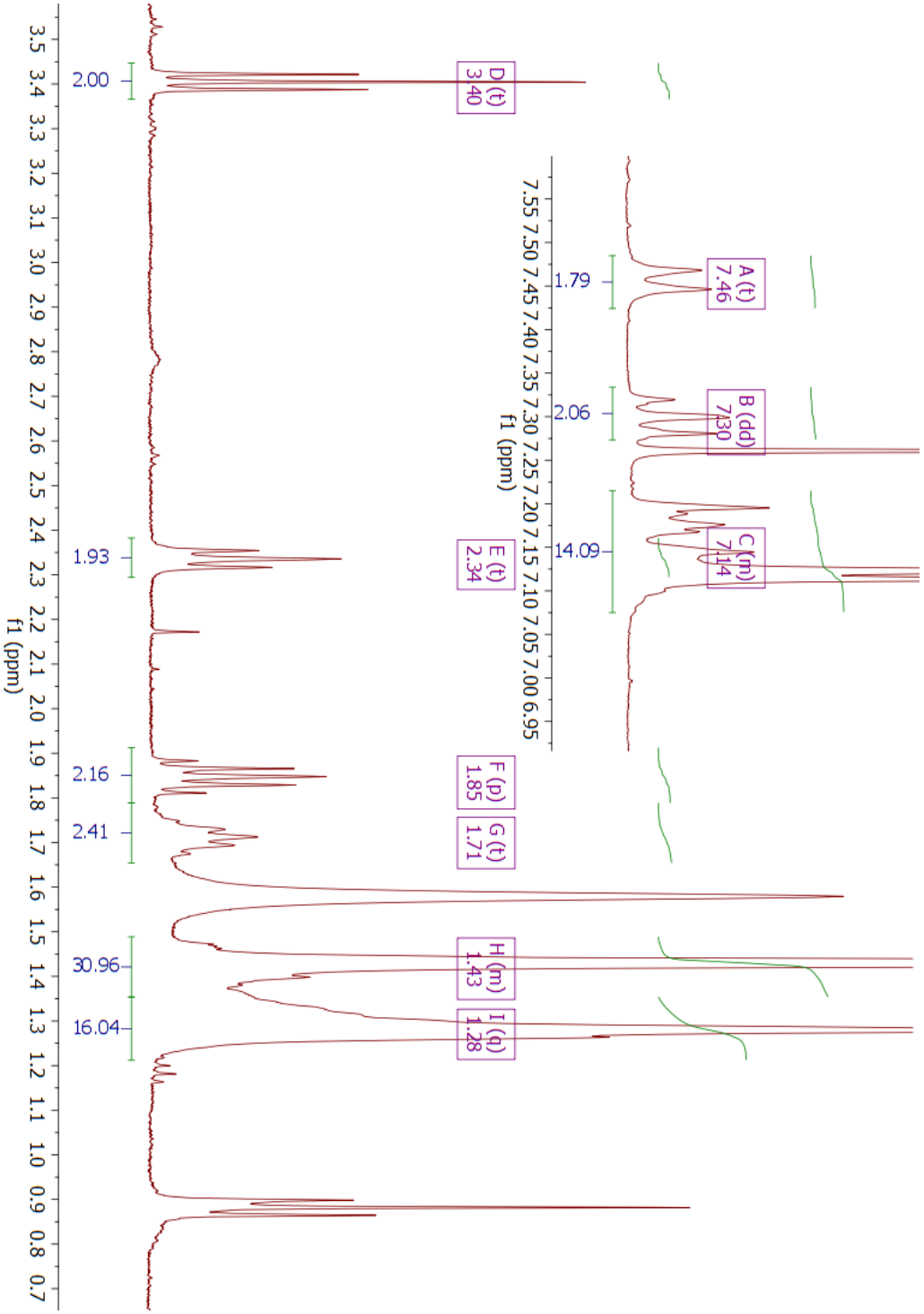

Figure A.21. ***tert-butyl (4-(12-bromododecanamido)phenyl)(4-((tert-butoxycarbonyl)(4-((tert-butoxycarbonyl)(phenyl)amino)phenyl)amino)phenyl)carbamate (11) ^{1}H NMR spectrum in $CDCl_3$***

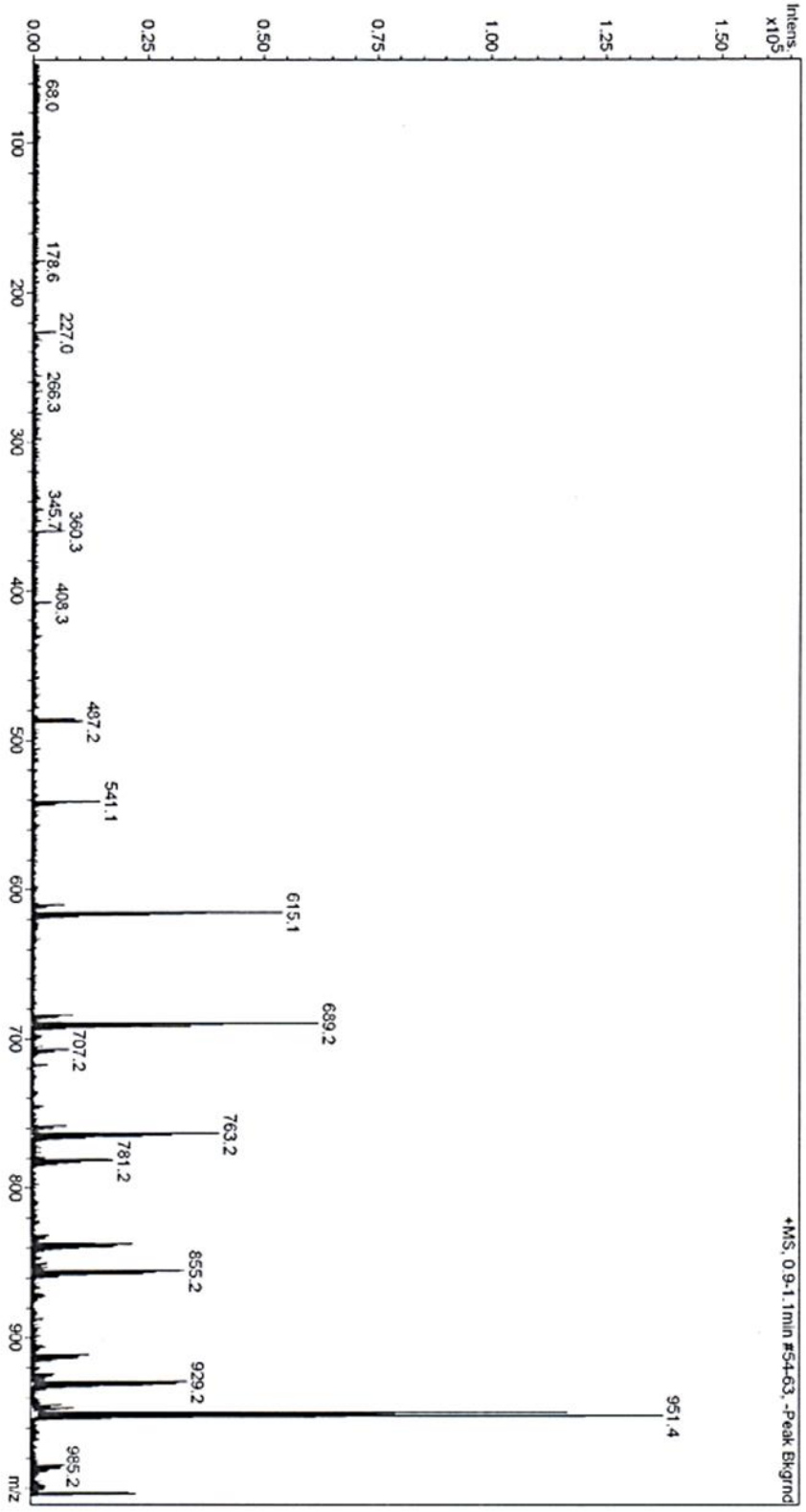

Figure A.22. ***tert-butyl (4-(12-bromododecanamido)phenyl)(4-((tert-butoxycarbonyl)(4-((tert-butoxycarbonyl)(phenyl)amino)phenyl)amino)phenyl)carbamate (11) Mass spectrometry***

12-bromo-N-(4-((4-((4-(phenylamino)phenyl)amino)phenyl)amino)phenyl)dodecanamide (12)

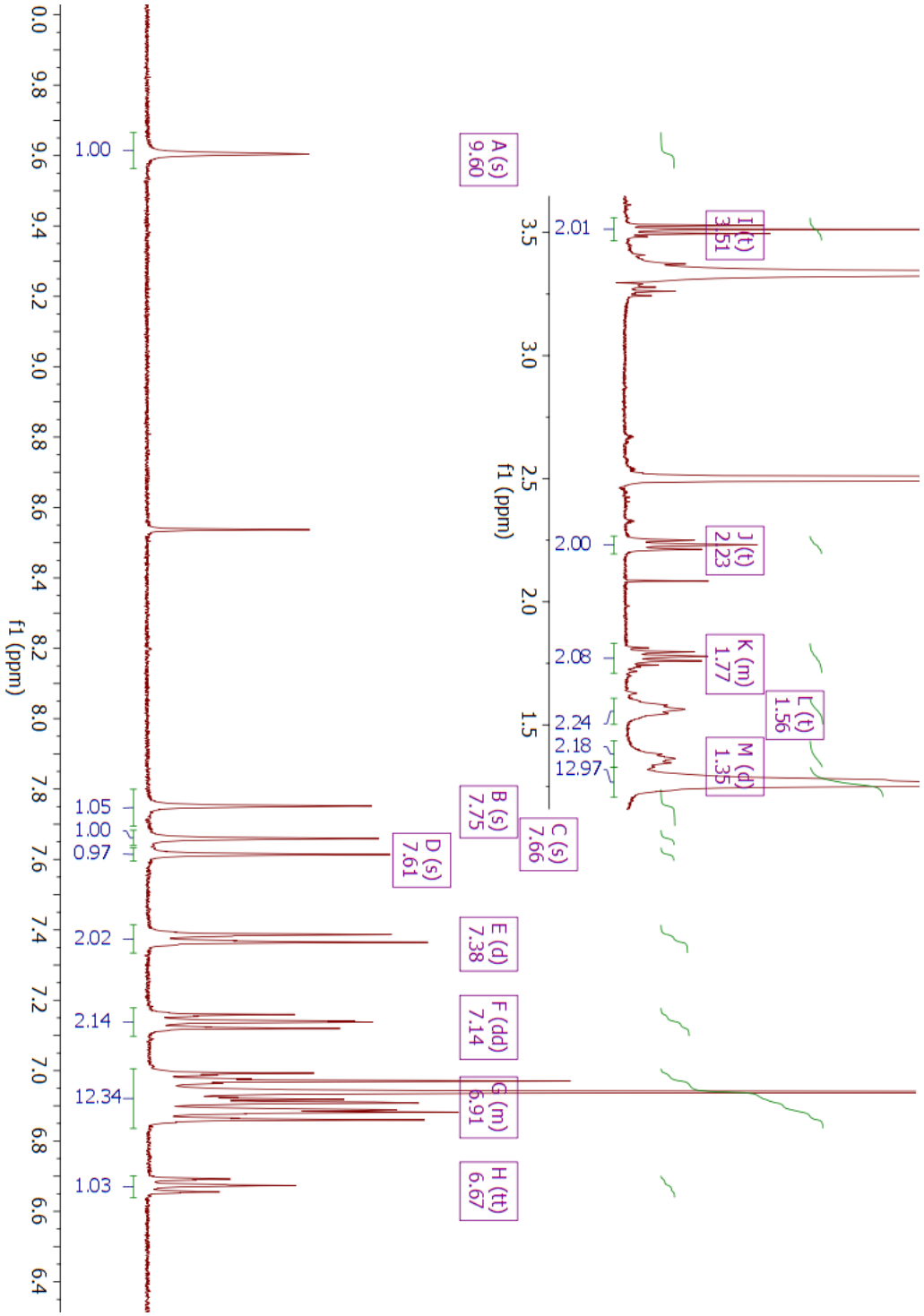

Figure A.23. ***12-bromo-N-(4-((4-((4-(phenylamino)phenyl)amino)phenyl)amino)phenyl)dodecanamide (12) ^{1}H NMR spectrum in DMSO-d$_6$***

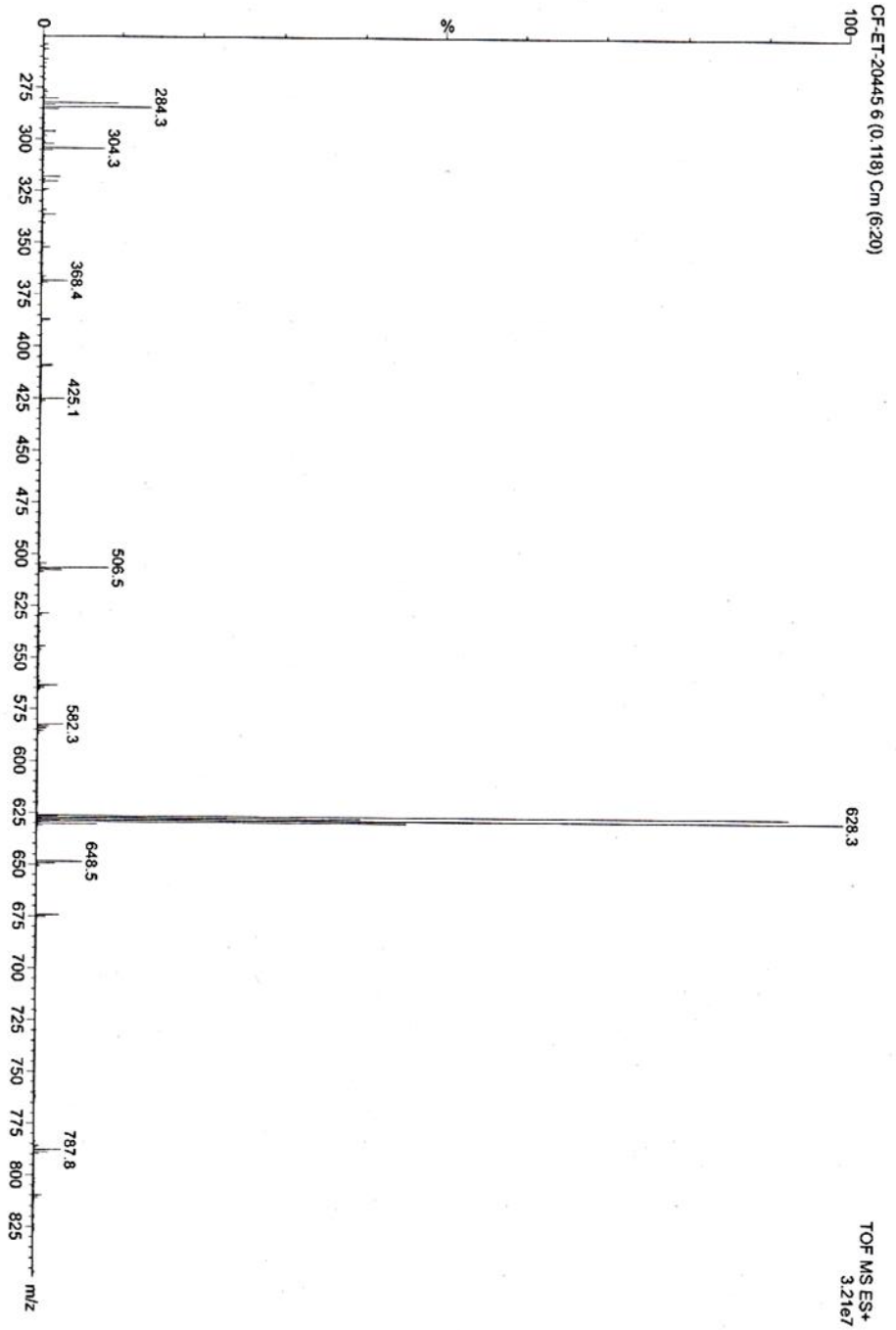

Figure A.24. ***12-bromo-N-(4-((4-((4-(phenylamino)phenyl)amino)phenyl)amino)phenyl)dodecanamide (12) Mass spectrometry***

12-bromo-N-(4-((4-(((1E,4E)-4-(phenylimino)cyclohexa-2,5-dien-1-ylidene)amino)phenyl)amino)phenyl)dodecanamide (13)

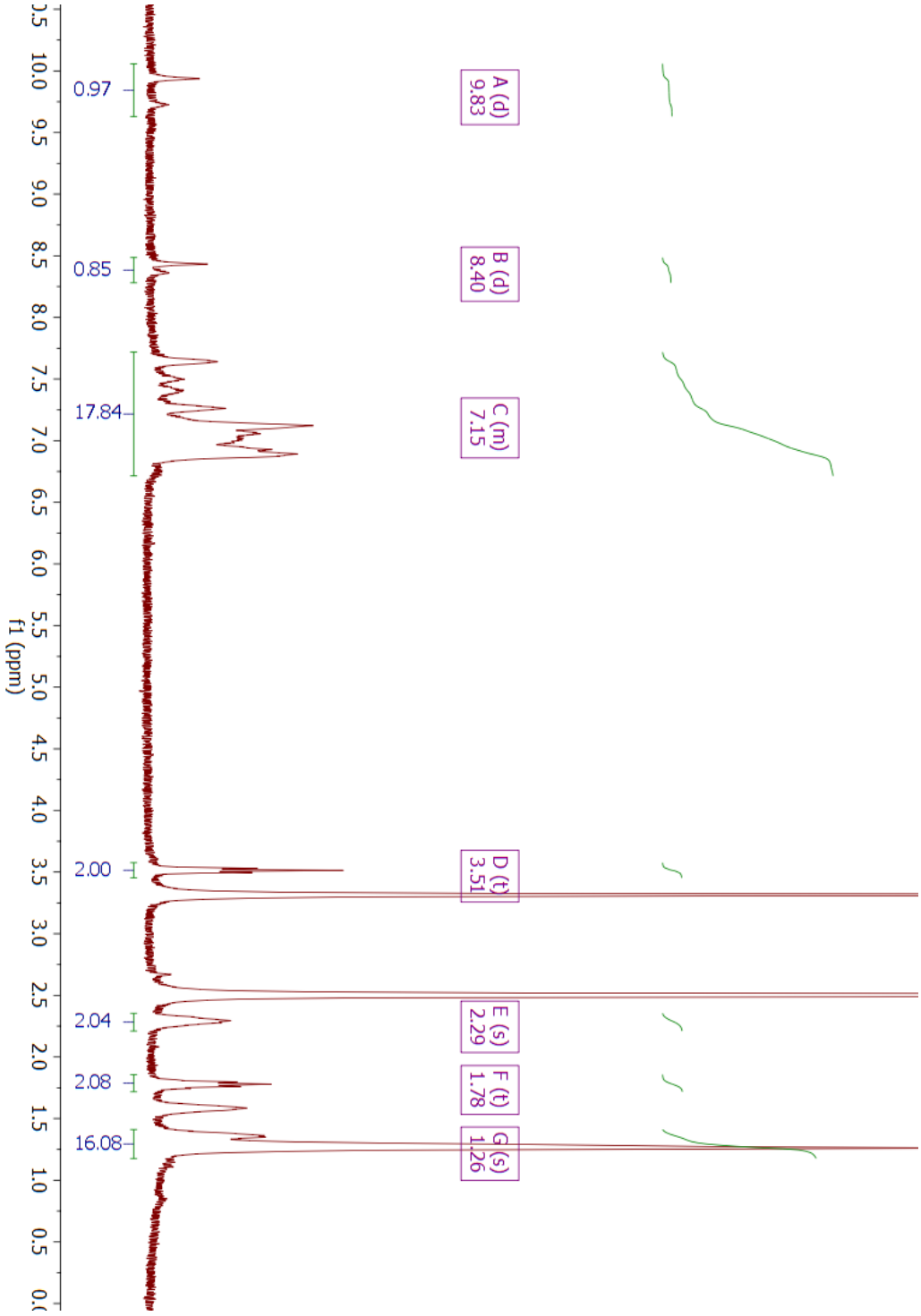

Figure A.25. ***12-bromo-N-(4-((4-(((1E,4E)-4-(phenylimino)cyclohexa-2,5-dien-1-ylidene)amino)phenyl)amino)phenyl)dodecanamide (13) ^{1}H NMR spectrum in DMSO-d_6***

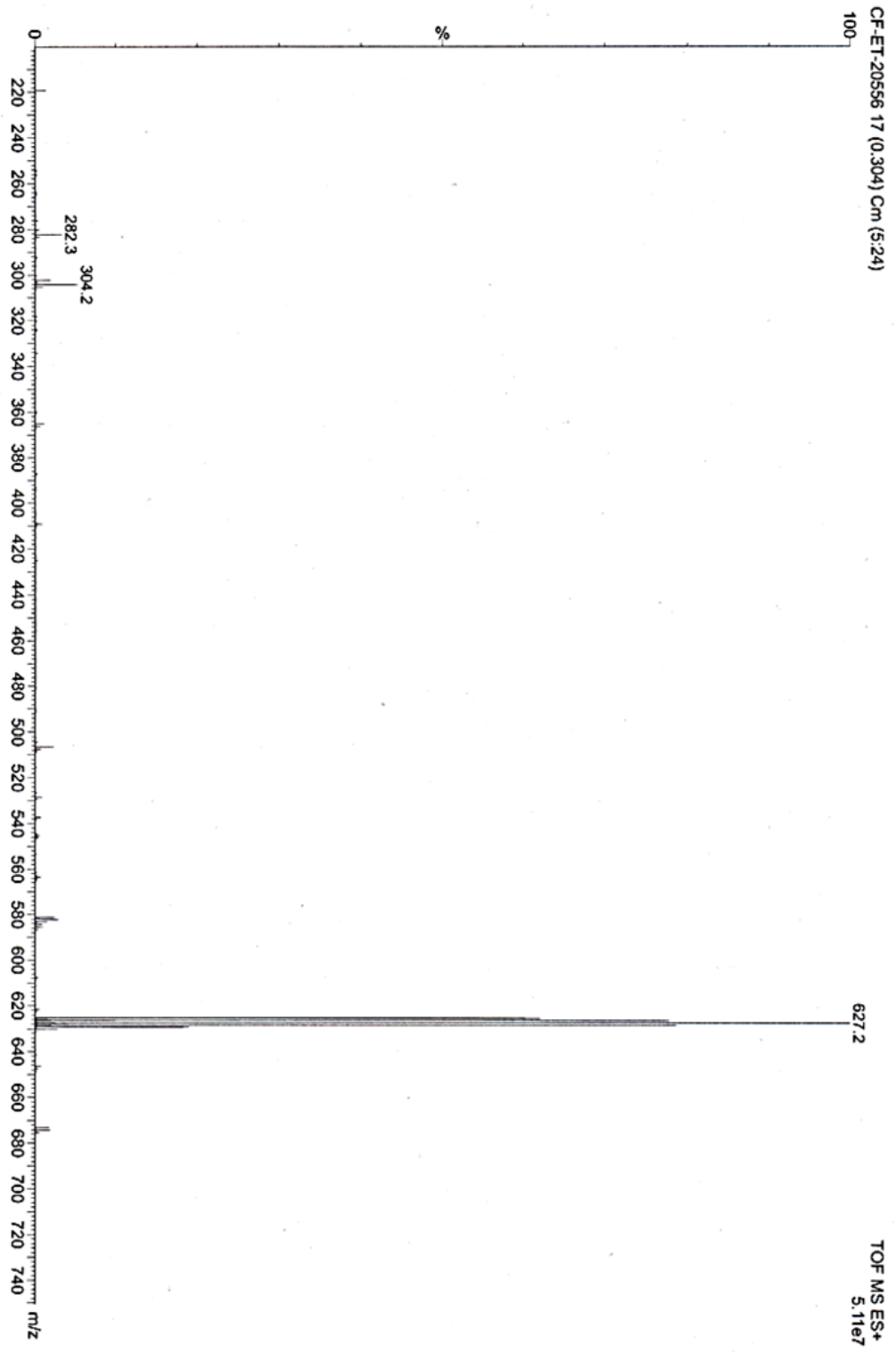

Figure A.26. ***12-bromo-N-(4-((4-(((1E,4E)-4-(phenylimino)cyclohexa-2,5-dien-1-ylidene)amino)phenyl)amino)phenyl)dodecanamide (13) Mass spectrometry***

EB TANI-C_{12}TAB (14)

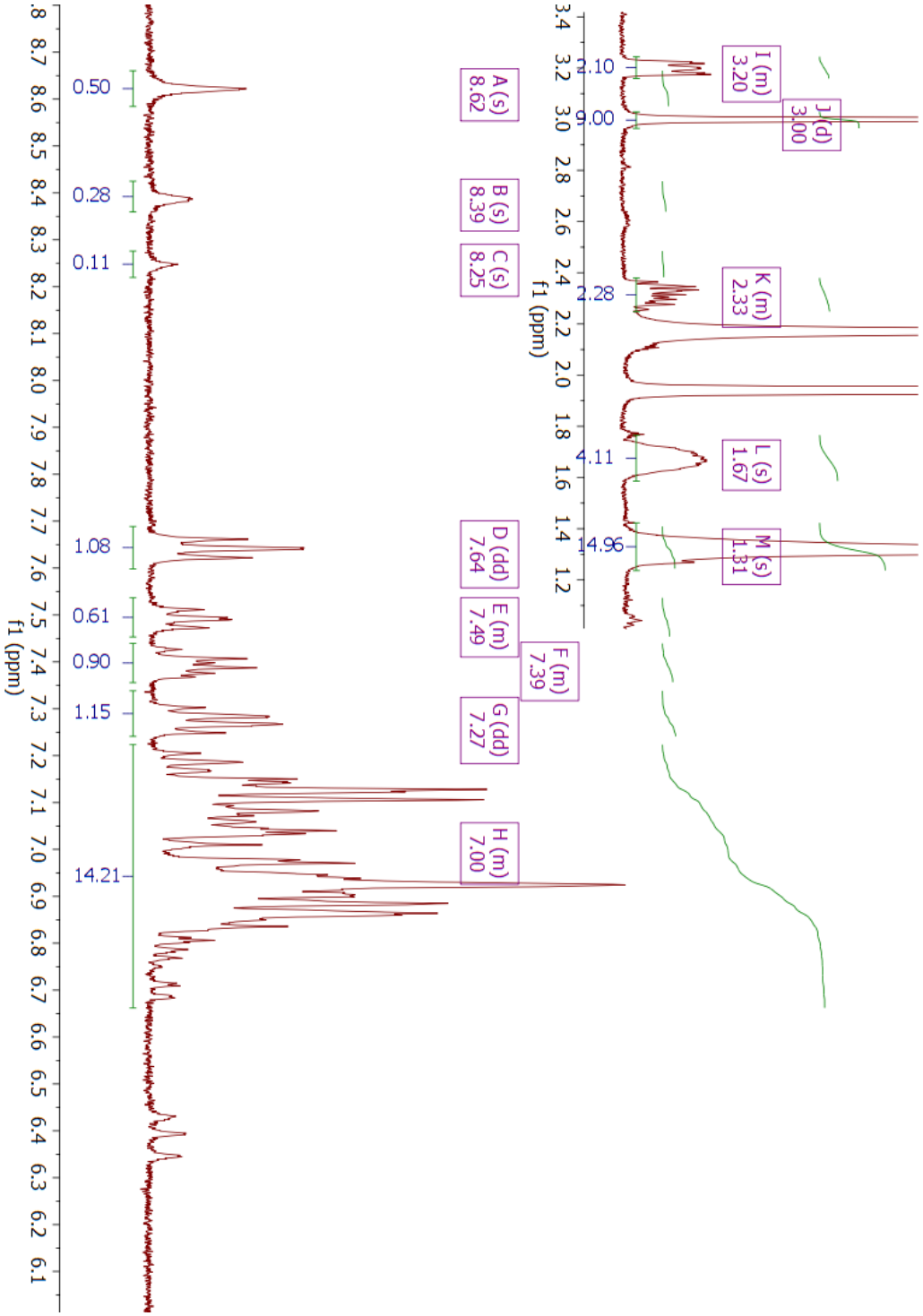

Figure A.27. ***EB TANI-C_{12}TAB (14) ^{1}H NMR spectrum in acetonitrile-d_3***

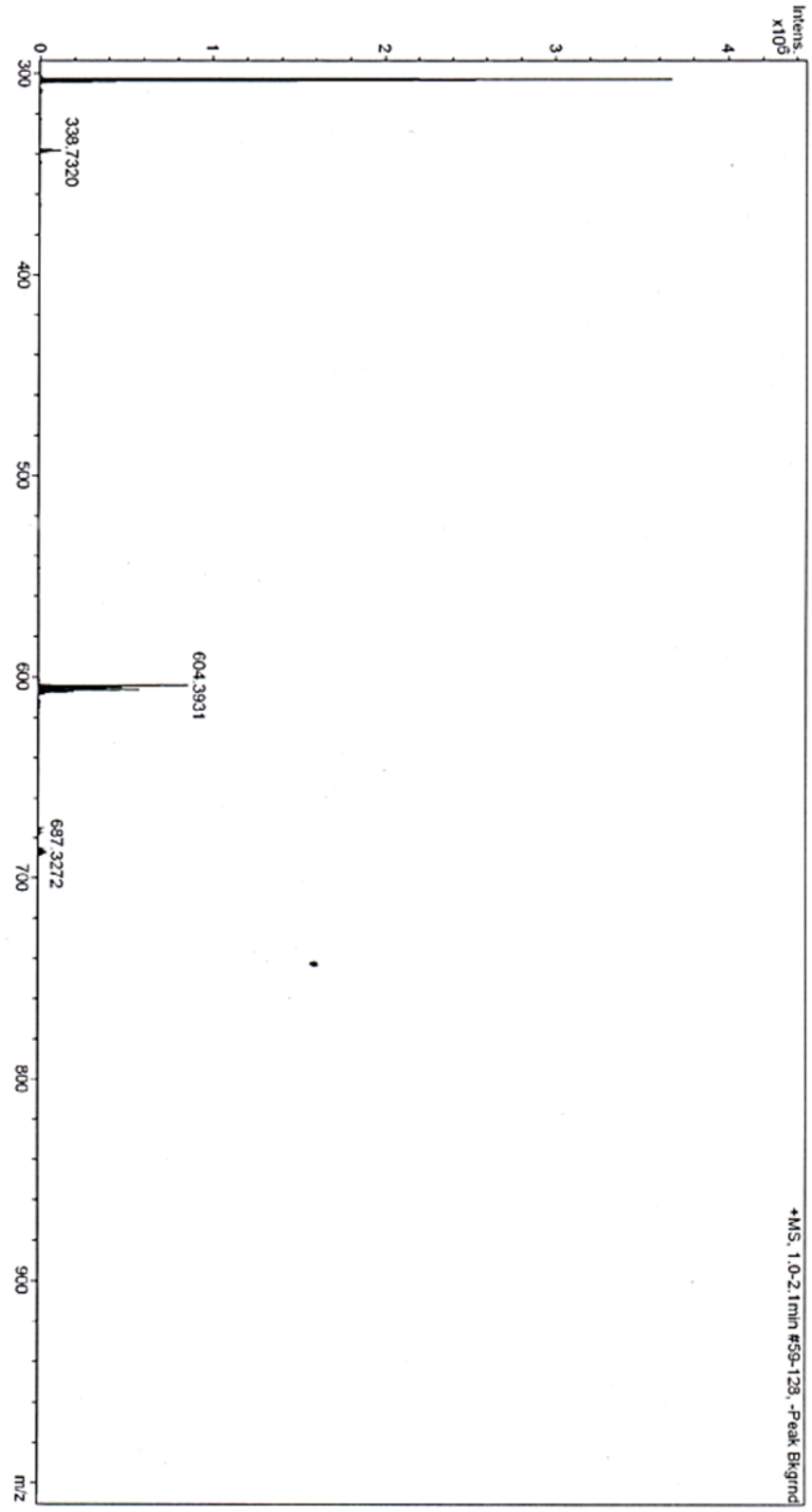

Figure A.28. ***EB TANI-C_{12}TAB (14) Mass spectrometry***

SYNTHESIS OF TANI-PTPB (EB)

EB TANI-PTPB (16)

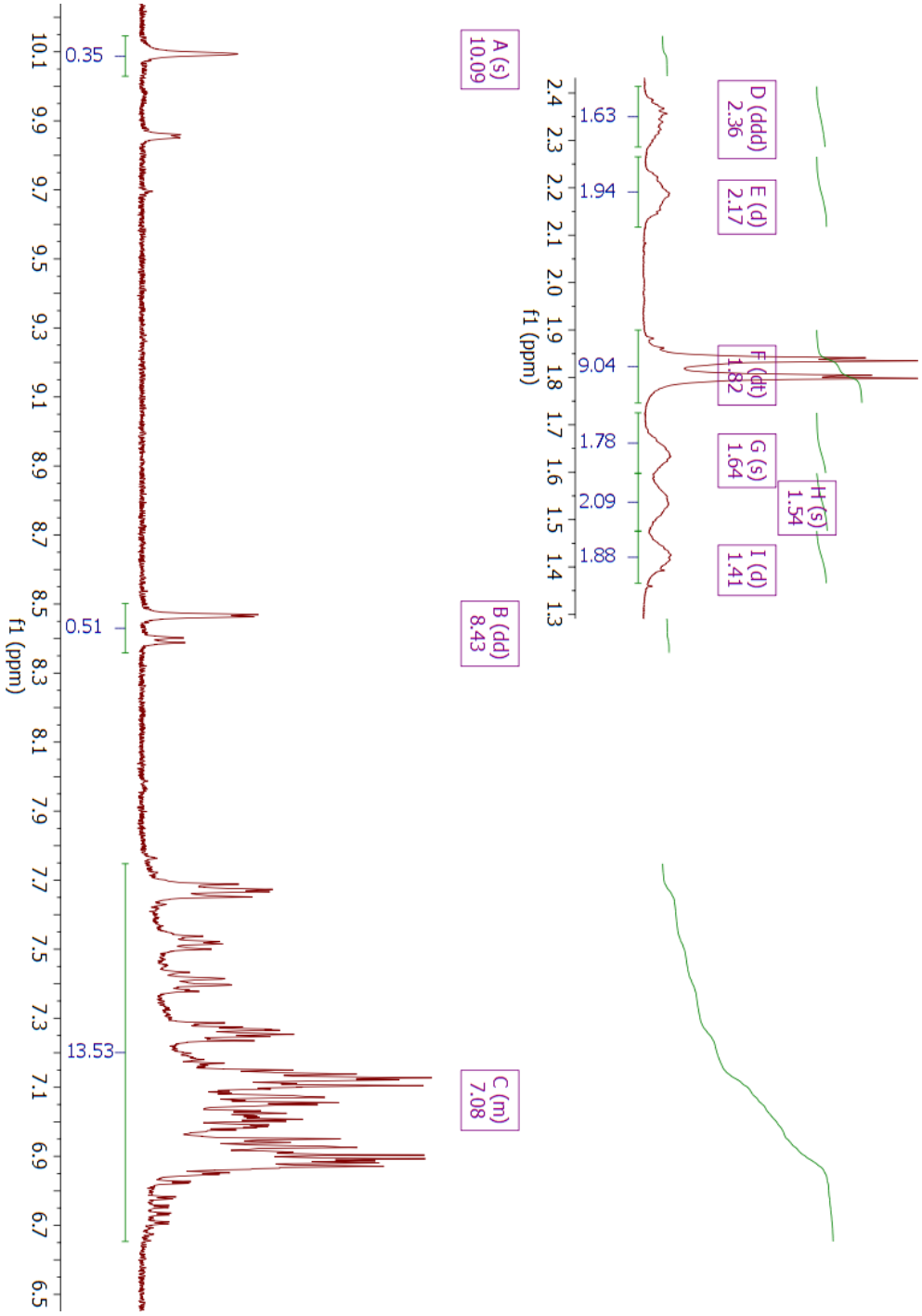

Figure A.29. ***TANI-PTPB (16) ^{1}H NMR spectrum in DMSO-d_6***

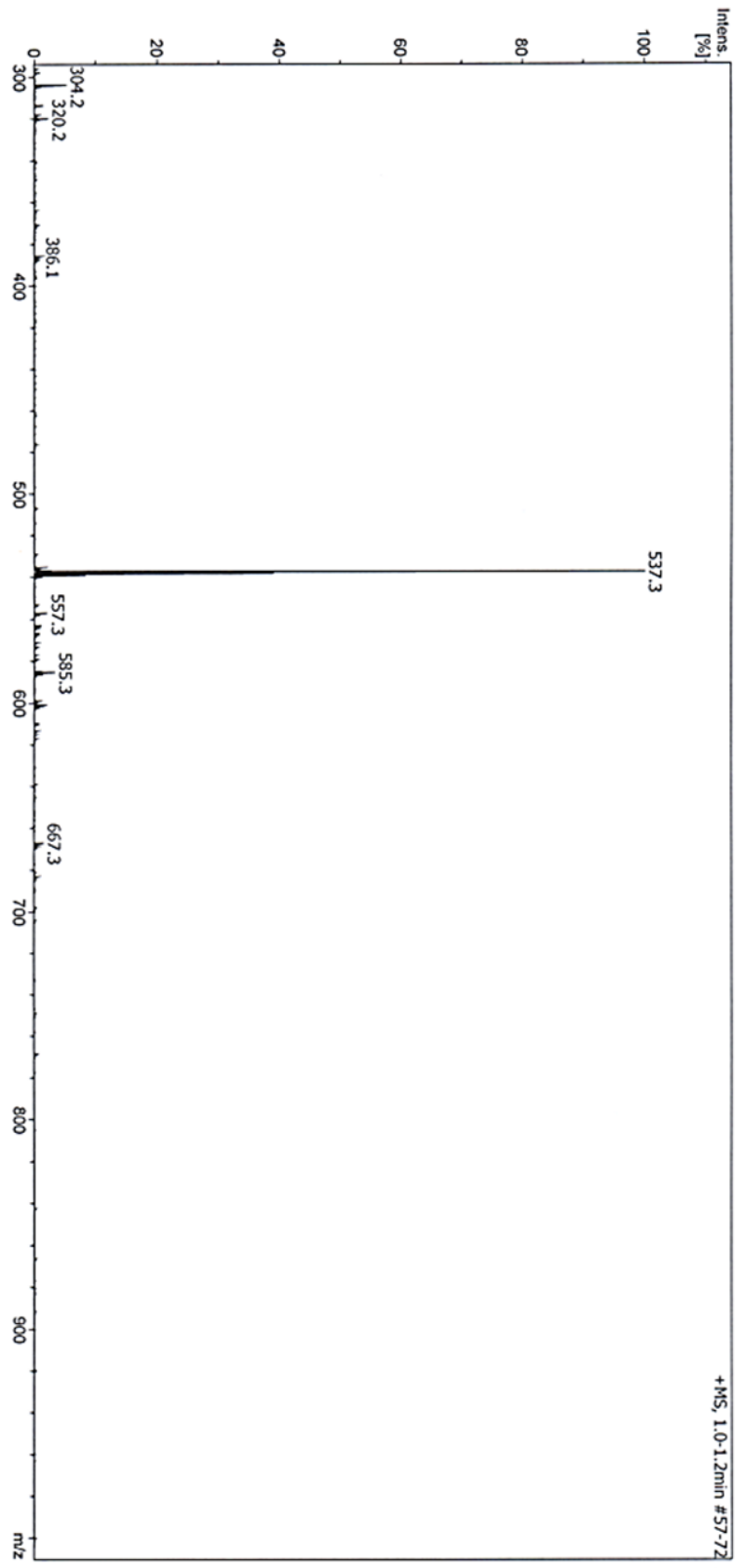

Figure A.30. ***TANI-PTPB (16) Mass spectrometry***

SYNTHESIS OF NH_2/NH_2 TANI

N^1-(4-nitrophenyl)-N^4-(4-((4-nitrophenyl)amino)phenyl)benzene-1,4-diamine (17)

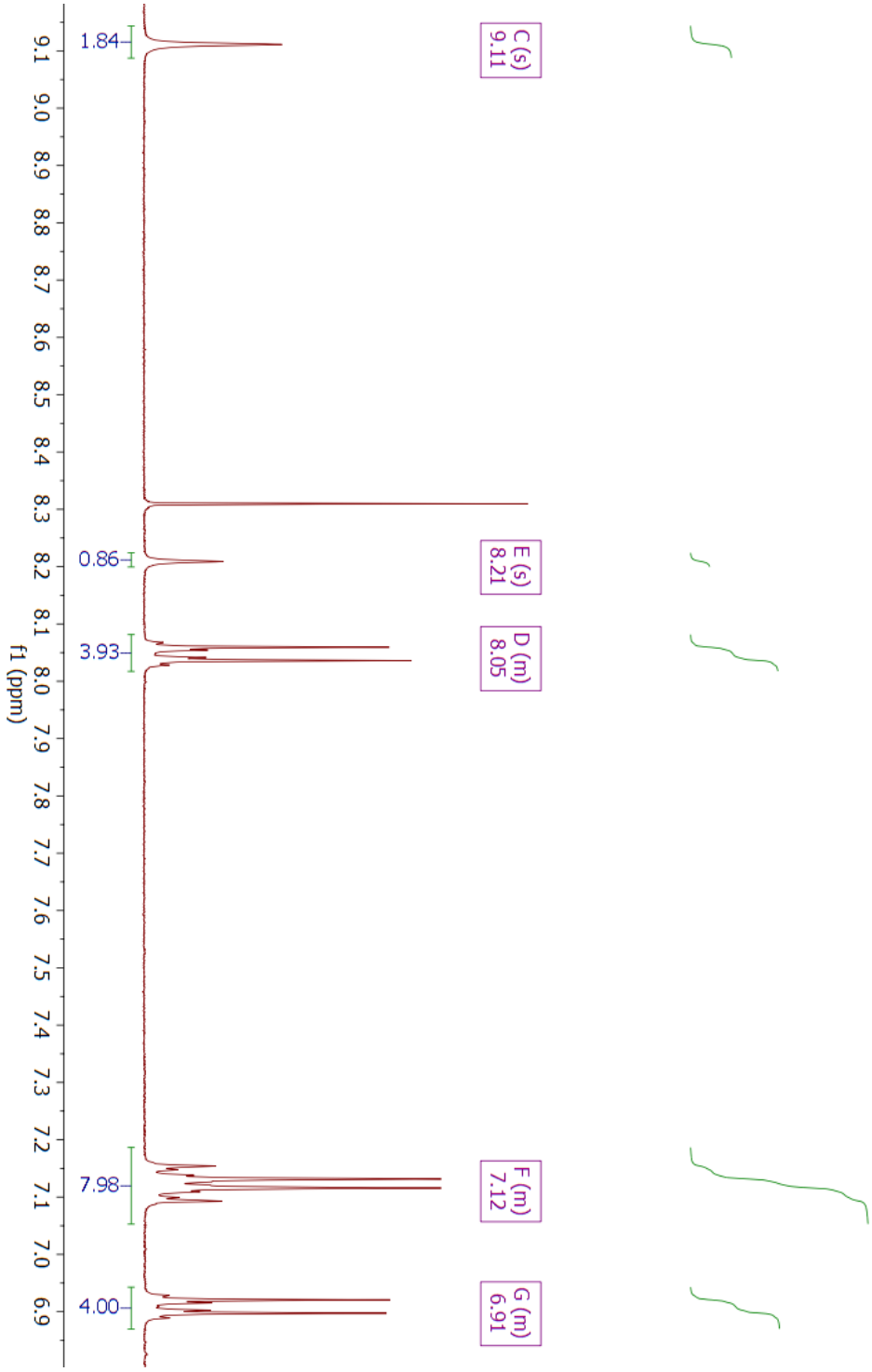

Figure A.31. ***N^1-(4-nitrophenyl)-N^4-(4-((4-nitrophenyl)amino)phenyl)benzene-1,4-diamine (17) ^{1}H NMR spectrum in DMSO-d_6***

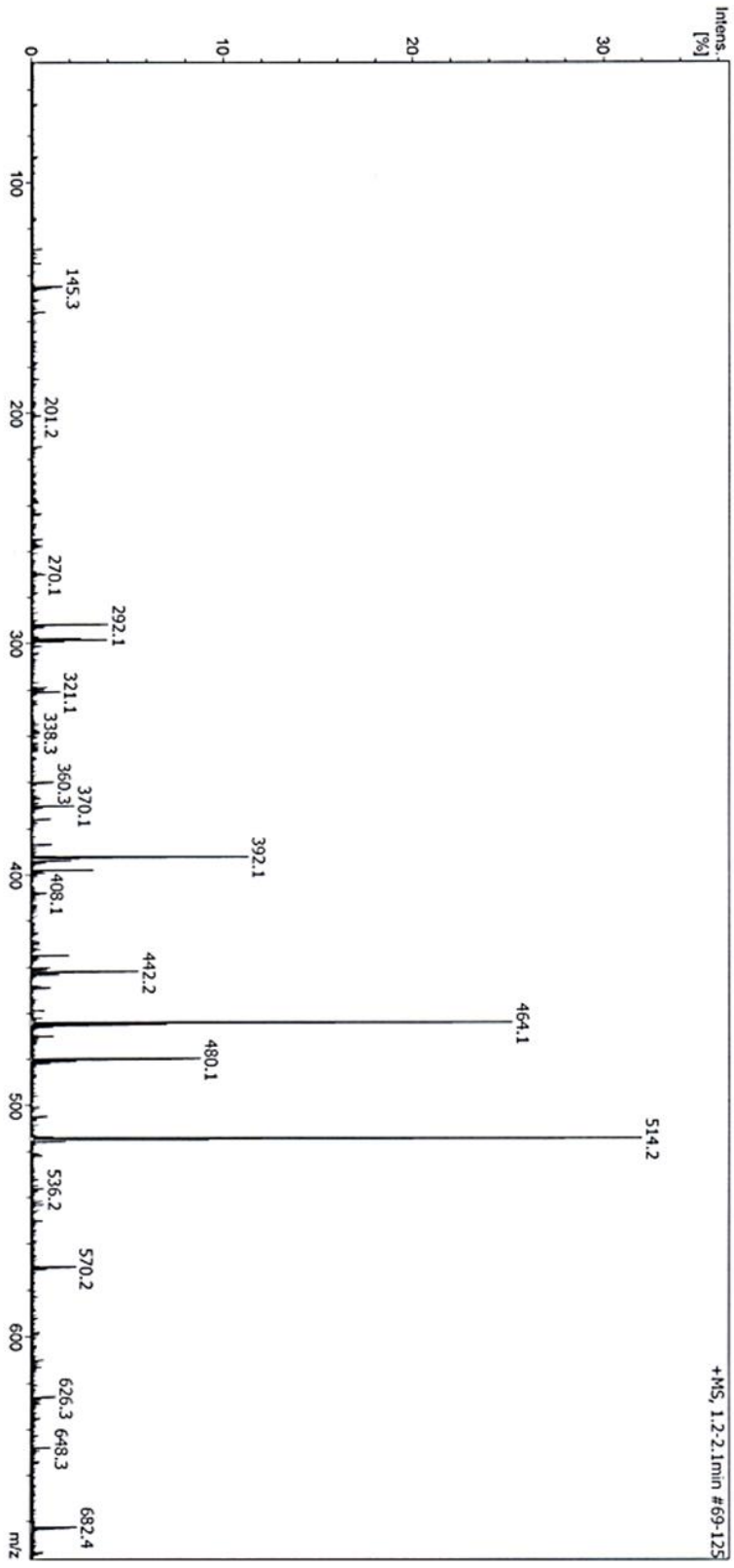

Figure A.32. ***N^1-(4-nitrophenyl)-N^4-(4-((4-nitrophenyl)amino)phenyl)benzene-1,4-diamine (17) Mass spectrometry***

tert-butyl (4-((tert-butoxycarbonyl)(4-((tert-butoxycarbonyl)(4-nitrophenyl)amino)phenyl)amino)phenyl)(4-nitrophenyl)carbamate (18)

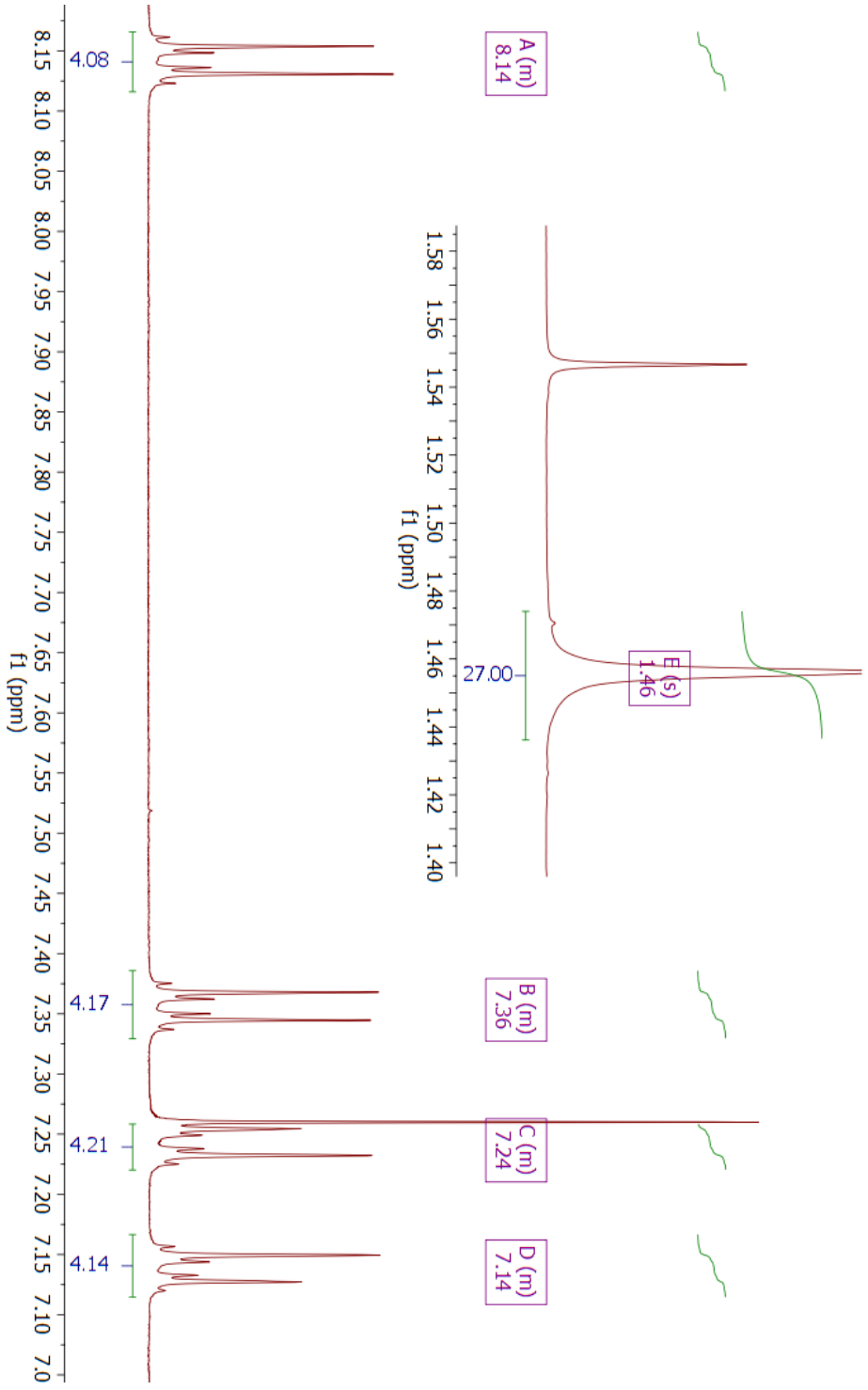

Figure A.33. ***tert-butyl (4-((tert-butoxycarbonyl)(4-((tert-butoxycarbonyl)(4-nitrophenyl)amino)phenyl)amino)phenyl)(4-nitrophenyl)carbamate (18) ^{1}H NMR spectrum in $CDCl_3$***

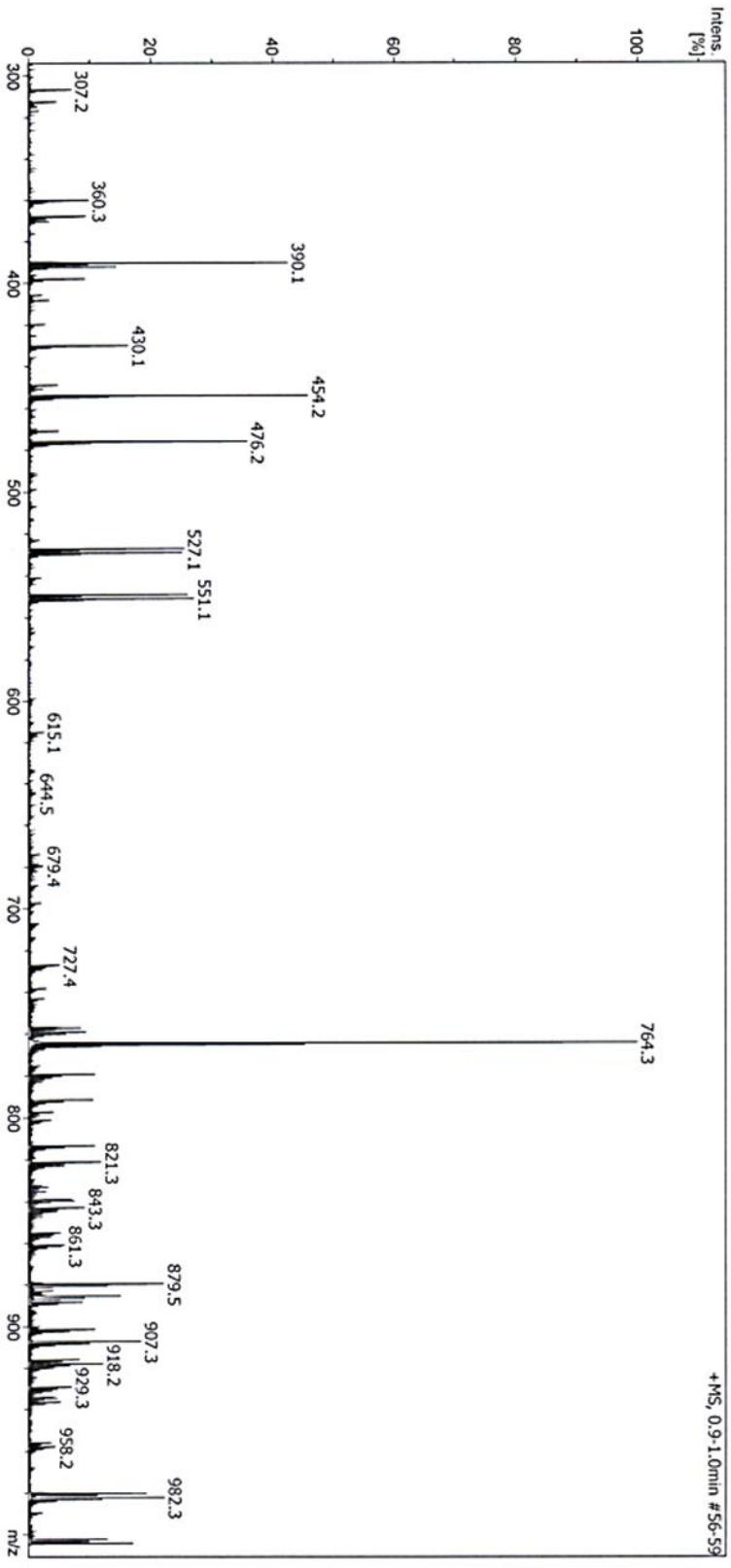

Figure A.34. ***tert-butyl (4-((tert-butoxycarbonyl)(4-((tert-butoxycarbonyl)(4-nitrophenyl)amino)phenyl)amino)phenyl)(4-nitrophenyl)carbamate (18) Mass spectrometry***

NH_2/NH_2 TANI (19)

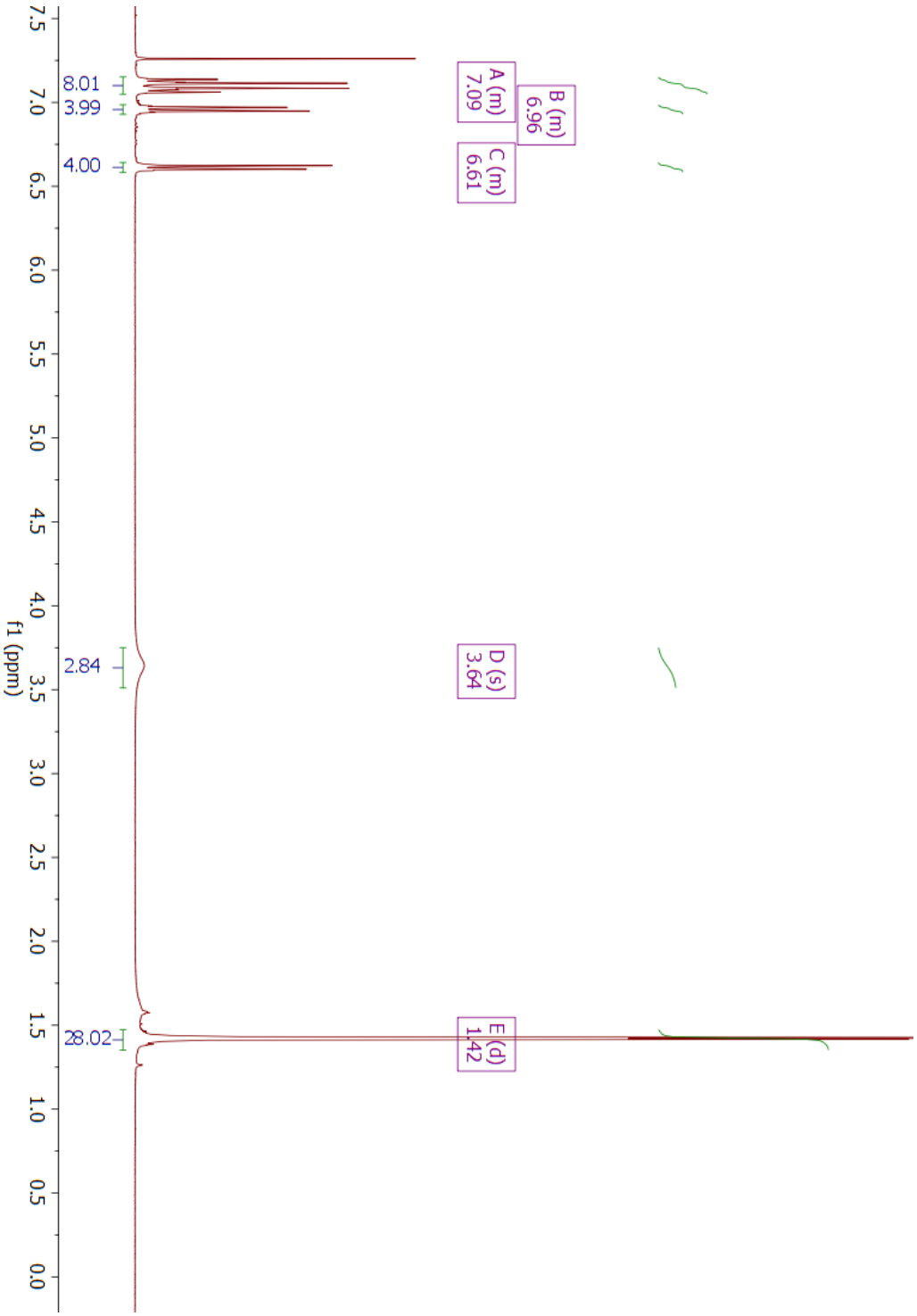

Figure A.35. ***NH_2/NH_2 TANI (19) ^1H NMR spectrum in $CDCl_3$***

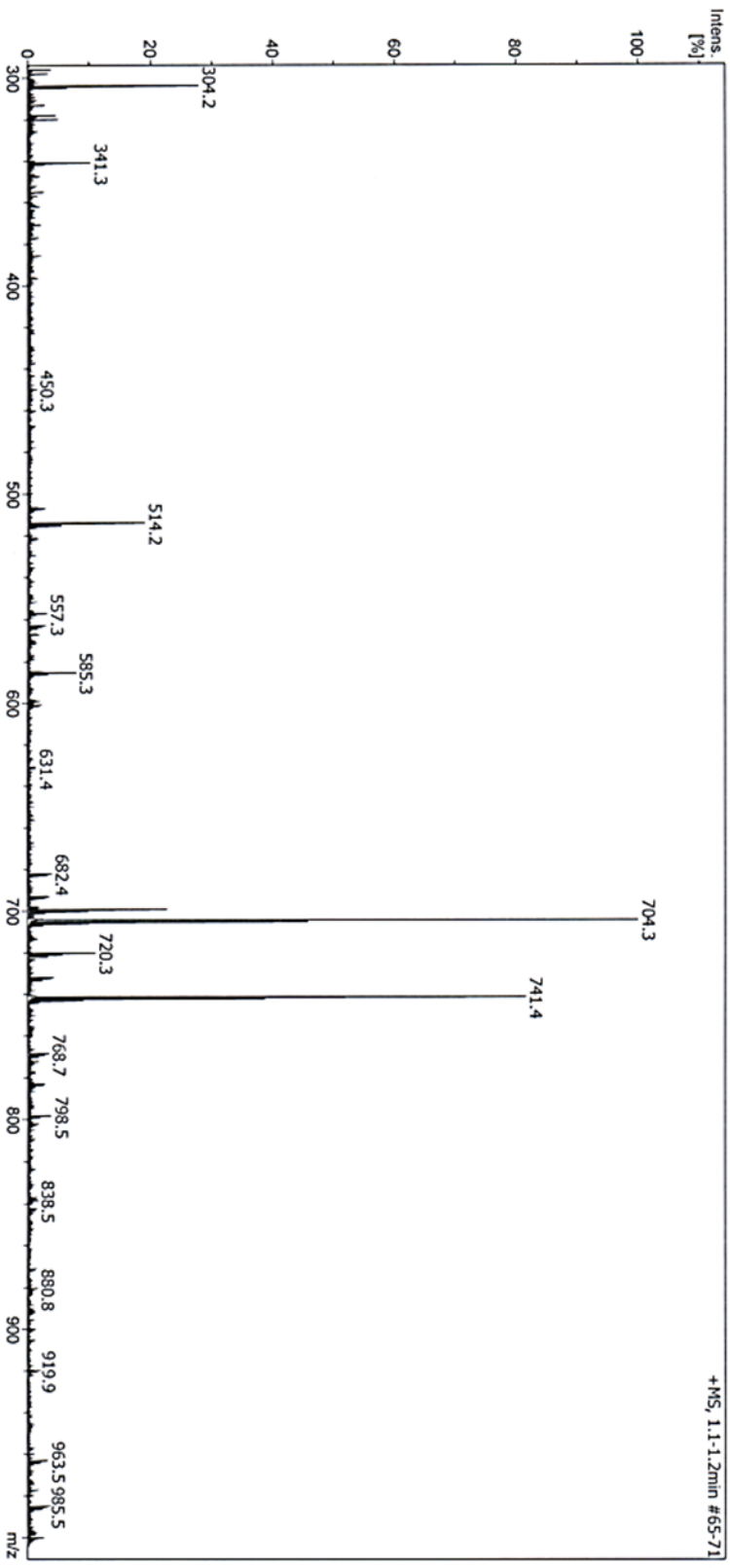

Figure A.36. ***NH_2/NH_2 TANI (19) Mass spectrometry***

SYNTHESIS OF TANI-(PTAB)$_2$ (EB)

tert-butyl (4-(6-bromohexanamido)phenyl)(4-((4-((4-(6-bromohexanamido)phenyl)(tert-butoxycarbonyl)amino)phenyl)(tert-butoxycarbonyl)amino)phenyl)carbamate (20)

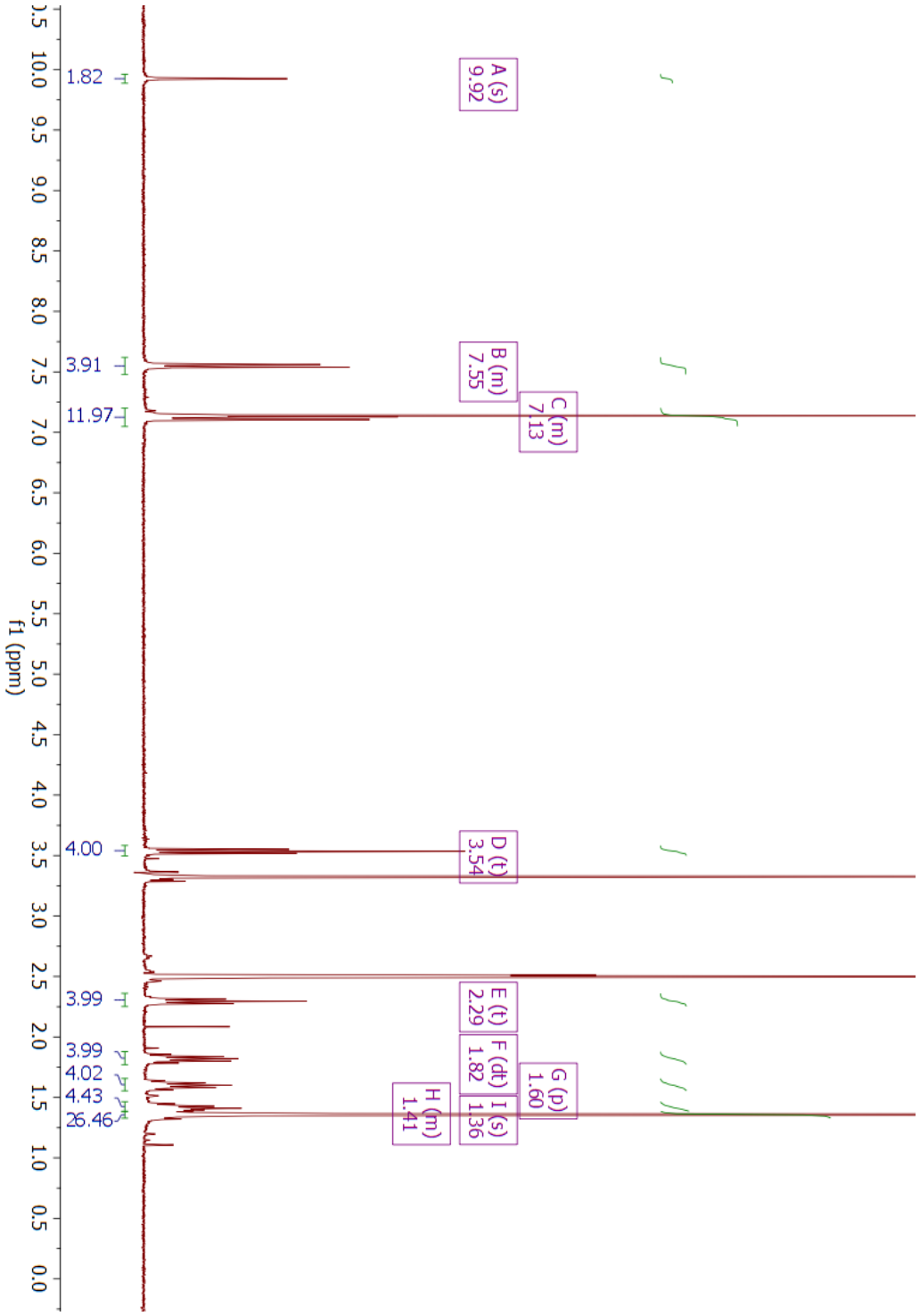

Figure A.37. ***tert-butyl (4-(6-bromohexanamido)phenyl)(4-((4-((4-(6-bromohexanamido)phenyl)(tert-butoxycarbonyl)amino)phenyl)(tert-butoxycarbonyl)amino)phenyl)carbamate (20) ^{1}H NMR spectrum in DMSO-d$_6$***

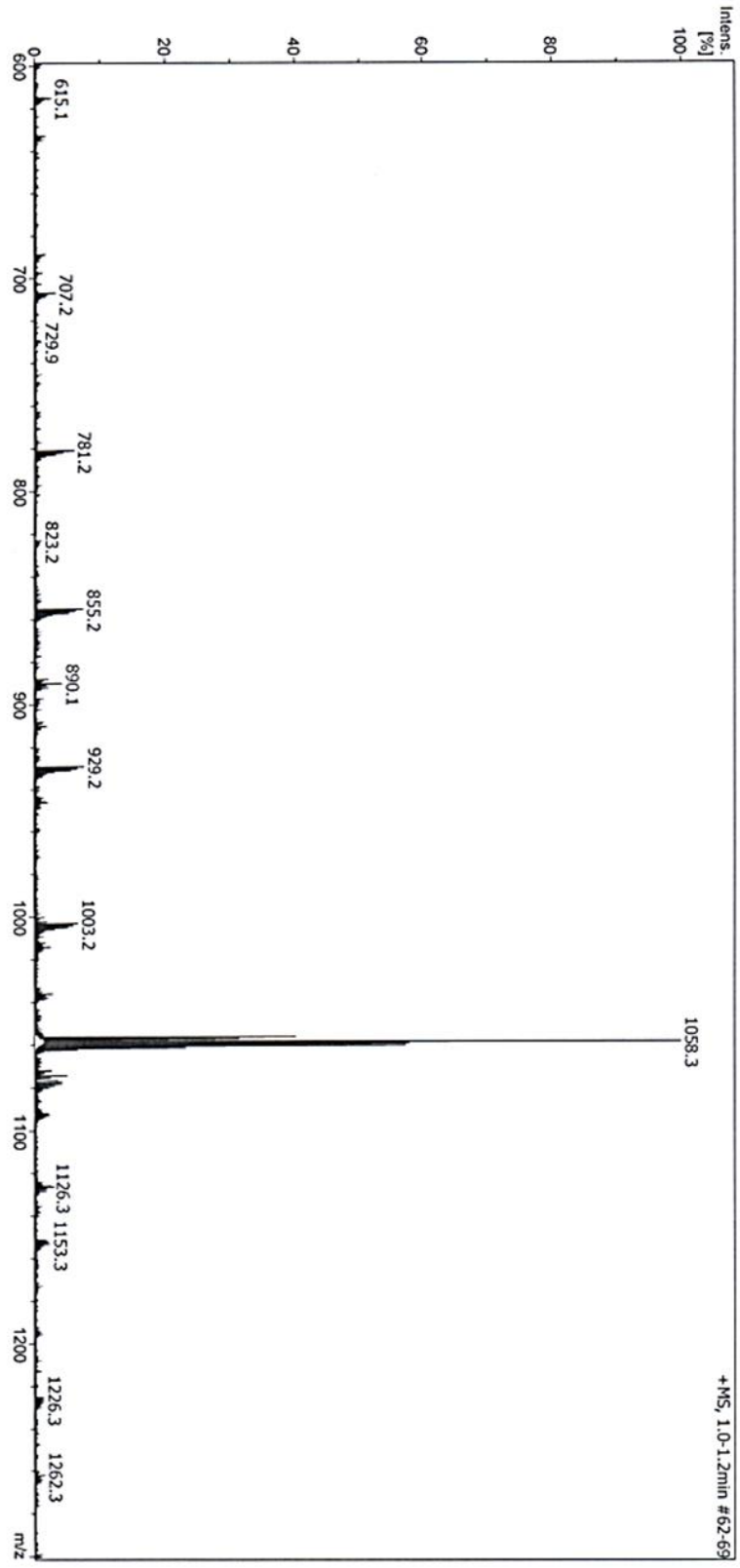

Figure A.38. ***tert-butyl (4-(6-bromohexanamido)phenyl)(4-((4-((4-(6-bromohexanamido)phenyl)(tert-butoxycarbonyl)amino)phenyl)(tert-butoxycarbonyl)amino)phenyl)carbamate (20) Mass spectrometry***

N,N'-(((azanediylbis(4,1-phenylene))bis(azanediyl))bis(4,1-phenylene))bis(6-bromohexanamide) (21)

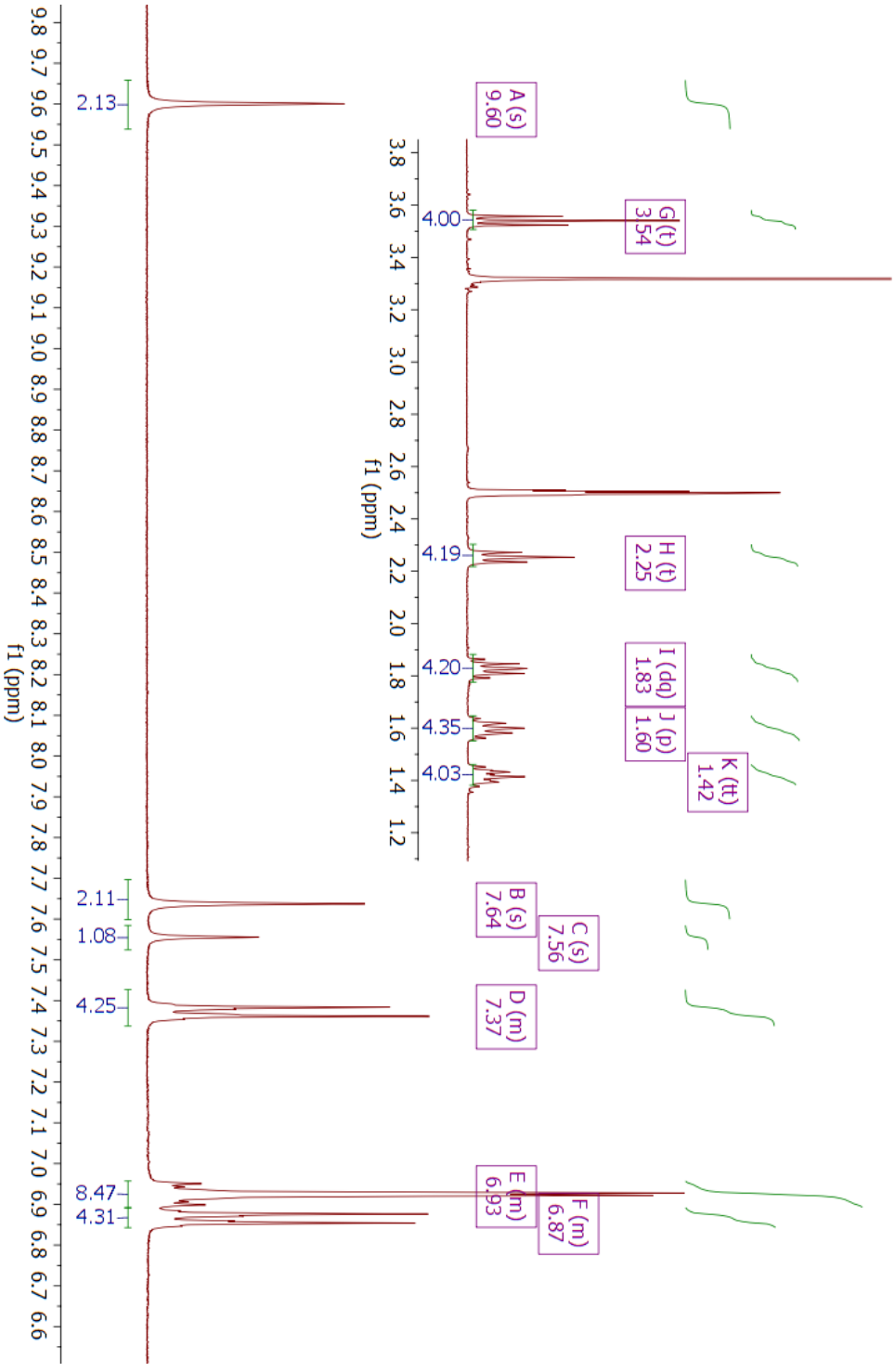

Figure A.39. ***N,N'-(((azanediylbis(4,1-phenylene))bis(azanediyl))bis(4,1-phenylene))bis(6-bromohexanamide) (21) ^{1}H NMR spectrum in DMSO-d_6***

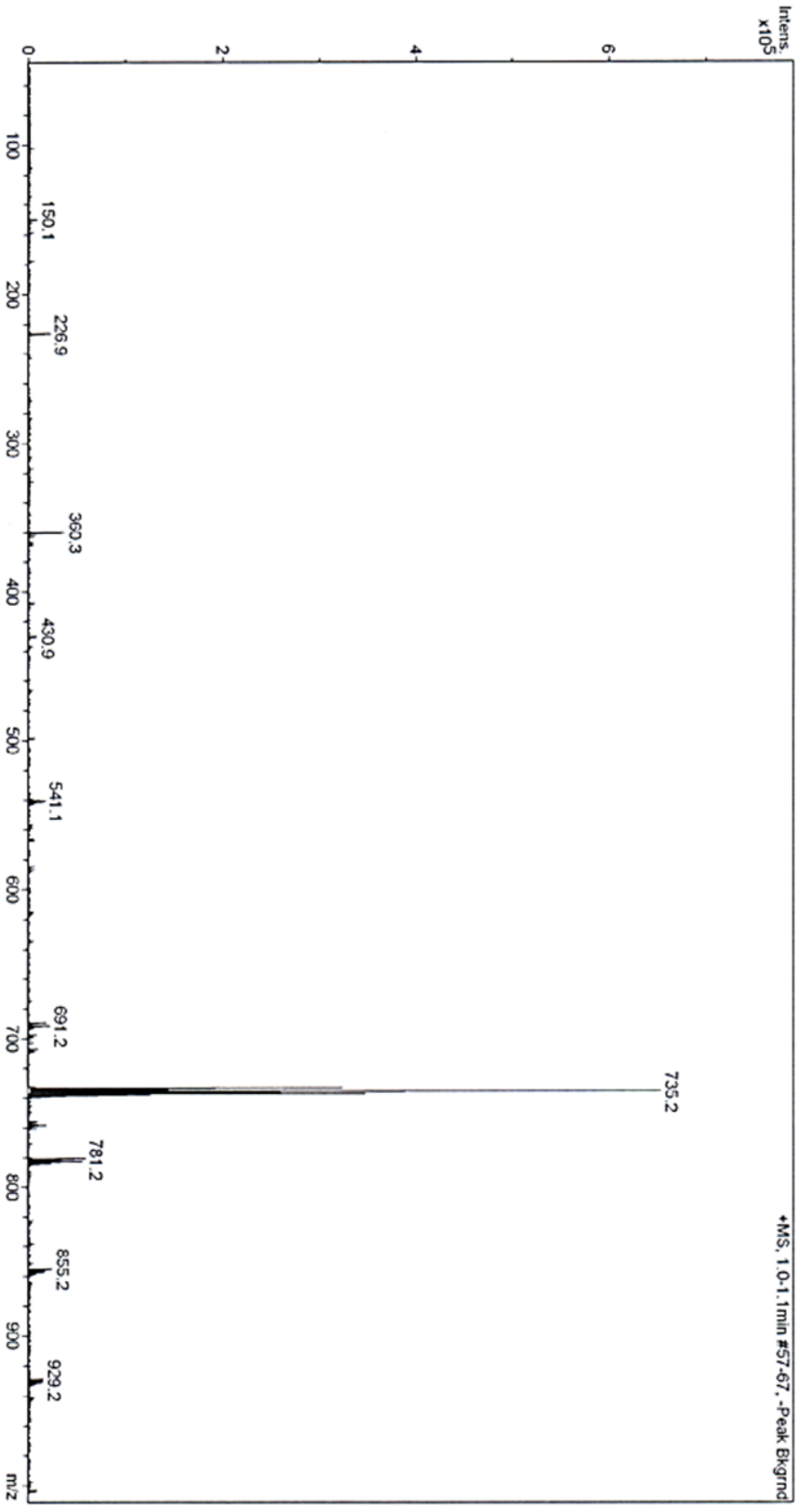

Figure A.40. ***N,N'-(((azanediylbis(4,1-phenylene))bis(azanediyl))bis(4,1-phenylene))bis(6-bromohexanamide) (21) Mass spectrometry***

6-bromo-N-(4-(((1E,4E)-4-((4-((4-(6-bromohexanamido)phenyl)amino)phenyl)imino)cyclohexa-2,5-dien-1-ylidene)amino)phenyl)hexanamide (22)

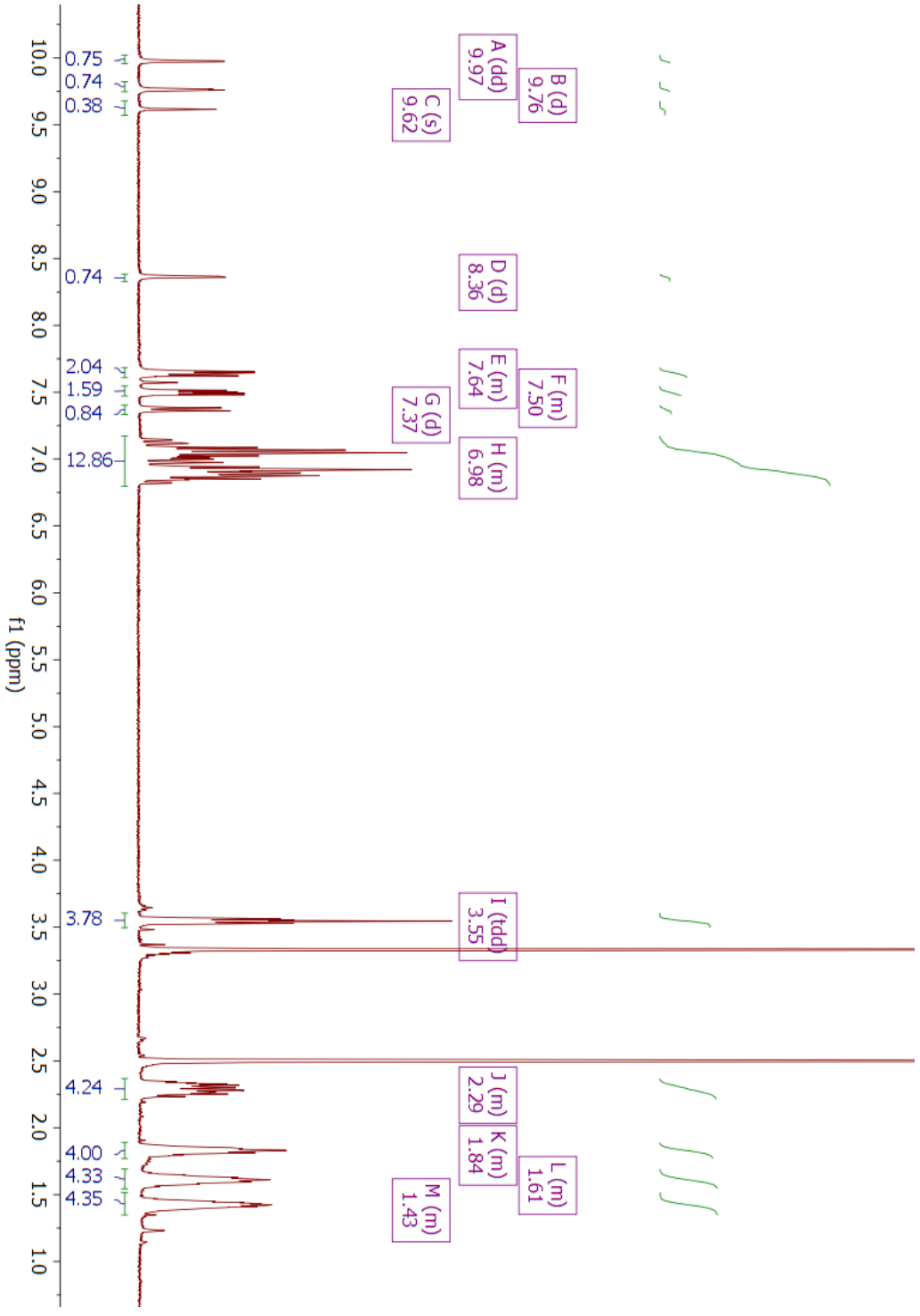

Figure A.41. ***6-bromo-N-(4-(((1E,4E)-4-((4-((4-(6-bromohexanamido)phenyl)amino)phenyl)imino)cyclohexa-2,5-dien-1-ylidene)amino)phenyl)hexanamide (22)*** ***^{1}H NMR spectrum in DMSO-d_6***

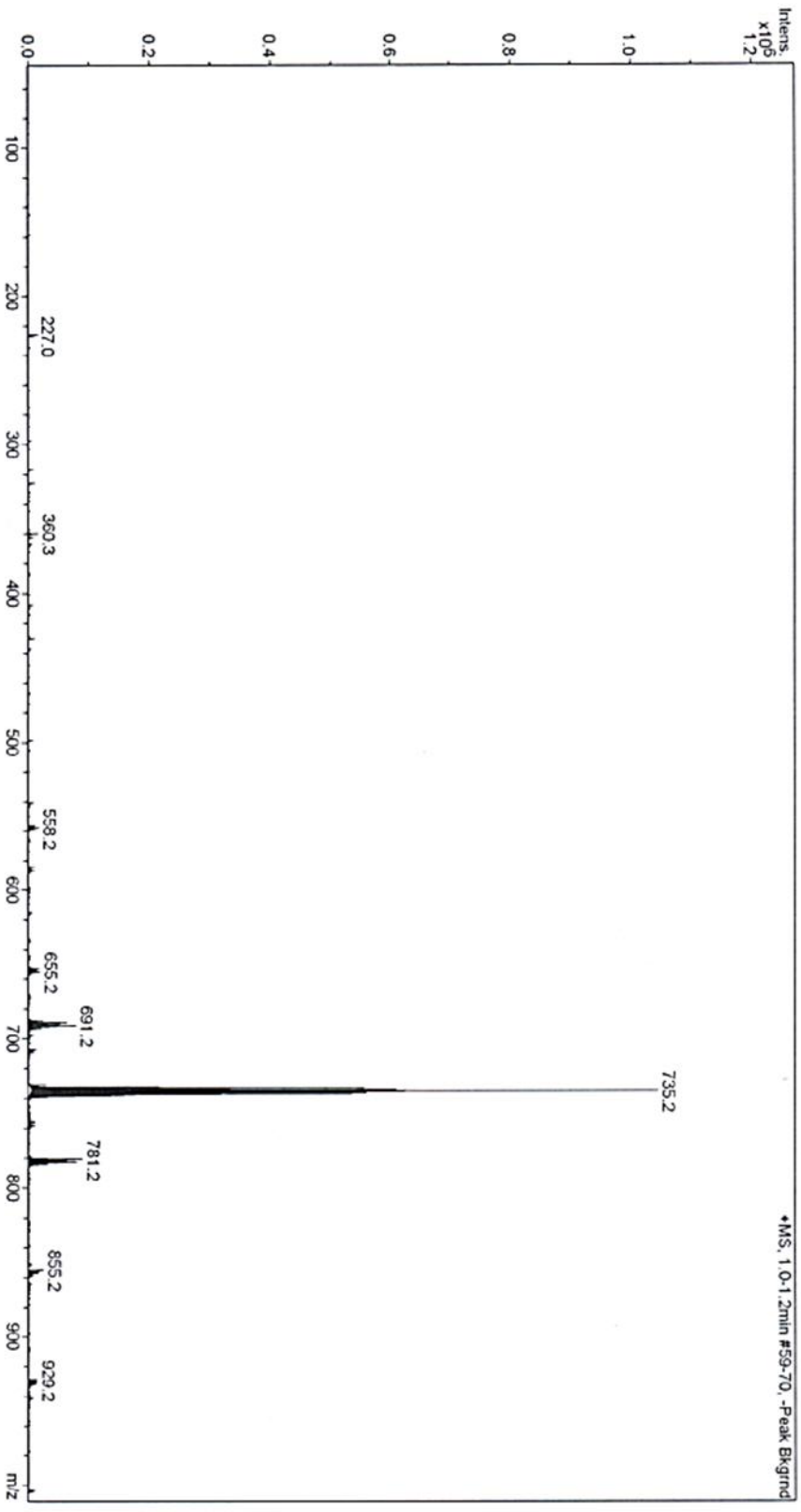

Figure A.42. ***6-bromo-N-(4-(((1E,4E)-4-((4-((4-(6-bromohexanamido)phenyl)amino)phenyl)imino)cyclohexa-2,5-dien-1-ylidene)amino)phenyl)hexanamide (22) Mass spectrometry***

EB TANI-$(PTAB)_2$ (23)

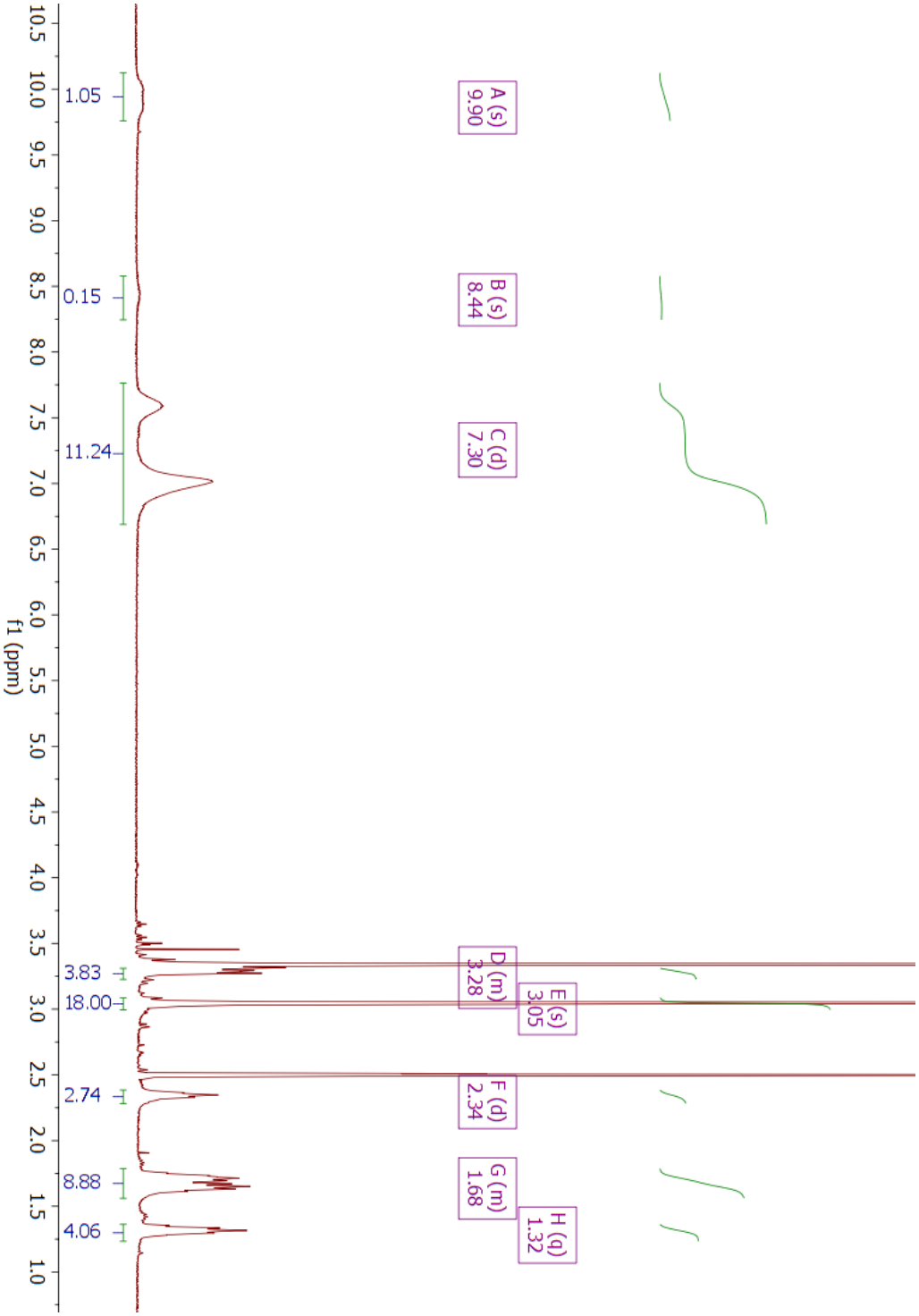

Figure A.43. ***EB TANI-$(PTAB)_2$ (23) ^1H NMR spectrum in DMSO-d_6***

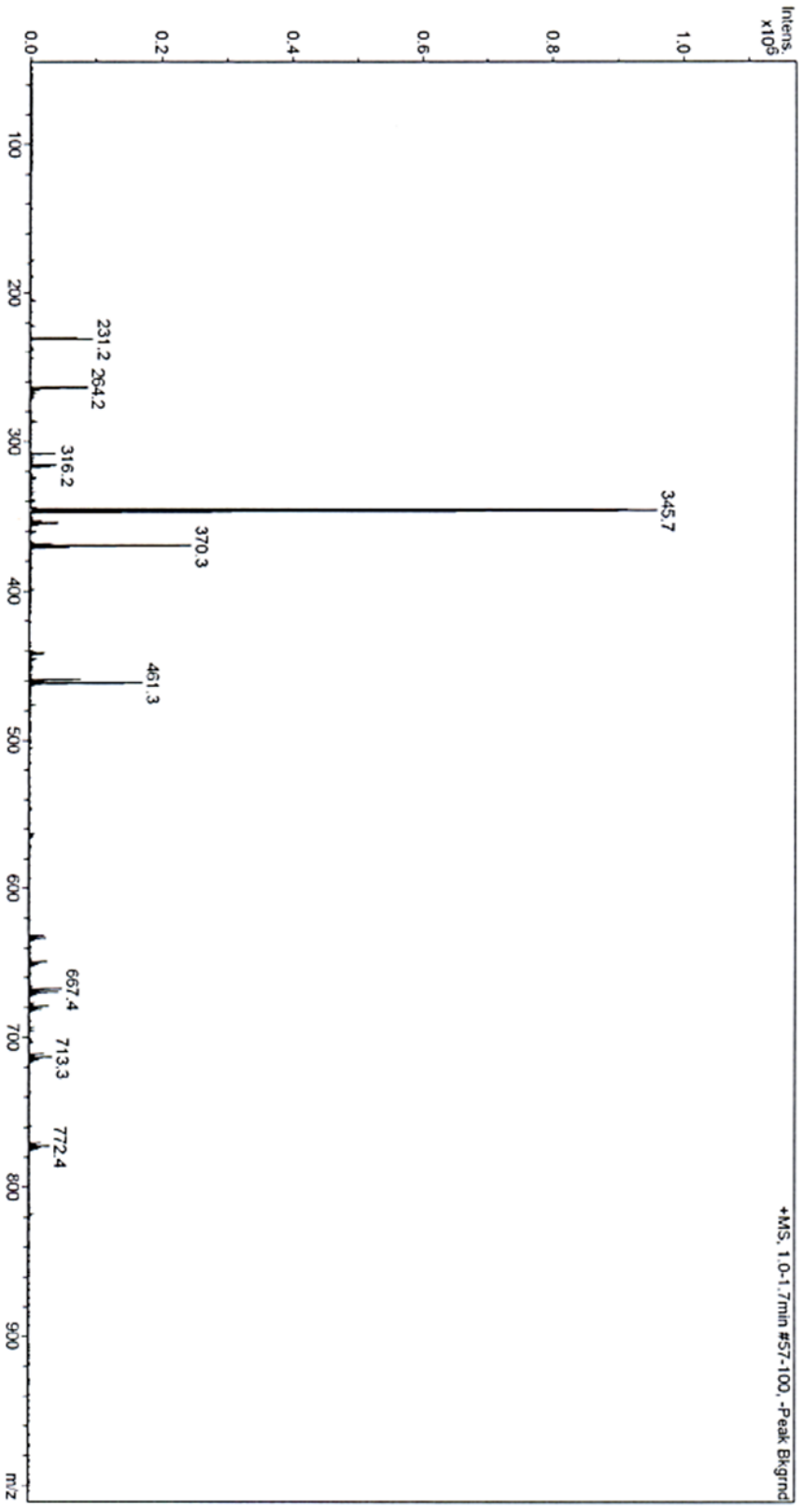

Figure A.44. ***EB TANI-(PTAB)$_2$ (23) Mass spectrometry***

SYNTHESIS OF MA-TANI-PTAB

NH_2-TANI-C_6Br

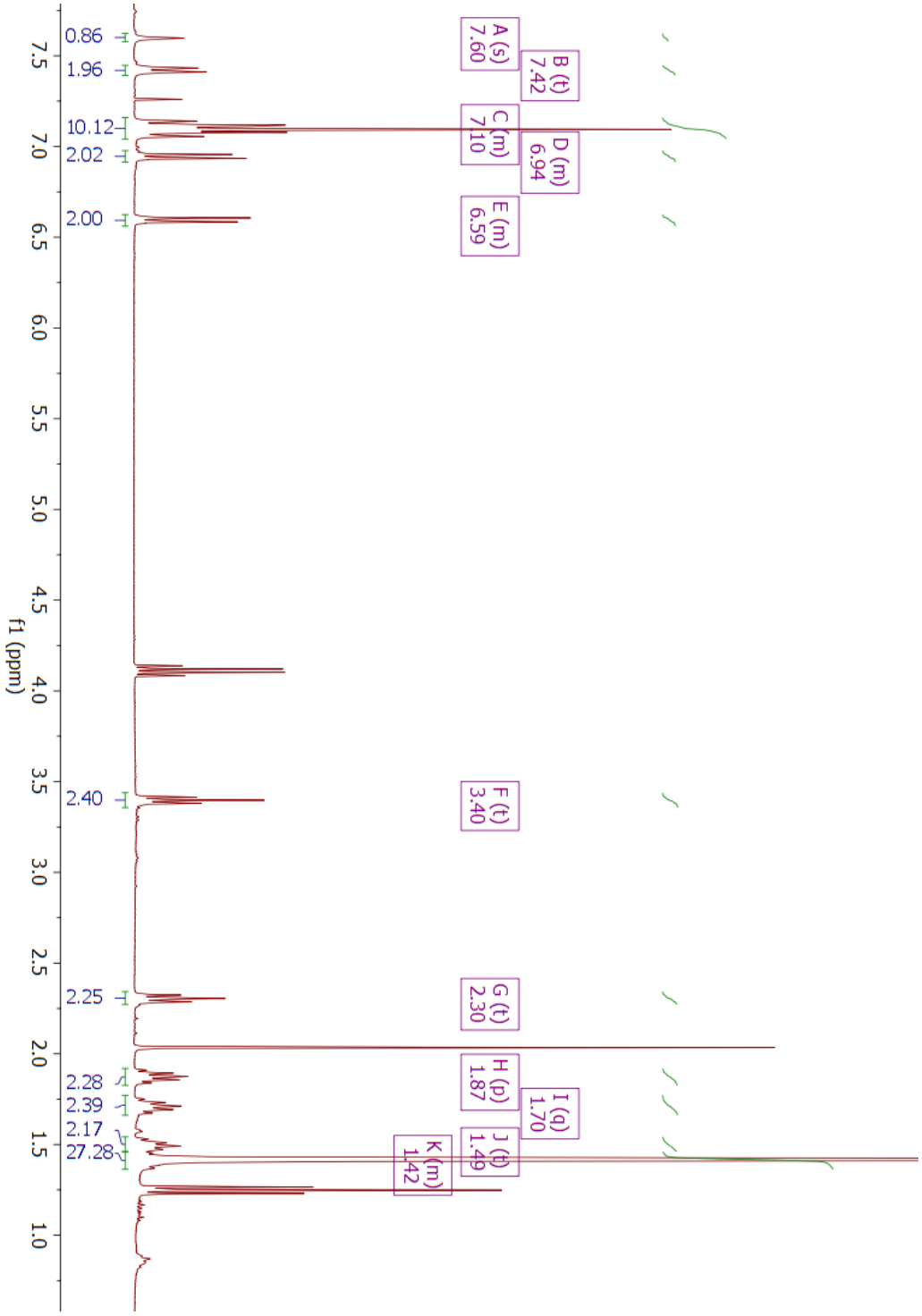

Figure A.45. ***NH_2-TANI-C_6Br (24) ^{1}H NMR spectrum in $CDCl_3$***

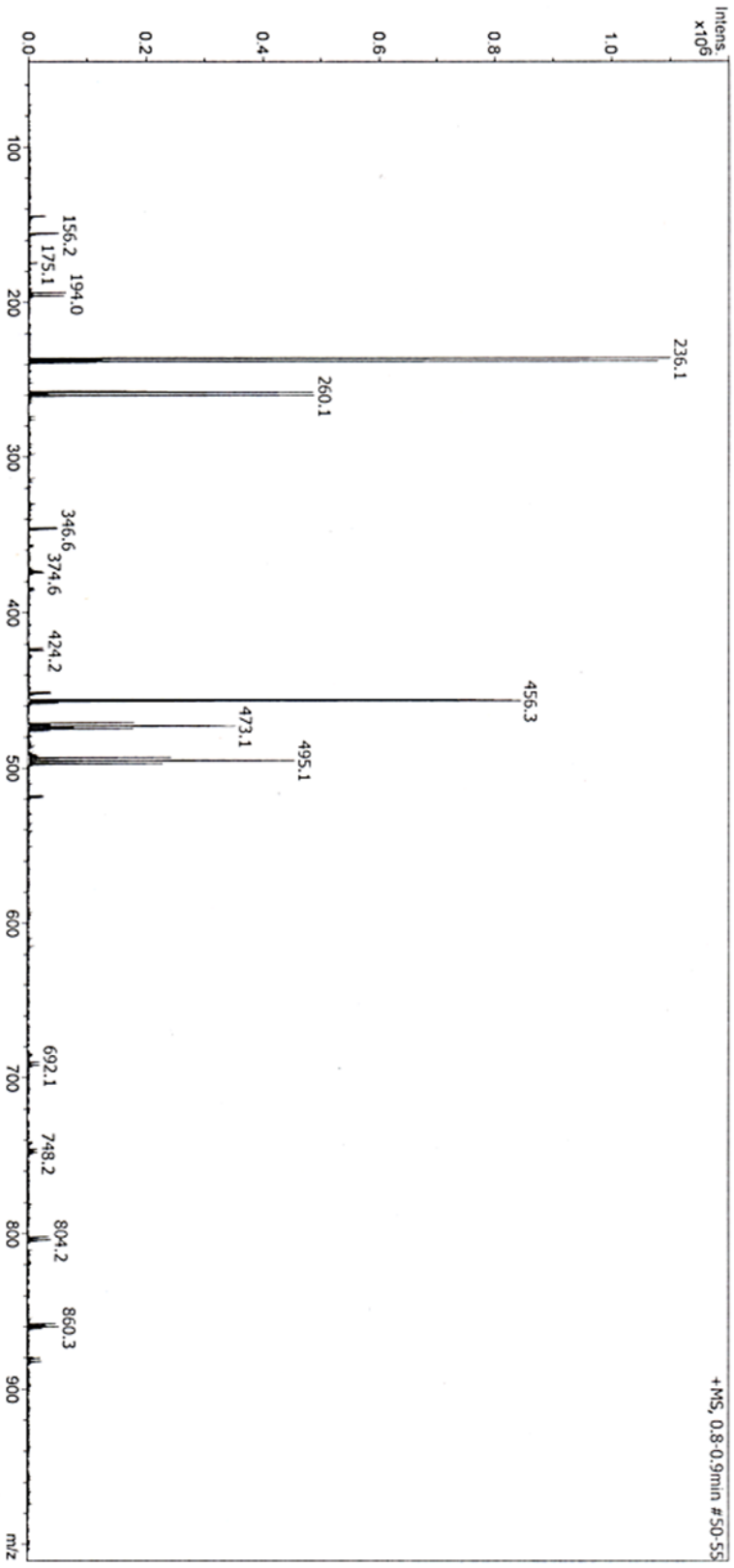

Figure A.46. ***NH_2-TANI-C_6Br (24) Mass spectrometry***

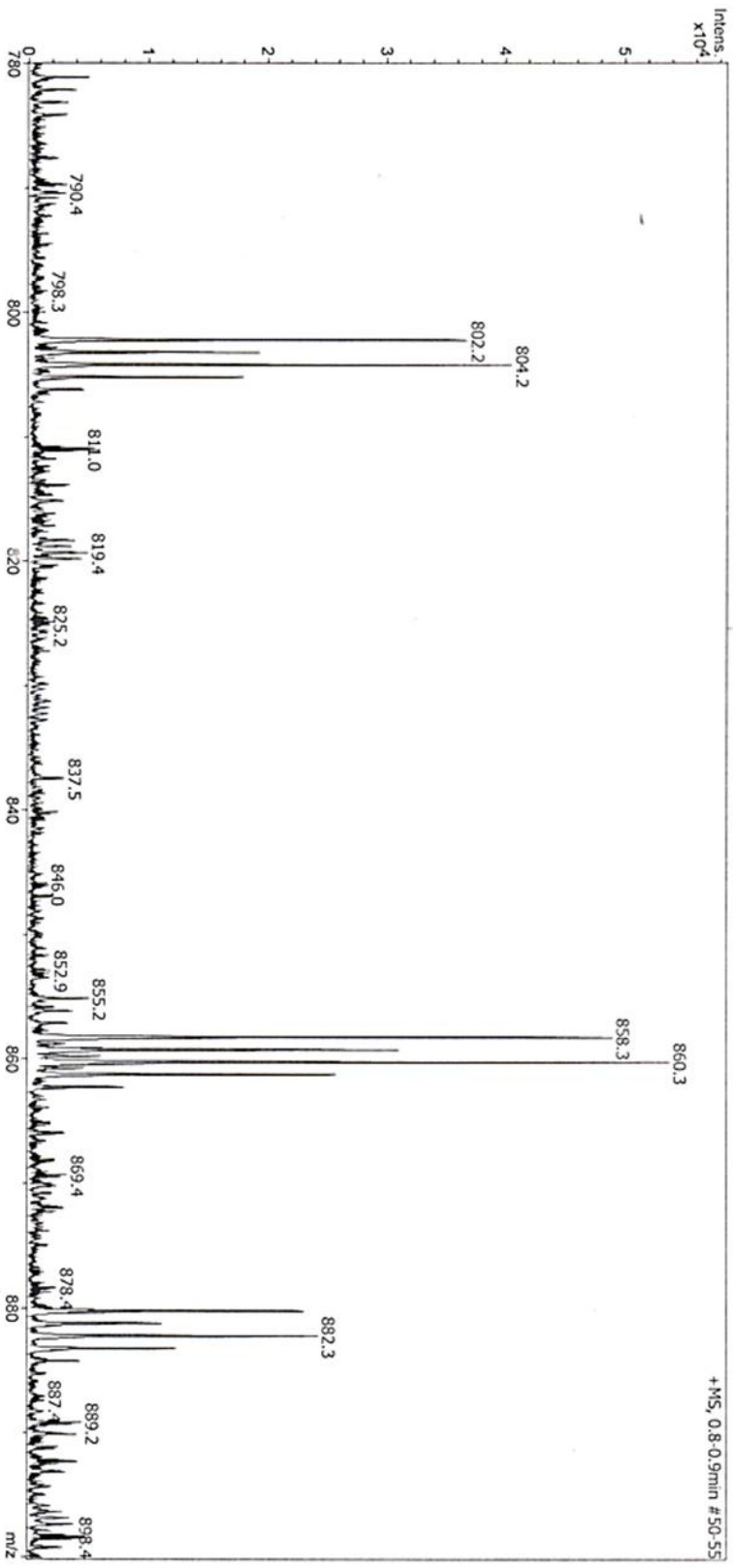

Figure A.47. ***NH₂-TANI-C₆Br (24) Mass spectrometry, expansion***

MA-TANI-C_6Br (25)

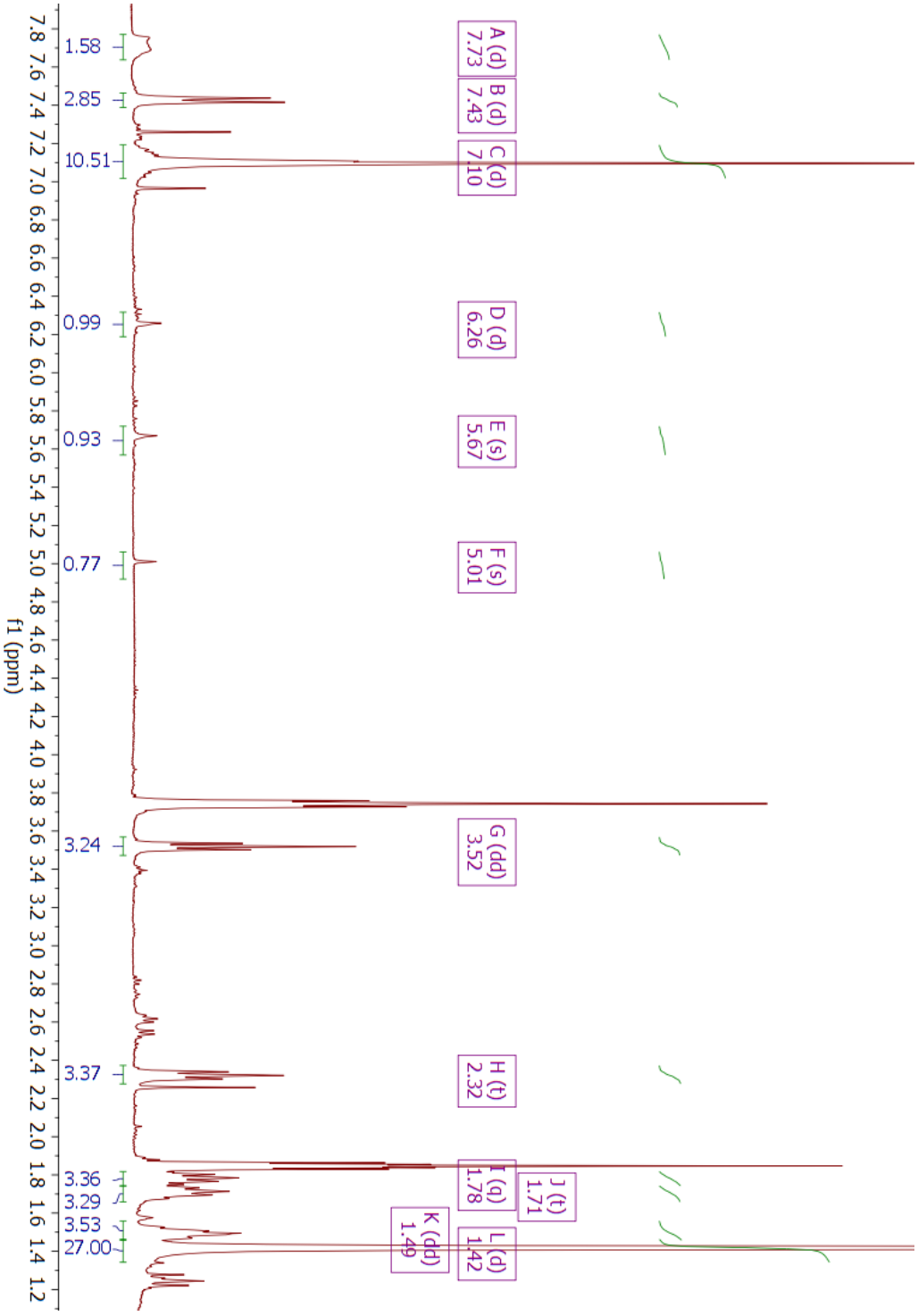

Figure A.48. ***MA-TANI-C_6Br (25) ^1H NMR spectrum in $CDCl_3$***

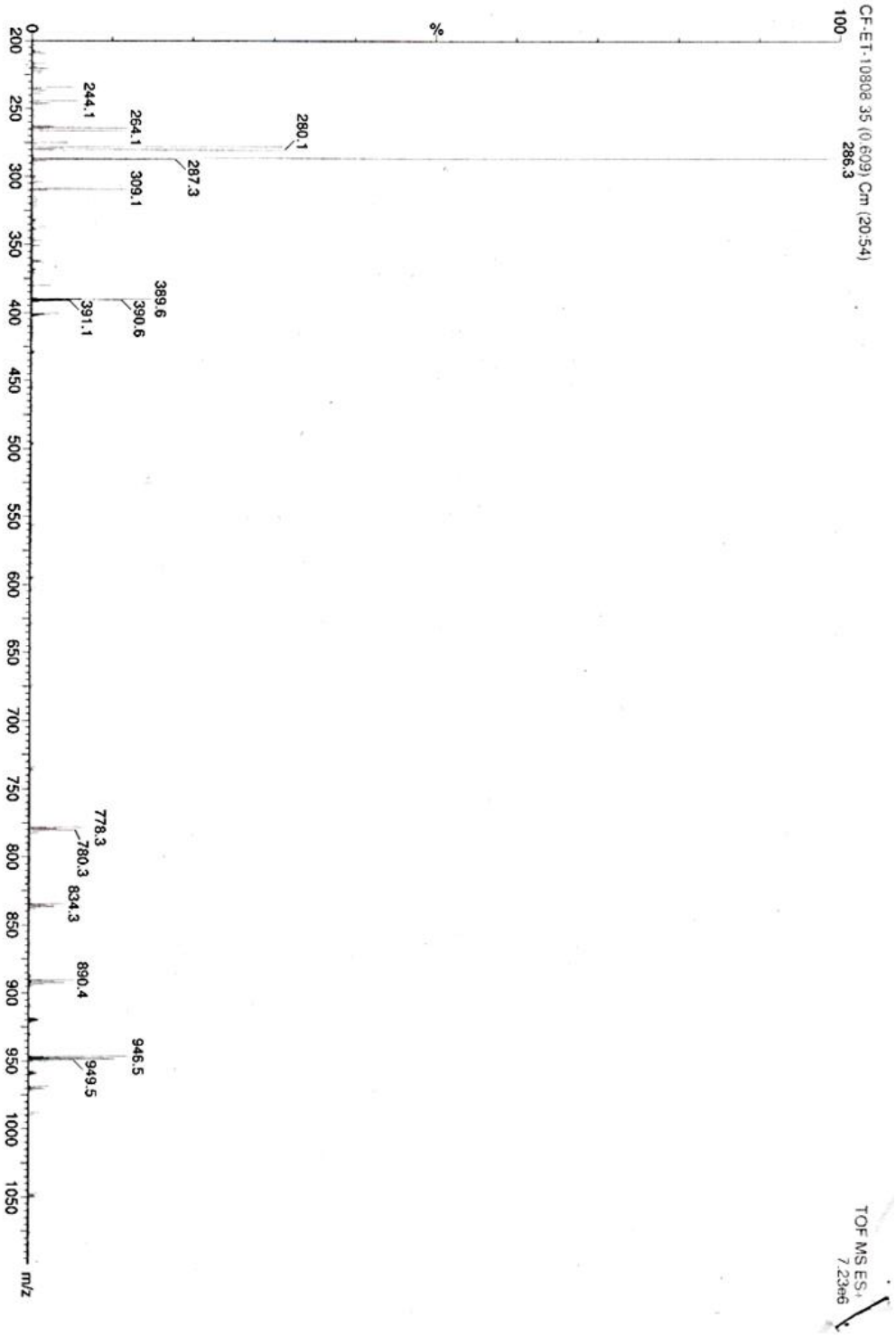

Figure A.49. ***MA-TANI-C₆Br (25) Mass spectrometry***

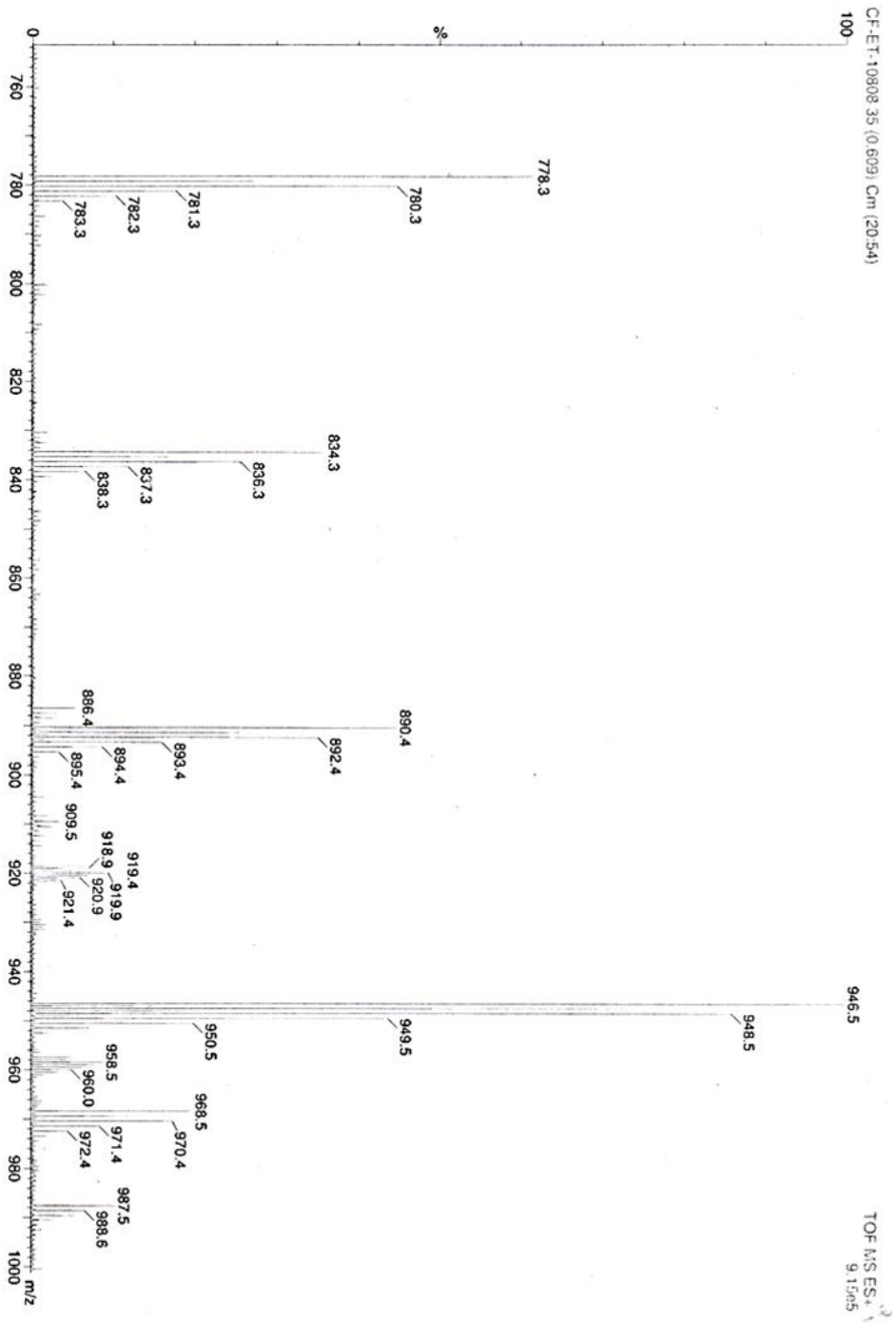

Figure A.50. ***MA-TANI-C_6Br (25) Mass spectrometry, expansion***

MA-TANI-NH_2 (26)

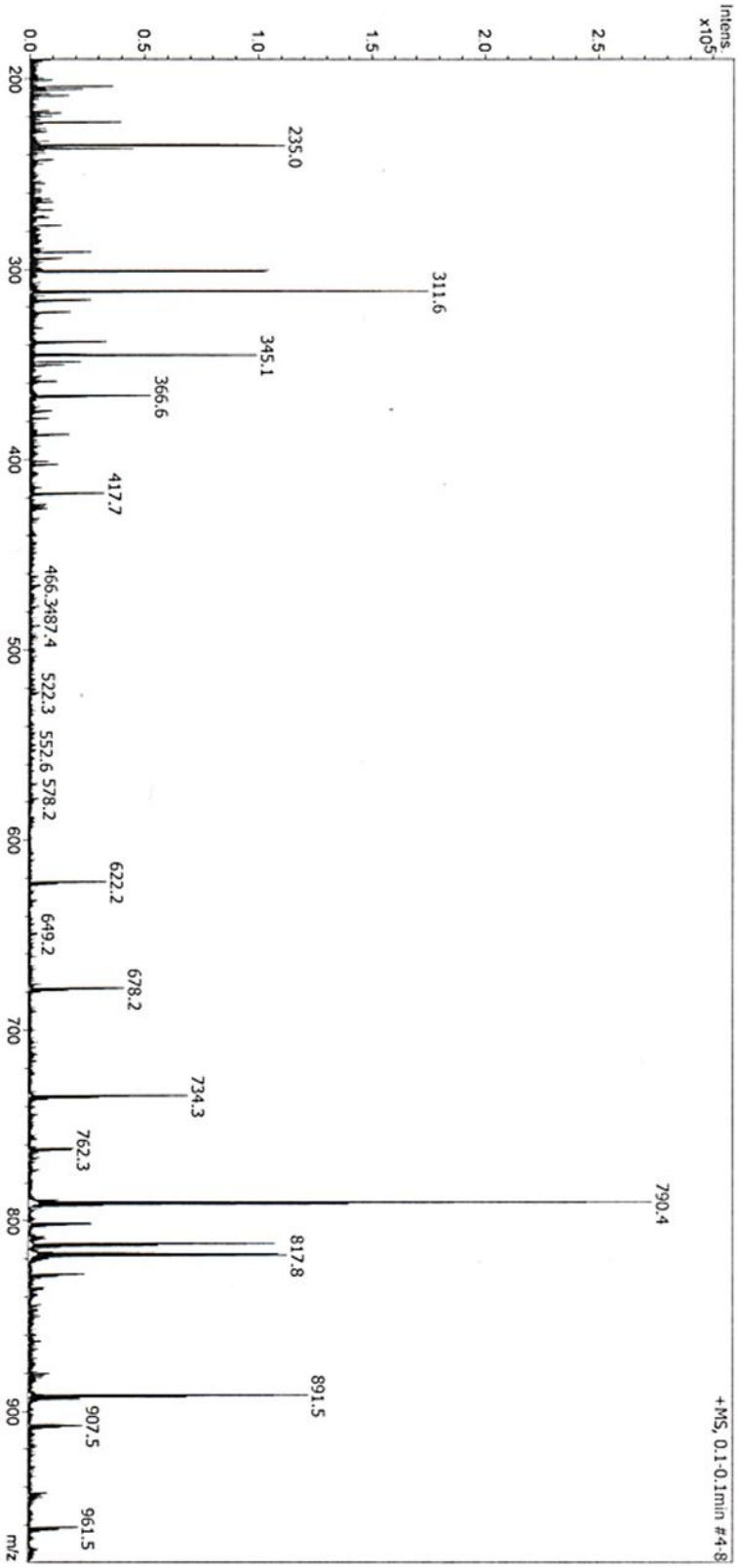

Figure A.51. ***MA-TANI-NH_2 (26) Mass spectrometry***

NH_2/CPh_2 TANI (28)

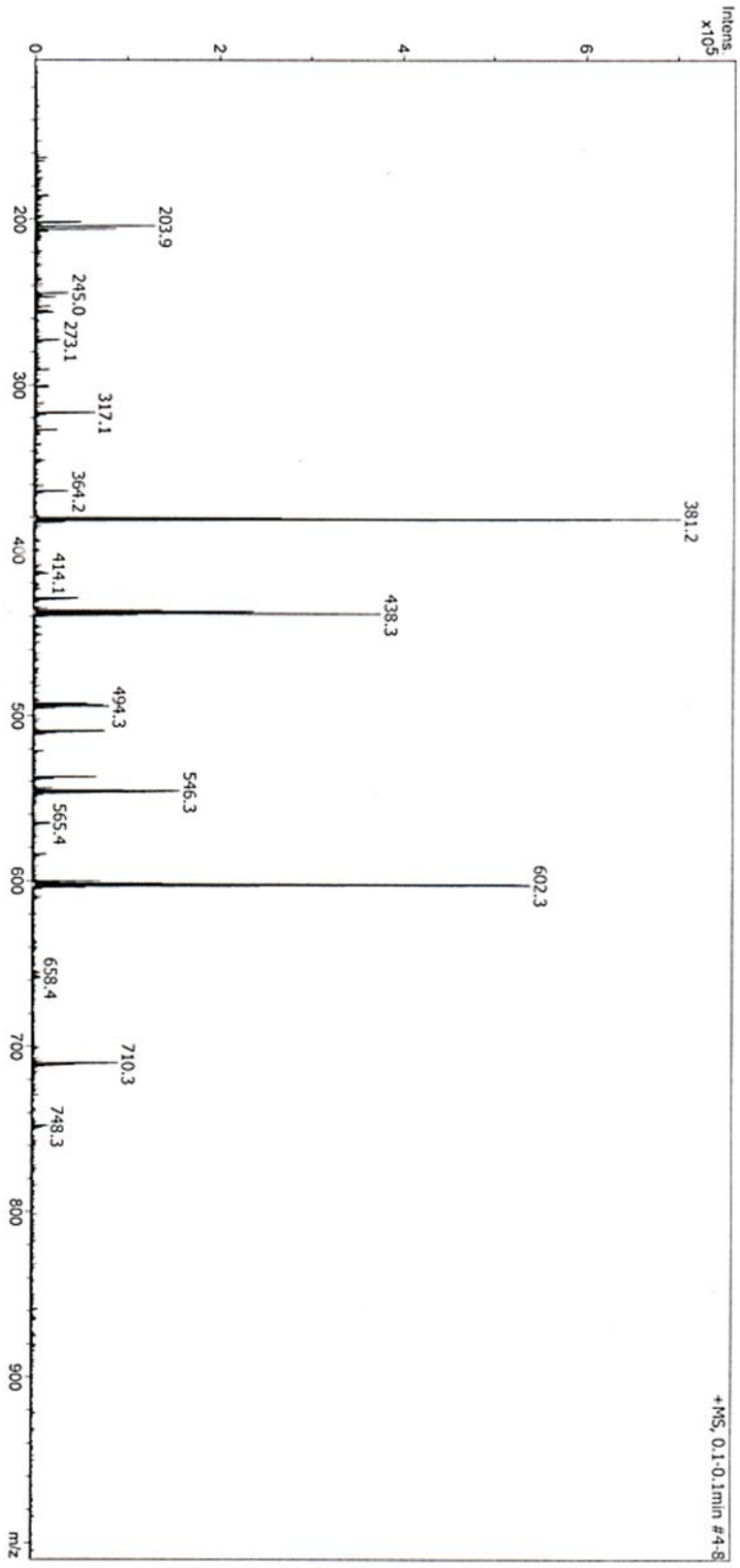

Figure A.52. ***NH_2/CPh_2 TANI (28) Mass spectrometry***

Activated molecular sieves, 110 °C, 48 hrs

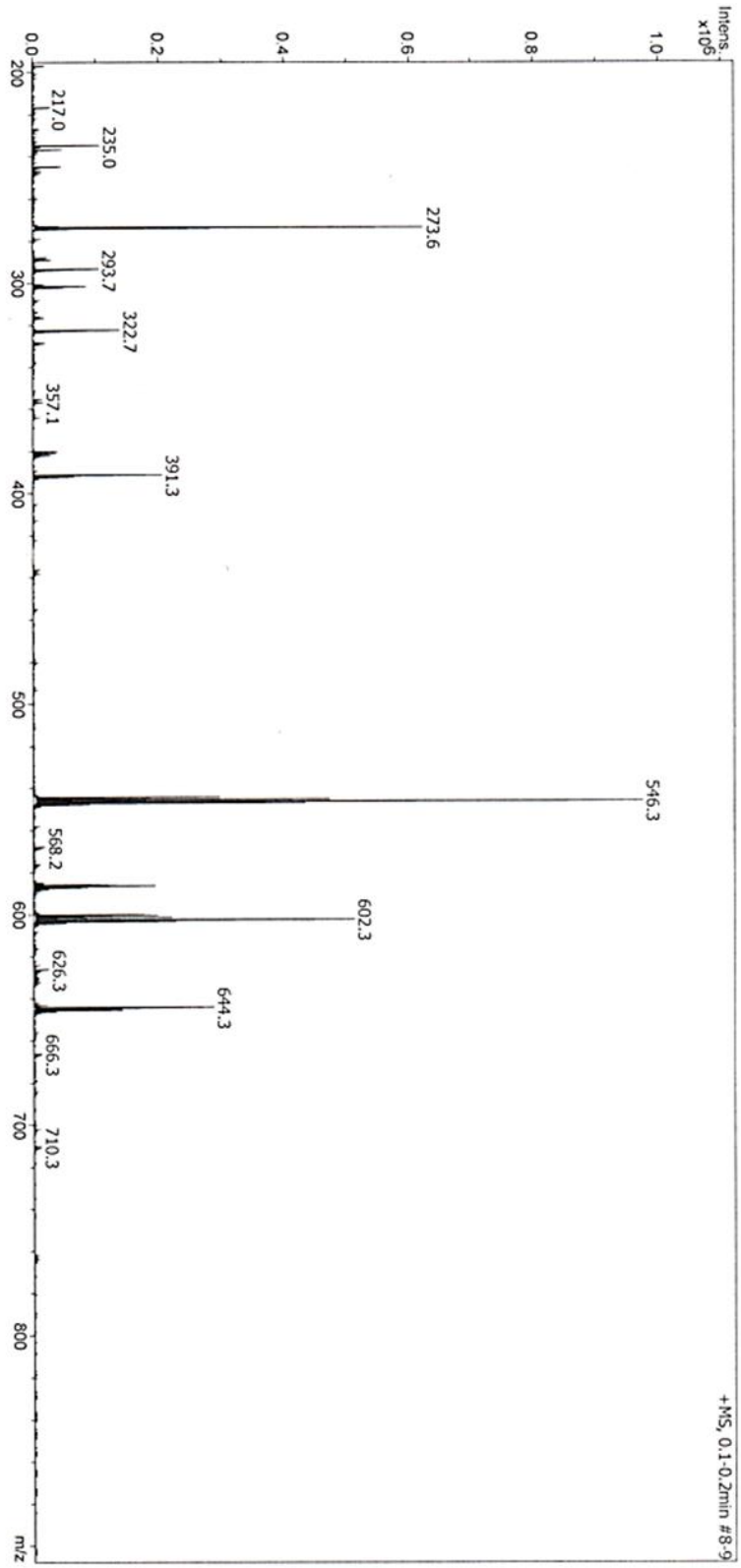

Figure A.53. ***NH_2/CPh_2 TANI (28) Mass spectrometry***

Activated molecular sieves, 70 °C, 24 hrs

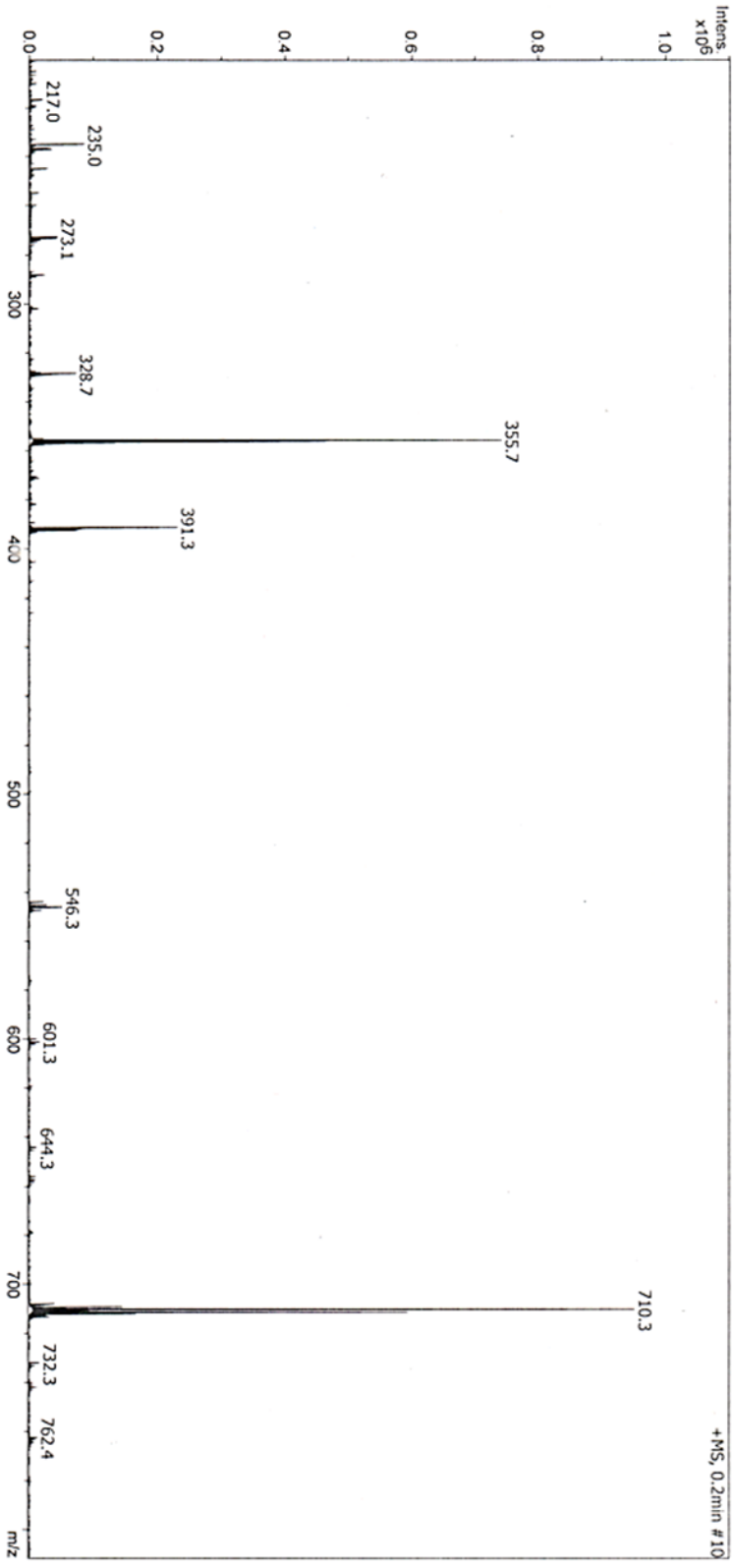

Figure A.54. ***NH_2/CPh_2 TANI (29) Mass spectrometry***

Activated molecular sieves, 70 °C, 24 hrs

MA-C_6-TANI-C_6-Br (30)

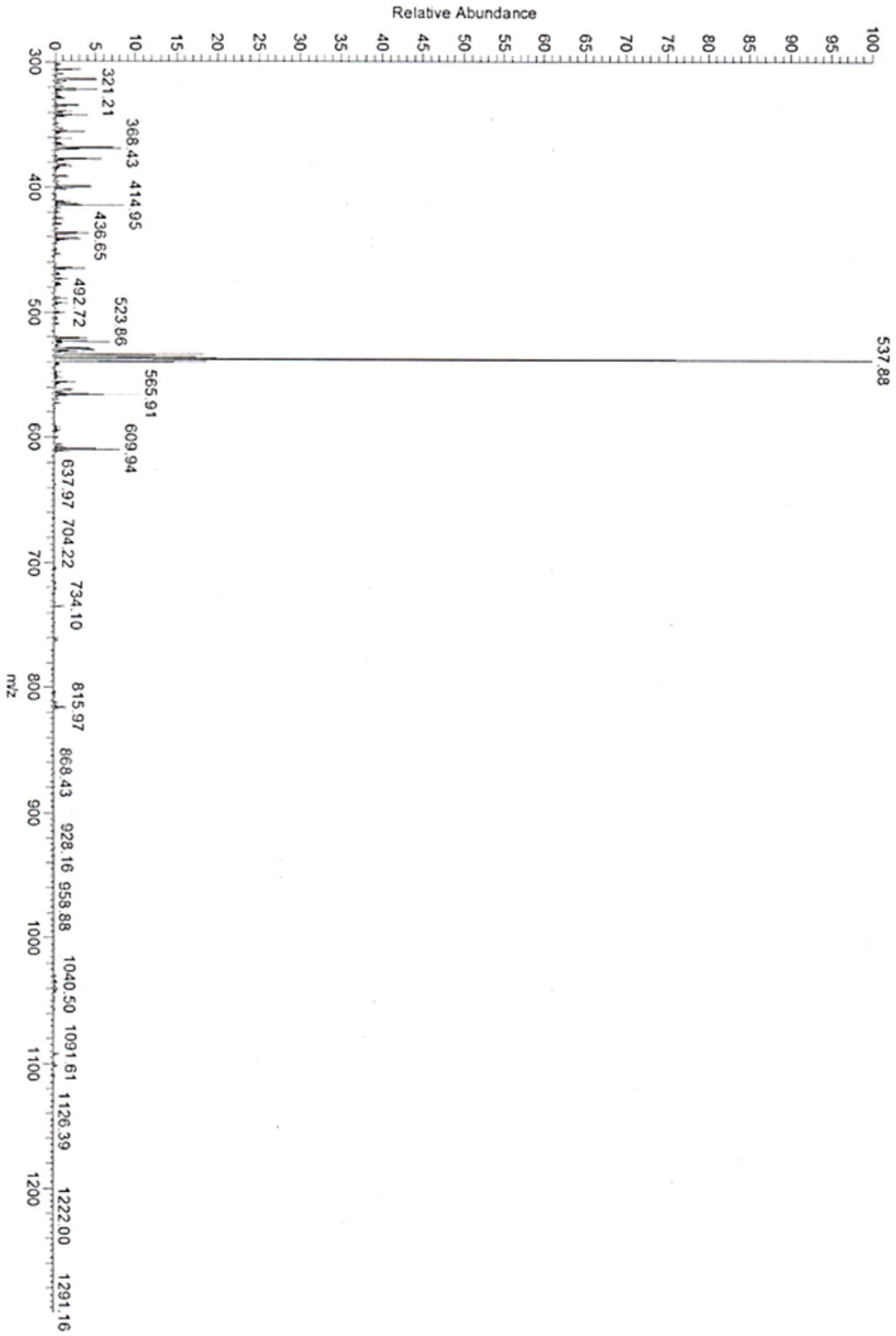

Figure A.55. ***MA-C_6-TANI-C_6-Br (30) Mass spectrometry***

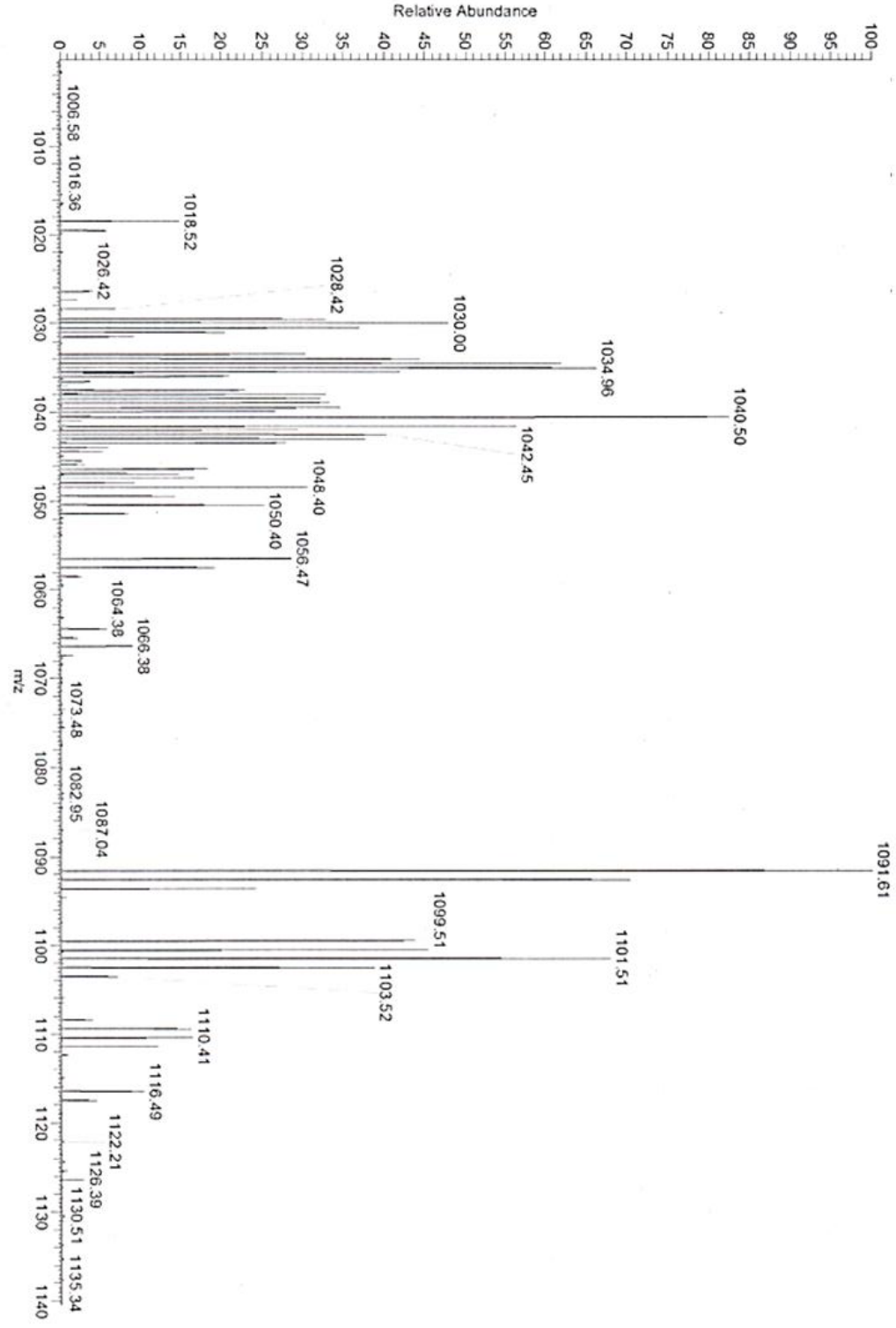

Figure A.56. ***MA-C6-TANI-C6-Br (30) Mass spectrometry, expansion***

Br-TANI-CPh$_2$ (32)

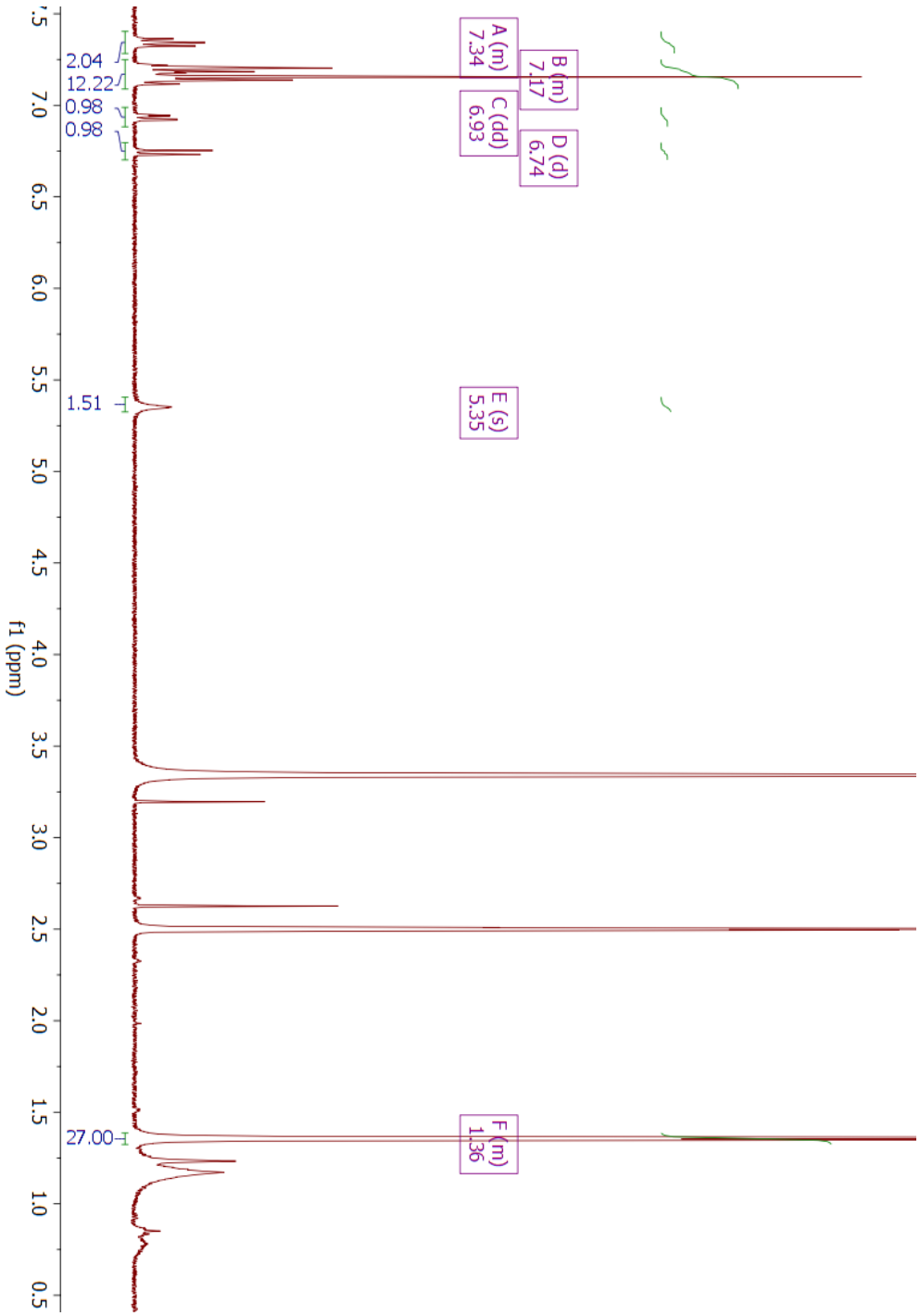

Figure A.57. ***Br-TANI-NH$_2$ (32) ^{1}H NMR spectrum in DMSO-d$_6$***

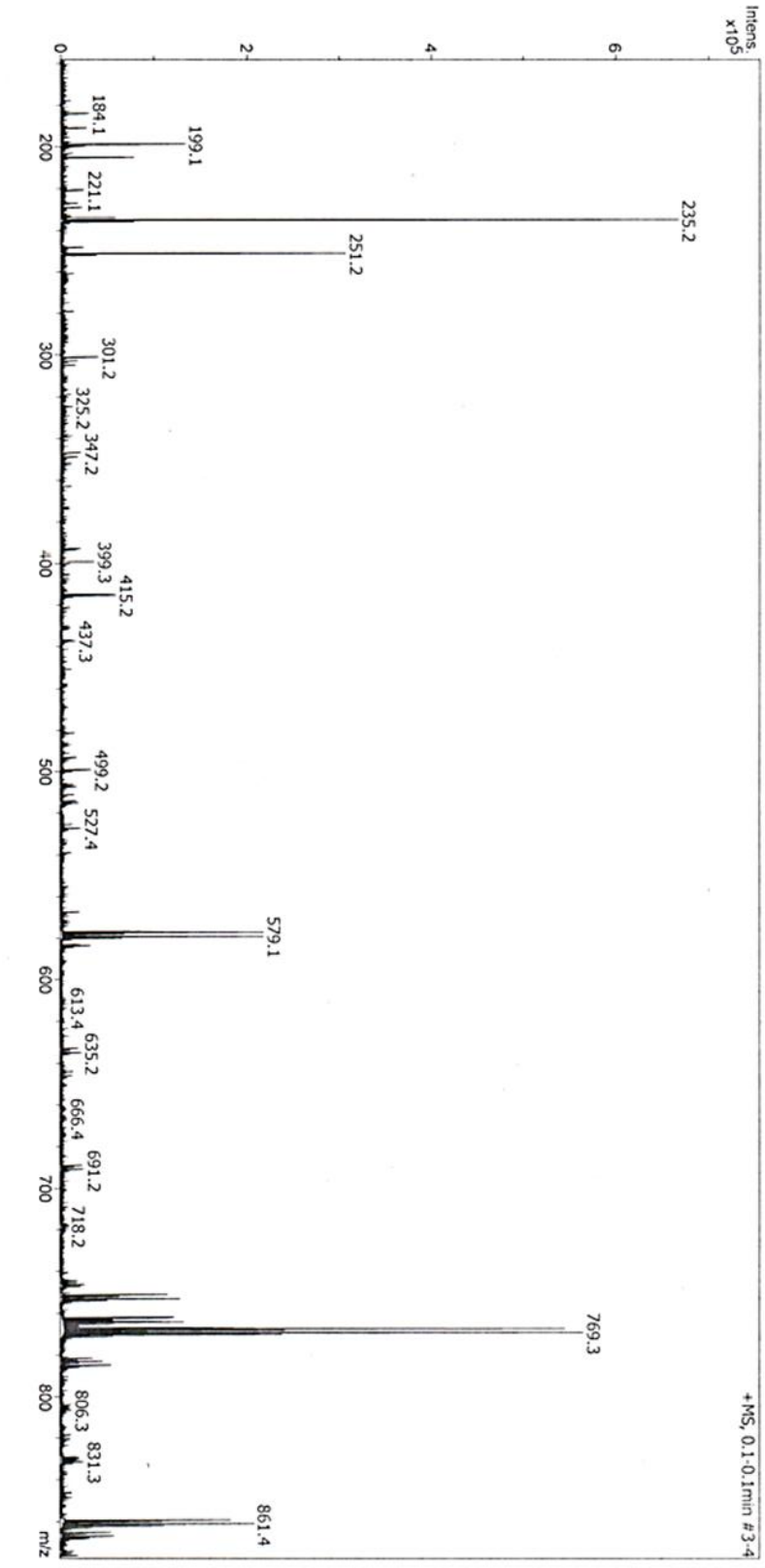

Figure A.58. ***Br-TANI-NH₂ (32) Mass spectrometry***

SYNTHESIS OF MA-11-2-TANI-PTAB

11-Bromoundecylmethacrylate (34)

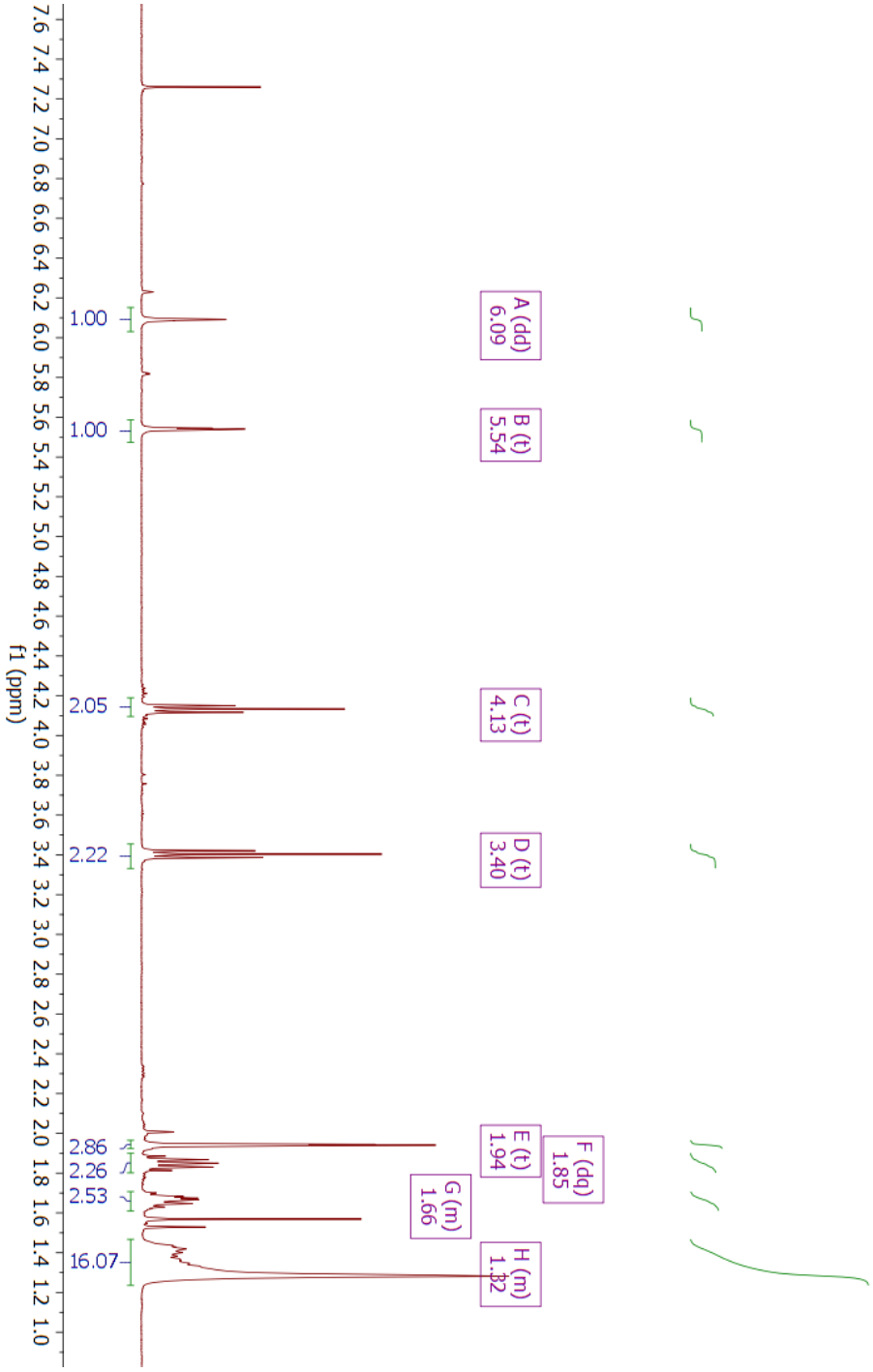

Figure A.59. ***11-Bromoundecylmethacrylate (34)*** ^{1}***H NMR spectrum in*** $CDCl_3$

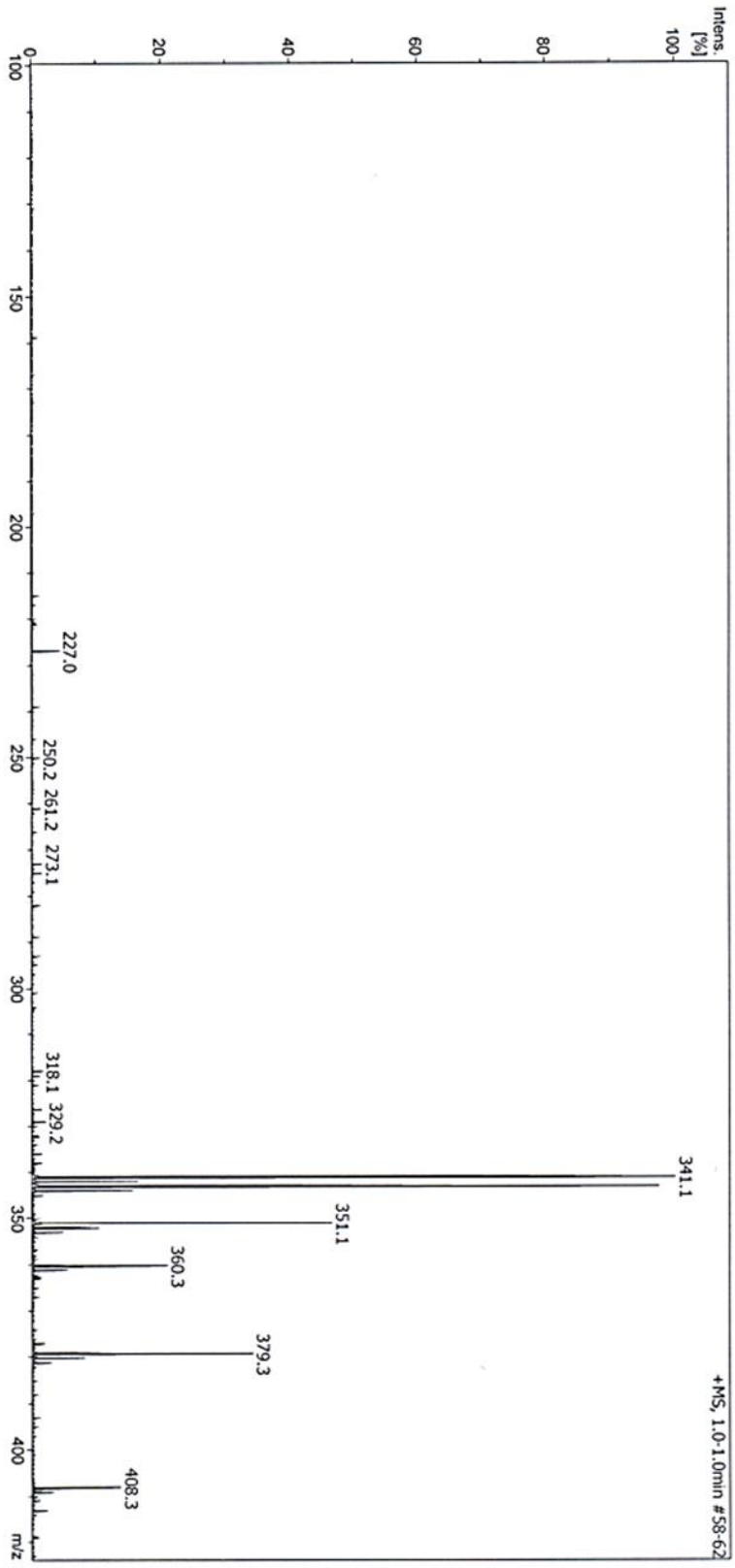

Figure A.60. ***11-Bromoundecylmethacrylate (34) Mass spectrometry***

MA-11-2 (35)

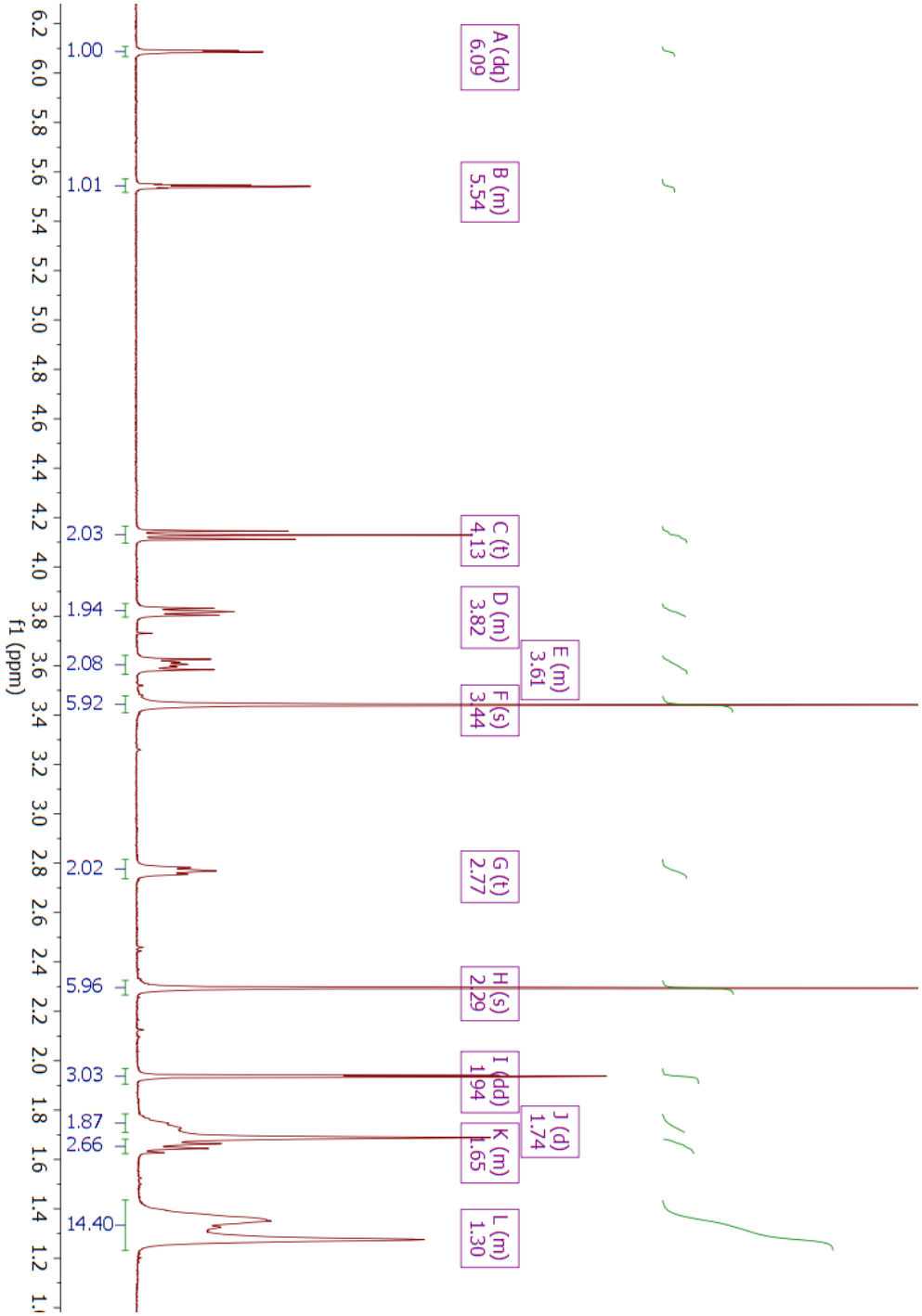

Figure A.61. ***MA-11-2 (35)*** ^{1}***H NMR spectrum in CDCl***$_3$

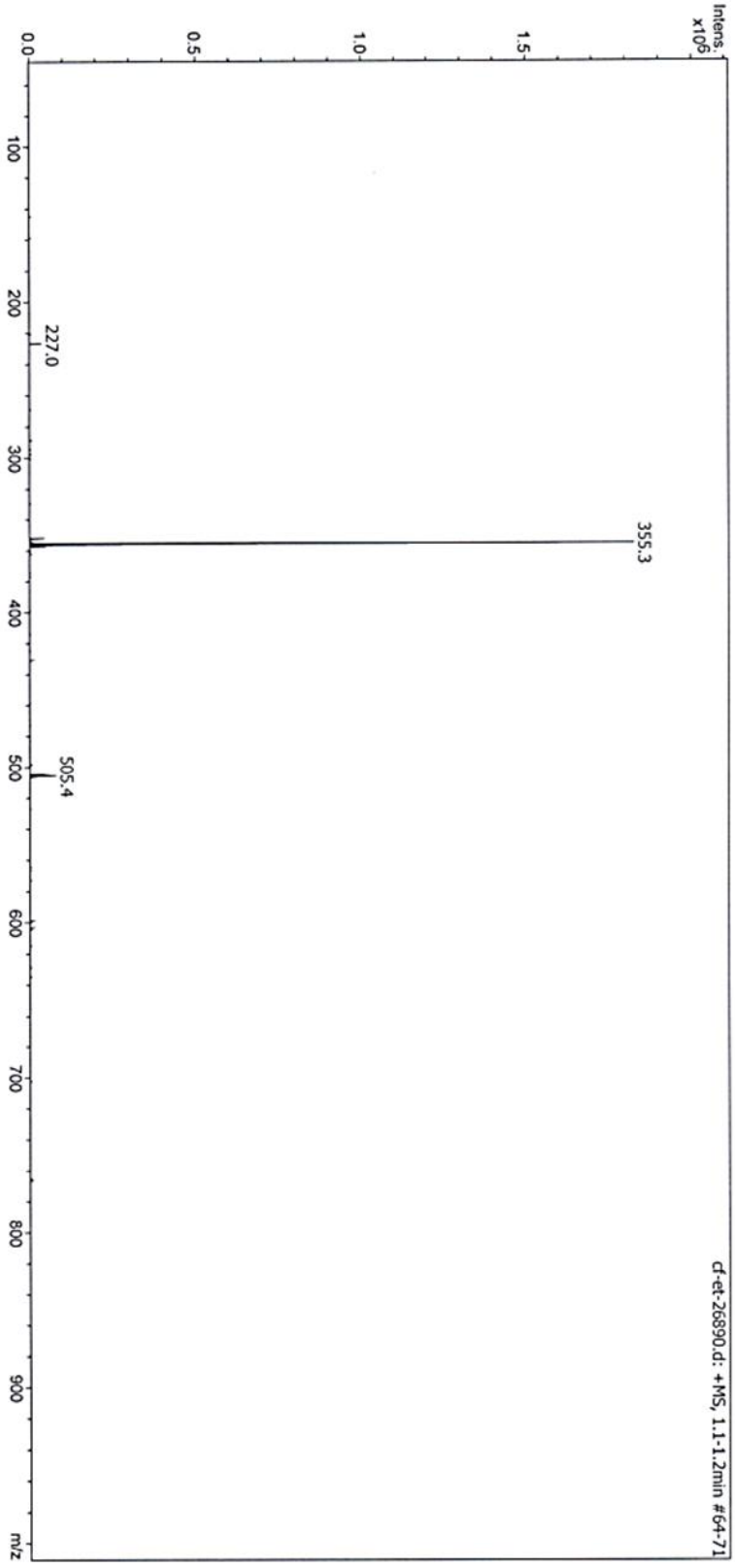

Figure A.62. ***MA-11-2 (35) Mass spectrometry***

SYNTHESIS OF MA-11-2-11-MA

MA-11-2-11-MA (36)

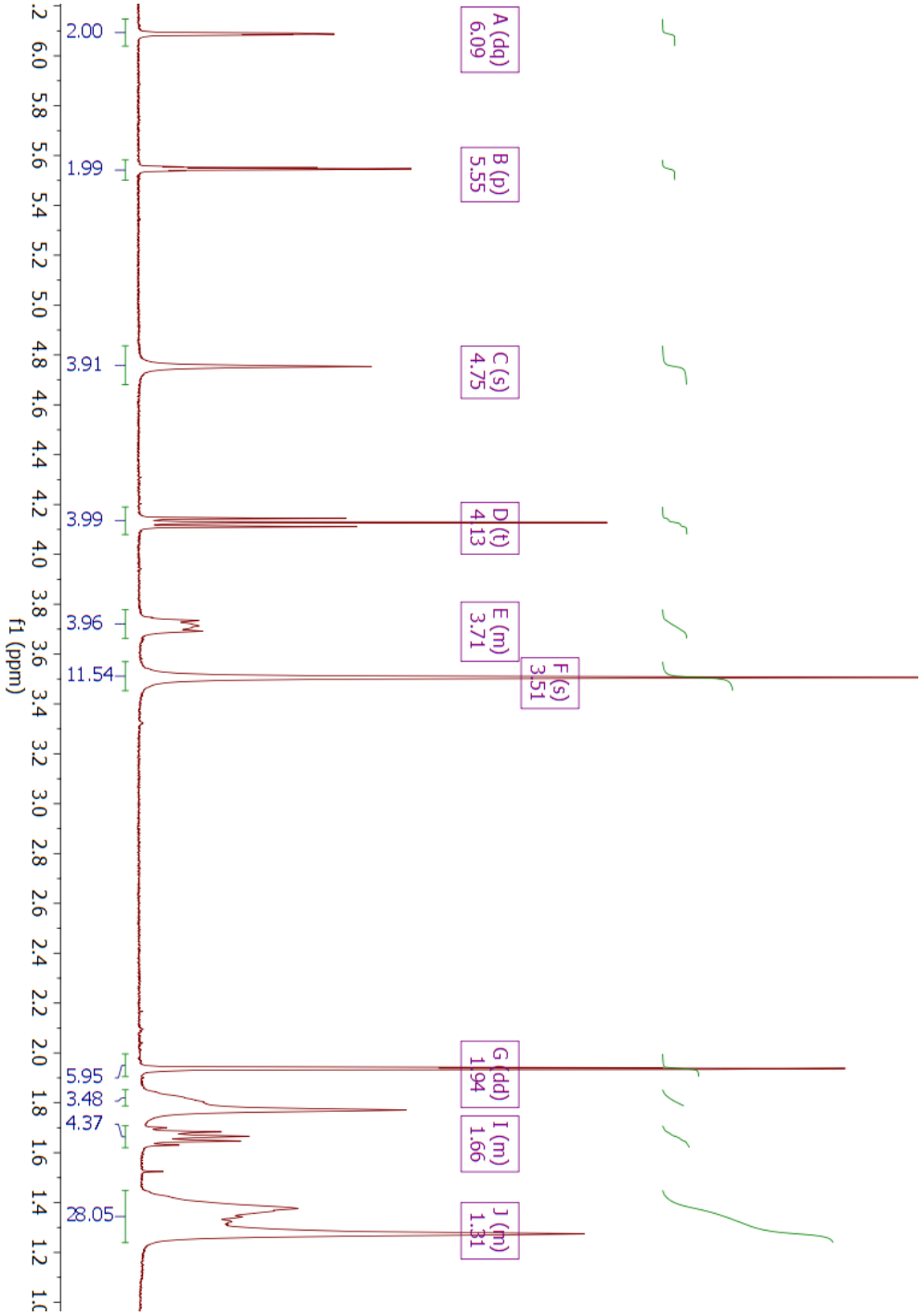

Figure A.63. ***MA-11-2-11-MA (36) ^{1}H NMR spectrum in $CDCl_3$***

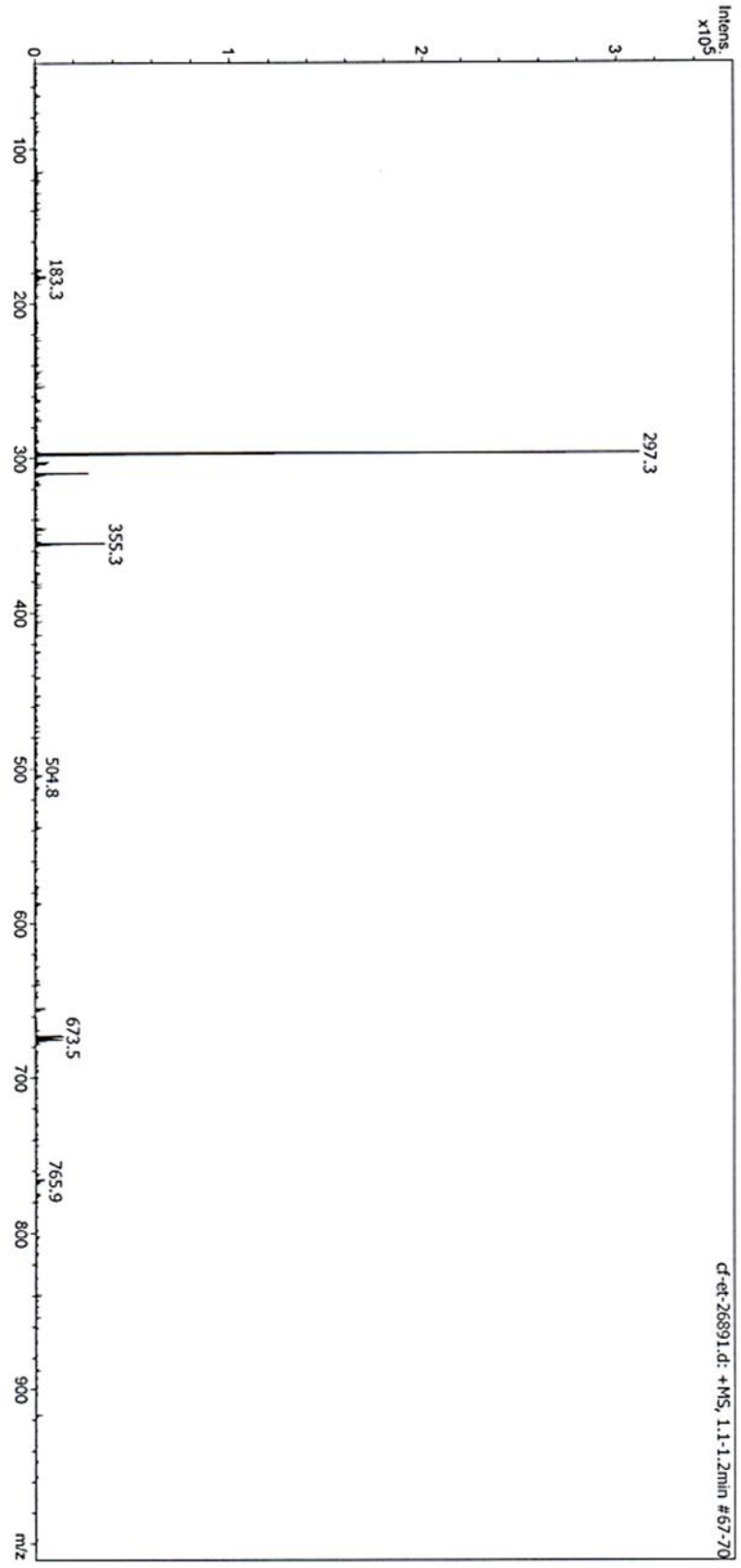

Figure A.64. ***MA-11-2-11-MA (36) Mass spectrometry***

Boc-MA-11-2-TANI-PTAB (38)

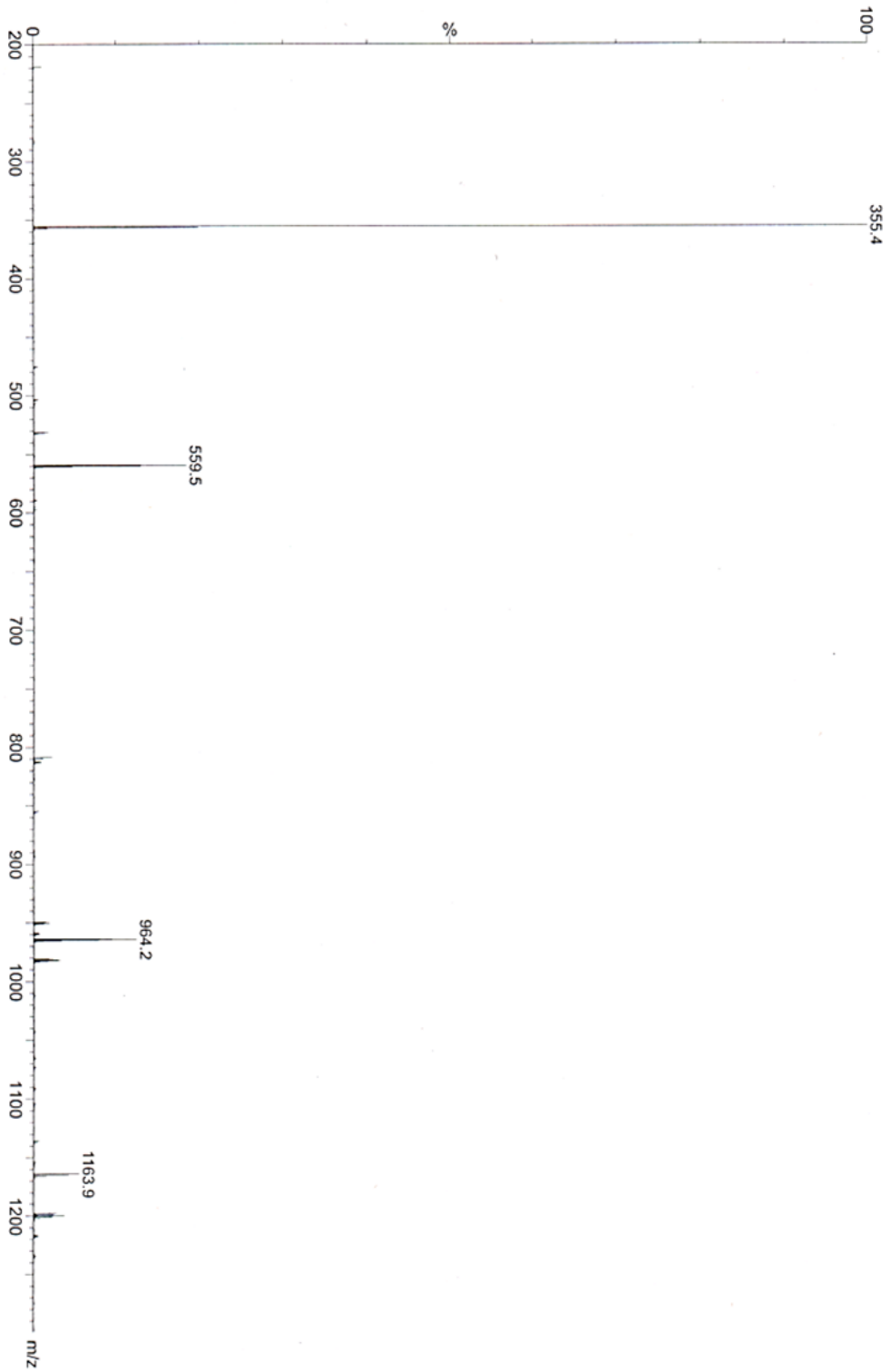

Figure A.65. ***Boc-MA-11-2-TANI-PTAB (38) Mass spectrometry***

Reaction of 7 and 35

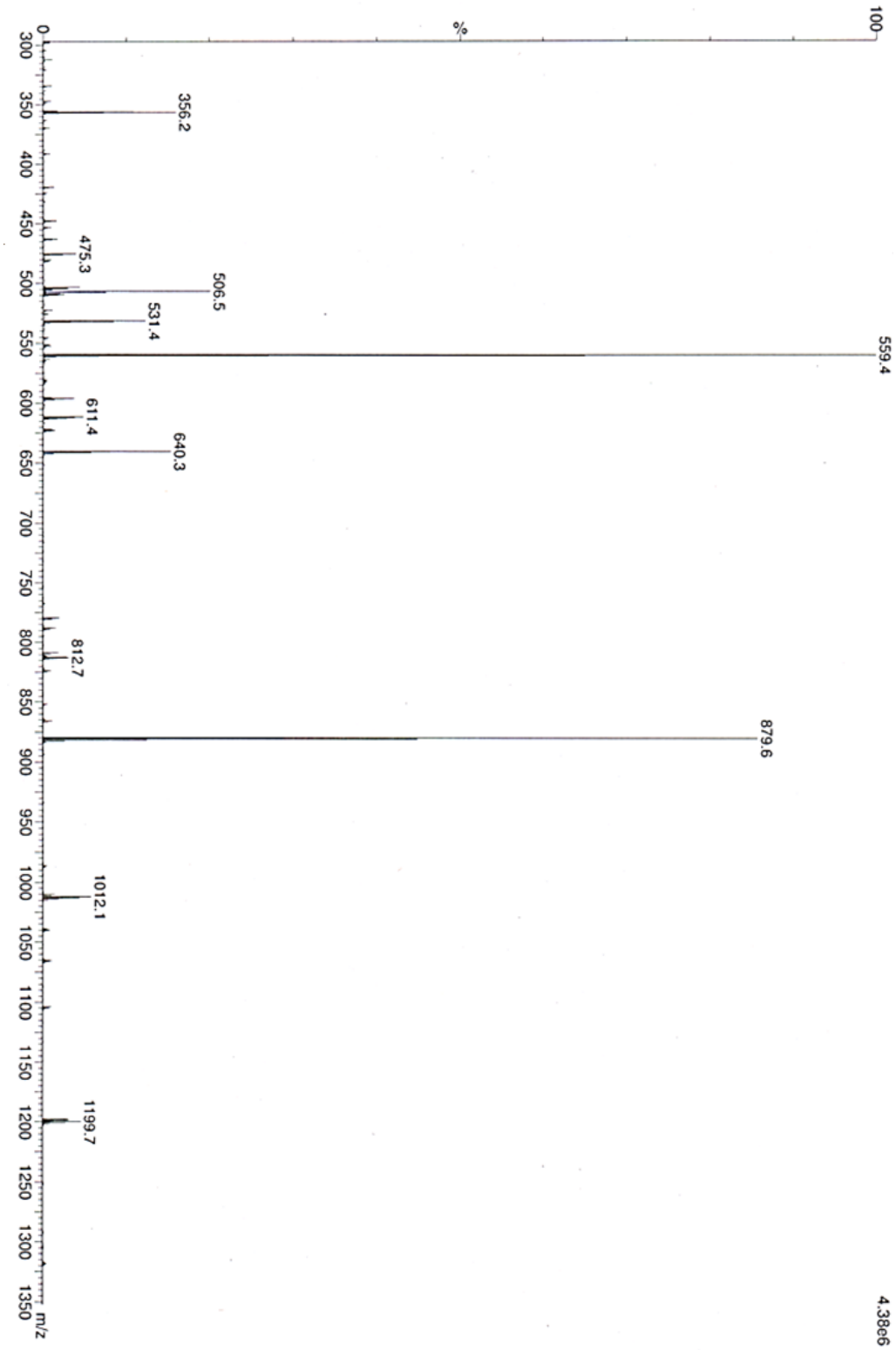

Figure A.66. ***Boc-MA-11-2-TANI-PTAB (38) Mass spectrometry***

Reaction of 39 and 34

NMe$_3$-2-TANI-PTAB (39)

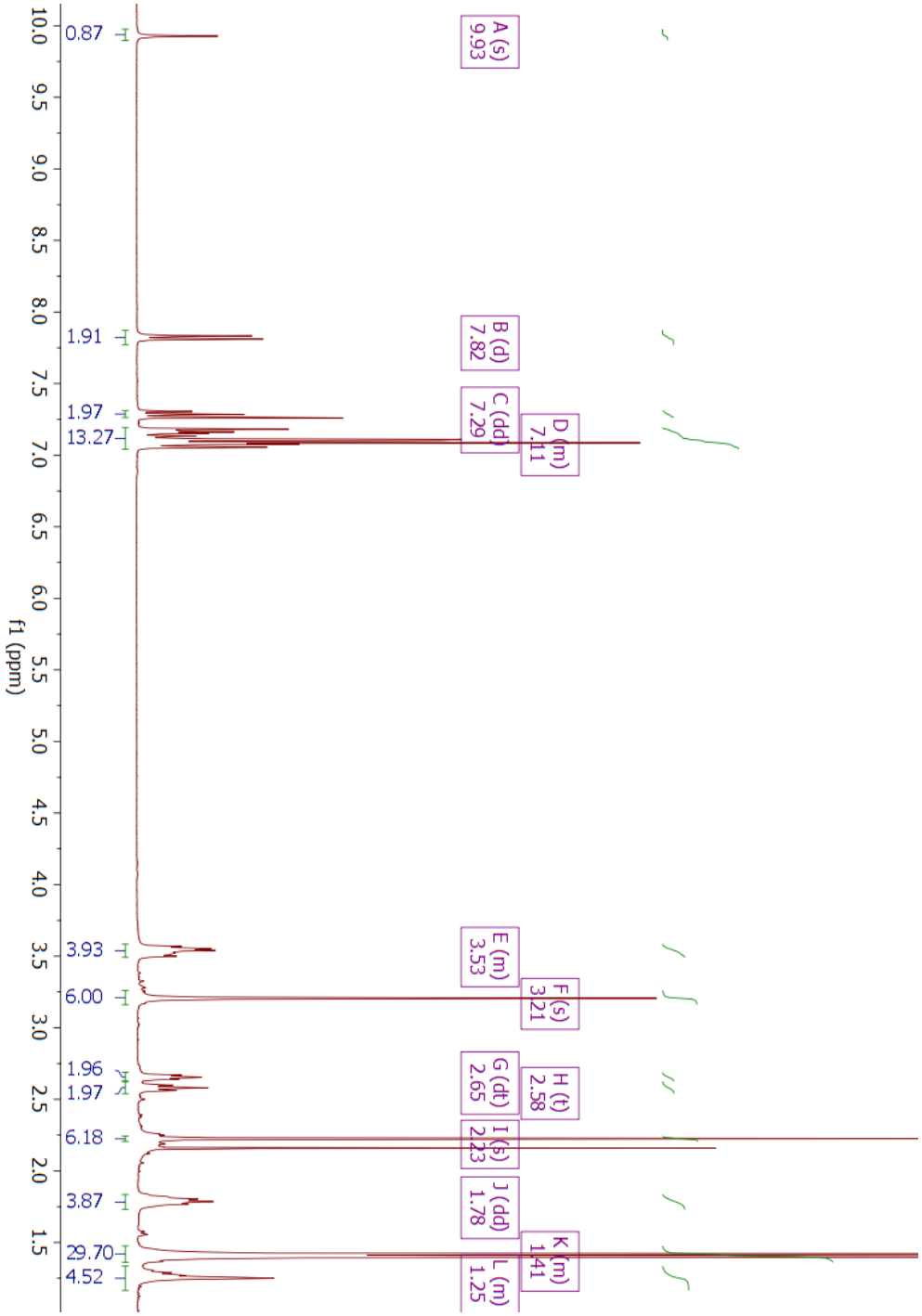

Figure A.67. ***NMe$_3$-2-TANI-PTAB (39) ^{1}H NMR spectrum in CDCl$_3$***

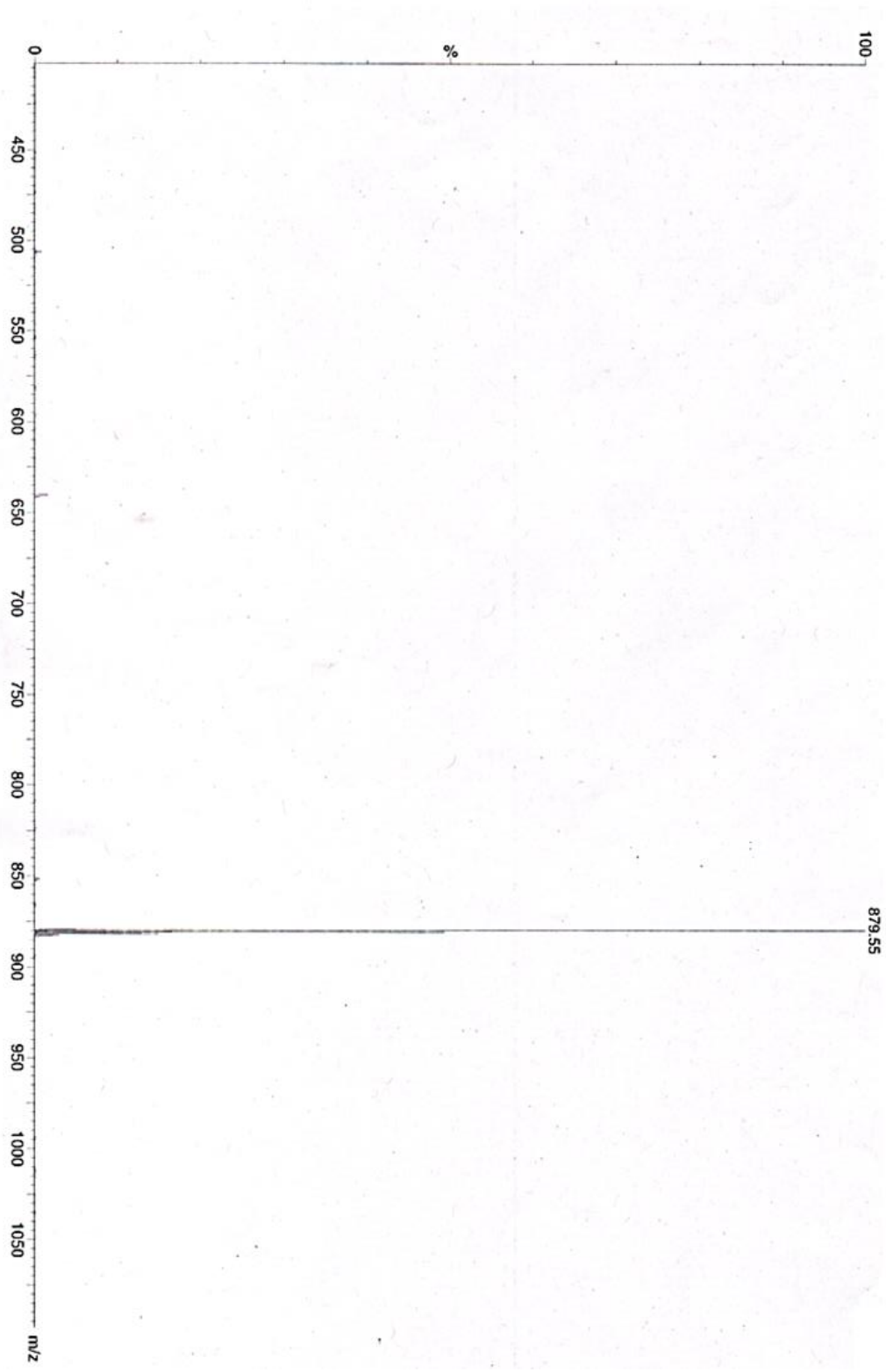

Figure A.68. ***NMe3-2-TANI-PTAB (39) Mass spectrometry***

NMe-2-NMe-TANI (40)

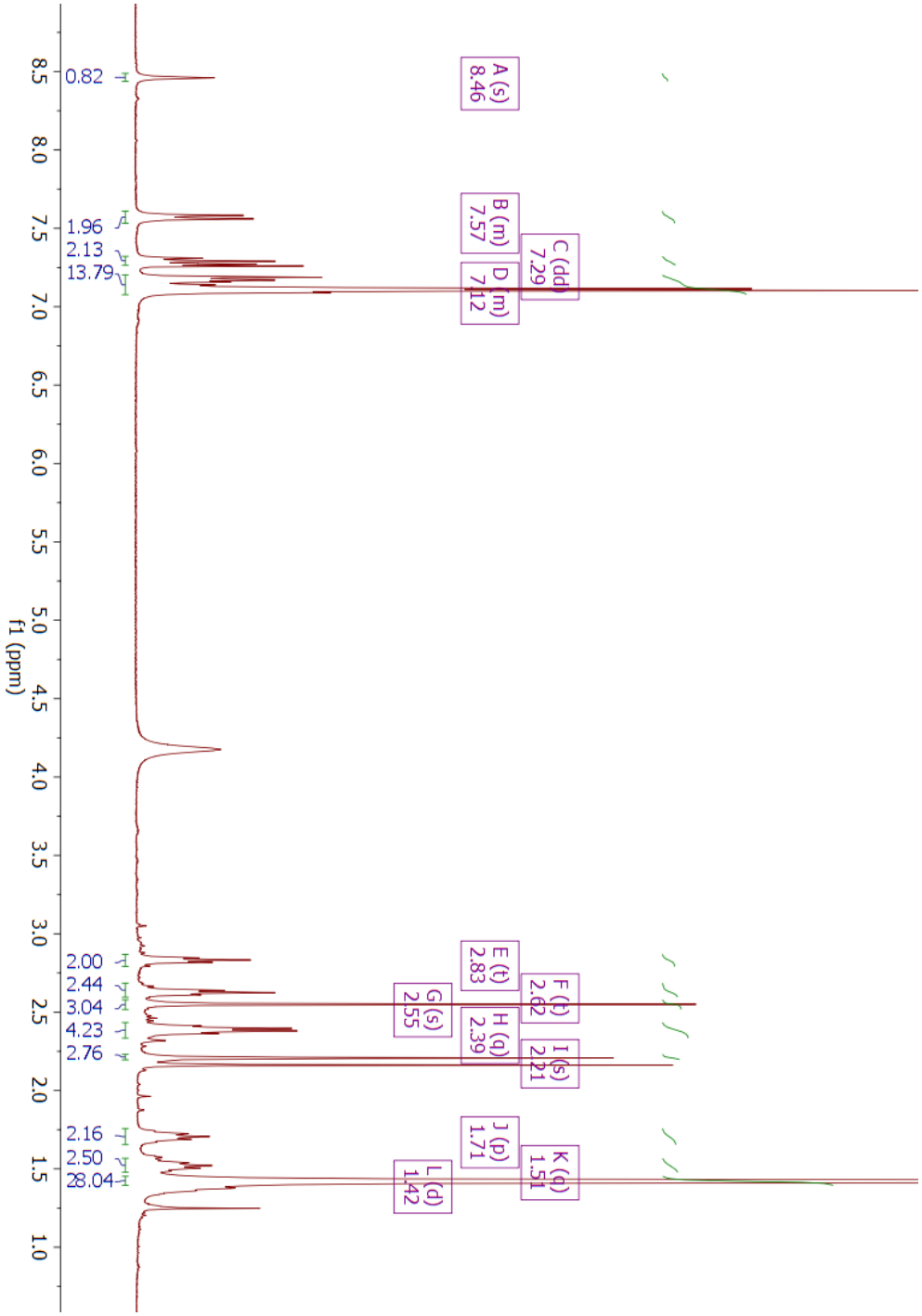

Figure A.69. ***NMe-2-NMe-TANI (40)*** ^{1}***H NMR spectrum in CDCl₃***

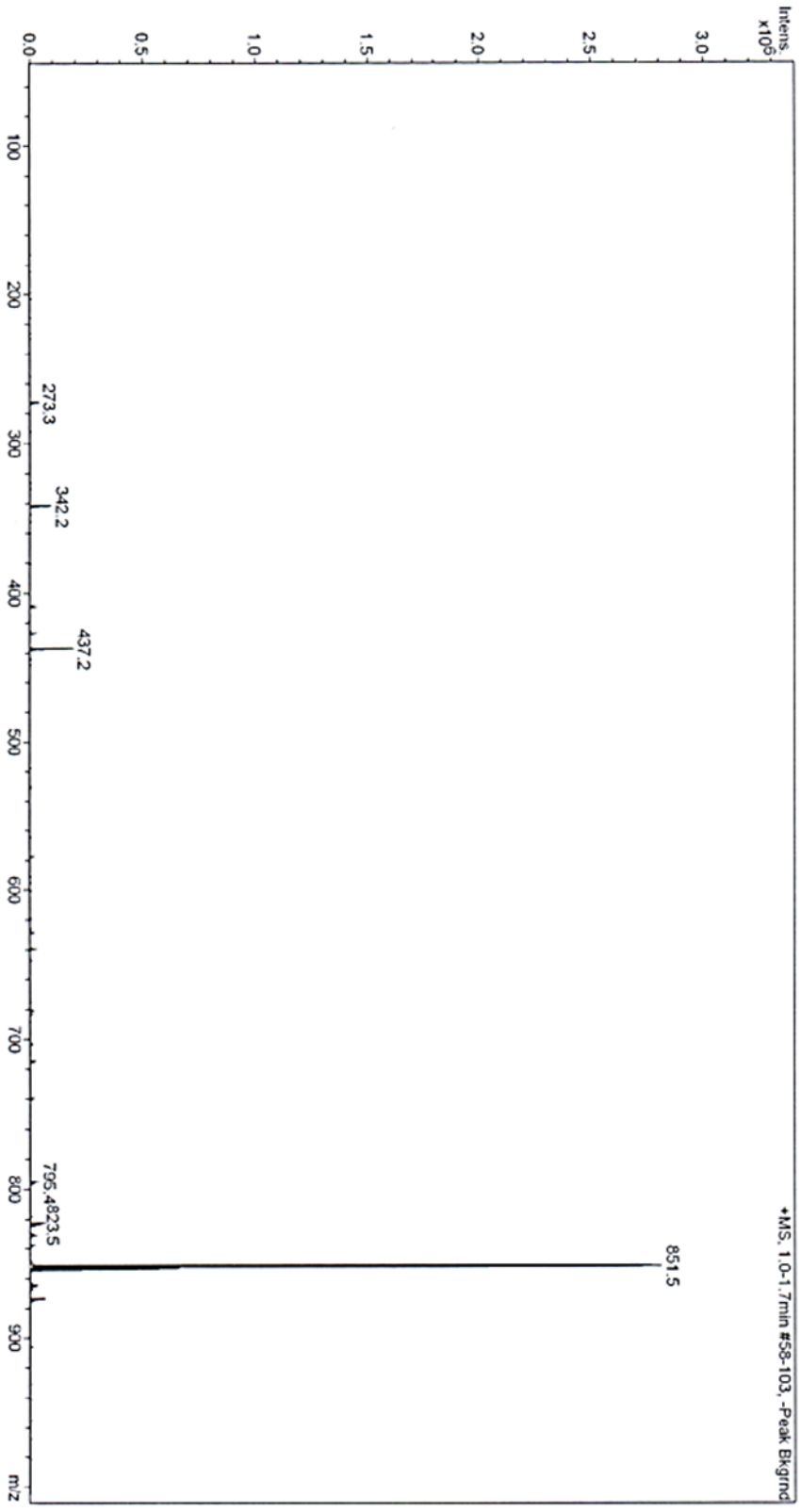

Figure A.70. ***NMe-2-NMe-TANI (40) Mass spectrometry***

MA-11-2-NMe-TANI (41)

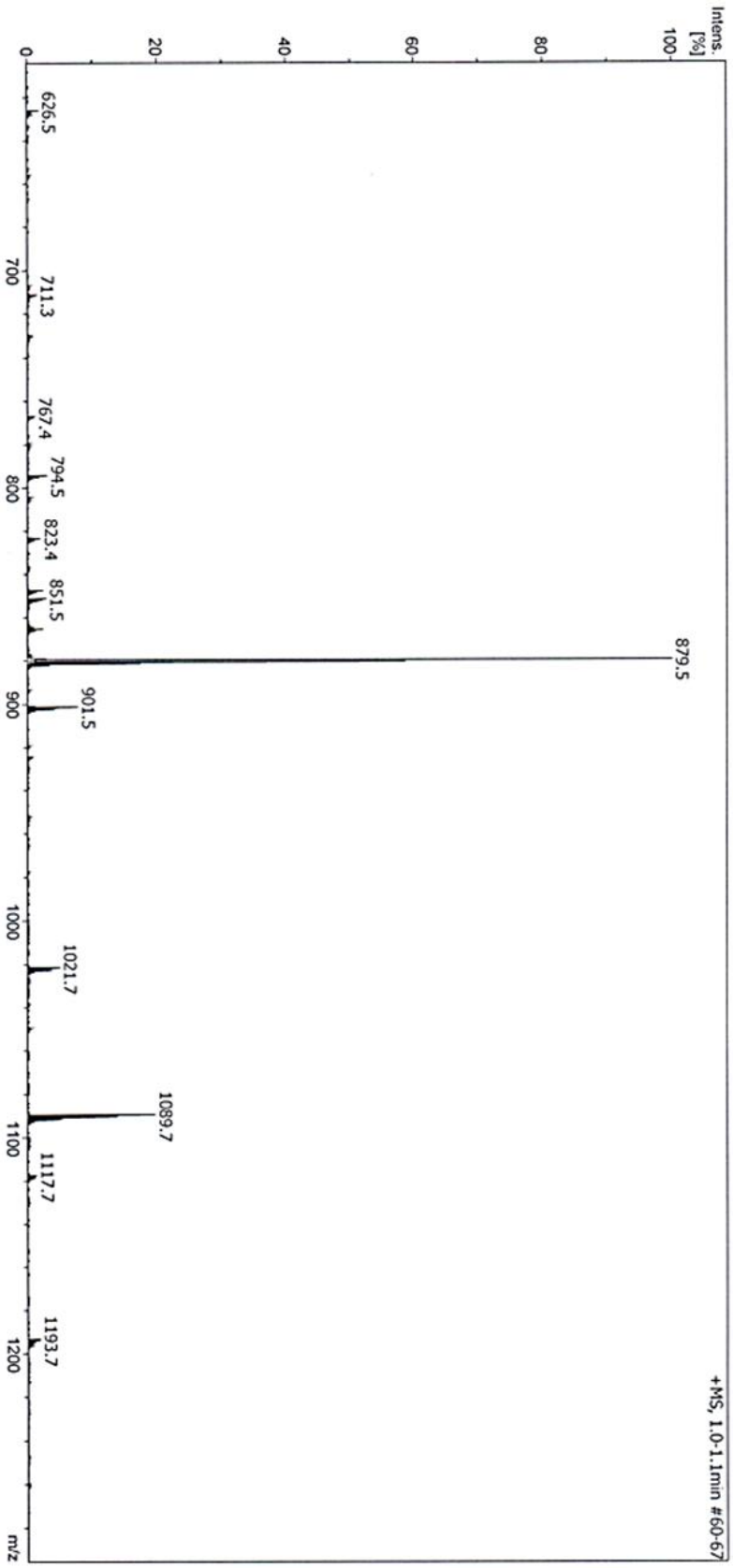

Figure A.71. ***MA-11-2-NMe-TANI (41) Mass spectrometry***

APPENDIX B

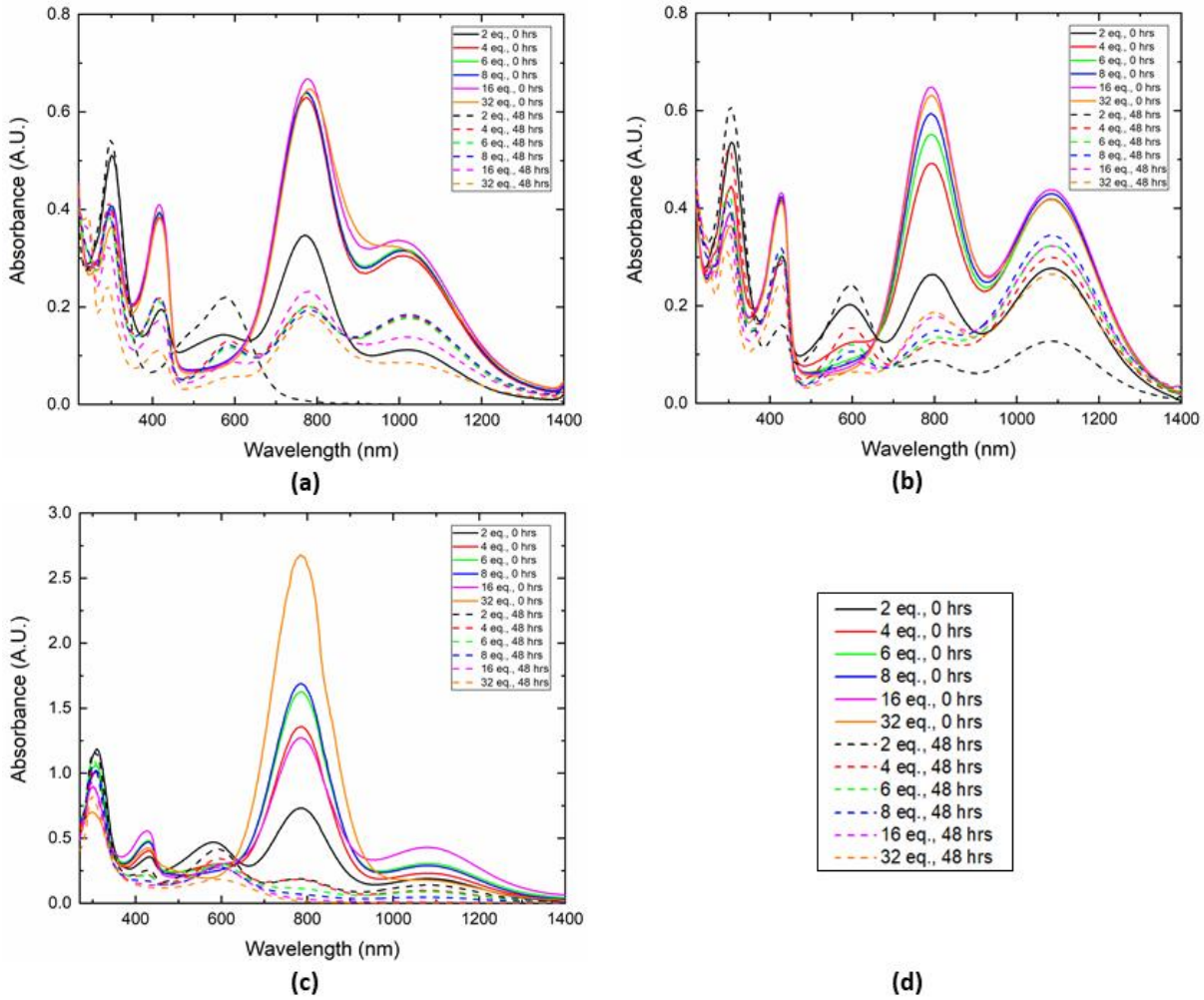

*Figure B.1. UV-Vis absorption spectra of ES **TANI-PTAB** (0.25 mM) doped with 2-32 eq. of **TFA**, (a) in water (b) in water/**PPO** (c) in water/**PPO**/**MO** (d) legend. Spectra recorded at 0 and 48 hrs.*

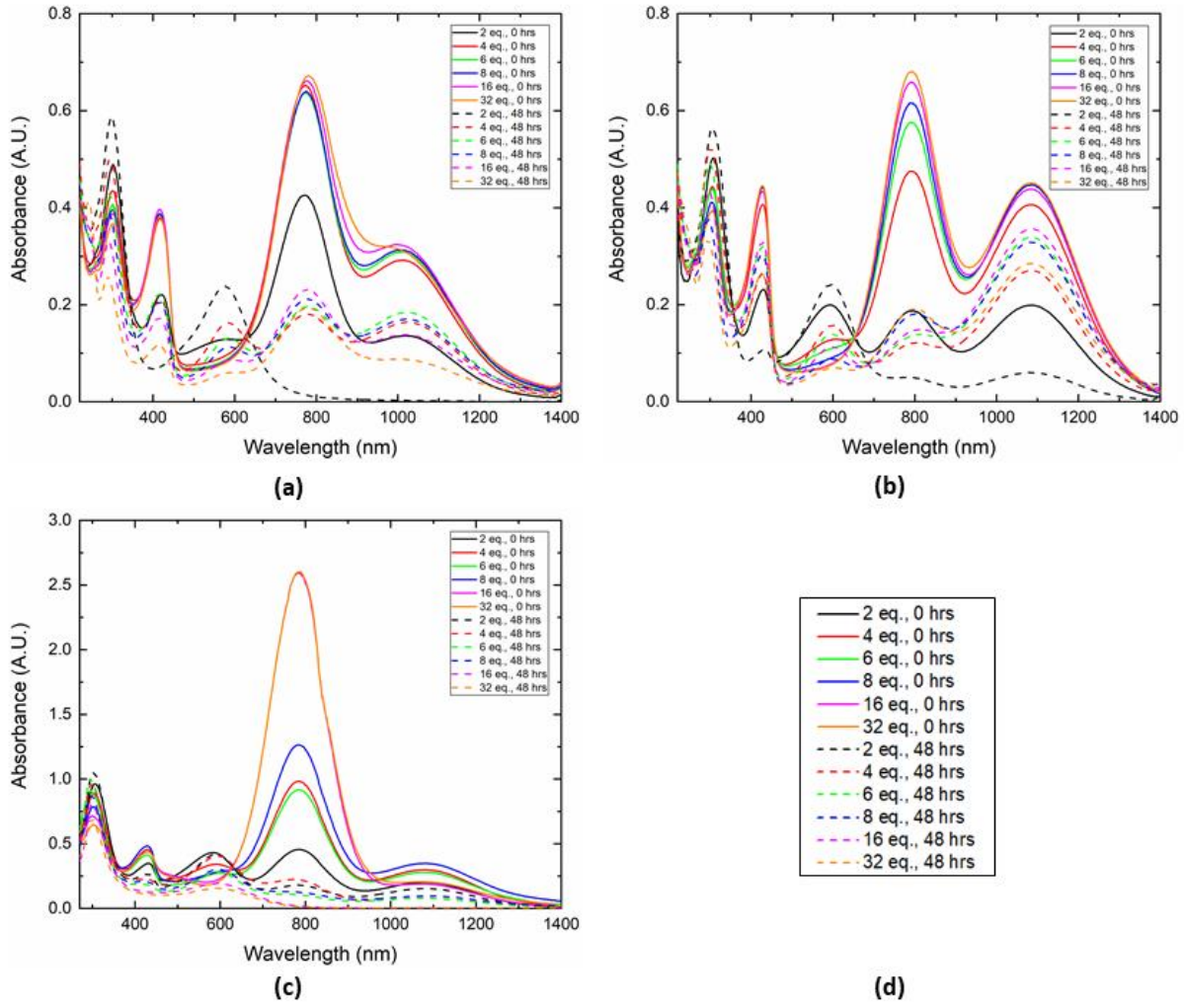

*Figure B.2. UV-Vis absorption spectra of ES **TANI-PTAB** (0.25 mM) doped with 2-32 eq. of **HCl**, (a) in water (b) in water/**PPO** (c) in water/**PPO**/**MO** (d) legend. Spectra recorded at 0 and 48 hrs.*

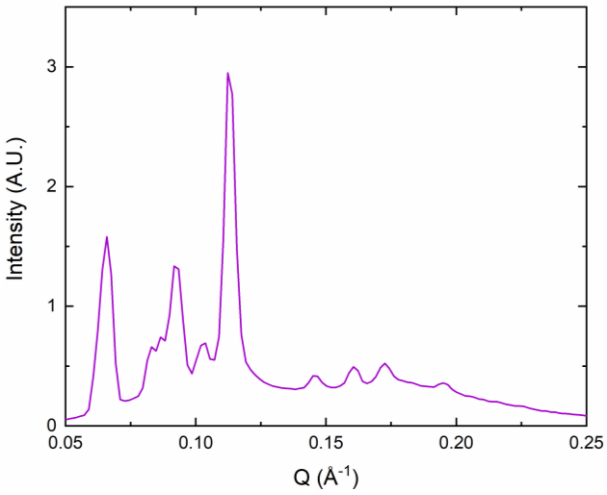

*Figure B.3. 1-D scattering pattern for **MO** containing EB **TANI-PTAB** (14 mm).*

*Table B.1. Lattice parameters for Pn3m cubic phases, prepared with **MO** and **PPO**. Samples were first prepared in the sponge phase using 20 % (v/v) **PPO** and were diluted to the Pn3m phase under centrifugation.*

Run no.	Lattice parameter (nm)
1	10.1
2	10.1
3	11.4
4	11.4
5	10.6
6	10.9
	Average = 10.75

*Table B.2. Lattice parameter calculation for a Pn3m cubic phase containing EB **TANI-PTAB** (2 mM).*

Peak no.	Q ($Å^{-1}$)	d (Å)	Peak ratio	d-spacing (nm)
1	0.0798	78.73666	√2	111.4
2	0.097	64.77511	√3	112.2
3	0.114	55.11566	√4	110.2
4	0.138	45.53033	√6	111.5
5	0.16	39.26991	√8	111.1
6	0.169	37.17861	√9	111.5
				Average = 111.3

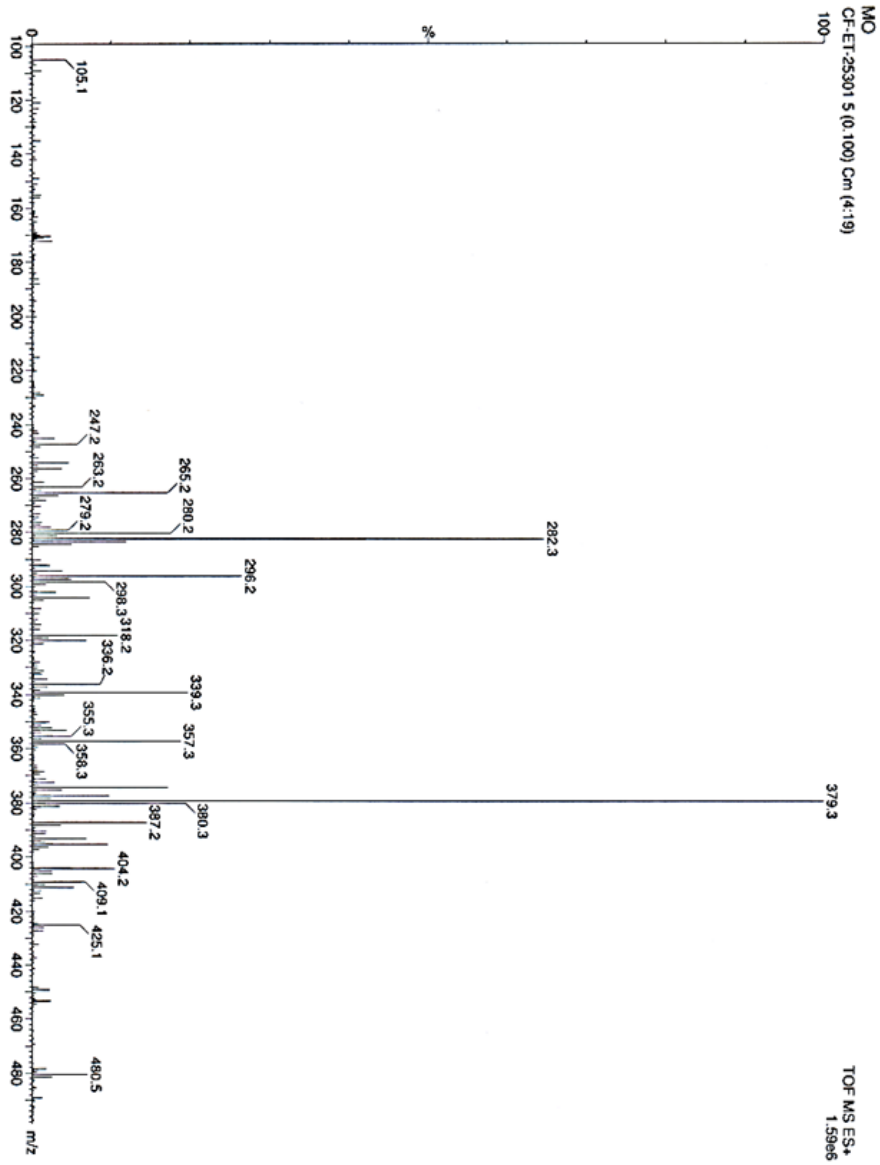

*Figure B.4. Monoolein (**MO**) from Danisco Mass Spectrometry*

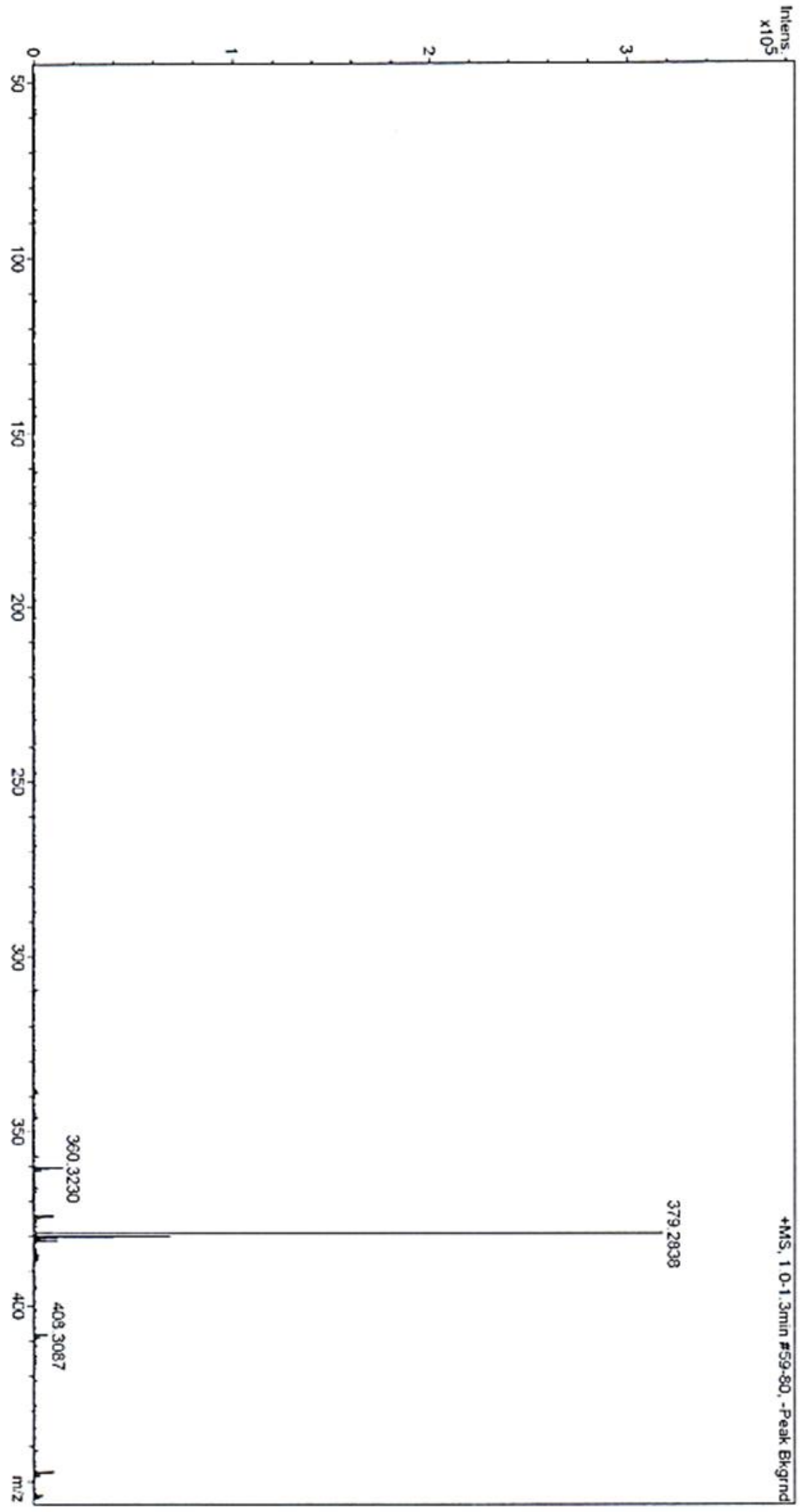

*Figure B.5. Pure Monoolein (**MO**) Mass Spectrometry*

APPENDIX C

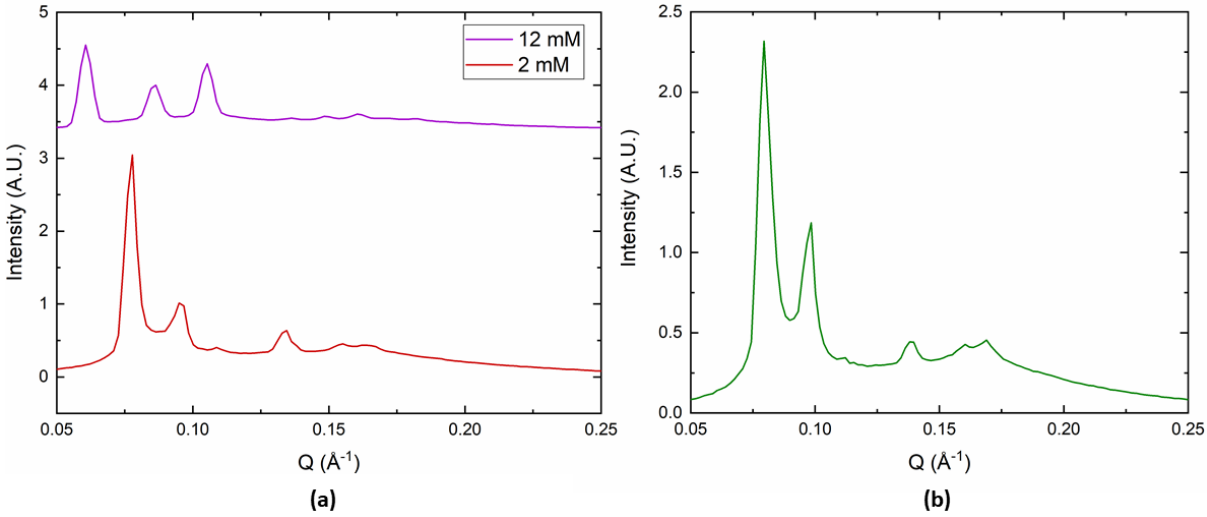

*Figure C. 1. 1-D scattering patterns for **MO** cubic phases containing (a) 2 mM and 12 mM **TANI-C12TAB** (EB) (b) 2 mM **TANI-C12TAB** (ES) doped with 4 molar equivalents of **CSA**.*

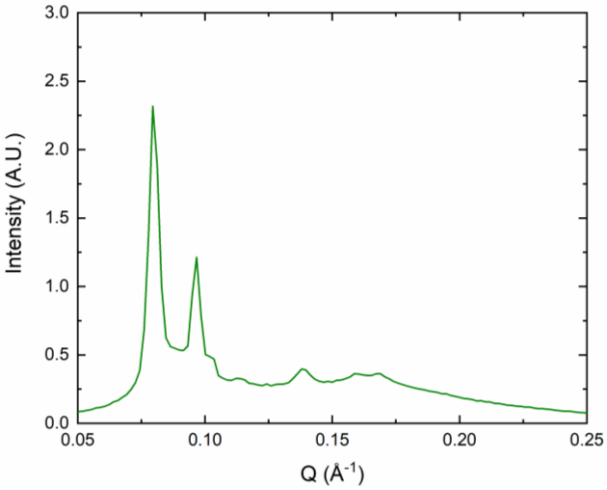

*Figure C. 2. 1-D scattering pattern for **MO** containing 2 mM **TANI-PTPB** (ES) doped with 4 molar equivalents of **CSA.***

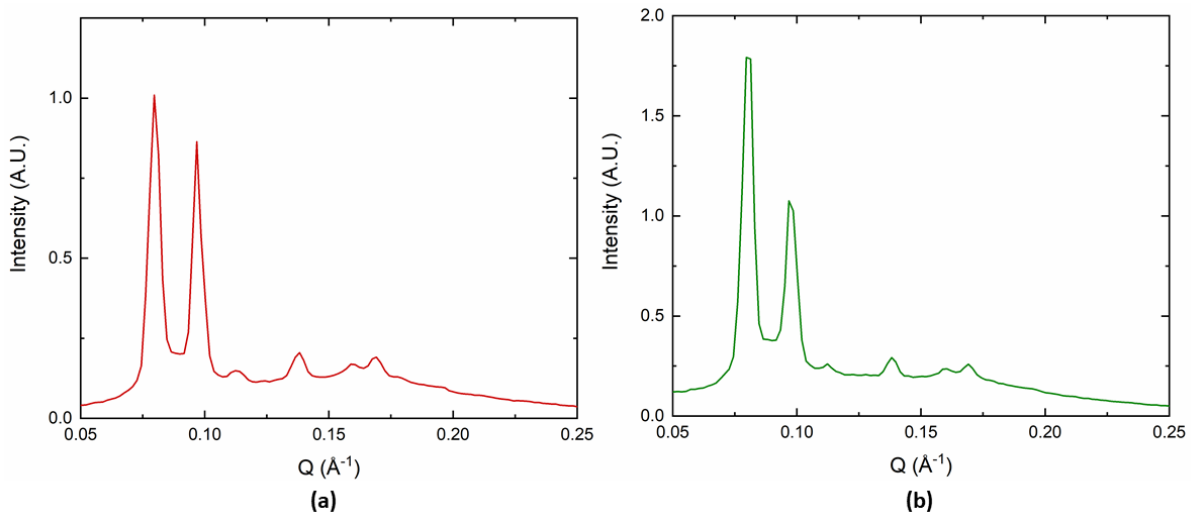

*Figure C. 3. 1-D scattering patterns for **MO** cubic phases containing (a) 10 mM **TANI-(PTAB)$_2$** (EB) (b) 10 mM **TANI-(PTAB)$_2$** (ES) doped with 4 molar equivalents of **NDS**.*

APPENDIX D

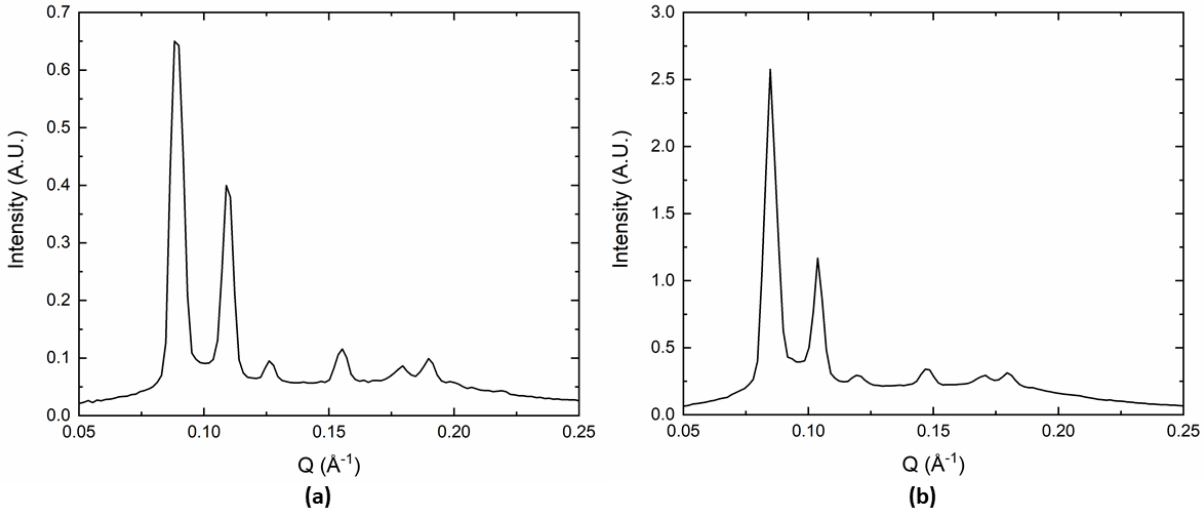

*Figure D. 1. 1-D scattering patterns for **MO** cubic phases containing (a) 24 mM **NDS** (b) 32 mM phytic acid.*

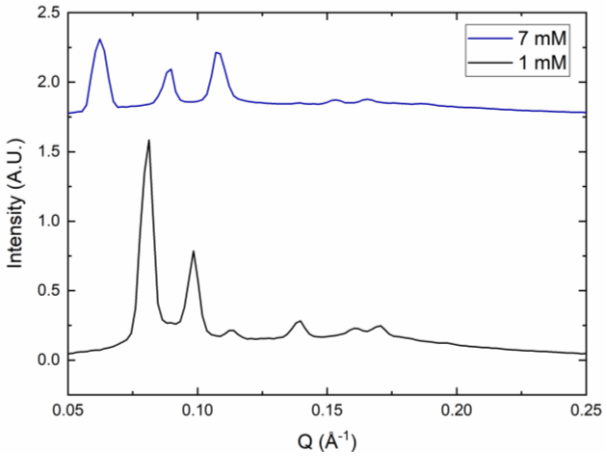

*Figure D. 2. 1-D scattering patterns for **MO** cubic phases containing 1 and 7 mM **MA-11-2-11-MA.***